NASA CONTRACTOR REPORT
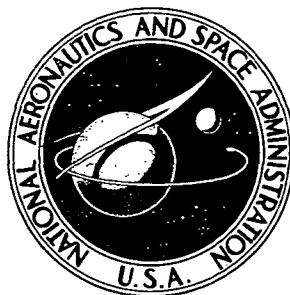
NASA CR-2382

DEVELOPMENT OF ACOUSTICALLY LINED EJECTOR TECHNOLOGY FOR MULTITUBE JET NOISE SUPPRESSOR NOZZLES BY MODEL AND ENGINE TESTS OVER A WIDE RANGE OF JET PRESSURE RATIOS AND TEMPERATURES

*by J. Atvars, G. C. Paynter, D. Q. Walker,
and C. F. Wintermeyer*

Prepared by
BOEING COMMERCIAL AIRPLANE COMPANY
Seattle, Wash. 98124
for Lewis Research Center

NATIONAL AERONAUTICS AND SPACE ADMINISTRATION • WASHINGTON, D. C. • APRIL 1974

1. Report No. NASA CR-2382	2. Government Accession No.	3. Recipient's Catalog No.
4. Title and Subtitle DEVELOPMENT OF ACOUSTICALLY LINED EJECTOR TECHNOLOGY FOR MULTITUBE JET NOISE SUPPRESSOR NOZZLES BY MODEL AND ENGINE TESTS OVER A WIDE RANGE OF JET PRESSURE RATIOS AND TEMPERATURES		5. Report Date APRIL 1974
		6. Performing Organization Code
7. Author(s) J. Atvars, G. C. Paynter, D. Q. Walker, and C. F. Wintermeyer		8. Performing Organization Report No. D6-60226
		10. Work Unit No.
9. Performing Organization Name and Address Boeing Commercial Airplane Company P. O. Box 3707 Seattle, Washington 98124		11. Contract or Grant No. NAS 3-15570
		13. Type of Report and Period Covered Contractor·Report
12. Sponsoring Agency Name and Address National Aeronautics and Space Administration Washington, D.C. 20546		14. Sponsoring Agency Code

15. Supplementary Notes

Final Report. Project Manager, Vernon H. Gray, V/STOL and Noise Division, NASA Lewis Research Center, Cleveland, Ohio

16. Abstract

An experimental program comprising model nozzle and full-scale engine tests was undertaken to acquire parametric data for acoustically lined ejectors applied to primary jet noise suppression. Ejector lining design technology and acoustical scaling of lined ejector configurations were the major objectives. Ground static tests were run with a J-75 turbojet engine fitted with a 37-tube, area ratio 3.3 suppressor nozzle and two lengths of ejector shroud (L/D = 1 and 2). Seven ejector lining configurations were tested over the engine pressure ratio range of 1.40 to 2.40 with corresponding jet velocities between 305 and 610 m/sec. One-fourth scale model nozzles were tested over a pressure ratio range of 1.40 to 4.0 with jet total temperatures between ambient and 1088°K. Scaling of multielement nozzle ejector configurations was also studied using a single element of the nozzle array with identical ejector lengths and lining materials. Acoustic far field and near field data together with nozzle thrust performance and jet aerodynamic flow profiles are presented in this report. The parametric variation of lining sound power insertion loss and tuning frequency is presented as a function of lining material and nozzle flow conditions. The directivity of far field acoustic radiation is found to be a critical factor in lining evaluation, as is noise generated downstream of the ejector exit plane. Geometric scaling of configurations is demonstrated, and the importance of flow similarity between scaled configurations is emphasized. Comparisons made between measured lining performance and the predicted performance based upon existing lined duct analysis procedures indicate good agreement in the lining core depth and tuning frequency relationship. However, measured attenuations are generally less than the predicted values by up to 3 dB. The bare 37-tube nozzle suffers a 2 to 3% thrust penalty relative to the conical nozzle, although static thrust augmentation is obtained with the ejector configurations. At a pressure ratio of 2.40, the 37-tube nozzle suppresses the overall sound power by 8 dB relative to the equivalent conical nozzle. With the L/D = 2 lined ejector this suppression increases to 15 dB. Calculated sideline perceived noise levels at 649 m (2128 ft) indicate a peak sideline PNL reduction of 10 PNdB with the 37-tube nozzle and 15 PNdB with the 37-tube nozzle and L/D = 2 lined ejector. Model-scale data indicate additional reductions of 2 to 3 PNdB for these configurations at a jet velocity of 800 m/sec. This velocity is above the operating range of the J-75 engine.

17. Key Words (Suggested by Author(s)) Acoustic linings Ejector performance Ejectors Acoustic scaling Jet noise suppressors Nozzles Thrust performance Nozzle performance		18. Distribution Statement Unclassified - unlimited Cat. o2	
19. Security Classif. (of this report) Unclassified	20. Security Classif. (of this page) Unclassified	21. No. of Pages 334	22. Price* $7.50

Page Intentionally Left Blank

CONTENTS

CONTENTS–Concluded

DEVELOPMENT OF ACOUSTICALLY LINED EJECTOR TECHNOLOGY

FOR MULTITUBE JET NOISE SUPPRESSOR NOZZLES

BY MODEL AND ENGINE TESTS

OVER A WIDE RANGE OF JET PRESSURE RATIOS AND TEMPERATURES

By J. Atvars, G. C. Paynter, D. Q. Walker, and C. F. Wintermeyer
Boeing Commercial Airplane Company

SUMMARY

An experimental program was undertaken by the Boeing Commercial Airplane Company to acquire an extensive, parametric set of data for acoustically lined ejectors applied to primary jet noise suppression. The program comprised model nozzle and full-scale engine tests. The major objective was to develop the technology of lined ejectors and in addition to demonstrate the possibility of scaling lined ejector performance.

Ground static engine tests were run using a Pratt and Whitney J-75 turbojet engine with a 37-tube, area ratio 3.3 suppressor nozzle and two lengths of ejector shroud (L/D = 1 and 2). Ejector area ratio was 4.3 and the ejectors were acoustically lined with perforated sheet and honeycomb cavity core material of various specifications. A total of seven full-scale ejector lining configurations were evaluated over the engine operating range (nozzle pressure ratios from 1.40 to 2.40 with corresponding primary flow velocities of 305 to 610m/sec). Equivalent one-fourth scale configurations were tested in a hot jet model test facility over a more extensive range of test conditions than was possible at full scale. The model-scale program also included two conical nozzles which were coupled to ejectors of L/D = 4 and 8 to investigate the single-element concept of scaling a multitube nozzle and ejector configuration. A total of 17 model-scale ejector lining configurations were evaluated over a range of nozzle pressure ratios between 1.40 and 4.0 with jet total temperatures between ambient and 1088°K (1500°F).

Acoustic far field and near field data together with nozzle thrust performance and jet aerodynamic flow profiles are presented in this report.

Parametric variations of lining sound power insertion loss and tuning frequency as a function of lining material specification and nozzle flow conditions are presented. The far field radiation

characteristics of ejectors are found to be critical in lining evaluations, as is the presence of noise generated downstream of the ejector exit plane. Comparisons are made between measured lining attenuation performance in the severe ejector environment and predicted performance based upon current lined duct analysis procedures (as used for turbomachinery noise reduction). The results indicate that lining tuning frequency may be predicted from the lined duct procedure, although the prediction of attenuation requires a more comprehensive understanding of the distribution of acoustic sources and the flow environment within the ejector. Measured attenuations, although low, were generally found to be within 3 dB of the predicted value. Predicted attenuations were in the range 4 dB to 12 dB, depending upon ejector length, lining material and nozzle total temperature and pressure conditions.

The nozzles and ejectors tested in this program may be geometrically scaled for acoustical and thrust performance evaluations, provided that aero- and thermodynamic flow similarity is maintained between the scaled configurations. Flow similarity is shown to be critical in the scaling of far field acoustic characteristics. The single-element concept of scaling lined ejectors did not provide results which were directly applicable to the equivalent multi-element nozzle and ejector configuration.

Static thrust measurements indicate that, with respect to the reference round convergent nozzle, the 37-tube suppressor nozzle suffers a 2%-3% thrust loss over the engine operating range. Thrust augmentation is obtained with the ejector configurations. A net thrust increase of 6% for the $L/D = 1$ ejector and 9% for the $L/D = 2$ ejector is obtained at a nozzle pressure ratio of 2.4 and jet temperature of $811°$ K ($1000°$F). The presence of acoustic linings in the ejector has a negligible effect on thrust performance.

The 37-tube nozzle suppresses the overall sound power from the J-75 engine by 3 dB at NPR = 1.40, increasing to 8 dB at NPR = 2.40. The unlined or hardwall ejector configurations provide no jet noise suppression relative to the 37-tube nozzle. However, the presence of an ejector has a marked influence on the directivity pattern of high-frequency jet noise, resulting in sharp maxima in intensity at about $120°$ from the engine inlet. The 37-tube nozzle with a lined $L/D = 2$ ejector suppresses jet noise by approximately 9 dB at NPR = 1.40 increasing to 15 dB at NPR = 2.40 relative to the reference conical nozzle.

Calculated 649m (2128 ft) sideline perceived noise levels showed that the peak sideline PNL of the J-75 engine at maximum thrust is reduced by 10 PNdB with the 37-tube nozzle installed; at the same power condition the lined $L/D = 2$ ejector configuration reduces the peak sideline noise by 15 PNdB. Model-scale data indicate additional reductions of 2-3 PNdB at a jet velocity of 800 m/sec which is above the range of the J-75 engine.

INTRODUCTION

The advent of commercial jet aircraft in the 1950s brought with it a new form of annoyance to the population in and around airports in the form of jet noise. The jet noise problem was, at that time, investigated extensively by both airframe and engine manufacturers. A temporary solution was found in the form of suppressor nozzles of various designs which improved the community acceptance of the early models of the 707 and DC-8 airplanes with tolerable penalties on performance and operating costs. The introduction of the turbofan engine concept, which obtained a greater thrust for higher mass flow at lower jet velocity (hence increased efficiency) offered a significant reduction in the jet noise problems. As a result, the jet noise suppression development effort by industry was considerably reduced. Jet noise suppression research was actively resumed during the 1960s when development of the SST reintroduced the turbojet engine together with the inherent jet noise problems.

The establishment of noise certification requirements for new airplanes (FAR 36) with the stated goal to further reduce aircraft noise levels in the future as new technology becomes available, has added to the need for continued research in engine noise reduction. Recent programs conducted by government and industry have provided basic knowledge of the mechanisms of fan and compressor noise generation. This knowledge has been applied to the development of some very successful fan noise attenuation techniques (e.g., using sound-absorbent liners inside engine ducts) for current and future generation subsonic commercial aircraft. The major barrier to further reduction of engine noise has once again become jet exhaust noise.

The work described in this report represents a continuation of efforts to develop new or additional techniques for jet noise suppression. Jet noise suppression research, which was conducted by Boeing during the SST program, has been reported extensively (refs. 1 and 2). The main effort concentrated on the development of an efficient multi-element suppressor nozzle. Some isolated tests demonstrated that jet noise could be further attenuated by adding an acoustically absorbent ejector shroud downstream of the multi-element mixer nozzle. Although a considerable level of sophistication has been achieved in the application of acoustic linings to turbomachinery noise reduction and reliable theoretical methods exist for the design of duct linings (ref. 3), these techniques have never been evaluated systematically for their usefulness in jet noise suppression. This program was conducted specifically to demonstrate the usefulness of acoustically lined ejectors for the absorption of jet noise and to provide some foundations for a lined ejector-suppressor technology.

To achieve this objective, Boeing performed a test program in which conical and 37-tube nozzles were used, model and full scale, to determine the jet noise suppression potential of

3

acoustically lined ejectors. A detailed description of the test program, hardware, and test techniques is given in this report. The test results obtained are first presented separately for the model-scale and the full-scale series under the subsections of acoustic far field data, near field data, thrust performance data, and flow survey data. Then the model- and full-scale results are compared and analyzed for scaling.

In carrying out the above work, large quantities of various jet noise and nozzle propulsion performance data were acquired and analyzed. Some innovative jet noise measurement techniques were also developed to eliminate ground reflection interference in the test data. Highlights of these additional results are also included in this report.

PROGRAM RATIONALE

Suppression of airplane engine jet noise has been the subject of continuing research and development for many years, by both industry and government laboratories as well as the academic world. Significant accomplishments have been achieved to date through the application of two basic techniques:

- Reduction of jet noise generation through the reduction of jet exit velocity, i.e., turbofan engines

- Various forms of mixing nozzles such as multitube or multilobe to induce more efficient mixing of the jet and a more rapid decay of jet velocity.

Similar progress has been made in the area of turbomachinery noise suppression. This has been accomplished by acoustically treating the engine interior passages (inlets and fan exhaust ducts) to absorb the turbomachinery noise before it is radiated from the engine.

The success of acoustically absorbent materials in reducing fan noise has led to the question of whether these materials could also be used to attack the jet noise problem. At first sight, there does not seem to be any easy or economical way to use sound absorbent materials for that purpose because jet noise is generated downstream of the primary nozzle. However, an examination of the problem shows a potential use for acoustic linings. High-frequency noise is attenuated more rapidly by the atmosphere than low-frequency noise, and, in addition, is easier to attenuate with acoustic liners. The characteristics of a multi-element nozzle are such that the predominant energy in the acoustic spectrum is of a higher frequency relative to a round convergent nozzle of the same flow area. Also, the source location of the predominant high-frequency noise is closer to the nozzle exit plane. The jet noise suppressor system concept is, therefore, a multi-element nozzle exhausting into an ejector shroud, the walls of which are acoustically lined. The linings may be designed to provide maximum attenuation at the frequencies of highest noise levels. The limiting feature of such a configuration is the noise produced downstream of the ejector exit plane, which cannot be attenuated by the ejector linings.

This concept has been verified experimentally (ref. 2) and shown to be a workable solution.

In order to develop this experimental concept into a viable design for airplane use it is essential that the noise suppression characteristics and the performance and weight penalties be optimized. The state of the art in optimizing multi-element jet noise suppressor nozzles is considerably more advanced than the corresponding ability to optimize a suppressor system comprising a suppressor nozzle and acoustically lined ejector. In spite of the fact that considerable theoretical and practical

experience exists in the application of acoustic linings to turbomachinery noise reduction on turbofan engines, the jet noise problem and related ejector-suppressor design variables are different enough from the turbomachinery case that work specifically addressed to the development of acoustic lining technology for jet noise suppression needs to be undertaken. As far as possible, use would be made of the experience gained with acoustic linings for fan noise reduction.

An experimental research program was designed to acquire a parametric set of data for a commonly used acoustic lining material—perforated sheet with a cellular cavity core and impervious backing sheet. The program was designed to answer the question of how these linings would perform in the severe environment of a primary jet flow. An existing hexagonal array 37-tube nozzle, which had been previously tested (ref. 1) and shown to be a good design, was selected as a reference nozzle for the program.

With the primary goal thus established, the program was expanded to include additional objectives that would benefit future work, namely:

- Conduct tests with both model- and full-scale hardware to demonstrate the feasibility of scaling lined ejector configurations.

- Determine the applicability of the existing fan duct lining design procedures to ejector lining designs.

- Take both near and far field acoustic and jet thermodynamic data to create a data bank that may contribute in the future towards the understanding of mean jet flow structure and noise source relationships for multi-element mixing nozzles and lined ejectors.

An extensive discussion of the principles of noise reduction by mixing nozzles and ejector nozzles is given by K. Eldred (ref. 4). A simplified model of the noise generated by a mixing nozzle and the equivalent noise reduction that is obtained with respect to a round convergent nozzle is shown in figure 1. It is postulated that the total noise from a multi-element mixing nozzle consists of the noise radiated by the individual tube flows before they coalesce at some downstream station, plus the noise radiated by the combined flow further downstream. The above model implies that the frequency spectrum of the premerging noise is primarily a function of the geometry and the jet velocity of a single element in the nozzle array, while the sound power level is some function of the number of elements in the nozzle array. If this is the case, then in an acoustically lined ejector the lining would be exposed in the premerging region to noise characteristic of the individual tubes. Thus, if the noise from one of these elements of the mixing nozzle were to be isolated then it would generate a spectrum shape representative in frequency distribution of the premixing noise. This principle would allow full-scale acoustic lining properties to be evaluated less expensively by conducting tests using a single element of a full-scale mixing nozzle and operating it in a model-scale facility.

In order to investigate this single-element scaling concept as well as expand the lined ejector technology data base, the program contained a segment of work in the model scale test facility using a combination of lined ejectors with single-tube nozzles of the same size as the elements of the full and one-fourth scale 37-tube nozzle arrays.

DESCRIPTION OF ACOUSTIC LININGS

RELATED PAST EXPERIENCE

Over the past few years considerable experience, both experimental and analytical, has been gained in the application of acoustic linings to engine inlets and fan exhaust ducts for the purposes of attenuating fan noise (ref. 5). Computerized design procedures have been developed at Boeing, based on the work of S. H. Ko (ref. 3), to predict the important lining and duct design parameters. The program basically solved the two-dimensional wave equation in a duct of a rectangular cross section which has two opposite walls lined with a single-layer lining. There can be uniform airflow in the duct, and it is assumed that the noise is generated upstream of the lined duct, with the sound energy being evenly (equal amplitude) distributed in all the propagating modes. The lining acoustic impedance (if it is known) can be input directly to the program, or it can be calculated within the program for the special case of a single-layer tuned resonator lining with a perforated plate face sheet in the presence of grazing flow. The latter case is solvable using a Boeing-developed semi-empirical impedance model (ref. 3) for perforated plates with grazing flow. In this model the single-layer lining consists of a perforated plate face sheet, with a thickness-to-hole diameter ratio of less than one, attached to a honeycomb core, and an impervious backing sheet.

DESIGN APPROACH

Considering previous experience it was decided to use the above design tool for perforated plate linings as the starting point for this program. Several fundamental differences were initially recognized to exist between linings in a fan exhaust duct and linings in an ejector surrounding a primary jet flow. The most significant of these were considered to be the characteristic distributed nature of jet noise within the ejector and the severe velocity and thermal gradients in the flow. In addition to influencing lining performance, the radial flow gradients at the ejector exit plane could also affect the way in which sound energy is radiated to the far field.

Since the acoustic performance of a lined ejector configuration can only be optimized for a given set of test conditions, a "design" case was identified based upon the takeoff power setting of the J-75 turbojet engine (the engine selected for the full-scale test program). Under static test conditions the takeoff power setting approximately corresponds to:

Nozzle pressure ratio = 2.4

Jet temperature = 811°K (1000°F)

Jet velocity   =   610m/sec (2000 ft/sec)

Sea level thrust   =   66,800 newtons (15,000 lbf)

The Boeing fan duct lining design procedure (ref. 3) was used to predict lining core depth and face sheet flow resistance (in terms of percent open area), for both model- and full-scale ejectors, to give maximum attenuation at a critical lining tuning frequency. The tuning frequency was chosen to correspond to the peak frequency associated with the jet noise of the 37-tube nozzle, at the design operating condition:

Model scale f_t =   8000 Hz

Full scale f_t =   2000 Hz

In order to broaden the aspect of the studies such that the optimum lining parameters could be verified experimentally, additional off-design lining configurations were chosen with the following parametric variations:

(a) Flow resistance ($R/\rho c$) : ("design" + 100%) and ("design" - 50%)

(b) Core depth (d) : (tuning frequency ± 1/2 octave)

The technique of obtaining "design" and "off-design" values of the lining flow resistance (percent open area) can best be illustrated by referring to figures 2 and 3, which summarize the predicted relationships between attenuation and flow resistance for the model- and full-scale ejectors, respectively. The main objective was to evaluate linings for which measurable changes in attenuation were predicted over the range of flow resistances selected.

As a result of these preliminary lining prediction studies, the linings listed in tables 1 and 2 were designed and fabricated for experimental evaluation in this program.

Lining material costs in the program were minimized by using simplified hardware designs. The choice of a hexagonal cross-sectional shape for the ejectors to approximate a cylinder enabled flat lining test panels to be used as shown by the full-scale example in figure 4.

DESCRIPTION OF THE TEST PROGRAM

Model- and full-scale test programs were structured to obtain the data and evaluate the concepts outlined. Full-scale tests were conducted at the Boeing Boardman, Oregon test facility. Model testing was carried out at the company's hot nozzle test facility in Seattle.

A Pratt & Whitney J-75 turbojet engine (without afterburner) was used for the full-scale evaluations. The engine was operated over a range of nozzle pressure ratios between 1.40 and 2.40 with corresponding gas total temperatures between 533°K (500°F) and 811°K (1000°F). The approximate range of jet velocities was 305 to 610m/sec (1000 to 2000 ft/sec). The maximum static thrust of the engine, as tested, was 66,800 newtons (15,000 lbf). The standard round convergent nozzle, with a centerbody, was tested to establish baselines for both propulsion and acoustic evaluations. The full-scale nozzle configurations tested comprised the 37-tube, area ratio 3.3 suppressor nozzle (approximately equal in geometric area to the standard conical nozzle) and the suppressor nozzle in conjunction with ejectors of two lengths in both hardwall (for reference) and various acoustically lined configurations.

The model-scale program was divided into two phases:

- One-fourth scale models of all the full-scale configurations, including the round convergent nozzle, were tested at conditions of nozzle pressure ratio and gas temperature corresponding to the nominal full-scale test points. In addition, the independent control of pressure and temperature at the model test facility allowed the one-fourth scale models to be evaluated over a wider range of nozzle operating conditions, and tests were conducted at nozzle pressure ratios between 1.40 and 4.00 and gas total temperatures between ambient and 1088°K (1500°F). The approximate corresponding range of jet velocities was between 229m/sec (750 ft/sec) and 855m/sec (2800 ft/sec).

- Two conical nozzles corresponding to single elements of the full- and model-scale 37-tube arrays were used to investigate the technique of evaluating acoustic linings in ejectors by the single-element concept. Each nozzle was tested with ejectors of length and lining characteristics, including hardwall, equivalent to those used with the related 37-tube arrays. Nozzle operating conditions similar to the one-fourth scale tests were used, although the use of water cooled nozzles enabled a limited amount of data to be acquired at gas total temperatures of 1643°K (2500°F).

A summary of the test configurations for this program is given schematically in figure 5.

The complete test program was planned to facilitate the comparison of engine and model-scale test data. For acoustic, propulsion performance, and jet flow field surveys, both data aquisition and reduction procedures were similar as were the relative measurement locations of most parameters. Experience has shown the characteristics of test facilities to be of particular importance in far field acoustic measurements. Both facilities in this program enabled acoustic data to be acquired in test arenas with smooth, fully reflecting surfaces and, with the use of ground level microphones, data could be easily corrected to "free field" conditions.

TEST FACILITIES

Model Scale

The hot nozzle test facility is a static test facility for the determination of exhaust nozzle propulsion performance and related, exterior noise fields. The facility has a maximum airflow capacity of 18.15 kg/sec (40 lb/sec) and can be used to measure axial thrusts up to 8900 newtons (2000 lbf) with a repeatability of 0.5% of the full-scale reading. Nozzle pressure ratios of 4.0 and total temperatures of 1643°K (2500°F) can be achieved for continuous operation. The design of the burner, however, produces relatively large temperature gradients, e.g., 167°K (300°F) gradient across the primary exit flow for an average total temperature of 1088°K (1500°F)]. Random temperature variations with time, at a given point, are ±16.7°K (30°F) at 1088°K (1500°F). Average primary total temperatures are determined from an area-weighted rake, containing seven shielded chromel/alumel thermocouples approximately 10cm upstream of the nozzle mounting flange. A similar rake arrangement for total pressure is located 180° from the temperature rake. The nozzle centerline is 1.83m (6 ft) above ground level.

The arena for acoustic measurements consists of a smooth, flat concrete surface as shown in figure 6. The arena is large enough to allow acoustic far field measurements to be made on a 15.2m (50 ft) radius centered on the test nozzle exit plane. Noise measurements are limited, however, to the quadrant of 90° to 180° from the nozzle inlet axis. Building surfaces in the vicinity of the test stand were covered with 10cm thick acoustically absorptive material to minimize sound reflection into the acoustic arena.

Full Scale

. The Boeing Boardman facility is a combined propulsion and acoustic static test facility for aircraft engines. An overall view of the test site is given in figure 7.

In this program the engine was mounted in the test stand with the engine centerline 3.61m (11.9 ft) above ground level, figure 8. The concrete test arena, machine finished to within 0.63cm

of flat, extends to a radius of 70m (250 ft) in the aft quadrant, centered on the engine exhaust nozzle. In the forward quadrant the concrete surface enables acoustic measurements to be made at a radius of 15.2m (50 ft) between 0° and 90° relative to the engine inlet centerline. Beyond the acoustic arena surface the terrain is flat rangeland free of obstructions.

Since the acoustical evaluations of this program were related explicitly to jet noise, an effort was made to minimize the possible interference from other sources of engine noise. An inlet muffler box was installed together with side barriers to attenuate engine inlet and case radiated noise, respectively, figure 9. The inlet muffler box, although used for all acoustic tests, was removed to enable the engine baseline configuration to be run for reference propulsion performance purposes.

Control of the engine was from a small building adjacent to the test stand; propulsion and acoustic data acquisition and reduction systems were located in a second building approximately 150m from the test stand.

All building and equipment surfaces in the vicinity of the test stand were covered with 10cm thick acoustically absorptive material to minimize sound reflection into the acoustic arena.

During the full-scale test program, mechanical difficulties were experienced with the J-75 engine. A replacement engine was required and, as will be seen later in the text, minor differences existed between the performance characteristics of the two engines. These differences, however, were small and the engine change did not adversely affect the results from the test program.

TEST HARDWARE

Model Scale

The one-fourth scale nozzles were a 15.2cm (6 in.) diameter round convergent nozzle, figure 10, and a scaled 37-tube, area ratio 3.3 array, figure 11. Simplified hexagonal ejectors, area ratio 4.3, with interchangeable interior panels were tested, figure 12, in conjunction with the 37-tube array. For the single-element concept of lining evaluation two additional conical nozzles, 10.9cm (4.3 in.) and 2.74cm (1.08 in.) diameters, typically shown in figure 13 were tested together with hexagonal ejectors, figures 14 and 15. For the single-element studies ejector geometry was chosen such that the radial distance from the nozzle lip to the ejector wall was the same as that for a tube in the outer row of the equivalent 37-tube nozzle and ejector. This gave ejector area ratios of 10 and 8.5 for the 10.9cm and 2.74cm diameter single nozzles, respectively.

A summary of model-scale nozzle geometry together with ejector dimensions is given in table 3.

Full Scale

The round convergent nozzle of the J-75 engine is 70.6cm (27.8 in.) diameter with a 27.4cm (10.8 in.) diameter centerbody. This reference configuration is shown in figure 16. The 37-tube suppressor nozzle, figure 17, has a hexagonal tube array (all nozzle centers equidistant) and an area ratio of 3.3.

Two lengths of area ratio 4.3 ejectors with hexagonal shapes matched to that of the 37-tube array were designed and tested. The ejector hardwall panels were designed to be interchangeable with acoustic lining test panels. The ejector installation on the engine rig is shown in figures 18 and 19. Figure 20 shows details of the ejector bellmouth entry and its relation to the 37-tube nozzle. The geometric properties of the test hardware are summarized in table 4. A representative full-scale acoustic test configuration comprising the 37-tube nozzle and L/D = 2 ejector is shown in figure 21.

Table 5 is a complete summary of the model- and full-scale configurations tested in this program.

INSTRUMENTATION

Acoustic Data System

Due to the similarity between model- and full-scale acoustic instrumentation, only the full-scale system will be described. Where any differences exist between the two systems the information relevant to the model-scale tests is included. Full-scale acoustic data were acquired over the frequency range 50 Hz to 10 kHz. As full-scale configurations were reproduced in the model program at one-fourth scale, model-scale data were acquired over the range 200 Hz to 40 kHz. All acoustic data were recorded on magnetic tape. Microphone arrays were divided into far field and near field.

Far Field Microphone Array

Microphones for the full-scale tests were located at a polar distance of 61m (200 ft), model scale 15.2m (50 ft), centered on the nozzle exit plane with microphones located at 10° increments from 80° to 150° with an additional microphone at 155° (note: in this program all angular locations are relative to engine or nozzle inlet centerline). Due to restrictions at the model test facility the microphone at 80° had to be omitted.

Sound energy radiated from the ejector inlet bellmouth was considered to be a potential noise source. For this reason four microphones, mounted at ground level, were located on a 15.2m arc at 60°, 70°, 8J° and 90°. Due to space restrictions at the model facility only one microphone could be used to monitor noise from the ejector bellmouth inlet. This microphone was located at nozzle centerline height in the near field.

Far field acoustic data in previous programs have been degraded by interference effects of sound reflected from the acoustic arena surface. This interaction of direct and reflected sound waves results in interference maxima and minima in measured spectra. In this program the microphone diaphragms were placed close to the reflecting arena surface such that both direct and reflected sound waves were in phase over the frequency range of interest. This technique allows spectra to be measured which are free field in shape but 6 dB above free field in level. Data are then easily corrected to free field levels for presentation (see appendix A). For the full-scale far field array the microphones were located in an inverted position with the diaphragm approximately 1.27cm (1/2 in.) above the concrete surface of the test arena, see figure 22. In the model facility, where the higher frequencies required a more exacting microphone installation, the microphone diaphragms were mounted flush with the test arena surface. Details of this type of microphone installation are shown in figures 23 and 24.

In addition to the microphones located at ground level, a number of microphones at both the full- and model-scale facilities were mounted at nozzle centerline height. Although the data from these microphones were not used in the acoustic evaluation of any configurations, comparisons were made between data from the ground level and engine centerline height microphones at a given location. As the use of ground level microphones is not well established, these comparisons provided a means of validating this method of data acquisition. In addition, the comparisons enabled acoustic shadowing of the ground microphones due to wind and temperature gradients in the test arena to be positively identified during full-scale testing.

Near Field Microphone Array

In both model- and full-scale tests an array of six microphones was used to investigate the pressure field close to the jet flow. Although the axial location of these microphones varied for different configurations, the locations were similar in terms of nondimensional distances for corresponding full- and model-scale configurations. The microphones were located on a line at 15° to the jet axis. In ejector configurations only three microphones were located downstream of the ejector exit plane. The other three microphones were relocated in water cooled, flush mounting jackets in the ejector walls to evaluate the dynamic pressure environment at the acoustic lining surface. Near field microphone arrays for the 37-tube nozzle, both with and without an ejector, are shown in figure 25. As mentioned in the previous section, an additional microphone was used in the model-scale tests to monitor noise radiated from the ejector inlet. This microphone is included figure 25.

Meteorological Monitoring

To minimize possible adverse influences of local meteorological conditions on the far field acoustic data, wind and temperature were continuously monitored at both test facilities. At the model-scale facility, wind speed and direction were recorded at a height of 2.14m, and temperature at heights of 0.3m and 1.83m above the arena surface. Both wind and temperature measurements were made at a distance of 16.7m at 125° to the nozzle inlet centerline. For full-scale tests, wind speed and direction, and temperatures at 0.3m and 1.83m, were monitored at a point 30m from the nozzle exit at 120° to the engine inlet centerline. An additional temperature measurement was made at 3.66m above the arena surface at 19m and 70°. It should be noted that microphones close to the ground were particularly susceptible to acoustic shadowing by wind and temperature gradients. Particular care was taken in this program to avoid this phenomenon.

The locations of microphones and meteorological stations for the full-scale test facility are shown in figure 26.

Flow Survey Instrumentation

Flow Mach number and velocity surveys were made for both model- and full-scale configurations at various locations downstream of the primary nozzle exit plane using continuously traversing total temperature and total pressure probes. Static pressures in the flow were assumed equal to the ambient value for bare nozzles; for ejector configurations, static pressures were assumed constant across any ejector section and equal to the ejector wall static pressure measured at the same axial location. With the ejector installed, access for the rakes was provided through the ejector wall on the centerline of, and normal to an acoustic test panel. The rakes were traversed radially to a point beyond the nozzle centerline for the conical nozzles and to a point beyond the boundary of the center tube of the array for the 37-tube nozzle. Examples of flow survey rake installations may be seen by reference to figure 12 (model scale) and figures 16 and 19 (full scale).

Wall static pressures within the ejectors were recorded from an array of pressure taps located axially along the centerline of one section of the ejector wall (in both hardwall and lined configurations). For model-scale ejectors these taps were located at 2.54cm increments along the constant area section of the ejector; full-scale, this increment was 10.2cm. Additional static pressure taps were located on the ejector bellmouth—at the highlight and at a point 2.54cm (10.2cm full scale) forward of the constant area ejector section. The bellmouth taps were aligned axially with the constant area section array.

Ejector wall temperatures were recorded from three flush-mounted thermocouples mounted axially at the ejector entrance, ejector center, and ejector exit planes. As with the pressure taps, the thermocouples were located along the centerline of one section of the ejector wall.

15

TEST PROCEDURES

Full-Scale Tests

During full-scale testing specific environmental criteria were observed to minimize the possible degradation of acoustic test data:

- No precipitation.

- Relative humidity and ambient temperature within the limits shown in figure 27. These limits were established such that corrections of acoustic data to standard day (15°C; 70%) conditions would be less than ± 2 dB up to 8000 Hz.

- Wind speed less than 4.7m/sec (15 ft/sec). This criterion was established as a guideline only. During testing, acoustic shadowing was found to occur when wind velocity components from the microphones to the source were as low as 1.5m/sec. Wind speed restrictions were therefore applied as necessary to avoid shadowing during testing.

Test conditions were selected to cover the engine operating range. These conditions were nominally described by the following engine pressure ratios: 1.40, 1.56, 1.80, 2.00, 2.20, and 2.40. To establish confidence in the data each test condition was established twice, except for jet wake surveys which were run once only.

For acoustic and propulsion performance test runs the engine was stabilized at each power condition. Immediately preceding any data acquisition, satisfactory conditions for acoustic testing were ensured by monitoring the signals from a microphone at ground level and one at engine centerline height located at the same angular position. An on-line display of the one-third octave band analysis of the signals from each microphone, together with the difference between the signals in each frequency band, enabled the presence of acoustic shadowing to be identified.

With satisfactory test conditions established, acoustic data from all microphones were recorded for 30 seconds. Engine performance parameters were sampled 10 times each before and after acoustic data acquisition. This procedure ensured a measure of engine stability over the recording period. Parameters related specifically to ejector configurations—bellmouth and wall static pressures, wall temperatures, and boundary layer total pressures—were sampled once only following each acquisition of engine performance parameters.

Wind speed and direction were continuously recorded while acoustic data were being taken. Ambient temperatures were taken with the engine performance data, and the relative humidity was measured prior to each test condition.

Jet wake surveys were not taken during acoustic testing. This procedure eliminated the possibility of interference from noise generated by the rake mechanism in the flow.

The procedure for acquisition of jet wake survey data was as follows:

- Stabilize engine at test condition.

- Acquire standard engine performance parameters.

- Initiate rake traverse and, at 2-second intervals, record P_T and T_T from each probe together with the rake position, P_{T7}, T_{T7}.

- Acquire data with rake traversing both into and out of the flow.

The rake traversing speed and data sampling rate combined to give a measure of flow parameters at 0.38cm increments across the jet wake. X-Y plotters enabled flow survey data to be monitored on-line to ensure satisfactory performance of the rake systems.

Model-Scale Tests

Test procedures for the model-scale program were similar to those used in full-scale testing. Similar environmental criteria were observed. The ambient temperature and relative humidity restrictions of figure 27 limit the corrections of the data due to atmospheric absorption to ± 2 dB at 40 kHz (from test day conditions to 15°C and 70% relative humidity). Since acoustic far field data were acquired at a radius of only 15.2m, it was considered unnecessary to provide a sophisticated on-line monitoring system for the identification of acoustic shadowing.

The range of nozzle operating conditions extended beyond the range of the J-75 engine test conditions, and a summary of the nominal conditions is given below.

Gas Total Temperature °K	°F	Nozzle Pressure Ratio				
Ambient	Ambient	1.4	1.6^X	2.2	3.0^X	4.0
533	500	1.4^*	1.6^X	2.2	3.0	4.0
589	600	1.6^*				
700	800	2.0^*				
755	900	2.2^*				
811	1000	1.4	1.6^X	2.2	2.4^{*X}	4.0
1088	1500	1.4	1.6^X	2.2	2.6^X	4.0
1643	2500^+	1.4		2.2		4.0

*   Nominal J-75 engine test conditions
x   Not used in single-element concept tests
+   Used only for 10.9cm diameter water cooled nozzle

Because of the wide range of test conditions, each point was established once only in the model program.

When nozzle operating conditions had stabilized at any given test point, 30 seconds of acoustic data were recorded from all microphone systems. Nozzle and ejector performance parameters were sampled once only, with the exception of thrust which was sampled five times, and nozzle total temperatures from the seven-probe rake which were sampled three times. For acoustic data runs performance parameters were sampled during acoustic data acquisition.

Jet wake survey data were acquired by following this procedure:

- Stabilize nozzle operating condition.

- Initiate rake traverse and continuously sample, at 20 channels/second, the parameters: rake position, P_T, P_S (ejector wall), and T_T.

- Acquire nozzle performance data during traverse.

- Continue traverse to beyond nozzle centerline, then reverse rake and continue to sample to point of traverse initiation.

Rake speed and sampling rate gave flow parameters at increments of approximately 0.13cm across the jet wake.

DATA REDUCTION

Acoustic Data

The recorded acoustic data were reduced using a General Radio No. 1921 spectrum analyzer coupled to a bank of parallel one-third octave band filters using a 16 second integration time. The sound pressure level output was true RMS with an analyzer resolution of 0.25 dB. The digitized results were automatically fed through a computer where system response corrections were made and then stored on digital magnetic tape. All spectral data were subsequently displayed in the form of machine plots. The digitized data were then edited and normalized for atmospheric absorption variations to a 15°C and 70% relative humidity standard day. Atmospheric absorption corrections up to the 10 kHz one-third octave band were applied using the standard curves in ARP 866 (ref. 6). Although the basic curves of atmospheric absorption in ARP 866 are not restricted to 10 kHz, the necessary curves for the higher frequencies are not included. In order to generate the absorption coefficients for model-scale test frequencies up to 40 kHz, the curves contained in ARP 866 data were extrapolated as described in appendix B. Spectra from the ground level microphones were lowered by 6 dB to give "free field" data, while data from the nozzle centerline height microphones were left uncorrected for ground reflection effects. Noise data in this final form were stored on digital magnetic tape for further analysis. Unless otherwise identified, all acoustic data presented in this report are free-field characteristics normalized to atmospheric conditions of 288°K (15°C) and 70% relative humidity.

Overall sound pressure levels (OASPL) presented for acoustic spectra are not measured values but are the computed sum of the measured one-third octave band levels.

Sound power levels (PWL) were calculated by the following method. Sound pressure levels from each microphone location were assumed to be constant in a 10° arc centered on the microphone. Assuming an axisymmetric sound field, an integral procedure was used to calculate the total sound power radiated through the surface of revolution about the jet axis described by the arc 75° to 158° at 61m radius for full-scale data and 85° to 158° at 15.2m radius for the model-scale data. Noise in the forward arc was assumed to be zero. (Note: atmospheric absorption of sound over the propagation distance was included to give the effective sound power of the source.)

Perceived noise levels (PNL) were calculated on a 649m (2128 ft) sideline for the subjective evaluation of the jet noise suppressor system. To do this, the desired one-third octave band spectra were first extrapolated by computerized techniques from their polar locations to the corresponding 649m sideline positions, taking into account the inverse square law and atmospheric absorption effects according to ARP 866. Ground absorption effects were not included in the extrapolation. Perceived noise levels were then computed according to the method described in ARP 865 (ref. 7).

Model-scale data were transformed in frequency and normalized for both measurement distance and nozzle size to full-scale values prior to the extrapolation and perceived noise calculations.

Propulsion and Jet Wake Data

The processing procedure for propulsion and jet wake data was essentially the same for model- and full-scale programs. The outputs from the data acquisition systems were a punched paper tape and a digital printout tape. The latter output was used for a "quick look" evaluation of the data during testing. The punched tape was processed through a computer where the data were transferred to digital magnetic tape. The data on the magnetic tape were then submitted as inputs to the propulsion and flow survey data reduction programs. Reduced and analyzed data were available in both printed listing and graphic forms.

Propulsion data. —Measured values of thrust, airflow (or more exactly flow meter parameters), fuel flow, primary gas total pressure and temperature, atmospheric pressure and temperature, primary nozzle flow area, local static pressures at various static tap locations, and local wall temperatures were input to the data reduction program. The program computed corrected thrust, corrected airflow, corrected fuel flow, primary flow ideal velocity and density (fully expanded jet), C_V and C_D (nozzle velocity and discharge coefficients), nozzle effective area, ideal thrust, and the ratios of local static and total pressures to ambient pressure. Machine plots were made of corrected thrust, corrected airflow, C_V, and C_D as functions of the nozzle pressure ratio. In addition, plots were made at each nozzle pressure ratio of the local static pressure distribution through the bellmouth and ejector.

Flow survey data. —For runs in which flow survey data were taken, probe position, probe total pressure and temperature, and the local static pressure were recorded on magnetic tape as the probe was traversed. These data were then input to the data reduction program in addition to the regular performance data input. The program computed local Mach number, static temperature, density, and velocity. Machine plots of total temperature and pressure, Mach number, velocity, and local static temperature as a function of distance from the nozzle centerline were generated.

RESULTS OF ACOUSTIC FAR FIELD TESTS

Similar procedures are adopted to evaluate the data from model- and full-scale test configurations. Acoustic power is used, both in overall and one-third octave band levels, to characterize the various configurations tested and to evaluate the installed performance of the ejector linings. The use of sound power reduction to assess lining performance may be directly related to the nature of the prediction procedures for lining attenuation discussed in an earlier section. Any significant changes in the directional characteristics of the radiated sound fields as a result of the configuration changes are also identified and presented in terms of sound pressure level and angular position. The effects of directivity changes are further presented in a later section where various configurations are evaluated in subjective terms of sideline perceived noise levels.

A round convergent (or conical) nozzle was tested to establish the acoustic baseline against which the overall performance of the 37-tube suppressor nozzle and lined ejector configurations could be evaluated. A sequence of comparisons was adopted to identify the relative acoustic performance of each component of the ejector-suppressor configuration:

- The noise suppression provided by the 37-tube nozzle was established by comparison to the equivalent flow area conical nozzle.

- Hardwall ejectors of L/D = 1 and 2 were tested to determine their influence upon the noise generation of the 37-tube nozzle and also to provide a reference for the evaluation of the acoustically lined ejectors.

- The performance of the various acoustic panels tested in the two ejector lengths was obtained by direct comparison of hardwall and treated configurations.

Due to the vast amount of data acquired during this program, only a limited and representative presentation of spectral and directivity data is contained in the main text; additional presentation of measured and derived results may be found in appendix C. All the data obtained on this contract are available on microfilm at NASA-Lewis Research Center, Cleveland, Ohio.

MODEL SCALE

In model test results, the validity of the highest three frequency bands (25, 31, and 40 kHz) in computed sound power spectra was considered suspect because the calculated power levels in these bands indicated an upward trend. This is the reverse of the general trend of spectrum shapes in this

frequency region. To compute sound power spectra, corrections are necessary to account for atmospheric absorption over the measurement distance. These corrections give a "source power" which is independent of measurement distance. Corrections in the frequency range above 10 kHz are based on an extrapolated version of ARP 866 as outlined in appendix B. Two factors could influence the validity of the data:

- The extrapolated values for absorption coefficients that have been applied overestimate the atmospheric losses.

- The data acquisition and/or reduction process provides a contribution, in terms of system noise, to the "measured" levels.

It has not been established with certainty if one or both of these factors contribute to this problem. However, extensive evaluations of the acoustic data system have been undertaken, including samples of narrow band on-line data for comparison with recorded data. None of these investigations has indicated any problem related to the data system. Therefore, the validity of the absorption coefficients or the way in which these are applied remains as the most likely source of error, although this has not been shown conclusively. Where applicable, overall sound power levels presented herein have been reduced to eliminate any contribution to the PWL from these suspect band levels.

Conical and 37-Tube Nozzle

Both the 15.2cm diameter conical and one-fourth scale 37-tube nozzles were tested at the same nominal total conditions of temperature and pressure. However, the rig installation of the 37-tube nozzle incorporated a diffuser section between the flow property (P_T, T_T) measurement station and the nozzle baseplate. The total head losses associated with this flow section resulted in nozzle total pressures that were less than the values indicated upstream (this is discussed more fully in a later section). This difference must be considered when the two nozzles are compared at the same nominal condition.

Where nozzle acoustic performance is compared as a function of jet velocity the following approach has been adopted:

- For the conical nozzle (and in subsequent tests of the 10.9cm and 2.74cm diameter nozzles) the ideal, fully expanded jet velocity is used based on the upstream measured total conditions.

● For the 37-tube nozzle, to account for the upstream flow losses, and losses in the nozzle, total pressure and temperature measurements were made over the range of operating conditions at the exit plane of four radially located tubes. The fully expanded jet velocity, computed from the average of these nozzle exit plane measurements, was then used to define the jet velocity for this nozzle. Figure 28 presents the calibration curves of measured velocity against indicated ideal velocity for various nozzle total temperatures.

Sound power spectra for the 15.2cm conical nozzle over the range of test conditions are shown in figure 29. The peaks in the spectra at high pressure ratios are attributed to shock-related noise with the characteristic decrease in frequency with increasing jet velocity for any given temperature condition. A corresponding series of sound power spectra for the one-fourth scale 37-tube nozzle is given in figure 30. For the majority of operating conditions the spectral distribution of acoustic energy may be related to the acoustic model of the two distinct regions of the jet—the initial mixing of the elemental jets (high frequency) and the downstream or coalesced flow (low frequency). Two characteristics of the multitube nozzle are to be noted: (1) at 1088°K and pressure ratios of 1.40 and 1.60 a marked change in spectrum shape was found with a more distinct peak in the region associated with the initial mixing of the individual jets, and (2) although the peak frequency associated with initial mixing increased with pressure ratio (or velocity) for given temperature conditions, this trend was not clearly evident when the jet velocity was increased at constant pressure ratio by increasing gas temperatures. Thus the frequency distribution of acoustic energy from the initial mixing of the jets was not related to jet velocity on the basis of simple Strouhal scaling [frequency = (constant x velocity) ÷ jet diameter] and the indication is that some other, possibly more complex, relationship must be determined to describe the frequency distribution of energy from this type of multi-element nozzle.

Shock-related noise was evident at only one test condition for the 37-tube nozzle: NPR = 3.0, T_T = ambient.

A summary of all test conditions for the 15.2cm conical and 37-tube nozzles, together with PWL and overall SPL as a function of angular position is given in table 6. It is to be noted that throughout table 6 the nozzle pressure ratios and gas total temperatures given refer to the nominal conditions only. The jet velocity term is precise and reflects the minor deviations from the nominal nozzle conditions established during testing.

The 37-tube nozzle was found to give a varying degree of sound suppression relative to the conical nozzle over the range of test conditions, primarily from a reduction in low-frequency energy. The overall acoustic performance of the conical and 37-tube nozzles are compared in figure 31 as a function of jet velocity. Sound power suppression by the 37-tube nozzle as a function of frequency is given in figure 32 for a representative range of nozzle flow conditions. At lower

pressure ratios an increase of up to 5 dB in high frequency (>4 kHz) energy was noted with the 37-tube nozzle, although at pressure ratios above 2.00 the increase was eliminated and sound energy suppression was measured over the entire frequency range. Because the actual nozzle total conditions compared are not exactly the same for the two nozzles, figure 32 must be regarded only as a qualitative representation of the 37-tube nozzle noise suppression performance.

37-Tube Nozzle With Hardwall Ejector

With the ejector installed, the flow from the nozzle expands to a local static pressure which is below the ambient pressure used to determine the nozzle pressure ratio. For this reason the flow attains a peak axial velocity within the ejector which is higher, for corresponding total conditions, than that attained when the ejector is not installed. In this program, where ejector and no-ejector configurations are compared on a basis of jet velocity, the following approach is adopted:

- For ejector configurations a characteristic velocity is determined which is the velocity that would be attained with the 37-tube nozzle without ejector operating at the same conditions of total temperature and pressure.

The static pressure conditions which exist at the nozzle exit plane, with the ejector installed, are described later.

Sound power spectra for the L/D = 1 and 2 hardwall ejectors are shown in figures 33 and 34. In general the sound power characteristics were similar to those of the 37-tube nozzle, and comparison with the bare nozzle at similar operating conditions identified the following ejector effects:

- A marginal reduction in high-frequency energy was noted, particularly for the L/D = 2 ejector. The induced secondary flow velocities are greater for the long ejector, and the resulting reduction in relative primary jet velocity may well contribute toward this reduction.

- At low conditions of temperature and pressure the L/D = 1 ejector gave a measurable increase in low-frequency energy as compared to the 37-tube nozzle.

- The L/D = 2 ejector provided low-frequency energy suppression at conditions of high primary jet velocity. The fully mixed exit conditions from the long ejector resulted in lower exit velocities and thus reduced noise levels in the part of the spectrum associated with this flow region. (Note: flow conditions at the ejector exit plane will be discussed in a later section.)

In summary, the relative acoustic performance of the 37-tube nozzle with the two lengths of hardwall ejectors installed is shown as a function of jet velocity in figure 35. Although overall PWL does not necessarily reflect the characteristic changes in spectral shape, it does demonstrate the consistent suppression, approximately 2 dB, from the $L/D = 2$ ejector as compared to the $L/D = 1$ ejector.

Although in overall terms the ejector had only a minor effect on the acoustic output of the 37-tube nozzle, the directional characteristics of the radiated sound energy were noticeably influenced by the ejector. This phenomenon is treated extensively in the section presenting full-scale data and is briefly identified and outlined in figure 36. It was found that, as opposed to the relatively uniform radiation of high-frequency energy from the 37-tube nozzle, with an ejector installed energy from source regions in the ejector was radiated preferentially, with a maximum level occurring generally at 120°-130° to the inlet. Low-frequency, or merged jet noise, generally associated with downstream regions of the flow were not influenced by the ejector. This was observed to a varying degree in the directivity of overall SPL, depending on the relative magnitude of the high-frequency energy.

The test conditions for the two hardwall ejector configurations, together with tabulated values of PWL and overall SPL as a function of angular position, are given in table 6.

37-Tube Nozzle With Lined Ejectors

The performance of each acoustic lining set was determined over the same range of nozzle temperatures and pressures used for the hardwall ejectors. The absorption characteristics at any given operating condition were determined by direct comparison of the one-third octave band sound power levels of hardwall and lined configurations. Two terms are introduced, as shown in figure 37, to define the absorption characteristics of a lining at a given nozzle operating condition:

- One-Octave Bandwidth Attenuation (or Insertion Loss): The level of attenuation at which the width of the one-third octave band attenuation spectrum is one octave. The use of this term tends to eliminate the minor variations in peak attenuation that can occur if attenuation is defined directly by the difference of two one-third octave band levels. It is important to note that where acoustic energy absorption by ejector linings is presented in terms of the total acoustic power absorbed, the term lining insertion loss rather than lining attenuation is used.

- Tuning Frequency: The center frequency of the one octave used to determine the attenuation level described above. This procedure allows the tuning frequency to be an interpolation between the preferred one-third octave band center frequencies.

25

For a nozzle pressure ratio of 2.4 (T = 811°K), representative spectra for L/D = 1 and 2 hardwall and lined ejectors are shown in figure 38. Included in this figure are the derived one-third octave band lining insertion loss spectra and a typical series of insertion loss spectra for a lined ejector over a range of pressure ratios at 811°K. The installed performance of the various model-scale acoustic test panels is summarized in figures 39 through 42, where one octave band insertion loss and tuning frequency are presented as a function of nozzle pressure ratio and temperature. The corresponding one-third octave band insertion loss spectra are presented in appendix C.

Certain observations may be made from the lining performance curves presented in figures 39-42:

- For the L/D = 1 ejector, lining insertion loss was relatively insensitive to the lining geometry at nozzle pressure ratios above 2.0, and tended to decrease from the values measured at NPR = 2.0.

- At pressure ratios below 2.0, linings in the L/D = 1 ejector exhibited a general trend of increasing insertion loss with increasing flow temperatures, although a range of 2-6 dB in insertion loss covered all lining configurations.

- For the 12% open area linings in the L/D = 1 ejector, tuning frequency varied inversely with lining core depth, although the proportional variation in tuning frequency was reduced at higher pressure ratios.

- Lining insertion loss increased with ejector length for a given lining, with a maximum of 10 dB at NPR = 2.0 to 2.4 (T = 811°K) for the 12% open area, 1.4cm core depth lining.

- For a given lining, tuning frequency did not appear to be a function of ejector length.

Lining performance over the range of nozzle conditions corresponding to the J-75 engine operating line is shown in figures 43 and 44. Only the linings equivalent to those tested full scale are indicated in these figures.

Discussions to follow in the section on scaling of lined ejector data indicate that the model-scale lining attenuation data for the L/D = 1 ejector may be limited in some respects and may not truly represent the ejector lining performance. Lining data shown in this section are presented as measured results only.

10.9cm Conical Nozzle and Lined Ejectors

In the single-element concept of ejector lining evaluation, the 10.9cm conical nozzle was representative of one element in the full-scale 37-tube nozzle array. The ejector lengths tested with this nozzle were equal to the full-scale configurations—1.32m and 2.64m. Only one lining set was tested in the 1.32m long ejector (12% open area, d = 2.54cm).

The baseline acoustic characteristics were established for the bare 10.9cm diameter nozzle although the results were not directly applied in the lining evaluations. Sound power spectra for the range of test conditions are presented in figure 45. A summary table of test conditions, together with PWL and overall SPL as a function of angular position are given in table 6 for the 10.9cm nozzle both with and without hardwall ejectors.

Acoustic lining performance was evaluated in a similar way to the one-fourth scale models, i.e., by direct comparison of lined and hardwall ejectors of the same length. For each lining set tested the sound power insertion loss characteristics were determined for each test condition. The single-element concept of scaling must be considered primarily as a tool to determine acoustic lining performance in the severe primary jet environment. The configurations tested, therefore, are not representative of any directly applicable hardware. For this reason, the determination of acoustic energy absorption by the lining is the prime objective and no study has been made of the other acoustic characteristics of the configuration such as directivity and the suppression afforded by the hardwall ejector relative to the bare conical nozzle.

Examples of the sound power spectra for the lined and hardwall ejectors (L/D = 4 and 8) are given in figure 46 together with the one-third octave band insertion loss spectra. A representative set of insertion loss spectra for the L/D = 8 ejector over a range of nozzle pressure ratios at 811°K is shown in figure 47. The acoustic performance of each lining set evaluated is given in figures 48 through 57 where one octave band insertion loss and tuning frequency are presented as a function of nozzle pressure ratio and temperature. The corresponding insertion loss spectra are presented in appendix C. The parametric results for the 10.9cm diameter nozzle and L/D = 8 lined ejectors are summarized in figures 58 through 61. Although the lining performance is dependent upon both lining depth and face sheet percent open area, some generalized observations can be made on each of these parameters separately. Figure 58 shows that the lining depth for maximum sound power suppression for the 12% open area lining decreases from 5.85cm to less than 2.5cm for increasing primary nozzle pressure ratio between 1.4 and 4.0. Conversely, figure 59 shows that for the 5.85cm deep lining the percent open area for maximum sound suppression increases from about 6% to 17% as the primary nozzle pressure ratio is increased from 1.4 to 4.0. Figures 60 and 61 confirm what had already been established in fan noise suppression work, that for a given duct L/D ratio, the lining depth is the major tuning parameter, with changes of face sheet percent open area being a second-order effect. As expected, the tuning frequency varies inversely with lining core depth.

2.74cm Conical Nozzle and Lined Ejectors ·

The single-element concept of ejector scaling was also applied to the one-fourth scale-model 37-tube nozzle. A 2.74cm diameter conical nozzle representing a single tube of the model 37-tube nozzle was tested in conjunction with two ejector lengths—30.5cm and 61cm. In addition, these configurations were inherently one-fourth scale models of the 10.9cm single-element tests described previously. However, this phase was limited to the evaluation of only one set of acoustic test panels (22% open area and 1.4cm core depth) in each of the ejector lengths. At the time of testing, this lining specification had shown the most promising attenuation characteristics in the 37-tube model tests and was chosen for this reason.

The acoustic characteristics of the bare 2.74cm diameter nozzle were initially established, and in figure 62 sound power spectra as a function of gas total temperature and pressure ratio are presented. The test conditions and values of PWL and overall SPL as a function of angular location are given in table 6 for the 2.74cm nozzle both with and without hardwall ejectors.

In figure 63 a comparison is made between the hardwall and lined ejectors for both lengths of ejector at a nozzle pressure ratio = 2.4 and $T_T = 811°$ K. Over the range of nozzle test conditions the lining performance is summarized, in terms of one-octave band insertion loss and tuning frequency, for both ejector lengths in figures 64 and 65. Because this test phase was limited to only one set of acoustic test panels no parametric studies of lining performance could be made. However, the results for this one set are compared, in the later section on scaling, to the results from both the model 37-tube configuration and the 10.9cm single-element configuration.

FULL SCALE

Full-scale engine configurations were evaluated over the full operating range of the J-75 engine, as previously outlined. Primary nozzle pressure ratio was varied between 1.4 and 2.4 with corresponding nominal gas total temperatures of 533°K to 811° K (500°F to 1000°F). The test data presented are average values from the two sets of data acquired at each test point. For full-scale test conditions the parameter of average jet velocity has been used to define V_J, thus:

$$V_J = \frac{\text{Measured thrust}}{\text{Measured mass flow rate}}$$

Available flow profile data indicated that this value of V_J was representative of the peak axial flow velocity for both conical and 37-tube nozzles. For ejector configurations, the jet velocity corresponding to any given test condition is defined as the velocity that would exist for the bare 37-tube nozzle operating at the same conditions of total pressure and temperature. This procedure is consistent with that used for the model-scale ejector configurations.

28

Although measures were taken to suppress noise radiated from the engine inlet and from the engine casing, it was not possible to eliminate from measurements noise generated in the turbine stage of the engine which is subsequently radiated from the primary nozzle. Turbine noise from the J-75 is predominantly discrete in nature with major components at the blade passing frequencies of the aft two rotor stages, and this provided a major contribution to measured acoustic spectra at low engine power settings in the frequency range 4-10 kHz. In analyses where overall sound power levels are used, the overall level has been reduced to account for the contribution from turbine noise. However, it must be noted that tabulated overall SPL and extrapolated PNL values have not been corrected for turbine noise contributions.

Reference Nozzles

The standard (non-afterburning) J-75 primary nozzle, which is a round convergent nozzle with a centerbody, was used to establish the overall acoustic baseline for the full-scale program. Acoustic power spectra for each of the engine test conditions are shown in figure 66. As with the model-scale data, the acoustic power spectra have been corrected for any atmospheric absorption losses (based directly upon ARP 866 for the full-scale data) that would occur over the 61m measurement distance. Turbine noise is evident at low pressure ratios, as mentioned in the previous section, at frequencies above 4 kHz.

The 37-tube suppressor nozzle was tested over the same range of test conditions as the conical except that the test point at NPR = 1.80 was not established. Sound power spectra for the five test points are given in figure 67. The characteristic spectrum associated with this type of nozzle—low- and high-frequency energy related to the coalesced flow and initial mixing regions, respectively—may be identified particularly at higher pressure ratios. At the low pressure ratios of 1.40 and 1.58, contributions to the spectra from turbine noise are again evident, although turbine noise was attenuated by approximately 5 dB as a result of transmission through the 37-tube nozzle.

Test conditions for the conical and 37-tube nozzles, together with PWL and overall SPL as a function of angular location, are given in table 7.

In figure 68 the overall acoustic power output of the conical and 37-tube nozzles are compared on the basis of jet velocity. The most significant observation is that apart from a redistribution of acoustic energy by the 37-tube nozzle there is also a net reduction in the overall acoustic energy for a given jet velocity. This suppression increased with jet velocity to a maximum of 8 dB at 610m/sec; below 305m/sec suppression was 3 dB or less. Maximum energy suppression occurred at a frequency corresponding to the peak of the conical nozzle acoustic spectrum, and in figure 69 suppression is shown as a function of one-third octave band frequency for the range of full-scale test conditions. As was noted with the model nozzle, the full-scale 37-tube nozzle gave a slight increase in acoustic

energy at high frequencies (>800 Hz) when compared to the conical nozzle. This increase was most marked at pressure ratios below 2.00 although the attenuation of discrete turbine noise by the 37-tube nozzle tended to obscure this trend in jet noise. No increase in high-frequency acoustic energy was found at NPR = 2.40.

1.32m and 2.64m Long Hardwall Ejectors

To establish a reference for the evaluation of the lined ejectors, both the L/D =1 (1.32m) and L/D = 2 (2.64m) ejectors were tested with hardwall panels installed.

Acoustic power spectra for the L/D = 1 and 2 hardwall ejectors are given in figures 70 and 71. As in the model configurations the spectral characteristics of the 37-tube nozzle were relatively unchanged by the presence of an unlined ejector, although the L/D = 2 ejector did provide a small but consistent amount of suppression in both the high- and low-frequency regions of the spectrum. The fully mixed exit flow conditions and consequently lower velocities could well account for the reduced level in low-frequency energy associated with the L/D = 2 ejector. A similar situation exists in the high-frequency region where the higher induced secondary velocities with the L/D = 2 ejector could, through the effect of lowering the relative primary jet velocity, account for the suppression measured.

The overall acoustic characteristics of the hardwall ejectors are presented in figure 72 as a function of jet velocity. A consistent reduction of approximately 2 dB in overall level was indicated for the L/D = 2 ejector as compared to the L/D = 1 ejector over the range of velocity conditions tested.

It was mentioned in the model-scale data section that the presence of an ejector had a marked effect on the directivity of high-frequency acoustic energy. This phenomenon was initially noted during the analysis of full-scale test data and for this reason is studied more extensively in this section. For a high and low engine thrust condition the directivities of overall SPL and selected one-third octave bands are shown in figures 73 and 74. Included in these figures are data from the 37-tube nozzle with and without an ejector and from the conical reference nozzle (for comparison). Figure 73 shows that the ejector has little effect on the radiation of low-frequency energy (below 250 Hz) from the 37-tube nozzle, suggesting that the predominant source of this energy is the low-velocity, large-diameter jet with the ejector exit as the effective nozzle. The character of this large jet would be similar (from the flow profile measurements) to some station in the coalesced flow region downstream of the bare 37-tube nozzle exit plane. Above 250 Hz, however, a redirection of acoustic energy is indicated with a distinct maximum at 120° to the inlet. Associated with this maximum is a significant decrease in energy at angles greater than 120°. It should be noted that from the computed power levels, the net change in acoustic energy is negligible (zero to 2 dB) relative to the 37-tube nozzle.

30

At the low power setting, figure 74, similar changes in directivity may be seen although not perhaps as clearly. The angle of maximum radiation is also less defined and tends to be between 120° and 130° to the inlet axis. The influence of the ejector on acoustic energy radiation is generalized in figure 75.

A simple model was studied to obtain some understanding of the changes in radiation characteristics of high-frequency energy due to the presence of an ejector. Figure 76 shows the model in diagrammatic form. It was assumed that all high-frequency acoustic energy is associated with the initial mixing of the elemental jets and that the most intense region of this source is located within the ejector length. These sources of acoustic energy are contained by the ejector walls and propagate (and are convected) downstream to the ejector exit where the energy is free to radiate to the far field. This idea is substantiated by the near field acoustic data (presented later) which show the most intense acoustic region to be at or immediately downstream of the ejector exit plane.

The model was investigated by computing acoustic ray paths through the flow gradients at the ejector exit using profiles measured during the program. This analytical exercise was qualitative only and is obviously subject to many qualifications. A diffuse sound field (energy propagating equally in all directions) was assumed to exist across the ejector exit plane. Five equidistant locations across the exit plane were considered, and ray paths were computed from each point for rays with initial directions between 90° and 0° relative to direction of flow. Forty-five ray paths (each at 2° increments) were computed from each point. This analysis, applied to the measured exit profiles at an NPR = 2.4, T_T = 811°K predicted that essentially a shadow zone would exist beyond 137° to the inlet while only a minimal amount of energy would be radiated to the 10° sector centered upon the 130° location. Assuming that the number of ray paths that terminated in each 10° sector is proportional in some way to the sound pressure level measured by the microphone at the center of that sector, a maximum SPL was predicted to occur at the 120° location—the same angle as indicated by measured data. While the SPL distribution forward of 120° could not be predicted even qualitatively without some prior knowledge of the actual acoustic energy distribution at the ejector exit, the significant fact is the prediction and measurement of a significant decay in acoustic intensity at angles greater than 120° to the inlet.

This study provides a plausible, initial explanation of the acoustic characteristics of the ejector configurations. Although not presented, the L/D = 1 ejector showed similar characteristics which were attributed, following this analysis, to the same phenomenon.

Lined Ejector Tests

The installed performance of each set of acoustic test panels was determined by direct comparison between hardwall and lined configurations. Sound power spectra for the L/D = 1 and 2 ejectors lined with panels of the same material specification (12% open area, 5.3cm core depth) are shown in figures 77 and 78. For a nozzle pressure ratio of 2.4 (T_T = 823° K) a direct comparison is made in figure 79 between the corresponding lined and hardwall configurations together with the derived lining insertion loss spectra. For each lining set, an insertion loss spectrum was obtained at each engine operating point and for example the series of spectra for the L/D = 2 ejector is shown in figure 80. Insertion loss spectra for all lining configurations tested are presented in appendix C.

As in the model-scale program, lining performance is described by the one-octave bandwidth insertion loss and the corresponding tuning frequency (see figure 37). For each of the lining sets tested, insertion loss and tuning frequency are presented as a function of nozzle pressure ratio in figures 81 and 82.

Although consistent and distinct differences were found between the various linings it must be emphasized that, for the L/D = 1 ejector, the total variation in insertion loss at any given test condition was 4 dB or less. A high degree of resolution is required, therefore, to identify the differences between the lining sets and this fact must be acknowledged in the interpretation of the results. However, the procedure adopted to determine insertion loss and tuning frequency—average data from two test runs, sound power levels, and the one-octave bandwidth definition of insertion loss must contribute to the credibility of the overall differences that are identified.

The following points are noted:

- For the 5.3cm core depth linings, insertion loss was a maximum at 6% open area. A decrease in insertion loss was noted for increasing surface sheet porosity.

- For a 3.8cm core depth, insertion loss increased with an increase in surface porosity from 12% to 22%.

- All linings provided an increase in insertion loss with increasing nozzle pressure ratio, with a maximum value indicated in the region NPR = 2.2 to 2.4.

- At the maximum NPR of 2.4, insertion loss by lining in the L/D = 2 ejector was still increasing.

- For the 12% open area lining, tuning frequency increased with decreasing core depth, as expected.

- In general, higher lining tuning frequencies were associated with higher nozzle pressure ratio.

- For a given core depth, the effective lining tuning frequency was influenced by surface sheet porosity.

- For the 5.3cm core depth 12% open area lining, an increase of ejector length from L/D = 1 to 2 provided an additional insertion loss of approximately 4 dB over the engine operating range.

- For the same lining (5.3cm, 12% open area) the effective tuning frequency was consistently lower for the L/D = 2 ejector than for the L/D = 1 ejector, although the difference was marginal.

The use of sound power insertion loss and the related tuning frequency has been adopted in this program for lining evaluations. This approach, as noted earlier, is consistent with the concept of the duct lining prediction procedure. Analysis of the test data has shown this to be the most valid approach for these studies as briefly discussed in the following paragraphs.

It is possible by arithmetic means to derive an attenuation spectrum for a lining configuration at each angle of measurement by the direct comparison of lined and hardwall configuration data. The values obtained at the angle of maximum sound radiation are often considered to be representative of lining performance. This alternative approach was studied and in figure 83 the derived attenuations and tuning frequencies as a function of angular location are shown for a lined configuration (12% open area, 5.3cm core depth, L/D = 2 ejector). Attenuation and tuning frequency were found to vary considerably with angular location, and no specific values could be confidently assigned to represent the lining performance. This was found to be true for all lining configurations.. Data corresponding to figure 83 for all L/D = 1 lined ejectors are presented in appendix C.

In all examples it was found that a marked change in the apparent lining characteristics occurred between angles of 110° and 120°. At 110° attenuation tended to be independent of nozzle pressure ratio; at 120° an increase in attenuation was found for higher pressure ratios. The reason for this phenomenon was investigated, and figure 84 is representative of the situation. Figure 84 shows measured one-third octave band sound pressure levels as a function of angular location for the frequency range in which the lining is effective. It was found that the presence of the lining influenced the directional characteristics of the radiated sound field above 1000 Hz. The angle of maximum energy radiated changed from 120° to 110°. By directly subtracting data on an angular basis this phenomenon results in an apparent decrease in attenuation at 110° and a significant

increase at 120° and above. The effect of this change is reflected in the one-octave band attenuation derived for each angle and inherently affects the determined value of tuning frequency. It is this feature of the measured data that accounts for the varying characteristics demonstrated in figure 83.

The effect of linings on directivity was considered in terms of the hardwall ejector concept outlined in figure 76. The directivity of the hardwall ejector was based on the equal distribution of acoustic energy at the ejector exit plane. With an acoustic energy absorber installed on the ejector walls this assumption is less likely to be correct. Higher acoustic intensities are more likely to exist towards the center of the ejector as a result of the absorption near the walls. A study of the refraction process indicated that energy from the center of the duct would be refracted further from the jet exit axis, and for the lined ejector this is the characteristic trend that was observed.

While the physical situation is complex, the foregoing concept is supported by the measured data and is presented as an initial step in understanding the acoustic mechanisms of ejector configurations.

RESULTS OF ACOUSTIC NEAR FIELD TESTS

Near field sound pressure levels were acquired in this program for two reasons: first, to examine the relative changes in jet noise source distribution that occur when the conical nozzle is replaced by the 37-tube nozzle, both with and without an ejector installed; and second, to acquire environmental information within the ejector for use in acoustic lining design procedures. Ejector wall sound pressure levels provide the necessary information for calculating the impedance of the ejector wall linings. Depending on the sophistication of the impedance calculation procedure, the results can be used either in the form of one-third octave band sound pressure levels or simply as overall sound pressure levels. Since these measurements were made in the presence of airflow, great care was necessary in making certain that the microphone installations were smooth with the ejector wall. This presented a problem in the one-fourth scale models where the microphone installation dimensions were relatively large with respect to the ejector dimensions. This problem manifested itself mainly in obtaining good repeatability of data between configuration changes where the microphone installations were removed and replaced. The resultant data scatter, however, did not normally exceed 3 dB. In the final analysis of lining attenuation performance, errors of this order in near field environment were found to be insignificant in terms of lining impedance calculations.

MODEL SCALE

Ejector wall measurements were normally taken at three axial stations, as identified in figure 25 and referred to in the text as ejector entrance, center, and exit locations. Measurements were taken in both hardwall and acoustically lined ejectors. A representative set of ejector wall sound pressure spectra for the three axial locations in the L/D = 1 hardwall ejector over a range of power settings is shown in figure 85. A number of qualitative trends can be observed in these data. Obviously, the spectral levels increase with increasing pressure ratio as well as with axial distance in the flow direction. Because the high-frequency noise sources are predominantly inside the ejector, the highest rate of increase of SPL with power setting is observed in the high-frequency part of the spectrum. The low frequencies, however, increase in level more significantly with change of axial location, as can be best seen in figure 86 for three different ejector configurations. This phenomenon may possibly be attributed to airflow effects over the microphone diaphragm.

A typical comparison of wall sound pressure spectra between a hardwall and a lined ejector is shown in figure 87. Although near the entrance of the ejector the two spectra appear to be almost identical, measurable differences occur in the data further downstream.

Samples of model-scale ejector wall sound pressure data appear in appendix C.

Near field sound pressure levels were measured with a microphone array at 15° to the jet exit axis as shown schematically in figure 25. In order to obtain accurate noise source location data for jet noise a much more extensive set of near field noise measurements would be required than were undertaken in this program. A simpler type of approach was taken to enhance the overall understanding of the results by providing qualitative, "apparent" noise source locations in the various jets and to indicate the dominant noise frequencies generated in the region where the lined ejectors would be installed. In other words, the near field noise data should be looked upon as giving an indication of the local noise environment for a projected lined ejector design.

In this test series the nozzle operating range covered both subsonic and supersonic jet velocities. Because convergent nozzles were used in this program, for some supercritical pressure ratios supersonic "screech" (discrete frequency) noise was generated which was most prevalent at ambient jet temperatures. For heated jets, supersonic "screech" was usually weak or nonexistent, at least in terms of one-third octave band analysis (ref. 8).

Examples of near field noise measurements for a supersonic and a subsonic condition corresponding to the extreme nozzle pressure ratio settings on the J-75 full-scale engine are shown in figures 88 and 89, where a nozzle pressure ratio of 2.4 indicates the lined ejector "design" case. The axial distance has been nondimensionalized with respect to an equivalent reference conical nozzle diameter of 16.5cm for all the configurations shown. This approach enables direct comparisons to be made between the near field noise measurements of the various configurations. A qualitative comparison between the conical nozzle and the 37-tube nozzle clearly shows the reduction of jet noise as well as the concentration of the apparent noise sources closer to the nozzle exit plane. The selected one-third octave band level data show the additional detail of how the acoustic energy for the 37-tube nozzle is concentrated in the higher frequency bands as compared with the reference conical nozzle. It is apparent from the figures that the peak noise generating region of the flow is only just contained within the short ejector ($x/D_e = 2$). Intuitively, therefore, it may be expected that the lining in the aft section of the long ejector, which extends to $x/D_e = 4$, would be more effective on a unit length basis for the maximum absorption of the jet noise.

Near field measurements beyond the exit plane of the ejectors indicate that the sound pressure field is a combination of noise from the jet in the immediate vicinity plus noise generated inside the ejector and radiating from the exit. In the overall sound power levels computed from the far field acoustic data, it was indicated that the $L/D = 2$ hardwall ejector was marginally quieter than the $L/D = 1$ ejector. The near field measurements close to the ejector exit plane support this earlier statement at a nozzle pressure ratio of 2.4, although at NPR = 1.40 no measurable difference between the ejectors was found in the near field.

A comparison of the axial distribution of high frequency energy in the near field is shown in figure 90 for the conical and 37-tube nozzles. For the same frequency bands it was found that energy from the 37-tube nozzle is located closer to the nozzle exit plane than for the conical nozzle. For the 37-tube nozzle these frequencies represent premerging noise and were found to be a maximum in the region of x/D_e = 1 downstream of the nozzle exit plane, or, in terms of the nozzle element dimension, six to seven element diameters downstream.

FULL SCALE

Ejector wall sound pressure levels were measured and analyzed at three axial locations corresponding to those already described in the model-scale section. In general, the full-scale ejector wall SPL data had less scatter and were considered to be of better quality than the model-scale data. For low power settings, however, turbine noise dominated the noise spectrum above about 4000 Hz. A representative set of ejector wall sound pressure spectra for the three axial locations in a L/D = 1 hardwall ejector are shown in figure 91 for a range of power settings. Figure 92 shows the relative change of spectral levels with microphone location in the two lengths of hardwall ejectors tested.

A typical comparison of wall sound pressure spectra between hardwall and lined ejectors is shown in figure 93. For both lengths of lined ejectors tested it can be seen that the presence of the lining mainly affected the midfrequency range of the spectrum. The frequency range affected corresponded closely to that at which the linings were tuned. The L/D = 2 ejector showed the largest influence at the ejector walls due to the lining. It should be noted that the response of the ejector wall microphones is influenced by local factors, and pressures at the wall may be reduced by the presence of lined surfaces in the vicinity of the microphone. For this reason, the reductions in surface dynamic pressure should not, in a direct way, be quantitatively related to lining attenuation as measured in the far field.

Examination of near field spectra for the 37-tube nozzle and hardwall ejector wall spectra over the first two nozzle diameters downstream of the nozzle exit plane revealed an interesting correlation of spectral shapes as shown in figure 94 for nozzle pressure ratios of 2.4 and 1.4, respectively. First of all, it has to be noted that the ejector hardwall spectra have been lowered by 8 dB with respect to the near field data for this comparison. This can be justified by the fact that the hardwall ejector spectral levels due to pressure doubling at the wall are 6 dB high with respect to free field, and the remaining 2 dB could be due to "reverberation" inside the ejector duct. As a result, it may be concluded from figure 94 that the noise generation process has not been changed significantly by the presence of the ejector over the initial length of x/D_e = 0 to x/D_e = 2.0. For the L/D = 2 ejector the comparison breaks down before x/D_e = 2.0, as shown in figure 95, indicating

that with increased ejector length and the associated changes in flow along the walls, additional factors are present that cannot be readily analyzed with the limited test data of this program.

Samples of full-scale ejector wall sound pressure data appear in appendix C.

Near field sound pressure levels were measured and analyzed in a similar fashion to that described under the model-scale studies. Examples of the near field distribution of jet noise for the high and low points on the J-75 engine operating line are shown in figures 96 and 97, the pressure ratio 2.4 being the lined ejector "design" case. The axial distance has been nondimensionalized with respect to an equivalent reference conical nozzle diameter (D_e) of 66cm. It was found that the 37-tube nozzle changes the near field noise level and redistributes it axially compared to the reference conical nozzle. On a one-third octave band basis it is apparent that the multitube nozzle near field sound pressure levels peak closer to the nozzle exit plane than the conical nozzle (for the same actual frequency), with the maximum sound energy being generated at higher frequencies. Immediately downstream of the ejector exit plane the near field comprises locally generated noise and noise generated within the ejector radiating to the far field. As with the model-scale configurations, the lower acoustic levels associated with the L/D = 2 ejector relative to the L/D = 1 are reflected in the near field one-third octave band measurements at NPR = 2.40. No significant differences in near field sound pressure levels were found for the two ejector lengths at NPR = 1.40.

In figure 98, the distribution of acoustic energy as a function of axial distance from the nozzle exit plane is shown for the conical and 37-tube nozzles. It must be noted that at NPR = 1.4 the 4 kHz band is influenced by turbine noise. For the full-scale 37-tube nozzle, the near field distribution of energy appeared to be less well defined at NPR = 2.40 than indicated by the corresponding model-scale data. Peak pressure levels occurred between $x/D_e = 1$ and $x/D_e = 2$. No explanation has been found for this difference although in general the changes that occur in near field characteristics as a result of the installation of the 37-tube nozzle are similar for both model- and full-scale configurations.

RESULTS OF THRUST PERFORMANCE TESTS

In addition to the acoustic evaluation of each nozzle configuration, data were acquired to determine relative propulsion performance of the configurations tested. Performance data were acquired to:

- Determine thrust and airflow characteristics of each nozzle.

- Obtain and present information to support trade studies in the design of ejector-suppressor configurations.

A summary of the geometric properties of the various nozzles tested is given in tables 3 and 4.

MODEL SCALE

The thrust, corrected to standard conditions, FGC, is plotted as a function of the nozzle pressure ratio for the 15.2cm conical nozzle, 37-tube bare nozzle, and the L/D = 1 and 2 hardwall ejector configurations in figures 99, 100, and 101. A conical diffuser was employed between the total head instrumentation and the baseplate for the 37-tube nozzle, which significantly lowered the total pressure at the nozzle as compared to the upstream measured value. The method described in reference 9 was used to correct the total pressure at the nozzle for losses associated with this diffuser. The relationship used was,

$$NPR_{actual} = 0.96 \, NPR_{measured}$$

The thrust performances of the various nozzles are compared at matched flow conditions. Nozzles of different geometry are said to be matched when they are geometrically sized to pass the same mass flux (primary) at the same NPR and total temperature. Friction and Vena Contracta effects reduce the effective nozzle exit area to something less than the geometric exit area; these effects are primarily a function of NPR and are generally different for different nozzles. A question therefore arises as to how the thrust performance of two nozzles of different geometry should be compared, since it is obvious that a simple comparison of FGC vs NPR for unmatched nozzles has little meaning in determining which type of nozzle has the best performance.

When evaluating nozzles for full-scale engine installation, it is necessary to consider overall engine performance, since the discharge characteristics of a set of nozzles of different geometry are in general not similar as a function of pressure ratio. In this approach, the thrust data for a given set

of nozzles are corrected for a match with one of the set at a given pressure ratio. To determine from model test data how a given set of nozzles will perform on a full-scale engine installation, it is necessary to correct the data for a match with one of the set at a selected pressure ratio.

Comparisons of matched model-scale thrust results, following the latter approach, are shown in figures 102, 103, and 104. An NPR = 2.4 (J-75 takeoff condition) was selected as the pressure ratio at which the nozzles would be matched. It was also decided to correct the thrust data of the various nozzles for a match with the 37-tube bare nozzle at NPR = 2.4. Thrust data for a given nozzle at a given NPR was corrected as follows:

$$FGC_{(matched)} = FGC \frac{A_{eff} \text{ 37-tube at NPR = 2.4}}{A_{eff} \text{ given nozzle at NPR = 2.4}}$$

where A_{eff} = coefficient of discharge multiplied by the nozzle geometric area.

It should be noted that, in the comparison of the model-scale conical and 37-tube nozzles, the major impact of the matching procedure results from the difference in the geometric flow areas between the two nozzles.

The matched thrust results indicate that the L/D = 2 ejector gives a higher thrust at a given NPR than the L/D = 1 ejector, the L/D = 1 ejector has a higher thrust than the conical nozzle, and the conical nozzle has a greater thrust than the suppressor bare nozzle. A more detailed presentation of the thrust performance variation is included in the later section on lined ejector data scaling. A discussion on ejectors used for thrust augmentation is given in reference 10.

The effect of acoustic lining material on the thrust of the L/D = 1 and 2 ejectors is shown in figure 105. The thrust of hardwall and lined ejectors (1.4cm depth, 22% open area) are compared as a function of NPR at ambient and 811°K total temperature. The greatest thrust loss, about 2%, occurred at an NPR of approximately 4.0 for the L/D = 2 ejector with the primary flow at ambient total temperature.

FULL SCALE

The corrected thrust, FGC, is plotted as a function of nozzle pressure ratio, NPR, for the conical, 37-tube, and the L/D = 1 and 2 hardwall ejectors in figure 106. The maximum thrust condition of NPR = 2.4 was again selected as the pressure ratio at which the nozzles would be matched. Following the matching procedure* described, thrust data for the 37-tube nozzle and the

---

*This procedure is valid for the J-75 engine and for other engines where for a given NPR, primary total temperature is only a weak function of primary mass flux.

L/D = 1 and 2 hardwall ejectors were corrected for match with the standard conical nozzle. The matched thrust results are also plotted in figure 106. The same performance trends with nozzle type were observed at full scale as in the model-scale tests.

The effect of acoustic lining material on the full-scale thrust performance is shown in figure 107 for L/D = 1 and 2 ejectors. A lining with a depth of 5.3cm and 12% open area had no directly measurable effect on the thrust of either the L/D = 1 or 2 ejectors (compared with the performance of the hardwall configuration). However, ejector wall static pressure distributions and ejector exit velocity profiles to be shown in the next section did indicate reduced secondary flow pumping and thus a marginal reduction in thrust performance.

RESULTS OF FLOW SURVEY TESTS

Flow profile data were acquired to help define the relationship between the flow characteristics and jet noise generation and propagation. The purpose of the flow survey data was to define qualitatively the flow regions and properties at various locations in the flow. Such properties include primary and secondary flows, shear layers, and relative mixing rates within the ejectors. Flow parameters related to the acoustic lining design procedures can also be obtained from the flow survey data.

MODEL SCALE

Wall surface pressure distributions for $L/D = 1$ and 2 hardwall ejectors are shown in figures 108 and 109. The pressure distributions presented are for total pressure and temperature conditions on the nominal J-75 engine operating line for nozzle pressure ratios up to and including 2.4. In addition, surface pressure distributions are presented for nozzle pressure ratios of 3.5 and 4.0 at a total temperature of $1088°K$ for the $L/D = 1$ and 2 hardwall ejectors. The minimum surface pressure was located on the ejector inlet bellmouth near the upstream end of the constant area ejector. The location of the minimum surface pressure was thought to be constant over the NPR range because local bellmouth curvature effects predominated. At a given total pressure and temperature, the minimum surface pressure for the $L/D = 2$ ejector was noticeably below that for the $L/D = 1$ ejector, indicating higher secondary velocities and greater induced secondary flows or pumping for the longer ejector. An interesting wall pressure distribution occurred between x/D of 0.1 and 0.3 for the $L/D = 2$ ejector operating at a nozzle pressure ratio of 4.0 and a total temperature of $1088°K$. This pressure distribution is thought to be caused by the expansion and contraction of the supersonic primary jet boundary near the primary nozzle exit.

The effect of acoustic lining on the surface pressure distribution of an $L/D = 2$ ejector at a nozzle pressure ratio of 2.4 and total temperature of $811°K$ is shown in figure 110. The minimum surface pressure for the 22% open area acoustic lining was 7% above that for the hardwall ejector, indicating a reduction in secondary induced flow and a loss in thrust performance.

Representative Mach number and velocity profiles at various stations downstream of the primary nozzle exit plane are shown in figures 111 and 112 for the 37-tube bare nozzle, figures 113 and 114 for the $L/D = 1$ hardwall ejector nozzle, and figures 115 and 116 for the $L/D = 2$ hardwall ejector nozzles.

The axial decay of peak velocity for the 37-tube nozzle and the 37-tube nozzle with L/D = 1 and 2 hardwall ejectors is shown in figure 117. The peak velocity decay for all three nozzles was characterized by an initially rapid rate of decay for x/D_e < 2, followed by a more gradual decay rate for $2 < x/D_e < 4$. The rate of decay was found to be a strong function of both the nozzle pressure ratio and the primary total temperature. An increase in the total temperature of the primary flow caused an increase in the rate of peak velocity decay; an increase in the nozzle pressure ratio caused a decrease in peak velocity decay rate. Nozzle type also influenced the rate of peak velocity decay; the L/D = 2 ejector with its increased rate of mixing had a more rapid rate of decay than did the 37-tube bare nozzle. The L/D = 1 and L/D = 2 ejectors had approximately the same rate of peak axial velocity decay.

In the previously presented Mach number and velocity profiles, the static pressure was assumed constant and equal to the values at the wall of the ejector or ambient for the 37-tube nozzle without ejector. This assumption is known to be incorrect near the primary nozzle exit plane when the primary flow is supersonic or where rapid flow turning takes place. An estimate was therefore made of the Mach number and velocity of the secondary flow between the tubes of the 37-tube suppressor nozzle. Assuming the local static pressure equal to ambient pressure, the computed Mach number and velocity between the tubes would be equal to zero; if the static pressure is assumed equal to the local static pressure measured at the end of the center tube of the array, and total pressure and temperature of the secondary flow are assumed equal to ambient conditions, the Mach number and velocity between the tubes may be estimated. These estimated values are presented as a function of nozzle pressure ratio in figure 118. Mach numbers up to 0.28 and velocities up to 91 m/sec were computed for the secondary, induced flow between the tubes.

FULL SCALE

Wall surface static pressure distributions for the L/D = 1 and 2 hardwall ejectors are shown in figures 119 and 120. The minimum surface pressure was located on the secondary inlet bellmouth near the primary nozzle exit plane. As with the model configurations the minimum surface pressure for the L/D = 2 ejector was noticeably below that for the L/D = 1 ejector. At a nozzle pressure ratio of 2.4, for example, the minimum surface pressure ratio (P_S/P_{amb}) for the L/D = 1 ejector was 0.91; for the L/D = 2 ejector the minimum was 0.83.

The effect of acoustic lining on the surface pressure distribution of the L/D = 2 ejector at a nozzle pressure ratio of 2.4 is shown in figure 121. The minimum surface pressure with the 12% area lining was approximately 1% above that for the hardwall ejector, which is an indication of reduced pumping and lower thrust performance. This indicated loss in thrust was too small to be recorded in the direct measurement of thrust.

Mach number and velocity profiles at stations downstream of the primary nozzle exit plane are shown in figure 122 for the conical nozzle, figure 123 for the 37-tube bare nozzle, figure 124 for the L/D = 1 hardwall ejector, and figure 125 for the L/D = 2 hardwall and lined ejectors. The effects of acoustic lining material on the Mach number and velocity profiles at two axial stations through the L/D = 2 ejector can be seen in figure 125. The Mach number and velocity profiles of hardwall and 12% open area linings are compared at a nozzle pressure ratio of 2.4 and although the effect of the lining is slight, the Mach and velocity profiles for the lined case are less full than those for the hardwall. This implies a lower exit momentum flux and hence a lower thrust for the lined ejectors—a similar indication to that obtained from the ejector wall static pressure distribution.

The axial decay of peak jet velocity is shown in figure 126 for the various full-scale configurations. As with the model-scale nozzles the peak velocity decay for the 37-tube bare and the L/D = 1 and 2 ejector nozzles was characterized by an initially rapid rate of decay for x/D_e < 2, followed by a more gradual rate of decay for $2 < x/D_e < 4$.

SCALING OF LINED EJECTOR DATA

Both near and far field acoustic data were scaled on a simple dimensional basis. Model- and full-scale configuration dimensions, together with the microphone measuring stations in the acoustic arena, were related by the geometric scaling factor of 1:4. Jet temperature and pressure conditions were established in the model program to correspond closely to the test conditions of the J-75 engine—these points were additional to those presented in the model-scale data section. For scaling purposes, acoustic frequencies were related by Strouhal number. This gave equivalent frequency ranges of 50 Hz to 10 kHz and 200 Hz to 40 kHz for full and model scale, respectively. Where sound power levels are presented, both full- and model-scale data have been normalized to a nozzle exit area of $1 m^2$.

Acoustic scaling is presented in the two subsequent sections—acoustic far field and near field. In addition, both model- and full-scale data are presented together in a later section in terms of sideline PNL.

ACOUSTIC FAR FIELD

Conical and 37-Tube Nozzles

The overall acoustic characteristics of the model- and full-scale nozzles are presented as a function of jet velocity in figure 127. Corresponding sound power spectra for these test points are shown in figures 128 and 129. In terms of absolute levels and spectral distribution, good agreement was found between the model- and full-scale configurations, although the following observations should be made:

- First, data from the 15.2cm reference conical nozzle appear consistently high by 1-2 dB when normalized with the full-scale data. To retain perspective on this difference, data from the 10.9cm nozzle have been included in figure 127. Data from the smaller nozzle however, tend to be consistently lower by 1-2 dB relative to the full scale nozzle. The observation is that each of these nominally conical nozzles has in fact a different physical geometry which may account for small differences in acoustic characteristics.

- Second, the comparison of the spectral distribution of acoustic energy of the model- and full-scale 37-tube nozzles improved with increasing nozzle pressure ratio. This results from two factors:

- Full-scale spectra are influenced, at low pressure ratios, by turbine and turbomachinery noise in the frequency range 4-10 kHz.

- Low-frequency energy levels were relatively high in the model-scale data and indications were that facility noise, probably burner generated, made some contribution to the data below 500 Hz.

With these reservations, agreement between the model- and full-scale test data was found to be good. The performance of the 37-tube nozzle as a sound power suppressor over the range of J-75 operating conditions is presented in figure 130 for both model- and full-scale nozzles. Suppression as a function of frequency for the corresponding conditions may be seen by reference to figures 32 and 69. Again, the correlation between model- and full-scale data is good.

37-Tube Nozzle With Hardwall Ejectors

With the hardwall ejectors installed (L/D = 1 and 2) the overall acoustic characteristics of both model- and full-scale test configurations are shown and compared in figure 131. It was noted earlier that the L/D = 2 ejector provided a marginal amount of suppression over the L/D = 1 ejector, and this consistent difference was found in both model- and full-scale data over the J-75 engine operating range. When normalized for nozzle area, good agreement was found in absolute sound power levels for the model- and full-scale data.

Sound power spectra corresponding to the points presented in figure 131 are shown in figures 132 and 133. Comparison of these spectra indicates similar trends that were observed and commented upon for the 37-tube nozzle without ejector.

Although the overall characteristics of the model- and full-scale hardwall ejectors displayed good agreement, a more detailed study of the directivity patterns of the model- and full-scale configurations indicated some differences—notably for the L/D = 1 ejector. Figure 134 compares far field SPL as a function of angular location over a range of frequencies. Both model- and full-scale configurations exhibit a peak intensity at 120° to the inlet, although the significant difference is that at larger angles (closer to the jet exit axis) the intensity decays from the peak more rapidly for the model ejector. Data presented later, related to the scaling of flow profiles and propulsion performance for the L/D = 1 ejector, indicate differences in the model- and full-scale configurations. It was outlined earlier that flow profiles at the ejector exit can significantly affect the far field directivity of sound radiated from the ejector. The dissimilar ejector exit profiles for the model- and full-scale L/D = 1 ejectors are held to account for the variations in directivity shown in figure 134. A corresponding comparison of the directivity characteristics for the L/D = 2 hardwall ejectors is shown in figure 135. Similar trends are seen, although the differences between model and full scale are somewhat less notable.

The relative directivity characteristics of hardwall and lined configurations are discussed further in the following section.

Acoustically Lined Ejector Configurations

The ability to scale acoustically lined ejectors was studied in three ways:

- Direct comparison of geometrically similar full and one-fourth scale model data (37-tube nozzle with lined ejectors).

- Assessment of the single-element scaling concept to evaluate the performance of linings to be used with a multitube array nozzle.

- A direct comparison of data from the geometrically similar 10.9cm and 2.74cm single-element configurations. Although somewhat limited in scope, this comparison provides additional evidence on the ability to geometrically scale acoustically lined configurations.

Geometrical scaling: 37-tube nozzles.—The insertion loss of comparable linings evaluated in both model- and full-scale ejectors may be directly compared by reference to figures 43 and 81. Although some similarity exists in the trend of increasing insertion loss with nozzle pressure ratio and ejector length, the model-scale linings in the L/D = 1 ejector do not exhibit the distinct variation in insertion loss with lining characteristics as was found in the full-scale configurations, particularly at nozzle pressure ratios above 2.0. No lining insertion loss greater than 5 dB was measured in the L/D = 1 model-scale ejector over the J-75 operating line. This characteristic was noted previously in figure 39 where lining insertion losses at pressure ratios above 2.0 were found to be relatively independent of lining material specification.

The following discussion outlines a possible explanation of the foregoing results. Figure 136 presents a qualitative picture of the ejector configurations as a noise source. High-frequency, initial flow mixing noise, which is generated within the ejector and can be attenuated by ejector linings, is radiated to the far field through the velocity and temperature gradients at the ejector exit plane. The directivity characteristics of the noise are sensitive to these gradients and, for the configurations tested in this program, have typically given peak sound pressure levels at 120° to the inlet. A rapid, progressive decay of intensities was noted at angles approaching the jet exit axis.

There is also noise generated downstream of the ejector by the fully or partially mixed primary and secondary flow exhausting from the ejector exit. This base jet, as it may be termed, generates noise which is primarily a function of the ejector exit diameter and the properties of the flow at

that point and which cannot be attenuated by linings within the ejector. The radiation characteristics from the base jet are generally similar to those of a round convergent nozzle.

For the evaluation of acoustic linings in ejectors, from the lining technology aspect, it is imperative that the noise level of the base jet be much lower than the noise levels of the lined ejector. If the base jet is not fully mixed then a precise prediction of the base jet noise levels is difficult, although intuitively it may be assumed that the levels will be above those for the fully mixed case—particularly at higher frequencies.

In terms of the space average sound pressure spectra, the SPL of the base jet may be well below the SPL of the lined ejector at frequencies of lining effectiveness. However, as a result of the different directivity characteristics of each source component, the SPL in frequency bands of maximum attenuation for lined ejectors may approach or be limited by the base jet at angles towards the jet exit axis. The spectral and directivity curves in figure 136 outline this phenomenon. If this occurs then the space integrated attenuation, or sound power insertion loss, for the linings will be lower than the true value. This is particularly relevant to this program as data showed that in general the maximum effect from the ejector linings at higher pressure ratios was found at angles greater than 120° to the inlet axis. This characteristic is typified by the full-scale data presented in appendix C, figures C-21 through C-26.

The model-scale L/D = 1 hardwall ejector data indicated a major factor that may result in this configuration being influenced more by base jet noise than the corresponding full-scale L/D = 1 ejector. It was shown in figure 134 that the differing ejector exit flow profiles between the model- and full-scale ejectors resulted in dissimilar directivity characteristics. The more rapid decay of intensity towards the jet exit axis for the model ejector gives hardwall noise levels which are closer to the base jet levels, thereby inherently reducing the magnitude of attenuation that can be measured.

The hypothesis of base jet interference is supported by the data presented in figure 137. In this figure, the directivity characteristics are compared for similarly lined model- and full-scale ejectors. For scaling of lining attenuation, the level of both model- and full-scale hardwall ejector curves appearing in figure 134 should be reduced by a similar amount when the ejectors are lined. This appears to occur in most frequency bands where the intensity for both the hardwall and lined model-scale ejector decays more rapidly from the peak level relative to the full-scale ejector data. However, in the 5000 and 6300 Hz frequency bands (1250 Hz and 1600 Hz full-scale) the model-scale data do not exhibit this trend, thereby indicating that the model-scale attenuation at these frequencies (which are at the peak of the lining attenuation spectrum) was limited at angles approaching the jet exit axis. It was further established that, although variations in SPL were found in other frequency bands for different lining configurations, the measured sound pressure levels in

the 5 kHz and 6.3 kHz frequency bands were essentially independent of lining material changes. This fact suggests that the SPL in these two bands was a result of a source not affected by lining absorption.

It is concluded that the base jet noise floor limited measured lining insertion loss in the model scale L/D = 1 ejector to approximately 5 dB at a pressure ratio of 2.40. Lining insertion loss above this nozzle pressure ratio was progressively limited by the increasing base jet noise levels to the point that at NPR = 4.0 only 3 dB or less was available. Below NPR = 2.40 the base jet became less dominant and at NPR = 1.40 and 1.60 the insertion losses measured were considered representative of the various lining materials.

The acoustic data acquired in this program have strongly emphasized the sensitivity of far field directivity characteristics to the ejector exit flow conditions. The preceding discussion has further emphasized the combined importance of ejector directivity effects and the presence of base jet noise in the evaluation of acoustic linings in ejectors. In the scaling of configurations it is imperative, therefore, that similarity in aerodynamic performance of the ejector configurations be achieved. It is apparent that, although the configurations in this program are geometrically scaled in overall terms, differences exist between them which resulted in dissimilar acoustic characteristics, the model-scale L/D = 1 ejector being less suitable for lining studies. This factor precludes the application of an ejector lining parametric study over the complete range of nozzle conditions of the model-scale program. However, ejector linings of low insertion loss performance (less than 5 dB), which are not severely limited by base jet noise, appear to scale well between model and full scale, as shown in figure 138. These data indicate that the acoustic characteristics of the linings in these ejector configurations may be scaled. Also shown in figure 138 is a comparison between model- and full-scale L/D = 2 lined ejector data. Scaling for this configuration appears good even though the model ejector gave insertion losses which were slightly lower, 1-2 dB, than the full scale ejector. Variations in lining tuning frequency for the model and full scale L/D = 2 ejectors were within one one-third octave band, and agreement between the configurations improves with increasing pressure ratio. Good lining performance scaling for the L/D = 2 ejectors may be directly related to the flow scaling between model and full scale, which was found to be substantially better for the L/D = 2 ejector, as compared to the L/D = 1 (see later section on flow survey data scaling).

Single-element scaling: 10.9cm and 2.74cm diameter nozzles. —Only one set of data is available from the single 10.9cm nozzle model tests where both lining specifications and ejector length may be compared directly to a full-scale configuration. This set is for a 12% open area (d = 5.85cm) lining and an ejector length of 2.64m. Lining insertion loss and tuning frequency, over the range of nozzle operating conditions, are compared directly in figure 139 for the two configurations.

Although both ejectors were 2.64m long, the ratio of L/D was different for the configurations: L/D = 2 full scale; L/D = 8 single element. This difference was reflected in the higher attenuations

achieved by the single-element ejectors. While the tuning frequencies were in reasonable agreement (within a one-third octave band), results indicated that the single-element configuration tuned at a consistently higher frequency. The variations of tuning frequency with pressure ratio were similar for both configurations.

The lining configurations tested in the 2.74cm single-element nozzle and ejector allowed direct comparison with results from the one-fourth scale 37-tube data for ejector lengths of 33cm and 66cm. For both ejector lengths the lining was 22% open area, 1.4cm core depth. Insertion loss and tuning frequency are shown as functions of nozzle pressure ratio in figures 140 and 141.

As with the 10.9cm nozzle, the single-element configuration with the inherently higher L/D ratio ejectors gave attenuation levels which were higher than those of the multitube nozzle configuration. Although different in magnitude, the characteristics of the insertion loss curves were similar for a given ejector length. Tuning frequencies were generally higher for the single-element configurations at a given nozzle condition, although this difference was in general no more than one one-third octave band. It should be noted that for these data the tuning frequency has been presented on a linear scale and some degree of caution must be exercised in the resolution available at these high frequencies (4-9 kHz).

Testing of single-element configurations has shown that the lining performance results are not directly applicable to the corresponding multi-element configurations. While this concept of scaling allows full-scale linings to be tested under model-scale conditions, there are many differences between the corresponding configurations. Two major variables between the single- and multi-element configurations were:

- Ratio of primary flow area to ejector cross-section area (ejector area ratio).

- Ejector L/D ratio for the same length of ejector.

Although the direct effects of area ratio on lining performance are not understood, the larger values of L/D for the single-element configurations must be a significant factor in increasing the measured levels of attenuation. Reducing the length of the single-element ejector to give equivalent L/D ratios is possible; however, this procedure would introduce another major variable, namely the relationship between the acoustic source distribution in the jet and the axial location and extent of the acoustic treatment. It has been assumed that, for a given element size and operating condition, the axial distributions of acoustic sources in the jet are comparable, whether the jet is a single element or one of an array. It was a basic consideration in the single-element concept that the lined ejectors should extend axially to the same distance for both single- and multi-element nozzles.

In general the single-element concept tests for lining evaluation were promising although there was no evidence that the data from these tests could be applied directly to equivalent lined ejector configurations with multi-element nozzles. The test results presented in the model-scale data section do indicate a potential for the use of a single-element ejector configuration as a tool to evaluate, on a more general basis, the performance of acoustic linings under conditions of primary jet flow. Where application to specific configurations is proposed and model testing is required, the use of geometrically scaled configurations is recommended.

Geometrical scaling: single-element nozzles.—The ability to geometrically scale lined ejector configurations is enhanced by a comparison between data from the 10.9cm and 2.74cm single-element configurations. Linings of 22% open area and corresponding core depths (5.85cm with 10.9cm nozzle and 1.4cm with 2.74cm nozzle) were both evaluated in single-element ejectors with L/D = 8. Figure 142 shows lining insertion loss and tuning frequency as a function of nozzle pressure ratio for the two scales of configuration. It is evident that the lining characteristics scale well. This comparison gives further confidence in the ability to scale acoustic lining results provided that the configurations themselves are geometrically scaled.

ACOUSTIC NEAR FIELD

Near field noise measurements were found to be extremely sensitive to microphone location, and in many cases the direct comparison between model- and full-scale data reflect this sensitivity. However, the comparisons are considered adequate to demonstrate a basic scaling ability in the near field environment of the jet flow.

Ejector wall sound pressure level spectra comparisons are shown in figures 143 and 144 for the two lengths of hardwall ejectors. Reasonable agreement is shown at all three measurement locations inside the ejectors if the turbine noise contribution in the full-scale data is ignored at the lower power setting. It is concluded that the ejector wall acoustic linings were exposed to a similar dynamic pressure field in both model- and full-scale configurations. Lining performance prediction analyses were undertaken using both model- and full-scale wall SPL spectra, and the analyses indicated minimal effects on predicted lining attenuations for the SPL variations measured.

Near field noise environment at corresponding locations near the free jet boundary of the model- and full-scale 37-tube nozzles are compared in figure 145. Again, except for turbine noise at low power setting, good agreement is shown between the data over the first two equivalent nozzle diameters from the nozzle exit plane. In figure 146 the near field environment downstream from the hardwall ejector exit plane is compared at model and full scale. The figure further indicates the basic ability to acoustically scale these configurations.

51

It is interesting to extend the data comparison beyond $x/D_e = 2$ for the conical and 37-tube nozzles. Figure 147 compares the overall sound pressure levels versus axial distance for both the conical and 37-tube nozzles. In general the scaling agreement is good for the two nozzles.

THRUST PERFORMANCE

For a given total pressure and temperature, the thrust of a given type of nozzle should be proportional* to the exit area of the nozzle. The exit area of the full-scale conical nozzle is 18.25 times that of the model-scale conical. The exit area of the full-scale 37-tube suppressor nozzle is 15.95 times that of the corresponding model-scale nozzle. A comparison of geometrically scaled model-scale and full-scale thrust data is shown in figure 148.

Model- and full-scale velocity and discharge coefficients, C_V and C_D, as a function of NPR and total temperature, are shown in figures 149 through 152 for the conical and 37-tube nozzles and $L/D = 1$ and 2 hardwall ejectors. Model scale C_V and C_D for the 37-tube and the ejector nozzle configurations were corrected for the diffuser head loss. Below NPR = 1.6, the engine surge bleed valve was open on the J-75 engine. A correction for the quantity of bleed air was made at the low power conditions according to available Pratt & Whitney information. It should be noted that this correction is necessary only in parameters that are computed from relationships involving measured primary mass flux. Curves of C_D and C_V for the J-75 engine are presented in band form as minor variations existed in the characteristics of the two J-75 engines used in the program. The bands include data from both engines. One dimensional ejector theory predicts a decrease in C_V (or thrust) with increasing primary total temperature at a given NPR; this predicted trend was observed for both the $L/D = 1$ and $L/D = 2$ model-scale ejectors.

Thrust differences of model- and full-scale nozzles with respect to the relevant conical nozzles are shown in figures 153 and 154. At NPR = 2.4 and T = 811°K the thrust of the $L/D = 2$ hardwall ejector is about 10% above that of the conical nozzle, the $L/D = 1$ hardwall ejector 5% above that of the conical nozzle, and the bare suppressor nozzle about 3% below the conical nozzle thrust. When comparison is made between model- and full-scale results it must be noted that, for a given NPR, flow total temperatures were not exactly the same for the corresponding configurations.

---

*Different boundary layer growth characteristics for model and full scale may cause minor differences between scaled model-scale thrust results and corresponding full-scale results.

The thrust augmentation of full- and model-scale, area ratio 4.32 ejectors was predicted with the one-dimensional theory from reference 9,* and comparisons between theory and experiment for augmentation as a function of NPR are shown in figure 155. Good agreement was obtained between the theory and the full-scale L/D = 2 hardwall ejector. The model-scale results for the L/D = 2 hardwall ejector were within 3% of the theory for 1.4<NPR<2.4; the difference between theory and experiment that exists at NPR = 2.0 is believed to be a result of data scatter. Augmentation for model- and full-scale L/D = 1 hardwall ejectors was 2%–4% below the predicted value, indicating incomplete mixing.

Secondary flow entrainment was also predicted from the one-dimensional theory, and the results of the analysis are compared with the range of results for the model- and full-scale L/D = 1 and 2 hardwall ejectors in figure 156. Experimental entrainment values were computed from the area averaged ejector exit velocity profile using the following relationship:

$$\frac{\dot{m}_s}{\dot{m}_p} = \frac{FG}{\dot{m}_p V_3} - 1$$

where

$\dot{m}_s$ =   entrained secondary mass flux

$\dot{m}_p$ =   primary mass flux

FG   =   measured thrust

V_3 =   area averaged ejector exit velocity at ejector exit, (as only a representative radial profile was used to compute V_3 some degree of error may be expected in this term).

Although the calculated values of entrainment at each test condition are based upon only one radial flow velocity profile in a nonaxisymmetric ejector flow, good agreement is found with the one-dimensional prediction. All calculated points were found to be within 7% of the predicted curve.

---

*The theory assumes that flow properties in the entering primary, entering secondary, and exiting mixed flow are uniform in a direction normal to the flow direction.

Present test results indicate that, for the J-75 operating line, the area ratio 4.3 ejector nozzles used in this study yield between 5% and 10% more thrust than a bare conical nozzle at static conditions depending upon ejector length. It must be appreciated that, due to the rapid increase of ram drag with flight Mach number, the net thrust of an ejector nozzle falls rapidly with increasing flight Mach number. For example, computed results shown in figure 157 for an area ratio 3.0 ejector illustrate the problem. At Mach numbers above 0.2, the ejector configuration yields less net thrust than the reference conical nozzle.

FLOW SURVEY

The ideal velocity, computed for an isentropic expansion of the exhaust gas to ambient pressure, is plotted as a function of nozzle pressure ratio and total temperature in figure 158. Although some differences existed in the fuel/air ratio between model and full scale, these differences did not result in a significant difference in the ideal velocity. Differences did exist, however, between the ideal velocities computed along the nominal engine operating line used in the model-scale program and those computed for the two engines; these differences are due to the slight variations in total temperature at a given nozzle pressure ratio for the different engine operating lines (nominal, J-75 number one, and J-75 number two). For ejector nozzle configurations, the peak primary jet velocity was above the computed ideal velocity. The local static pressure at the primary nozzle exit in the ejector configurations is typically well below ambient pressure. Thus, the pressure ratio through which the primary flow expands is greater than the ratio of total to ambient pressure used to compute the ideal velocity. This implies that the peak velocity reached by the primary flow is above the computed ideal velocity.

Ejector wall surface static pressure distributions for model- and full-scale L/D = 1 and 2 hardwall ejectors are compared in figures 159 and 160. For the L/D = 2 ejector, the model- and full-scale wall surface pressures agree well at nozzle pressure ratios of 1.4 and 2.4. For the L/D = 1 ejector, however, minimum model-scale surface pressures were as much as 5% below the corresponding full-scale surface pressures at a nozzle pressure ratio of 2.4.

Mach number and velocity surveys at several axial locations are compared in figures 161 and 162 for L/D = 1 and 2 hardwall ejectors. Model-scale Mach numbers and velocities at the ejector exit are noticeably below the corresponding full-scale values near the axis of the ejector. For the L/D = 1 ejector, the secondary flow Mach numbers and velocities near the primary nozzle exit plane were somewhat above the corresponding full-scale values. When comparisons are made of flow profiles from model- and full-scale configurations, it must be noted that no account has been taken of the differences in NPR that occur due to the model-scale nozzle diffuser total pressure loss. Care should be taken if quantitative comparisons are to be made.

The area averaged ejector exit Mach numbers, M_3, are compared with the results of the one-dimensional theory in figure 163. The model-scale data for the L/D = 2 ejector compare well with theory. Full-scale data compare well with theory for the L/D = 2 ejector at nozzle pressure ratios of 2.0 and 2.4, but are somewhat low at 1.4. Both model- and full-scale data for the L/D = 1 ejector fall below the values predicted over the 1.4–2.4 pressure ratio range.

The area averaged ejector exit velocities are also shown in figure 163. The exit velocity for any given configuration varied approximately linearly with nozzle pressure ratio.

The secondary flow Mach numbers, M_2, at the primary nozzle exit plane are compared with the one-dimensional theory in figure 164. Experimental values of M_2 were computed from the wall static pressure distribution. Model- and full-scale data for the L/D = 2 ejector are generally higher than the theory predicts. The model-scale L/D = 1 ejector data agree fairly well with the theory; the full-scale L/D = 1 ejector data fall below the theoretically predicted line.

Model- and full-scale peak axial velocity decay are compared in figure 165 for the various nozzle configurations. The model-scale axial decay rate was substantially higher for both the 37-tube and the L/D = 2 ejector nozzle configurations.

Flow properties computed or measured in the model-scale L/D = 2 ejector compared well with the corresponding full-scale data. Substantial differences in flow properties were noted, however, between the model- and full-scale L/D = 1 ejectors. The model-scale L/D = 1 ejector had a higher entrainment rate than the full-scale L/D = 1 ejector. This implies that a longer ejector was necessary for complete mixing at full scale than at model scale. Probable reasons for the different mixing rates that were observed between model and full scale include differences in free-stream turbulence or boundary layer properties at the start of mixing. It is not within the scope of this program to investigate in more detail the many factors that could contribute to these differences. However, it is important that the differences be noted with respect to both the acoustical and propulsion performance aspects of configuration scaling.

COMPARISON OF PREDICTED AND MEASURED
LINED EJECTOR ATTENUATION

REVISED PREDICTION PROCEDURE

The computerized, fan duct lining prediction procedure described earlier was refined during this contract. The refinements were made to the computer program and not to the theoretical model of reference 3, and were carried out independently of this lined ejector program. The changes made and their impact on the predicted lining results are as follows.

The most important change to the prediction procedure concerned the duct airflow Mach number and temperature inputs. Initially the computer program assumed uniform or plane flow profiles in the duct and consequently used one set of Mach number and temperature inputs for both the average flow conditions in the duct as well as the grazing conditions at the lining surface and temperature in the lining cavity. In the revised form, two input values are used to provide a more realistic description of the flow conditions in the duct where the average free-stream values of Mach number and temperature may be significantly different from those at the lining surface. This is more representative of the situation in the ejector where the entrained ambient air maintains the wall temperature well below the free-stream value. The lower temperatures (and consequently speed of sound) in the lining cavity result in an effectively deeper lining than if the free-stream temperature is used, causing the lining to tune to a lower frequency than predicted by the earlier version of the computer program.

At the beginning of the program, it was necessary to assume a number of ejector environment values to be used in the prediction procedure. Since experimental data have now been acquired, measured values of ejector environment have been used in rerunning the prediction program. It was found, however, that the originally assumed inputs were not substantially different from the subsequently measured data and the resultant changes in predicted performance due to these variations were found to be second order.

In its original form the prediction program calculated attenuation levels for discrete frequencies. The revised procedure calculates the attenuation over one-third octave bandwidths. This change was found to have a negligible effect on predicted one-octave bandwidth insertion loss for the linings.

The foregoing discussion is summarized by a typical example in figure 166. The initially predicted insertion loss spectrum was tuned to a frequency of 2000 Hz. The revised predicted spectrum tunes at a lower frequency of approximately 1150 Hz, primarily as a result of the lower

ejector wall temperature input. For comparison, the corresponding measured insertion loss spectrum shows that the lowering of the tuned frequency in the prediction procedure improves considerably the agreement between measured and predicted values. When predicted lining performance is presented, the revised procedure has been used unless otherwise specified.

37-TUBE NOZZLE WITH LINED EJECTORS

Attenuation spectra were originally predicted for the design engine power setting of nozzle pressure ratio of 2.4 and jet temperature of 811°K. Because the measured data cover an extensive range of power settings, additional attenuation spectra were predicted over the J-75 engine operating line to evaluate the lining performance trends with nozzle pressure ratio. There are a number of ways of comparing the measured and predicted lining results. The basic data in the form of measured and predicted insertion loss spectra for a range of nozzle pressure ratios between 1.4 and 2.4 and different linings and ejector lengths both model and full scale are shown in figures 167 through 170.

The impedance expression for a normally reacting acoustic lining material may be generalized in the form:

$$\underbrace{\frac{Z}{\rho c} = \frac{R}{\rho c} + i\frac{X}{\rho c}}_{\text{face sheet}} \underbrace{- i \cot \frac{(2\pi fd)}{c}}_{\text{cavity}}$$

where:

 Z = acoustic impedance

 R = resistance

 X = reactance

 ρc = characteristic impedance of air

 f = frequency

 d = cavity depth

 c = speed of sound

57

The first grouped term represents the normalized impedance of the face sheet material and the second term the impedance of the cavity core. Actual lining performance has to be evaluated relative to the predicted performance in terms of both tuning frequency and attenuation.

The frequency at which maximum attenuation occurs is generally referred to as the lining tuning frequency. Each term in the above impedance expression contributes to the prediction of lining tuning frequency and the ability to predict this value reflects the credibility of the lining impedance model for ejector application. The representative results presented in figures 167 through 170, summarized for all model- and full-scale linings in figures 171 and 172 indicate a generally good agreement (within a one-third octave band) between measured and predicted tuning frequency. It is interesting to note, however, that for model-scale linings where the insertion loss is thought to be limited by base jet noise there is a trend for the measured tuning frequency to become higher than the predicted value for increasing nozzle pressure ratios. This trend may be seen in figure 167 for the 12% lining (d = 1.4cm and 1.9cm) and 6% lining (d = 1.4cm); corresponding full-scale data do not exhibit this trend.

The impedance term related to the lining cavity may be evaluated as a separate entity using the measured results. The cavity impedance becomes infinite at frequencies where $d = \lambda/2$ (λ = wave length) or multiples thereof. At these frequencies the lining absorption theoretically becomes zero and if analyzed over one-third octave bandwidths minima will occur in the attenuation spectrum. In practice only the first one or two minima can be clearly seen in the attenuation spectrum. Consequently, an agreement between measured and predicted results in terms of the frequency at which the first minimum occurs is indicative of agreement of lining tuning characteristics. This agreement is clearly seen in figures 167 through 170. The one-third octave band in which the "first minimum" occurs can also be calculated from:

$$d = \lambda/2$$

or

$$f = c/2d$$

where c = speed of sound in the cavity.

From the average of measured values of temperature at the lining surface, speeds of sound of 358m/sec and 342m/sec have been computed for the model-scale and full-scale ejectors, respectively. With these values for c and the appropriate cavity depths shown in figures 167 through 170, it was found that the "first minimum" should occur in the 12,500 Hz and 3150 Hz bands for model and full scale, respectively. This correlates well with the measured results shown in figures 167 through 170.

The insertion loss spectra in figures 167 through 170 are not only a function of the lining face sheet impedance, but are also related to the jet noise distribution within the ejector. However, the predicted spectra are strictly related to the fan duct noise model, in which all the acoustic energy is generated upstream of the lined section. Thus, with currently available technology, the predicted insertion losses are expected to be higher than those measured, as shown by the results. The important factor, however, is whether both the measured and predicted lining performance follow the same trends with face sheet porosity and nozzle pressure ratio, thereby indicating an ability to predict optimum lining configurations. Figures 171 and 172 compare the attenuation trends with engine power setting for both model- and full-scale results, with reasonable agreement shown. This agreement is subject to the limitation of base jet noise, discussed earlier, which may limit the measured attenuations for model-scale $L/D = 1$ ejector lining, particularly at NPR > 2.0. In figure 173 the special case of the design engine power setting is shown for both model- and full-scale results as a function of lining face sheet porosity or percent open area. From the full-scale results the trend is for the predicted optimum percent open area to be slightly higher than measured.

10.9CM DIAMETER NOZZLE WITH LINED EJECTORS

Insertion loss spectra have been predicted for the design engine power setting of NPR = 2.4 and jet temperature of 811°K and are presented together with the corresponding measured results in figures 174 through 176 for all the configurations tested. As with the 37-tube nozzle configurations, good agreement is found between measured and predicted tuning frequency in terms of the "first minimum" in the insertion loss spectra associated with infinite cavity impedance. Evaluating the tuning frequency on the basis of peak insertion loss, the results have been presented as a function of cavity depth and percent open area in figure 177. Good agreement, to within a one-third octave band, can be seen for the 12% open area linings as a function of cavity depth, although this agreement tends to deteriorate the increasing core depth. Agreement between prediction and measurement is also good for the higher percent open area linings for a fixed cavity depth; however, at low percent open areas the differences become progressively larger than a one-third octave bandwidth tolerance. For the 10.9cm nozzle and $L/D = 8$ ejector, a comparison of measured and predicted insertion loss spectra (figs. 174 and 175) in terms of tuning frequency indicates that measured attenuations may have been limited by base jet noise. As outlined in the previous section, the presence of base jet noise has the effect of increasing the measured tuning frequency relative to the predicted value. This trend was noted in Figures 174 and 175 for low tuning linings (d = 5.85 and 8.6cm) and for linings with high insertion loss characteristics (6% and 12% open area). Both low tuning frequency and high attenuation emphasize the base jet noise limitation and as a result the differences between measured and predicted values of tuning frequency in figure 177 are attributed to base jet noise.

As for the 37-tube nozzle results, the measured attenuation levels are expected to be lower than predicted. This may be more evident with the 10.9cm nozzle configurations because of the very long duct lengths tested (L/D = 8) and the inherently higher levels of predicted attenuation. The insertion loss comparisons are summarized in figure 178 and show at least qualitative agreement. Again the measured optimum lining face sheet percent open area appears to be slightly lower than the predicted value.

2.74CM DIAMETER NOZZLE WITH LINED EJECTORS

Lining insertion loss spectra have been predicted for a range of engine power settings including the design case of nozzle pressure ratio of 2.4 and jet temperature of 811°K. The predicted results are presented together with the corresponding measured results in figure 179 for the two ejector lengths tested. Again, good agreement is shown between measured and predicted-tuning frequency in terms of the "first minimum" in the spectra associated with the condition of infinite cavity impedance. Evaluating the tuning frequency at the point of maximum lining insertion loss, however, it is found that the agreement with predictions is not as good as for the previous nozzle and ejector configurations. No rational explanation can be given for the larger than expected discrepancies, except to note that in figure 142 the scaled performance of the linings in the 10.9cm and 2.74cm nozzle single-element ejectors displayed good agreement. This may suggest that the predicted performance curves for the 2.74cm nozzle ejector linings are the source of the discrepancy.

ACOUSTIC PERFORMANCE OF THE 37-TUBE/LINED
EJECTOR JET NOISE SUPPRESSOR SYSTEM

In this section the results of the program are presented in an overall way to show the jet noise suppression that has been achieved on the J-75 engine and, over a wider range of nozzle conditions, for the model-scale nozzles. The results are presented in terms of sound power suppression and also in subjective terms of perceived noise level reduction. For PNL reduction the data have been extrapolated to a sideline of 649m (2128 ft). As noted in the section on data reduction, a simple extrapolation procedure has been used based only upon distance and atmospheric attenuation; no account has been taken of excess ground attenuation or of any effects related to flight or airplane velocity. The PNL data presented are for one engine only, and for this reason the absolute levels must be interpreted with caution. The data, however, do provide a relative subjective evaluation taking into account source directivity, source energy frequency distribution, and a factor for atmospheric absorption over a realistic propagation distance. The PNL suppression values should, however, be quite representative of an airplane installed configuration.

SOUND POWER REDUCTION

Calculated sound power spectra were presented earlier for the various model- and full-scale test configurations. Examples of sound power suppression spectra for the model- and full-scale 37-tube nozzles over the J-75 engine operating line are shown in figures 32 and 69. The results indicate that, relative to the reference nozzle, the 37-tube nozzle suppresses the jet noise from the engine exhaust and that this suppression occurs mainly over the lower jet noise frequencies. The amount of suppression varies, however, increasing with increasing power setting within the operating range of the J-75 engine.

Representative insertion loss spectra for the full-scale acoustic linings with respect to hardwall ejectors were shown in figures 79 and 80. The linings attenuated jet noise at intermediate frequencies between 400 and 3000 Hz and showed secondary suppression peaks between 3000 and 6000 Hz. Consequently, the combination of the 37-tube nozzle with the acoustically lined ejectors exhibits a broadband suppression characteristic as shown in figures 180 and 181. One way to summarize the results is to look at the overall sound power suppression for the configurations as a function of V_J as shown in figures 182 and 183 for full and model scale, respectively.

61

The full-scale results in figure 182 show that the overall sound power suppression achieved on the J-75 engine at maximum power is approximately as follows:

37-tube nozzle	8 dB
37-tube nozzle with L/D = 1 lined ejector (6% open area, d = 5.33cm)	12 dB
37-tube nozzle with L/D = 2 lined ejector (12% open area, d = 5.33cm)	15 dB

The above result for the L/D = 1 lined ejector represents the highest suppression achieved from the lined configurations tested. Only one lined configuration for the L/D = 2 ejector was tested in the program. For the lined ejectors, the rate of increase of jet noise suppression declines with increasing nozzle pressure ratio. This results from the increasing domination of the overall sound power level by low-frequency noise generated downstream of the ejector exit plane.

The model-scale results for the 37-tube nozzle in figure 183 show that the sound power suppression is clearly a function of jet temperature as well as jet velocity. It is also evident that higher levels of sound power suppression can be achieved with the 37-tube nozzle at conditions outside those defined by the J-75 engine operating line.

PERCEIVED NOISE LEVEL REDUCTION

Typical examples of perceived noise levels calculated on a 649m sideline for the design engine power setting of NPR = 2.4 and jet temperature of 811° K are shown in figures 184 and 185 for full-scale and model-scale results. Where the data were available, extrapolations are included in figure 184 from the 15.2m radius microphone array in the forward quadrant. The sideline noise levels are shown on a linear distance scale for the various suppressor configurations; the lining configurations that gave highest attenuations are presented for both model- and full-scale L/D = 1 ejectors. In addition to the relative amounts of noise suppression at various sideline points, figures 184 and 185 indicate the significant changes in directivity between conical nozzle, hardwall ejectors, and the acoustically lined ejectors, the progression of the noise peak being from 140° to 120° and then to 110° from the engine inlet axis, respectively. Because of this inherent change of sideline noise directivity, one way of evaluating the jet noise suppression from static tests is to compare the peak or maximum perceived noise level (PNLM) for each suppressor component. Results from the full-scale and model-scale tests are presented in this form for the J-75 engine operating conditions in figure 186. The results are plotted as a function of jet velocity (V_J) rather

than pressure ratio to eliminate discrepancies in the actual values of nozzle pressure ratio and jet temperature established between the full-scale and model-scale configurations. Model-scale results covering the complete range of nozzle pressure ratios and jet temperatures tested are presented for all the suppressor components in figures 187 and 188. It is apparent that the noise levels at a given V_J are a function of jet temperature and the generalized data in figures 187 and 188 may be used to extract noise data for other engines with operating lines differing from the J-75.

From the data presented in figure 186, the relative acoustical performance of each of the suppressor system components may be directly derived as shown in figure 189. The full-scale data do not extend to the zero axis at the lower jet velocities due to the attenuation of turbine noise, which is not present in the model-scale results. At the higher jet velocities, the L/D = 1 lined ejector does not appear to offer much advantage over the 37-tube nozzle. This is a result of the hardwall ejectors being noisier than the 37-tube nozzle, as shown in figures 184 and 185, and thus lining effectiveness is not shown to its full advantage. The maximum sideline perceived noise level reduction achieved statically on the J-75 engine with the 37-tube nozzle and L/D = 2 acoustically lined ejector (12% open area, d = 5.33cm linings) is shown to be approximately 15 PNdB. The PNL reduction from the corresponding model-scale configuration operating at the same nominal condition of NPR = 2.4 (811° K) was 13 PNdB. From the slope of the curve it could be speculated that even higher values of noise reduction could be achieved with such a system on engines operating at a jet velocity above 610m/sec.

PNL suppression for the model-scale 37-tube nozzle is presented in figure 190 as a function of jet temperature and velocity. It is shown that higher values of suppression are achieved at jet velocities above the J-75 engine range, with a maximum indicated reduction of 13 PNdB at a velocity of 850m/sec. Comparison (from figs. 187 and 188) at this velocity may also be made for the L/D = 2 lined ejector and an additional reduction of 3 PNdB, relative to the maximum suppression on the J-75 operating line, is indicated.

It has already been shown that statically the ejector configurations generate higher thrust than the bare nozzles for a given nozzle pressure ratio. To account for these changes in thrust, the sideline perceived noise levels have been presented versus corrected gross thrust for the J-75 engine as shown in figure 191. Taking the unsuppressed J-75 engine maximum thrust of 66,800 newtons (15,000 lb) as a reference (100%) the noise suppression can be presented as a function of equal thrust as shown in figure 192. Although this approach does not change measurably the 37-tube nozzle suppression results, it is favorable to the lined ejector suppression values showing a maximum jet noise suppression of 16.5 PNdB for the L/D = 2 acoustically lined ejector. The effectiveness of the acoustic linings as jet noise absorbers are also shown for the configurations by subtracting the lined ejector results from the corresponding hardwall ejector data. For the "design" case of 100% gross thrust, acoustic linings in the L/D = 1 ejector contribute 4 PNdB and in the L/D = 2 ejector 7 PNdB to the sideline jet noise reduction.

In the above discussion the lined ejector configurations presented were those that gave the lowest sideline PNLM values. It is of interest, however, to look at the sideline results of the other lining configurations tested in the L/D = 1 ejector as summarized in figure 193. It was found, for example, that for the 12% open area linings a core depth of 5.3cm is approximately the optimum value in terms of sideline noise suppression for this ejector diameter. However, it can also be seen that for a 5.3cm deep lining a percent open area less than 12% is better at the design power setting of NPR = 2.4.

A summary of PNL data for both the conical and 37-tube nozzles, and the hardwall and lined ejectors is presented in tables 8 and 9 for model- and full-scale configurations, respectively.

CONCLUSIONS

ACOUSTICALLY LINED EJECTOR DESIGN TECHNOLOGY

The major objectives of the program were to experimentally evaluate the application of current duct lining design procedures and scaling relationships to the design of acoustically lined ejectors for jet noise suppression. For the configuration tested it was concluded that the basic design procedure for acoustically lined ducts with airflow may be applied to ejectors for the determination of the lining tuning frequency and attenuation relationships. Lining sound power insertion loss was lower than predicted although it was indicated that the lining impedance model, incorporating the effect of grazing flow, may be used to determine the optimum face sheet open area. Lining attenuation was less than predicted for two main reasons:

- The acoustic sources are distributed within the ejector and are not located upstream of the ejector entrance as the lining prediction procedure assumes.

- Noise generated downstream of the ejector exit plane, which cannot be attenuated by the lining, may have prevented the true measurement of lining attenuation.

An accurate prediction of lining sound power insertion loss requires a quantitative description of the acoustic source distribution in the ejector together with a knowledge of the way in which acoustic energy propagates within the severe flow environment of the ejector. This program has demonstrated measured lining attenuation to be a complex function of lining tuning frequency, far field directivity, pressure ratio, and ejector flow characteristics. The determination of true lining performance for lining technology applications requires a full understanding of all the relationships between these variables.

SCALING OF ACOUSTICALLY LINED EJECTORS

It may be concluded from this program that acoustically lined ejector configurations can be geometrically scaled provided that flow similarity, in both aerodynamic and thermal properties, is maintained. Although geometrical scaling was undertaken in this program, differences did exist between model- and full-scale configurations that resulted in dissimilar flow properties within corresponding ejectors. This fact precluded a direct demonstration of lining performance scaling for L/D = 1 lined ejector configurations. Excellent agreement was found in the acoustic characteristics of the model- and full-scale 37-tube suppressor nozzles.

The concept of lining studies using a single element of a multitube array with the ejector lengths and lining materials of the related multitube nozzle installation was evaluated. The results indicate a good potential for the use of this type of configuration for fundamental lining studies. However, direct application of the single tube results to the acoustic performance of the ejector with the multi-element nozzle was not possible.

NOZZLE THRUST PERFORMANCE

Static thrust measurements indicated that the 37-tube nozzle suffered a 2%-3% thrust penalty relative to the reference conical nozzle over the J-75 operating range. Thrust augmentation was measured with the ejectors installed. A net thrust gain of 6% for the L/D = 1 ejector and 9% for the L/D = 2 ejector relative to the conical nozzle was indicated at an engine pressure ratio of 2.40 at 811°K. Model-scale data showed thrust augmentation to be a function of primary flow temperature, with augmentation decreasing with increasing temperature and nozzle pressure ratio. First-order prediction of the ejector thrust performance was possible using a one-dimensional ejector mixing prediction procedure.

The presence of acoustic lining in the ejectors was found to have a negligible effect upon the thrust performance of the ejector nozzle configurations.

JET NOISE SUPPRESSION

The 37-tube, area ratio 3.3 suppressor nozzle was found to suppress the overall sound power output from the equivalent round convergent nozzle. This suppression increased with jet velocity and, for the J-75 engine, was 3 dB at NPR = 1.40 and 8 dB at NPR = 2.40. The installation of an unlined or hardwall ejector gave no additional suppression relative to the 37-tube nozzle, although the presence of the ejector had a marked effect upon the far field radiation characteristics of noise generated within the ejector length. Directivity was found to be primarily influenced by velocity and temperature gradients at the ejector exit plane and, in general, a distinct maximum in intensity occurred between 110° and 130° to the nozzle inlet axis. The presence of acoustic linings in the ejector was found to change directivity relative to the hardwall ejector.

Extrapolation of the static test data to a 649m sideline distance enabled reductions in perceived noise levels to be calculated. The results showed that, relative to the round convergent nozzle, the 37-tube nozzle reduced the peak sideline PNL by 10 PNdB at a nozzle pressure ratio of 2.4. With the acoustically lined L/D = 2 ejector this reduction increased to 15 PNdB. Model-scale

data indicated that an improvement in PNL reduction by up to 3 PNdB could be achieved with these nozzles at jet velocities up to 800m/sec—above the range of the J-75 engine.

The changes in directivity pattern caused by the hardwall ejectors resulted in peak sideline perceived noise levels up to 2 PNdB above the levels from the 37-tube nozzle. This feature reduced, by a corresponding amount, the potential effectiveness of the acoustic linings in reducing sideline perceived noise levels.

RECOMMENDATIONS

This program has demonstrated the ability of a multi-element nozzle and lined ejector shroud to suppress and attenuate primary jet noise. Optimization of the acoustical performance of such a suppressor system requires an understanding of many interdependent phenomena. To achieve this goal, the following recommendations are made:

- Analytical and experimental programs should be undertaken to develop an understanding of the relationship that exists between lining absorption and the acoustic source distribution and flow gradients within the ejector.

- Ejector flow mixing analyses and measurements should be studied in relation to ejector acoustic radiation characteristics and to the noise generated downstream of the ejector exit plane.

- More extensive parametric variations on ejector area ratio and ejector axial location, suppressor nozzle design, and ejector lining materials should be undertaken.

- Lined ejector concepts should be fully investigated for application to low-velocity noise suppression.

The use of small, geometrically scaled, lined ejector nozzles for acoustical evaluations has been shown to be feasible. However, when scaled configurations are to be used, it is recommended that considerable attention be given to achieving flow similarity between the different scales of nozzle. The far-field acoustical characteristics of ejectors in this program were found to be extremely sensitive to the flow field within and, notably, at the exit plane of the ejector. The single-element concept for scaling of a multitube nozzle array with a lined ejector cannot, on the basis of results from this program, be recommended as a directly applicable acoustical scaling technique for lined ejector evaluations.

Until the acoustical performance of lined ducts containing distributed noise sources and severe mean gas property gradients can be quantified, and the interdependence of mean gas flow properties and far-field acoustic radiation characteristics of ejectors evaluated, it is recommended that existing lined duct analysis procedures be used for ejector lining applications. The following guidelines for lining design are provided:

- The bare suppressor nozzle must be evaluated to determine acoustic energy spectral characteristics, acoustic source distribution, and the near-field dynamic pressure field.

- The desired lining tuning frequency is established by taking into account the characteristic nozzle spectrum at the design operating condition and the distance from the engine at which noise suppression will be evaluated (to account for the atmospheric attenuation of sound at the higher frequencies).

- The minimum ejector length should be adequate to shroud the jet noise sources which are to be attenuated.

- Using available lined duct design procedures, linings may be optimized for maximum attenuation at the design frequency. Lining impedance calculations require a description of the ejector environment:

  - mean flow properties may be estimated from analytical flow mixing programs.

  - dynamic pressures at the ejector wall are closely related to the near-field measurements on the bare nozzle.

- Iterative procedures to optimize ejector geometry (length and diameter), noise suppression, and both aerodynamic and propulsion performance can be undertaken to achieve an optimum noise suppression nozzle and ejector system.

Caution is recommended, however, in the direct application of predicted lining attenuations. Jet noise generated downstream of the ejector exit plane can effectively limit the attenuation achieved by the ejector linings. However, assuming fully mixed flow conditions at the ejector exit plane and taking the ejector exit to be equivalent to a round nozzle, an estimate may be made for base jet noise levels using flow mixing analyses and empirical jet noise prediction procedures. While this approach may underestimate base jet noise if the ejector exit flow is not fully mixed, it may be used to give an initial indication of the limitations of a lined-ejector system. If in-flight predictions are to be made, relative velocity effects must be considered in the base jet noise estimates. In addition to limitations by base jet noise, the directivity characteristics of the suppressor nozzle may change significantly when an ejector is installed. These changes, which may be unique to a particular configuration, can effectively reduce the acoustical performance of lined ejectors when results are compared to the noise reduction characteristics of the bare suppressor nozzle.

APPENDIX A

USE OF GROUND LEVEL MICROPHONES
FOR MEASUREMENT OF FAR FIELD JET NOISE

It is desirable to present ground static jet noise measurements in terms of the free-field sound pressure level. However, for microphones located above a reflecting plane, the combination of direct and reflected (from the area surface) sound waves results in a wave interference phenomenon at the microphone. This interference results in maxima and minima in the measured spectrum at frequencies which are primarily a function of the microphone height, source height, and the distance between the source and microphone. The effect of a reflecting plane on the propagation and measurement of jet noise was investigated theoretically and experimentally by W. L. Howes (ref. 11). Howes measured ground reflection fluctuations in jet noise spectra as large as 10 dB from peak to valley in one-third octave bandwidth spectra, where the source and receiver were both above a ground plane. He suggested a technique for correcting such jet noise spectra to free-field levels if the measurements were made in the presence of a perfect reflector ground plane. Recent Boeing practice, however, has been to measure free-field or reflection (interference)-free jet noise spectra directly rather than to use a correction procedure. Limited success with direct measurement of free-field spectra has been achieved by using:

- Vertical microphone arrays, or

- Microphones close to a flat, smooth, concrete ground surface covering the whole acoustic test arena.

The latter technique of ground level microphones has been used routinely for full-scale measurements up to frequencies of 10 kHz. Figure A-1 shows the theoretically predicted ground reflection interference as a function of frequency for a microphone at engine centerline height and at the same polar distance over a flat reflecting surface as in the J-75 engine tests. Also shown is the curve for a microphone 1.27cm above the ground plane. Assumptions made in the above prediction were that the noise emanated from a point source, that it was statistically stationary, and that the microphones were in the far field. Figure A-1 clearly illustrates the potential difficulty of correcting the high-level microphone spectrum to free field.

However, the figure also shows that as the microphone is brought close to the reflecting ground plane, the frequency at which the first minimum occurs shifts to higher frequencies. For a microphone only 1.27cm above the ground plane and for the test geometry in this program the reflection effects become measurable only above 20 kHz. Consequently, in the full-scale test

program SPL spectra measured with ground microphones were assumed free of reflection interference up to 10 kHz, but 6 dB above free field in level, a correction which is easily applied.

Figure A-2 shows similar curves calculated for the model-scale test geometries with the ground microphone height of 0.63cm, which is the minimum practical distance that the center of the microphone diaphragm could be brought to the ground surface. For model-scale testing, 0.63cm is not close enough to obtain reflection-free data between 40 and 80 kHz. Although in this program 40 kHz was, strictly speaking, the upper frequency limit, a broader requirement of 80 kHz was used to make certain that the reflection interference effects were moved well beyond 40 kHz frequency in the model-scale spectra. This requirement caused the ground microphones to be flush mounted in the ground surface, i.e., zero height. Flush mounting of microphones in the ground plane eliminated the reflection interference effects; however, it created a new problem in that microphone response corrections at near grazing sound incidence had to be determined, because of the absence of such information in the manufacturer's users manual. The investigation of corrections appropriate to flush-mounted grazing incidence microphones was conducted in two parts as follows:

- First, in an anechoic indoor facility the model-scale test arena and noise source microphone relationships were reproduced on a one-fifth geometric scale and tests conducted with a 2.54cm diameter cold jet noise source to determine the difference in the B&K 4136 microphone response with and without the presence of a ground plane.

- Second, a study was made of test data obtained for a conical reference nozzle at the hot nozzle test facility Comparisons were made between jet centerline height and ground level microphones above 10 kHz after normalizing both to free-field levels (i.e., by subtracting 3 dB and 6 dB, respectively).

Measured sound pressure level data from flush-mounted microphones referenced to free field for both indoor and outdoor tests gave similar quantitative results. There was a definite trend of response rolloff with frequency above 16 kHz as shown in figure A-3. From a brief survey of the literature, references 12, 13, and 14, it was concluded that the observed trends in figure A-3 were to be expected. The high-frequency rolloff of the flush-mounted microphone to a grazing incidence wave is caused by the tendency for positive and negative portions of a sound wave occurring simultaneously on the microphone diaphragm to cancel as the wave length approaches the microphone effective diameter. This cancellation effect is part of the free-field response correction as given by Bruel and Kjaer for the 4136 microphone at grazing incidence, but the B&K curve also includes the effect of disturbance to the sound field caused by the microphone body itself. This latter effect must be removed from the correction for the flush-mounted microphone.

In reference 13 an expression of the form $(\sin \omega \ell/\lambda)/(\omega \ell/\lambda)$ is derived for the frequency response of a rigid rectangular piston of length, ℓ, flush mounted in a flat plate at grazing incidence to a sinusoidal sound wave, producing a rolloff response similar to that found in the test data in figure A-3. Considering that the B&K 4136 diaphragm is round and nonrigid it was necessary to use an expression similar to one derived in reference 14 involving a Bessel function to estimate the effective diameter of the microphone diaphragm (the geometric diameter for the B&K 4136 microphone diaphragm is 0.445cm):

$$20 \log_{10} \frac{p_m}{p_o} = 20 \log_{10} 2 \left[\frac{2J_1(\omega D_c/\lambda)}{\omega D_c/\lambda} \right], dB$$

where:

p_m =   measured pressure

p_o =   free-field pressure in absence of microphone or reflecting surfaces

ω =   angular velocity $(2\pi f)$

λ =   wavelength of sound

D_c =   effective diameter of microphone

J_1 =   first order Bessel function

Solution of the above equation for the first zero response ($p_m = 0$) gives $D_c = 1.22$. The published curve for the B&K 4136 microphone for 90° incidence free-field correction drops off abruptly above 50 kHz and appears, when plotted on linear coordinates, to extrapolate to zero at approximately 110 kHz, which would give an effective diameter of approximately 0.376cm and provide a reasonable fit with the experimental data as shown in figure A-3. This calculated microphone response curve was used in processing the model test data from the ground microphones. It must be emphasized that the response corrections have been developed for the particular microphone/jet relationship used in this program and will not necessarily apply to other arrangements without further investigation.

The use of ground microphones has enabled reflection-free, smooth jet noise spectra to be measured over the range of model-scale frequencies, in contrast to the jagged spectrum shape produced by microphones at a level equal to the nozzle centerline height as shown in figure A-4. Statistical analysis of data from 66 paired spectra (centerline versus ground microphone) showed

that the ground microphone measured 2.9 dB higher than the centerline microphones for frequencies above 10 kHz, which agrees with the predicted value of 3.0 dB. However, in the body of data accumulated in this program, there are many individual cases of larger deviations that are not readily explained. In some cases equipment and facility noise floors are suspected to be the major causes of disagreement. Similarly, there are numerous cases where almost perfect agreement occurs between predicted differences between centerline and ground microphones.

Another phenomenon was noted during the evaluation of the ground microphone technique that may partly contribute to deviations observed in the test data. It was determined during laboratory tests that the high-frequency response of the B&K 4136 microphone at 90° incidence is not necessarily symmetrical about the principal axis. For example, when a group of 11 microphones were tested at 63 kHz at grazing incidence it was found that the angular variations in the response of three microphones was greater than 3 dB, while five microphones had less than 1 dB. The effect was negligible below 40 kHz.

APPENDIX B

ATMOSPHERIC ABSORPTION OF SOUND IN THE FREQUENCY RANGE 10-40 kHz

It is currently accepted that ARP 866 presents the most qualified procedure for the calculation of absorption of sound by the atmosphere over a wide range of temperature and humidity. The frequency range covered by ARP 866 is 31 Hz to 10 kHz with absorption values presented as a function of one-third octave band center frequency.

Since the emphasis in this program was on acoustic scaling, it was necessary to take account of atmospheric absorption in both model- and full-scale test programs. The model-scale program therefore extends the absorption requirements to 40 kHz, and at the present time this information is not generally available.

Four figures, B-1 to B-4, present the basic information contained in ARP 866. While this standard has been designed for the frequency range 31 Hz to 10 kHz, there is no apparent reason why the parametric relationships cannot be extrapolated, where necessary, to extend the range of application to 40 kHz. The procedure has been incorporated to the extent shown in figures B-1, B-2, and B-3. (Note that figure B-4 is independent of frequency.)

A computer program has been developed which tabulates absorption rates over the same range of temperature and relative humidity as ARP 866 but with an extension of the frequency range to 40 kHz. While certain doubts must exist in this procedure, which has not been experimentally validated, it is essential that some estimate be made of absorption where model- and full-scale data are to be compared. For this reason the approach outlined has been adopted.

74

APPENDIX C

TEST DATA

This appendix contains additional, supporting model- and full-scale test data. These data, which are presented graphically, are as follows:

APPENDIX D

SYMBOLS

A   Area, cm^2 or m^2

AR   Area ratio: for nozzle $= \dfrac{\text{area enclosed by perimeter of nozzle array}}{\text{primary flow area}}$

                     for ejector $= \dfrac{\text{ejector cross-sectional area}}{\text{primary nozzle flow area}}$

C_D Discharge coefficient $= \dot{m}_p / \dot{m}_{p\ ideal}$

C_f Friction coefficient $= \tau_w / \frac{1}{2} \rho V^2$, where τ_w = wall shear stress, N/m^2

C_V Velocity coefficient $= FG/\dot{m}_p V_{ideal}$

c   Speed of sound, m/sec

D   Diameter, cm or m

D_c Microphone effective diameter

D_e Equivalent diameter, cm or m

d   Lining core depth, cm

FG   Measured gross thrust, Newtons

FGC   Corrected gross thrust, FG/δ, Newtons

f   Frequency, Hz

f_t Tuning frequency, Hz

H   Acoustic lining separation, cm or m

J_1 First order Bessel function

L   Length, cm or m

L/D   Ejector length-to-diameter ratio

M_2 Secondary flow Mach number at primary exit plane

M_3 Area averaged flow Mach number at ejector exit plane

$\dot{m}_p$ Primary flow mass flux, kg/sec

$\dot{m}_{p\ ideal}$ Ideal primary mass flux, kg/sec

$\dot{m}_s$ Secondary (entrained) flow mass flux, kg/sec

NPR   Nozzle pressure ratio, nominal

NPR_{act} Nozzle pressure ratio, actual

OASPL   Overall sound pressure level, dB (re $20\mu\,N/m^2$)

P_{amb} Ambient static pressure, N/m^2

P_S Static pressure, N/m^2

P_T Total pressure, N/m^2

P_{T_p} Primary flow total pressure, N/m^2

P_{T7} Total pressure at turbine exit, N/m^2

PNL   Perceived noise level, PNdB

PNLM   Maximum (peak) perceived noise level, PNdB

PWL   Sound power level, dB (re 10^{-13} watts)

p_m Measured pressure, N/m^2

p_o Free-field pressure, N/m^2

R   Resistive component of acoustic impedance, rayls (MKS)

SPL	Sound pressure level, dB (re $20\mu N/m^2$)
T, T_T	Total temperature, °K
T_{T_P}	Primary flow total temperature, °K
T_{T7}	Total temperature at turbine exit, °K
V	Velocity, m/sec
V_3	Area averaged flow velocity at ejector exit plane, m/sec
V_{ideal}	Ideal, fully expanded jet velocity, m/sec
V_J	Jet velocity, m/sec
V_{max}	Fully expanded jet velocity based on total pressure and temperature measured by rake immediately downstream of nozzle exit plane
X	Reactive component of acoustic impedance, rayls (MKS)
x,y	Distance, cm or m
Z	Specific acoustic impedance, rayls (MKS)
λ	Wavelength of sound, m
δ	Ratio of ambient to reference pressure
θ	Angle from engine or nozzle inlet axis, degrees
ϕ	Thrust augmentation ($FGC_{ejector}/FGC_{primary\ nozzle}$)
ρ	Density, kg/m^3
ρc	Characteristic impedance of air, rayls (MKS)
ω	Angular velocity, rad/sec

78

REFERENCES

1. Wright, C. P.; Morden, D. B.; and Simcox, C. D.: SST Technology Follow-On Program—Phase I, A Summary of the SST Jet Noise Suppression Test Program. FAA Report AD900-399L, The Boeing Company, Seattle, Washington, February 1972.

2. Lu, H. Y.; Morden, D. B.; Benefiel, R. L.; and Simcox, C. D.: SST Technology Follow-On Program—Phase I, Performance Evaluation of an SST Noise Suppressor Nozzle System. FAA Report AD900-400L, The Boeing Company, Seattle, Washington, February 1972.

3. Ko, S. H.: Acoustic-Wave Attenuation in Lined Rectangular Ducts with Uniform Flow and Shear Flow. D6-25485. The Boeing Company, Seattle, Washington, August 1971.

4. Eldred, K. M.; et al.: Suppression of Jet Noise with Emphasis on the Near Field. Tech. Documentary Report ASD-TDR-62-578, Flight Dynamics Laboratory, Aeronautical System Division, Air Force Systems Command, Wright-Patterson Air Force Base, Ohio, February 1963.

5. Anon: Study and Development of Turbofan Nacelle Modifications to Minimize Fan-Compressor Noise Radiation. NASA CR-1711, Vols. 1 through 7, The Boeing Company, Seattle, Washington, 1970.

6. Anon: Standard Values of Atmospheric Absorption as a Function of Temperature and Humidity for Use in Evaluating Aircraft Flyover Noise. SAE ARP 866, August 1964.

7. Anon: Definitions and Procedures for Computing the Perceived Noise Level of Aircraft Noise. SAE ARP 865, August 1969.

8. Simcox, C. D.: Effect of Temperature and Shock Structure on Choked Jet Noise Characteristics. AIAA Paper No. 71-585, AIAA 4th Fluid and Plasma Dynamics Conference, June 1971.

9. Eshbach, Ovid W., ed.: Handbook of Engineering Fundamentals, Vol. 1, Ch. 6. John Wiley and Sons, Inc., Second Edition, 1952.

10. Kennedy, E. D.: Mixing of Compressible Fluids. ASME Journal of Applied Mechanics, pp. 335-338, 1961.

11. Howes, W. L.: Ground Reflection of Jet Noise. NASA Technical Report R-35, January 1958.

12. Anon: Quarter-Inch Condenser Microphones, Type 4135/36. Bruel and Kjaer Instructions and Applications Book, 1969.

13. Morgan, W. V.; Sutherland, L. C.; and Young, K. J.: The Use of Acoustic Scale Models for Investigating Near Field Noise of Jet and Rocket Engines, WADD Technical Report 61-178, April 1961.

14. White, P. H.: Effect of Transducer Size, Shape, and Surface Sensitivity on the Measurement of Boundary Layer Pressures. J. Acous. Soc. Am., Vol. 41, No. 5, 1967.

TABLE 1.—MODEL-SCALE LININGS

Nozzle	Ejector Diameter, D, cm	Length, L, cm	Lining design variable Core depth, d	Flow resist, $R/\rho c$	Acoustic lining Open area, %	Core depth, d, cm
37 tube	33	33	Design	Design	12	1.4
			+ 1/2 octave	Design	12	0.9
			- 1/2 octave	Design	12	1.9
			Design	+ 100%	6	1.4
			Design	- 50%	22	1.4
			Design	- 67%	30	1.4
		66	Design	Design	12	1.4
			Design	- 50%	22	1.4
10.9-cm conical	33	264	Design	Design	12	5.85
			+ 1 octave	Design	12	2.54
			+ 1/2 octave	Design	12	3.81
			- 1/2 octave	Design	12	8.60
			Design	+ 100%	6	5.85
			Design	- 50%	22	5.85
		132	+ 1 octave	Design	12	2.54
2.74-cm conical	7.62	30.5	Design	Design	22	1.4
		61	Design	Design	22	1.4

TABLE 2.—FULL-SCALE LININGS

Nozzle	Ejector Diameter, D, cm	Length, L, cm	Lining design variable Core depth, d	Flow resist, $R/\rho c$	Acoustic lining Open area, %	Core depth, d, cm
37 tube	132	132	Design	Design	12	5.33
			+ 1/2 octave	Design	12	3.81
			- 1/2 octave	Design	12	7.62
			Design	+ 100%	6	5.33
			Design	- 50%	22	5.33
			+ 1/2 octave	- 50%	22	3.81
		264	Design	Design	12	5.33

81

TABLE 3.–MODEL-SCALE HARDWARE

Nozzle	Nozzle convergence half angle, deg	Nozzle diameter, cm	Nozzle area, cm²	Ejector diameter, cm	Ejector length, cm	Remarks
15.2-cm conical	10	15.2	182	–	–	Reference nozzle
37-tube	5	37 at 2.74 equispaced 4.75-cm centers	219	33	33 66	Tube length = 17.7 cm Tube OD = 3.18 cm ID = 2.80 cm Base plate dia = 66 cm
10.9-cm conical	7	10.98	94.5	33	132 264	Water-cooled nozzle, exit lip radius ≈ 0.476 cm
2.74-cm conical	3.25	2.74	5.89	7.62	30.5 61	Water-cooled nozzle, exit lip radius ≈ 0.16 cm

TABLE 4.–FULL-SCALE HARDWARE

Nozzle	Nozzle convergence half angle, deg	Nozzle diameter, cm	Nozzle area, cm²	Ejector diameter, cm	Ejector length, cm	Remarks
J-75 conical (with centerbody)	12	OD = 70.6 ID = 27.5	3325	–	–	Reference nozzle
37-tube	12	37 at 11.0 equispaced 19.0-cm centers	3510	132	132 264	Tube length - 89 cm Tube OD = 12.7 cm ID = 12.4 cm Base plate dia = 140 cm

TABLE 5.—TEST CONFIGURATIONS
Model-Scale Test

Configuration	Nozzle	Ejector Diameter, cm	Length, cm	Acoustic lining Open area, %	Core depth, cm
1	15.2-cm conical	—	—	—	—
2	37 tube	—	—	—	—
3		33	33	—	—
4				12	0.9
5				12	1.4
6				12	1.9
7				6	1.4
8				22	1.4
9				30	1.4
10			66	—	—
11				12	1.4
12				22	1.4
13	10.9-cm conical	—	—	—	—
14		33	264	—	—
15				12	2.54
16				12	3.81
17				12	5.85
18				12	8.60
19				6	5.85
20				22	5.85
21			132		
22				12	2.54
23	2.74-cm conical	—	—	—	—
24		7.62	30.5	—	—
25				22	1.4
26			61	—	—
27				22	1.4

Full-Scale Test

Configuration	Nozzle	Ejector Diameter, cm	Length, cm	Acoustic lining Open area, %	Core depth, cm
1	70.6-cm conical	—	—	—	—
2	37 tube	—	—	—	—
3		132	132	—	—
4				12	3.81
5				12	5.33
6				12	7.62
7				6	5.33
8				22	5.33
9				22	3.81
10			264	—	—
11				12	5.33

TABLE 6. MODEL SCALE TEST DATA SUMMARY

15.2-cm Round Convergent Nozzle

NPR	T_T, °K	V_J, m/sec	Angle from inlet centerline, deg — Overall sound pressure level, dB re 20 μN/m^2								PWL, dB re 10^{-13} watt
			90	100	110	120	130	140	150	155	
1.4	Ambient	210	89.1	90.1	92.1	91.9	92.9	93.4	93.2	93.6	133.8
1.6		248	94.6	95.8	97.3	97.6	98.4	99.1	99.7	100.2	139.5
2.2		317	106.4	106.6	107.4	107.2	108.2	109.5	110.7	111.5	150.3
3.0		370	117.9	118.0	118.7	120.4	120.3	120.4	123.5	124.0	160.1
4.0		409	120.9	121.1	121.8	122.3	122.2	122.1	124.9	126.6	164.7
1.4	533	307	95.8	97.4	99.3	100.3	102.6	104.7	106.1	106.3	143.3
1.6		358	100.0	101.8	103.9	105.6	107.9	110.5	111.8	111.8	148.7
2.2		448	108.9	110.1	111.5	114.5	117.8	121.3	123.5	124.0	159.0
3.0		532	120.6	120.1	120.4	122.0	125.7	129.7	130.1	131.1	166.0
4.0		584	122.8	122.3	123.6	125.0	129.1	132.5	132.0	133.1	169.6
1.6	589	381	100.8	102.5	105.0	107.8	110.6	113.5	114.8	114.5	151.2
2.0	700	499	107.3	109.5	113.2	115.8	120.1	124.0	124.5	124.3	160.8
2.2	755	548	110.9	113.1	115.2	119.4	123.7	127.5	126.8	125.9	164.0
1.4	811	384	99.8	101.3	105.4	106.7	109.8	112.7	113.5	113.3	150.3
1.6		450	104.3	106.0	109.1	111.6	115.6	119.1	119.0	118.7	155.9
2.2		570	111.1	113.6	116.1	120.2	125.2	127.6	125.9	125.0	164.2
2.4		603	114.3	116.0	117.4	122.3	127.9	129.0	126.8	125.6	166.2
4.0		748	124.2	124.9	125.9	130.4	135.4	135.4	133.1	130.5	172.7
1.4	1088	442	105.5	107.4	109.7	114.0	117.6	118.5	119.2	117.6	156.4
1.6		508	108.8	110.9	113.2	118.8	122.7	123.6	122.8	121.0	161.1
2.2		669	115.8	118.4	121.4	127.3	129.6	127.8	125.8	124.1	167.5
2.6		734	119.1	121.0	122.9	129.6	131.0	129.0	126.7	125.7	169.3
4.0		863	125.5	126.0	128.3	134.6	134.9	132.9	131.0	128.9	173.9

10.9-cm Round Convergent Nozzle

NPR	T_T, °K	V_J m/sec	Angle from inlet centerline, deg — Overall sound pressure level, dB re 20 μN/m^2								PWL, dB re 10^{-13} watt
			90	100	110	120	130	140	150	155	
1.4	Ambient	228	84.2	82.6	85.2	84.3	86.0	87.2	87.2	86.9	127.1
2.2		340	102.9	99.9	101.9	101.2	102.8	104.5	105.7	105.9	145.2
4.0		434	120.0	115.7	117.1	116.7	117.9	119.1	121.7	123.0	159.9
1.4	533	310	91.3	90.7	94.3	94.7	97.0	99.5	99.6	99.3	137.7
2.2		458	105.1	104.0	107.1	108.9	112.9	115.8	116.6	116.2	153.4
4.0		589	119.8	117.7	120.7	122.1	126.1	128.3	126.1	126.4	165.9
1.6	589	386	97.4	97.0	100.7	102.2	105.2	107.7	108.0	107.9	145.5
2.0	700	495	104.7	104.7	108.4	111.4	115.4	117.8	117.1	116.8	154.9
2.2	755	553	108.2	108.1	112.4	115.1	119.6	121.4	119.1	118.3	158.5
1.4	811	392	97.6	96.2	101.4	102.2	105.6	107.2	107.2	106.7	145.2
1.6		449	100.1	99.1	105.0	105.7	110.4	112.0	112.4	112.6	149.8
2.2		571	107.6	106.6	112.8	115.0	120.1	120.6	118.8	117.2	158.3
2.4		601	109.7	108.3	114.6	116.9	122.1	122.8	118.9	118.9	160.2
4.0		731	119.5	117.4	122.4	124.4	128.4	126.4	124.7	123.2	166.4
1.4	1088	444	100.4	99.6	105.5	106.4	110.7	111.3	111.2	110.5	149.5
2.2		655	111.4	112.1	117.8	120.6	123.0	121.5	119.6	117.1	161.5
4.0		852	120.3	118.5	125.2	128.4	129.1	126.7	124.7	123.2	168.3
2.2	1643	821	116.1	116.4	123.6	124.4	123.7	121.5	118.7	117.2	164.3
4.0		1057	121.3	122.0	129.3	129.3	128.9	126.6	124.2	123.0	170.3

TABLE 6.—Continued
2.74-cm Round Convergent Nozzle

NPR	T_T, °K	V_J, m/sec	\multicolumn{8}{c}{Angle from inlet centerline, deg}	PWL, dB re 10^{-13} watt
---	---	---	90	100	110	120	130	140	150	155	
			Overall sound pressure level, dB re 20μ N/m^2	
1.4	Ambient	233	71.7	72.0	80.3	74.2	80.4	76.8	77.6	77.7	121.0
2.2		352	87.5	88.7	90.2	89.4	93.3	94.5	96.0	96.3	134.8
4.0		440	102.9	102.5	103.3	102.3	102.9	104.5	106.8	108.1	147.3
1.4	533	299	83.4	84.9	82.5	82.4	85.1	87.4	88.2	87.5	127.0
2.2		458	90.1	91.4	94.5	96.8	100.6	103.2	105.2	104.5	142.0
4.0		584	103.8	104.1	106.9	107.9	111.2	113.8	113.7	112.7	154.8
1.6	589	381	83.9	85.7	88.6	89.6	92.5	94.9	96.3	95.9	133.6
2.0	700	490	89.9	92.1	95.7	98.6	103.2	105.2	105.9	104.8	143.4
2.2	755	545	93.4	94.4	98.8	101.9	106.9	109.2	108.8	108.3	147.2
1.4	811	378	83.7	84.8	89.0	89.8	93.4	94.2	94.2	92.7	133.0
1.6		448	88.0	88.7	92.8	94.3	97.9	99.5	100.8	100.1	138.2
2.2		563	94.3	95.4	100.3	102.4	107.4	107.8	108.5	108.1	147.1
2.4		590	95.2	97.3	101.6	105.2	110.6	112.4	112.0	108.9	150.8
4.0		716	102.9	104.0	107.4	111.7	115.6	113.8	113.1	112.3	154.1
1.4	1088	435	87.4	88.8	94.4	95.0	98.2	98.4	98.6	95.1	138.0
2.2		645	96.0	97.7	103.9	107.5	111.2	108.9	108.3	107.7	150.0
4.0		839	104.7	105.4	110.2	115.9	117.0	114.4	113.3	111.3	155.7

37-Tube Nozzle

NPR	T_T, °K	V_J, m/sec	\multicolumn{8}{c}{Angle from inlet centerline, deg}	PWL, dB re 10^{-13} watts
---	---	---	90	100	110	120	130	140	150	155	
			Overall sound pressure level, dB re 20μ N/m^2	
1.4	Ambient	210	87.7	89.5	86.2	89.7	91.0	90.9	89.1	88.9	132.0
1.6		250	91.9	93.7	89.9	94.6	95.3	94.3	92.8	93.2	136.0
2.2		316	99.8	101.8	96.7	101.9	102.7	102.3	101.8	102.2	146.2
3.0		363	111.1	111.8	110.4	110.2	112.4	112.3	110.9	113.4	155.1
3.5		378	111.6	113.1	108.0	111.4	111.7	111.7	112.4	113.7	156.1
1.4	533	293	93.0	95.7	92.6	97.6	97.7	96.9	95.1	95.2	138.1
1.6		342	97.3	100.0	96.7	101.7	101.6	101.1	99.8	100.1	142.5
2.2		436	103.7	107.0	104.5	109.7	109.7	110.6	109.7	109.1	151.2
3.0		500	110.3	112.0	110.9	114.6	115.1	115.7	116.4	116.7	157.3
4.0		552	113.8	115.4	113.6	117.0	118.4	119.6	121.3	121.7	160.5
1.6	589	360	99.0	101.6	104.0	104.6	104.2	103.7	102.1	101.7	145.6
2.0	700	467	104.6	109.5	109.2	111.0	110.8	111.1	110.7	110.6	153.0
2.2	755	515	107.0	111.2	111.5	113.3	113.4	113.9	113.9	113.7	155.5
1.4	811	344	98.4	100.7	97.6	102.4	101.0	100.5	98.5	98.5	142.6
1.6		416	102.0	105.1	102.5	107.6	106.4	106.6	105.1	105.1	148.0
2.2		544	108.3	110.9	111.9	113.3	113.9	114.3	113.9	113.7	155.8
2.4		567	109.1	111.6	109.5	114.5	114.5	115.7	115.4	115.3	156.5
4.0		692	115.1	117.2	114.8	120.0	121.7	124.6	125.4	125.4	163.4
1.4	1088	387	107.1	109.5	109.3	108.5	107.2	107.6	105.9	105.3	150.7
1.6		493	111.7	114.0	112.7	111.7	111.6	111.9	109.8	109.5	155.4
2.2		639	111.7	115.1	114.1	116.5	116.9	117.5	116.9	116.1	159.4
2.6		715	112.7	116.0	116.5	117.5	118.2	119.5	120.1	119.5	160.9
3.7		836	115.9	118.7	120.9	121.5	124.8	127.0	126.8	126.0	165.8

The NPR listed in this table is a nominal value. Because of a total pressure loss in the diffuser upstream of the 37-tube nozzle, the actual NPR is less than indicated. The following relationship: NPR$_{ACT}$ = NPR x 0.96 (see text) is used to account for these losses and where relevant the term NPR$_{ACT}$ is used to present experimental data.

TABLE 6.--Continued

37-Tube Nozzle With L/D = 1 Hardwall Ejector

NPR*	T_T, °K	V_J, m/sec	Angle from inlet centerline, deg								PWL, dB re 10^-13 watt
			90	100	110	120	130	140	150	155	
			Overall sound pressure level, dB re 20μN/m^2								
1.4	Ambient	210	90.3	89.7	90.7	91.0	91.2	91.3	90.0	89.2	132.7
1.6		252	93.5	93.5	94.8	95.0	95.3	95.1	93.7	93.0	136.7
2.2		320	100.7	101.7	102.9	102.5	102.9	101.8	100.8	100.0	148.7
3.0		366	111.6	112.1	112.2	112.1	112.1	110.7	109.9	110.0	157.5
3.5		381	111.8	112.8	112.9	112.8	113.1	112.9	112.4	112.2	158.3
1.4	533	297	95.3	96.0	97.1	97.9	98.3	96.2	95.1	94.4	138.6
1.6		342	98.5	99.3	100.2	101.4	101.8	99.2	98.1	97.5	142.2
2.2		439	105.0	106.1	107.5	109.3	108.3	106.6	105.2	104.5	151.6
3.0		502	110.7	111.8	113.1	115.0	114.5	113.6	113.1	112.8	158.8
4.0		555	114.9	116.3	117.1	119.0	118.8	119.5	120.1	120.1	163.0
1.6	589	360	100.3	100.9	101.7	103.8	103.6	100.6	99.2	98.6	143.9
2.0	700	470	105.5	107.6	109.0	111.5	109.6	106.8	105.0	104.8	151.4
2.2	755	517	108.4	110.3	112.1	115.5	112.2	110.0	108.2	107.8	155.0
1.4	811	345	98.9	100.5	101.4	103.5	101.7	98.4	96.9	96.5	143.0
1.6		446	102.8	104.1	106.2	109.0	105.8	101.9	100.5	100.1	147.8
2.2		534	109.4	111.1	113.6	116.6	112.9	110.2	108.7	108.4	156.0
2.4		558	110.8	112.7	115.0	117.6	114.7	112.0	111.0	110.6	157.6
4.0		700	117.0	118.0	120.2	121.2	121.8	123.1	125.4	125.2	164.2
1.4	1088	397	102.3	104.9	106.7	108.8	104.4	100.9	99.8	99.8	147.5
1.6		473	106.7	109.4	111.3	113.6	108.2	105.2	103.4	103.4	152.6
2.2		622	113.4	115.7	118.2	118.6	115.9	114.6	113.0	111.4	160.4
2.6		679	115.9	118.0	119.7	120.0	119.0	118.2	117.4	116.5	162.7
4.0		820	118.8	120.4	122.6	122.6	124.7	126.6	128.4	128.0	167.3

37-Tube Nozzle With L/D = 2 Hardwall Ejector

NPR*	T_T, °K	V_J, m/sec	Angle from inlet centerline, deg								PWL, dB re 10^-13 watt
			90	100	110	120	130	140	150	155	
			Overall sound pressure level, dB re 20μN/m^2								
1.4	Ambient	217	85.0	86.5	87.9	87.9	90.0	89.7	87.5	86.6	130.0
2.2		320	98.5	99.8	100.7	100.7	101.8	100.3	97.3	97.9	145.0
3.5		387	104.4	106.0	107.7	106.9	107.1	106.2	106.3	106.1	149.5
1.4	533	302	92.6	93.9	96.3	97.6	98.4	95.7	93.7	93.0	137.7
2.2		436	101.0	103.2	105.6	107.1	106.9	103.6	102.4	102.1	147.7
4.0		549	112.2	113.5	115.4	116.7	116.6	117.3	118.1	118.1	158.7
1.6	589	364	95.7	98.1	99.7	102.0	102.7	98.8	97.0	96.3	141.8
2.0	700	467	102.3	105.0	107.7	109.5	108.0	105.1	103.3	102.5	148.9
2.2	755	517	104.5	107.5	110.2	113.7	109.9	108.0	104.9	105.1	152.1
1.4	811	345	94.8	96.5	99.6	100.6	100.6	97.7	94.8	95.7	140.5
1.6		418	98.3	101.5	104.5	106.2	104.6	100.7	99.1	97.8	145.3
2.2		538	105.7	107.3	112.0	114.9	110.3	107.1	106.1	104.8	153.2
2.4		564	107.0	109.9	113.3	115.8	112.1	108.5	108.0	106.8	154.7
4.0		692	113.3	115.4	117.7	117.7	118.2	119.0	120.5	120.0	160.1
1.4	1088	400	98.8	101.1	104.8	105.0	102.5	99.5	98.8	98.2	144.4
2.2		610	108.0	111.5	116.3	116.7	111.7	109.2	108.1	107.1	156.3
4.0		808	114.2	116.4	120.0	118.7	119.8	121.6	123.0	123.2	161.9

*NPR$_{ACT}$ NPR x 0.96

86

TABLE 6.—Continued

10.9-cm-Round Convergent Nozzle With L/D = 4 Hardwall Ejector

NPR	T_T, °K	V_J, m/sec	Angle from inlet centerline, deg								PWL, dB re 10^{-13} watt
			90	100	110	120	130	140	150	155	
			Overall sound pressure level, dB re 20μN/m²								
1.4	Ambient	231	88.0	89.4	91.4	89.9	90.0	89.5	88.6	88.0	131.4
2.2	↓	343	102.4	102.7	104.2	104.6	105.5	105.1	104.2	103.5	146.3
4.0	↓	438	115.1	115.9	118.4	117.6	117.3	118.7	116.6	115.9	159.0
1.4	533	313	93.3	95.6	96.4	96.8	98.5	98.6	96.8	95.7	138.3
2.2	↓	463	108.2	109.2	110.8	113.4	118.3	115.4	110.9	109.9	155.1
4.0	↓	592	120.6	120.9	121.8	123.6	124.6	124.9	122.6	121.9	165.0
1.6	589	384	98.6	100.6	101.8	104.1	106.5	106.1	102.3	101.3	145.0
2.0	700	503	107.7	110.3	111.8	116.5	118.9	116.4	111.8	110.9	156.2
2.2	755	549	110.3	113.1	115.9	118.9	121.4	119.4	115.4	113.2	159.1
1.4	811	384	105.8	107.3	108.8	111.0	107.3	106.4	102.5	101.3	149.2
1.6	↓	442	103.5	105.8	108.0	110.3	113.8	111.0	107.5	106.0	151.1
2.2	↓	573	112.3	114.2	117.4	121.0	122.6	119.5	116.4	114.7	160.4
2.4	↓	600	114.2	115.7	118.9	122.7	125.4	120.8	117.8	116.3	162.6
4.0	↓	731	120.2	122.3	125.2	128.5	128.2	126.9	124.9	123.1	167.9
1.4	1088	437	102.6	105.5	107.2	110.0	112.0	108.8	105.5	104.0	149.8
2.2	↓	662	115.3	118.3	121.2	123.8	123.5	120.0	116.5	115.8	162.7
4.0	↓	848	122.5	125.2	127.4	129.4	129.0	127.2	125.0	123.7	169.5

10.9-cm Round Convergent Nozzle With L/D = 8 hardwall Ejector

NPR	T_T, °K	V_J, m/sec	Angle from inlet centerline, deg								PWL, db re 10^{-13} watt
			90	100	110	120	130	140	150	155	
			Overall sound pressure level, dB re 20μN/m²								
1.4	Ambient	230	79.5	81.1	83.4	83.8	86.1	85.2	85.8	84.0	126.8
2.2	↓	340	100.1	100.1	103.8	103.9	106.2	104.8	102.5	100.8	146.0
4.0	↓	433	109.0	107.7	110.9	110.8	115.5	112.1	112.6	110.9	153.4
1.4	533	308	87.3	88.0	91.4	92.2	96.2	95.9	95.6	92.4	134.7
2.2	↓	467	105.1	105.9	108.6	110.6	115.0	113.7	109.8	106.4	152.5
4.0	↓	590	116.3	116.8	119.8	121.3	126.3	119.7	118.4	116.0	163.8
1.6	589	414	93.8	94.9	98.4	100.2	104.0	103.9	101.6	98.8	142.1
2.0	700	498	102.0	103.9	108.2	111.1	117.7	113.8	109.9	107.1	153.5
2.2	755	552	107.1	108.7	112.3	116.2	122.1	116.7	112.3	109.8	157.7
1.4	811	387	94.6	95.6	99.5	101.2	106.5	104.7	102.2	99.3	143.4
1.6	↓	446	98.2	99.4	104.0	106.4	111.7	109.3	106.1	103.4	148.3
2.2	↓	577	107.3	108.5	114.0	117.5	123.2	116.3	113.1	109.9	158.7
2.4	↓	599	108.8	110.0	116.3	119.1	126.2	117.5	114.5	111.4	161.3
4.0	↓	731	117.0	118.0	123.2	124.9	128.0	121.1	120.6	118.0	165.8
1.4	1088	433	97.6	98.4	102.2	104.4	110.1	106.9	104.2	101.2	146.5
2.2	↓	667	109.8	111.8	117.3	119.5	125.6	116.5	114.8	111.3	161.1
4.0	↓	848	117.8	118.7	125.1	127.3	128.6	121.6	121.1	118.4	167.3
2.2	1644	823	111.7	114.2	119.4	121.6	123.3	116.5	115.4	112.2	160.8
4.0	↓	1050	118.5	120.6	126.9	128.9	127.1	121.5	122.1	119.9	167.8

TABLE 6.—Concluded

2.74-Cm Round Convergent Nozzle With L/D = 4 Hardwall Ejector

NPR	T_T, °K	V_J, m/sec	Angle from inlet centerline, deg								PWL, dB re 10^{-13} watt
			90	100	110	120	130	140	150	155	
			Overall sound pressure level, dB re 20 μN/m²								
1.4	Ambient	232	79.0	80.6	83.6	79.9	80.6	80.8	82.7	82.5	124.3
2.2		351	90.5	92.5	95.7	93.1	95.1	94.7	94.3	94.5	137.0
4.0		438	102.0	101.2	104.3	101.4	103.5	105.4	107.6	107.5	147.0
1.4	533	306	83.5	84.4	87.5	86.2	87.7	87.1	86.7	86.6	128.2
2.2		459	95.1	95.5	99.1	100.1	102.4	99.1	98.7	97.8	141.6
4.0		586	102.9	103.4	107.8	107.4	110.7	110.5	110.8	109.2	151.4
1.6	589	378	87.5	89.0	92.2	91.6	93.5	92.5	91.0	90.9	133.4
2.0	700	489	94.5	96.2	100.8	101.5	102.9	99.4	98.3	96.8	142.1
2.2	755	542	101.9	104.8	106.5	109.8	110.0	104.6	103.8	102.4	149.8
1.4	811	376	87.0	88.5	92.5	91.5	94.4	91.5	91.2	90.0	133.4
1.6		445	91.5	92.9	97.3	97.8	99.3	95.1	95.1	94.0	138.4
2.2		567	99.5	102.1	106.7	107.7	108.2	103.3	102.9	100.3	148.2
2.4		589	103.0	103.8	108.7	108.1	107.3	102.5	101.8	100.0	148.8
4.0		717	105.0	106.1	112.5	113.4	115.5	111.9	111.1	110.0	154.8
1.4	1088	431	91.5	93.2	97.5	98.2	98.6	95.6	94.1	93.3	138.3
2.2		650	102.1	104.7	110.5	110.7	108.3	104.5	103.5	102.7	150.9
4.0		838	107.1	108.9	115.1	114.6	114.2	112.2	111.2	109.9	156.3

2.74-Cm Round Convergent Nozzle With L/D = 8 Hardwall Ejector

NPR	T_T, °K	V_J, m/sec	Angle from inlet centerline, deg								PWL, dB re 10^{-13} watt
			90	100	110	120	130	140	150	155	
			Overall sound pressure level, dB re 20 μN/m²								
1.4	Ambient	231	71.6	72.0	75.8	73.4	74.5	75.5	75.7	76.4	119.6
2.2		349	85.8	88.0	93.7	90.9	93.5	91.0	89.0	88.6	134.3
4.0		436	95.4	96.0	99.8	97.6	98.4	98.2	99.3	99.3	141.4
1.4	533	306	78.8	80.8	84.7	84.2	86.9	86.3	84.7	84.3	126.2
2.2		458	92.2	95.0	97.8	98.7	101.4	97.7	95.1	93.7	140.3
4.0		588	99.3	102.7	105.2	105.7	105.6	103.3	102.7	102.1	147.9
1.6	589	380	84.4	86.1	90.3	90.3	92.9	90.8	88.9	87.6	131.8
2.0	700	491	91.4	94.4	98.4	99.8	102.7	97.3	94.6	94.1	140.6
2.2	755	542	96.7	99.0	104.5	106.9	108.2	101.8	98.4	97.1	146.8
1.4	811	377	85.8	87.4	91.4	91.2	94.9	91.9	89.5	89.5	133.1
1.6		444	89.3	91.6	95.7	96.7	99.6	94.9	92.6	91.1	137.6
2.2		562	98.7	101.2	105.1	107.5	109.7	103.1	99.6	98.6	148.1
2.4		587	99.4	102.2	107.7	108.2	108.3	102.4	99.6	97.7	148.3
4.0		717	103.4	104.5	110.3	111.5	108.6	105.1	104.4	103.7	151.6
1.4	1088	440	88.5	91.1	95.5	97.0	98.7	93.7	91.9	91.1	137.1
2.2		659	99.6	103.4	109.2	109.9	107.9	102.3	99.4	98.4	149.8
4.0		845	105.0	107.8	113.1	113.7	108.8	105.9	105.5	104.9	154.1

TABLE 7.—FULL-SCALE TEST DATA SUMMARY

| Configuration | NPR | T_T, °K | V_j, m/sec | Angle from inlet centerline, deg | | | | | | | | | PWL dB re10⁻¹³ watt |
| | | | | 80 | 90 | 100 | 110 | 120 | 130 | 140 | 150 | 155 | |
				Overall sound pressure level, dB re 20 μN/m²									
Conical nozzle	1.4	595	310	96.7	99.4	101.0	102.9	103.0	104.0	105.4	105.5	104.9	156.2
	1.56	628	365	99.9	101.9	103.6	105.7	106.7	106.9	110.5	111.4	111.1	161.1
	1.8	673	433	103.6	105.1	107.1	109.2	111.5	114.5	116.8	118.5	117.9	167.1
	2.0	723	488	105.6	107.6	109.9	112.2	115.2	118.6	121.5	123.3	122.0	171.3
	2.2	761	540	109.8	110.6	113.1	115.3	118.6	122.8	126.0	126.1	124.5	175.0
	2.4	823	587	113.6	113.8	115.3	118.1	121.3	126.0	128.4	127.2	125.5	177.3
37-tube nozzle	1.4	595	299	94.4	95.8	97.1	98.8	99.8	99.8	98.3	97.7	96.3	152.6
	1.58	628	367	98.1	99.6	101.1	102.9	104.5	104.4	103.3	102.8	101.9	157.5
	2.0	673	478	103.9	105.5	107.2	109.4	111.5	111.7	111.9	112.3	112.1	164.8
	2.2	761	530	106.6	107.8	109.6	111.9	113.5	114.2	114.6	115.2	115.1	167.4
	2.4	823	583	108.9	110.0	111.3	113.9	114.4	115.4	116.1	116.8	117.0	168.9
37-tube nozzle with L/D=1 hardwall ejector	1.4	595	292	92.6	94.3	97.8	98.8	100.0	99.9	96.5	94.9	93.0	152.4
	1.56	628	351	95.9	97.4	100.8	102.6	104.0	103.2	100.0	98.5	96.7	156.2
	1.8	673	417	99.2	101.6	104.6	106.8	108.4	107.3	104.2	102.8	101.8	160.2
	2.0	723	472	102.5	104.6	109.4	110.3	112.2	111.4	108.3	107.1	106.4	164.2
	2.2	761	519	105.5	107.8	110.3	113.2	115.4	114.6	112.1	111.1	110.8	167.2
	2.4	823	573	108.1	110.3	112.7	115.8	117.5	116.7	115.1	114.7	114.9	169.8
37-tube nozzle with L/D = 2 hardwall ejector	1.4	595	291	91.3	93.2	95.4	97.5	100.0	99.8	95.7	93.4	92.7	151.5
	1.56	628	349	94.0	96.3	98.4	100.7	103.2	102.5	98.2	96.2	95.3	154.8
	1.8	673	415	97.2	99.9	102.2	105.0	107.8	106.4	101.7	99.8	99.0	158.8
	2.0	723	471	100.6	103.1	105.3	108.2	111.5	109.5	105.1	103.3	103.2	162.2
	2.2	761	521	103.6	106.3	108.5	111.3	114.7	111.9	108.5	107.4	107.5	165.4
	2.4	823	573	106.8	109.2	111.0	113.9	117.6	114.5	111.8	111.2	112.1	168.3
Conical nozzle (repeat)	1.4	595	316	96.2	98.8	101.0	102.0	102.7	104.0	105.2	105.5	105.1	156.1
	1.56	628	372	99.6	101.2	103.7	105.8	106.9	108.7	110.5	111.2	111.0	161.1
	1.8	673	439	102.8	104.8	107.2	109.5	111.7	114.6	117.0	118.4	118.0	167.2
	2.0	723	491	106.1	107.2	109.5	112.1	114.9	118.4	121.5	123.1	122.0	171.2
	2.2	761	543	108.9	110.1	112.4	115.2	118.3	122.5	125.9	125.8	124.5	174.7
	2.4	823	590	112.6	113.3	115.0	118.1	121.3	126.1	128.7	127.3	125.7	177.4

TABLE 8.—SCALE-MODEL TEST DATA EXTRAPOLATED TO A 649-M SIDELINE DISTANCE

Conical, 37-Tube, and Hardwall Ejector Configurations

Configuration	NPR	Jet temp, °K	Angle from nozzle inlet, θ, deg
			90	100	110	120	130	140	150	155
			Perceived noise level, PNdB
15.2-cm conical nozzle	1.4	533	78.6	80.1	81.2	81.2	81.4	79.9	76.5	74.5
	1.6	589	84.1	85.7	87.3	89.2	89.9	90.0	87.5	85.3
	2.0	700	91.1	93.3	96.0	97.5	100.0	101.6	99.3	97.3
	2.2	755	–	97.1	98.4	101.2	103.9	105.8	101.9	98.9
	2.4	811	98.9	100.4	100.7	104.4	108.4	107.6	101.9	98.7
	4.0	1088	109.8	110.2	111.5	116.8	115.4	110.9	105.3	101.3
37-tube suppressor nozzle	1.4	533	77.1	79.8	80.8	79.7	77.6	74.3	68.4	66.0
	1.6	589	83.5	85.9	87.1	87.0	84.4	81.0	75.2	72.2
	2.0	700	89.6	92.3	92.7	93.6	91.6	89.3	84.3	81.2
	2.2	755	91.6	94.5	95.2	96.0	94.4	92.2	87.4	84.2
	2.4	811	93.8	96.1	97.5	97.3	95.7	93.8	88.8	85.8
	3.7	1088	100.8	103.6	104.8	104.8	104.4	103.9	100.3	97.7
L/D = 1 hardwall ejector	1.4	533	75.0	77.3	78.2	78.7	77.7	71.8	65.9	63.2
	1.6	589	81.8	83.9	84.2	85.7	83.4	76.6	70.8	67.8
	2.0	700	89.5	92.1	92.6	94.4	90.8	84.6	77.7	75.0
	2.2	755	92.9	95.1	95.8	98.5	93.4	87.8	81.0	78.2
	2.4	811	95.8	97.4	98.9	100.5	95.9	90.2	83.8	80.9
	4.0	1088	104.1	105.4	106.5	105.4	104.5	103.4	101.9	99.1
L/D = 2 hardwall ejector	1.4	533	73.7	77.1	78.8	78.7	77.9	71.0	65.1	61.6
	1.6	589	78.7	81.9	82.8	84.1	82.8	74.9	69.2	65.9
	2.0	700	86.8	89.4	91.6	92.3	89.0	82.1	75.7	72.1
	2.2	755	89.4	92.2	94.5	96.6	91.0	85.3	77.5	74.8
	2.4	811	92.1	95.0	97.5	98.7	93.6	86.5	81.3	76.7
	4.0	1088	99.8	101.8	104.7	101.9	100.0	98.3	95.2	93.3

Lined Ejector Configurations, L/D = 1

\multicolumn{2}{c}{Ejector configuration}	NPR	Jet temp, °K	\multicolumn{8}{c}{Angle from nozzle inlet, θ, deg}
Open area, %	Depth, cm			90	100	110	120	130	140	150	155
				Perceived noise level, PNdB
6	1.4	1.4	533	73.2	76.7	77.2	78.1	76.7	71.3	65.5	62.7
		1.6	589	78.7	82.6	83.3	84.0	81.0	75.7	69.7	66.7
		1.8	645	84.3	87.5	88.5	89.4	84.5	79.1	73.5	70.4
		2.0	700	89.3	91.2	92.6	92.2	87.9	83.7	77.3	73.7
		2.2	755	90.8	93.2	96.2	95.3	90.9	86.7	79.9	76.6
		2.4	811	92.4	96.0	96.7	95.4	91.3	86.3	81.2	77.2
		4.0	1088	100.4	103.3	104.4	102.7	102.0	99.9	97.0	94.7
12	0.9	1.4	533	74.1	77.7	77.8	78.2	77.5	72.0	65.9	63.0
		1.6	589	79.6	83.0	83.3	83.8	81.8	75.9	69.9	67.5
		1.8	645	83.7	87.7	89.2	89.5	84.9	80.5	73.8	71.2
		2.0	700	89.8	90.8	91.9	92.1	87.8	84.2	77.5	74.2
		2.2	755	90.5	92.5	95.0	95.3	90.7	86.7	80.7	76.2
		2.4	811	91.7	94.2	96.2	95.8	90.2	86.2	81.3	77.7
		4.0	1088	100.5	102.5	104.7	103.4	102.2	100.0	96.9	94.7

TABLE 8.—Concluded

Ejector configuration		NPR	Jet temp, °K	Angle from nozzle inlet, θ, deg							
Open area, %	Depth, cm			90	100	110	120	130	140	150	155
				Perceived noise level, PNdB							
12	1.4	1.4	533	73.4	76.1	76.7	77.0	74.8	70.4	64.6	61.7
		1.6	589	78.1	81.4	82.7	83.7	80.7	74.8	69.1	66.2
		1.8	645	83.8	86.8	87.5	88.3	82.4	78.4	73.0	69.8
		2.0	700	87.4	90.1	91.5	91.9	85.7	82.1	76.4	73.0
		2.2	755	90.2	92.6	93.7	94.4	88.6	85.1	78.9	75.3
		2.4	811	92.3	95.2	97.1	96.1	91.0	87.2	81.5	78.1
		4.0	1088	100.8	103.1	105.1	103.3	102.1	100.4	96.8	94.4
12	1.9	1.4	583	73.4	76.6	77.4	77.9	76.8	71.1	65.3	62.4
		1.6	589	79.4	82.6	83.7	84.5	81.3	75.3	69.4	66.5
		1.8	645	84.8	87.9	88.7	89.5	85.3	79.2	73.9	70.8
		2.0	700	88.0	90.8	92.5	92.6	88.4	82.7	76.6	73.3
		2.2	755	90.5	93.4	95.8	95.9	91.9	96.9	79.8	77.2
		2.4	811	91.9	95.1	97.6	97.0	92.2	86.6	81.3	77.5
		4.0	1088	101.3	103.5	104.9	103.1	101.8	100.1	96.7	94.4
22	1.4	1.4	533	73.9	76.3	77.0	78.4	77.9	—	65.9	62.6
		1.6	589	80.3	82.8	83.2	83.9	81.8	—	70.1	67.3
		2.0	700	87.7	90.5	91.0	91.8	87.5	—	76.6	73.4
		2.2	755	90.8	93.5	94.3	94.7	90.0	—	79.3	76.1
		2.4	811	89.1	92.7	93.2	93.8	89.4	84.2	78.6	76.3
		4.0	1088	98.0	100.8	101.1	100.1	99.4	98.8	95.9	93.6
30	1.4	1.4	533	74.2	75.6	77.5	78.0	76.6	70.9	65.4	63.0
		1.6	589	80.0	82.0	82.4	84.7	82.4	76.0	69.4	67.6
		2.0	700	87.6	90.0	91.1	90.6	86.9	82.0	76.1	73.4
		2.2	755	90.9	92.5	94.1	95.7	90.3	85.6	79.1	76.8
		2.4	811	93.2	95.4	97.2	97.9	92.5	87.5	82.1	79.3
		4.0	1088	103.0	105.4	105.5	105.6	103.5	103.0	99.2	98.2

Lined Ejector Configurations, L/D = 2

Ejector configuration		NPR	Jet temp, °K	Angle from nozzle inlet, θ, deg							
Open area, %	Depth, cm			90	100	110	120	130	140	150	155
				Perceived noise level, PNdB							
12	1.4	1.4	533	70.4	73.0	75.2	77.0	76.7	69.7	64.1	60.4
		1.6	589	75.8	78.8	80.6	81.2	80.5	73.3	68.5	65.0
		1.8	645	79.0	82.0	84.8	86.4	84.1	77.3	72.9	68.7
		2.0	700	83.6	86.3	89.0	90.0	86.4	81.5	75.6	71.2
		2.2	755	—	89.1	91.5	92.6	88.7	85.2	78.5	73.7
		2.4	811	88.7	91.6	94.3	94.8	91.6	87.3	80.8	76.6
		4.0	1088	96.9	99.7	101.6	100.3	99.7	97.7	95.4	93.0
22	1.4	1.4	533	70.2	71.0	74.0	74.8	76.3	69.8	64.0	62.8
		1.6	589	75.6	76.6	79.8	81.3	80.6	73.1	68.2	65.7
		2.0	700	82.7	85.0	88.7	89.5	84.5	78.9	74.3	71.1
		2.2	755	84.8	86.5	90.8	91.2	86.6	81.4	76.5	73.6
		2.4	811	87.0	88.3	92.3	92.7	87.2	82.6	77.9	74.7
		4.0	1088	97.0	97.9	101.5	99.4	99.1	98.1	95.3	93.5

TABLE 9.–J-75 ENGINE TEST DATA EXTRAPOLATED TO 649 M SIDELINE

Configuration	NPR	Jet temp, °K	Angle from engine inlet, θ, deg — Perceived noise level, PNdB										
			60	70	80	90	100	110	120	130	140	150	155
Conical nozzle (First engine)	1.4	595	74.0	76.6	79.4	80.8	81.9	82.7	82.9	82.4	80.3	77.4	73.4
	1.56	628	78.7	80.9	84.4	86.0	87.3	88.5	89.4	89.3	88.2	86.1	83.0
	2.0	723	84.9	87.0	89.8	91.7	93.3	94.9	96.7	98.2	98.6	96.6	94.2
	2.2	761	88.5	90.4	93.3	95.0	96.8	98.6	100.5	102.4	103.2	100.2	96.2
	2.4	823	93.7	94.9	97.1	98.1	99.5	101.0	102.7	105.6	105.9	101.4	97.2
Conical nozzle (Second engine) (start of series)	1.4	595	74.0	76.5	78.9	81.1	82.7	83.8	84.2	83.3	81.4	77.6	73.8
	1.56	628	77.2	80.1	82.7	84.8	86.3	87.5	88.4	88.5	86.9	84.6	81.7
	1.8	673	—	—	86.4	88.7	90.5	92.0	93.5	94.3	93.9	92.5	90.2
	2.0	723	84.4	86.8	89.3	91.6	93.6	95.3	97.3	98.7	99.1	98.4	95.1
	2.2	761	88.0	90.1	93.8	94.8	97.2	98.7	100.8	103.2	104.3	101.4	97.7
	2.4	823	93.3	95.1	97.6	98.0	99.7	101.7	103.4	106.6	107.1	102.5	98.6
Conical nozzle (Second engine) (end of series)	1.4	595	—	—	78.7	80.7	82.7	83.7	83.7	83.3	81.1	77.6	74.3
	1.56	628	—	—	82.5	84.3	86.6	87.9	88.5	88.4	86.8	84.4	82.0
	1.8	673	—	—	86.2	88.4	90.7	92.4	93.6	94.4	94.1	92.4	90.4
	2.0	723	—	—	89.7	91.1	93.3	95.3	97.0	98.3	99.0	97.9	94.9
	2.2	761	—	—	92.9	94.4	96.4	98.5	100.3	102.7	104.1	101.0	97.6
	2.4	823	—	—	96.6	97.7	99.2	101.6	103.4	106.7	107.4	102.5	98.7
37-tube suppressor nozzle	1.4	595	74.9	76.5	77.9	79.1	80.5	81.5	81.7	80.0	75.5	71.2	66.4
	1.56	628	78.9	80.4	81.9	83.6	84.9	86.2	86.8	84.8	80.9	76.3	71.9
	1.8	673	—	—	—	—	—	—	—	—	—	—	—
	2.0	723	84.7	86.5	88.0	89.9	91.1	92.9	94.0	92.6	89.9	85.9	82.3
	2.2	761	87.2	88.8	90.4	91.9	93.6	95.4	96.2	95.2	92.9	88.6	85.0
	2.4	823	89.9	91.2	92.5	94.1	95.4	97.4	97.2	96.7	94.2	90.1	86.3
L/D = 1 hardwall ejector	1.4	595	72.6	74.4	75.3	77.5	80.6	81.4	81.7	79.7	73.3	68.1	62.7
	1.56	628	75.3	77.4	79.3	81.3	84.7	85.8	86.3	83.5	77.3	71.6	66.5
	1.8	673	—	—	82.9	85.8	88.6	90.2	90.9	88.1	82.3	76.0	71.3
	2.0	723	80.8	83.1	86.5	89.0	93.3	93.8	94.6	92.6	86.6	80.5	75.5
	2.2	761	84.6	86.9	89.7	92.2	94.5	96.7	97.9	95.8	90.4	84.4	79.9
	2.4	823	88.1	90.1	92.5	94.6	96.9	99.3	100.0	97.7	93.2	87.6	83.7

TABLE 9.—Continued

Configuration	NPR	Jet temp, °K	Angle from engine inlet, θ, deg — Perceived noise level, PNdB										
			60	70	80	90	100	110	120	130	140	150	155
L/D = 1 lined ejector (12% open area; d = 7.6cm)	1.4	595	72.0	72.5	74.0	75.6	78.0	79.6	80.4	77.6	72.2	66.9	61.5
	1.56	628	74.0	75.2	77.3	79.3	81.7	83.4	84.5	80.5	74.8	69.7	64.8
	1.8	673	–	–	80.9	83.4	85.7	88.0	88.8	83.9	78.5	73.2	68.3
	2.0	723	77.8	80.1	84.3	86.8	89.4	91.4	92.1	87.7	82.4	76.6	72.0
	2.2	761	81.7	83.7	87.3	89.4	91.6	94.0	94.2	90.7	86.1	79.9	76.5
	2.4	823	85.5	87.0	90.1	92.4	94.2	96.5	96.6	94.1	89.9	83.7	81.3
L/D = 1 lined ejector (6% open area; d = 5.3cm)	1.4	595	–	–	74.6	75.8	78.3	79.3	79.9	77.2	71.6	66.0	61.0
	1.56	628	–	–	77.0	79.1	80.9	82.6	83.5	79.4	73.8	68.4	63.8
	1.8	673	–	–	80.3	83.4	86.2	87.9	88.4	82.9	78.0	72.7	67.7
	2.0	723	–	–	83.7	86.2	88.5	90.2	89.9	85.1	80.6	75.2	70.7
	2.2	761	–	–	86.9	88.9	90.4	93.2	91.6	87.8	83.8	78.8	75.9
	2.4	823	–	–	89.3	90.9	93.1	95.1	93.0	90.8	87.6	83.0	80.6
L/D = 1 lined ejector (12% open area; d = 5.3cm)	1.4	595	71.6	72.5	73.4	75.4	77.8	79.4	79.8	77.9	72.0	66.7	61.4
	1.56	628	73.7	75.3	76.7	78.5	81.5	83.4	83.0	81.2	75.3	70.9	65.6
	1.8	673	–	–	79.6	83.1	85.6	87.4	87.8	83.9	78.5	73.6	68.7
	2.0	723	77.8	80.0	83.5	86.1	88.8	90.7	90.7	86.8	81.8	77.0	72.4
	2.2	761	82.0	83.8	86.0	88.7	91.4	93.1	92.0	89.3	84.6	79.6	76.2
	2.4	823	84.9	86.7	88.9	90.9	93.8	95.7	94.3	92.2	87.8	83.6	81.0
L/D = 1 lined ejector (22% open area; d = 5.3cm)	1.4	595	–	–	74.1	76.5	78.5	79.7	80.7	78.6	72.9	68.0	63.0
	1.56	628	–	–	77.8	80.3	82.8	84.2	85.1	82.1	76.4	71.6	67.1
	1.8	673	–	–	81.2	84.2	86.7	88.5	89.3	85.6	80.1	75.4	71.0
	2.0	723	–	–	84.6	87.2	89.7	91.3	92.0	88.1	82.9	78.5	74.3
	2.2	761	–	–	87.9	90.5	92.8	94.5	94.7	91.4	86.5	81.6	77.5
	2.4	823	–	–	90.5	92.8	94.8	96.8	97.2	93.9	89.7	84.8	82.1
L/D = 1 lined ejector (22% open area; d = 3.8cm)	1.4	595	–	–	73.3	75.7	77.5	78.9	80.2	78.1	72.2	67.0	62.3
	1.56	628	–	–	76.7	79.1	80.8	82.8	84.3	81.2	75.5	70.7	65.8
	1.8	673	–	–	79.8	83.1	84.9	87.4	89.0	84.8	79.0	73.9	69.4
	2.0	723	–	–	82.7	86.1	88.1	90.4	91.4	86.6	81.9	77.3	73.4
	2.2	761	–	–	86.2	88.9	90.6	93.2	93.1	88.9	84.7	80.2	76.9
	2.4	823	–	–	88.9	91.1	93.3	95.4	94.9	91.3	87.9	83.1	81.9

93

TABLE 9.– Concluded

Configuration	NPR	Jet temp, °K	Angle from engine inlet, θ, deg										
			Perceived noise level, PNdB										
			60	70	80	90	100	110	120	130	140	150	155
L/D = 1 lined ejector (12% open area; d = 3.8cm)	1.4	595	—	—	74.6	76.8	78.6	79.9	80.2	78.3	72.7	67.7	63.0
	1.56	628	—	—	77.7	80.4	82.1	83.7	84.0	81.3	75.6	71.0	66.5
	1.8	673	—	—	81.2	84.0	85.9	87.8	88.6	85.8	79.7	75.7	71.0
	2.0	723	—	—	84.6	87.4	89.4	91.6	92.0	88.1	82.9	78.7	74.6
	2.2	761	—	—	87.3	90.2	91.9	94.3	94.4	90.4	85.8	81.4	77.3
	2.4	823	—	—	90.2	92.3	93.9	96.6	96.6	92.9	88.2	84.7	82.1
L/D = 2 hardwall ejector	1.4	595	—	—	74.6	76.7	78.8	80.2	81.7	79.7	72.7	66.5	62.0
	1.56	628	—	—	77.9	80.5	82.4	84.0	85.3	82.7	75.3	69.3	65.0
	1.8	673	—	—	81.3	84.3	86.4	88.4	90.1	87.1	79.2	72.8	68.6
	2.0	723	—	—	84.7	87.5	89.6	91.6	93.9	90.4	82.8	76.2	72.4
	2.2	761	—	—	87.8	90.4	92.7	94.7	96.9	92.9	86.2	79.9	76.1
	2.4	823	—	—	90.9	93.1	95.2	97.6	100.1	95.7	89.6	83.4	80.3
L/D = 2 lined ejector (12% open area; d = 5.3cm)	1.4	595	70.2	71.1	71.8	72.9	74.5	75.7	76.8	75.4	69.2	63.5	59.5
	1.56	628	72.1	73.4	74.7	76.5	77.8	79.5	81.1	77.8	71.7	66.2	62.3
	1.8	673	—	—	76.1	78.9	81.0	83.3	86.0	79.7	74.2	68.6	64.8
	2.0	723	75.4	76.8	79.0	82.1	84.4	86.7	88.0	82.1	77.0	71.7	68.0
	2.2	761	80.6	81.6	83.6	85.6	87.4	89.9	89.9	84.7	80.7	76.0	73.2
	2.4	823	82.6	83.6	85.3	87.8	89.8	91.6	90.9	87.2	84.4	80.3	78.3
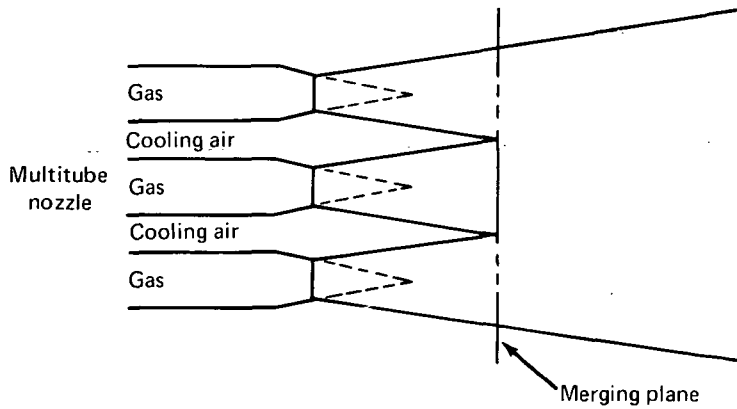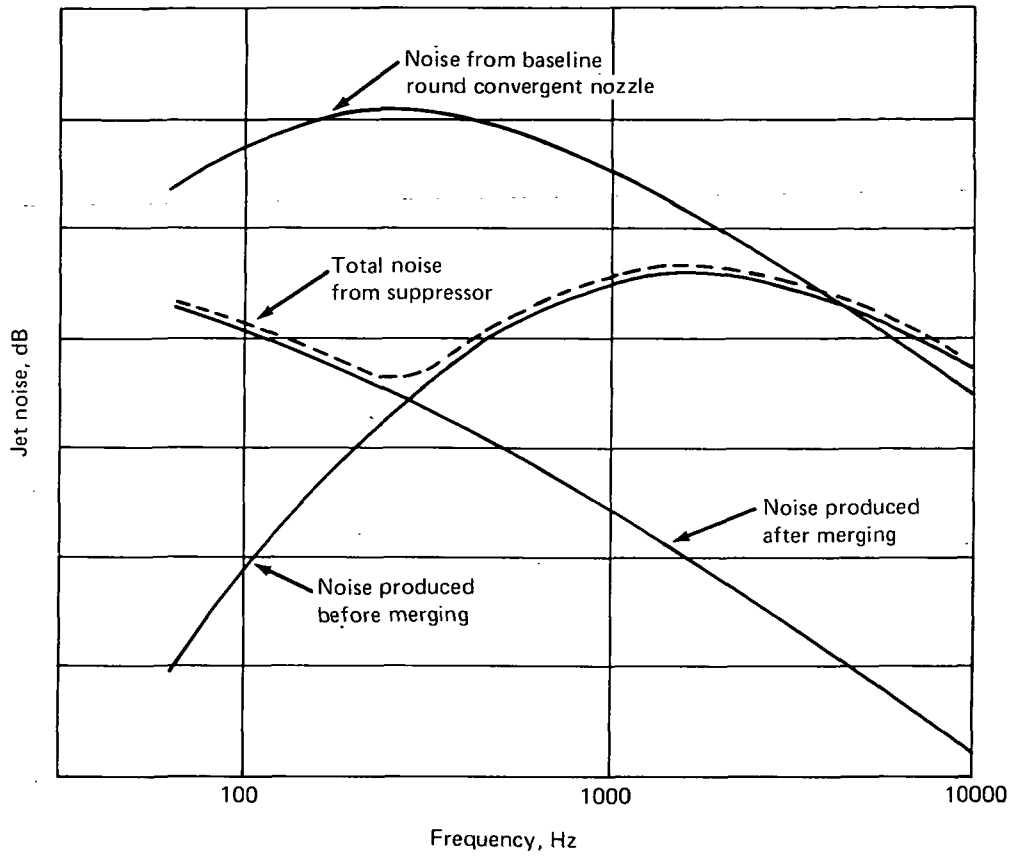
FIGURE 1.—MULTITUBE NOZZLE JET NOISE SPECTRUM
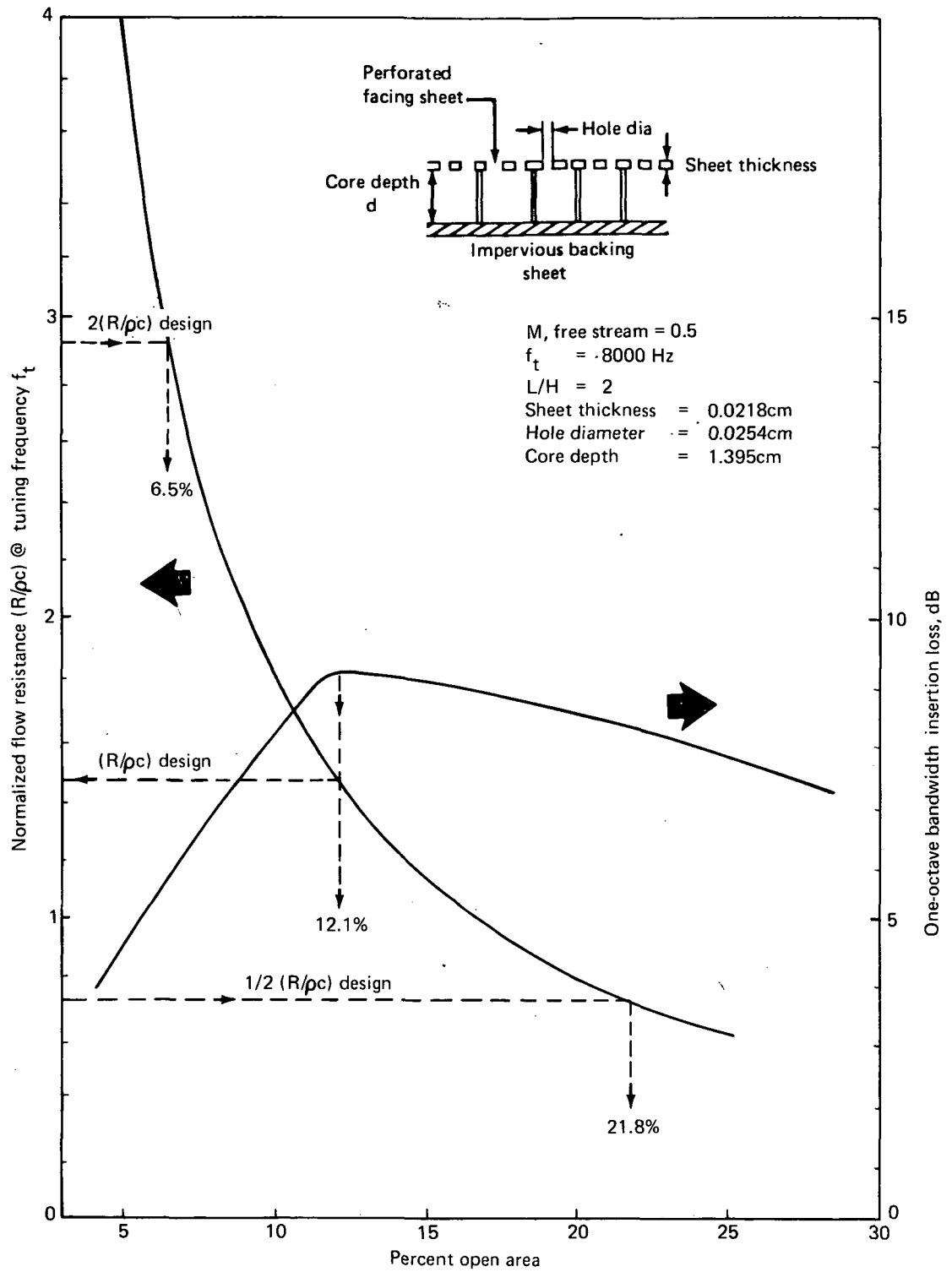
FIGURE 2.—PREDICTED LINING ATTENUATION FOR MODEL-SCALE 37-TUBE NOZZLE AND 33-CM- LONG EJECTOR
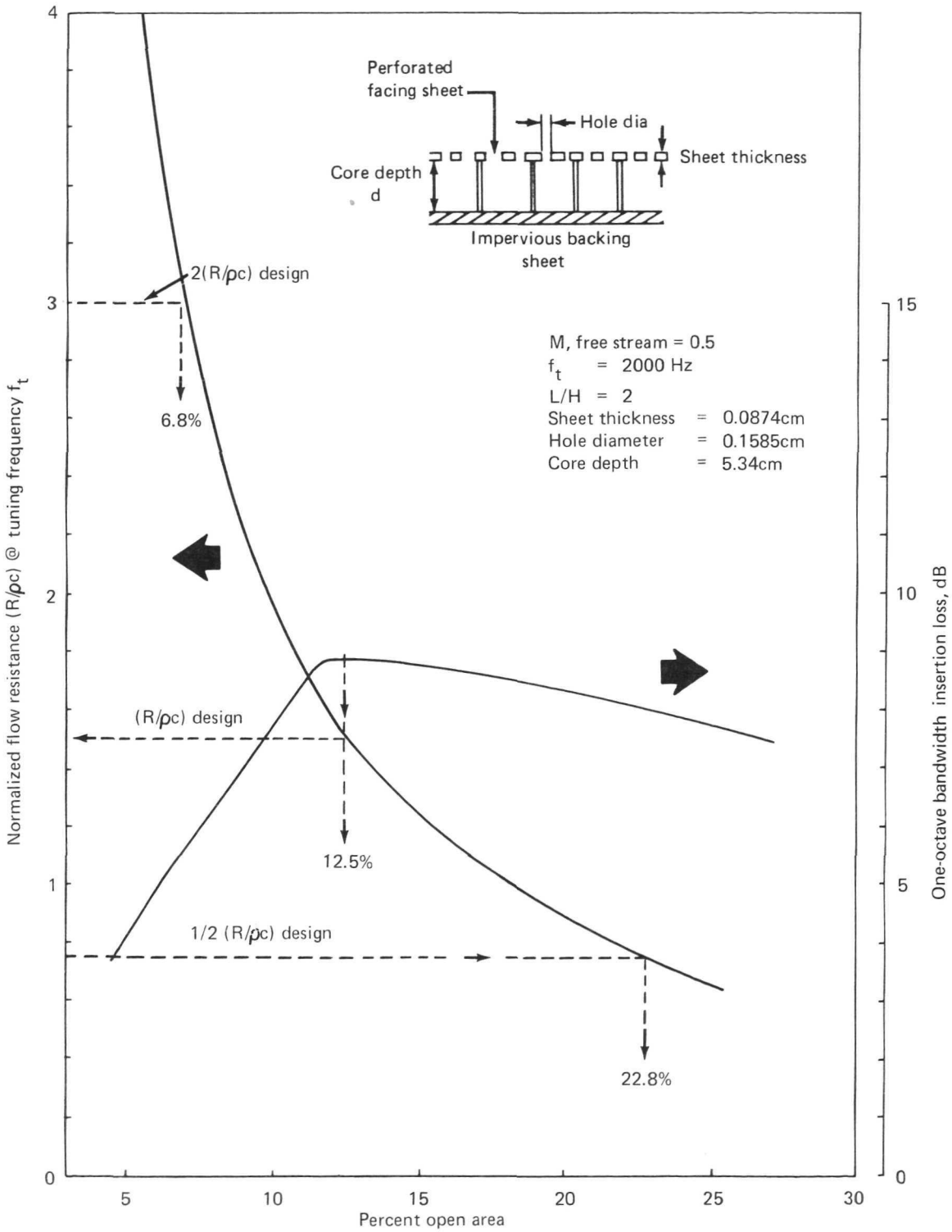
FIGURE 3.—PREDICTED LINING ATTENUATION FOR FULL SCALE 37-TUBE NOZZLE AND 1.32-M-LONG EJECTOR
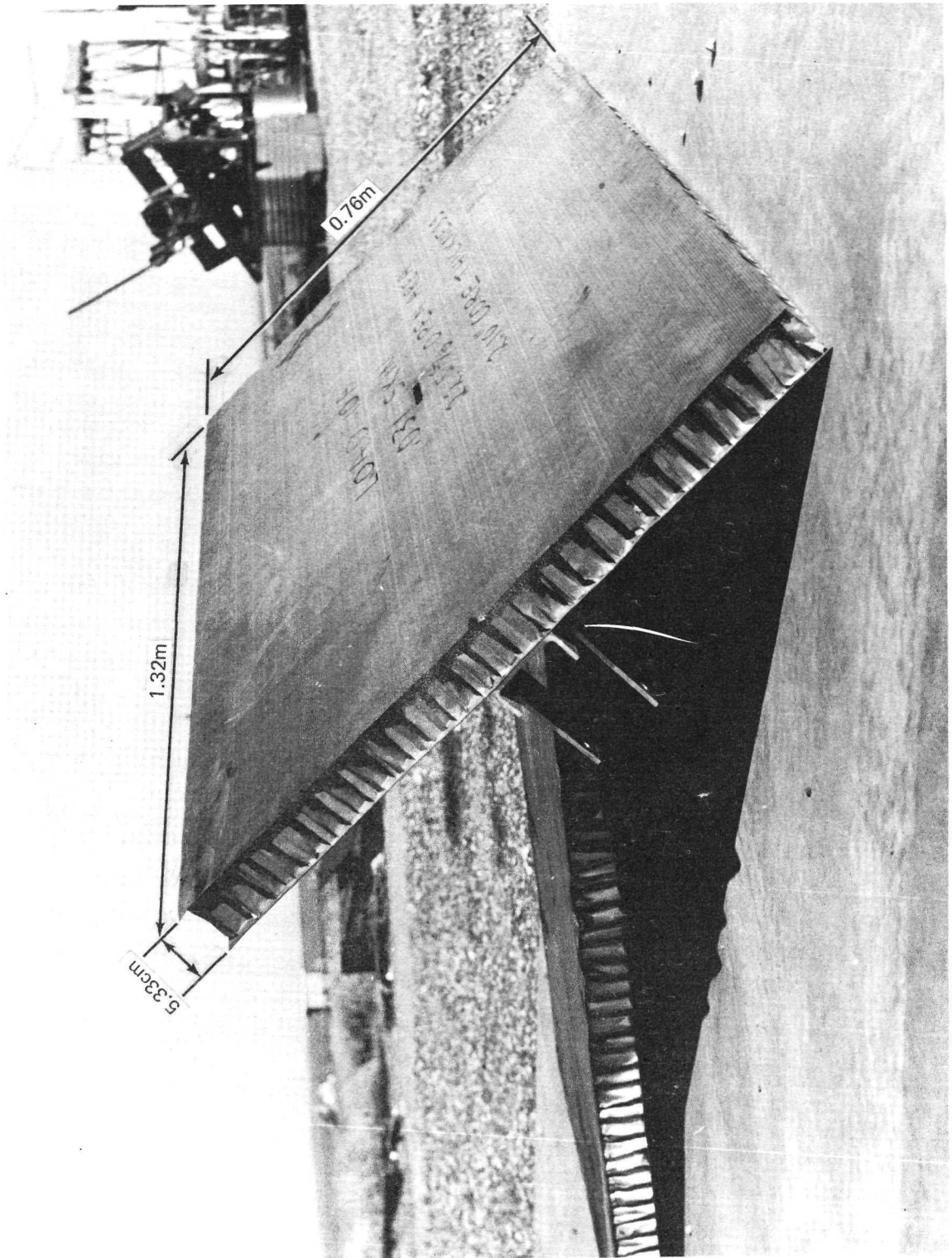
FIGURE 4.—TYPICAL FULL-SCALE ACOUSTIC LINING TEST PANEL

Round convergent
nozzle

37-tube suppressor nozzle

Centerbody in
full-scale J-75
nozzle only

Area ratio   3.3

37-tube with ejectors (L/D = 1; L/D = 2), ejector
area ratio = 4.3; hardwall and lined
(Ejector D ≡ diameter of inscribed circle)

Single element scaling

Ejector lengths and linings are the same as used with
related 37-tube arrays
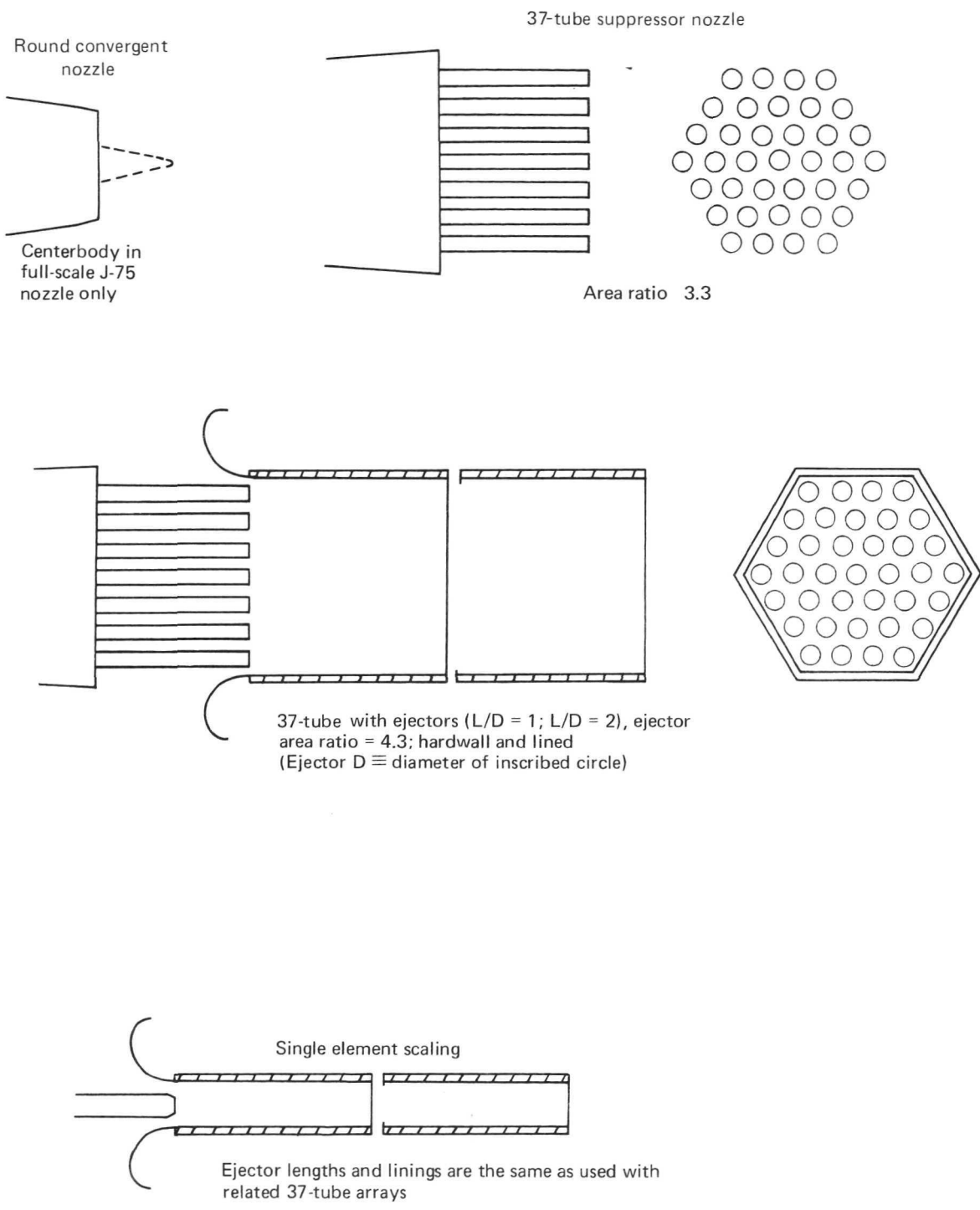
FIGURE 5.—SCHEMATIC SUMMARY OF NOZZLE AND EJECTOR TEST CONFIGURATIONS

99
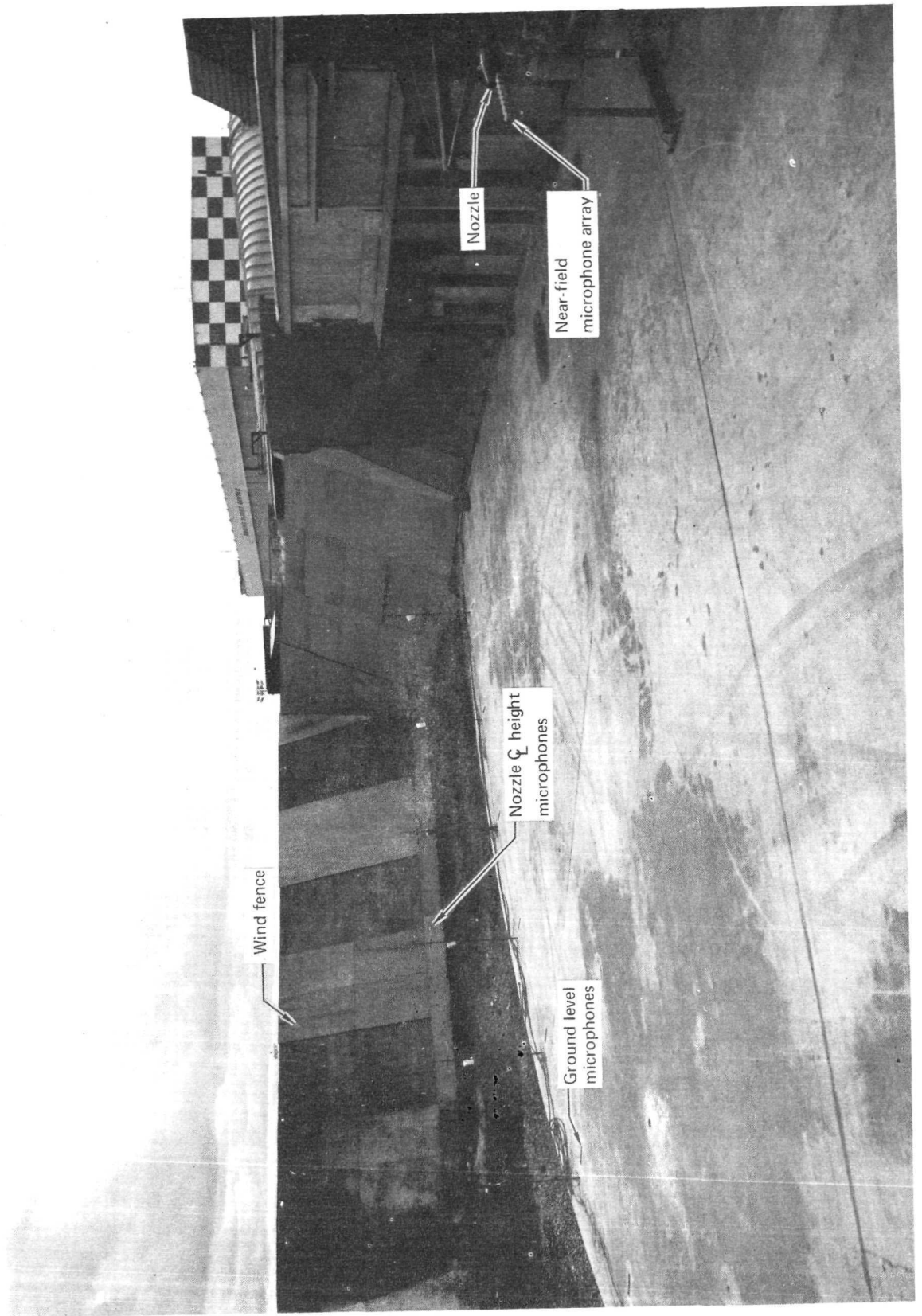
FIGURE 6.–MODEL-SCALE ACOUSTIC TEST ARENA AT THE HOT NOZZLE TEST FACILITY
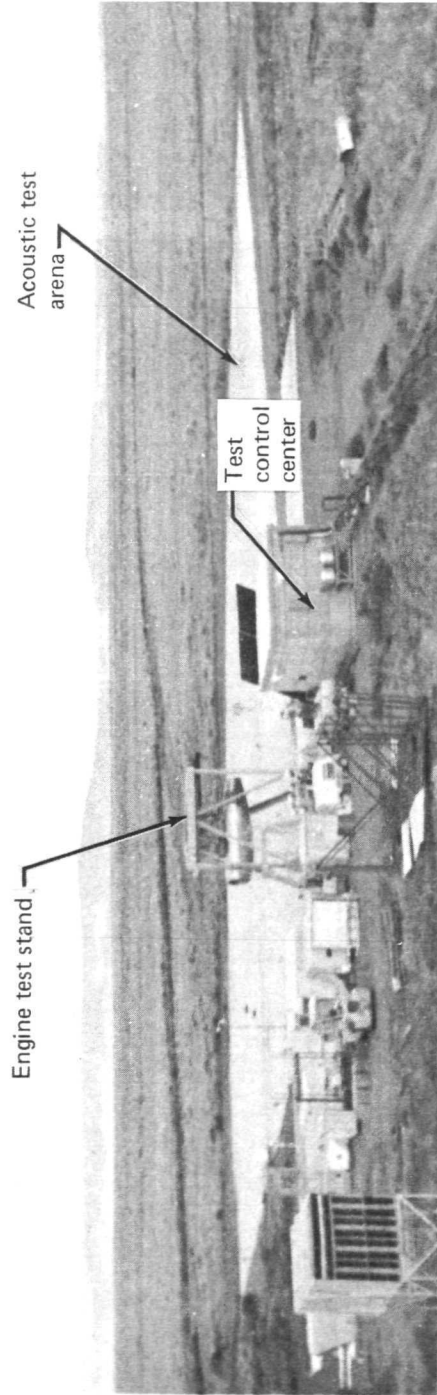
FIGURE 7.—FULL-SCALE ACOUSTIC TEST ARENA AT THE BOARDMAN ENGINE TEST FACILITY

Acoustic test arena

Test control center
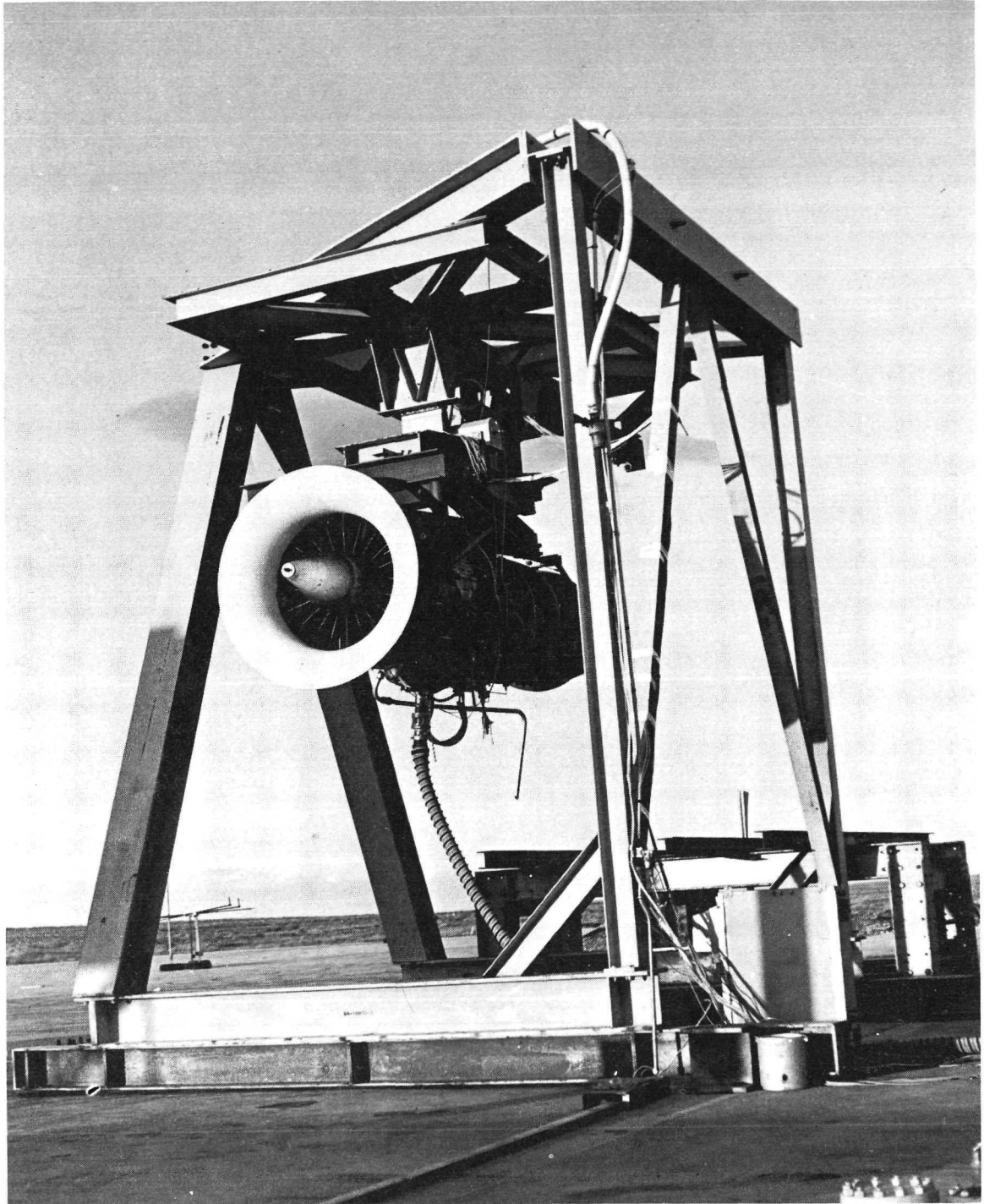
Engine test stand

FIGURE 8.—J-75 TEST ENGINE INSTALLATION FOR PERFORMANCE BASELINE RUN

Inlet muffler

Exhaust nozzle

Engine side Baffles
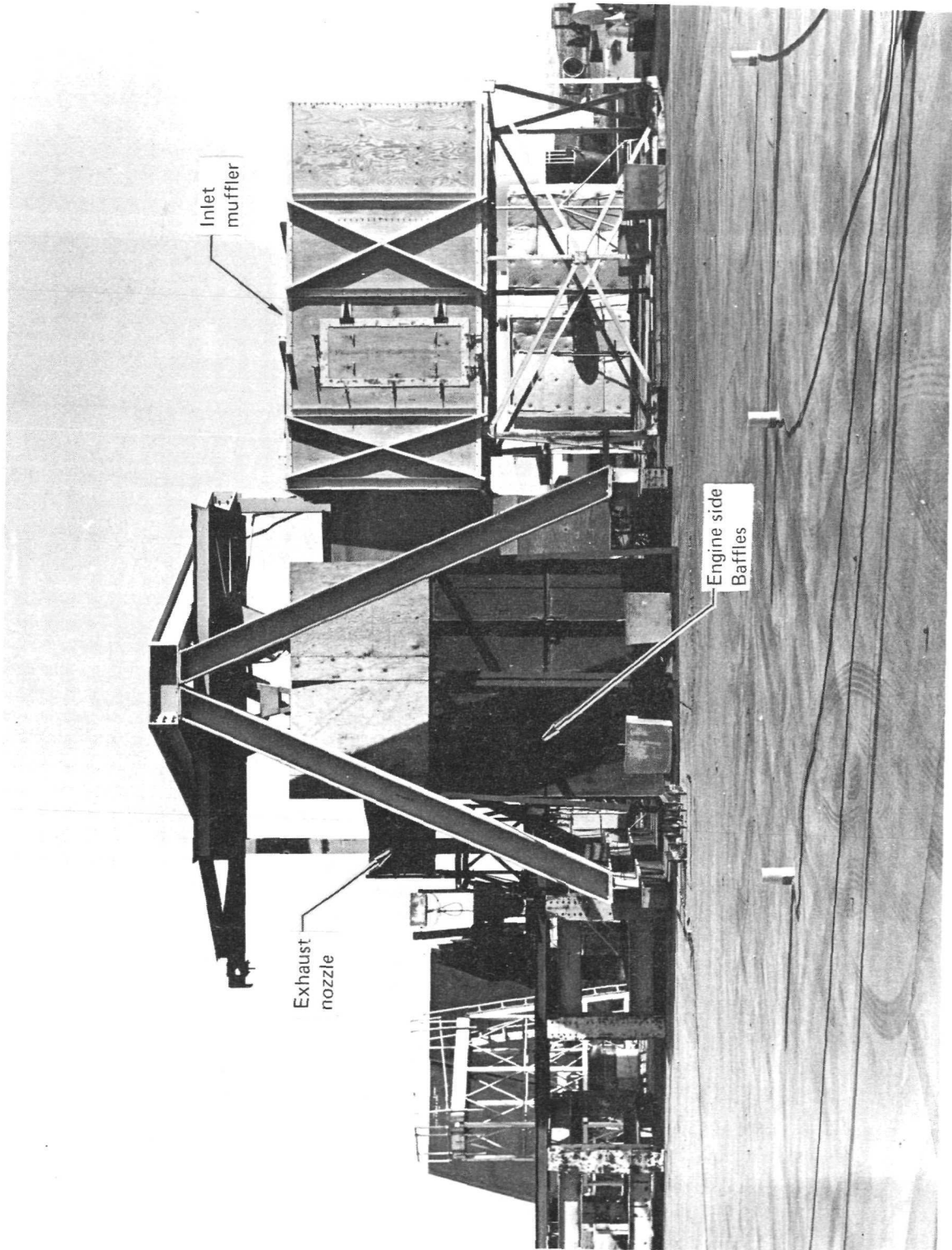
FIGURE 9.—J-75 ENGINE TEST STAND SET UP FOR ACOUSTIC RUN
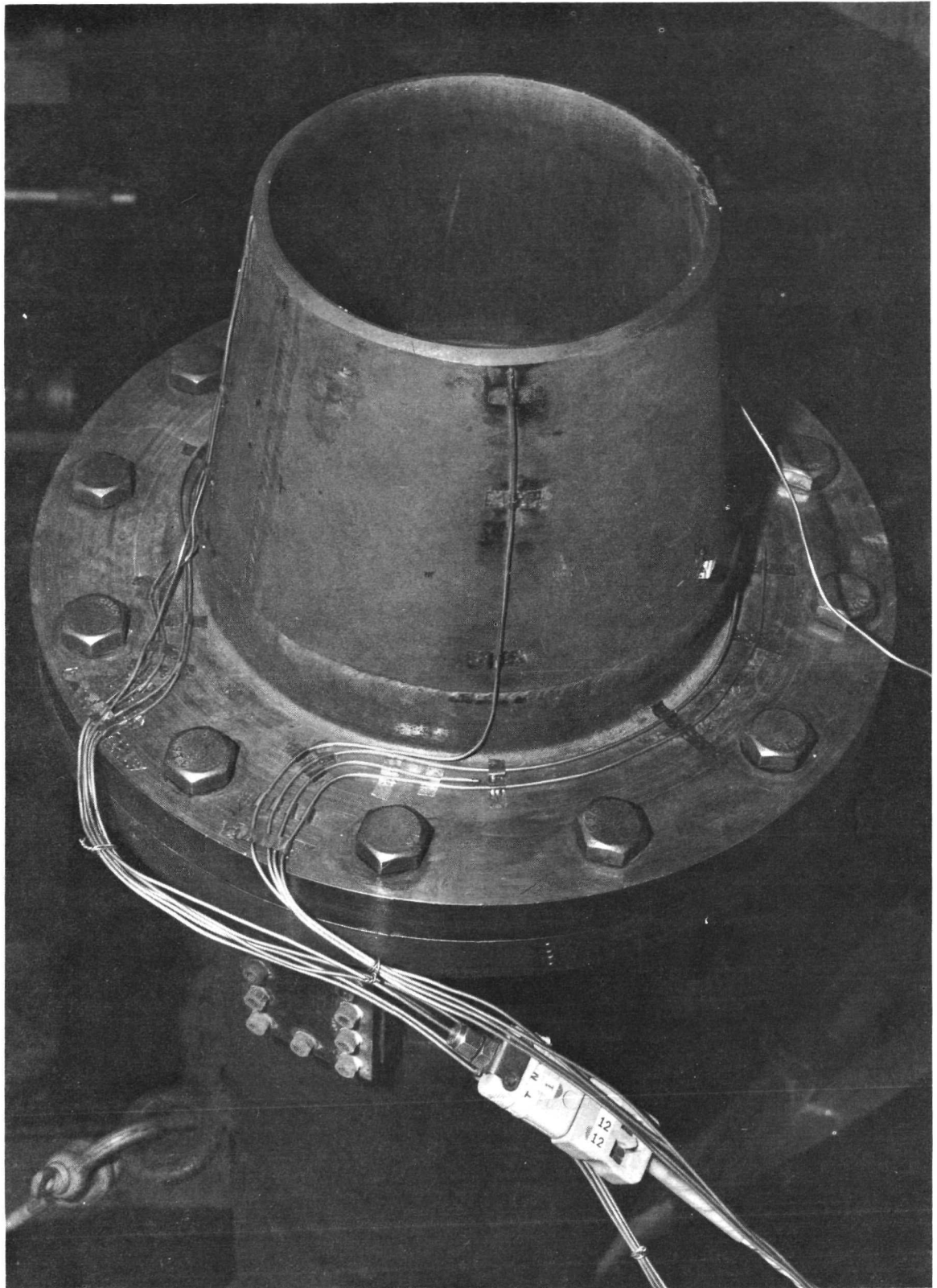
FIGURE 10.—MODEL-SCALE 15.2-CM—DIAMETER CONICAL REFERENCE NOZZLE
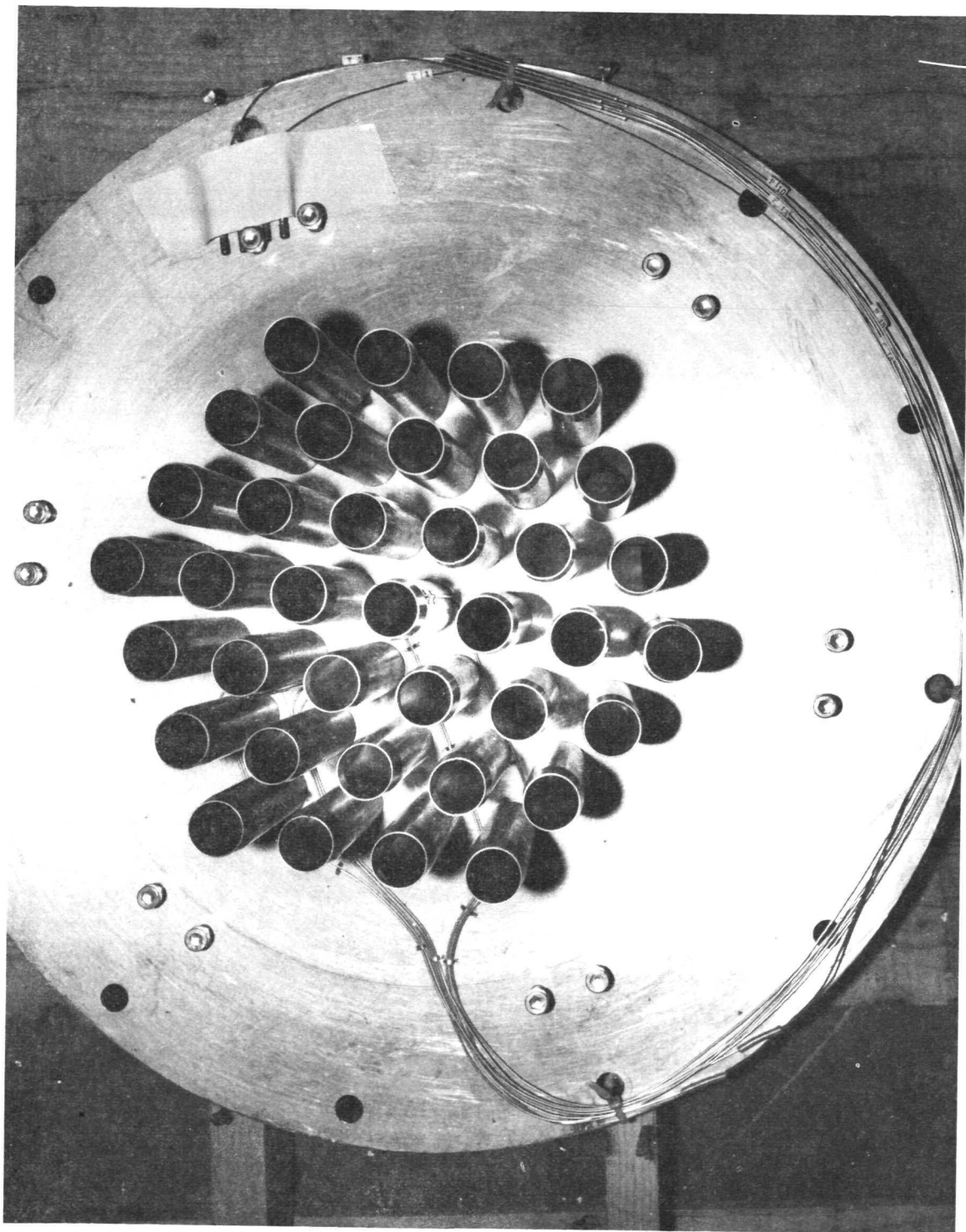
FIGURE 11.— MODEL-SCALE 37-TUBE SUPPRESSOR NOZZLE

Flow survey
traversing
mechanism & probe

33 cm

3.81 cm radius

7.62 cm
radius

Acoustic lining panel

Base plate
diameter = 66 cm

Ejector diameter 33 cm
(inscribed circle
of hexagonal
ejector section)

Ejector $\mathcal{C}_L$

Tube length
17.7 cm

Plan Section on Ejector Centerline
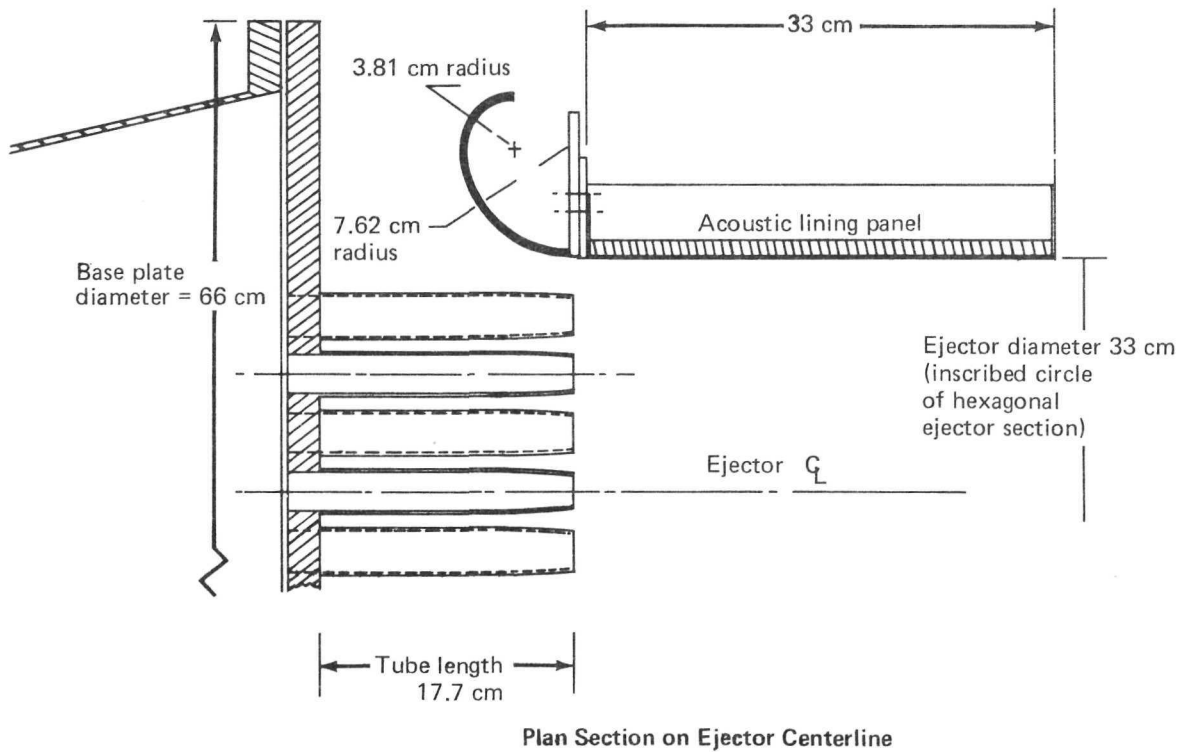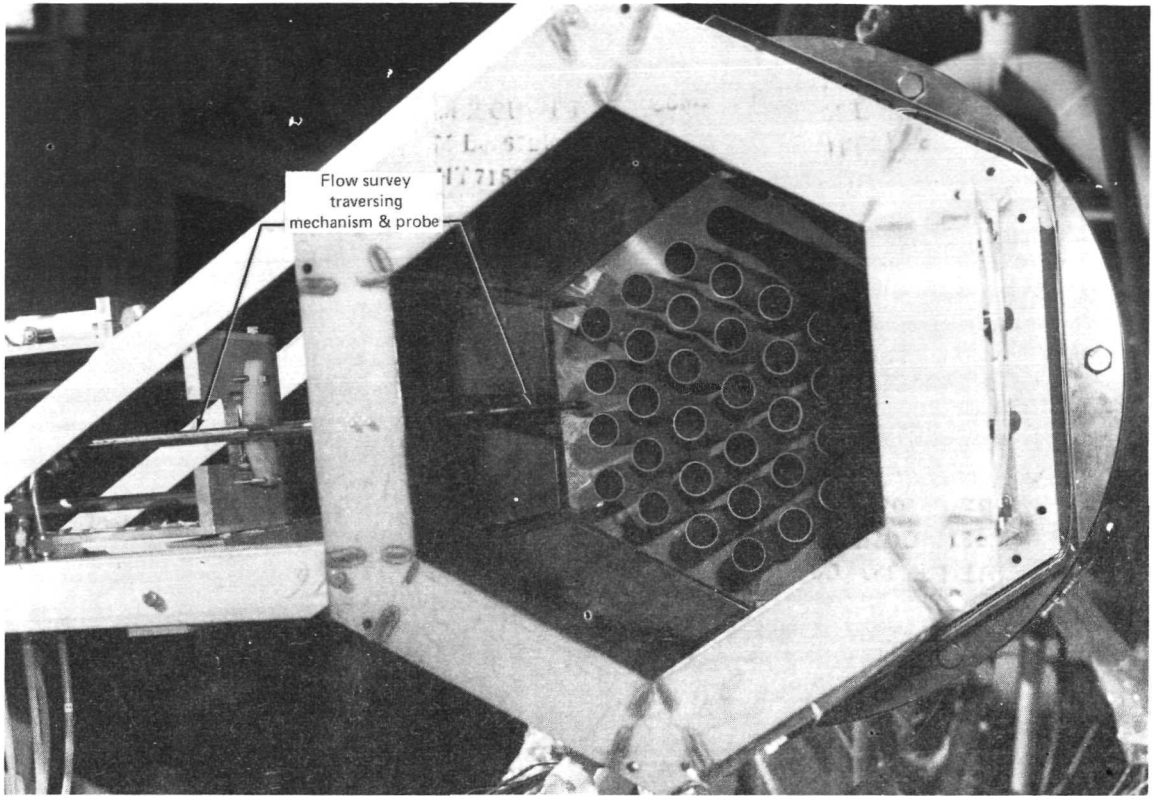
FIGURE 12.— MODEL SCALE L/D = 1 EJECTOR INSTALLATION

106
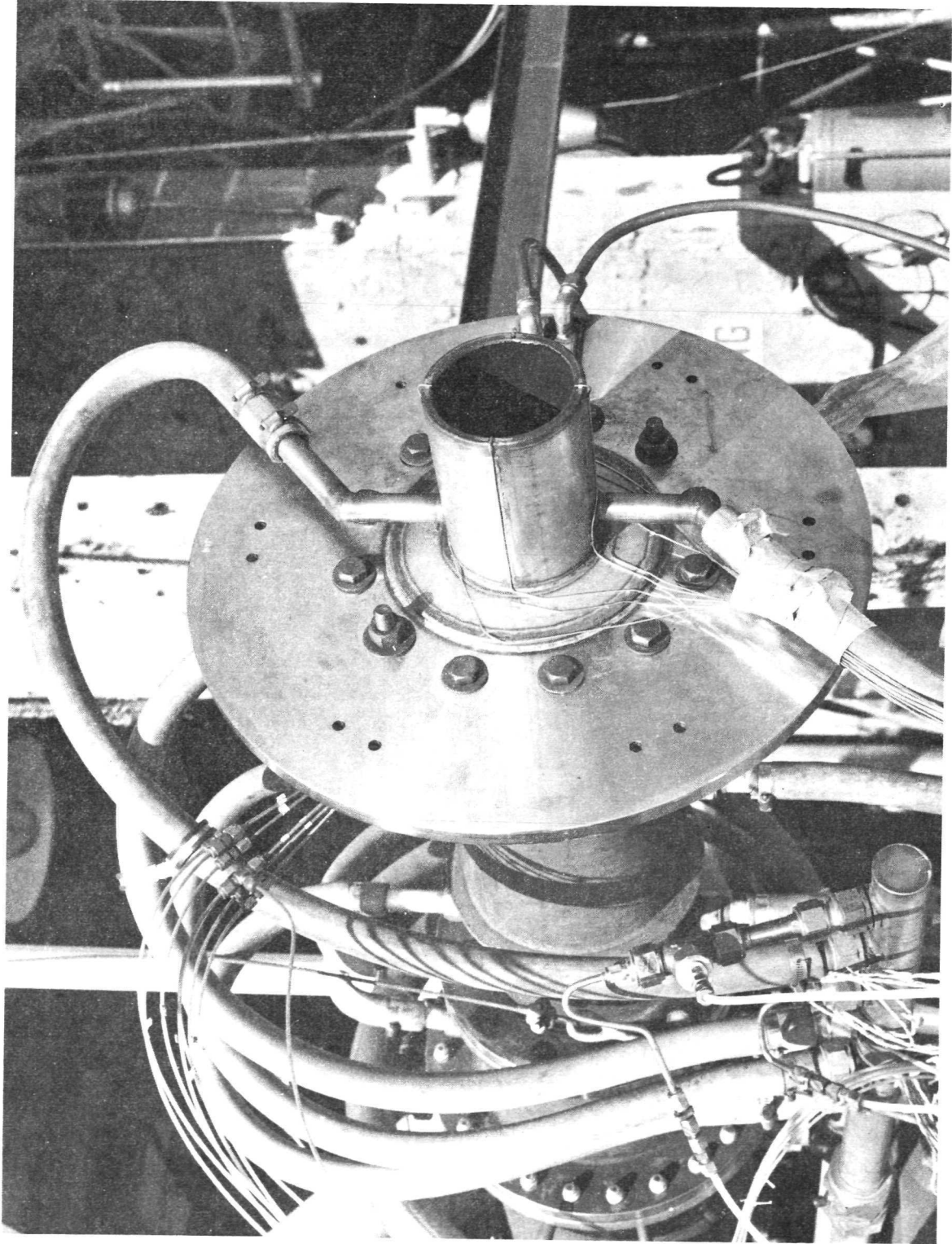
FIGURE 13.—MODEL-SCALE 10.9-CM-DIAMETER WATER COOLED CONICAL NOZZLE
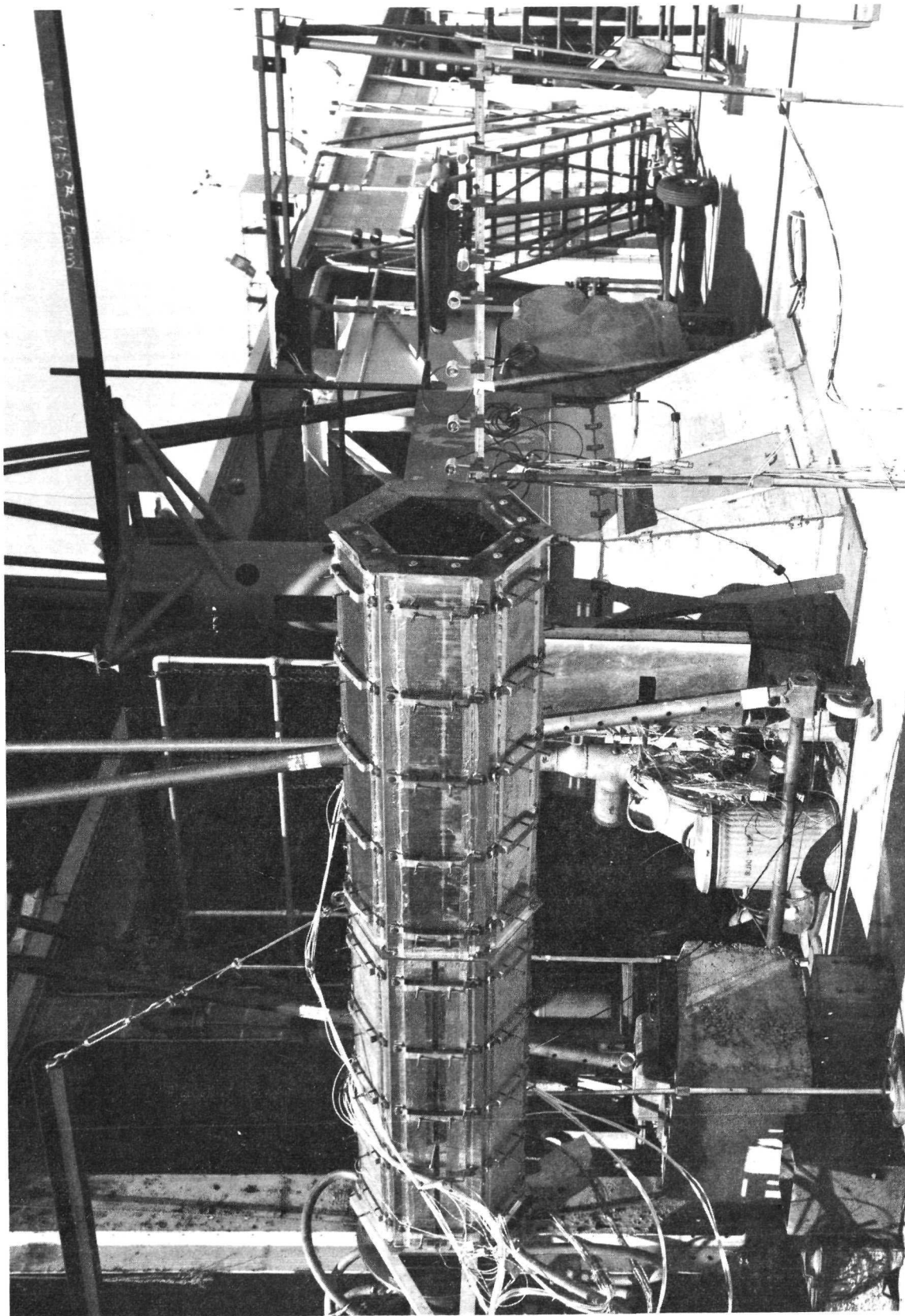
FIGURE 14.—MODEL-SCALE L/D = 8 EJECTOR INSTALLATION FOR 10.9-CM-DIAMETER NOZZLE
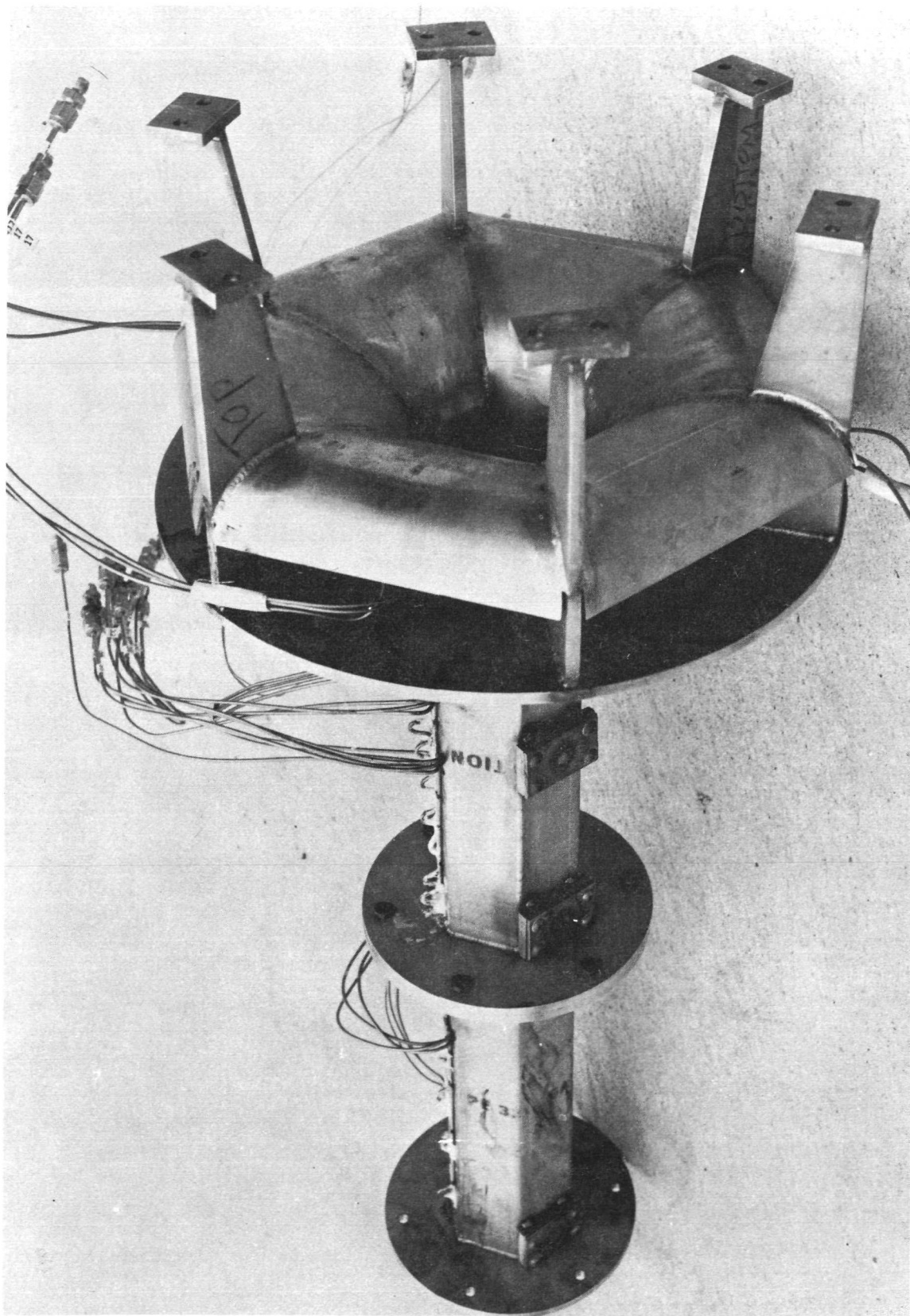
FIGURE 15.—MODEL-SCALE L/D = 8 EJECTOR FOR 2.74-CM-DIAMETER NOZZLE
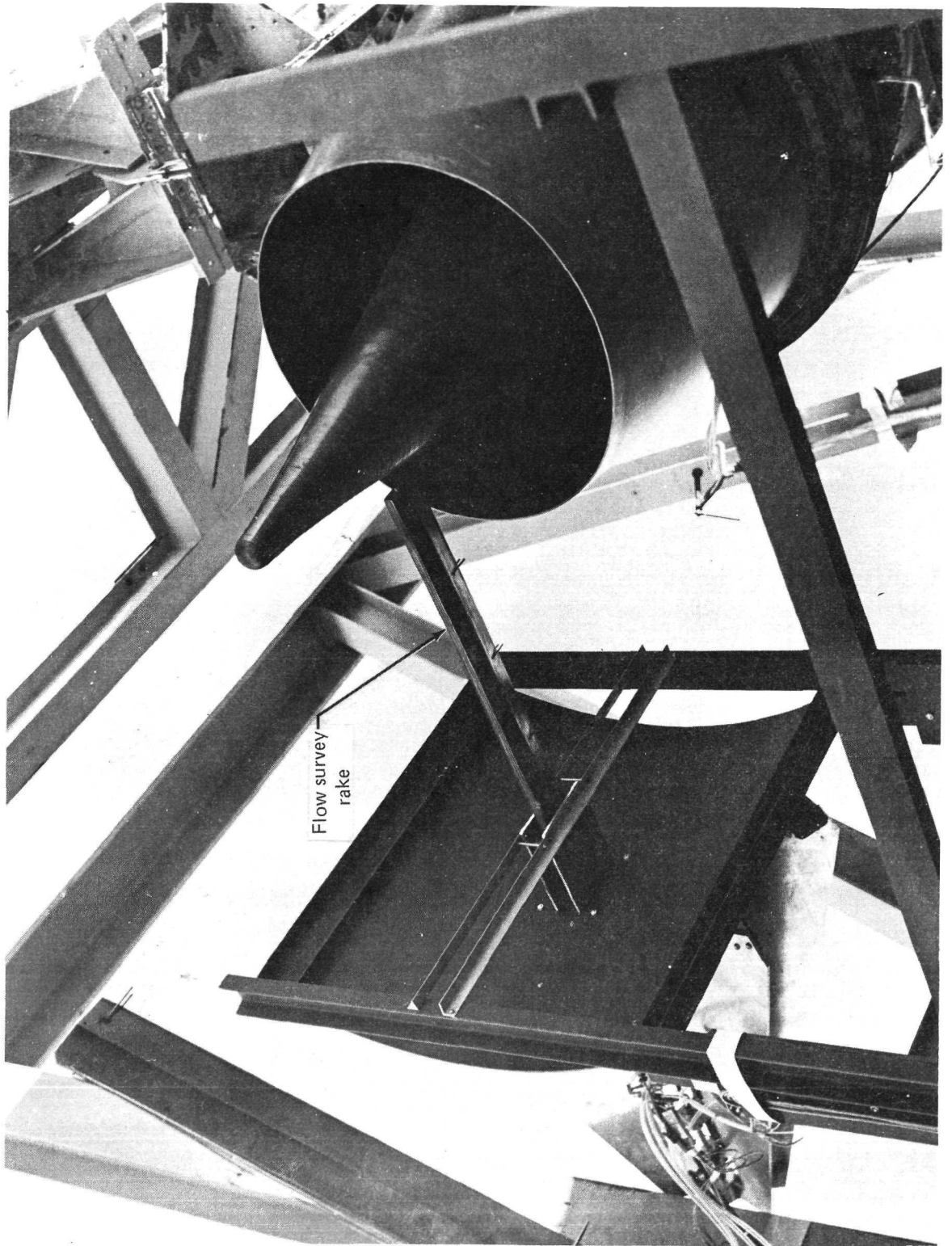
Flow survey rake

FIGURE 16.—J-75 ENGINE REFERENCE NOZZLE SET UP FOR A FLOW SURVEY TEST
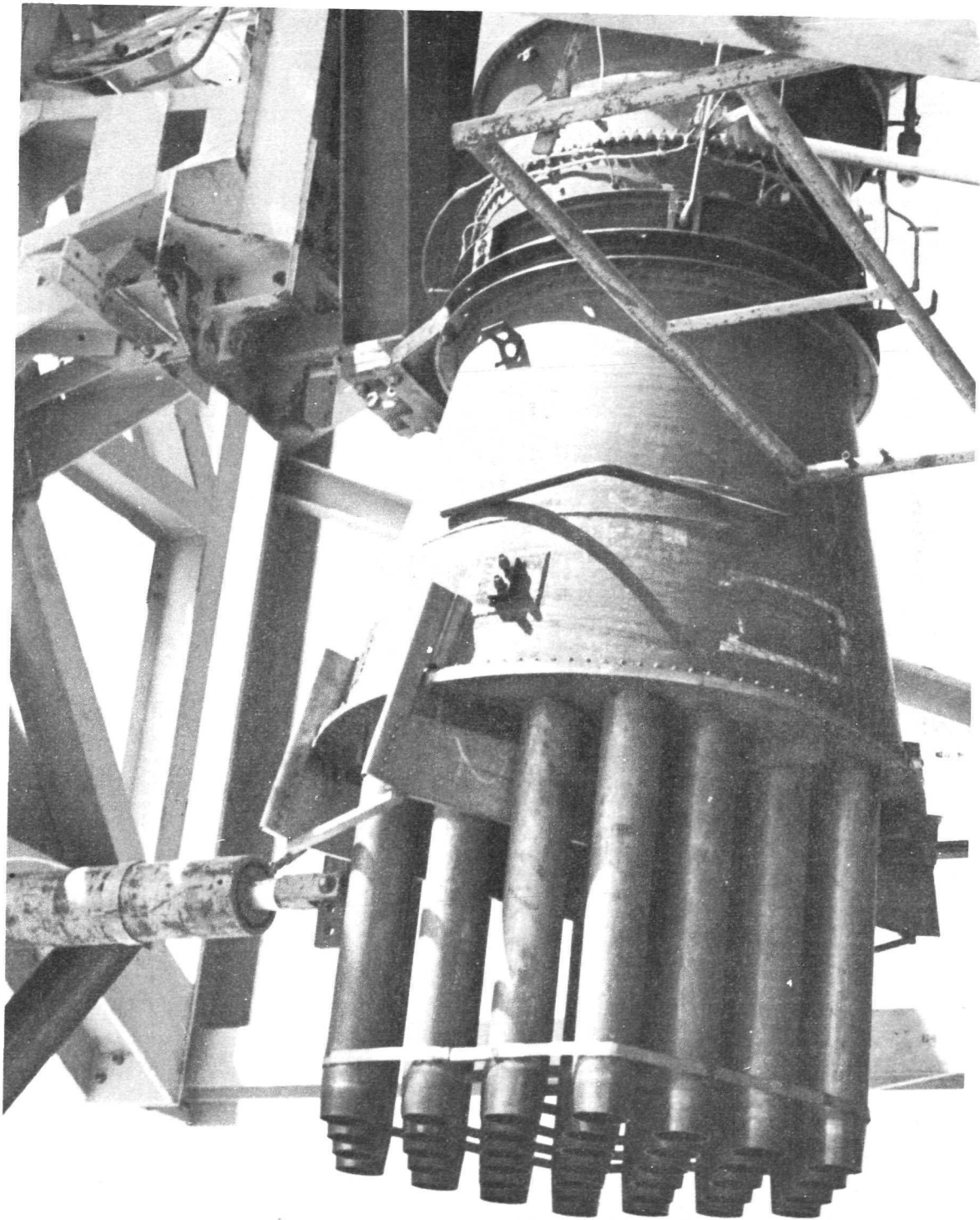
FIGURE 17.—FULL-SCALE 37-TUBE SUPPRESSOR NOZZLE

111

15.24 cm radius

Ejector Bellmouth inlet

Ejector length
132 cm
(and 264 cm)

30.5 cm radius

Ejector diameter = 132 cm
(inscribed circle of hexagonal
ejector section)

Baseplate
diameter = 140 cm

Ejector C_L

Tube length
89 cm
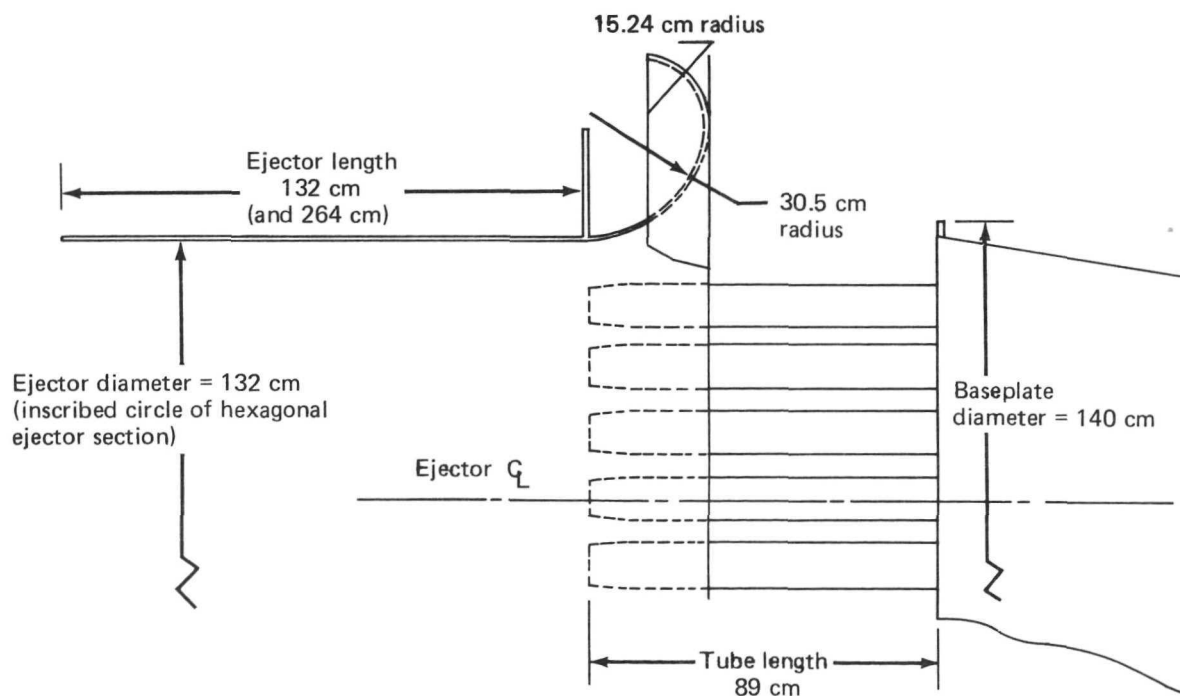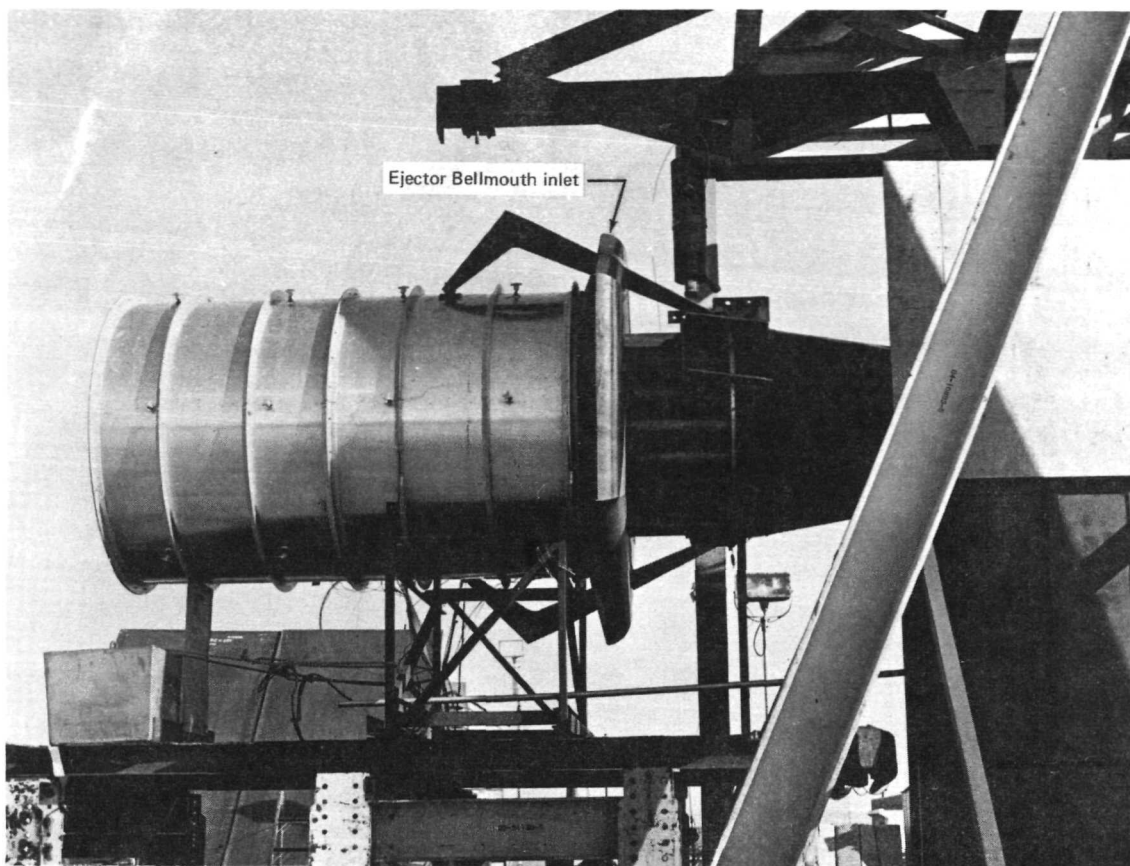
Plan Detail on Ejector Centerline

FIGURE 18.—FULL-SCALE EJECTOR INSTALLATION

Flow survey
traversing
mechanism
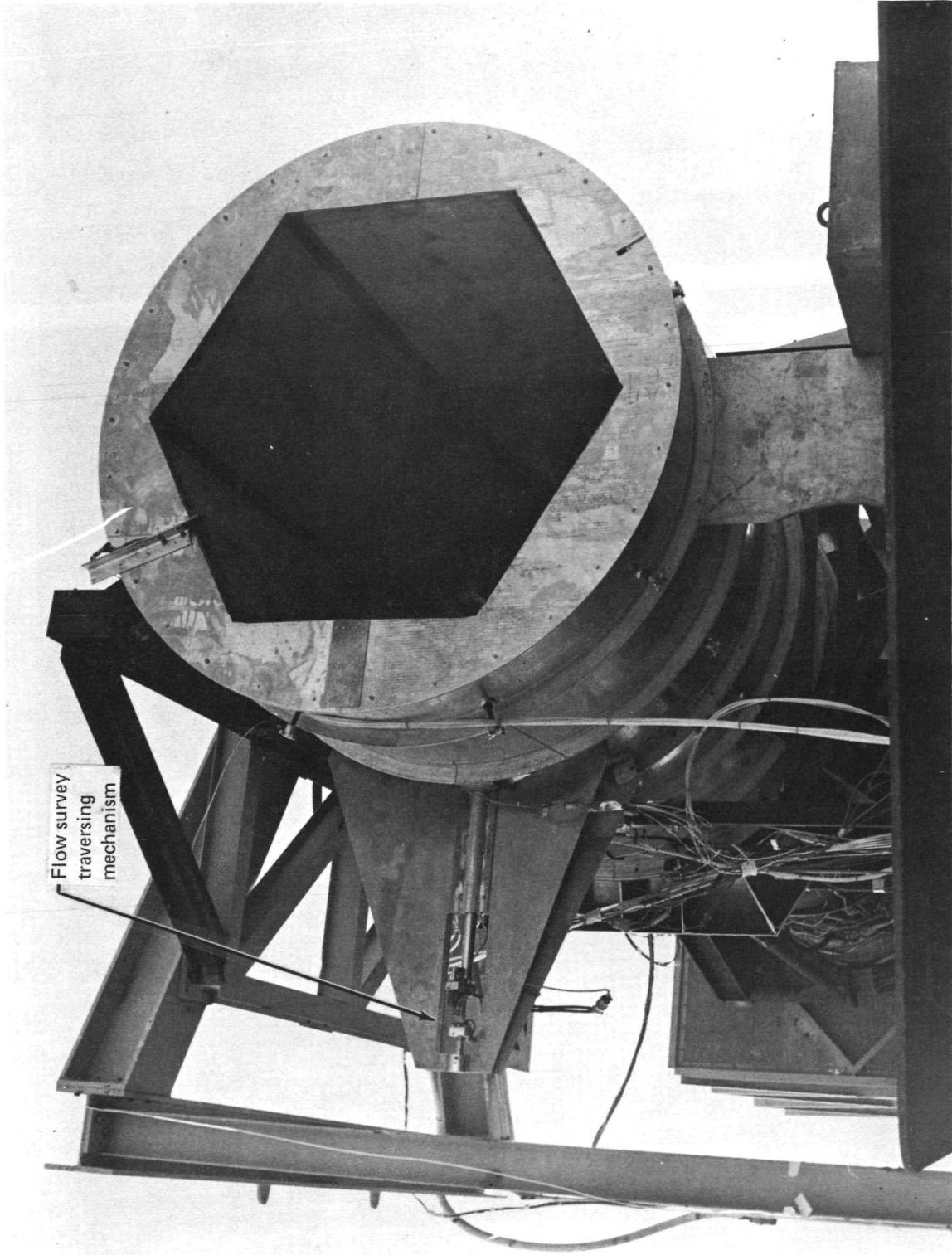
FIGURE 19.—FULL-SCALE EJECTOR, END VIEW

113

Ejector
bellmouth
inlet
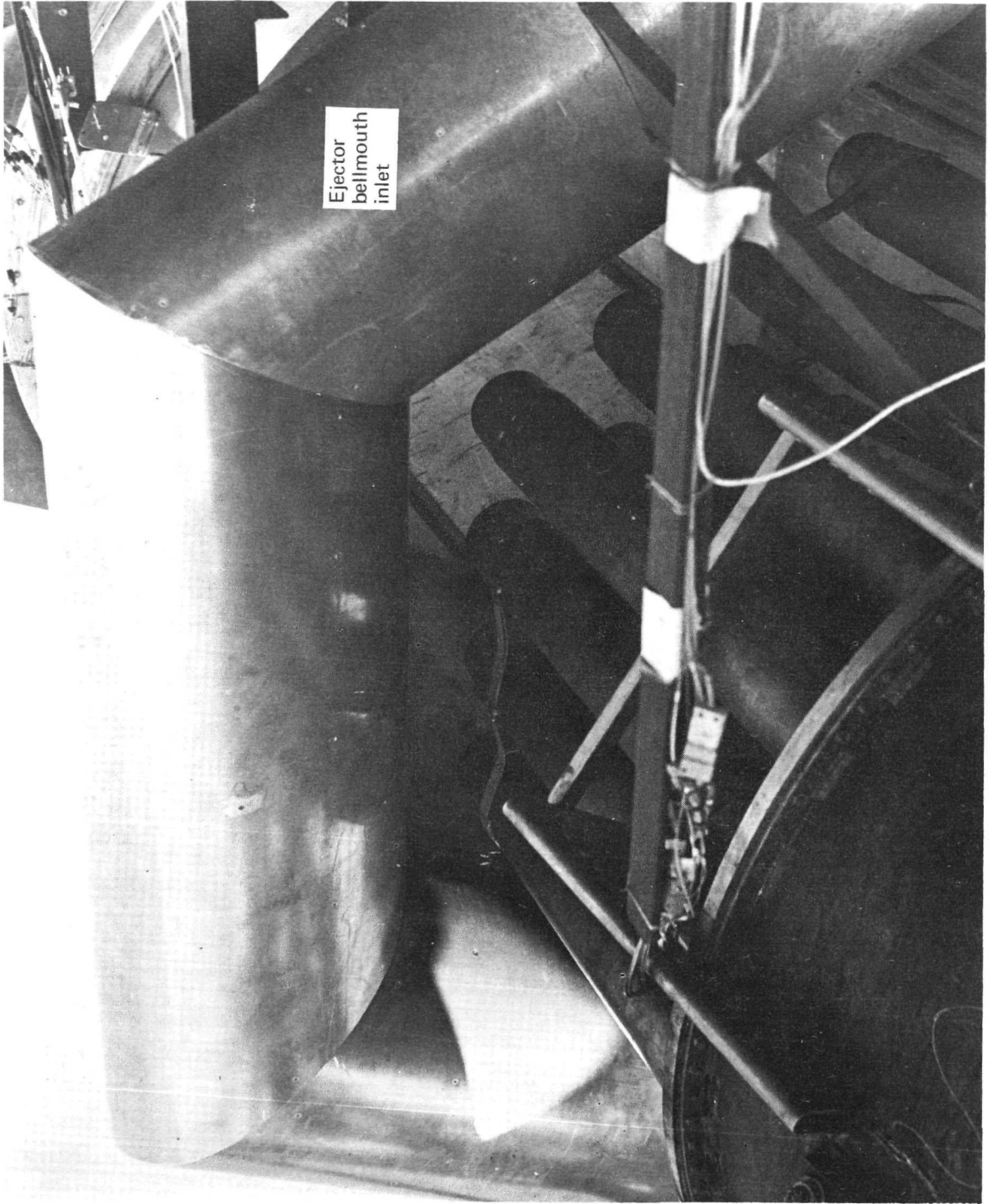
FIGURE 20.—FULL-SCALE EJECTOR BELLMOUTH ENTRY

114
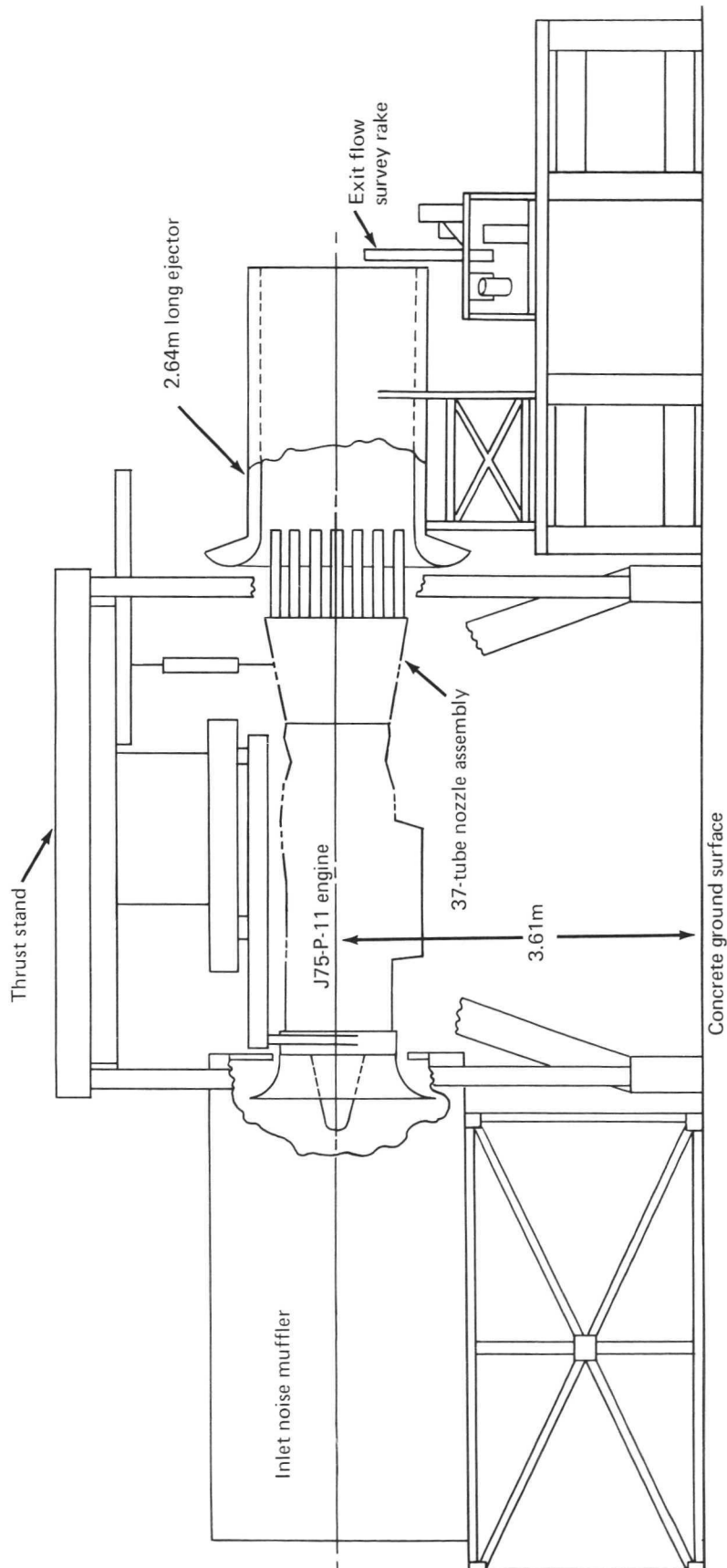
FIGURE 21.– TYPICAL J-75 ENGINE INSTALLATION FOR ACOUSTIC TESTS

115

Wind shield

Microphone
diaphragm
parallel to
and 1.27cm
above ground
surface

Test arena
surface

Mounting
plate
(flush with ground
surface)
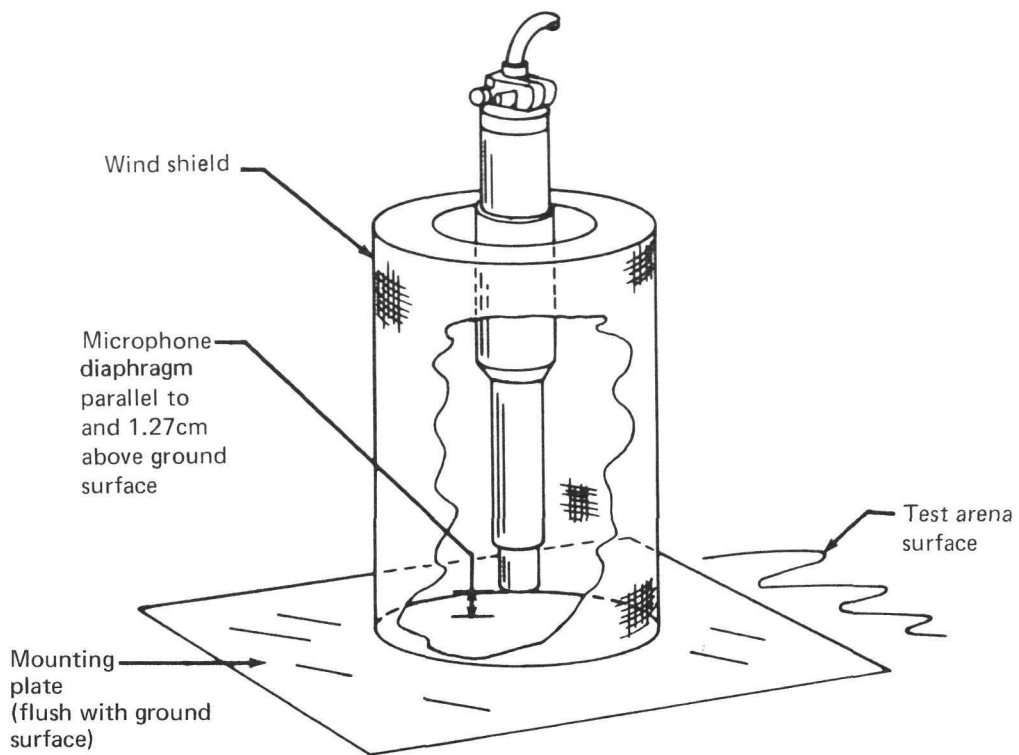
FIGURE 22.—FAR FIELD GROUND-LEVEL MICROPHONE INSTALLATION FOR FULL-SCALE TESTING

Microphone button
flush with concrete
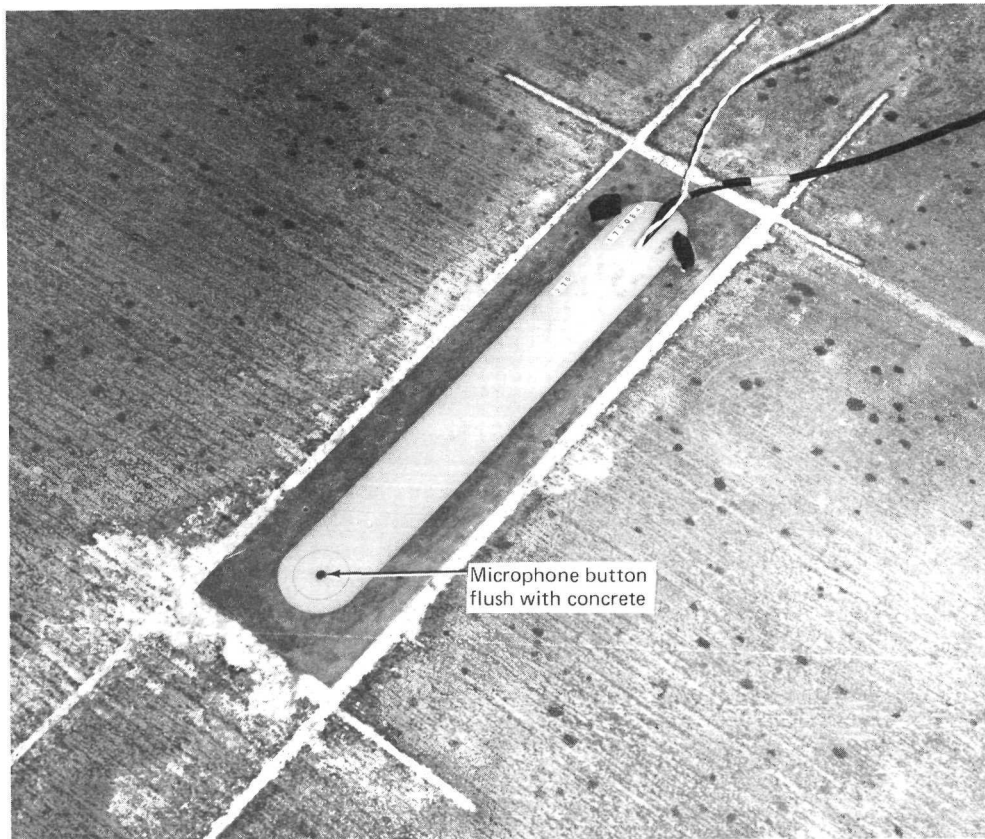
FIGURE 23.—FAR FIELD GROUND-LEVEL MICROPHONE INSTALLATION FOR MODEL-SCALE TESTING

116

Heater

Microphone
button

2 (in.)

1

Preamplifier
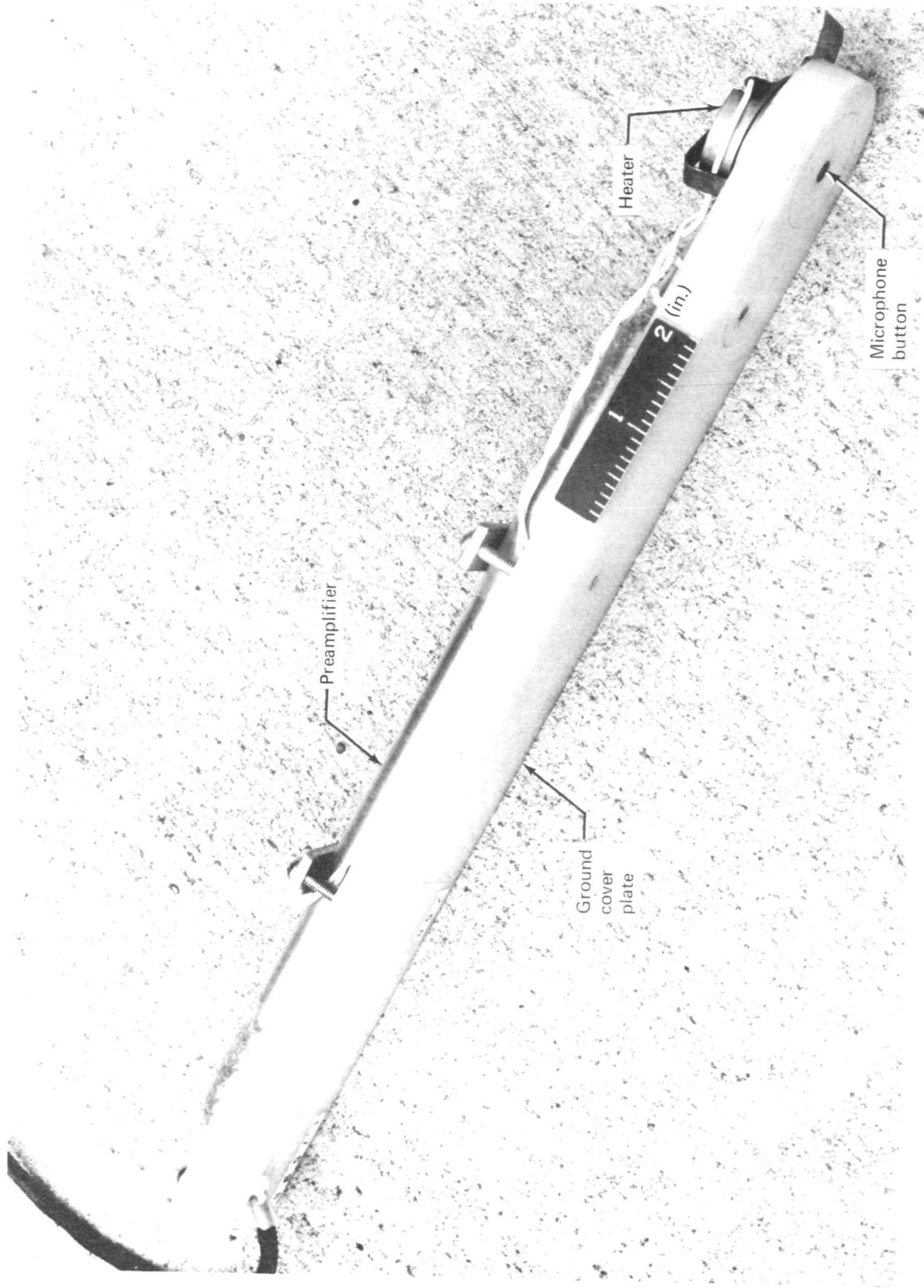
Ground
cover
plate

FIGURE 24.—FAR FIELD GROUND-LEVEL MICROPHONE UNIT FOR **MODEL-SCALE TESTING**

117
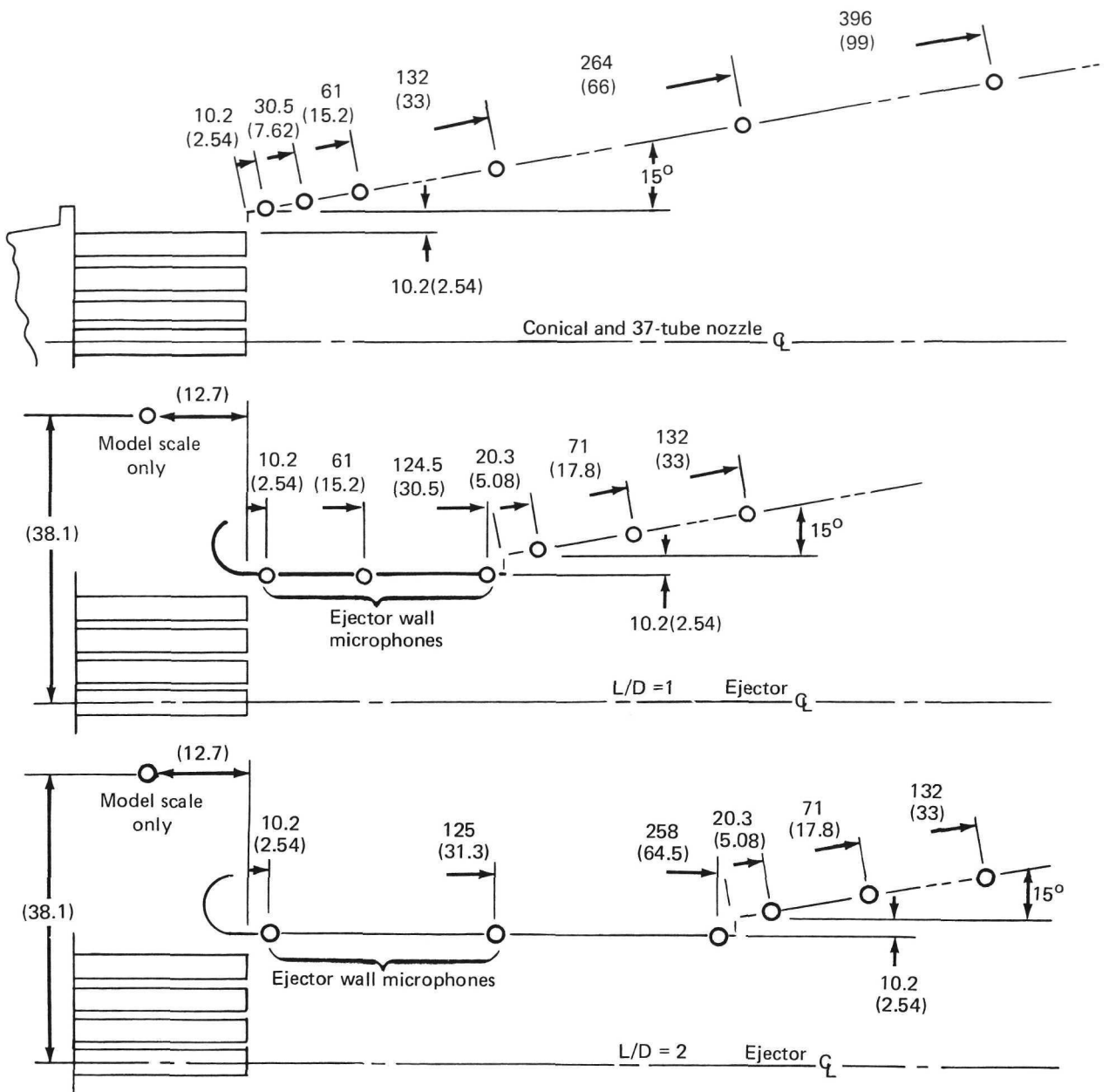
Dimensions in cm

( ) Figures in parentheses refer to model scale

FIGURE 25.—NEAR FIELD MICROPHONE ARRAYS FOR FULL- AND MODEL-SCALE TESTS
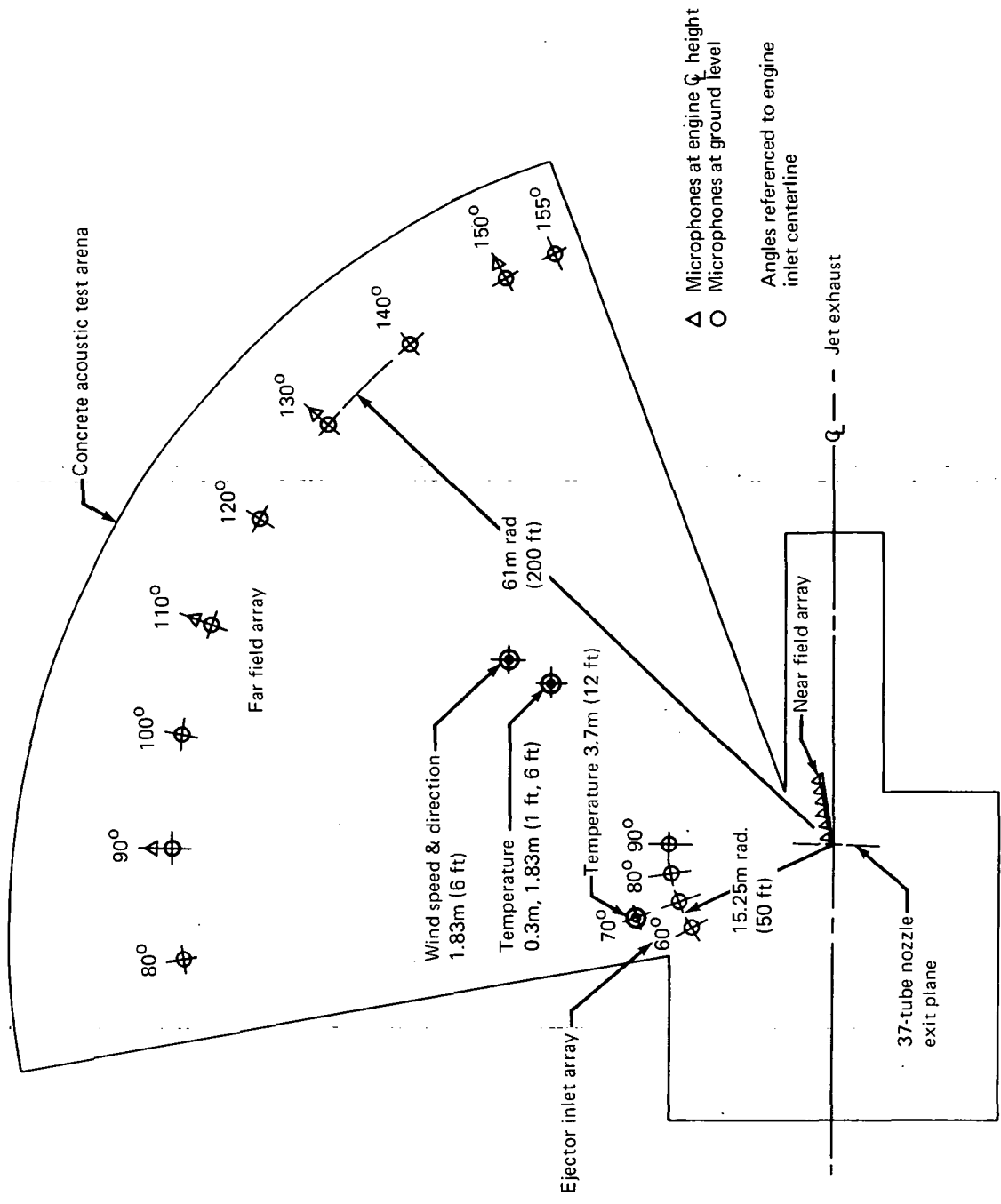
FIGURE 26.—FAR FIELD MICROPHONE ARRAY FOR FULL-SCALE TESTS

119
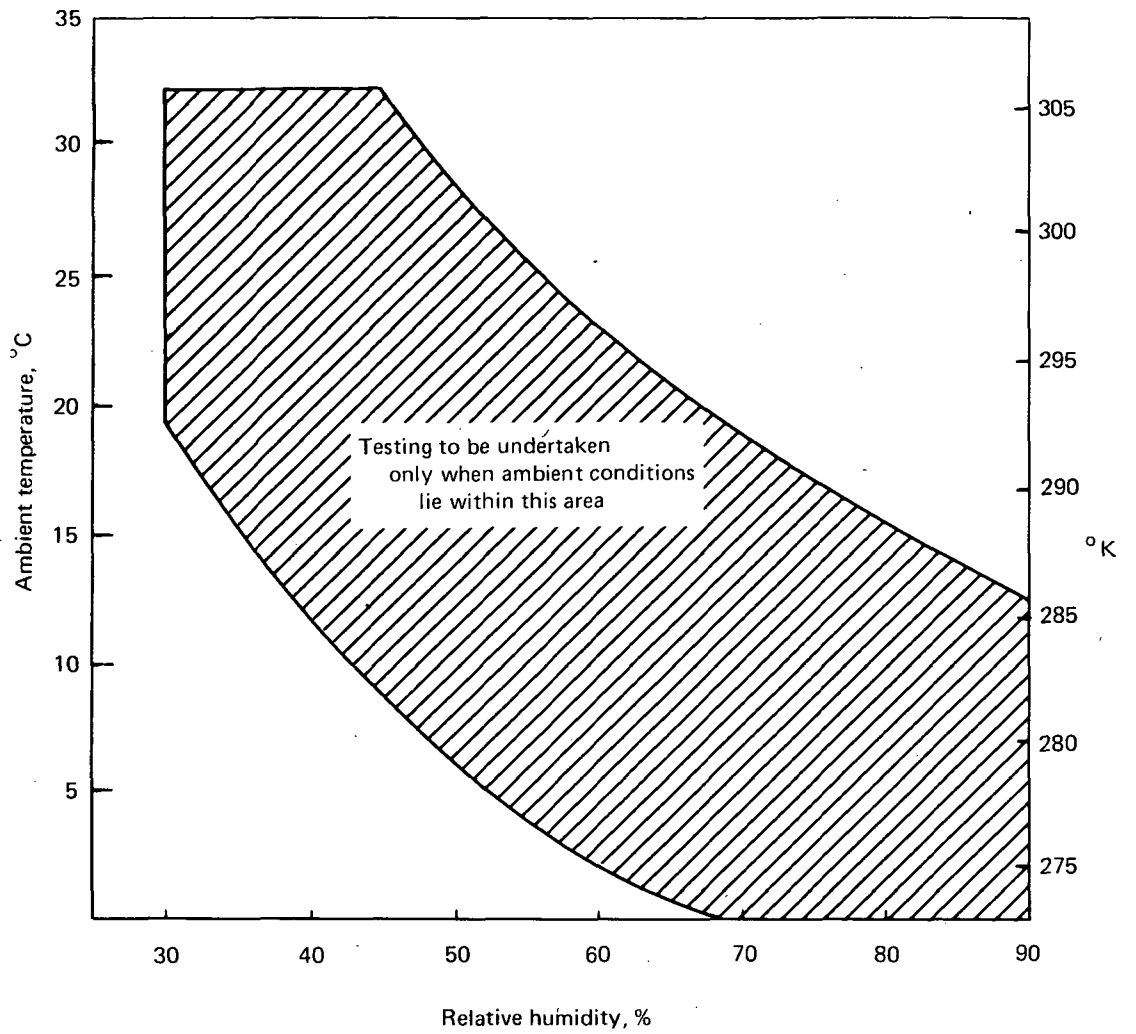
FIGURE 27.—TEMPERATURE AND RELATIVE HUMIDITY RESTRICTIONS FOR ACOUSTIC TESTING
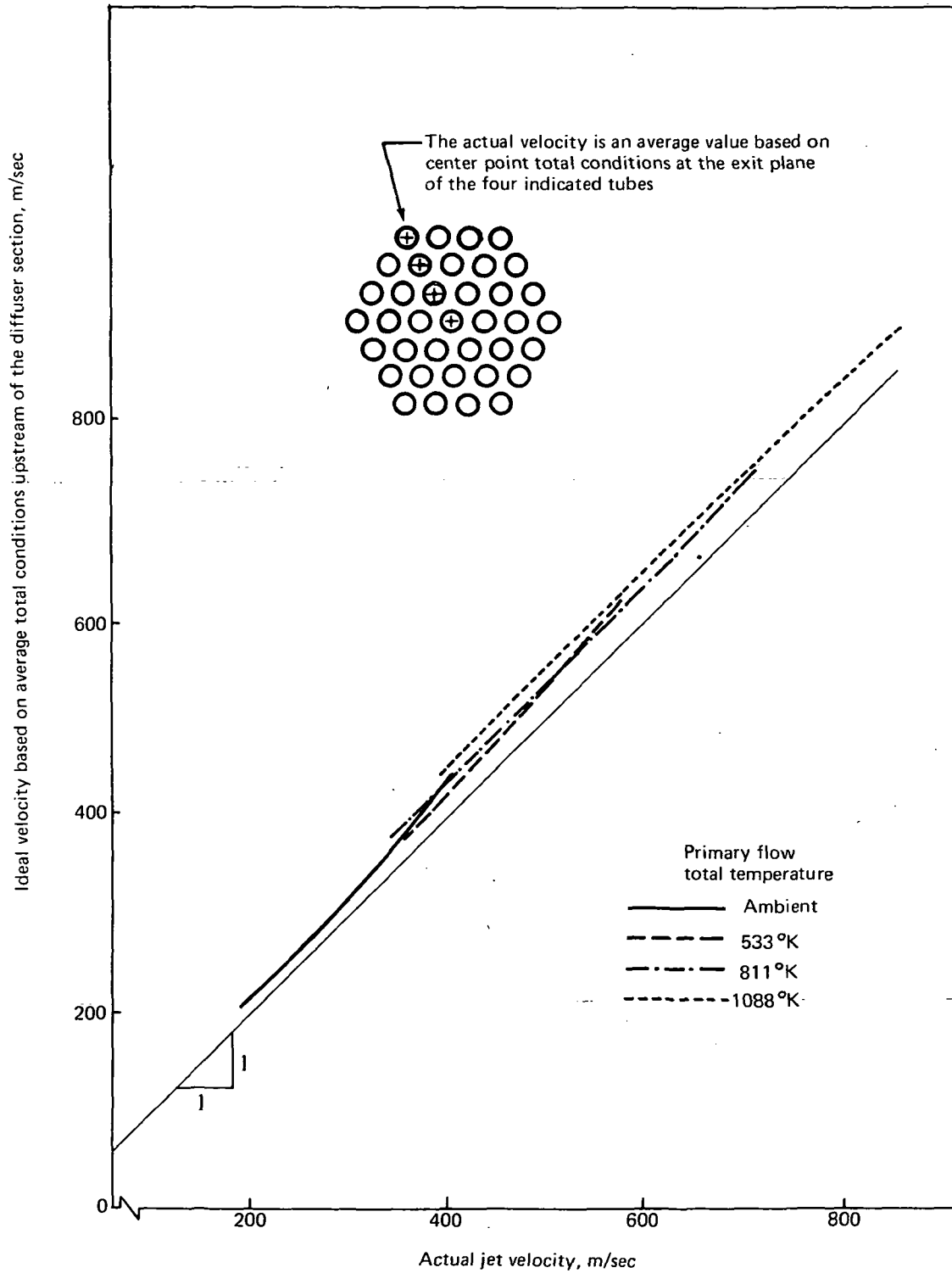
FIGURE 28.–JET VELOCITY FOR THE MODEL-SCALE 37-TUBE NOZZLE
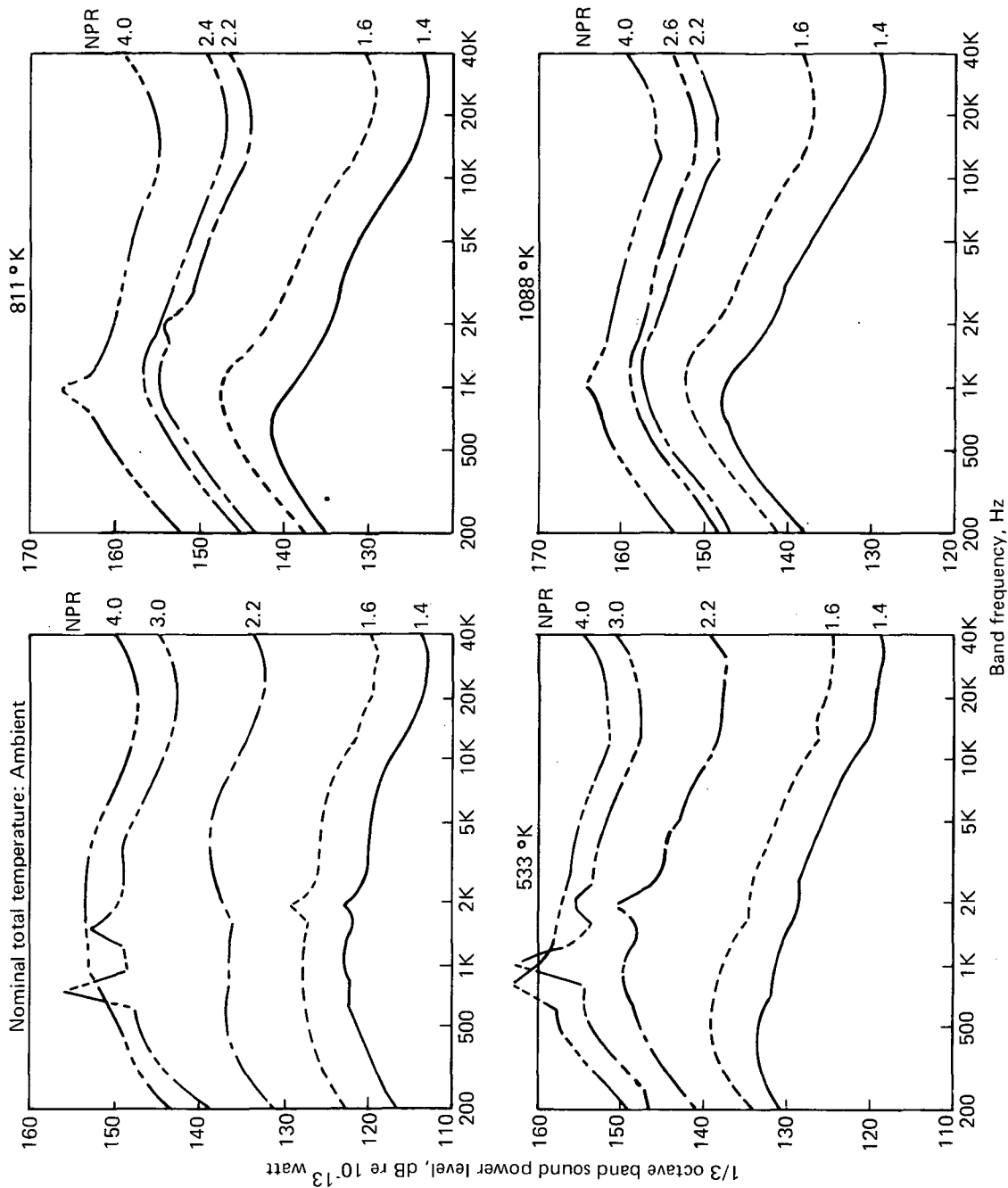
FIGURE 29.–SOUND POWER SPECTRA FOR MODEL-SCALE 15.2-CM-DIAMETER CONICAL REFERENCE NOZZLE

122
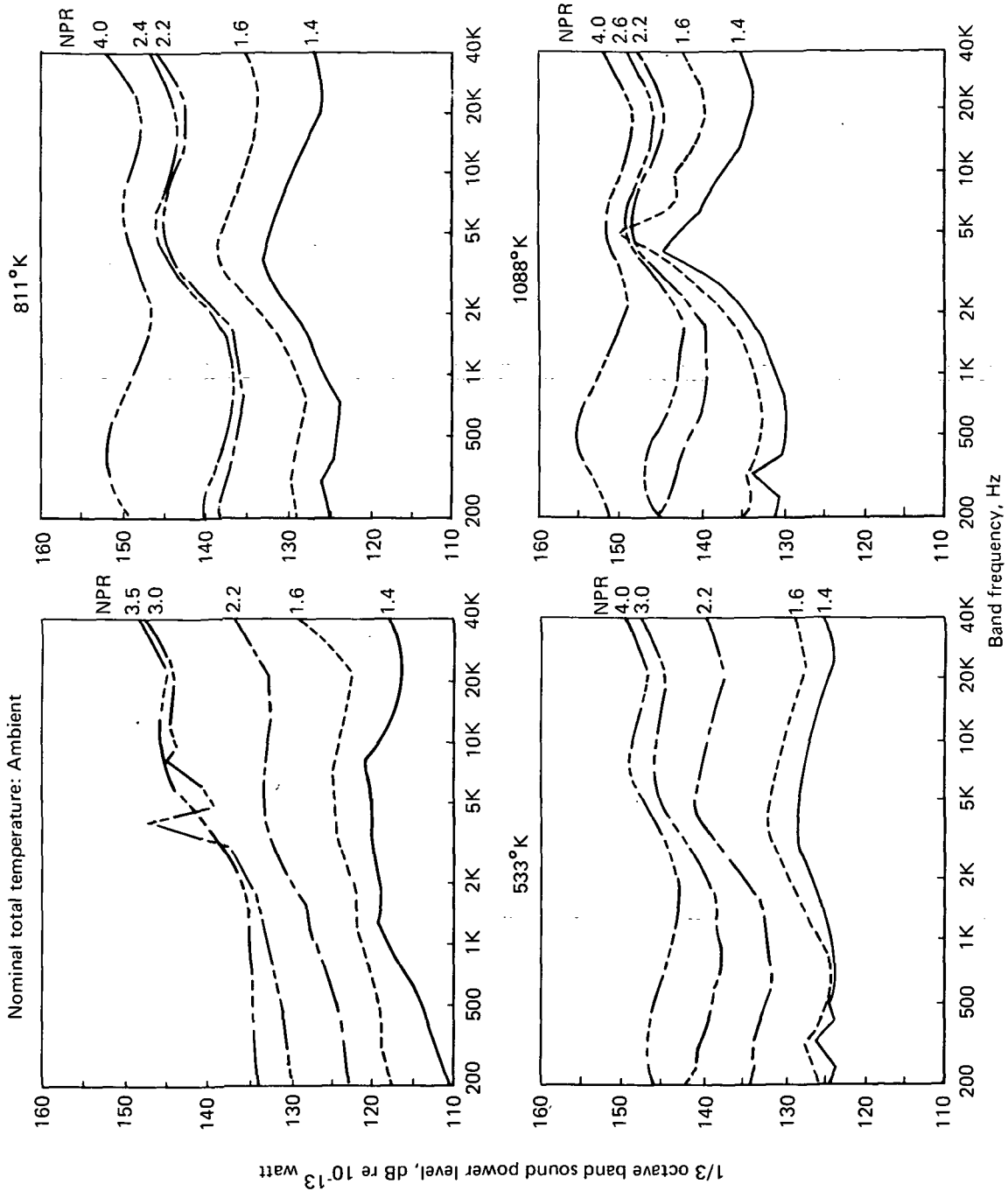
FIGURE 30.—SOUND POWER SPECTRA FOR MODEL-SCALE 37-TUBE SUPPRESSOR NOZZLE

123
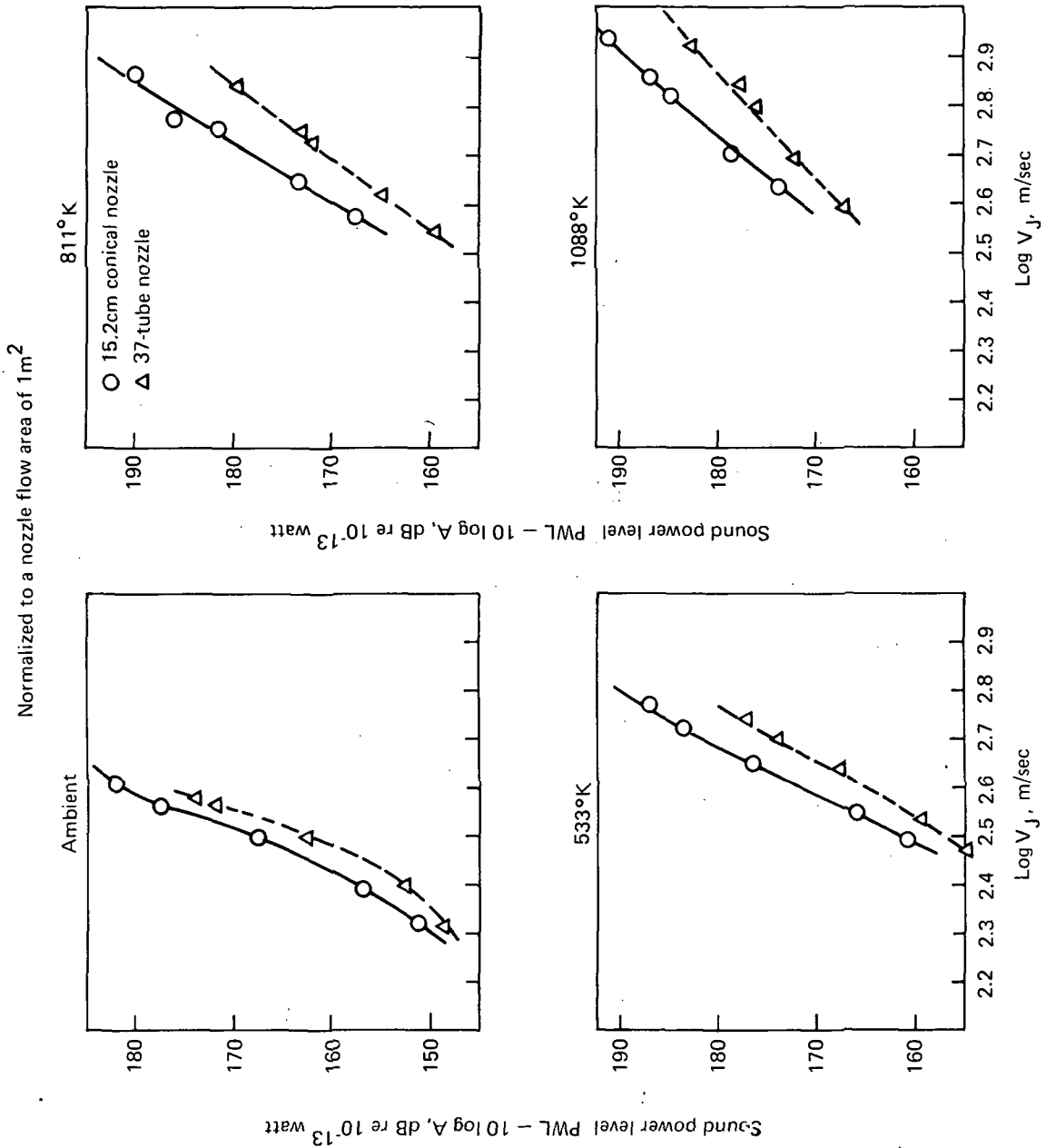
FIGURE 31.—NORMALIZED OVERALL SOUND POWER FOR MODEL-SCALE REFERENCE
CONICAL AND 37-TUBE SUPPRESSOR NOZZLES

124
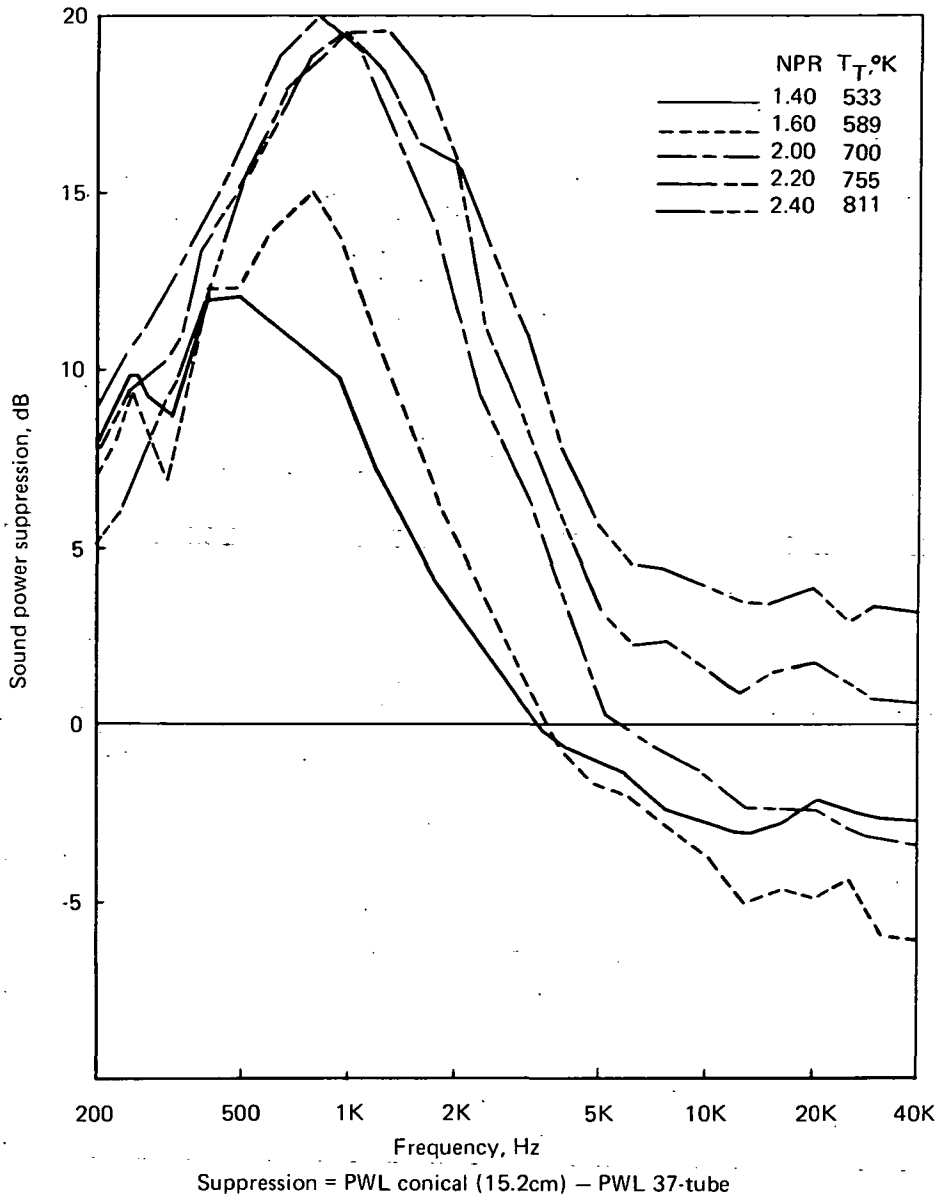
FIGURE 32.—SOUND POWER SUPPRESSION WITH MODEL-SCALE 37-TUBE NOZZLE

125
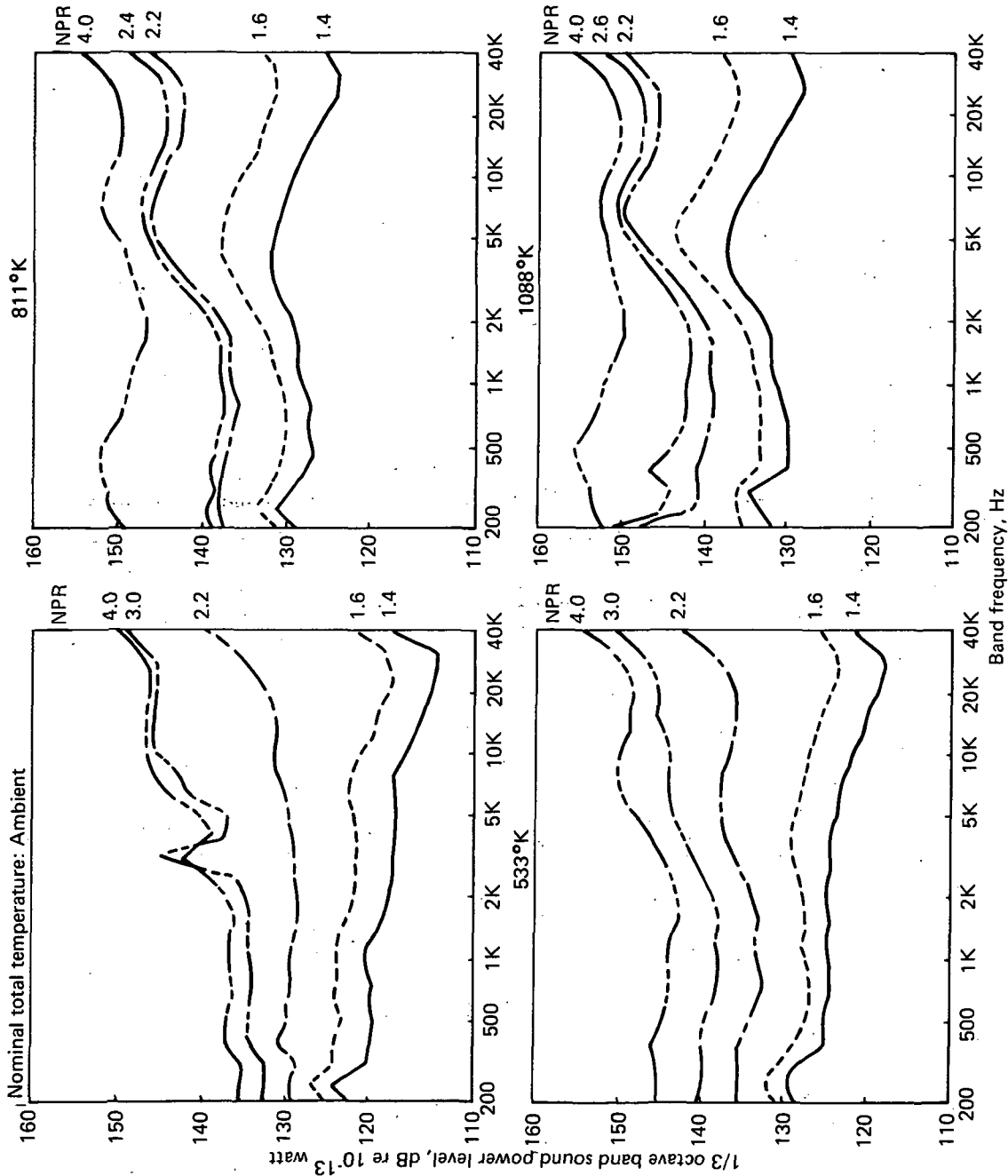
FIGURE 33.—SOUND POWER SPECTRA FOR MODEL-SCALE 37-TUBE NOZZLE WITH L/D = 1 HARDWALL EJECTOR
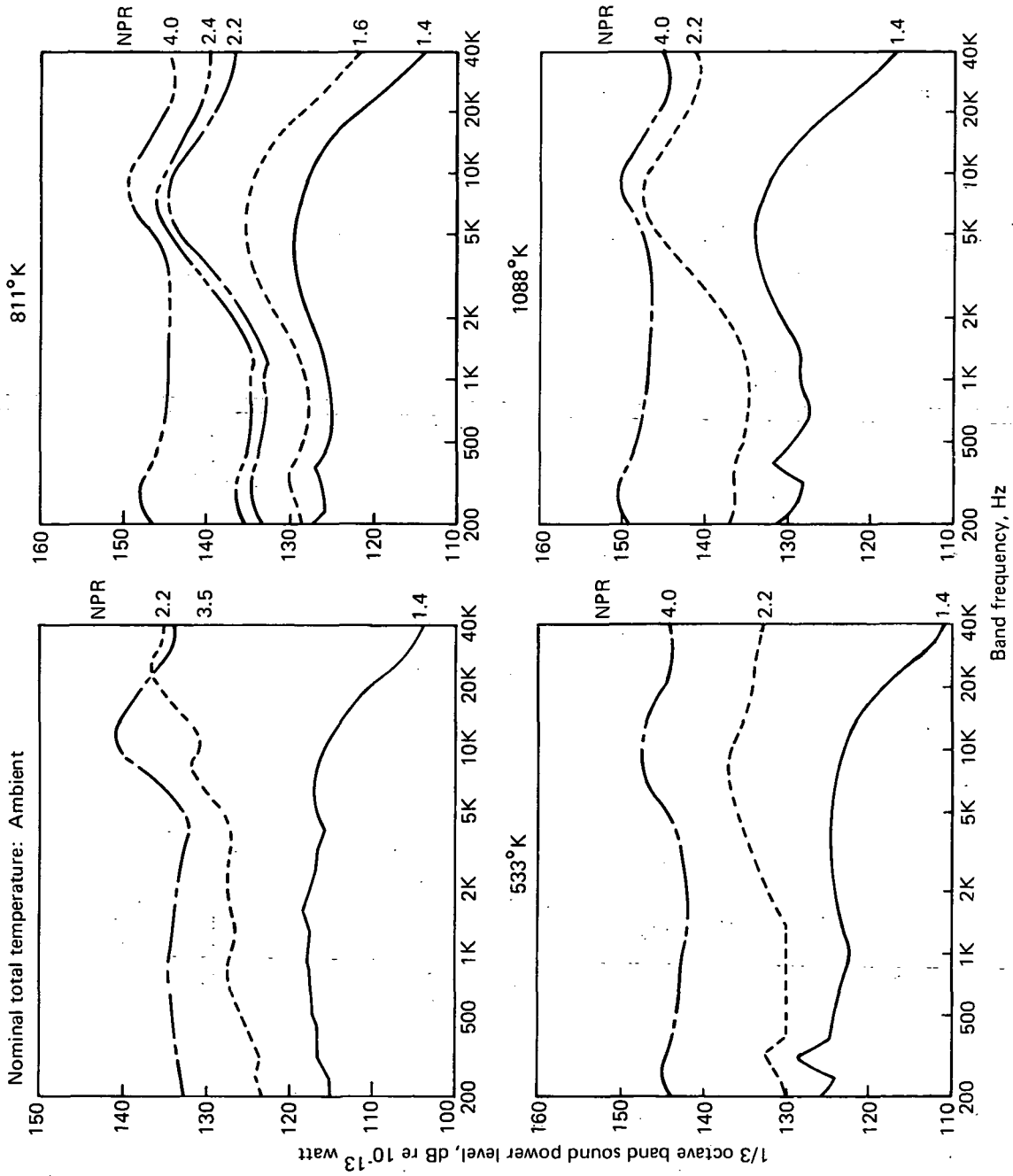
FIGURE 34.—SOUND POWER SPECTRA FOR MODEL-SCALE 37-TUBE NOZZLE WITH L/D = 2 HARDWALL EJECTOR

O 37-tube nozzle + hardwall ejector, L/D = 1

△ 37-tube nozzle + hardwall ejector, L/D = 2

Normalized to a nozzle flow area of 1m²
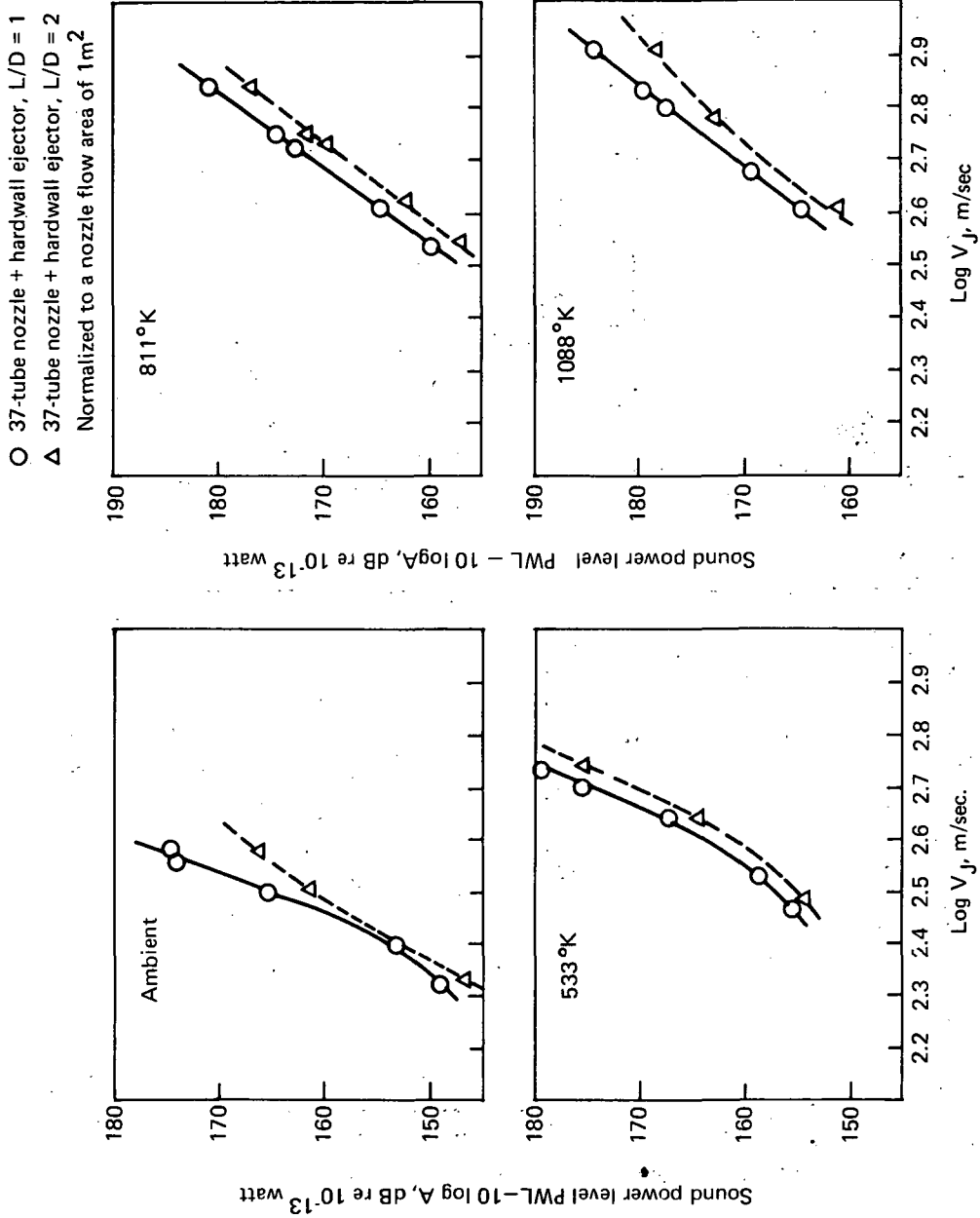
FIGURE 35.—NORMALIZED OVERALL SOUND POWER LEVEL FOR MODEL-SCALE 37-TUBE NOZZLE WITH L/D = 1 AND L/D = 2 HARDWALL EJECTORS

128
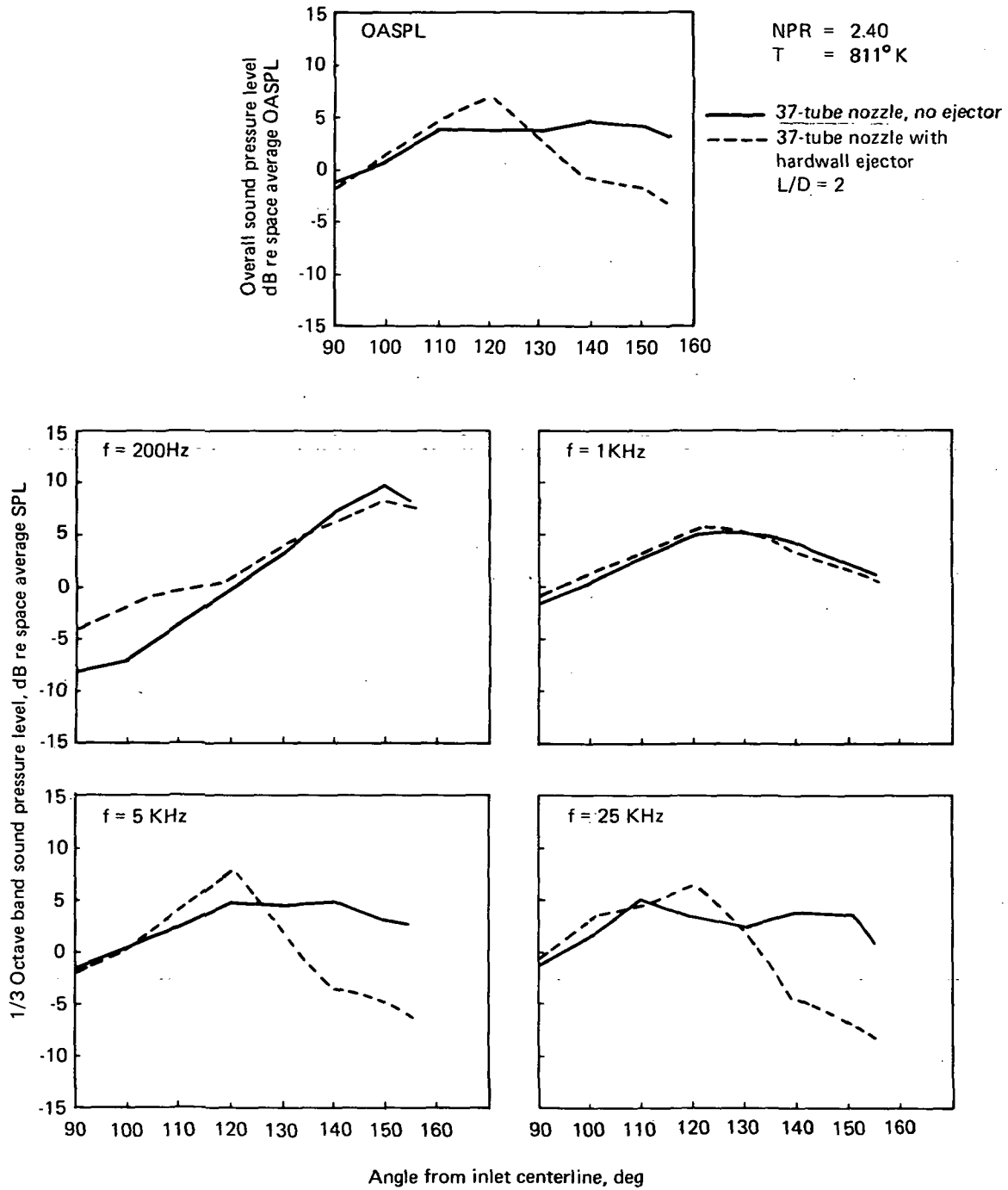
FIGURE 36.—THE EFFECT OF A HARDWALL L/D = 2 EJECTOR UPON THE ACOUSTIC RADIATION
CHARACTERISTICS (MODEL-SCALE)

FIGURE 37.—DEFINITION OF ACOUSTIC LINING ATTENUATION TERMS
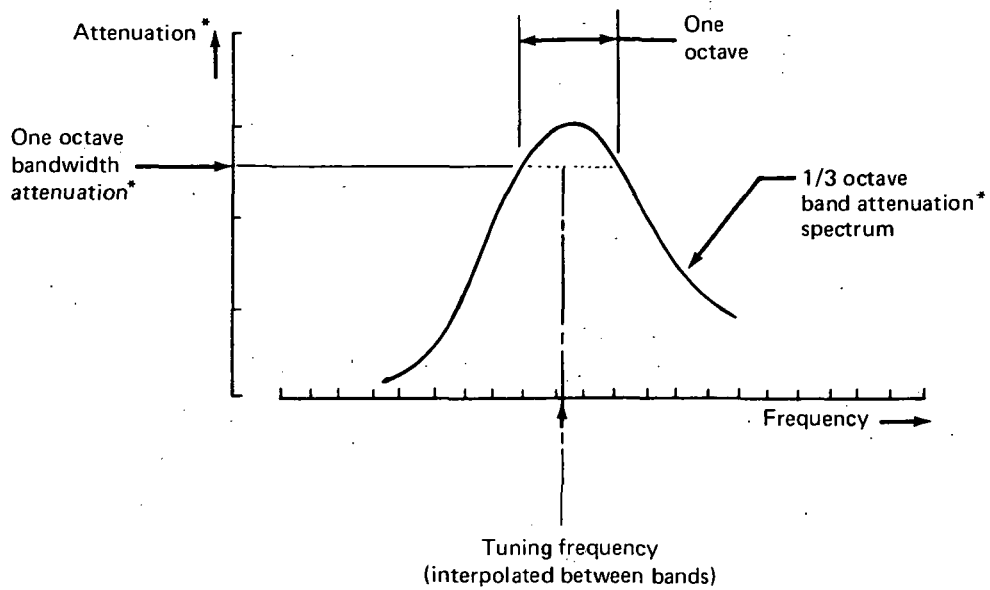
*Insertion loss replaces the term attenuation if sound power
level reductions are considered.

130
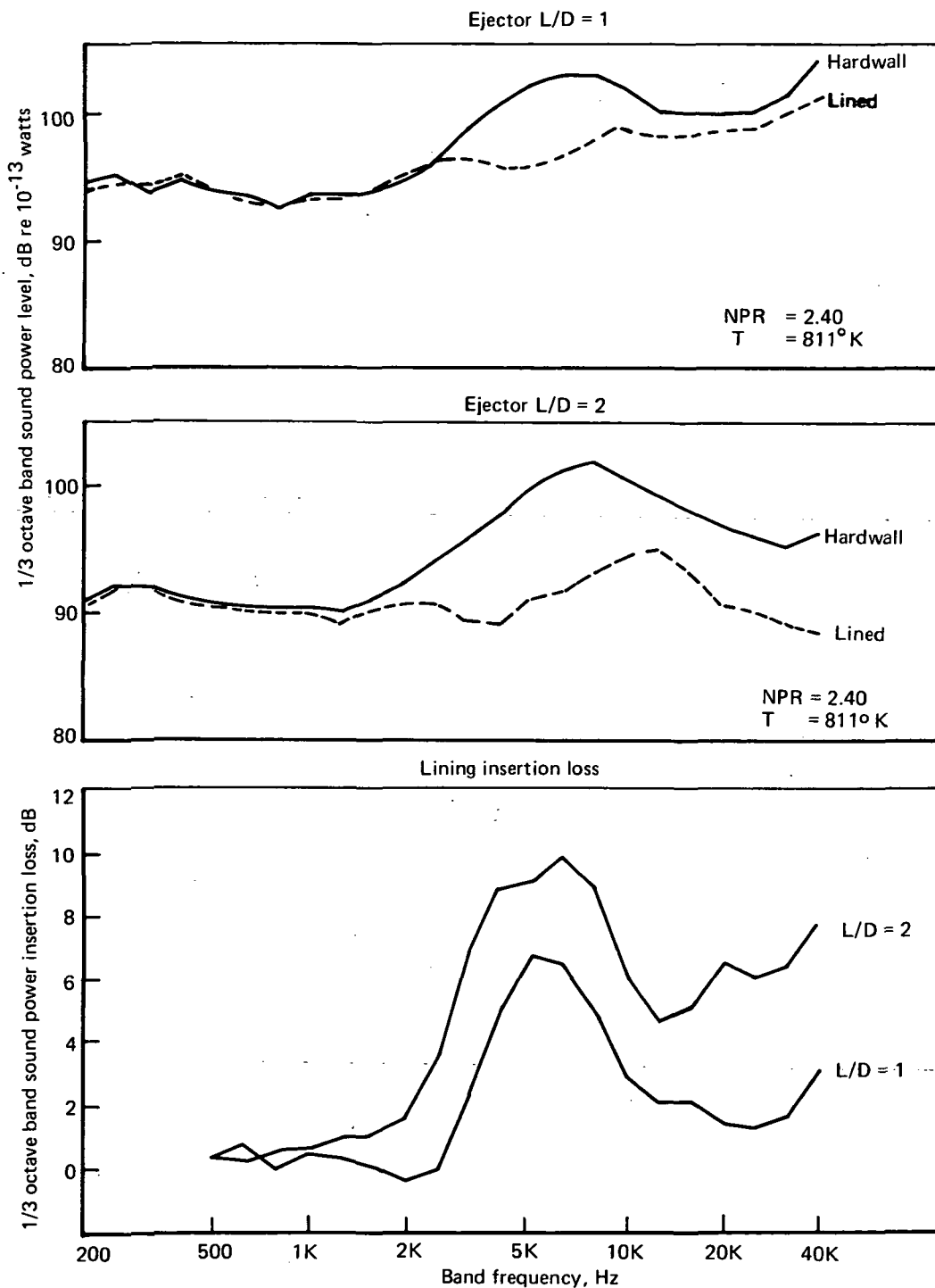
A.—Comparison of the acoustic performance of lined and
   hardwall L/D = 1 and L/D = 2 ejectors (22% open area,
   d = 1.4-cm lining)

FIGURE 38.—EXAMPLE OF LINING PERFORMANCE FROM MODEL-SCALE TEST
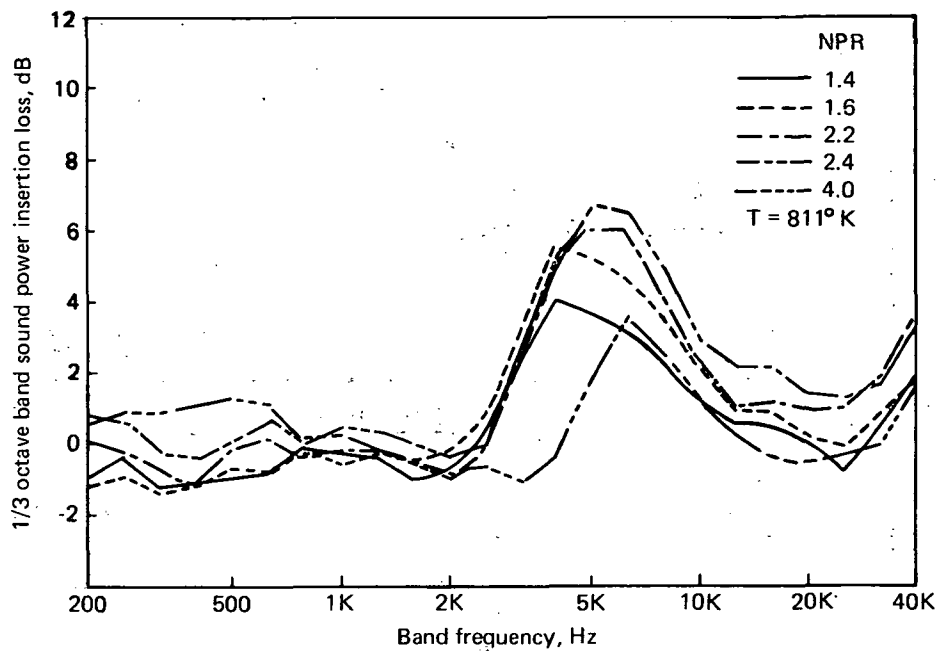
B.—Sound power insertion loss spectra with model scale
lined L/D = 1 ejector (22% open area; d = 1.4 cm)

FIGURE 38.—Concluded
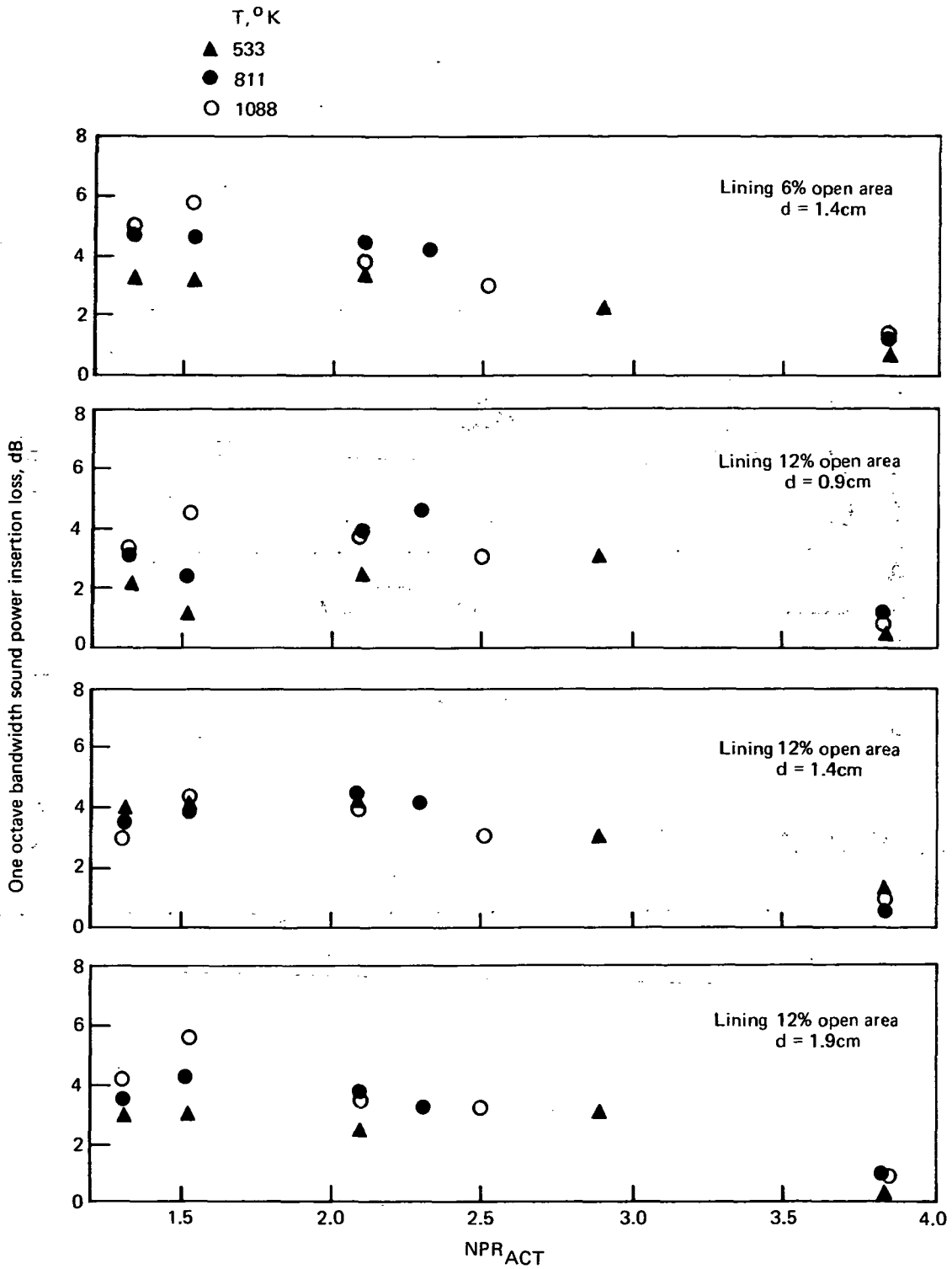
FIGURE 39.—SOUND POWER INSERTION LOSS FOR MODEL-SCALE 37-TUBE NOZZLE
WITH L/D = 1 LINED EJECTOR

133
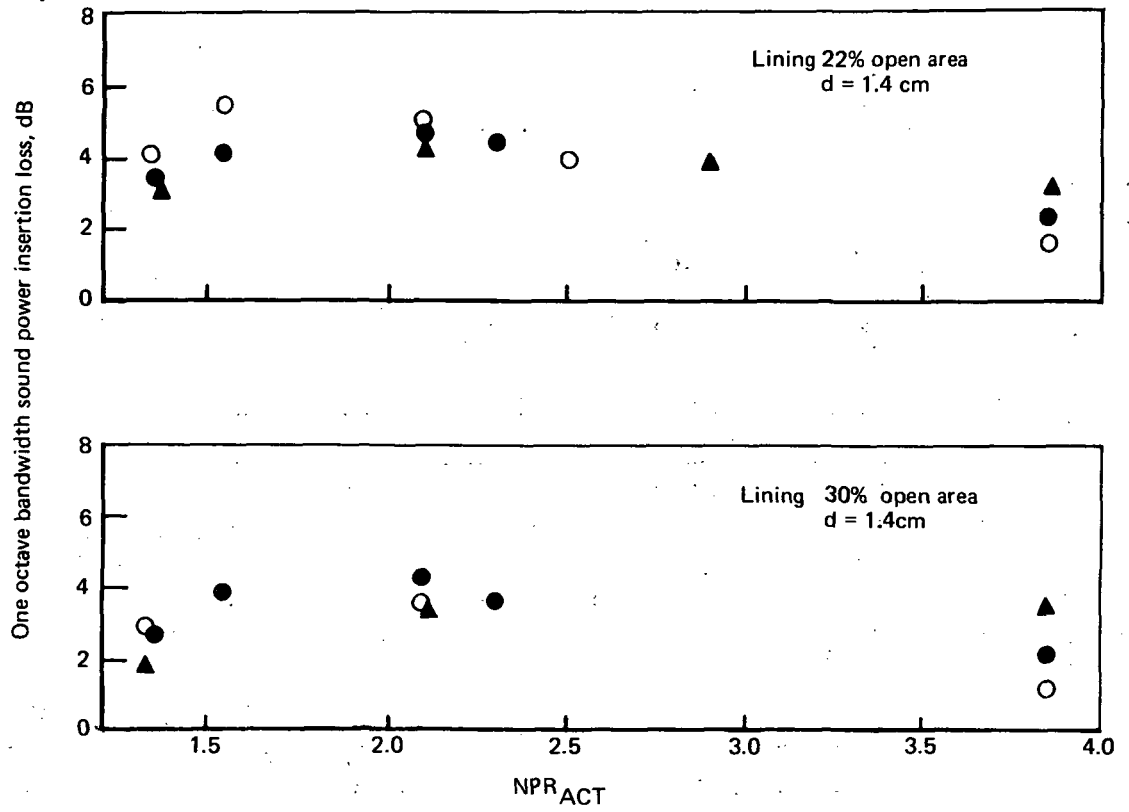
FIGURE 39.—Concluded
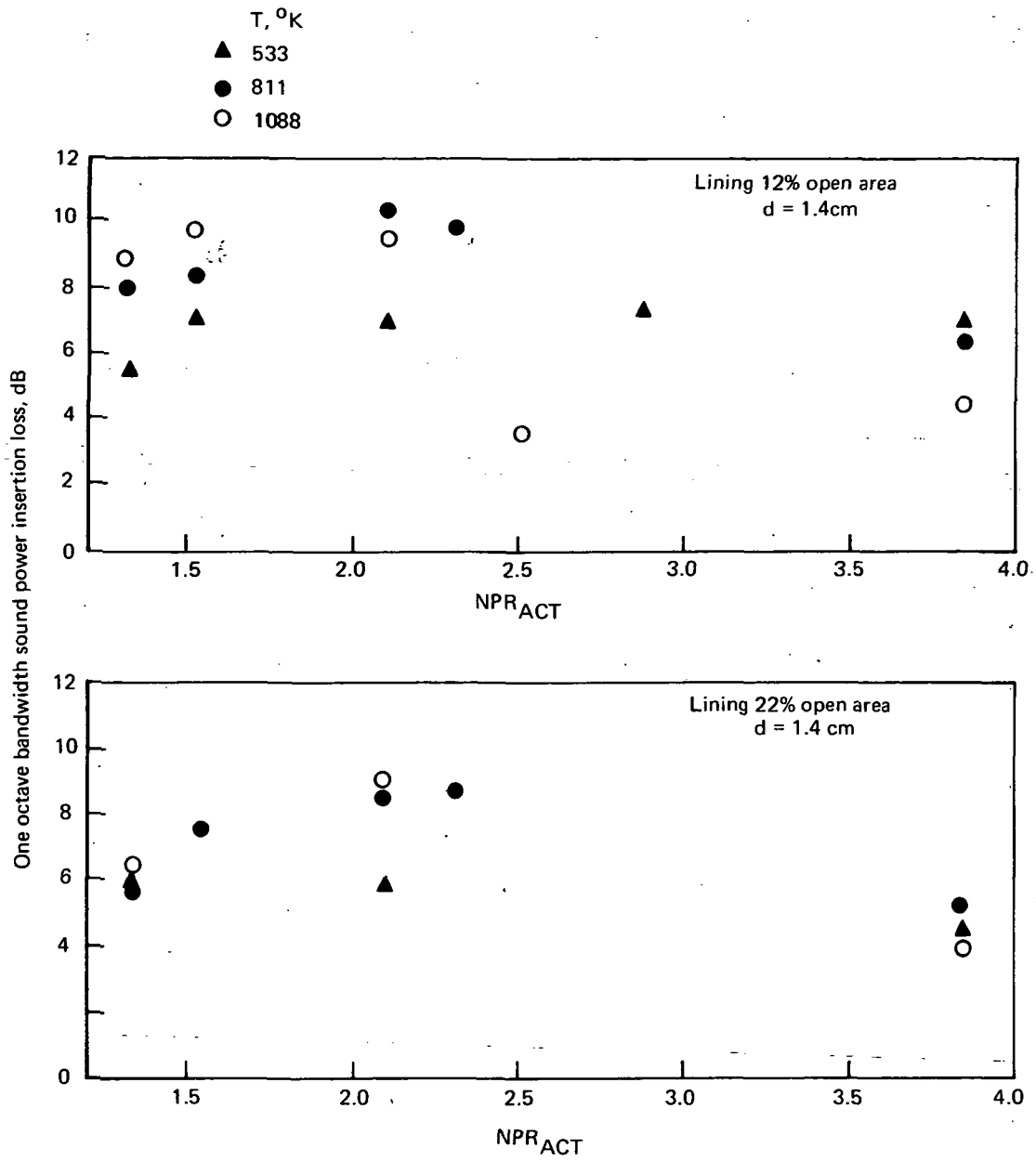
FIGURE 40.—SOUND POWER INSERTION LOSS FOR MODEL-SCALE 37-TUBE NOZZLE
WITH L/D = 2 LINED EJECTOR
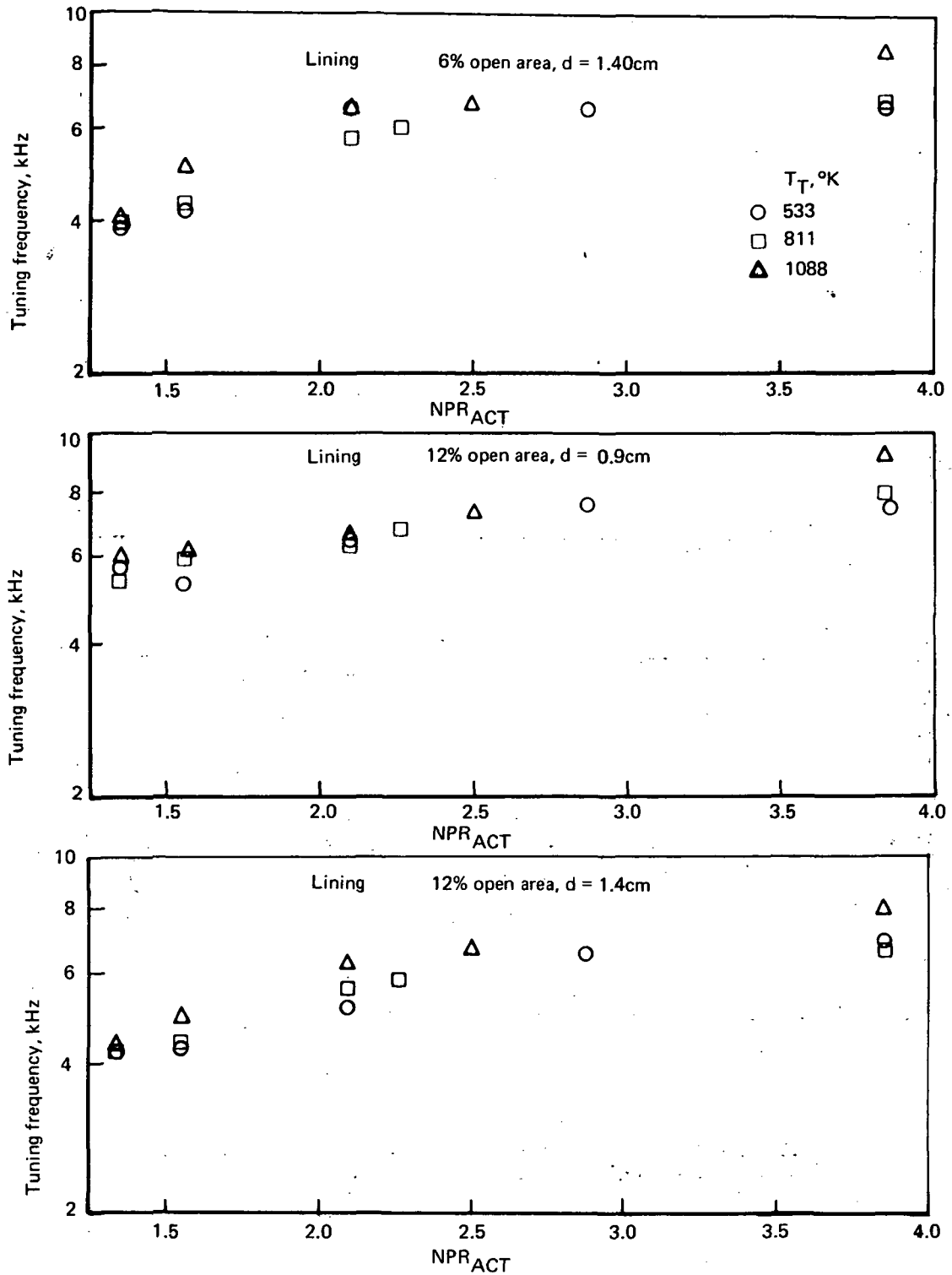
FIGURE 41.—TUNING FREQUENCIES FOR MODEL-SCALE 37-TUBE NOZZLE WITH
L/D = 1 LINED EJECTORS
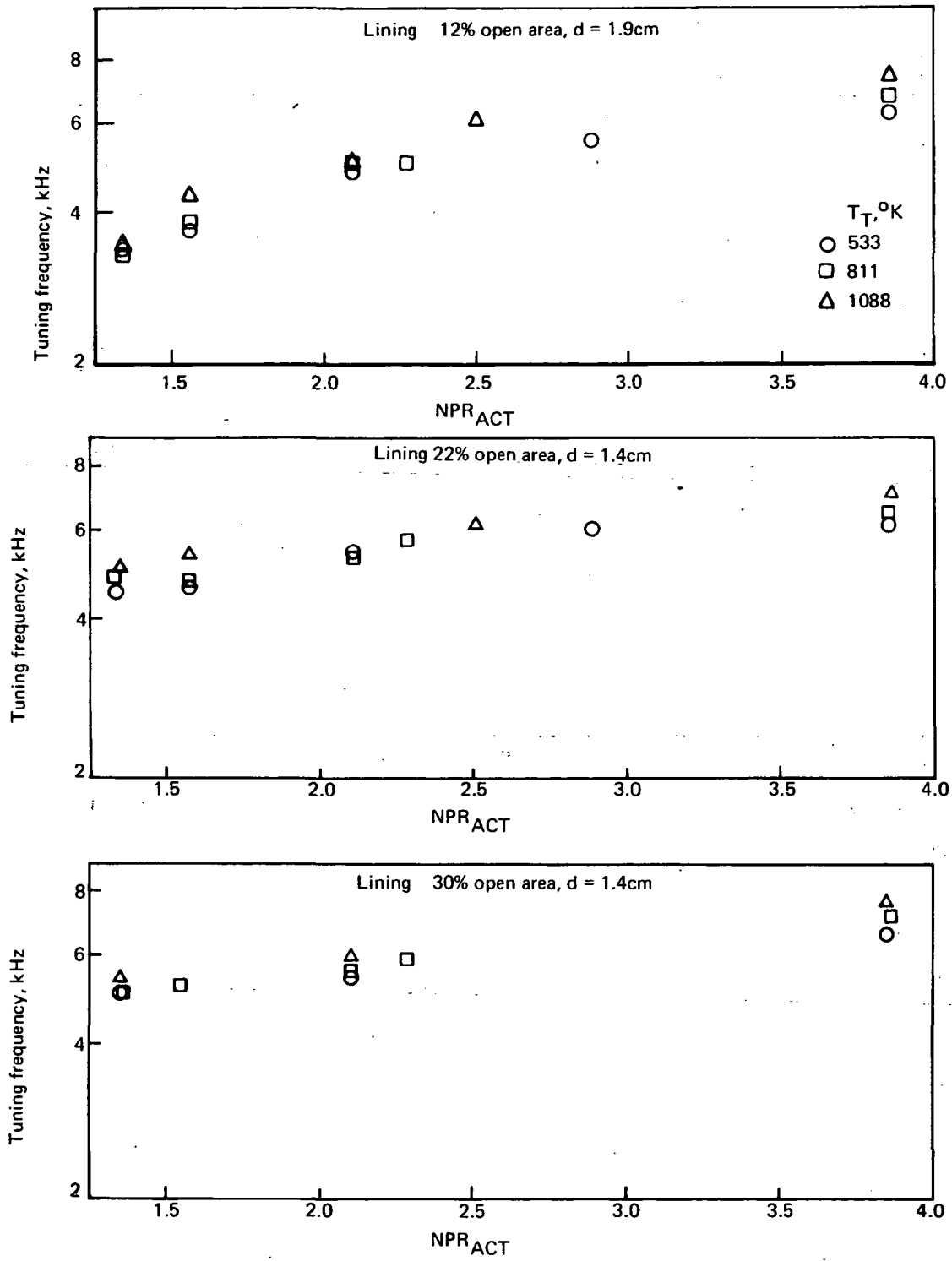
FIGURE 41.—Concluded

137
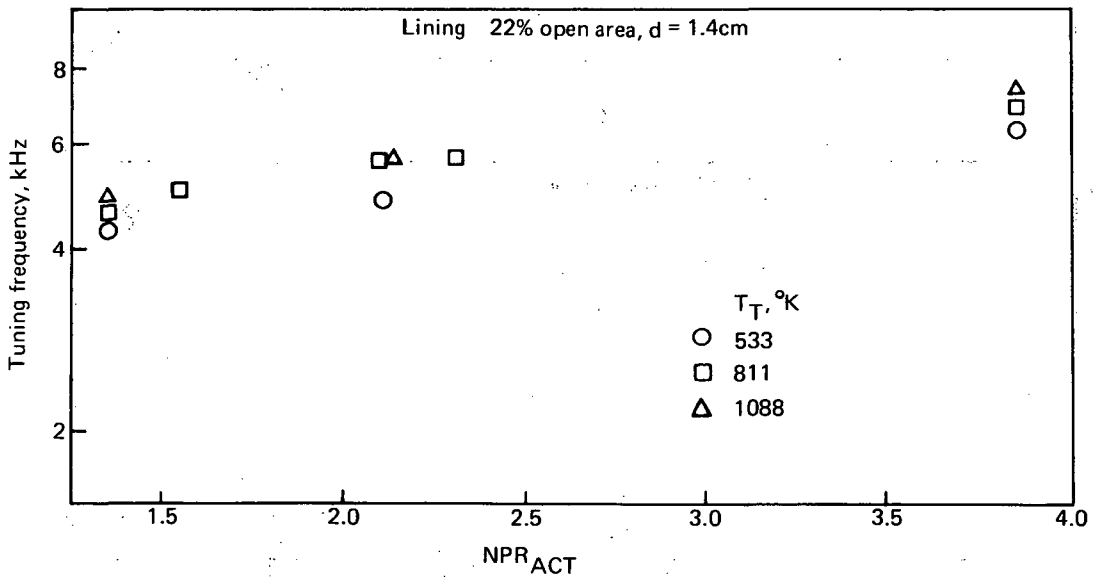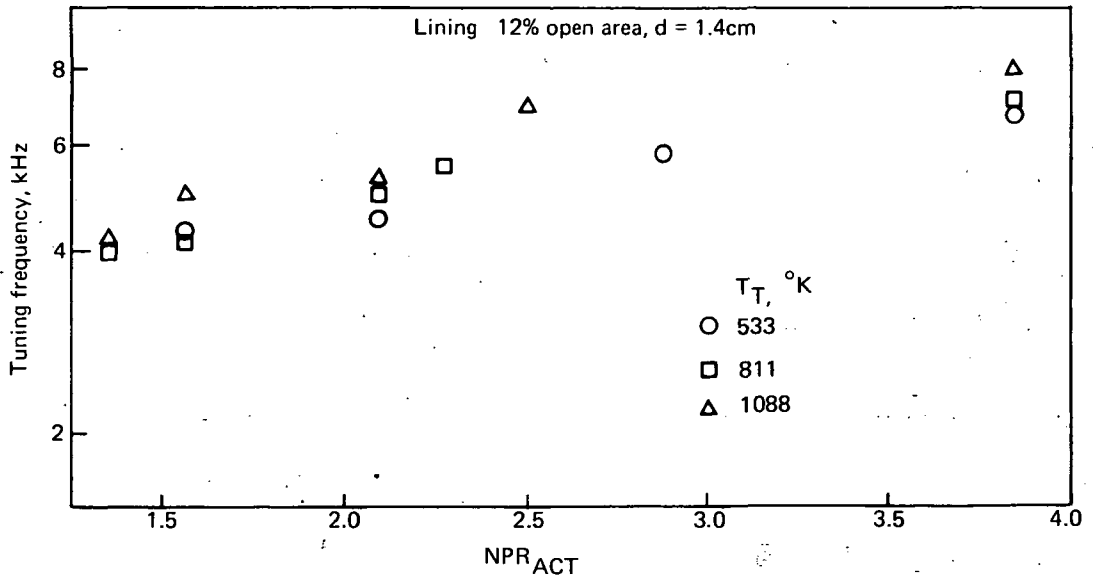
FIGURE 42.—TUNING FREQUENCIES FOR MODEL-SCALE 37-TUBE NOZZLES WITH
L/D = 2 LINED EJECTORS

	Open area, %	Core depth, cm	Ejector L/D
O	12	1.4	2
□	12	1.4	1
△	6	1.4	1
◇	22	1.4	1
●	12	1.9	1
◆	12	0.9	1
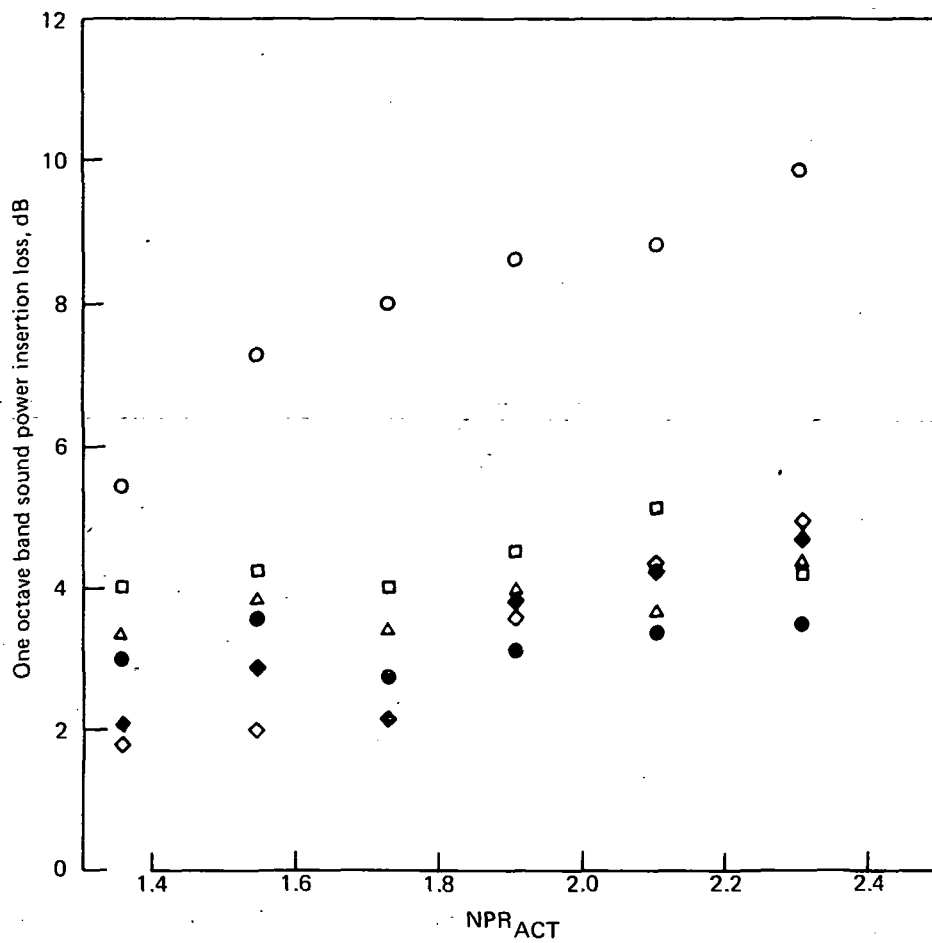
FIGURE 43.—INSERTION LOSS OF MODEL-SCALE LININGS FOR THE
J-75 ENGINE OPERATING CONDITIONS
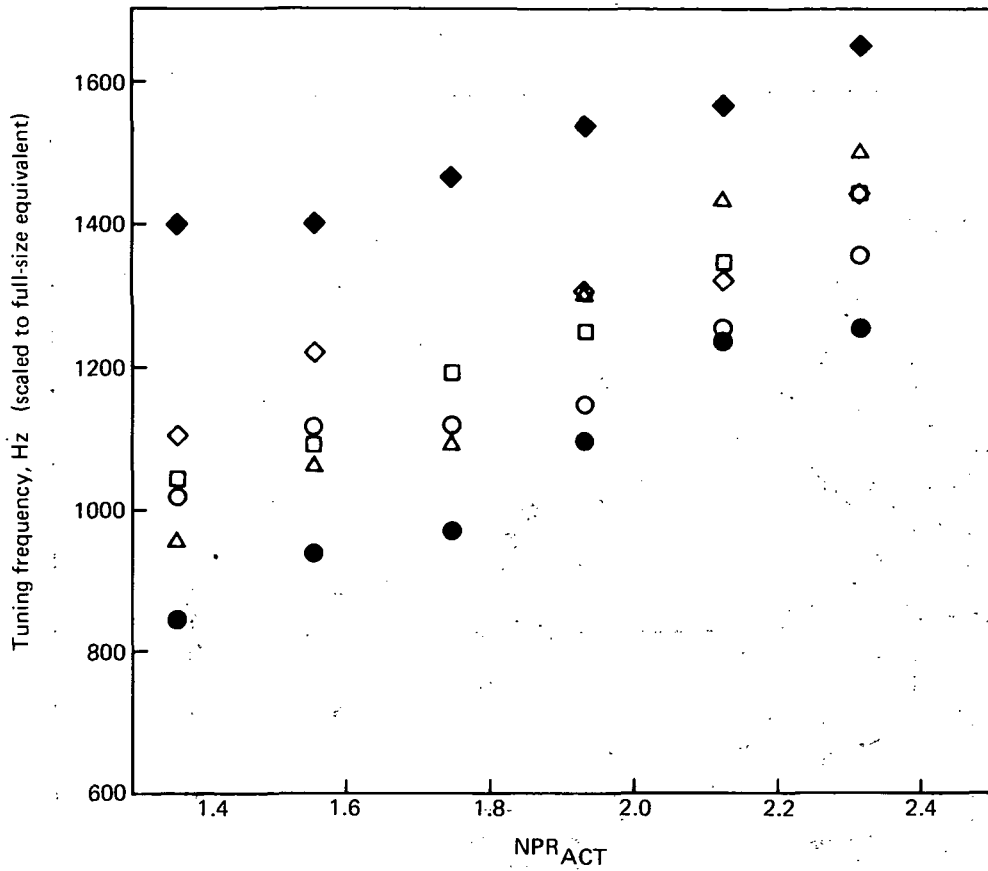
Open area, %	Scaled core depth, cm	Actual core depth, cm	L/D
○ 12	5.6	1.4	2
□ 12	5.6	1.4	1
△ 6	5.6	1.4	1
◇ 22	5.6	1.4	1
● 12	7.62	1.9	1
◆ 12	3.81	0.9	1

FIGURE 44.—TUNING FREQUENCY OF MODEL-SCALED LININGS
FOR THE J-75 ENGINE OPERATING CONDITION
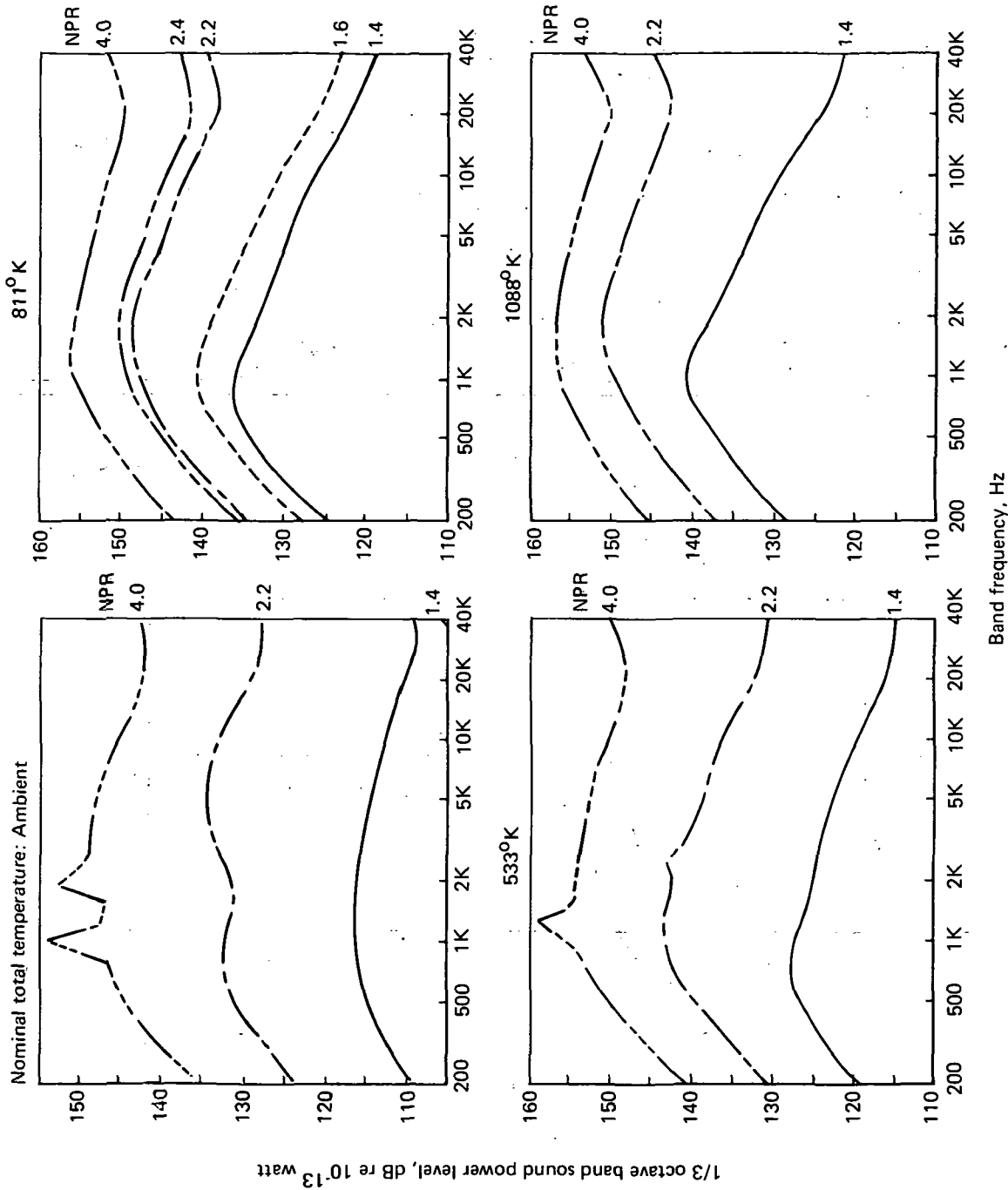
FIGURE 45.—SOUND POWER SPECTRA FOR MODEL-SCALE 10.9-CM-DIAMETER CONICAL NOZZLE

141
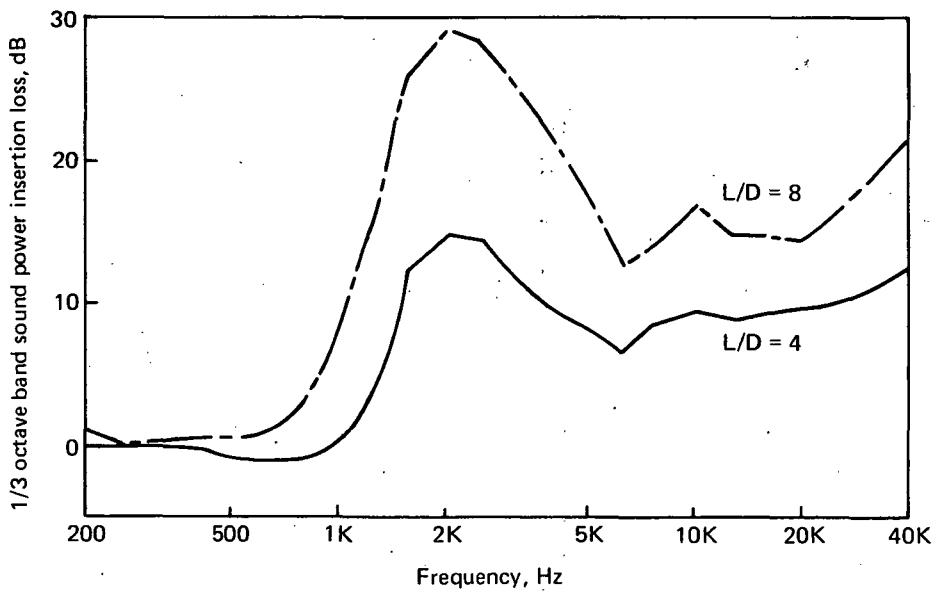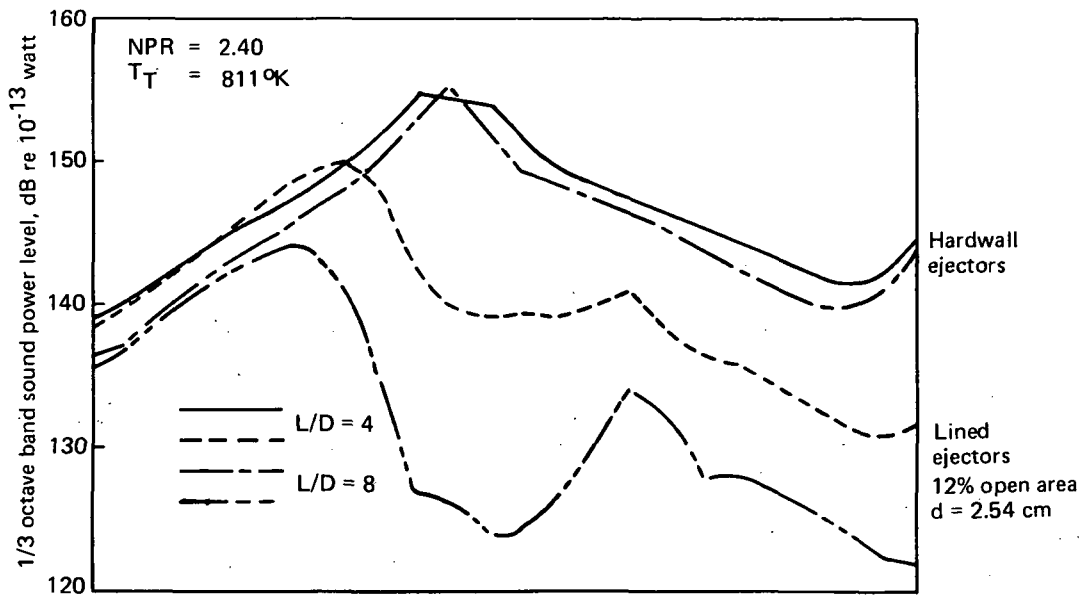
FIGURE 46.—COMPARISON OF THE ACOUSTIC PERFORMANCE OF LINED AND HARDWALL
EJECTORS WITH THE 10.9-CM-DIAMETER NOZZLE

142
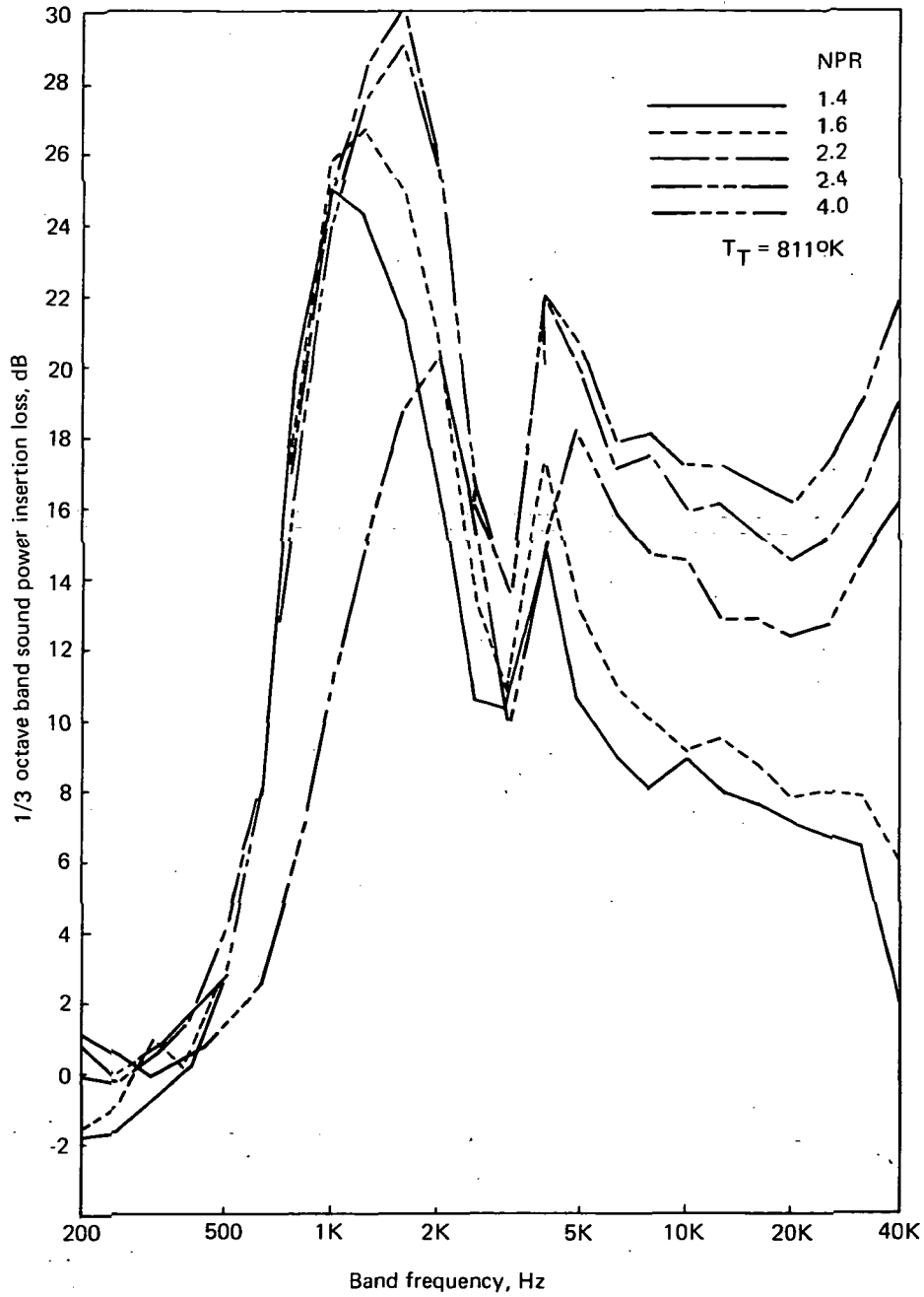
FIGURE 47.—SOUND POWER INSERTION LOSS SPECTRA WITH 12% OPEN AREA LINING
IN THE L/D = 8 EJECTOR AND 10.9-CM-DIAMETER NOZZLE (d = 5.85 CM)
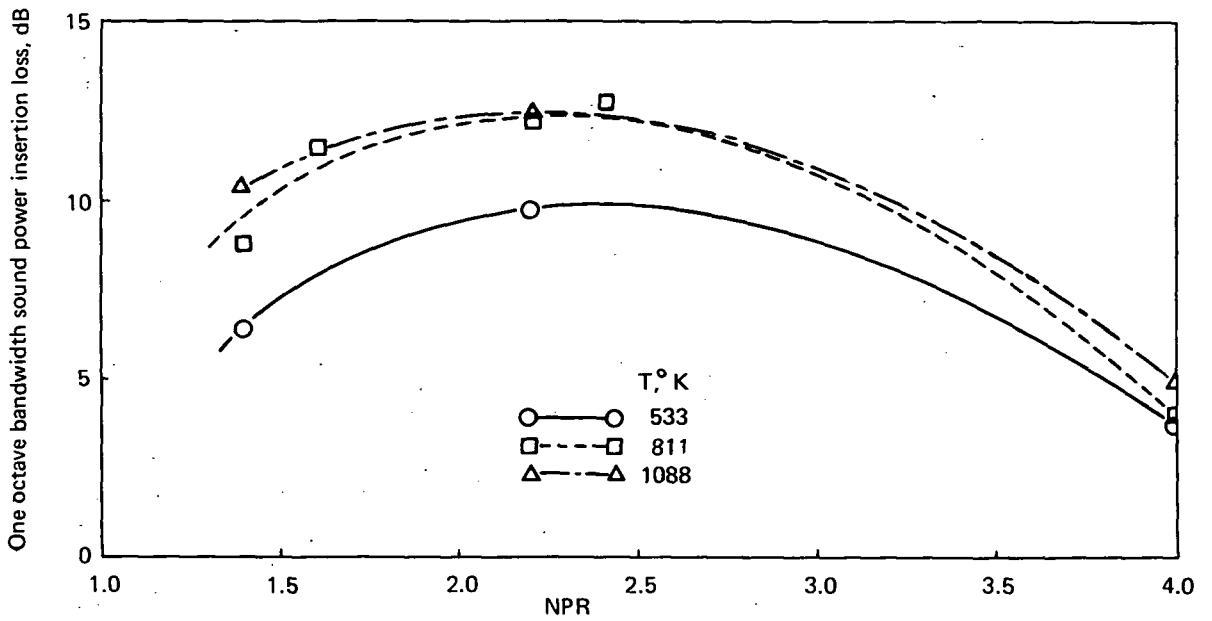
FIGURE 48.—SOUND POWER INSERTION LOSS WITH 12% OPEN AREA LINING IN THE L/D = 4 EJECTOR AND 10.9-CM-DIAMETER NOZZLE (d = 2.54 CM)
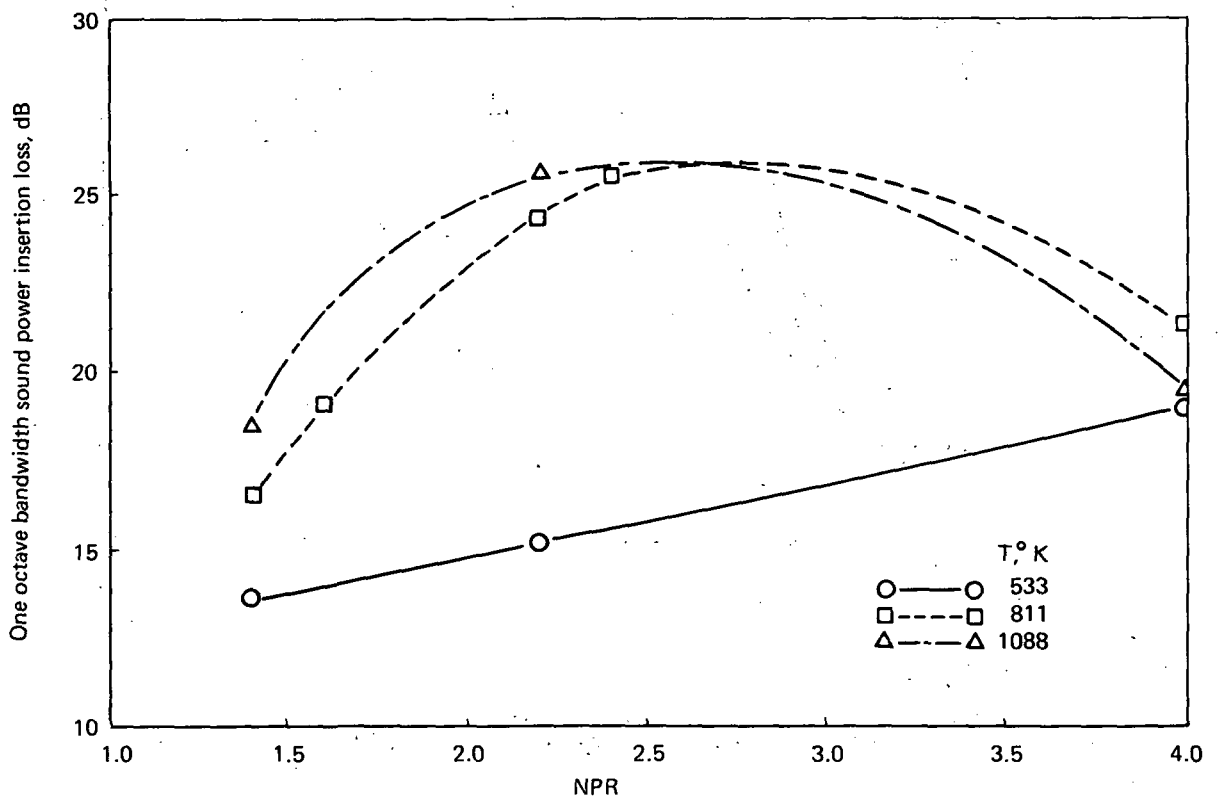
FIGURE 49.—SOUND POWER INSERTION LOSS WITH 12% OPEN AREA LINING IN THE L/D = 8 EJECTOR AND 10.9-CM-DIAMETER NOZZLE (d = 2.54CM)

144
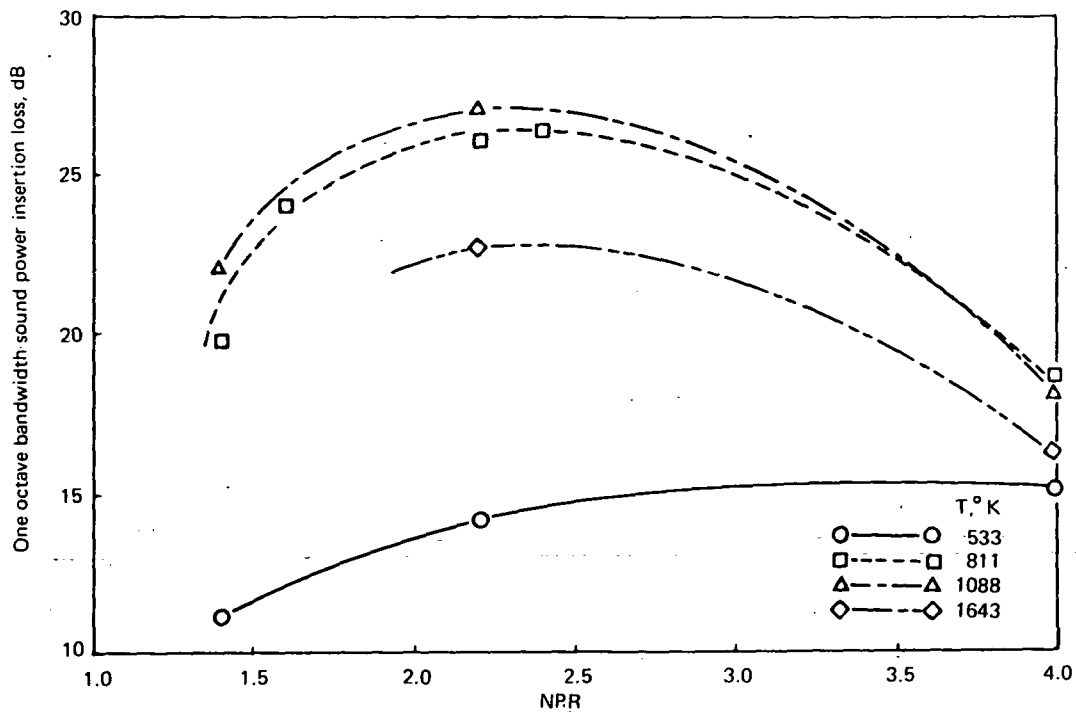
FIGURE 50.—SOUND POWER INSERTION LOSS WITH 12% OPEN AREA LINING IN THE L/D = 8 EJECTOR AND 10.9-CM-DIAMETER NOZZLE (d = 3.81CM)
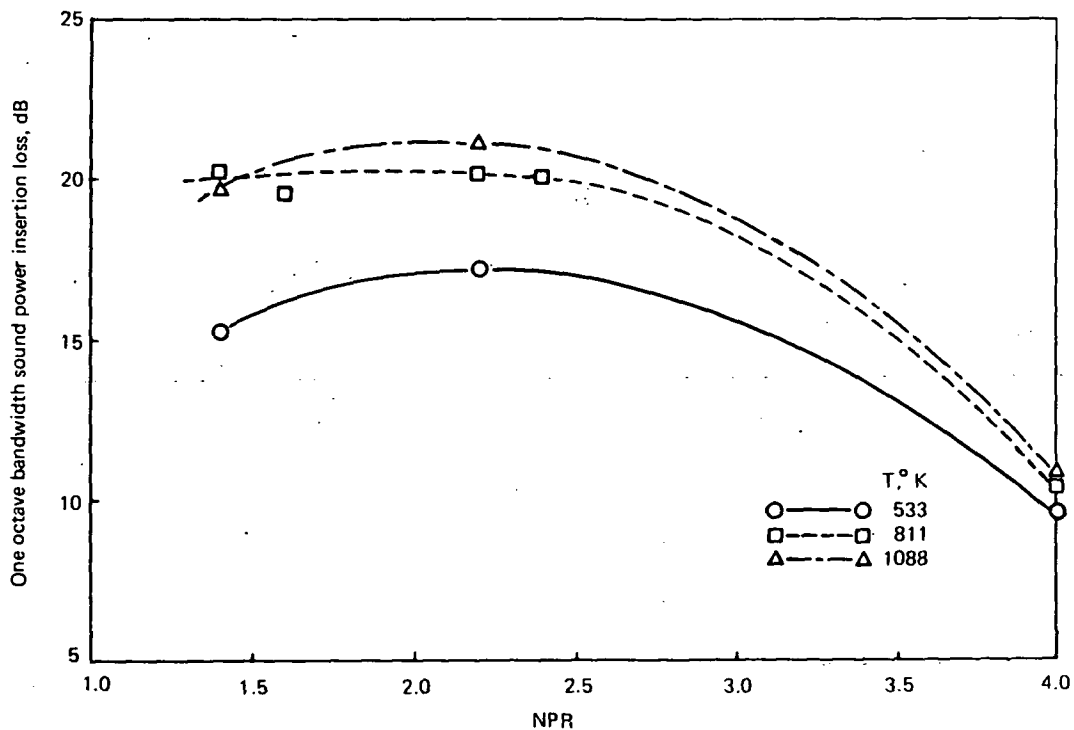
FIGURE 51.—SOUND POWER INSERTION LOSS WITH 12% OPEN AREA LINING IN THE L/D = 8 EJECTOR AND 10.9-CM-DIAMETER NOZZLE (d = 8.6CM)

145
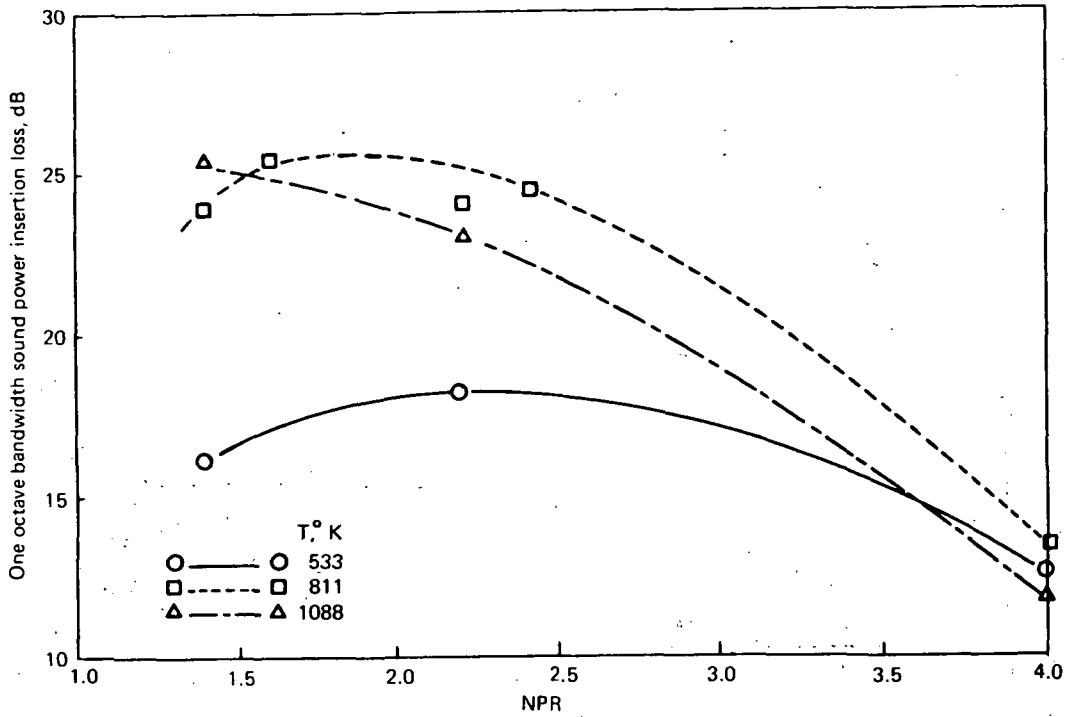
FIGURE 52.—SOUND POWER INSERTION LOSS WITH 6% OPEN AREA LINING IN THE L/D = 8 EJECTOR AND 10.9-CM-DIAMETER NOZZLE (d = 5.85CM)
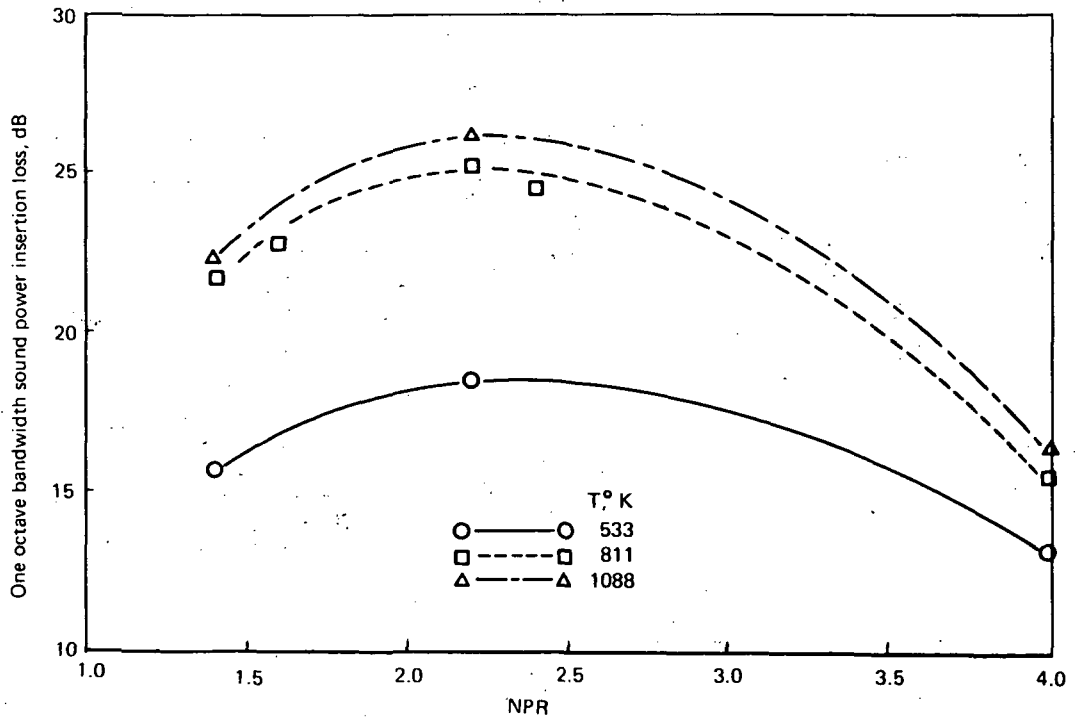
FIGURE 53.—SOUND POWER INSERTION LOSS WITH 12% OPEN AREA LINING IN THE L/D = 8 EJECTOR AND 10.9-CM-DIAMETER NOZZLE (d = 5.85CM)

146
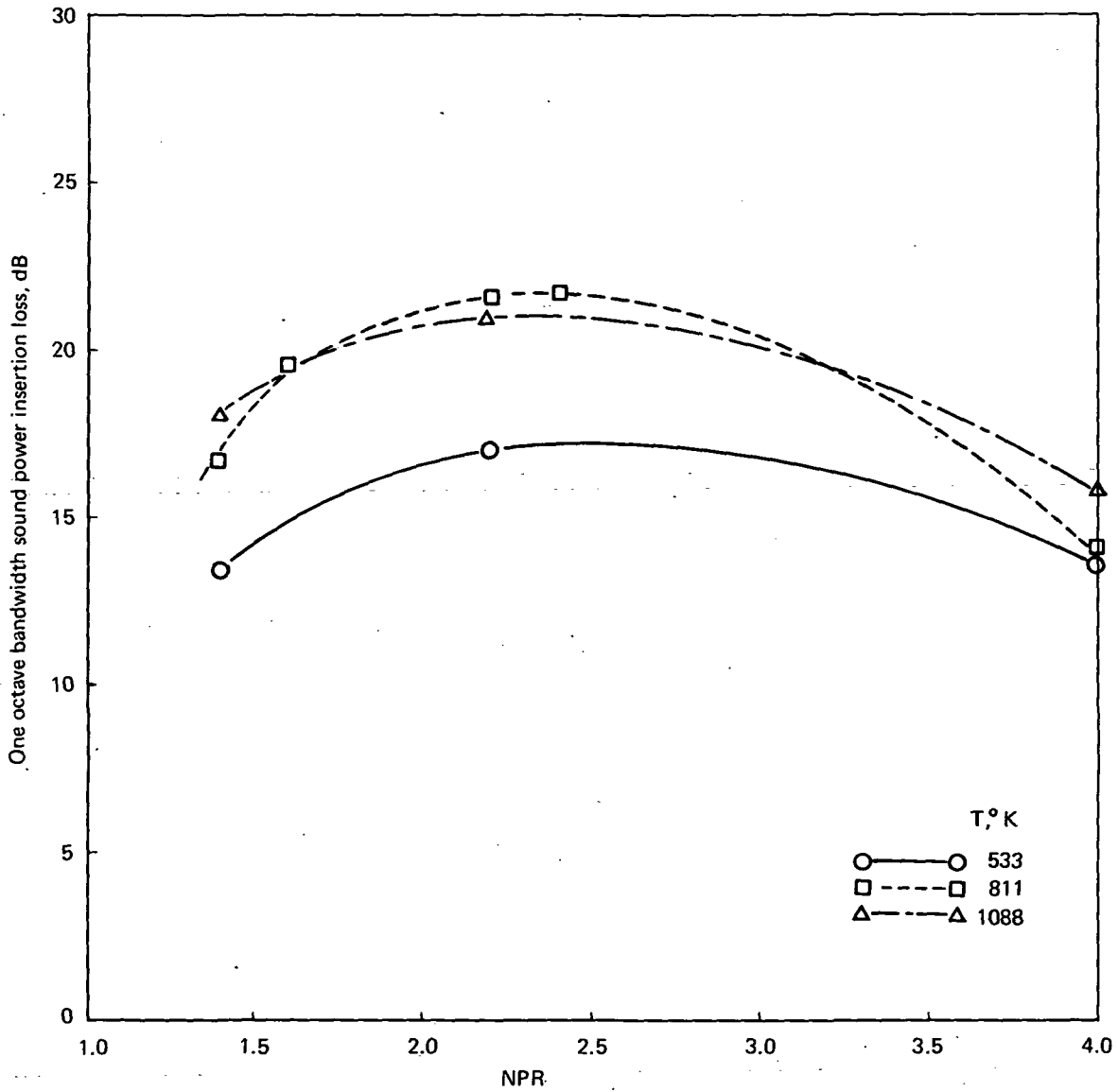
FIGURE 54.—SOUND POWER INSERTION LOSS WITH 22% OPEN AREA LINING IN THE L/D = 8 EJECTOR AND 10.9-CM-DIAMETER NOZZLE (d = 5.85 CM)
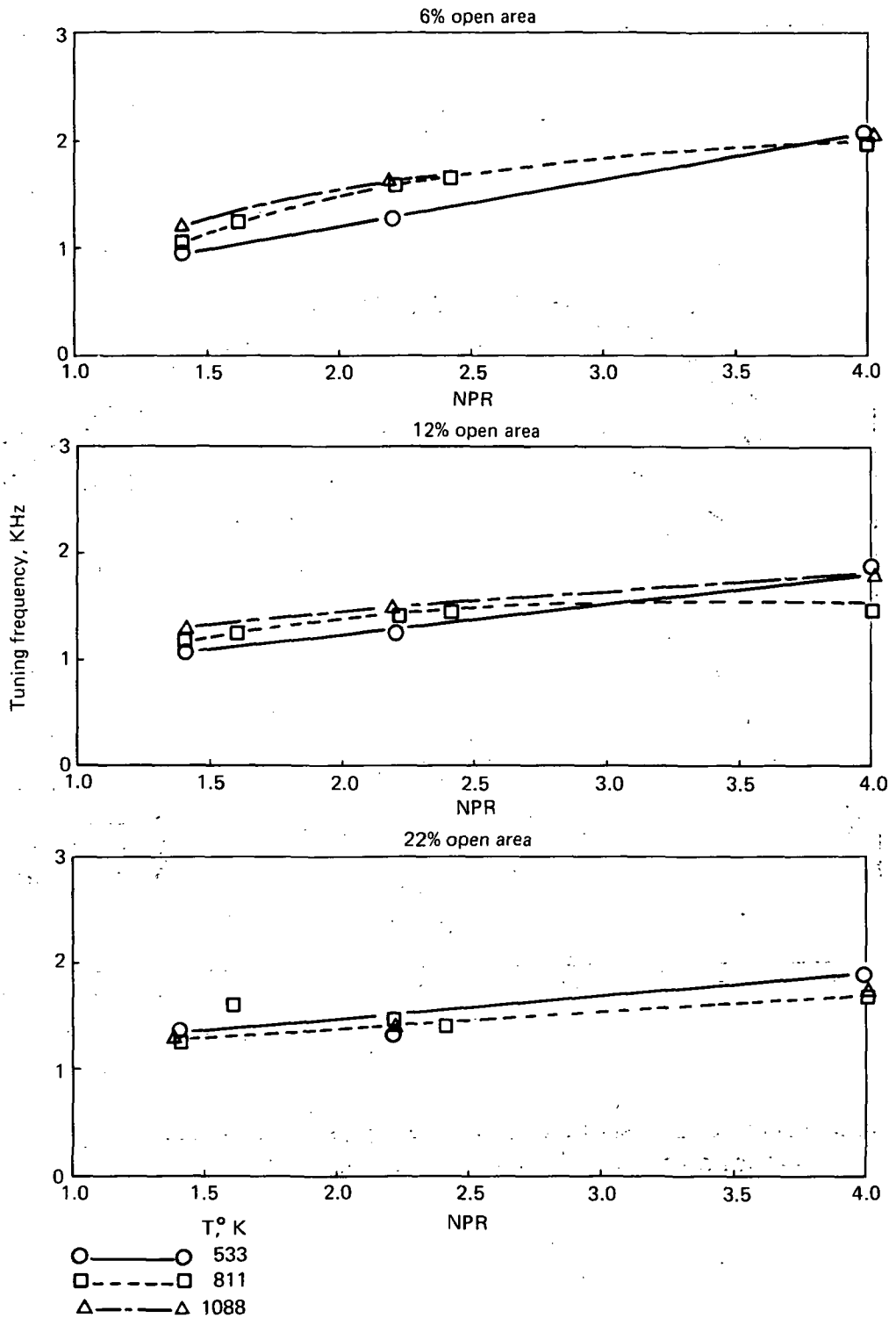
FIGURE 55.—TUNING FREQUENCY FOR 5.85-CM-DEEP LININGS IN THE L/D = 8 EJECTOR AND 10.9-CM-DIAMETER NOZZLE
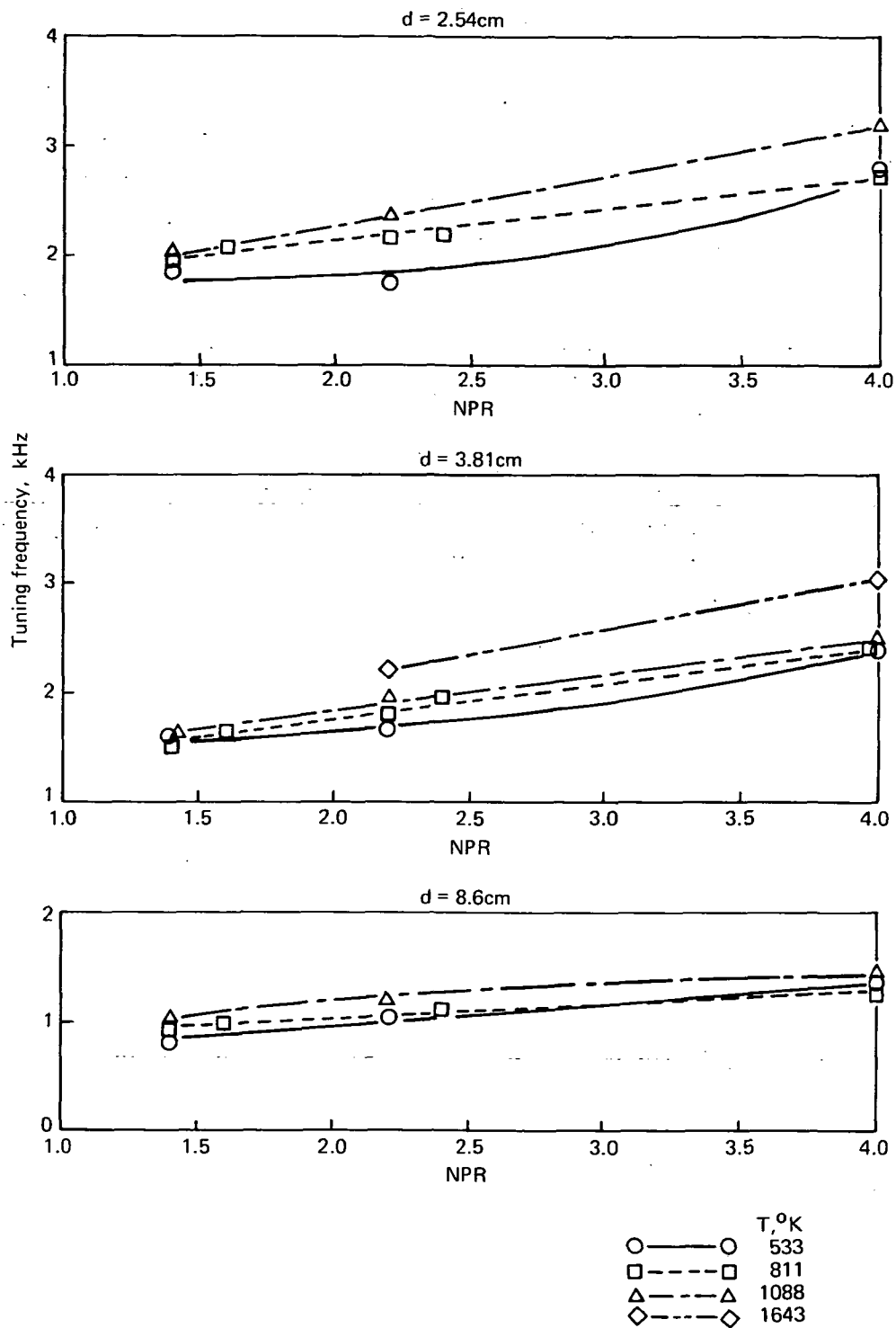
FIGURE 56.—TUNING FREQUENCY FOR 12% OPEN AREA LININGS IN THE L/D = 8 EJECTOR
AND 10.9-CM-DIAMETER NOZZLE
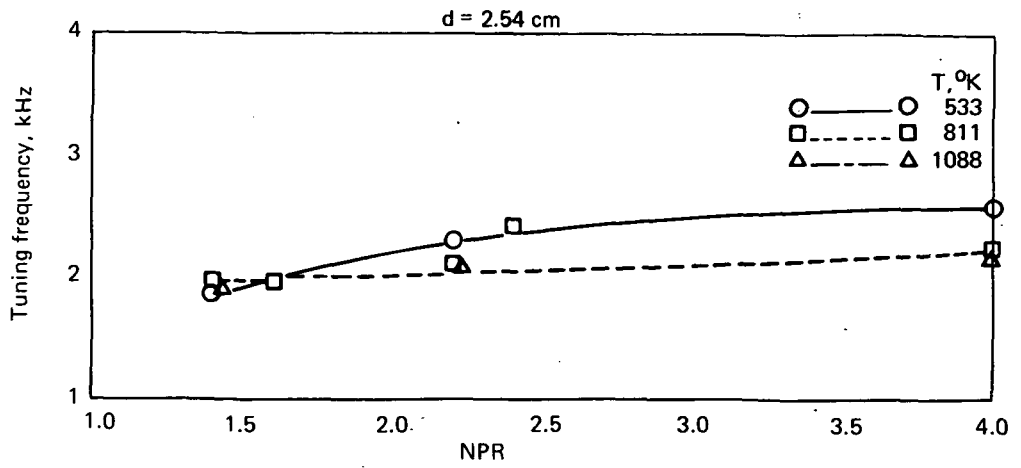
FIGURE 57.–TUNING FREQUENCY FOR 12% OPEN AREA LINING IN THE L/D = 4 EJECTOR
AND 10.9-CM-DIAMETER NOZZLE
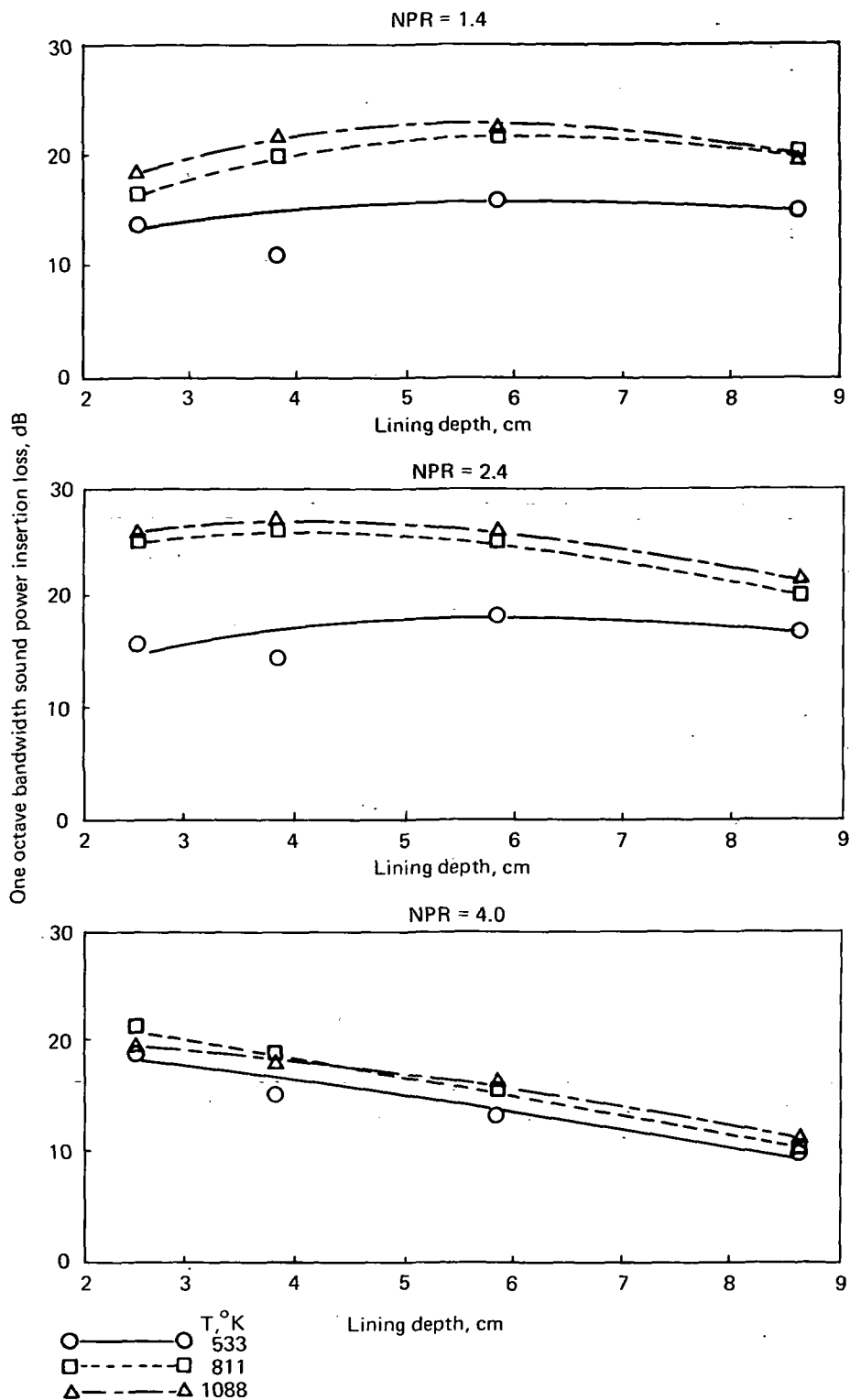
FIGURE 58.—SOUND POWER INSERTION LOSS AS A FUNCTION OF LINING DEPTH FOR 12% OPEN AREA LININGS IN THE L/D = 8 EJECTOR AND 10.9-CM-DIAMETER NOZZLE
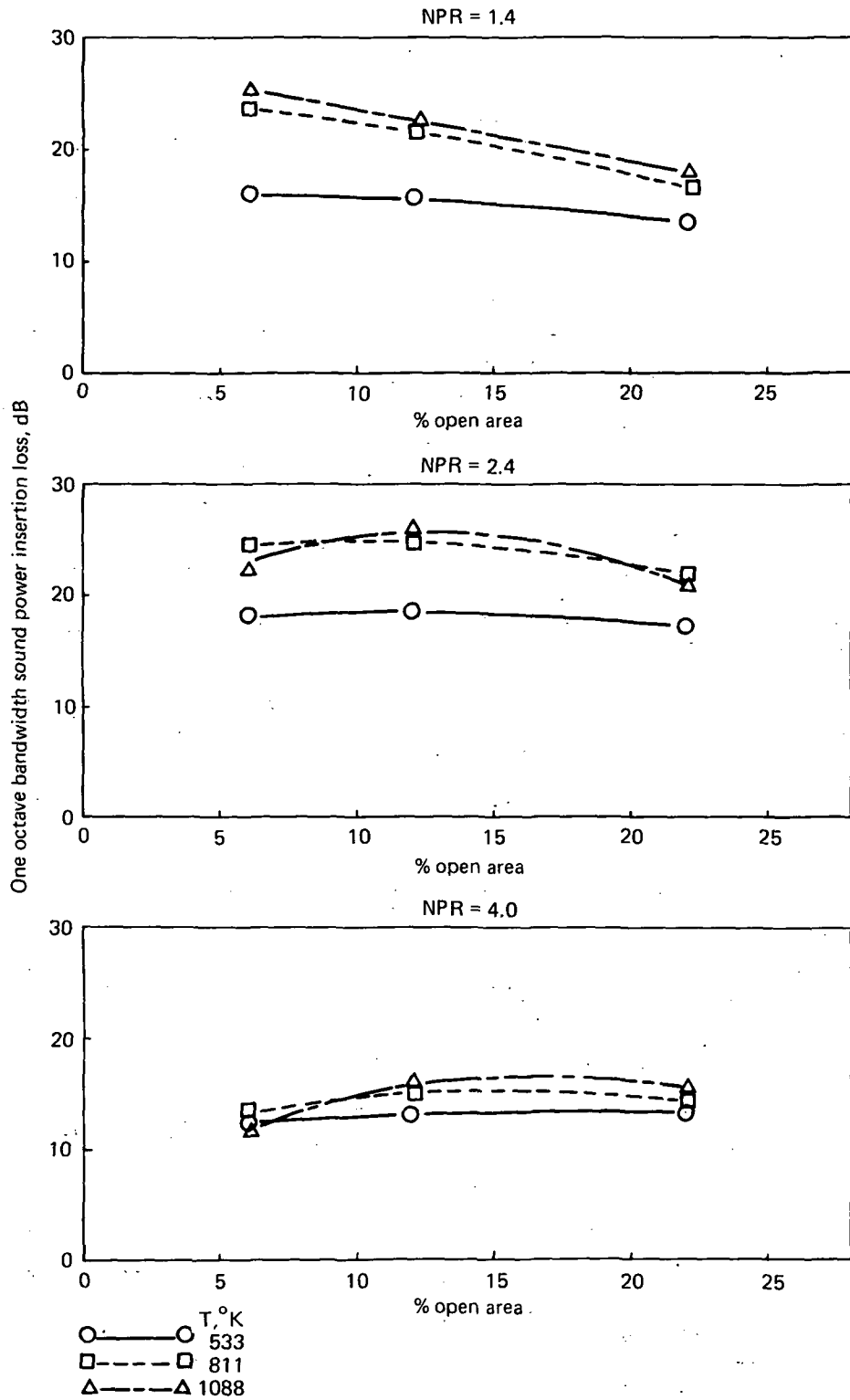
FIGURE 59.—SOUND POWER INSERTION LOSS AS A FUNCTION OF LINING % OPEN AREA FOR 5.85-CM-DEEP LININGS IN THE L/D = 8 EJECTOR AND 10.9-CM-DIAMETER NOZZLE
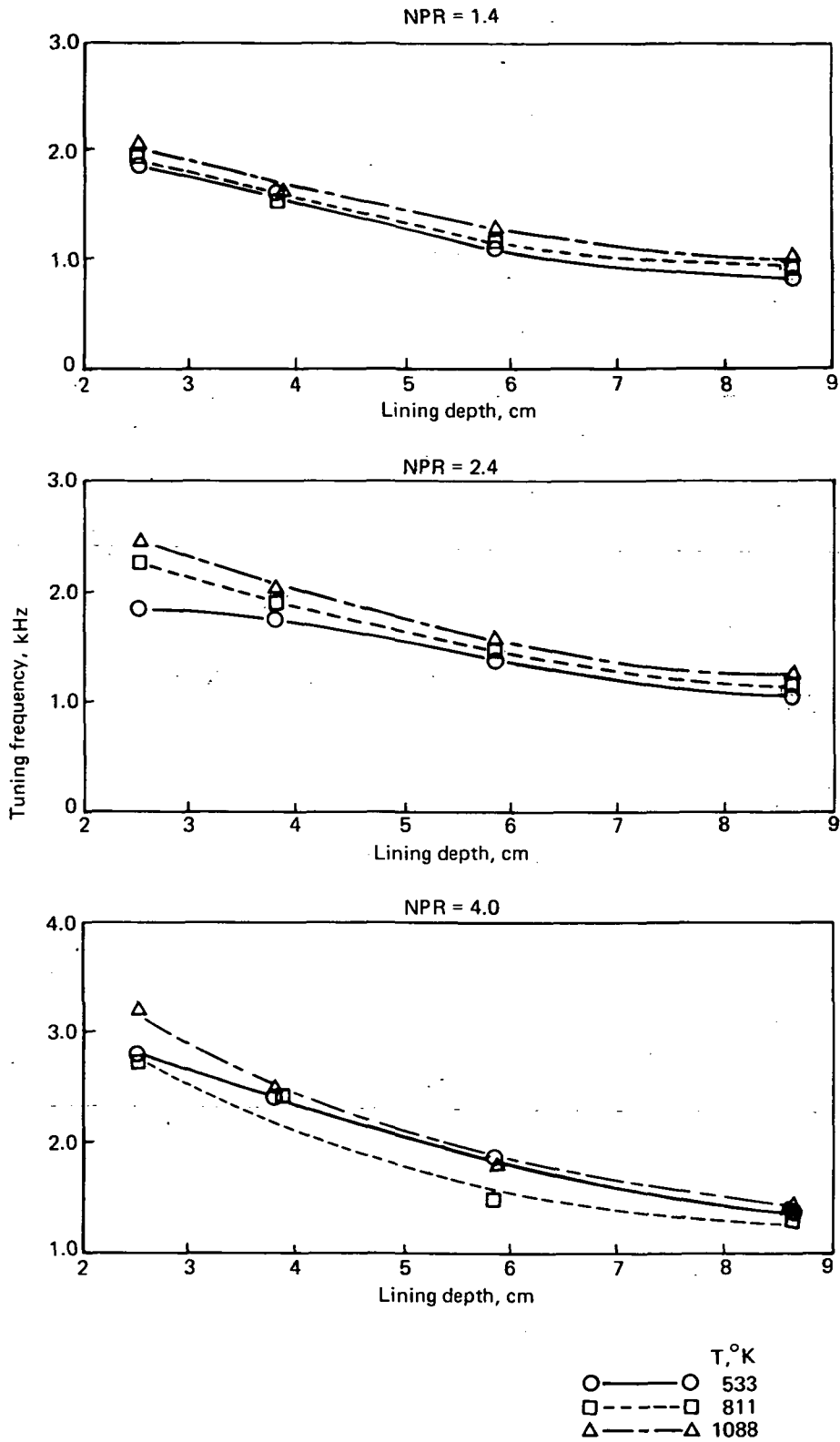
FIGURE 60.–TUNING FREQUENCY AS A FUNCTION OF LINING DEPTH FOR 12% OPEN AREA LININGS IN THE L/D = 8 EJECTOR AND 10.9-CM-DIAMETER NOZZLE

153
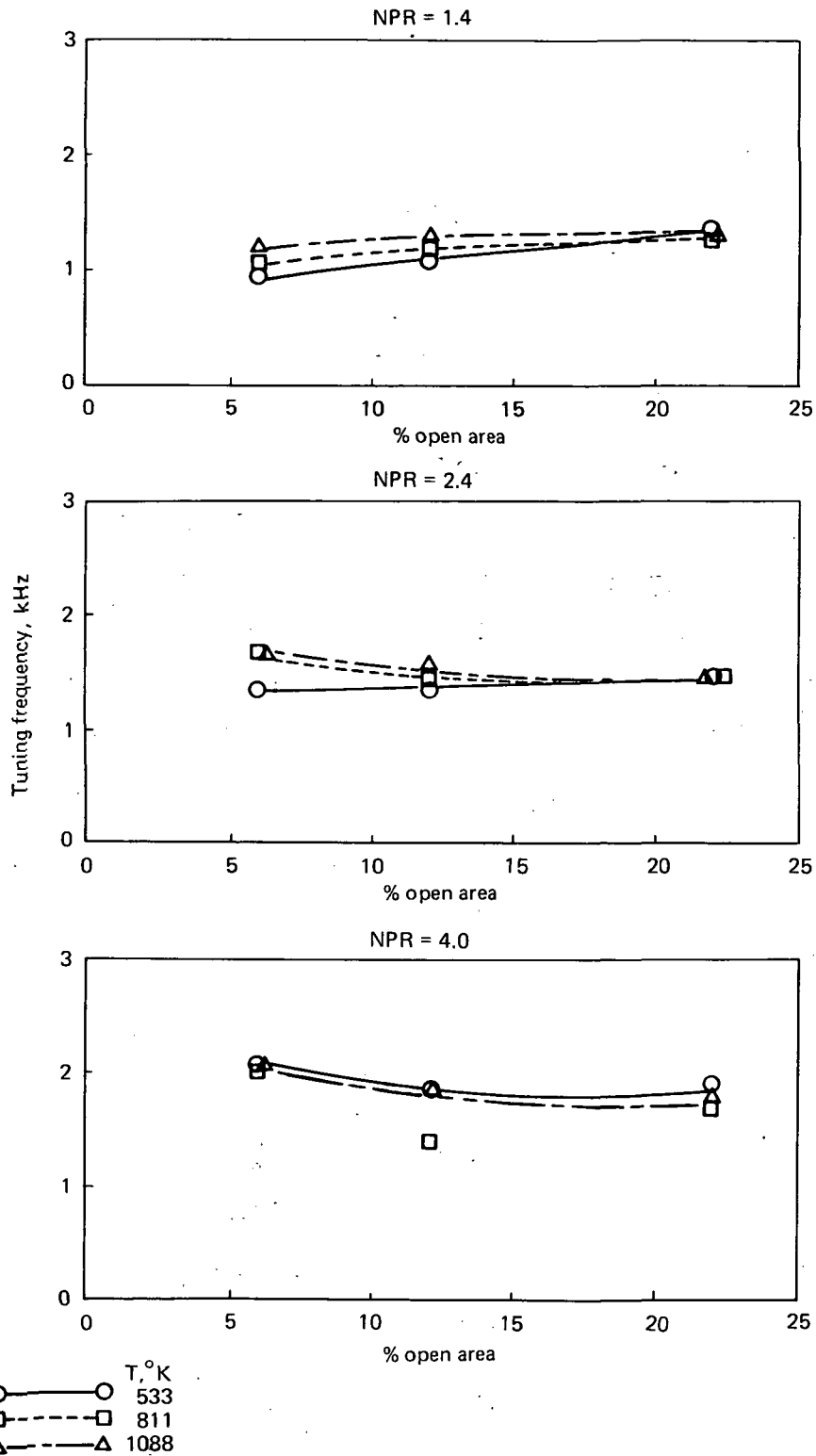
FIGURE 61.—TUNING FREQUENCY AS A FUNCTION OF LINING % OPEN AREA FOR 5.85-CM-DEEP LININGS IN THE L/D = 8 EJECTOR AND 10.9-CM-DIAMETER NOZZLE
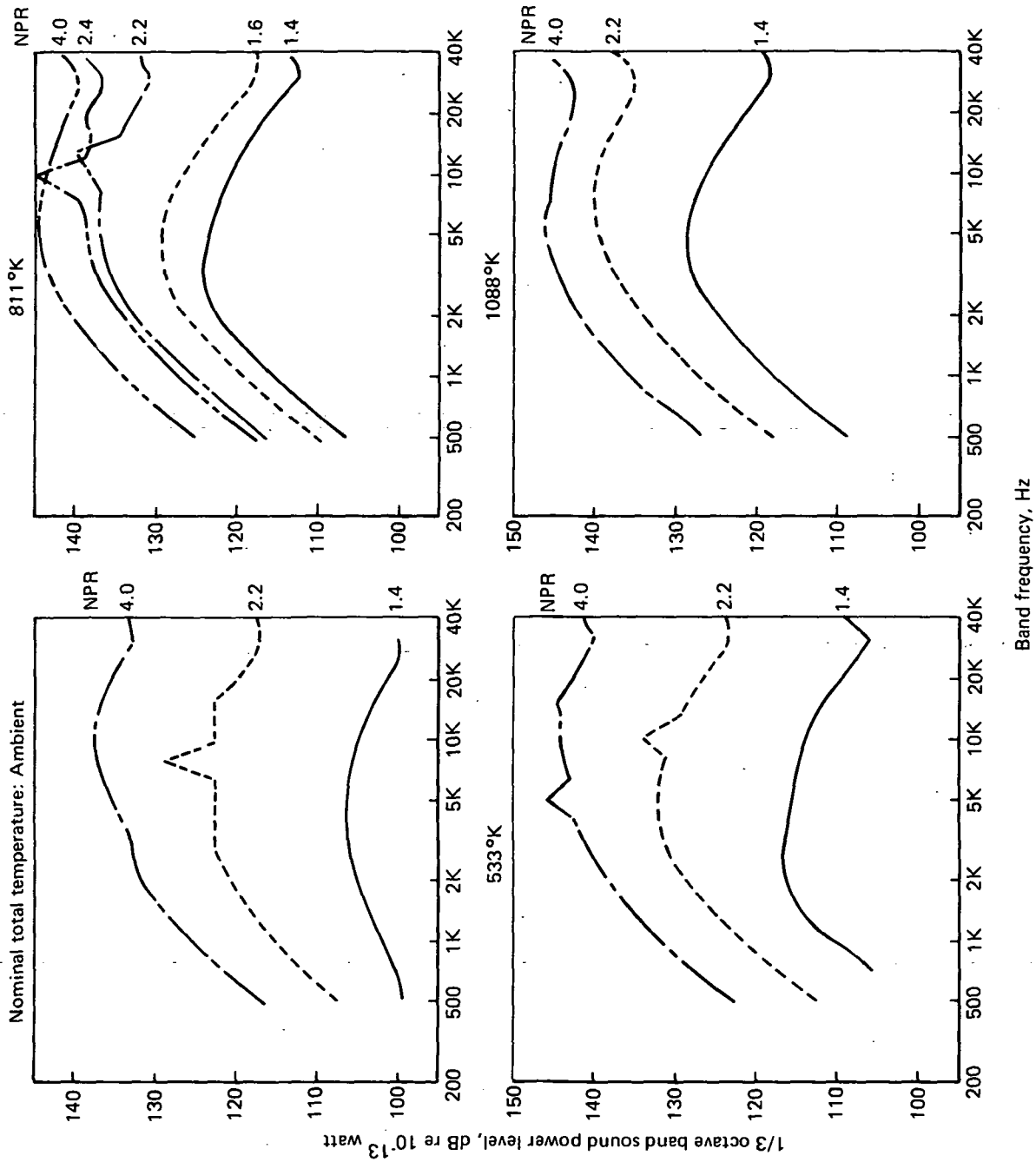
FIGURE 62.—SOUND POWER SPECTRA FOR THE MODEL-SCALE 2.74-CM-DIAMETER CONICAL NOZZLE

155
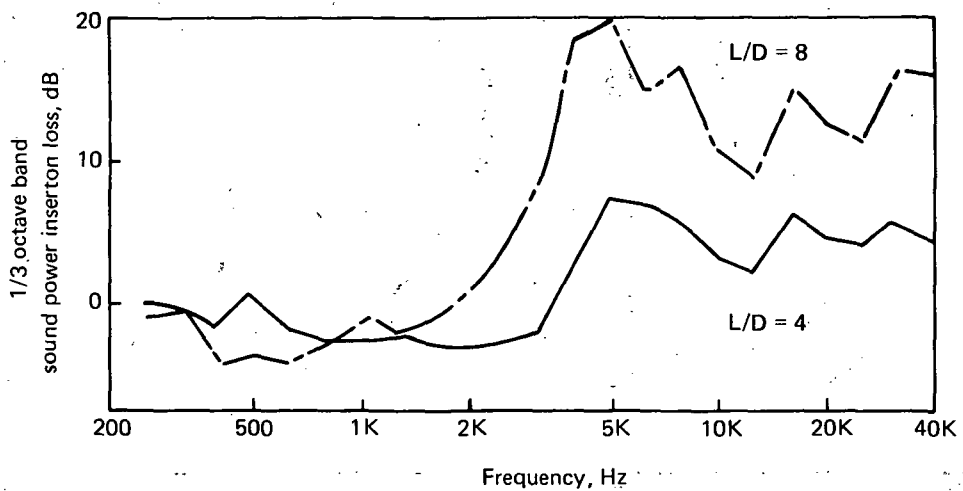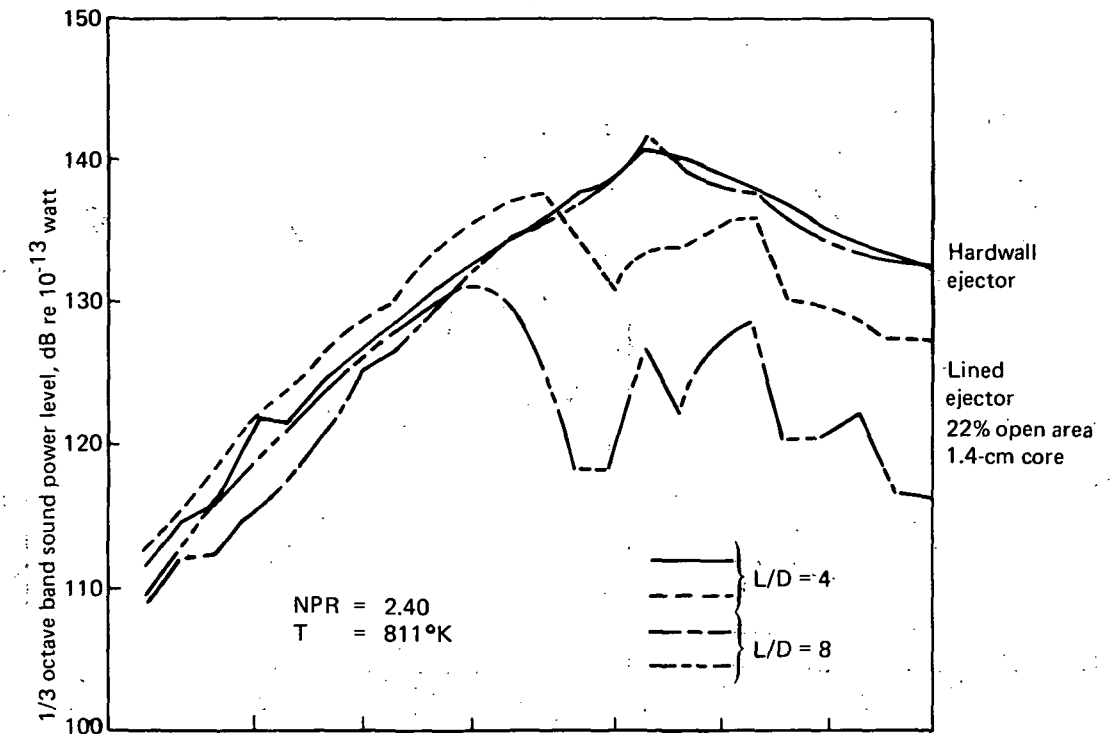
FIGURE 63.—COMPARISON OF THE ACOUSTIC PERFORMANCE OF LINED AND HARDWALL
EJECTORS WITH THE 2.74-CM-DIAMETER NOZZLE

156
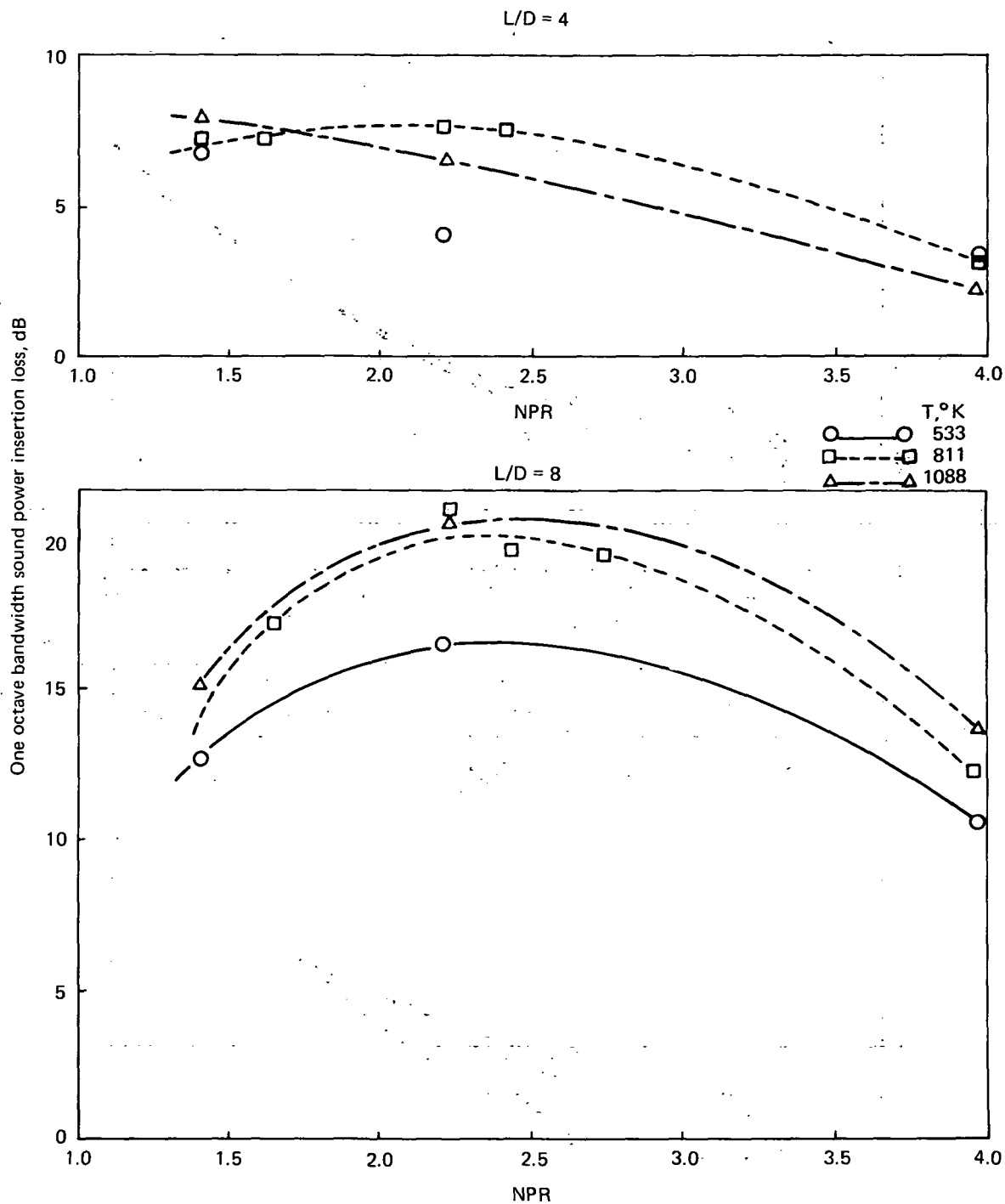
FIGURE 64.–SOUND POWER INSERTION LOSS WITH 22% OPEN AREA LININGS IN THE L/D = 4 AND
L/D = 8 EJECTORS AND 2.74-CM-DIAMETER NOZZLE (d = 1.4 CM)

157
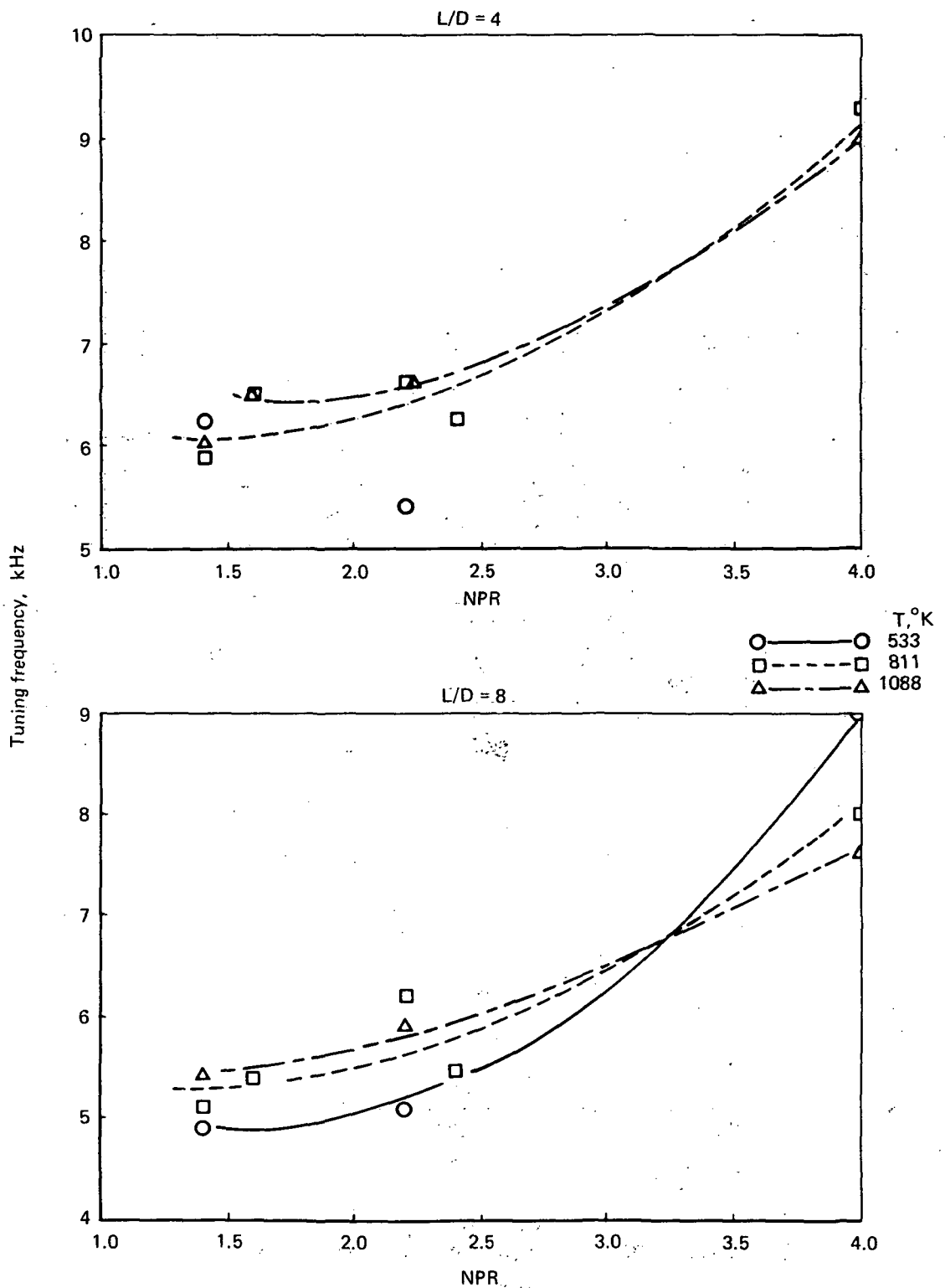
FIGURE 65.—TUNING FREQUENCY FOR 22% OPEN AREA LININGS IN THE L/D = 4 AND
L/D = 8 EJECTORS AND 2.74-CM-DIAMETER NOZZLE (d = 1.4 CM)
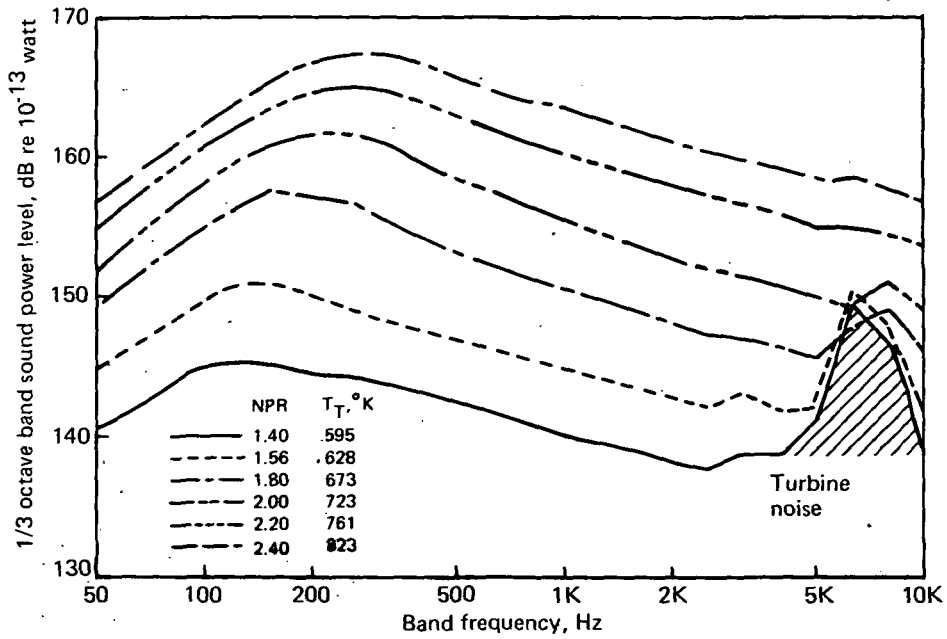
FIGURE 66.—SOUND POWER SPECTRA FOR THE J-75 ENGINE WITH REFERENCE CONICAL NOZZLE
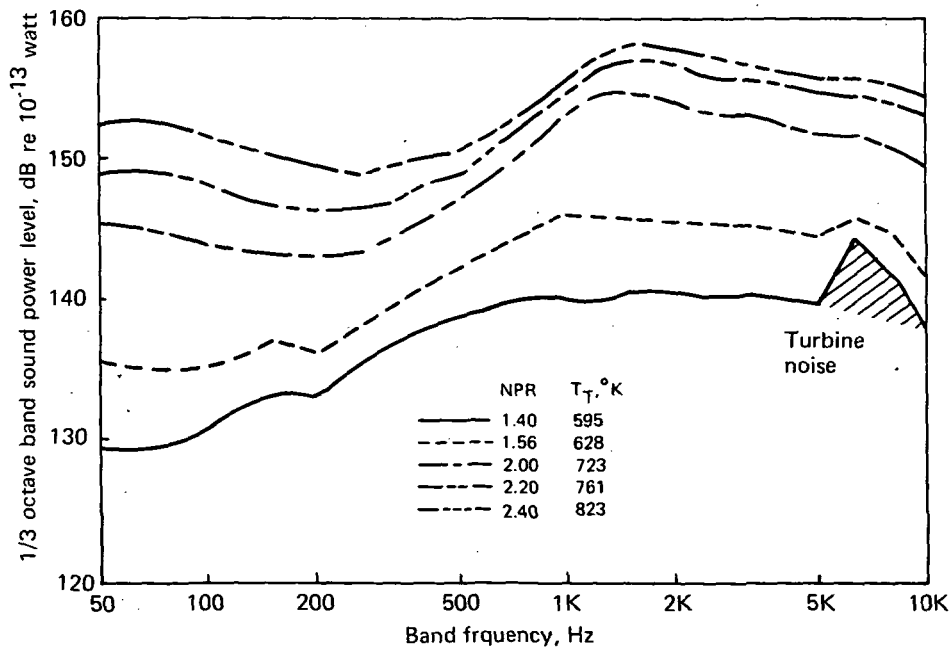
FIGURE 67.—SOUND POWER SPECTRA FOR THE J-75 ENGINE WITH 37-TUBE SUPPRESSOR NOZZLE
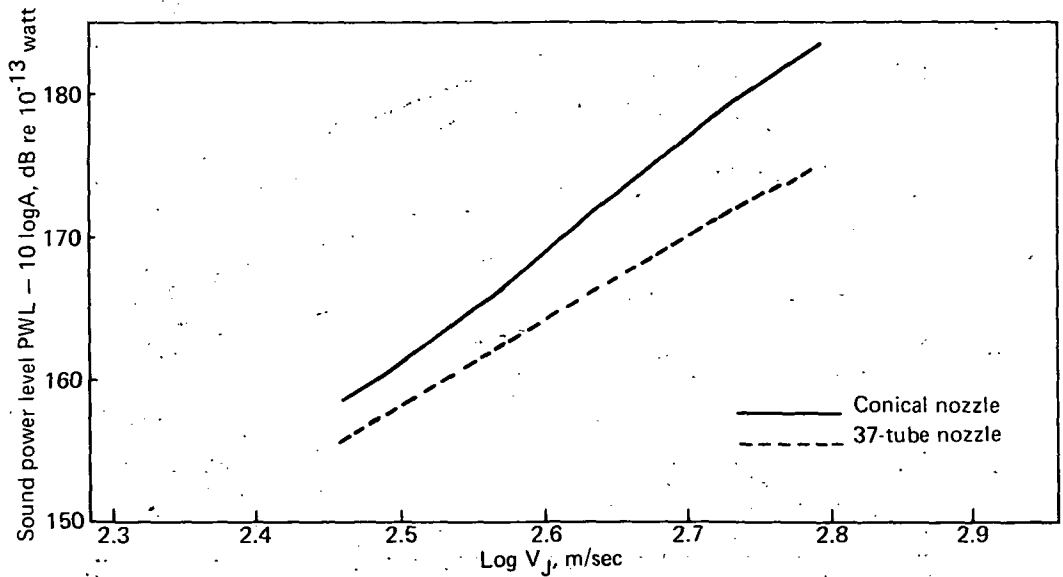
FIGURE 68.—OVERALL SOUND POWER LEVELS FOR THE FULL SCALE CONICAL AND 37-TUBE NOZZLES AS A FUNCTION OF JET VELOCITY (NORMALIZED TO A FLOW AREA OF 1 M^2)

Suppression = PWL conical nozzle — PWL 37-tube nozzle
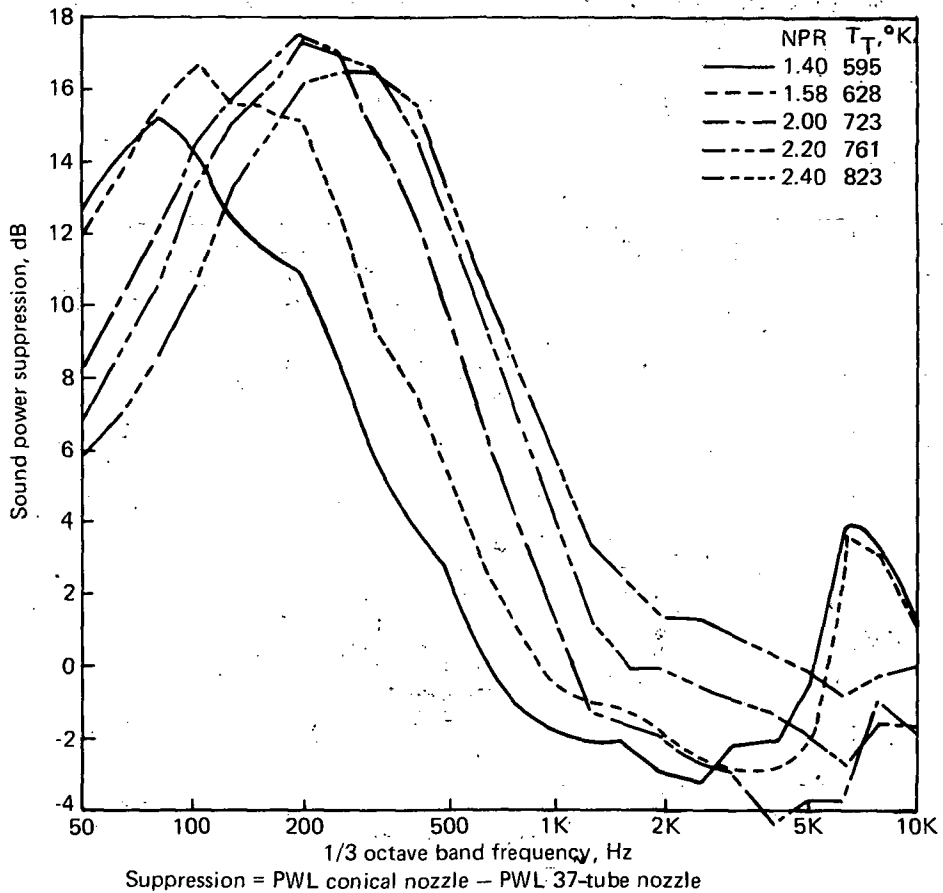
FIGURE 69.—SOUND POWER SUPPRESSION SPECTRA FOR THE FULL-SCALE 37-TUBE NOZZLE
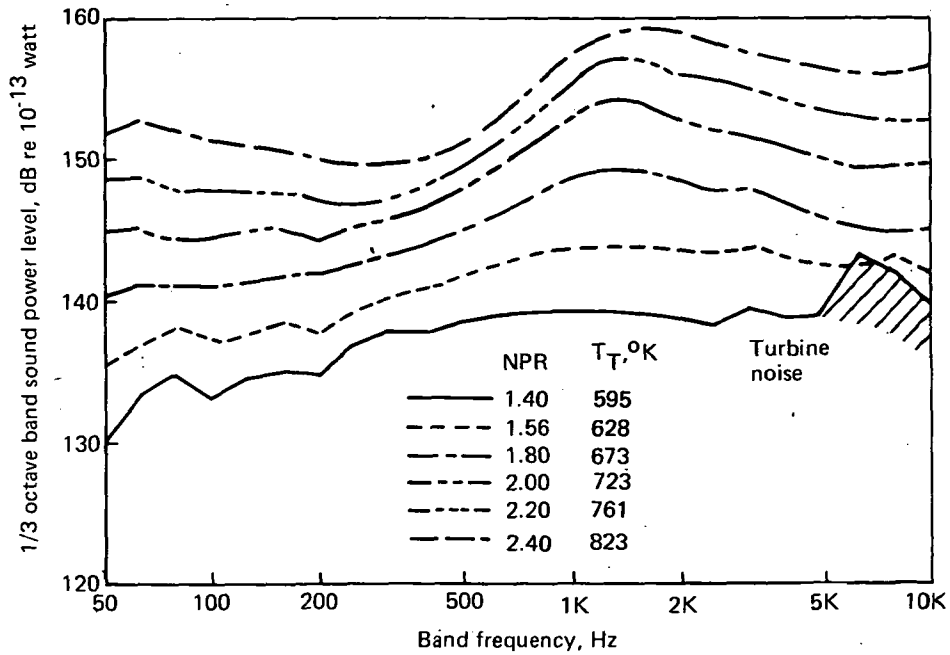
FIGURE 70.–SOUND POWER SPECTRA FOR FULL-SCALE 37-TUBE NOZZLE
WITH L/D = 1 HARDWALL EJECTOR
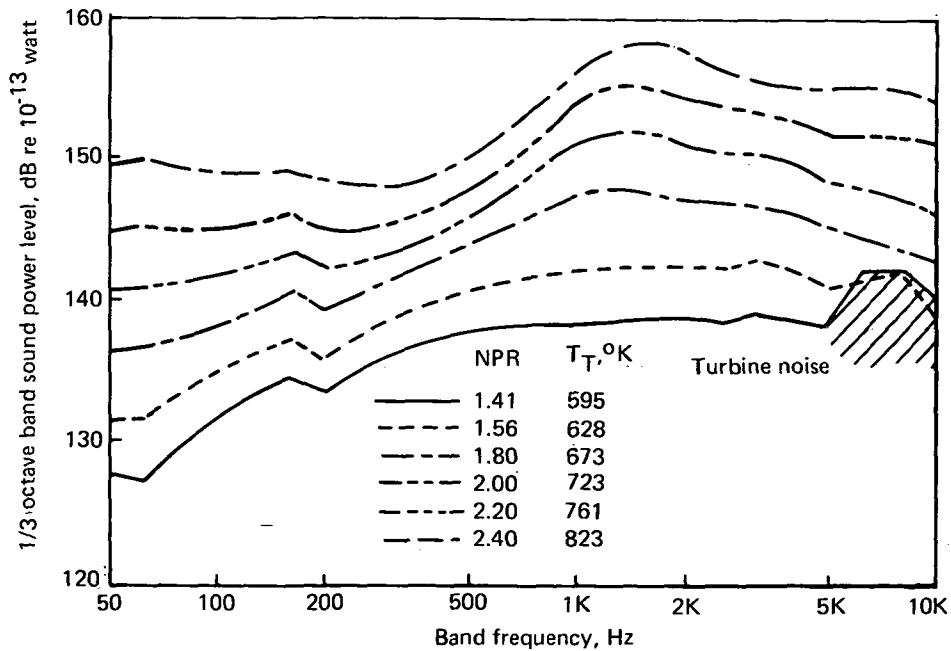
FIGURE 71.–SOUND POWER SPECTRA FOR FULL-SCALE 37-TUBE NOZZLE WITH
L/D = 2 HARDWALL EJECTOR

161
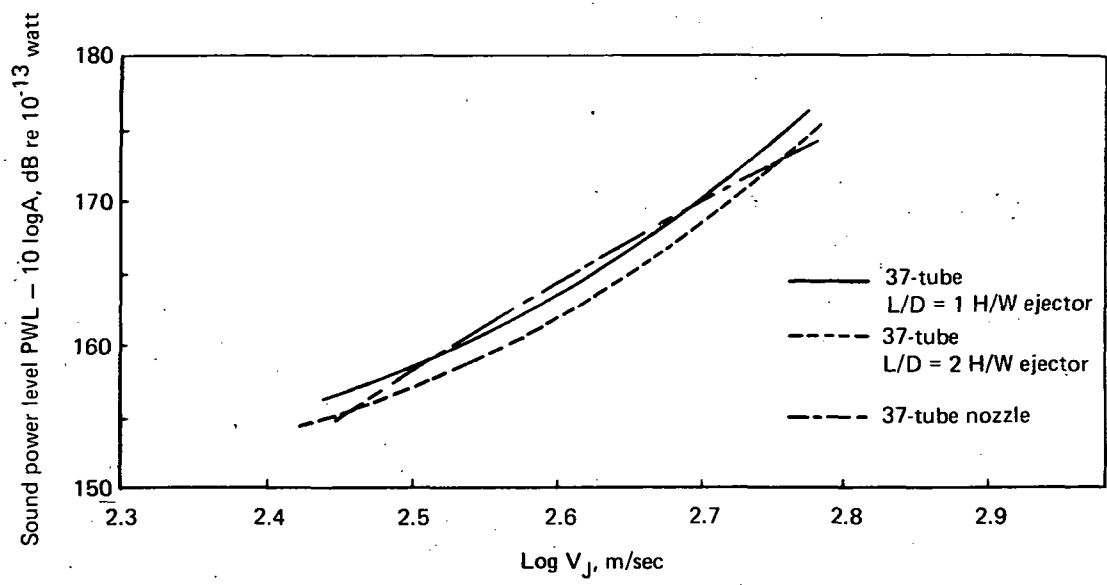
FIGURE 72.—SOUND POWER LEVELS FOR THE FULL-SCALE 37-TUBE NOZZLE AND L/D = 1 AND L/D = 2 HARDWALL EJECTORS (NORMALIZED TO A FLOW AREA OF 1 M²)
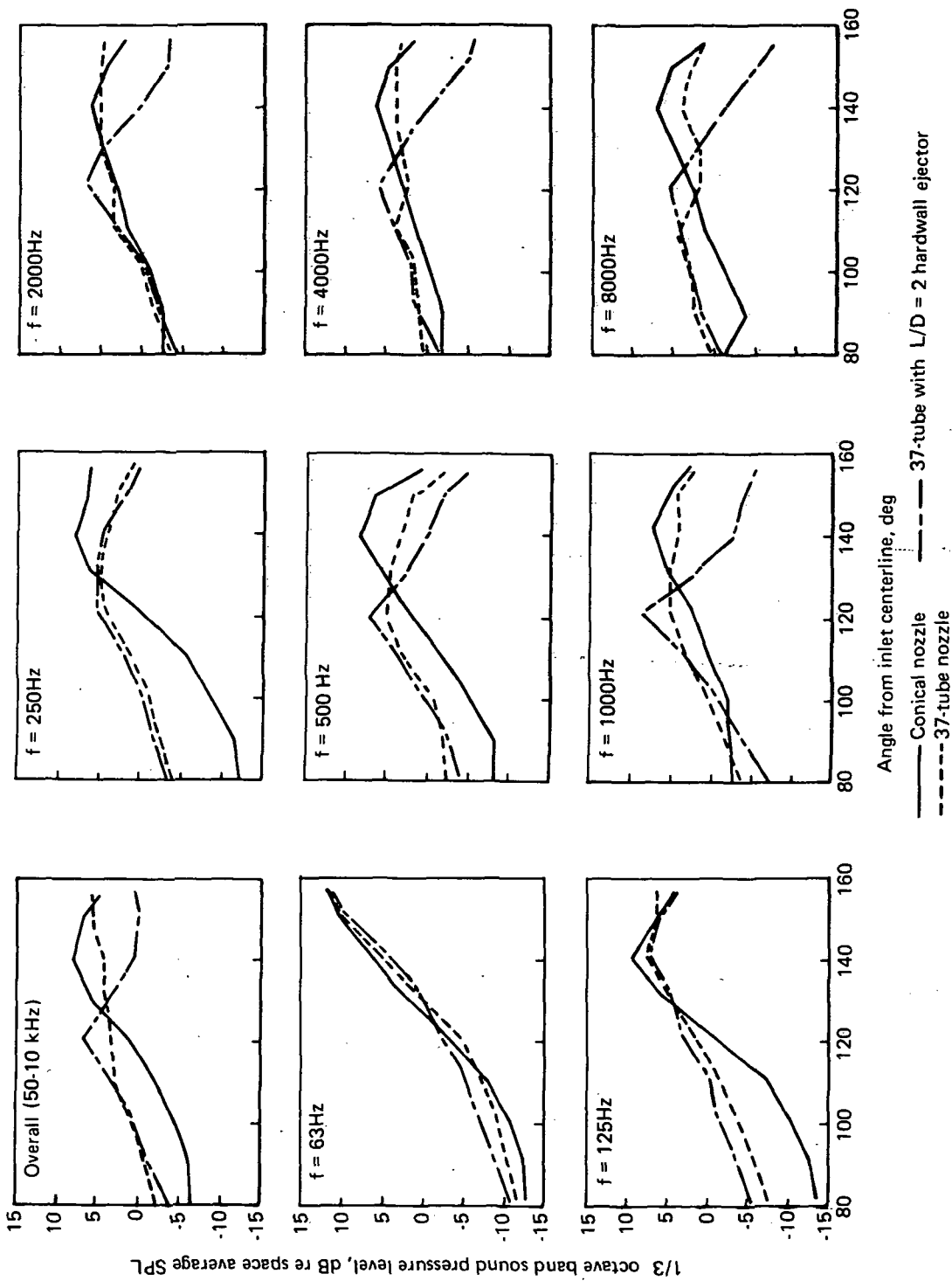
FIGURE 73.—CHANGES IN DIRECTIVITY AS A FUNCTION OF FREQUENCY BETWEEN FULL-SCALE CONICAL, 37-TUBE AND L/D = 2 HARDWALL EJECTOR AT NPR = 2.4 AND T = 823° K

163
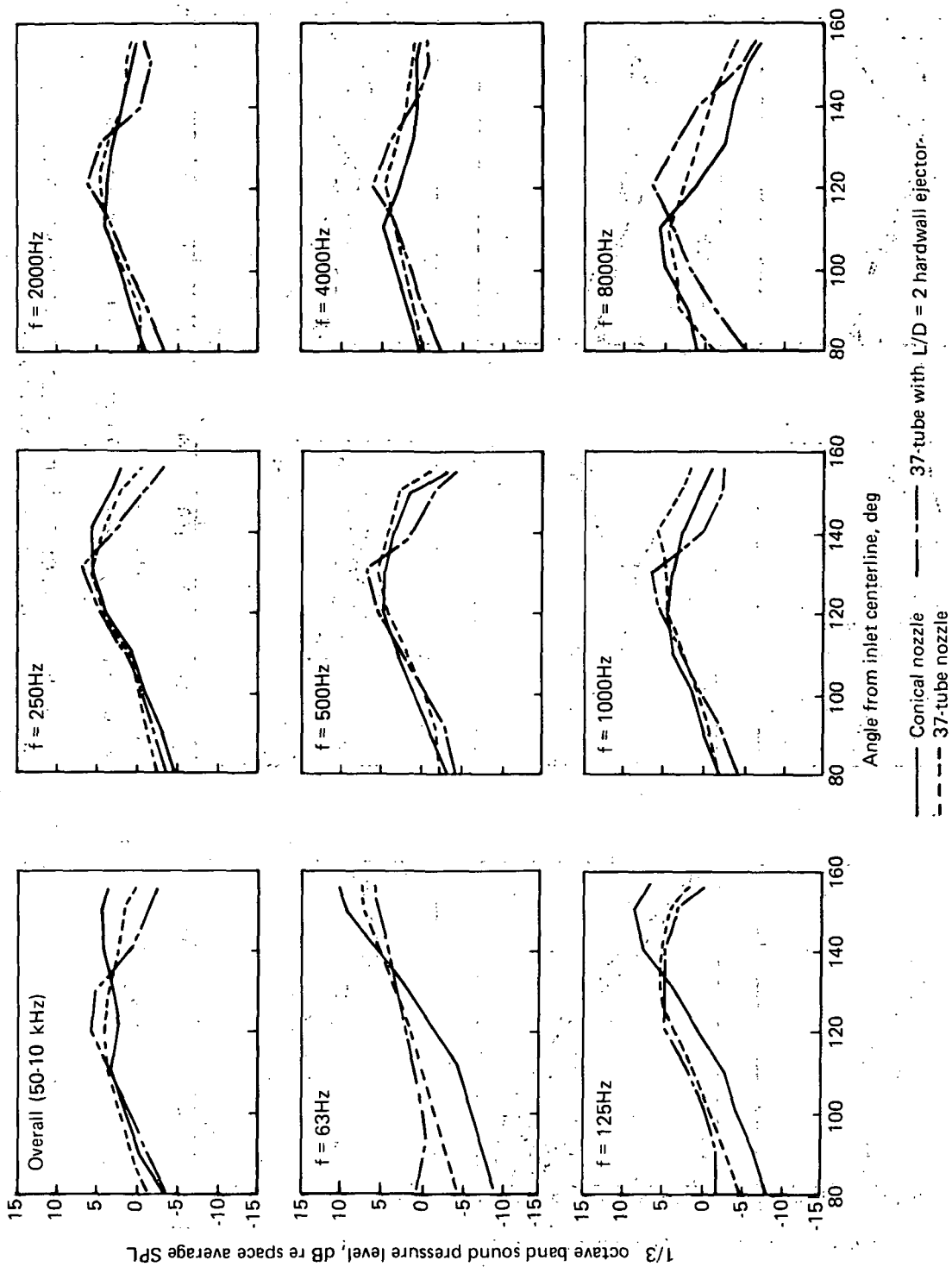
FIGURE 74.–CHANGES IN DIRECTIVITY AS A FUNCTION OF FREQUENCY BETWEEN FULL-SCALE CONICAL, 37-TUBE AND L/D = 2 HARDWALL EJECTOR AT NPR = 1.4 AND T = 595° K
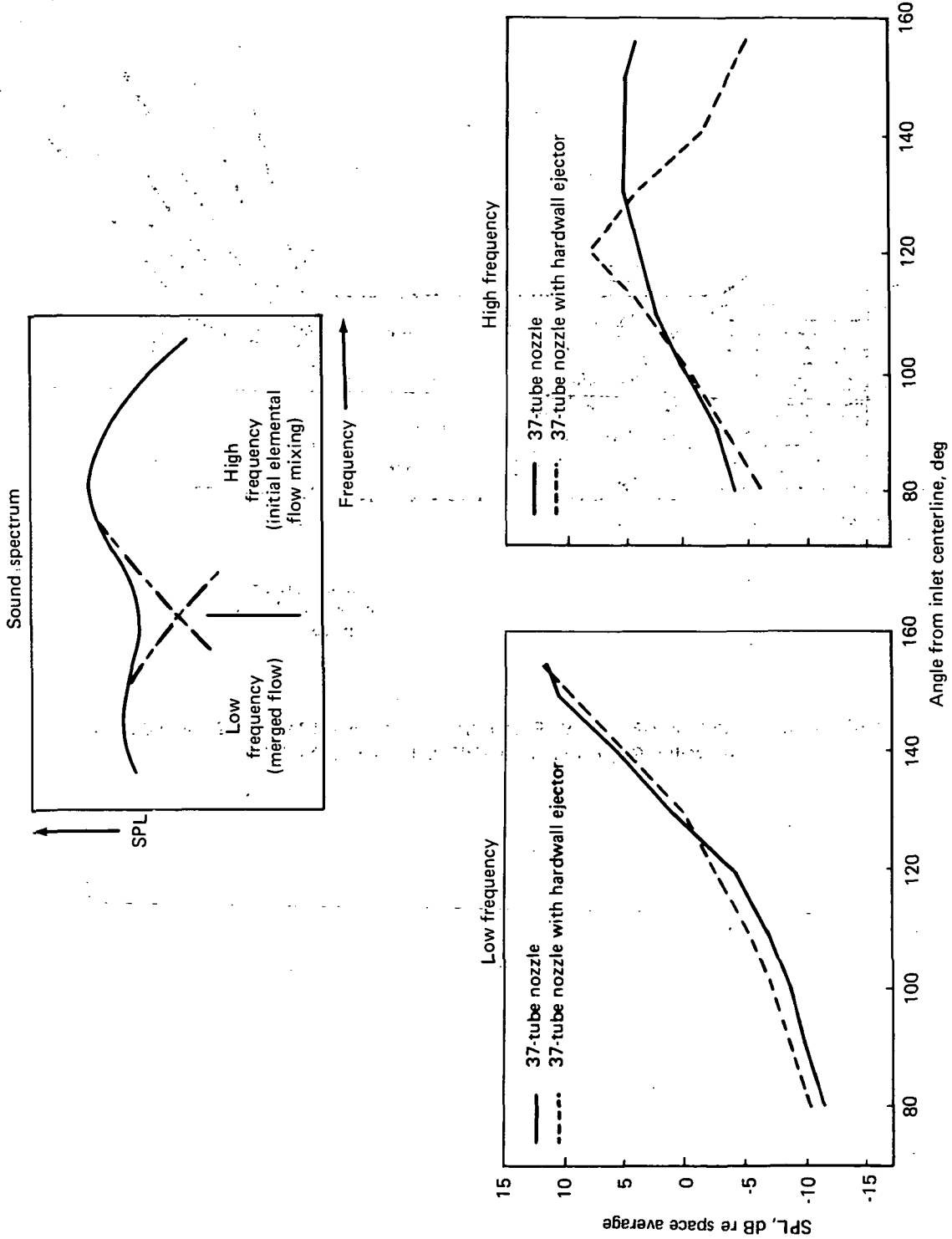
FIGURE 75.—INFLUENCE OF EJECTOR UPON RADIATED SOUND FIELD

165
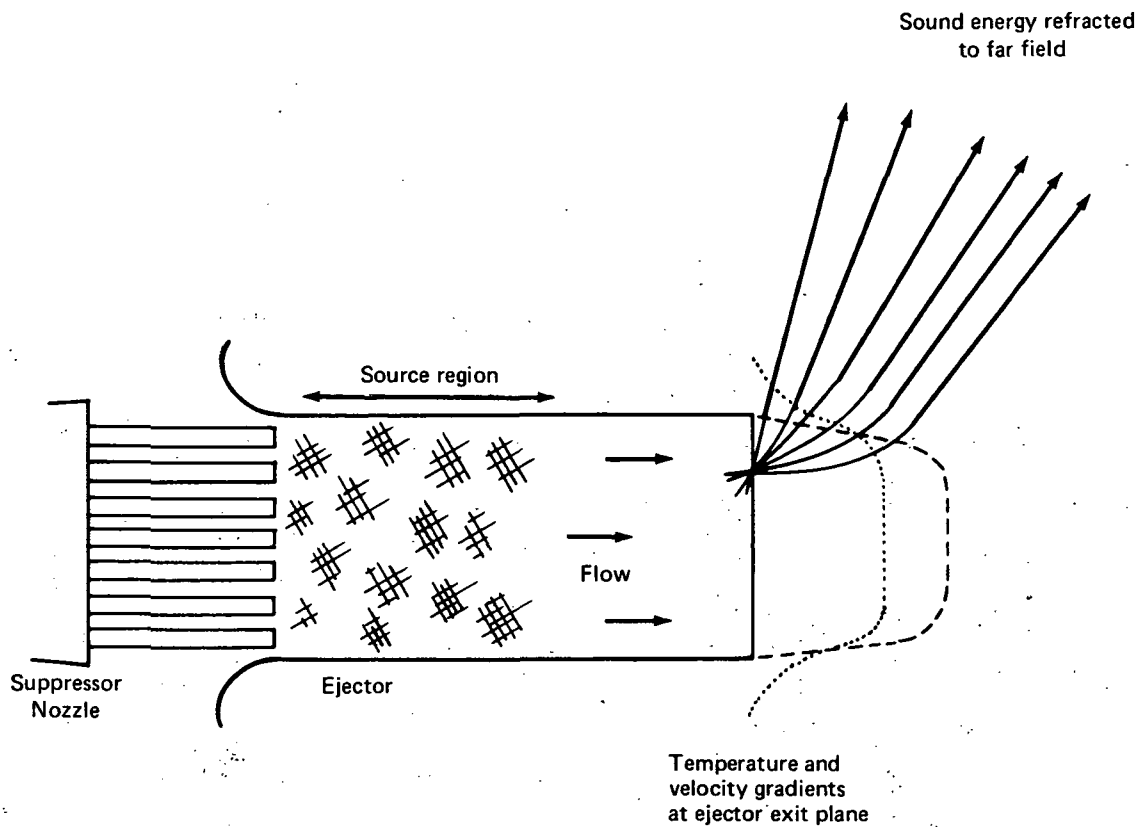
FIGURE 76.—SIMPLE MODEL OF AN EJECTOR CONFIGURATION AS A SOUND SOURCE
(FOR NOISE GENERATED WITHIN EJECTOR LENGTH)
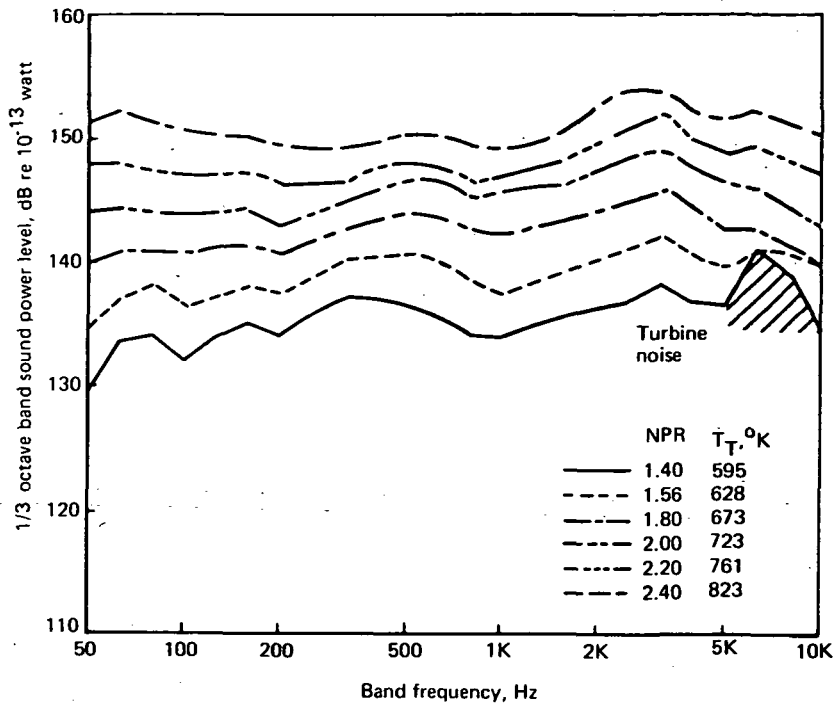
FIGURE 77.—SOUND POWER SPECTRA FOR FULL SCALE 37-TUBE NOZZLE WITH
L/D = 1 LINED EJECTOR (12% OPEN AREA; d = 5.33 CM)
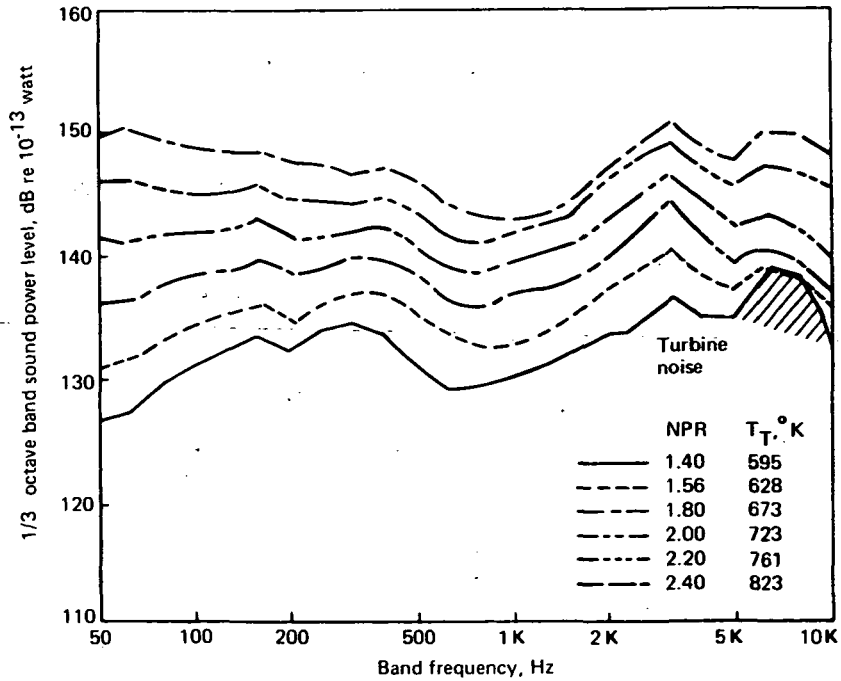
FIGURE 78.—SOUND POWER SPECTRA FOR FULL SCALE 37-TUBE NOZZLE WITH
L/D = 2 LINED EJECTOR (12% OPEN AREA; d = 5.33 CM)
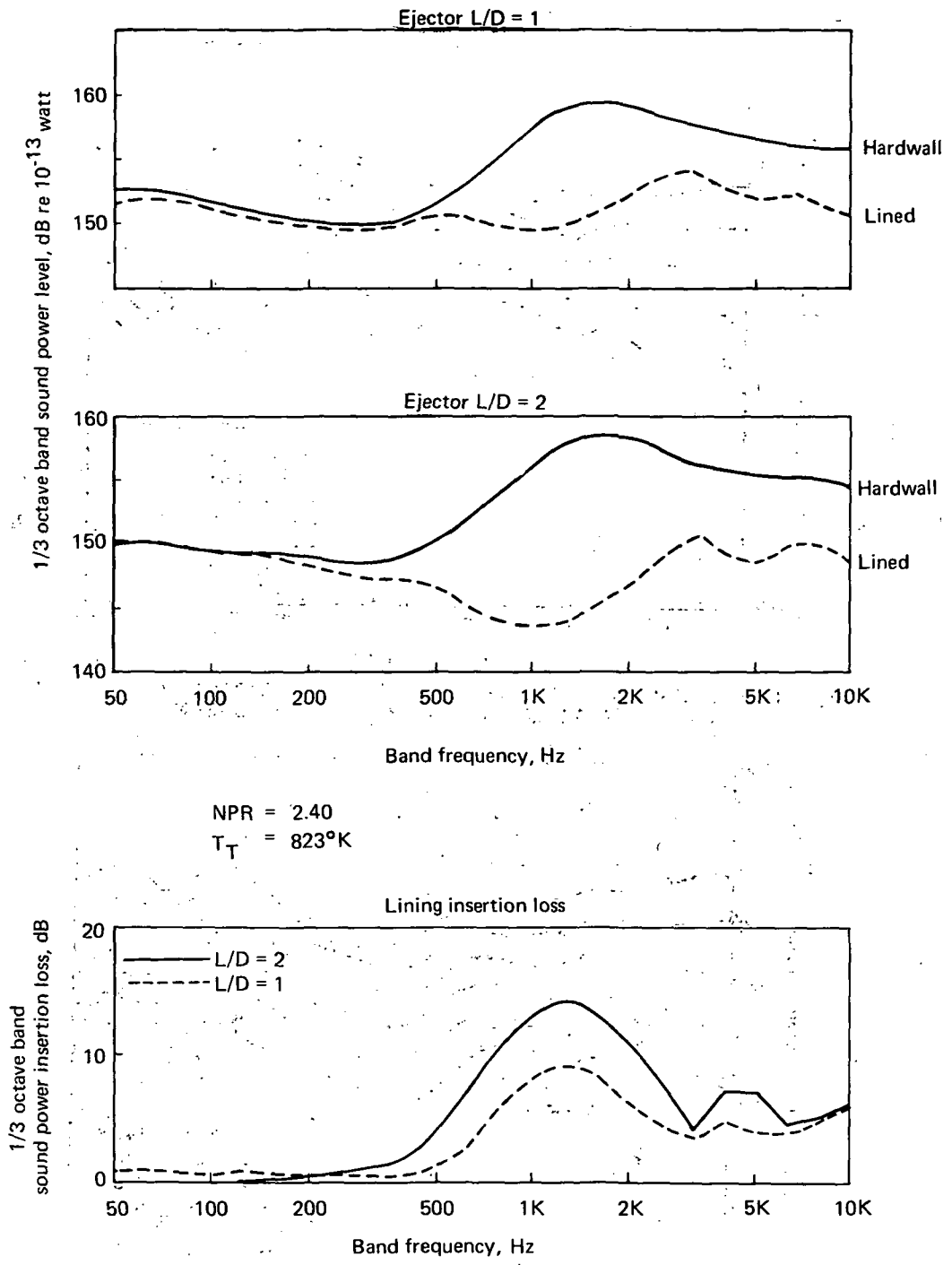
FIGURE 79.—COMPARISON OF THE ACOUSTIC PERFORMANCE OF LINED AND HARDWALL
L/D = 1 AND L/D = 2 EJECTORS (12% OPEN AREA; d = 5.33 CM LININGS)

168
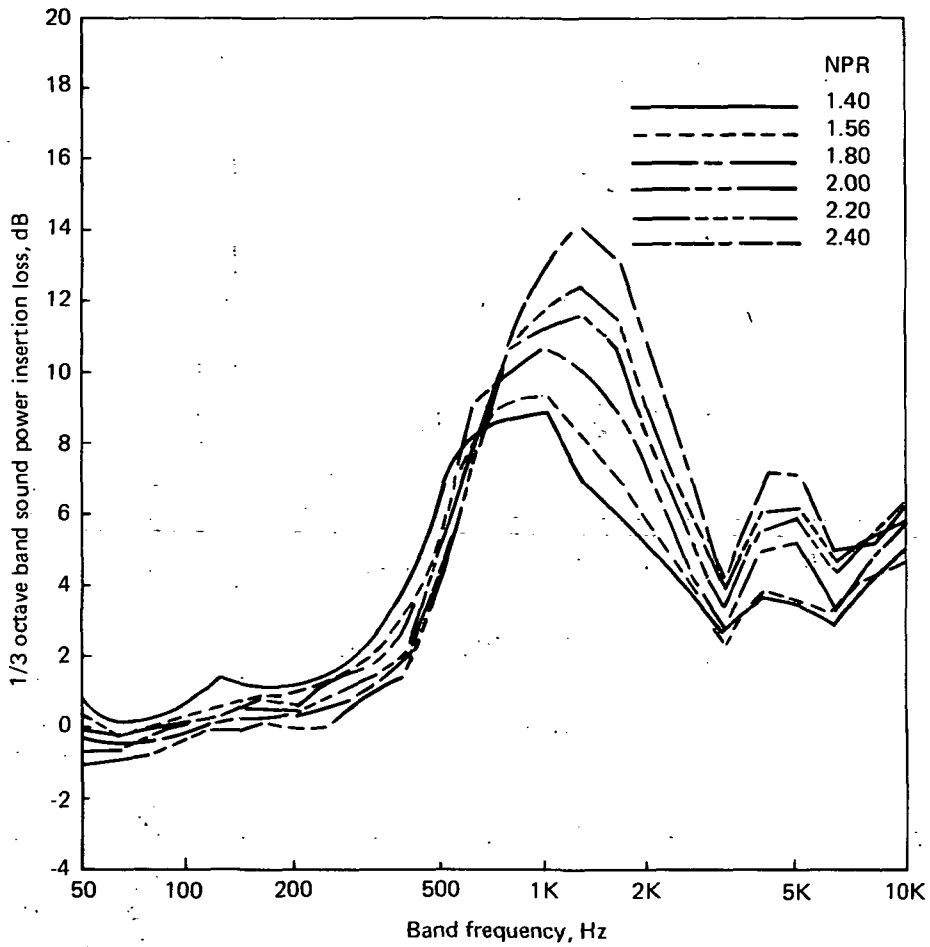
Insertion loss = PWL Hardwall — PWL lined

FIGURE 80.—SOUND POWER INSERTION LOSS SPECTRA FOR FULL-SCALE LINED
L/D = 2 EJECTOR (12% OPEN AREA; d = 5.33 CM)

FIGURE 82.—TUNING FREQUENCY FOR FULL-SCALE
ACOUSTIC LININGS
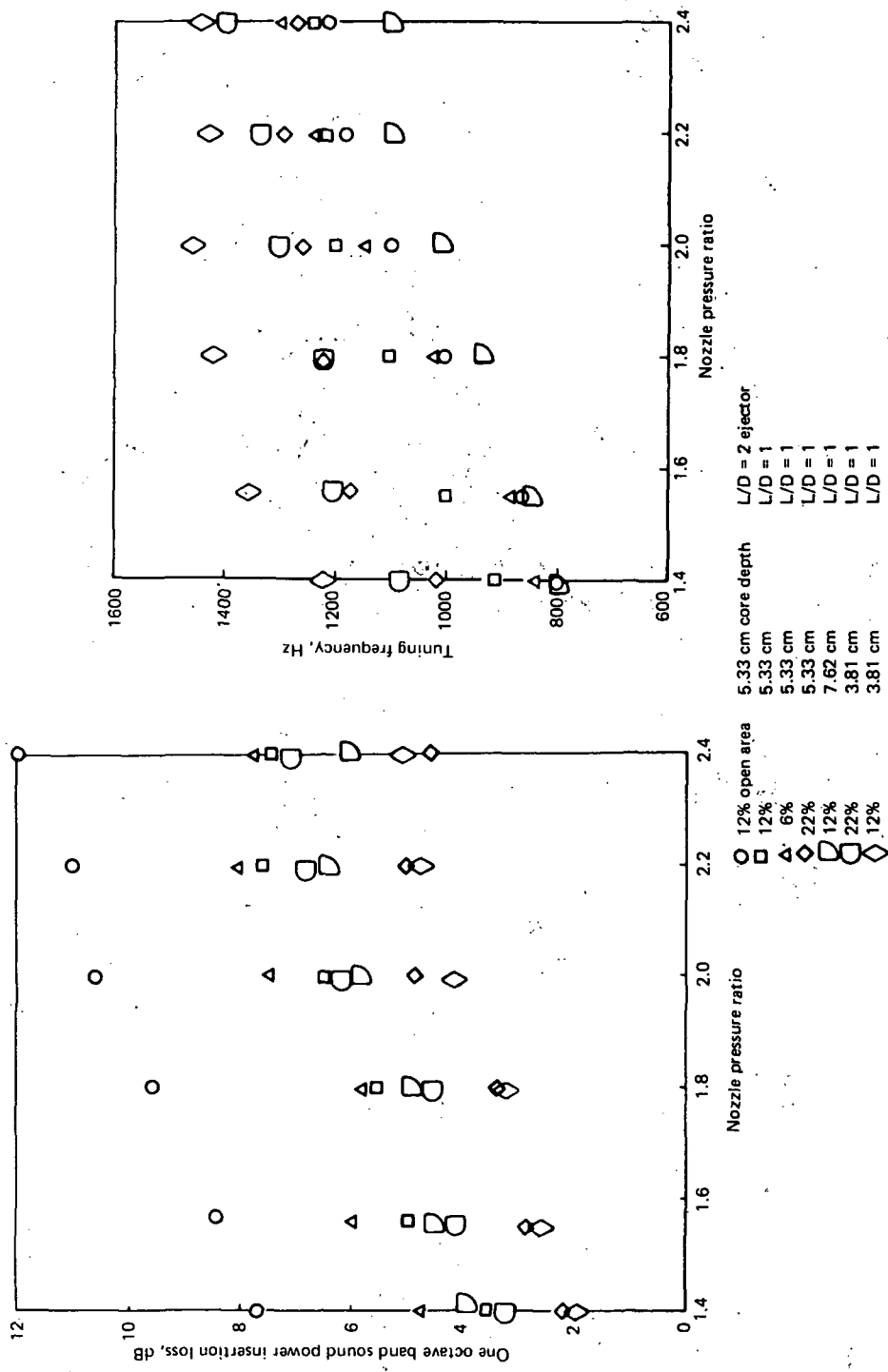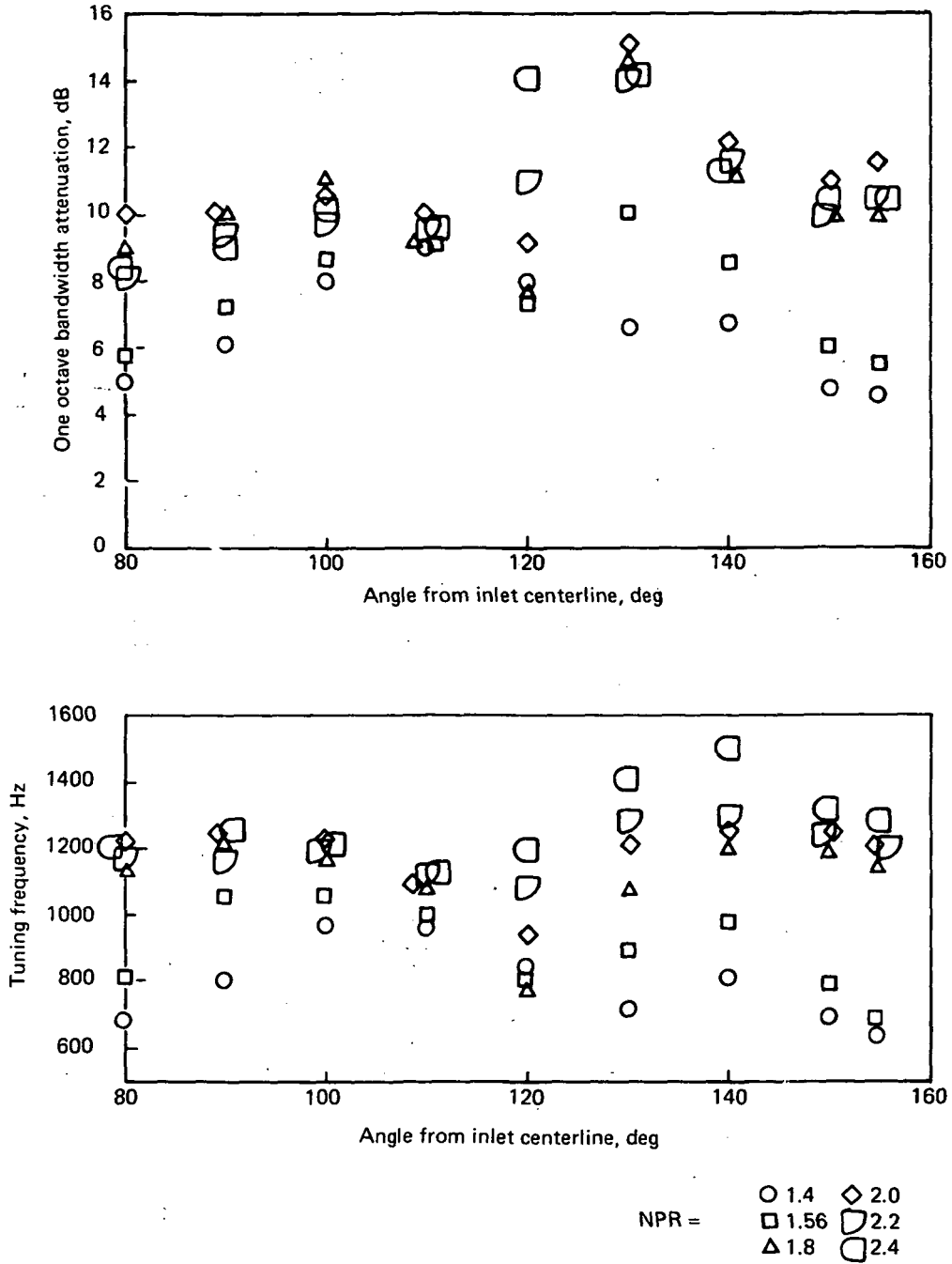
FIGURE 81.—SOUND POWER INSERTION LOSS FOR FULL-SCALE
ACOUSTIC LININGS

FIGURE 83.—FULL-SCALE LINING ATTENUATION AND TUNING CHARACTERISTICS AS A FUNCTION OF
ANGLE FOR THE L/D = 2 EJECTOR (12% OPEN AREA; d = 5.33 CM)

171
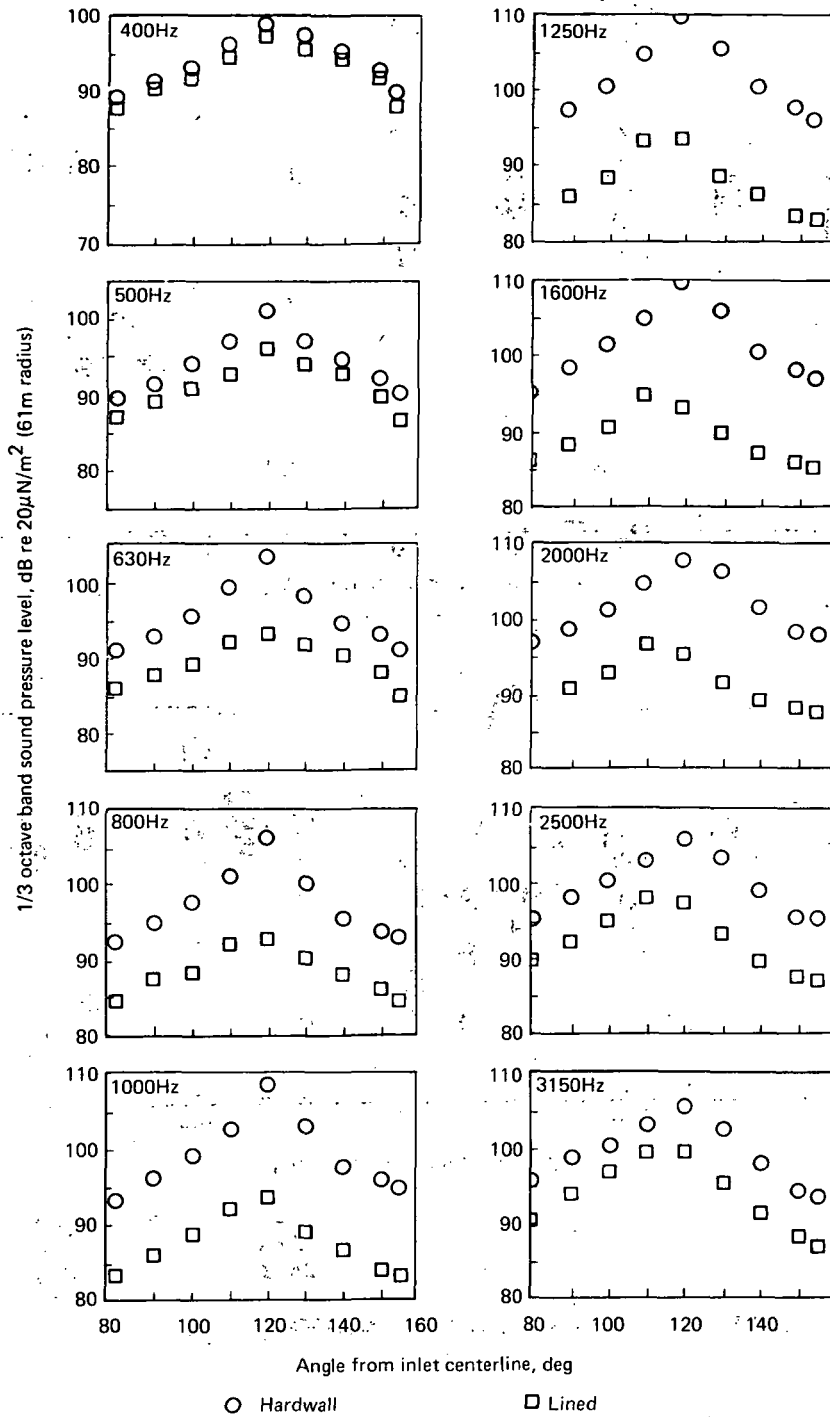
FIGURE 84.—EFFECT OF LINING ON SOUND FIELD DIRECTIVITY FOR
THE FULL SCALE L/D = 2 EJECTOR (12% OPEN AREA; d = 5.33 CM)

Ejector entrance

1/3 octave band sound pressure level, dB re $20\mu N/m^2$

Symbol	NPR	Jet temp, °K	Overall SPL, dB
	1.4	533	143.5
	1.6	589	148.6
	2.0	700	152.8
	2.2	755	156.0
	2.4	811	157.3
	4.0	1088	157.8

Ejector center

Symbol	NPR	Jet temp, °K	Overall SPL, dB
	1.4	533	149.5
	1.6	589	153.4
	2.0	700	160.1
	2.2	755	162.7
	2.4	811	163.3

Ejector exit

Symbol	NPR	Jet temp, °K	Overall SPL, dB
	1.4	533	151.1
	1.6	589	155.1
	2.0	700	161.5
	2.2	755	164.0
	2.4	811	165.6
	4.0	1088	170.1

Band center frequency, Hz

FIGURE 85.- MODEL-SCALE EJECTOR WALL SPL SPECTRA IN THE L/D = 1 HARDWALL EJECTOR (37-TUBE NOZZLE)

173
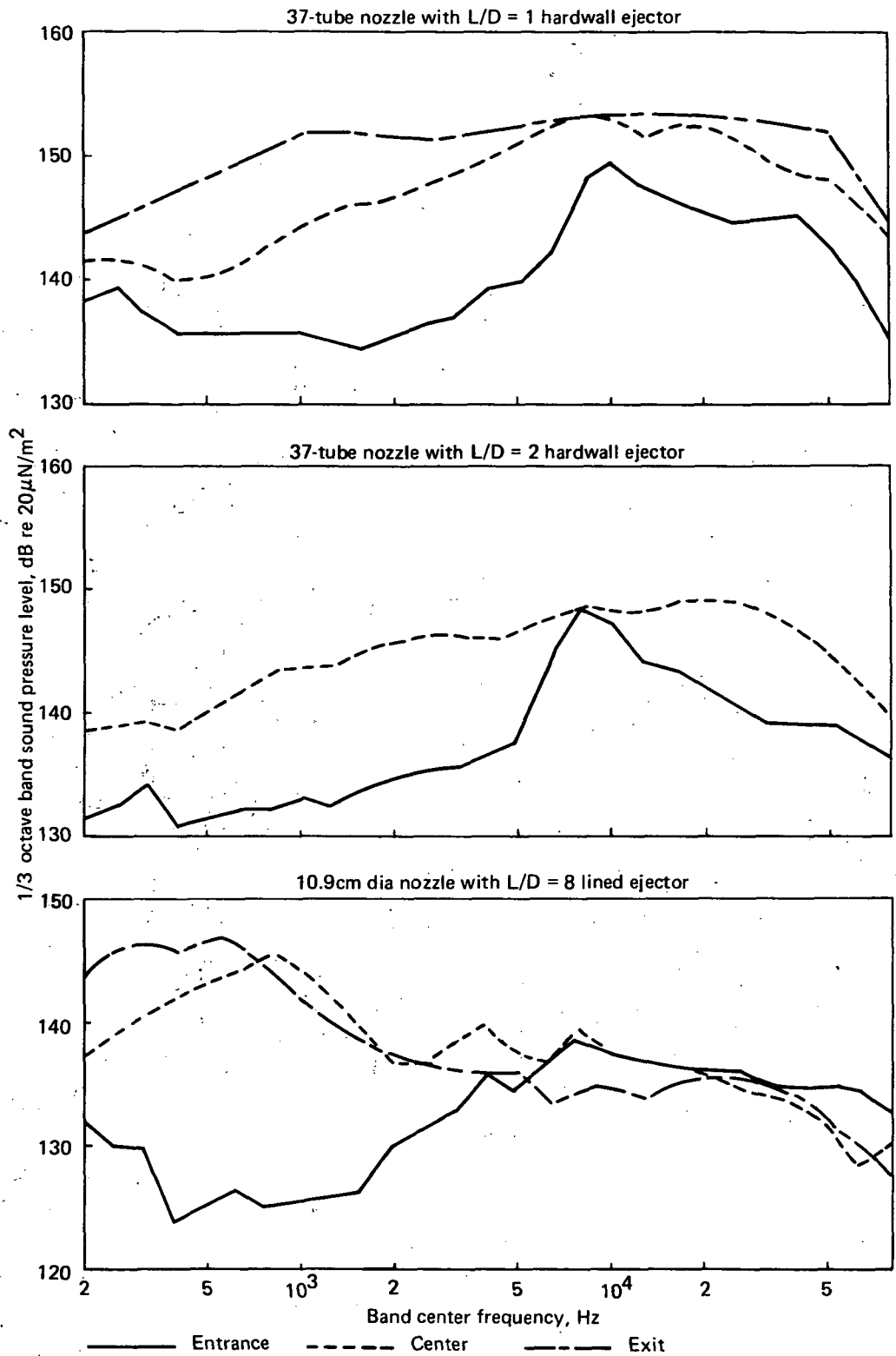
FIGURE 86.–MODEL-SCALE EJECTOR WALL SPL SPECTRA FOR VARIOUS EJECTORS AT
NPR = 2.4 AND T = 811°K

174
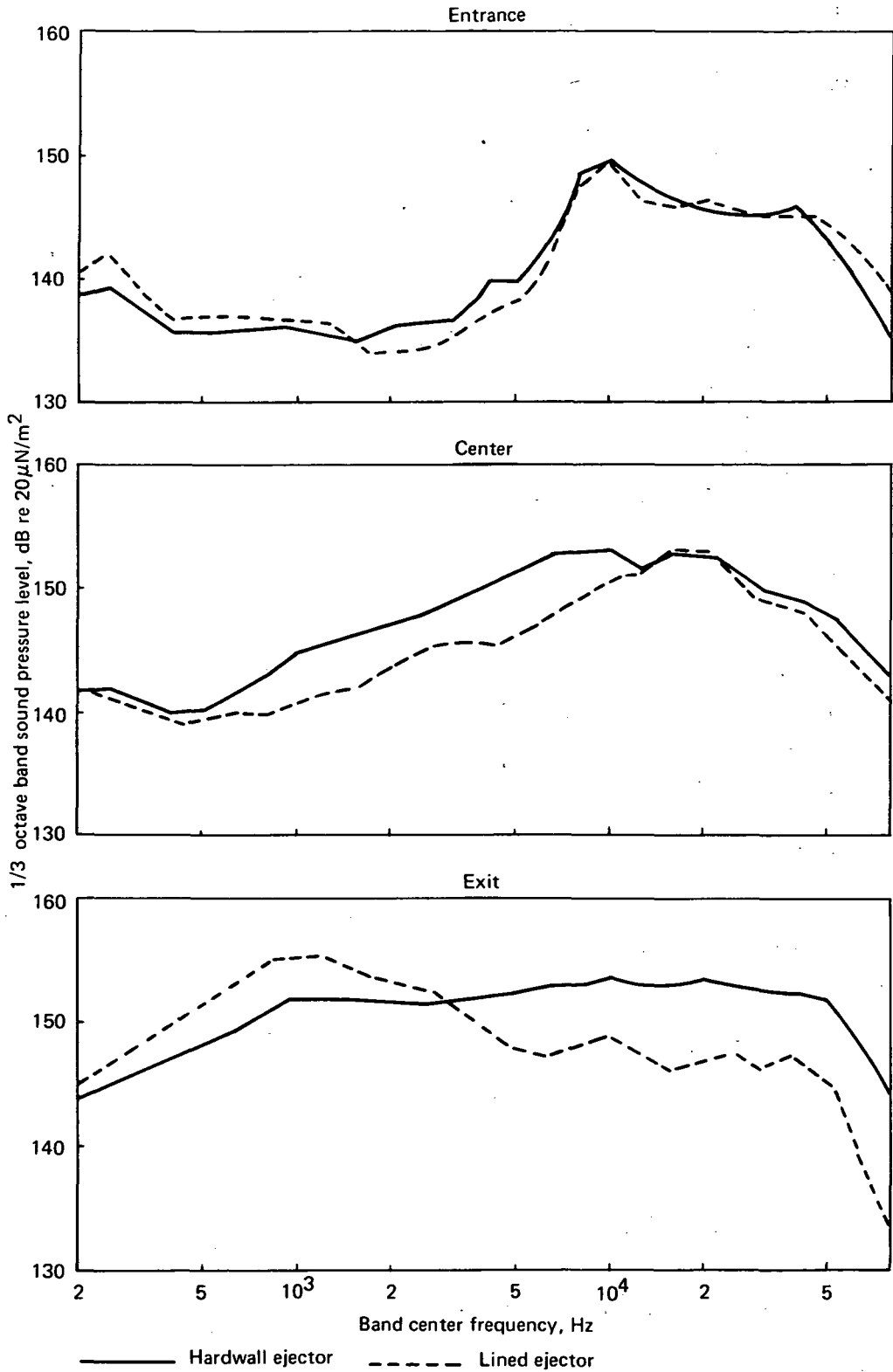
FIGURE 87.—MODEL-SCALE EJECTOR WALL SPL SPECTRAL COMPARISON BETWEEN HARDWALL AND LINED L/D = 1 EJECTORS AT NPR = 2.4 AND T = 811°K

175
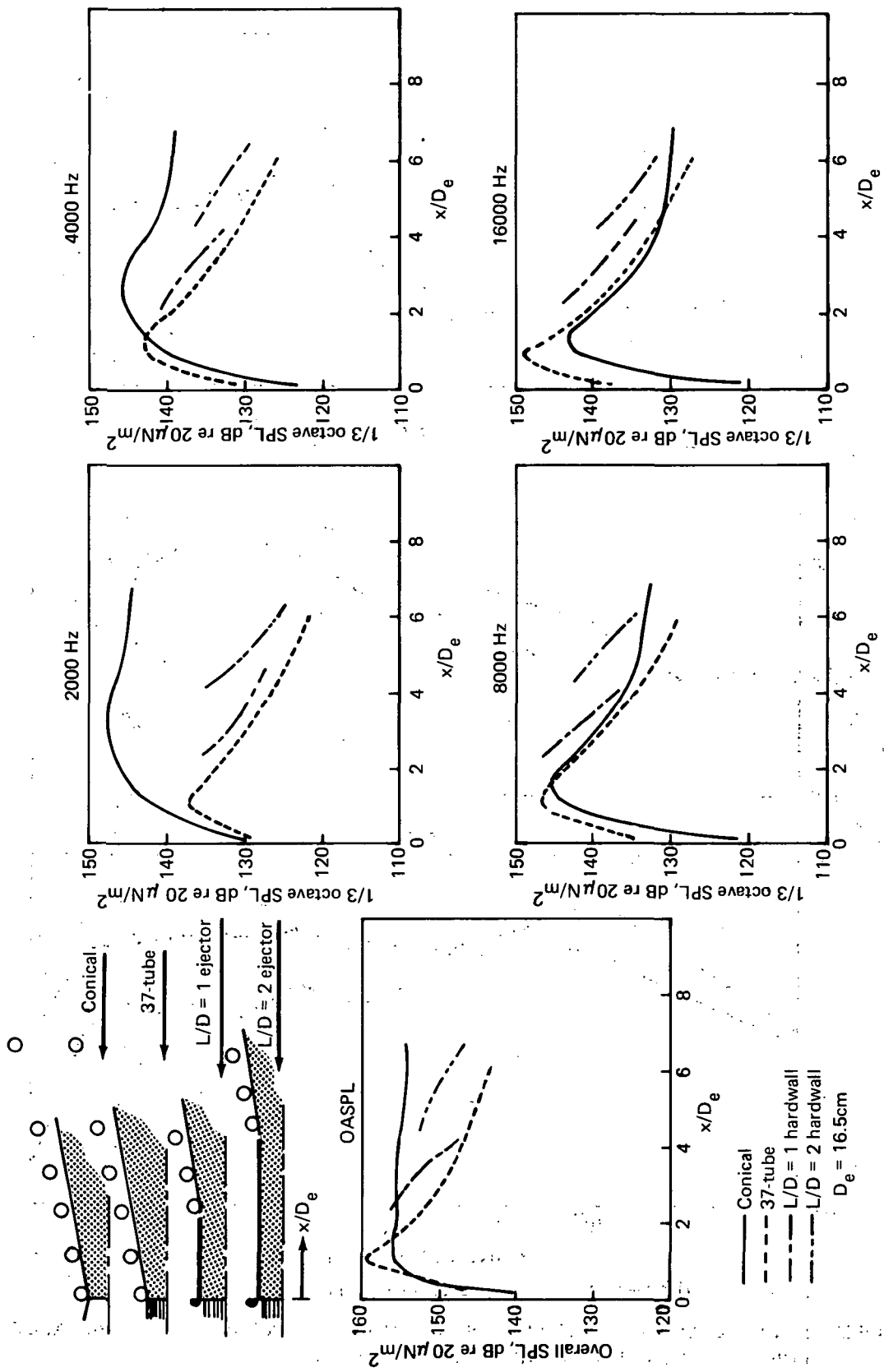
FIGURE 88.—MODEL-SCALE NEAR FIELD JET NOISE ENVIRONMENT AT NPR = 2.4 AND T = 811°K

176
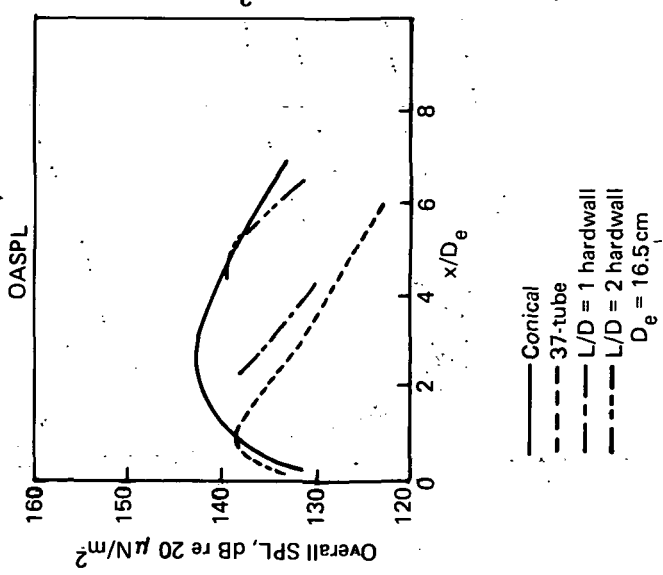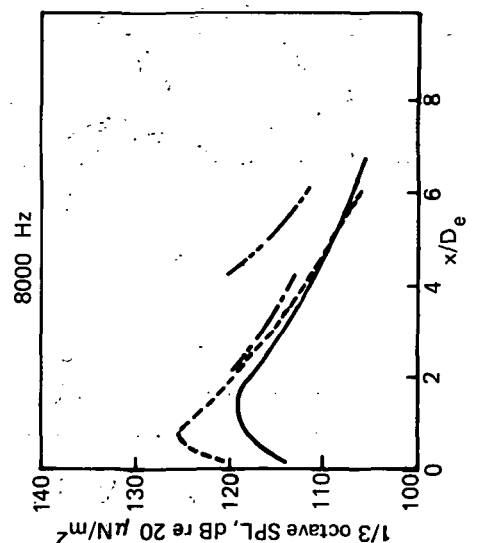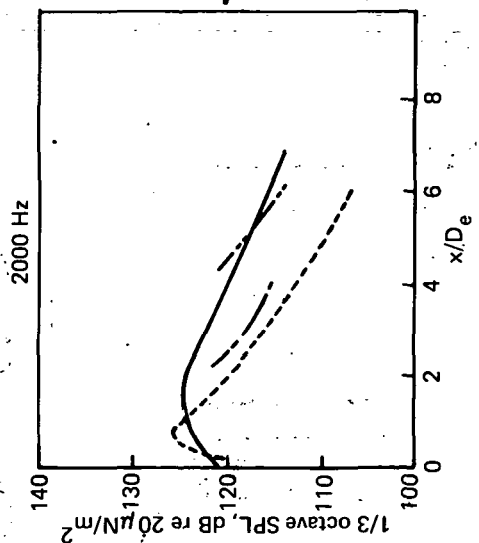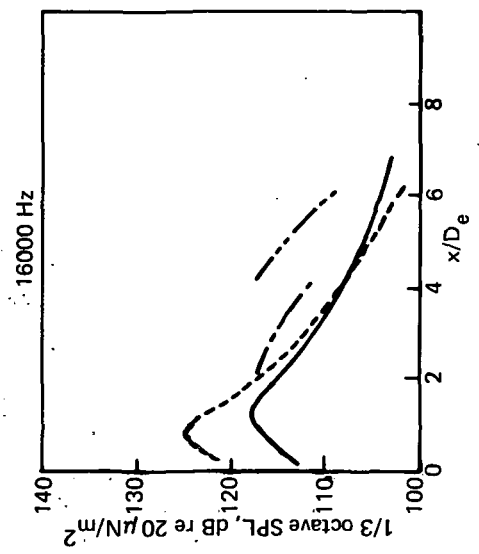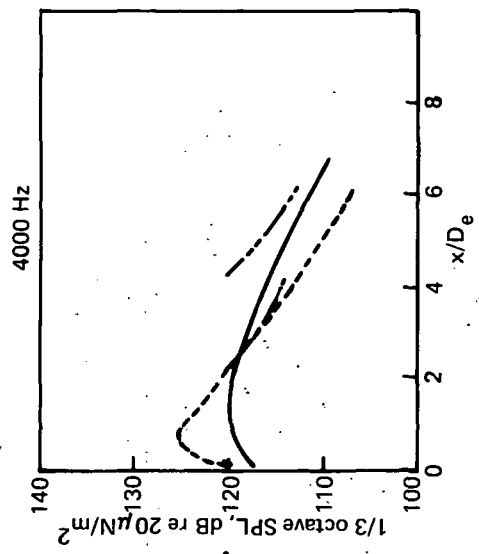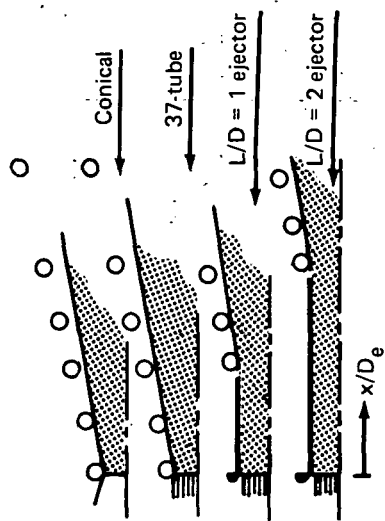
FIGURE 89.—MODEL-SCALE NEAR FIELD JET NOISE ENVIRONMENT AT NPR = 1.4 AND T = 533°K

177
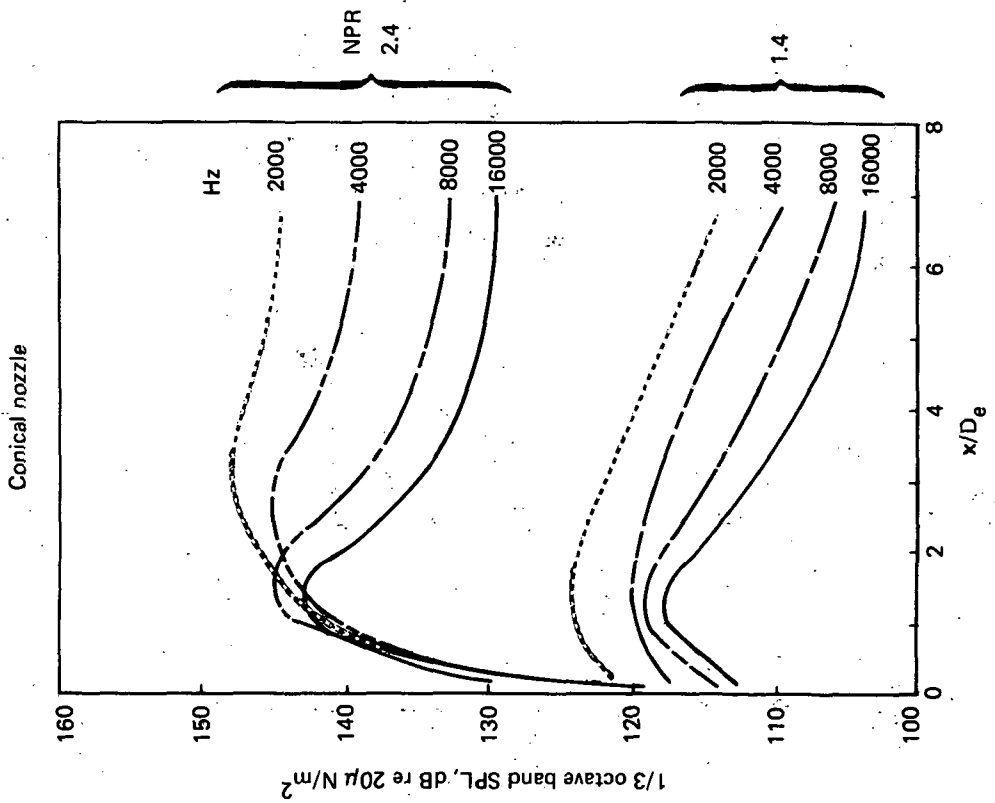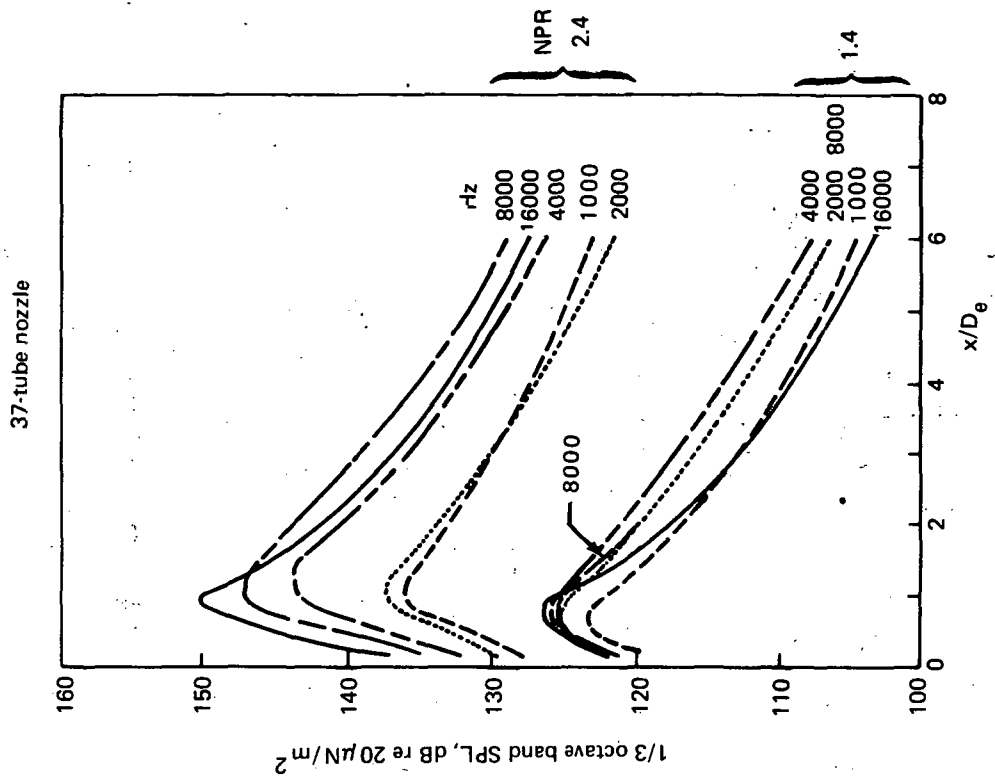
FIGURE 90.–MODEL-SCALE "APPARENT" NOISE SOURCE LOCATIONS FOR THE
CONICAL AND 37-TUBE NOZZLES

$D_e = 16.5$ cm
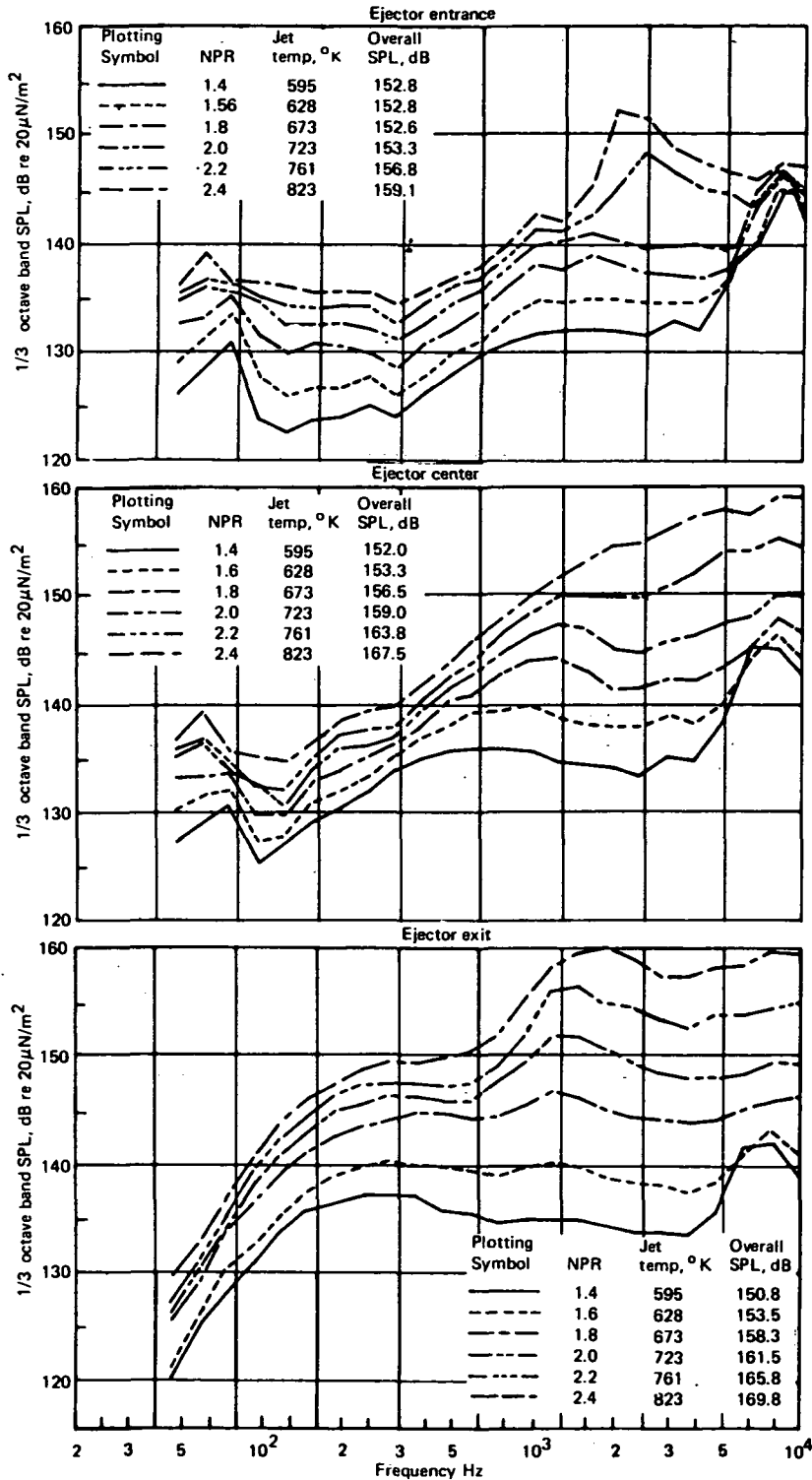
FIGURE 91.—FULL-SCALE EJECTOR WALL SPL SPECTRA IN THE L/D = 1 HARDWALL EJECTOR

179
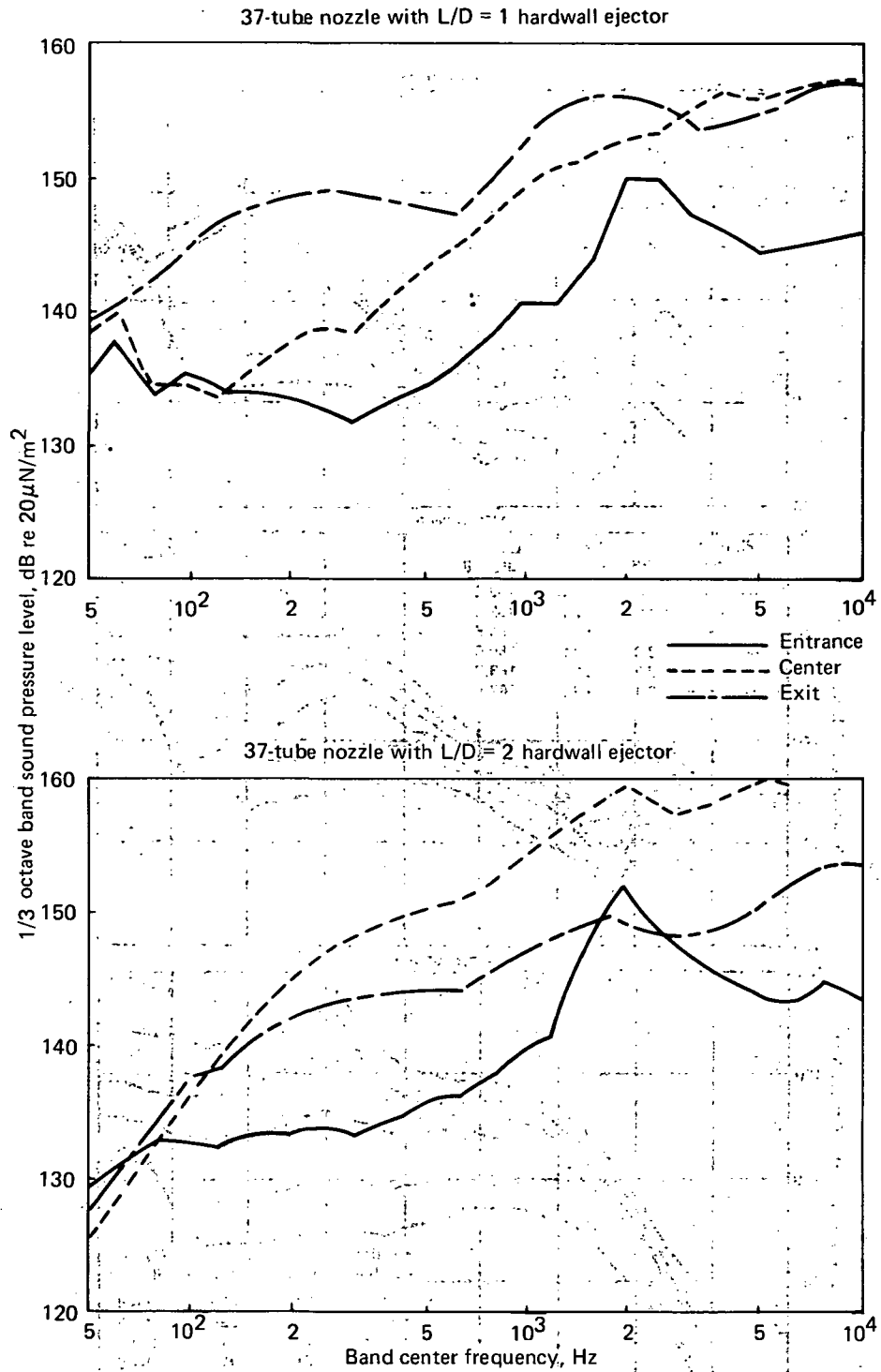
FIGURE 92.—FULL-SCALE EJECTOR WALL SPL SPECTRA FOR VARIOUS EJECTORS AT
NPR = 2.4 AND T = 823° K
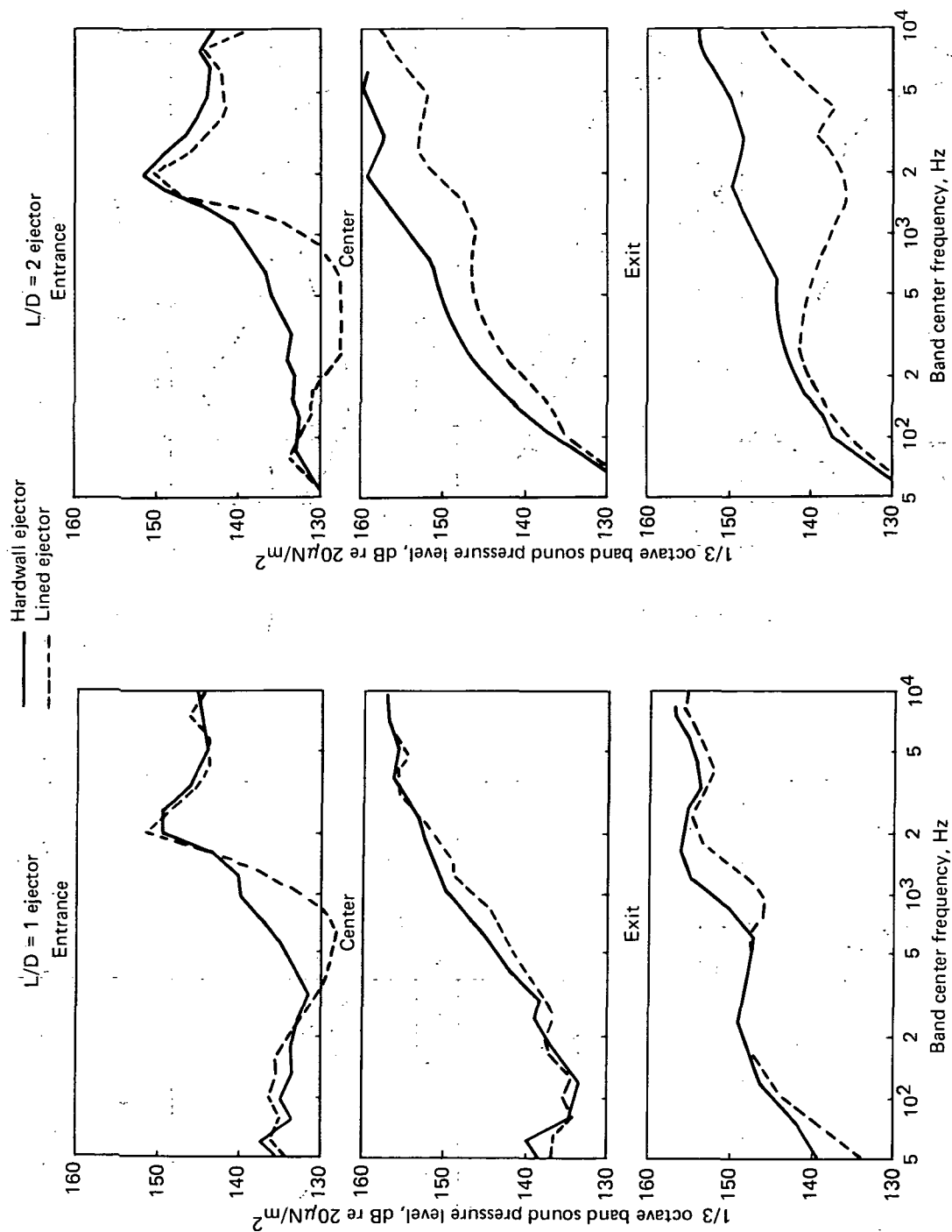
FIGURE 93.—FULL-SCALE EJECTOR WALL SPL SPECTRAL COMPARISON BETWEEN HARDWALL AND LINED EJECTORS AT NPR = 2.4 AND T = 823° K

181
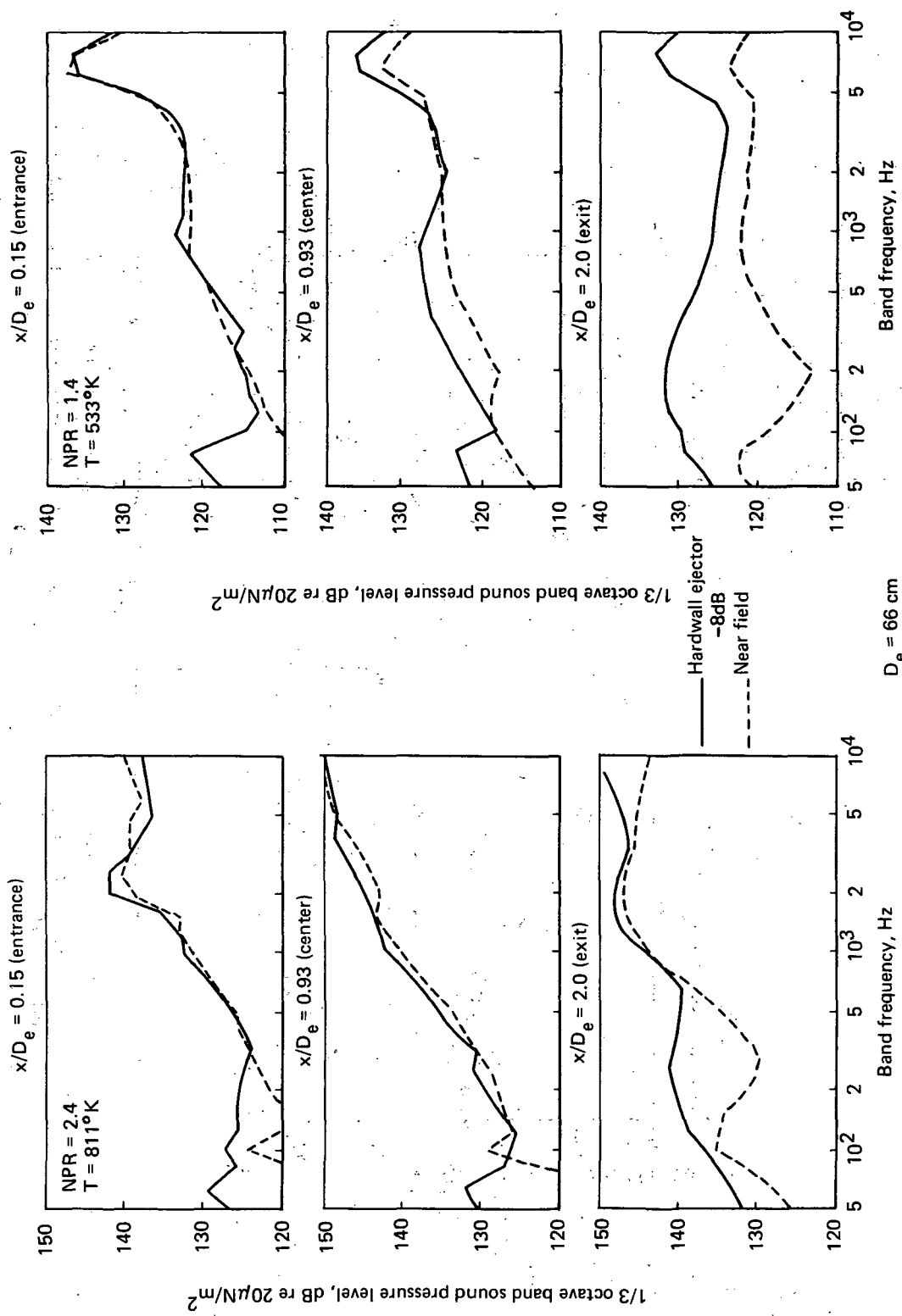
FIGURE 94.–FULL-SCALE NEAR FIELD JET NOISE ENVIRONMENT COMPARISONS BETWEEN 37-TUBE NOZZLE AND L/D = 1 HARDWALL EJECTOR

182
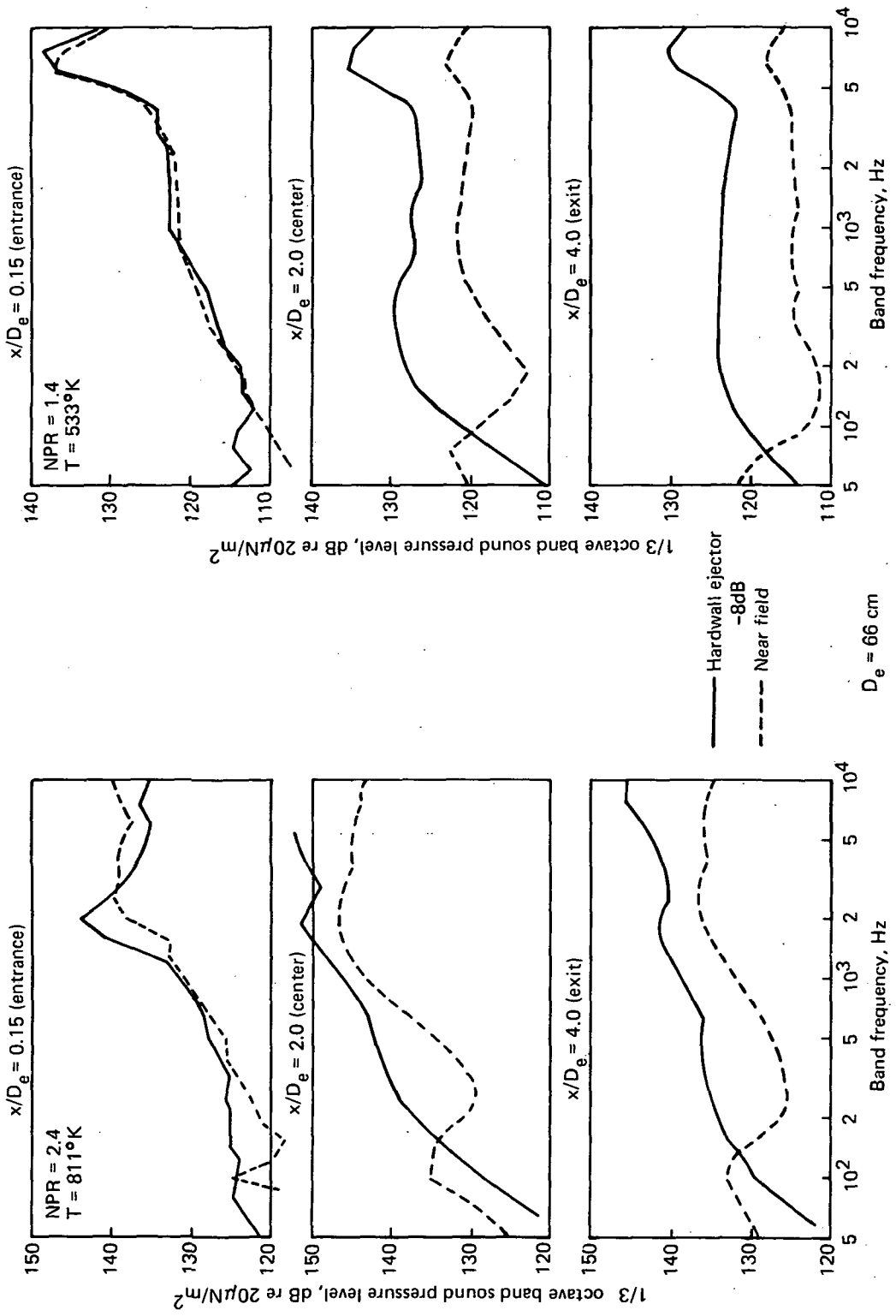
FIGURE 95.–FULL-SCALE NEAR FIELD JET NOISE ENVIRONMENT COMPARISONS BETWEEN 37-TUBE NOZZLE AND L/D = 2 HARDWALL EJECTOR

183
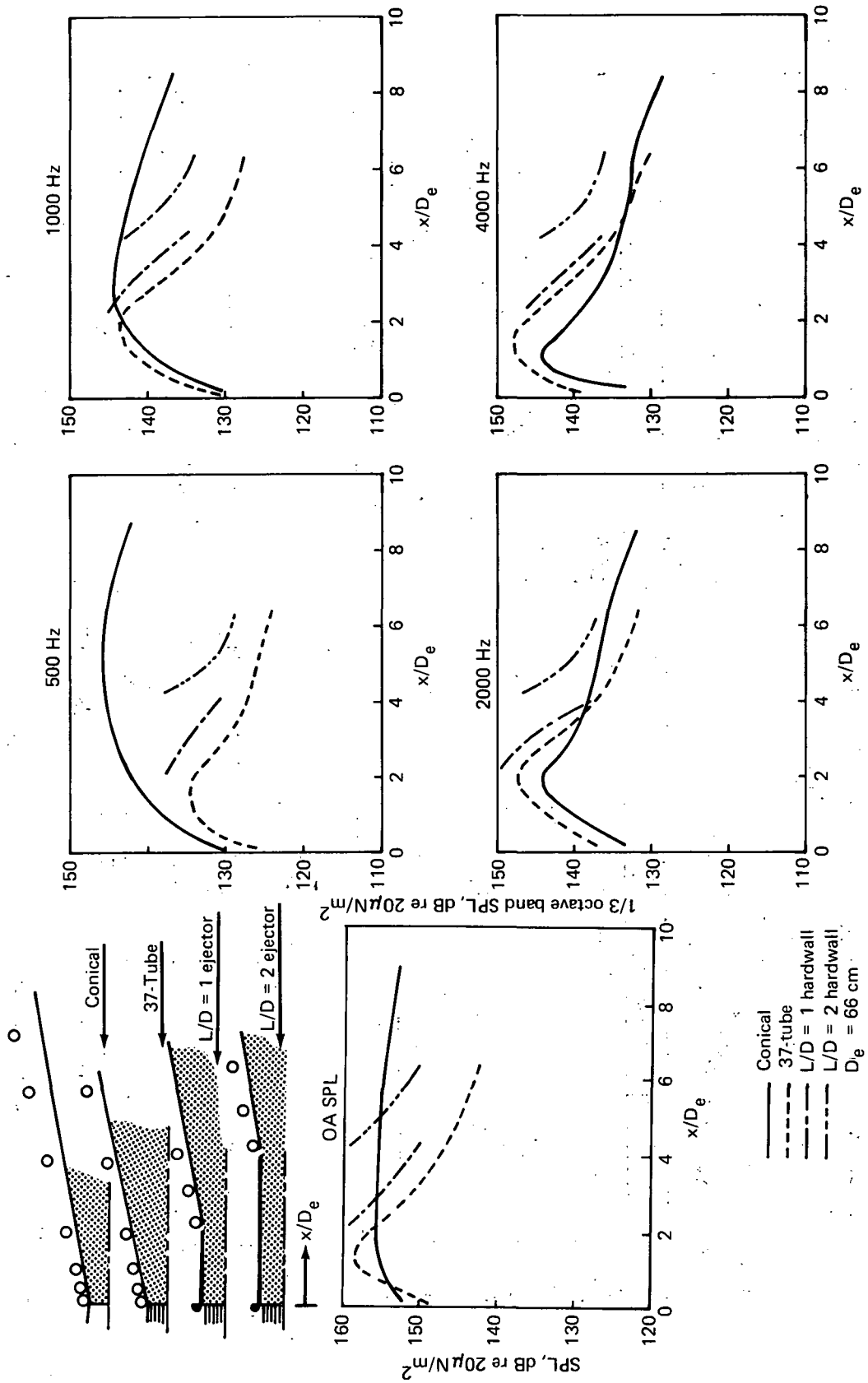
FIGURE 96.– FULL-SCALE NEAR FIELD JET NOISE ENVIRONMENT AT NPR = 2.4 AND T = 823° K

184
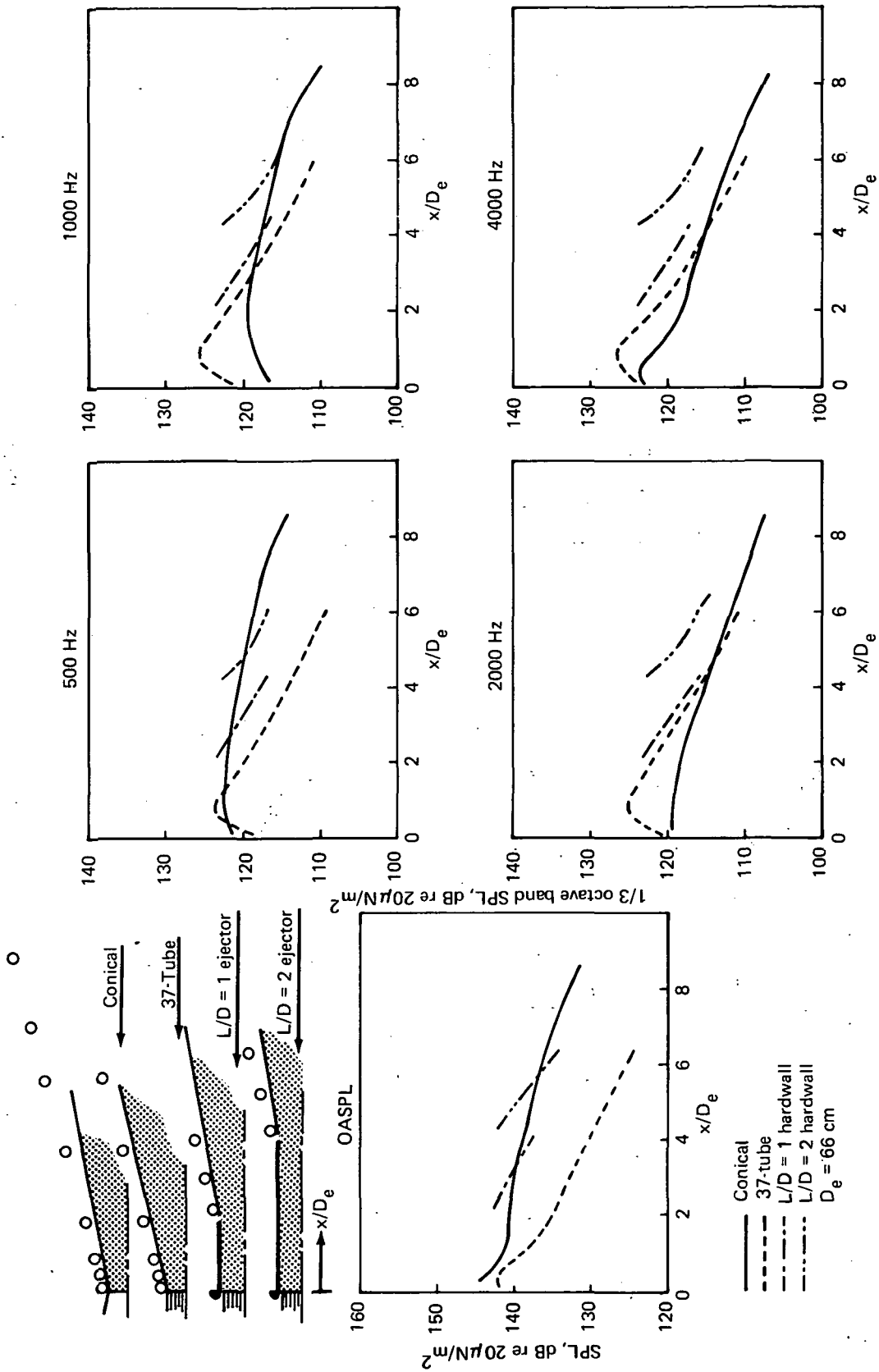
FIGURE 97.– FULL-SCALE NEAR FIELD JET NOISE ENVIRONMENT AT NPR = 1.4 AND T = 595°K

185
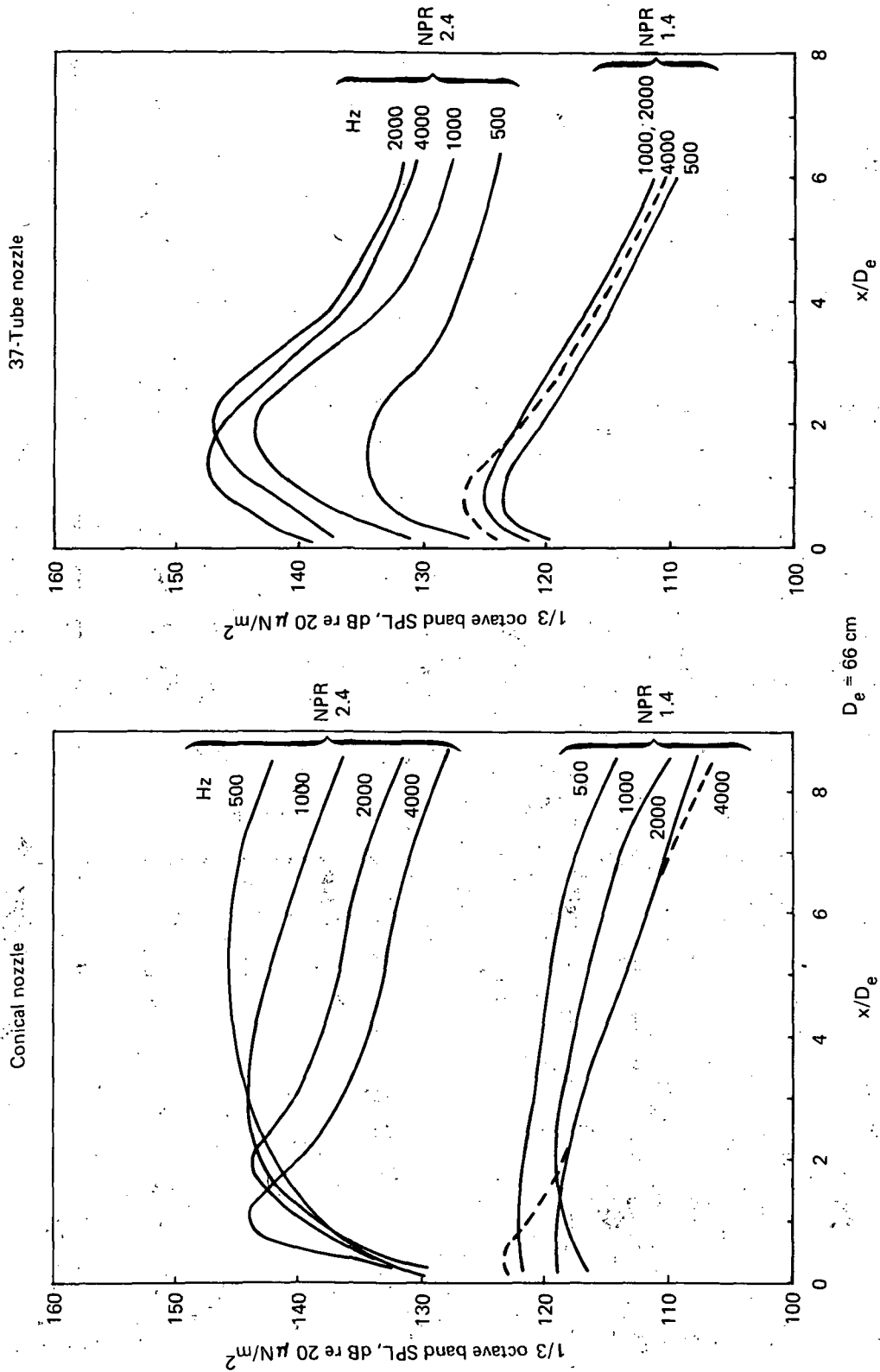
FIGURE 98. "APPARENT" NOISE SOURCE LOCATIONS FOR THE FULL-SCALE CONICAL AND 37-TUBE NOZZLES
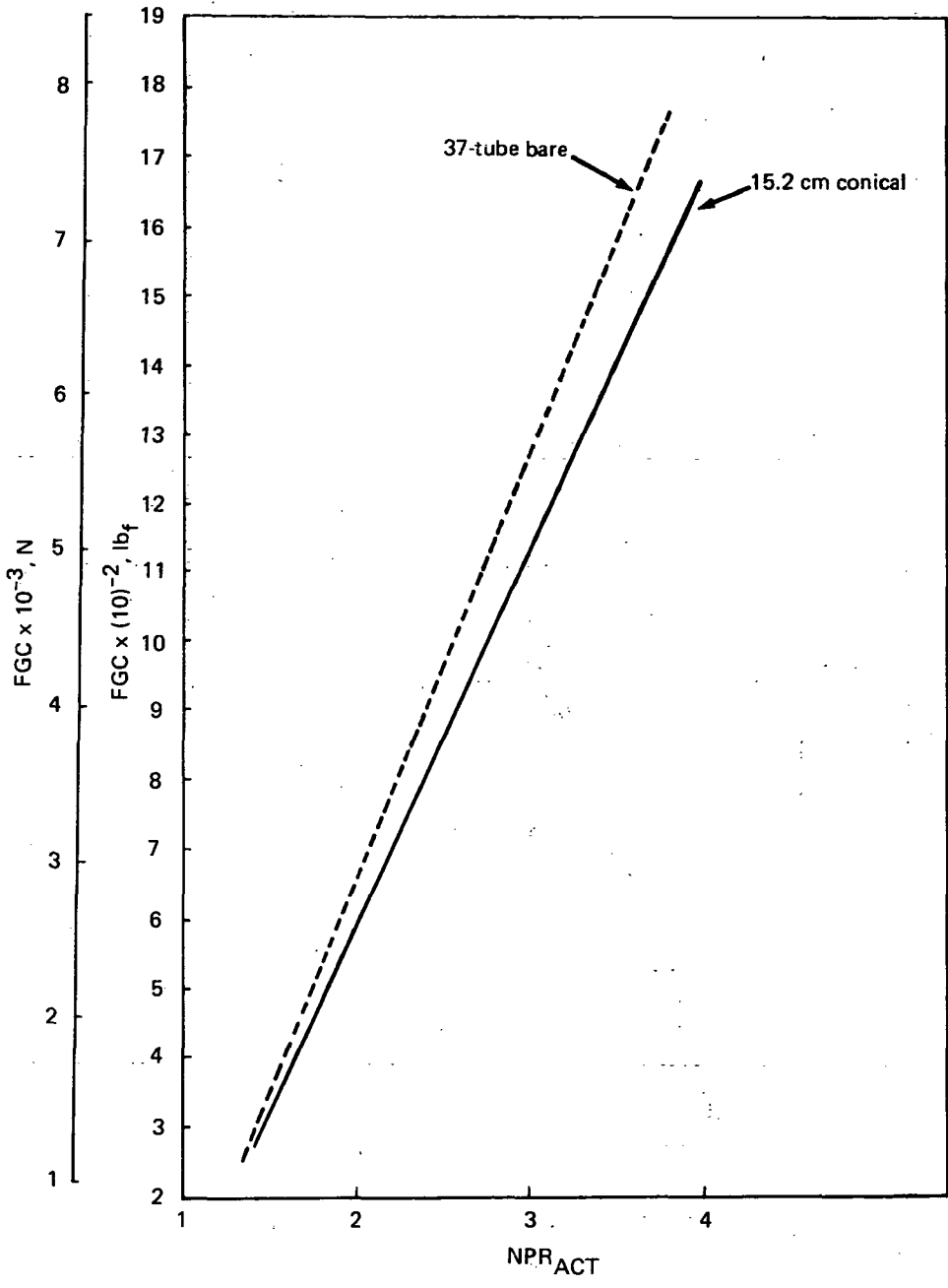
FIGURE 99.— MODEL-SCALE CORRECTED GROSS THRUST FOR CONICAL AND 37-TUBE NOZZLES

187
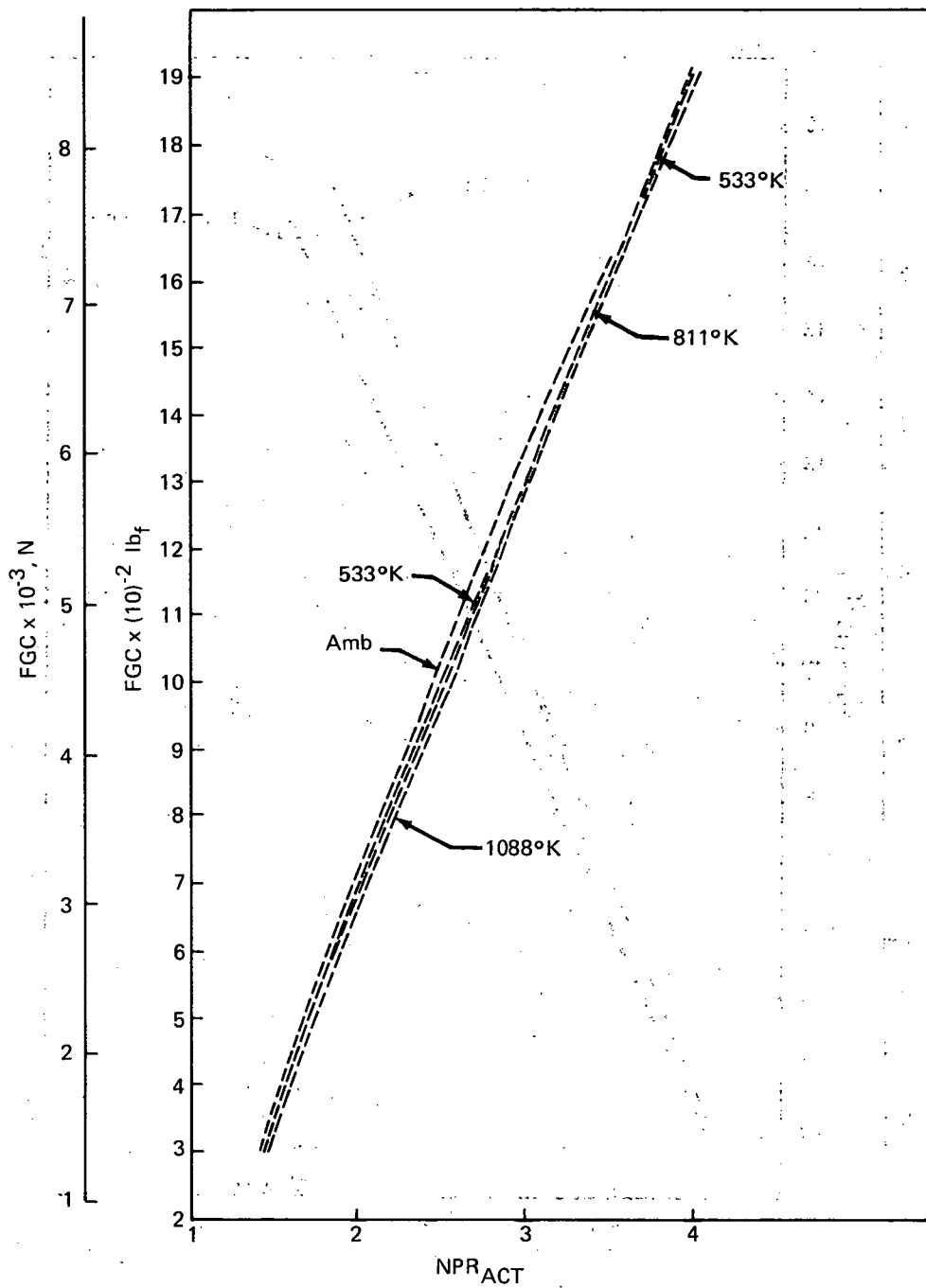
FIGURE 100. — MODEL-SCALE CORRECTED GROSS THRUST FOR THE L/D = 1 HARDWALL EJECTOR
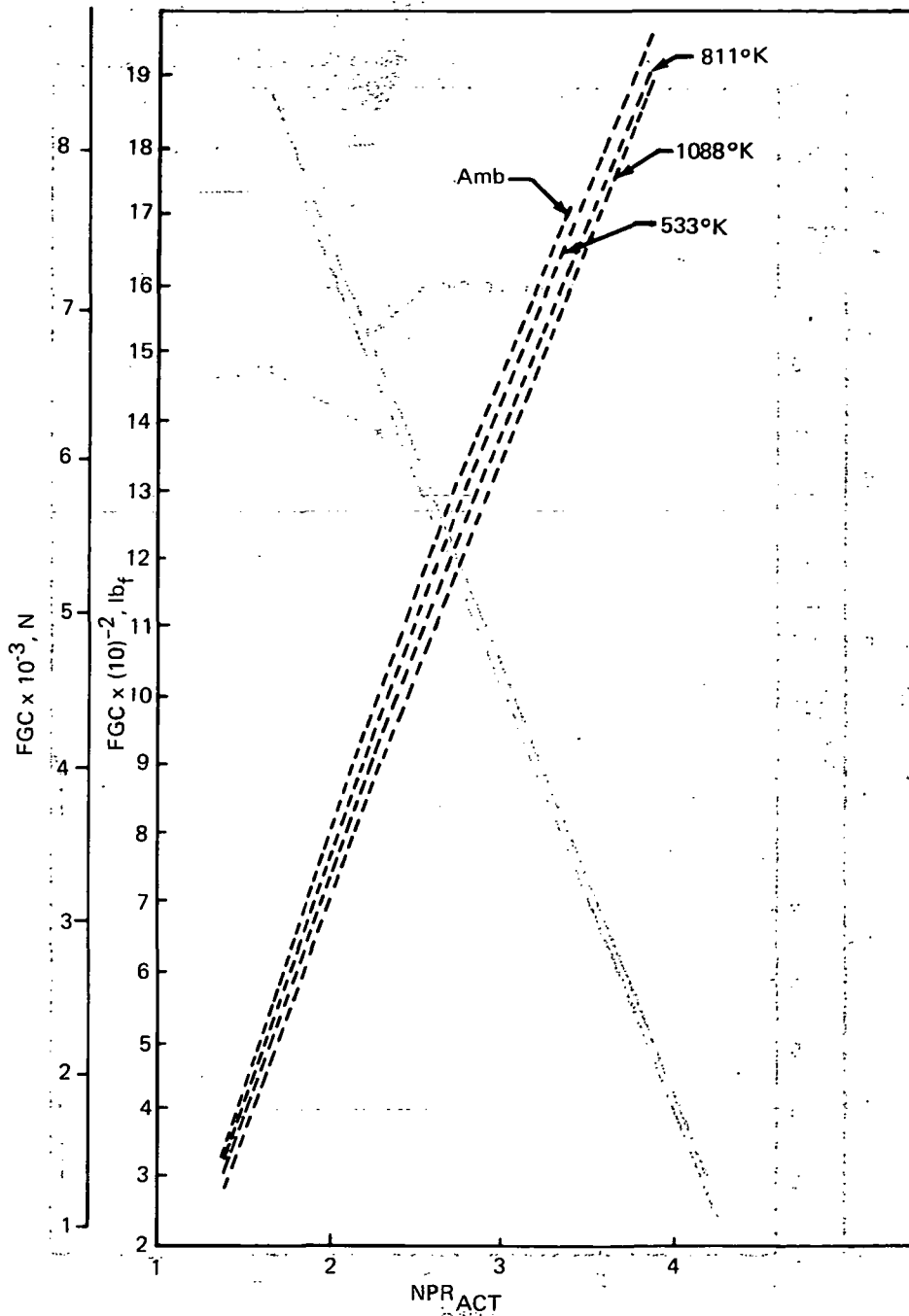
FIGURE 101.— MODEL-SCALE CORRECTED GROSS THRUST FOR THE L/D = 2 HARDWALL EJECTOR
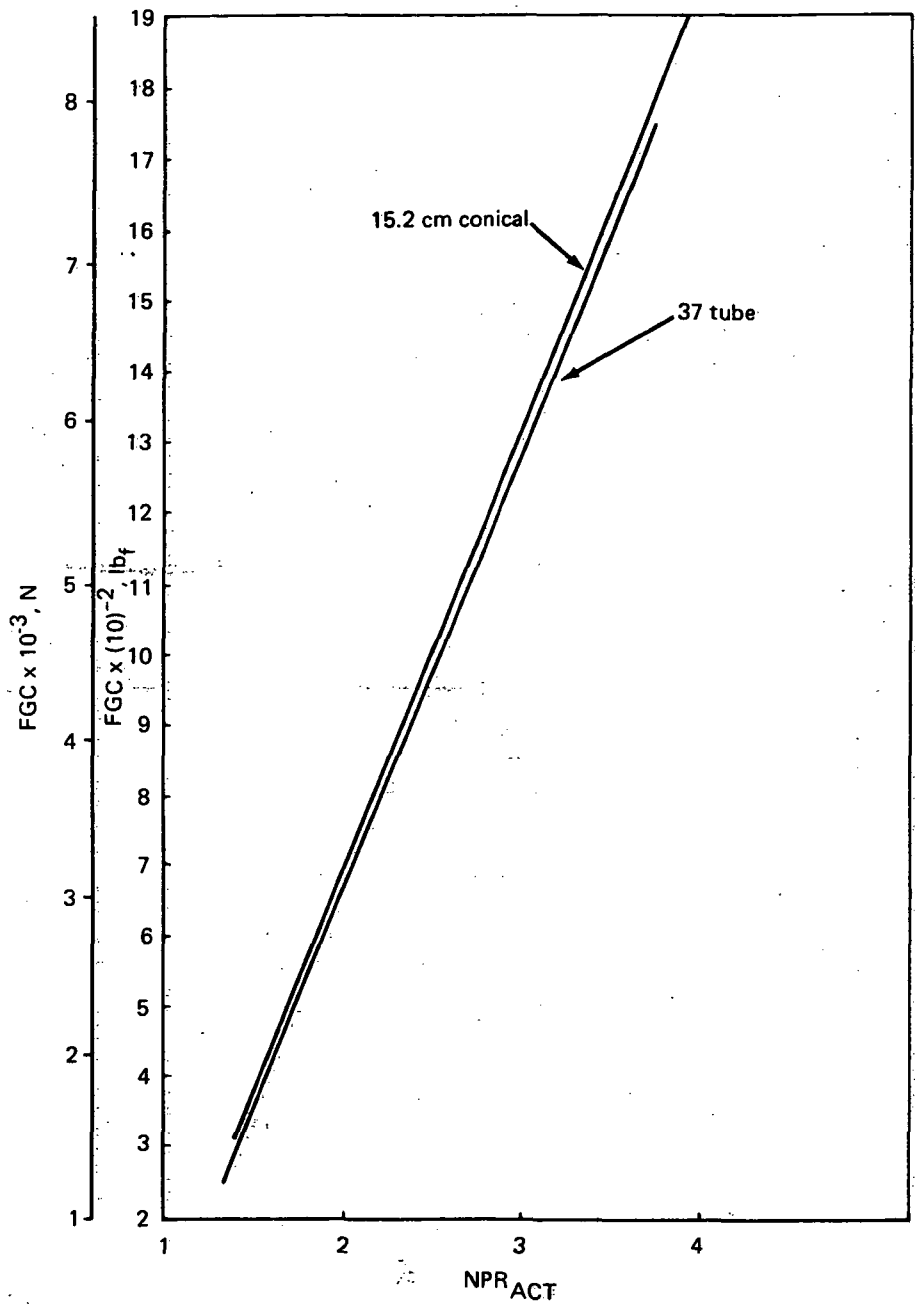
FIGURE 102.— MODEL-SCALE CORRECTED GROSS THRUST COMPARISON BETWEEN THE CONICAL
AND 37-TUBE NOZZLES "MATCHED" AT NPR$_{ACT}$ = 2.4
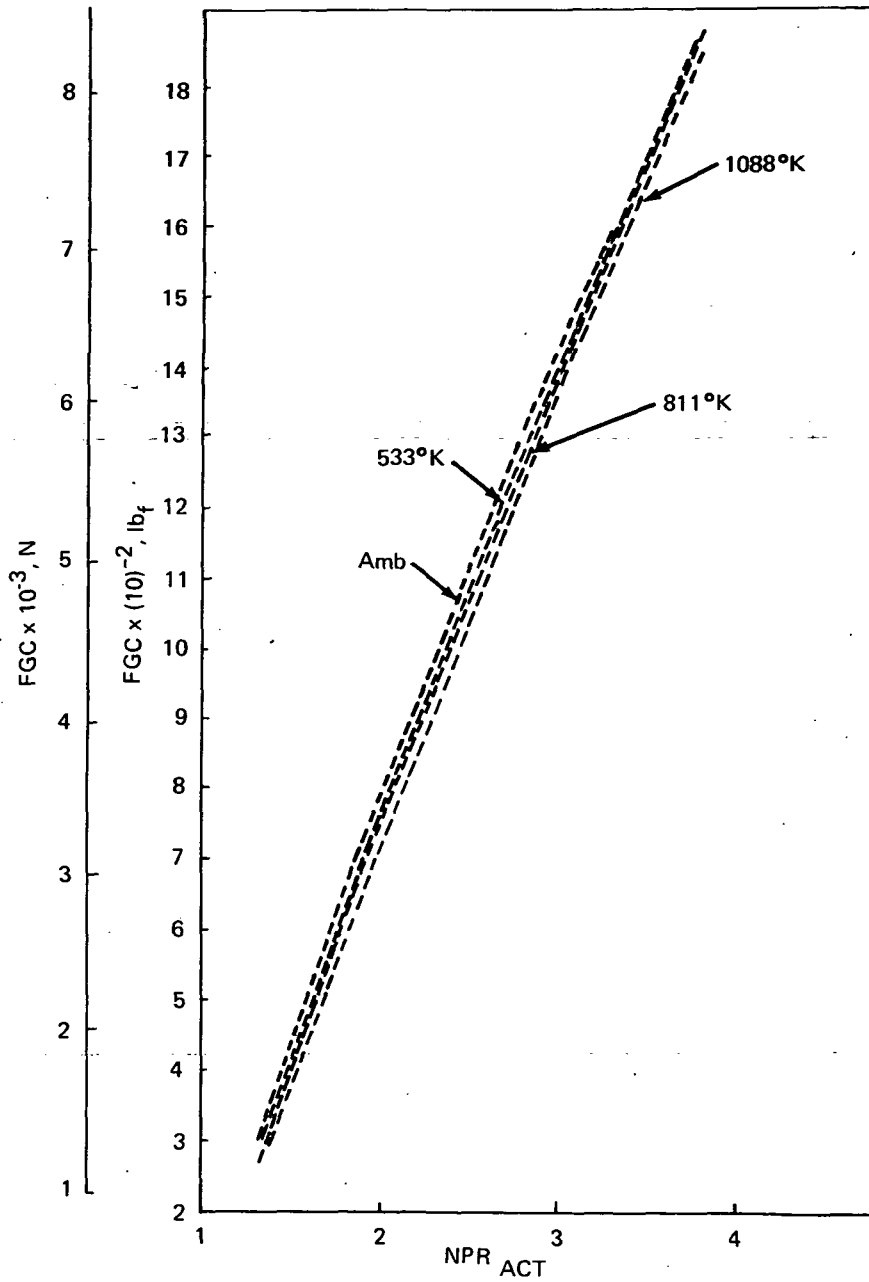
FIGURE 103.– MODEL-SCALE CORRECTED GROSS THRUST FOR THE L/D = 1 HARDWALL EJECTOR "MATCHED" TO THE 37-TUBE NOZZLE AT NPR_{ACT} = 2.4
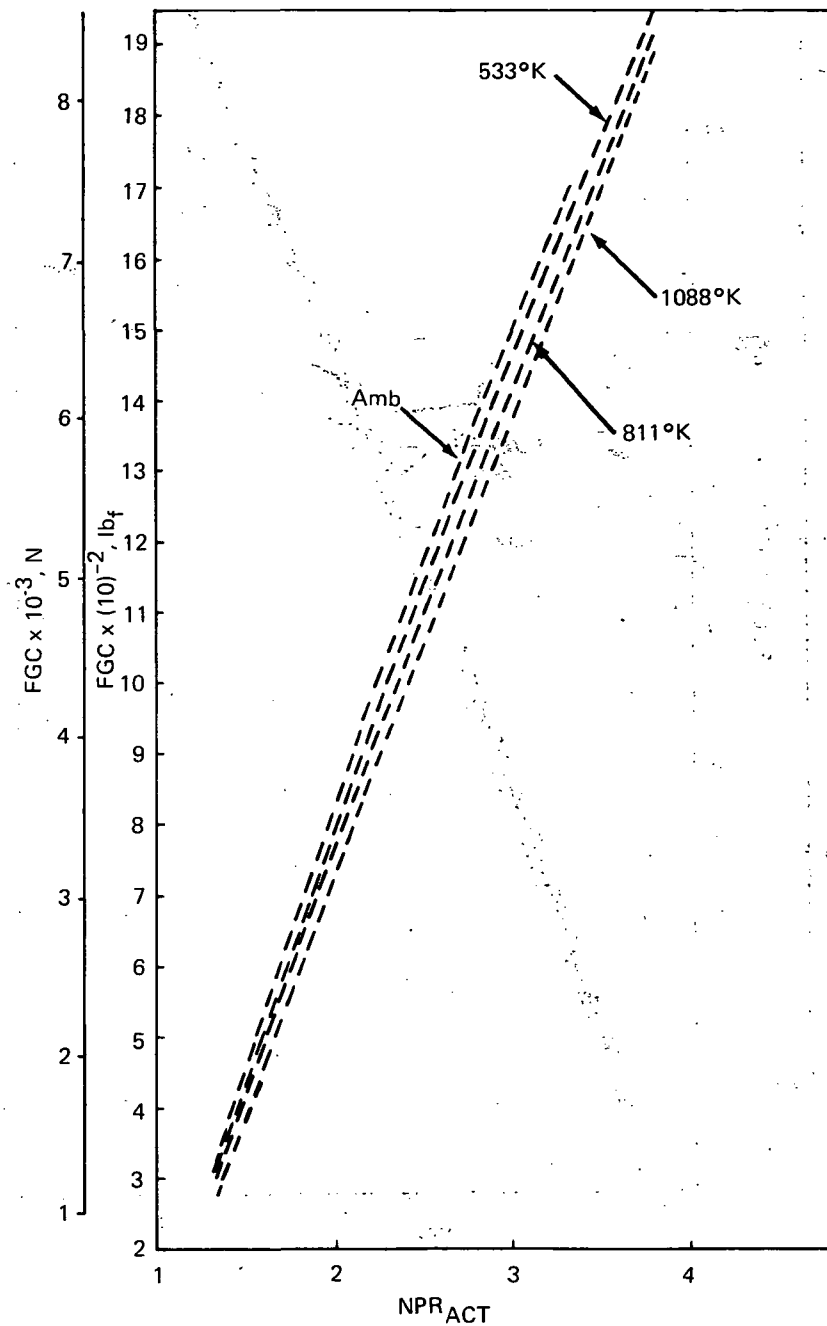
FIGURE 104.— MODEL-SCALE CORRECTED GROSS THRUST FOR THE L/D = 2 HARDWALL EJECTOR "MATCHED" TO THE 37-TUBE NOZZLE AT NPR_{ACT} = 2.4
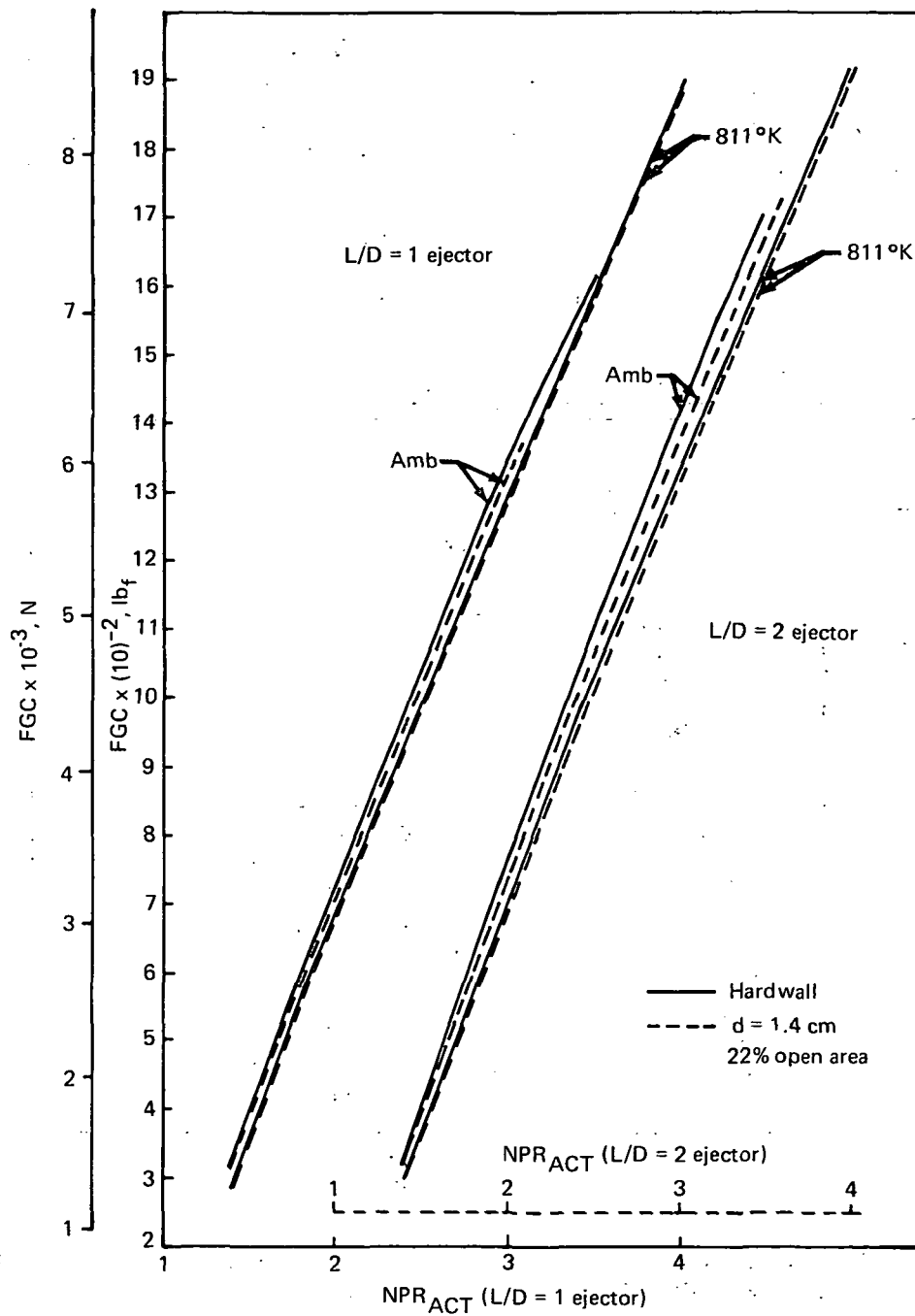
FIGURE 105.— THE EFFECT OF ACOUSTIC LINING ON THE THRUST OF L/D = 1 AND L/D = 2
MODEL-SCALE EJECTORS

193
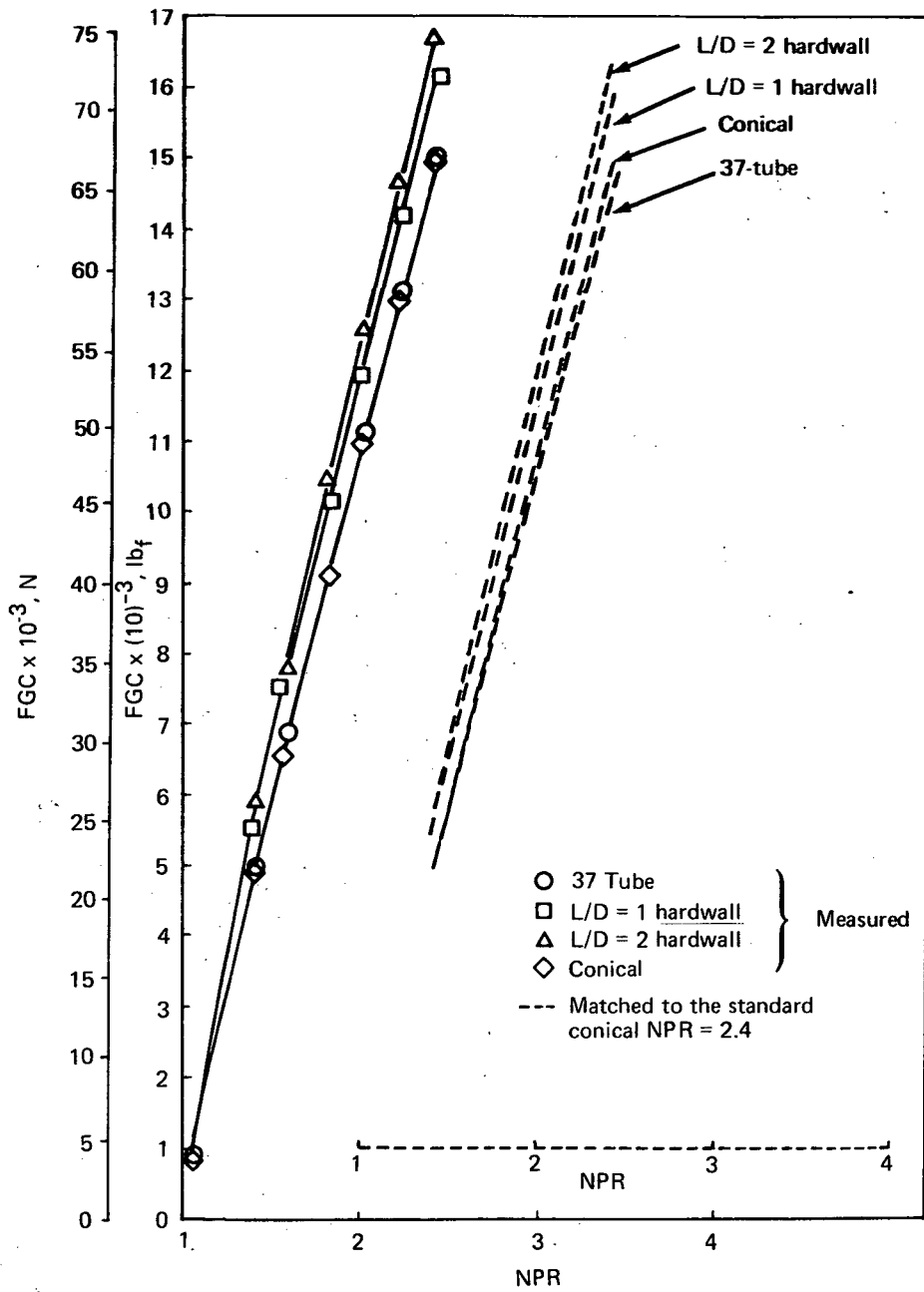
FIGURE 106.— FULL-SCALE MEASURED AND "MATCHED" CORRECTED GROSS THRUST FOR ALL NOZZLE CONFIGURATIONS.

194
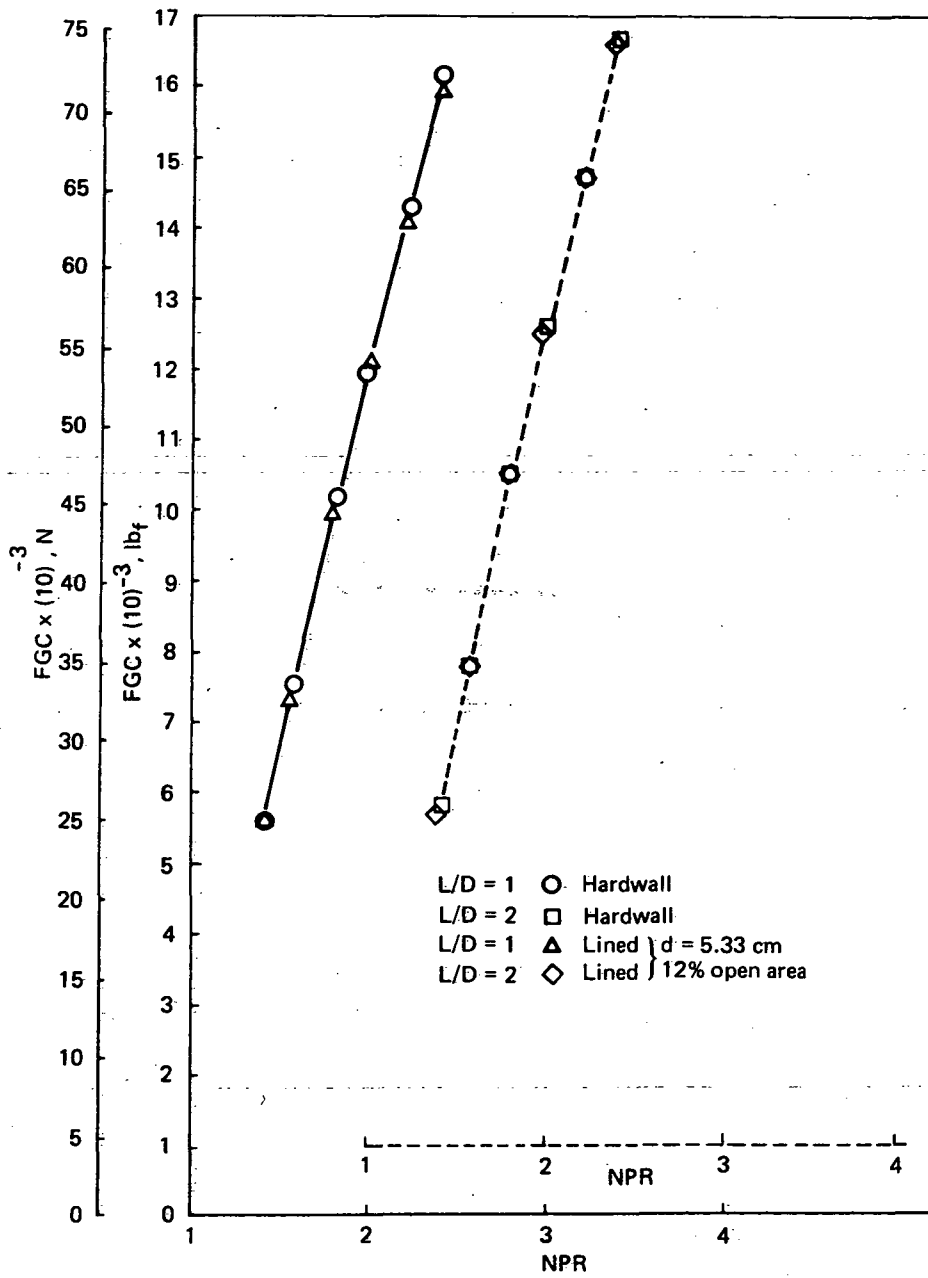
FIGURE 107.— THE EFFECT OF ACOUSTIC LINING ON THE THRUST OF L/D = 1 AND L/D = 2 FULL-SCALE EJECTORS

195
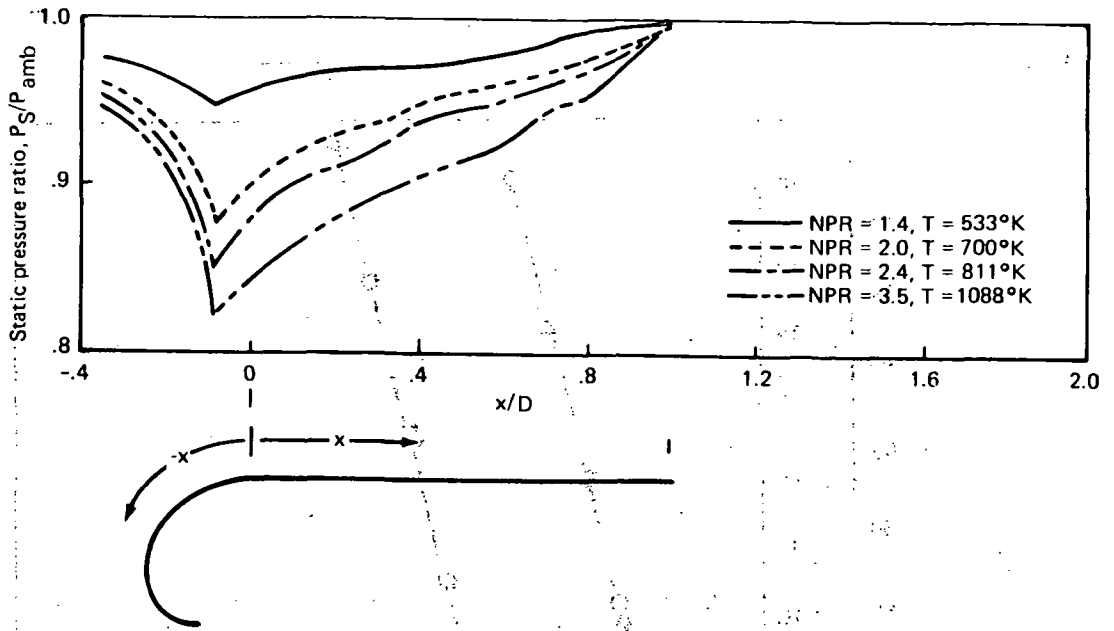
FIGURE 108. — MODEL-SCALE EJECTOR WALL STATIC PRESSURE DISTRIBUTIONS FOR L/D = 1 HARDWALL EJECTOR
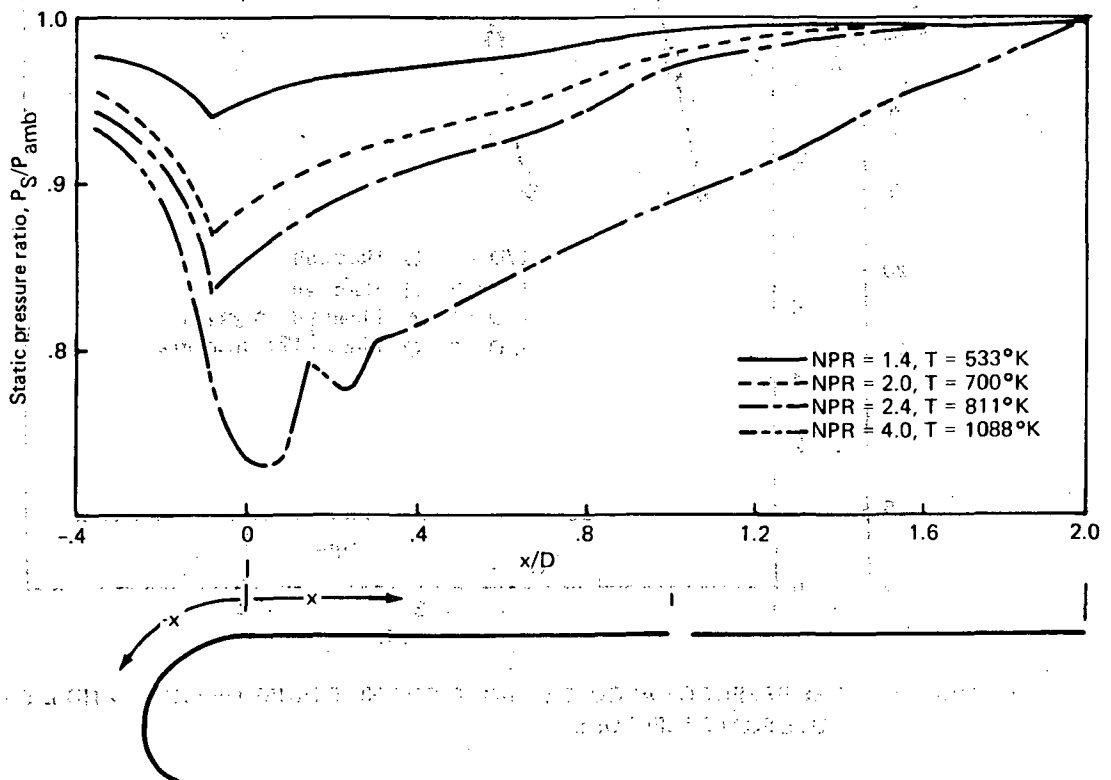
FIGURE 109. — MODEL-SCALE EJECTOR WALL STATIC PRESSURE DISTRIBUTIONS FOR L/D = 2 HARDWALL EJECTOR

196
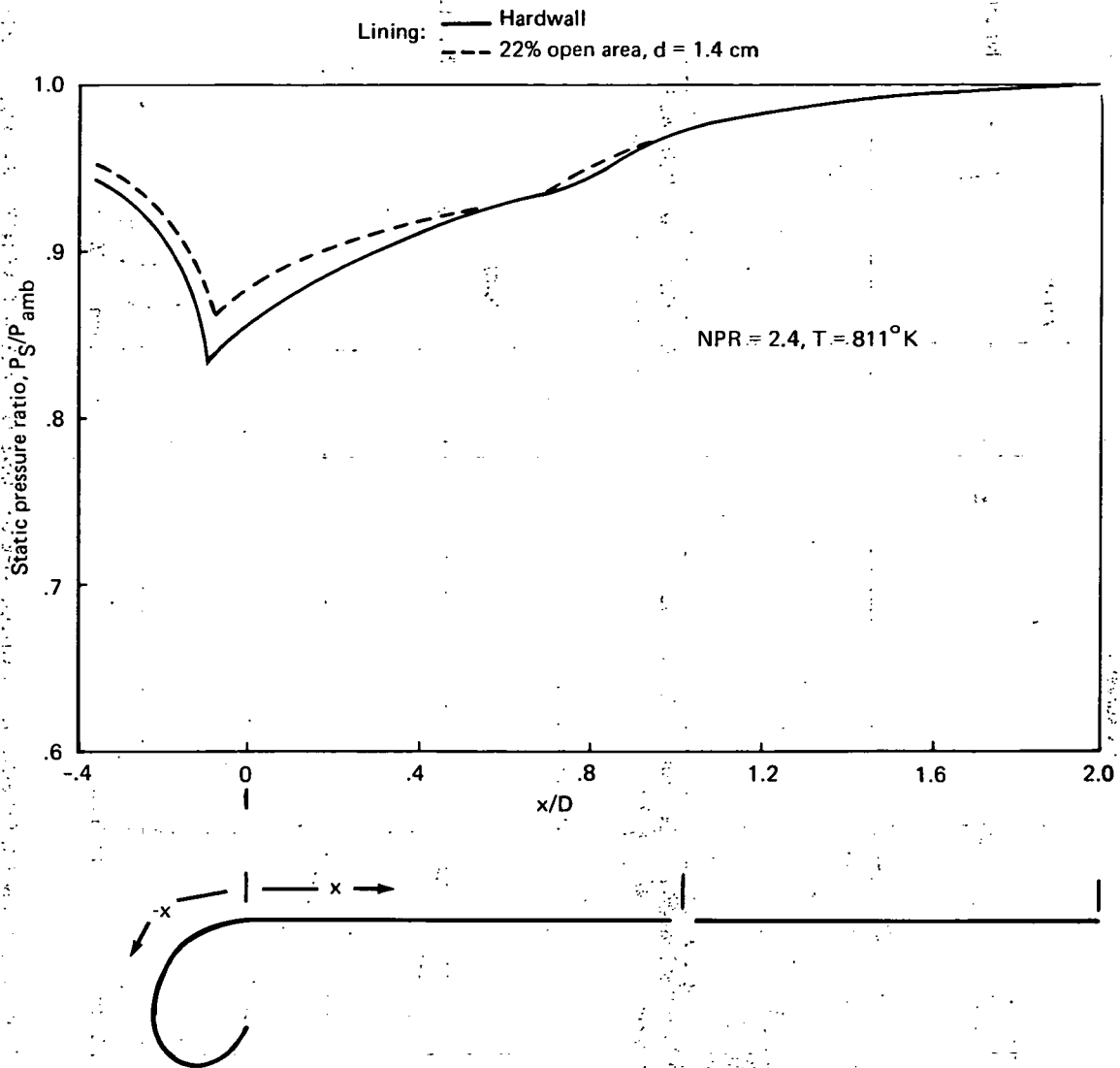
FIGURE 110. — THE EFFECT OF ACOUSTIC LINING ON THE WALL STATIC PRESSURE OF THE MODEL-SCALE L/D = 2 EJECTOR
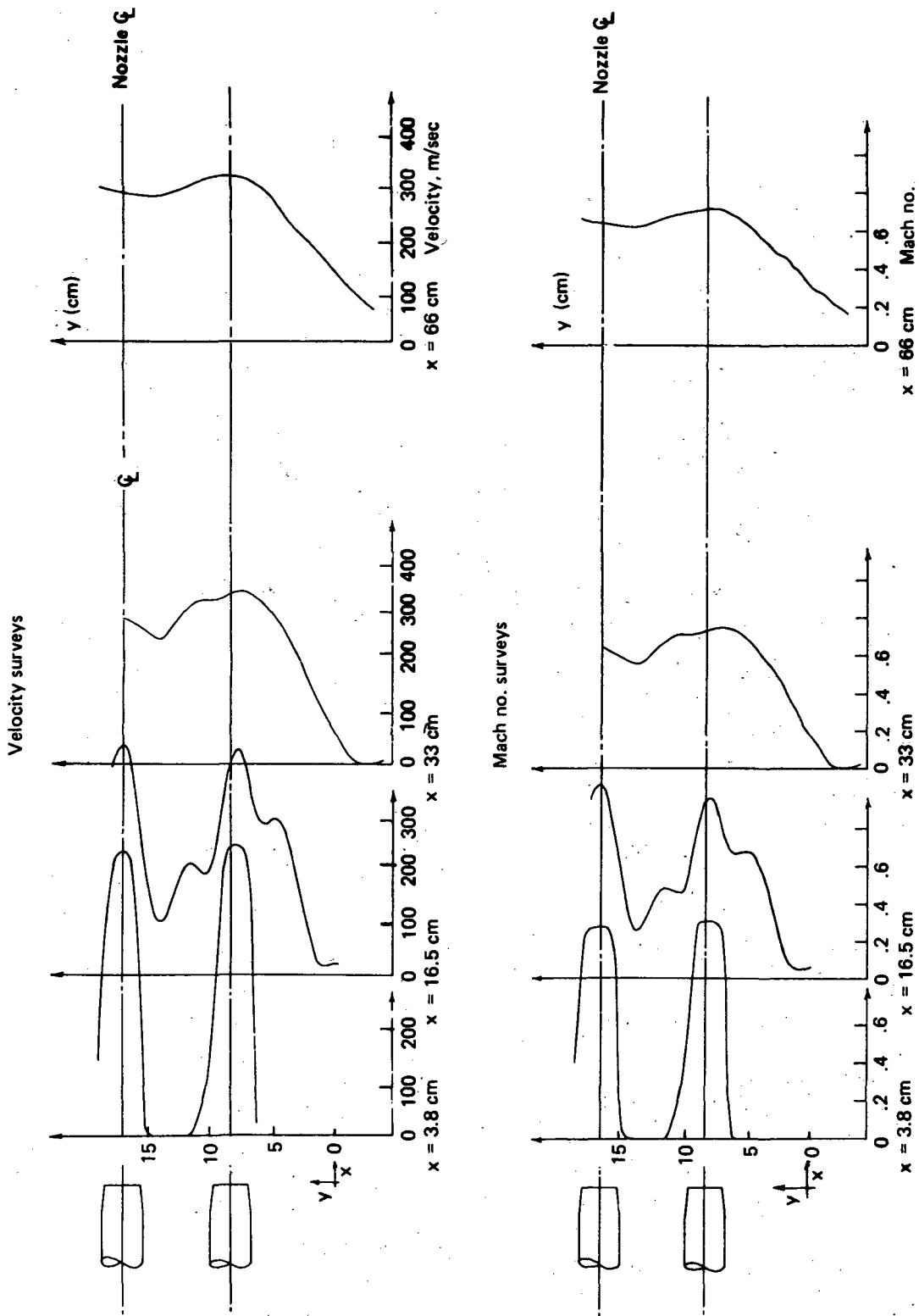
FIGURE 111.– MODEL-SCALE VELOCITY AND MACH NUMBER SURVEYS ACROSS THE 37-TUBE NOZZLE JET AT NPR = 2.4 AND T = 811°K
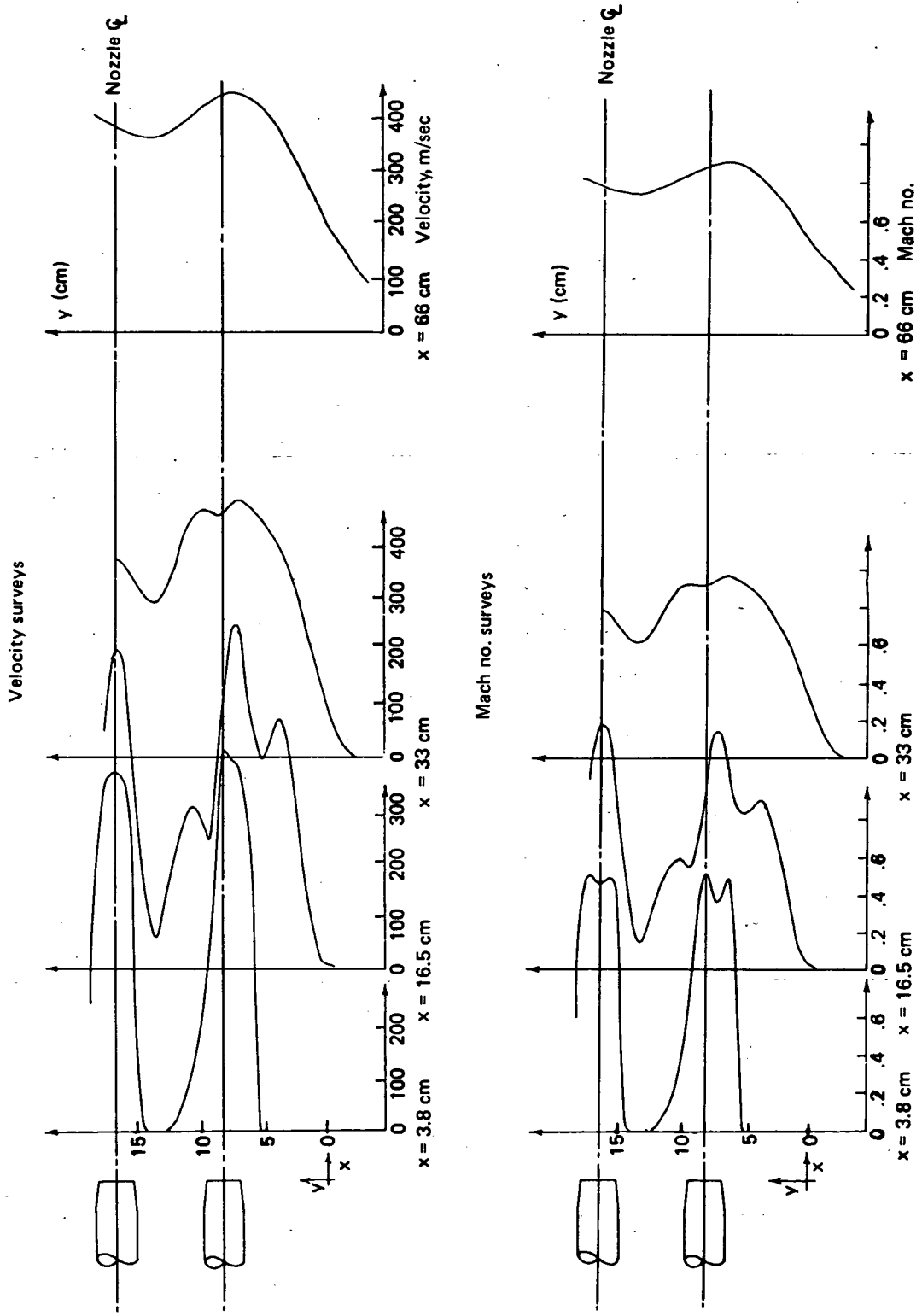
FIGURE 112. — MODEL-SCALE VELOCITY AND MACH NUMBER SURVEYS ACROSS THE 37-TUBE NOZZLE JET AT NPR = 3.5 AND T = 1088°K

199
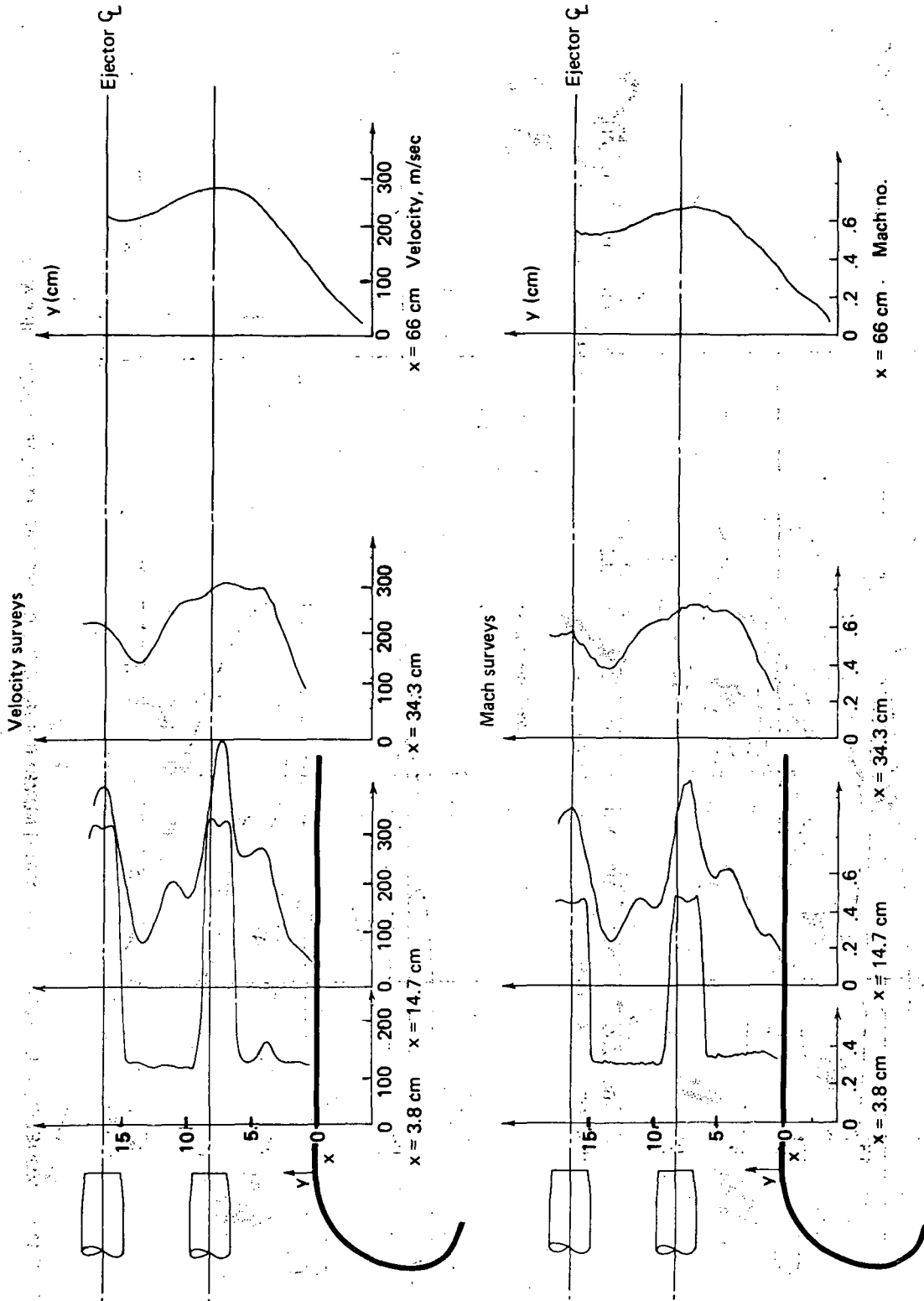
FIGURE 113.– MODEL-SCALE VELOCITY AND MACH NUMBER SURVEYS ACROSS THE FLOW OF THE L/D = 1 EJECTOR AT NPR = 2.4 AND T = 811° K
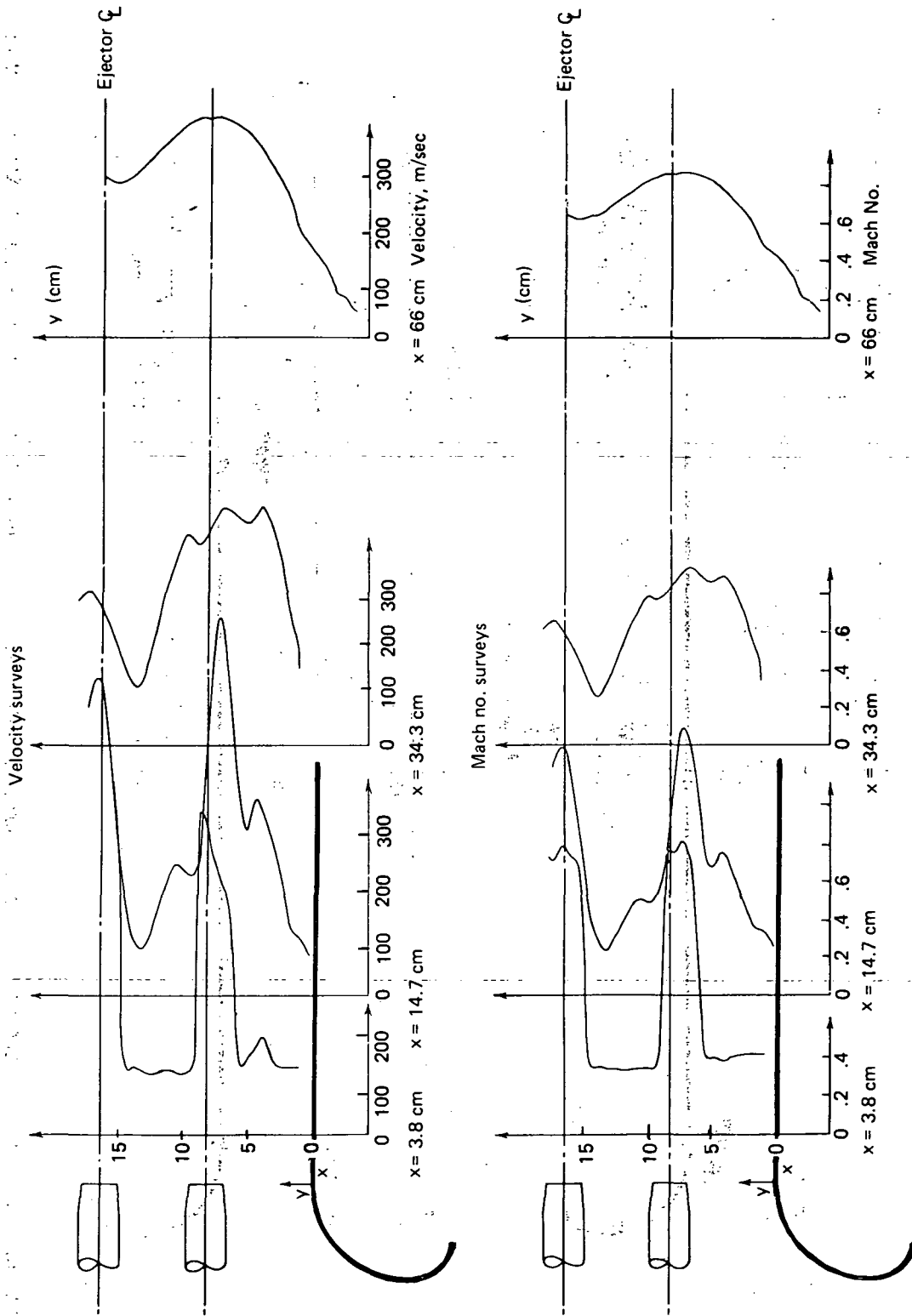
FIGURE 114.– MODEL-SCALE VELOCITY AND MACH NUMBER SURVEYS ACROSS THE FLOW OF THE L/D = 1 EJECTOR AT NPR = 3.5 AND T = 1088° K
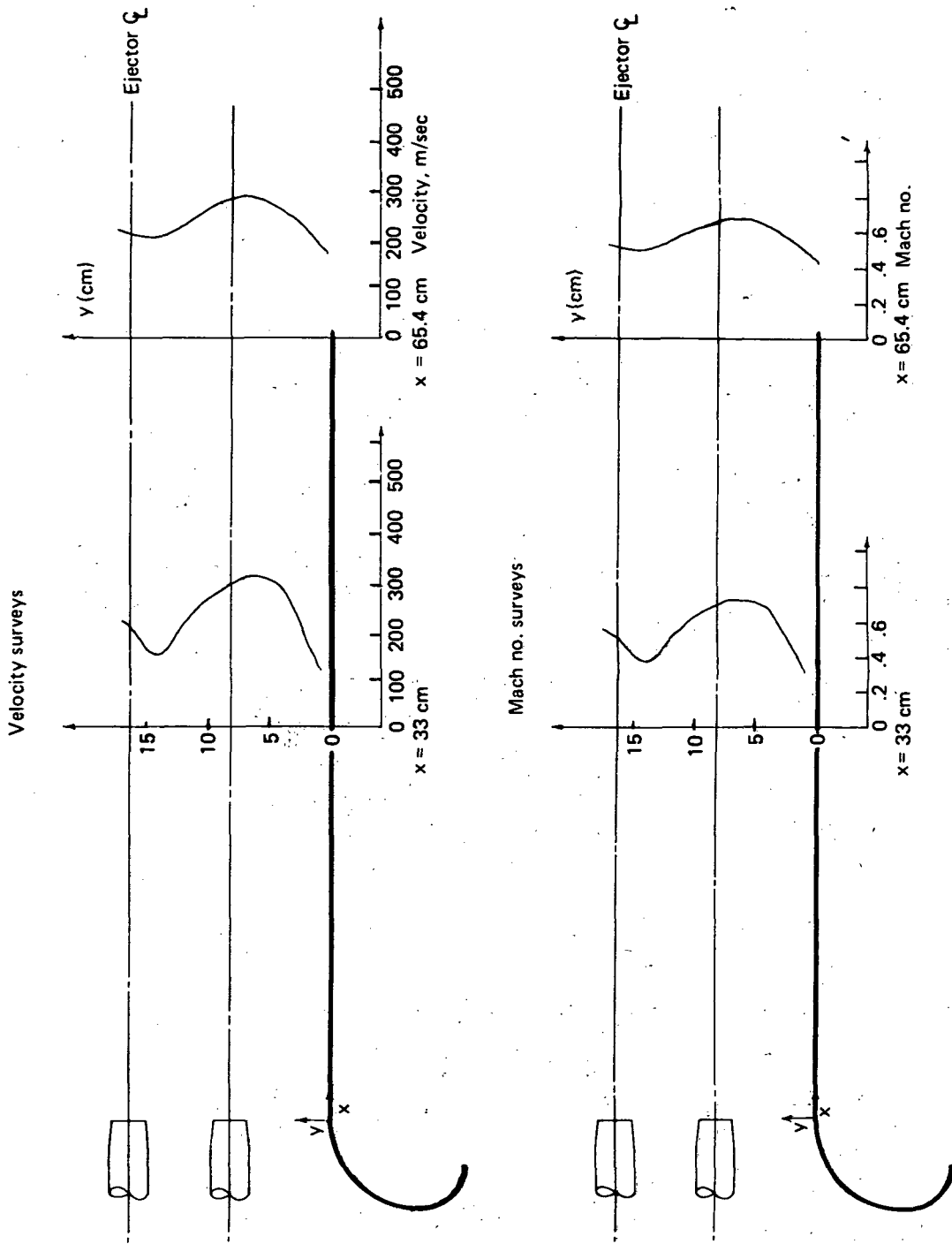
FIGURE 115.– MODEL-SCALE VELOCITY AND MACH NUMBER SURVEYS ACROSS THE FLOW OF THE L/D = 2 EJECTOR AT NPR = 2.4 AND T = 811° K
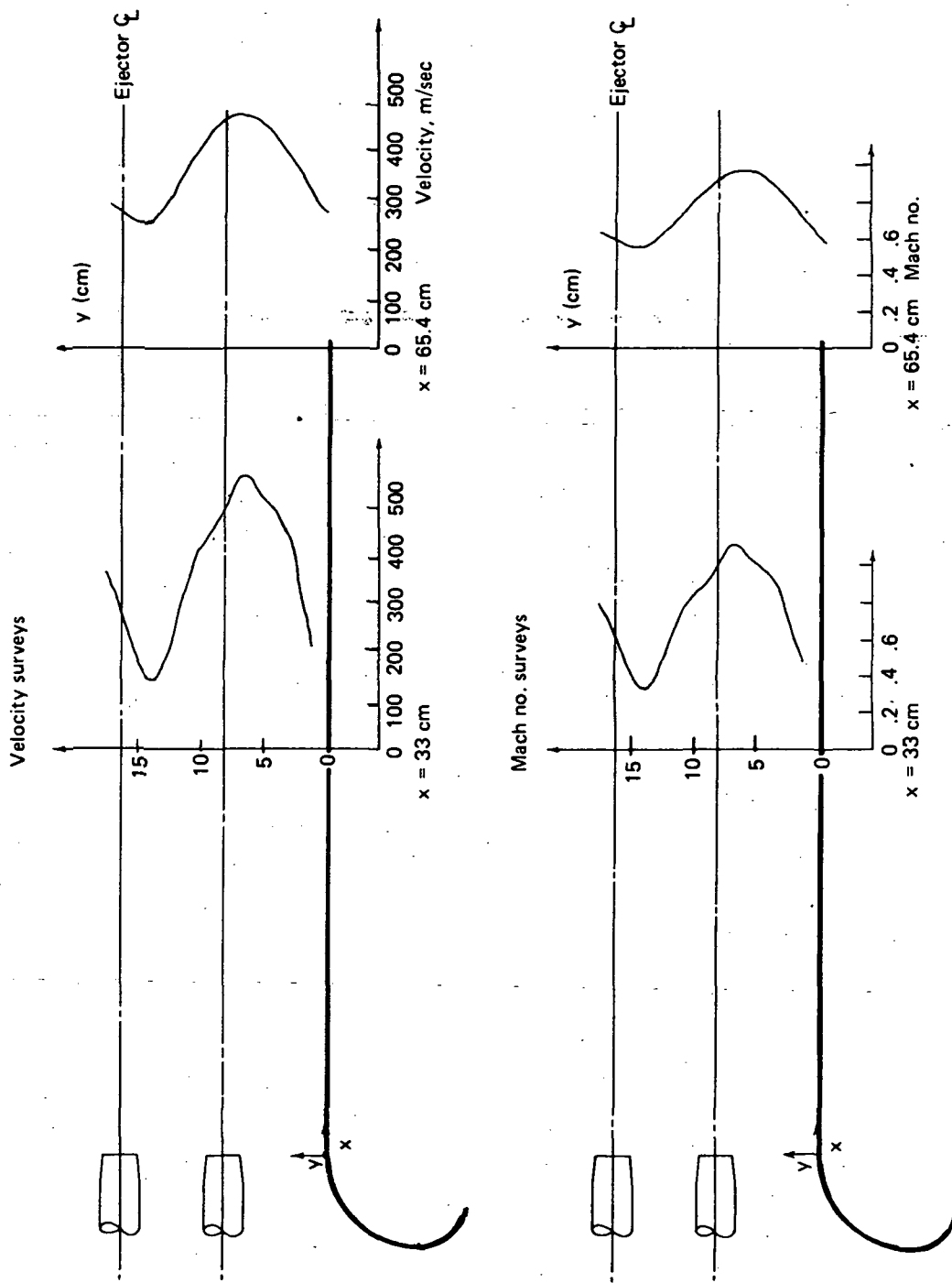
FIGURE 116. – MODEL-SCALE VELOCITY AND MACH NUMBER SURVEYS ACROSS THE FLOW OF THE L/D = 2 EJECTOR AT NPR = 4.0 AND T = 1088° K

203
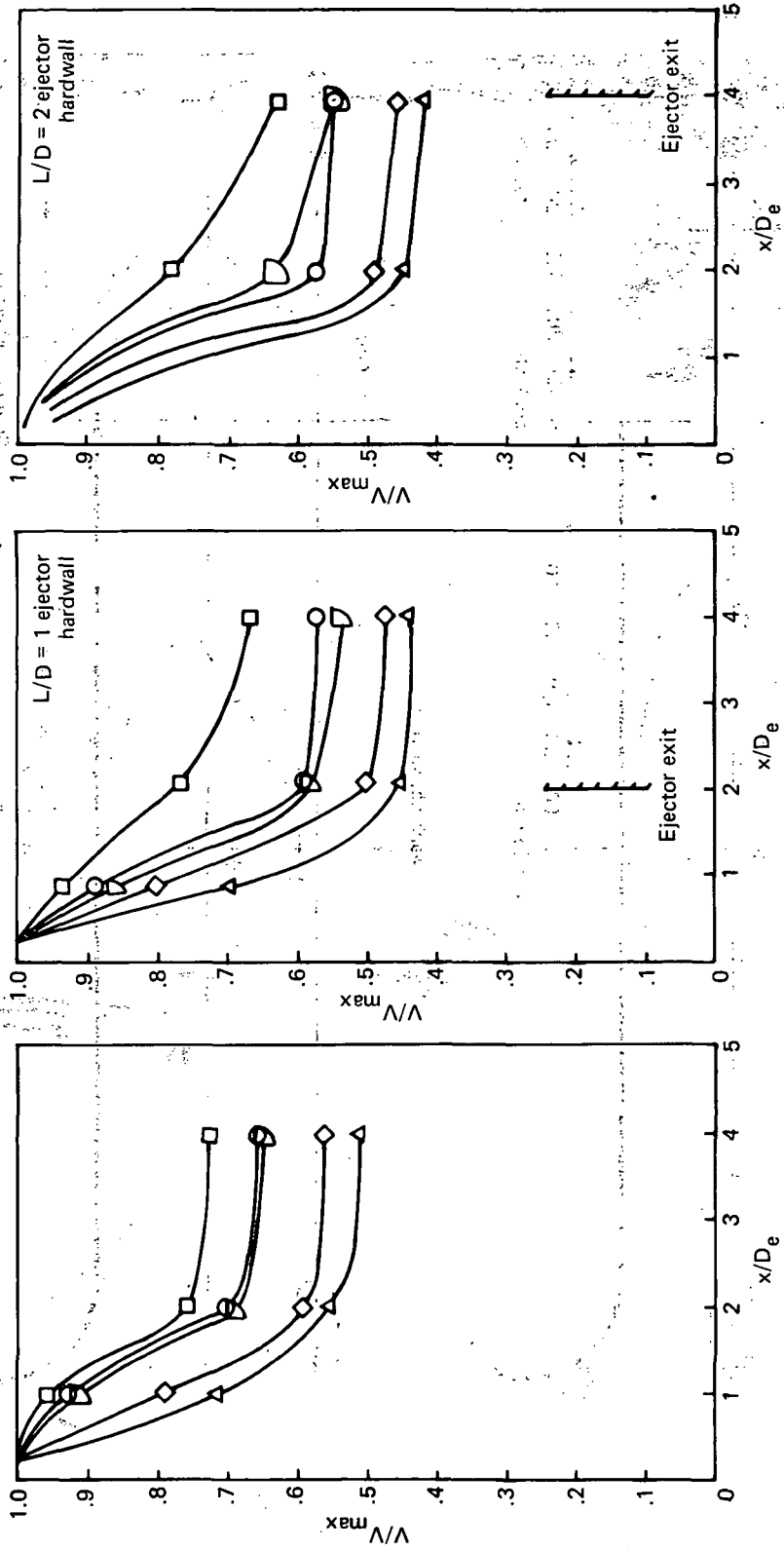
FIGURE 117. – MODEL-SCALE JET PEAK VELOCITY DECAY FOR THE 37-TUBE NOZZLE,
L/D = 1 AND L/D = 2 EJECTORS

Mach no. was obtained from P_S/P ambient where P_S = static pressure at center tube exit.

M = Mach number between tubes

V = velocity between tubes, m/sec
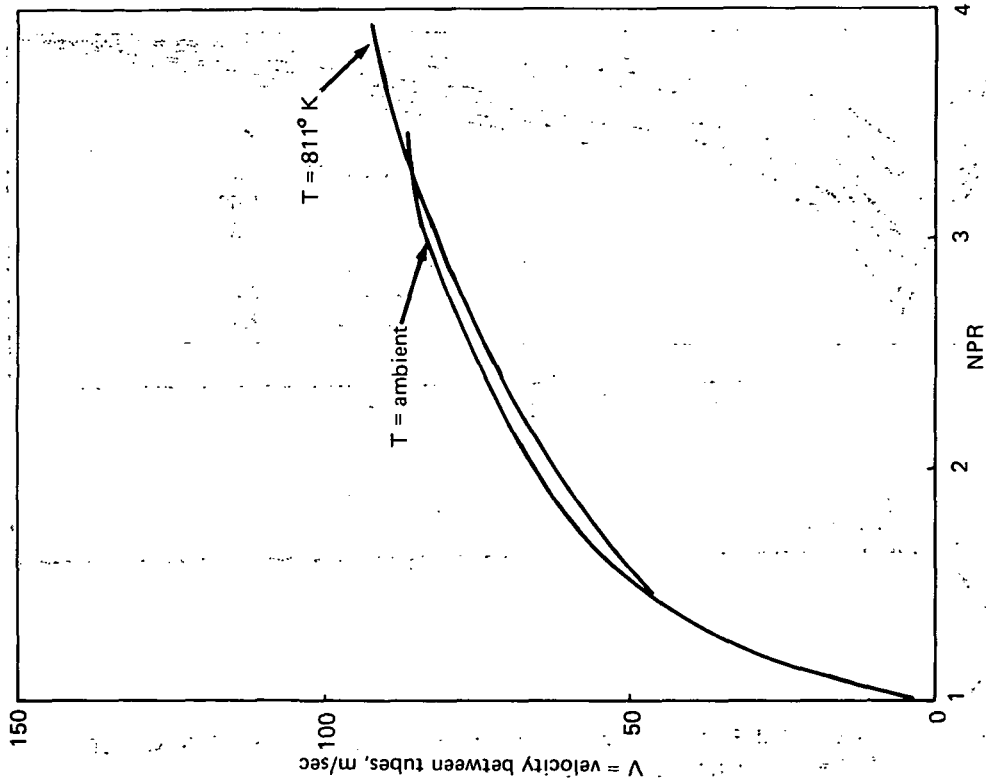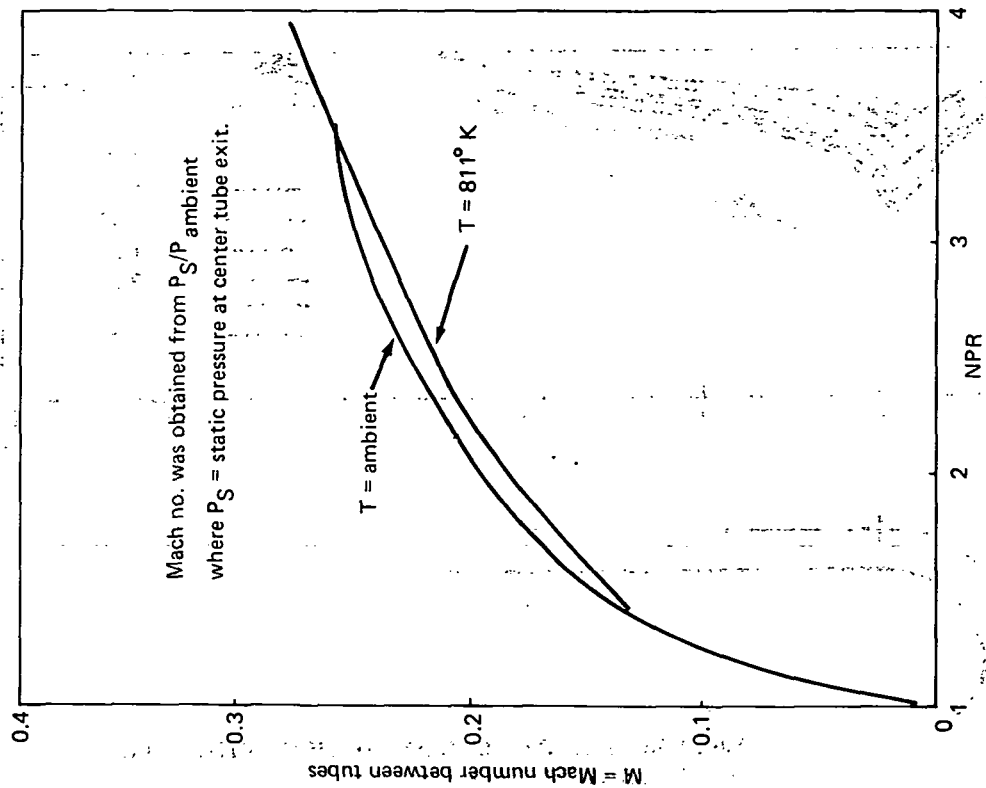
FIGURE 118.– MODEL-SCALE ESTIMATED FLOW VELOCITY AND MACH NUMBER BETWEEN THE TUBES OF THE 37-TUBE NOZZLE

205
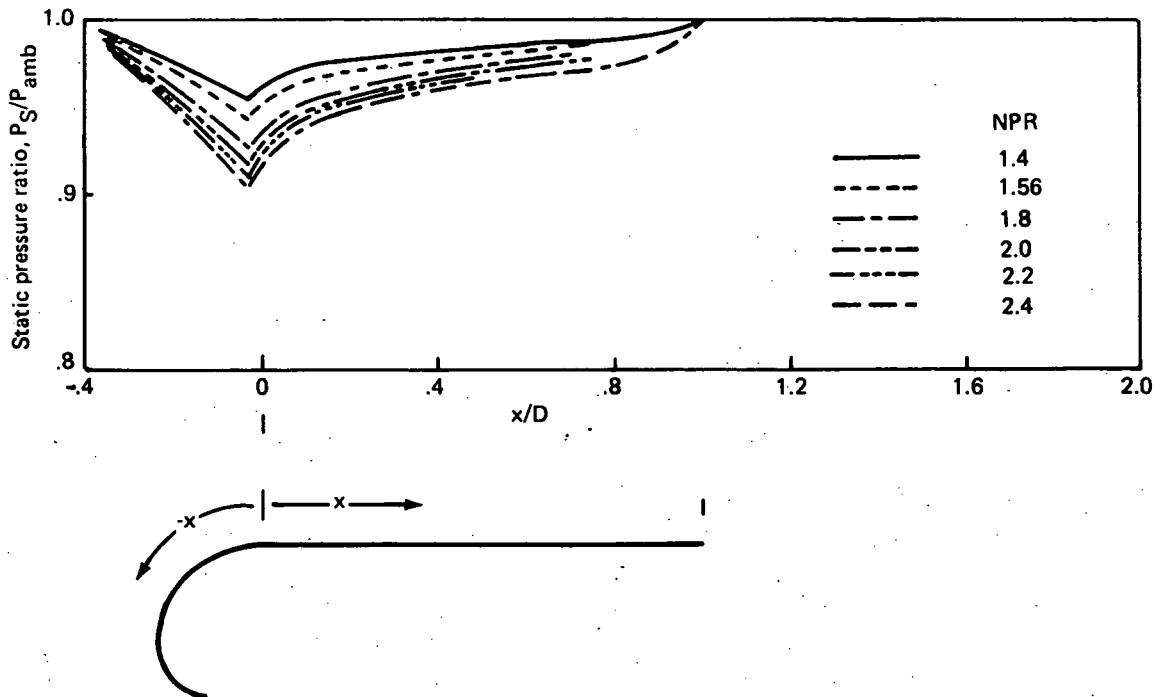
FIGURE 119. – FULL-SCALE EJECTOR WALL STATIC PRESSURE DISTRIBUTIONS FOR
L/D = 1 HARDWALL EJECTOR
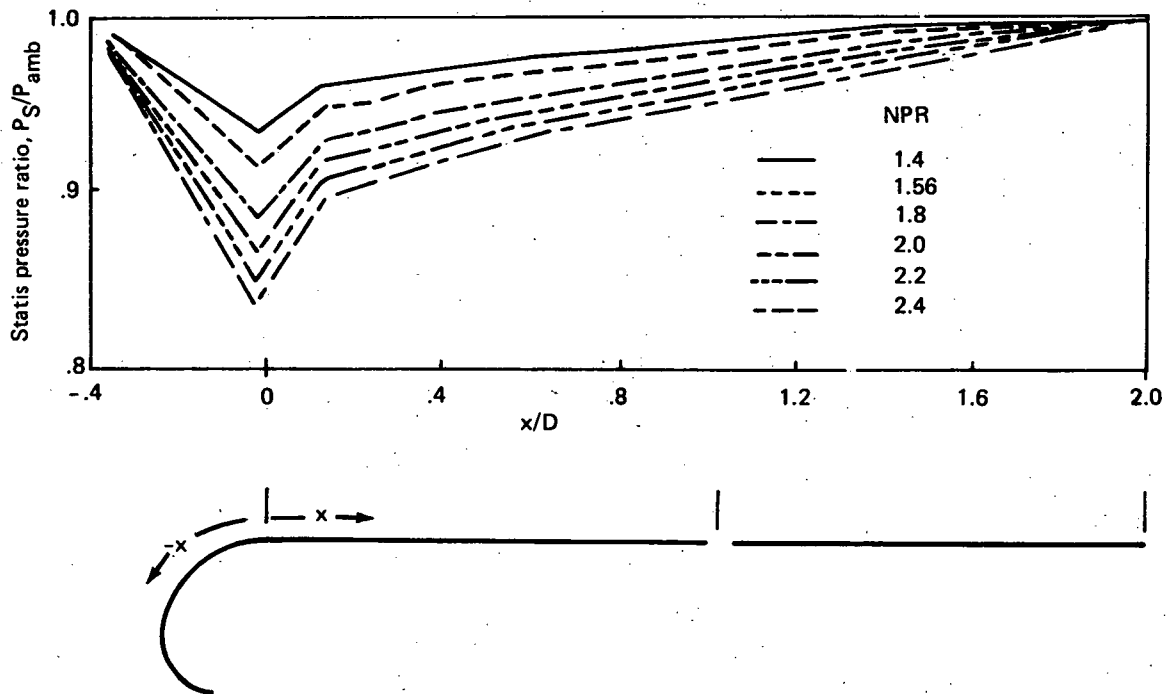
FIGURE 120. – FULL-SCALE EJECTOR WALL STATIC PRESSURE DISTRIBUTIONS FOR
L/D = 2 HARDWALL EJECTOR

206
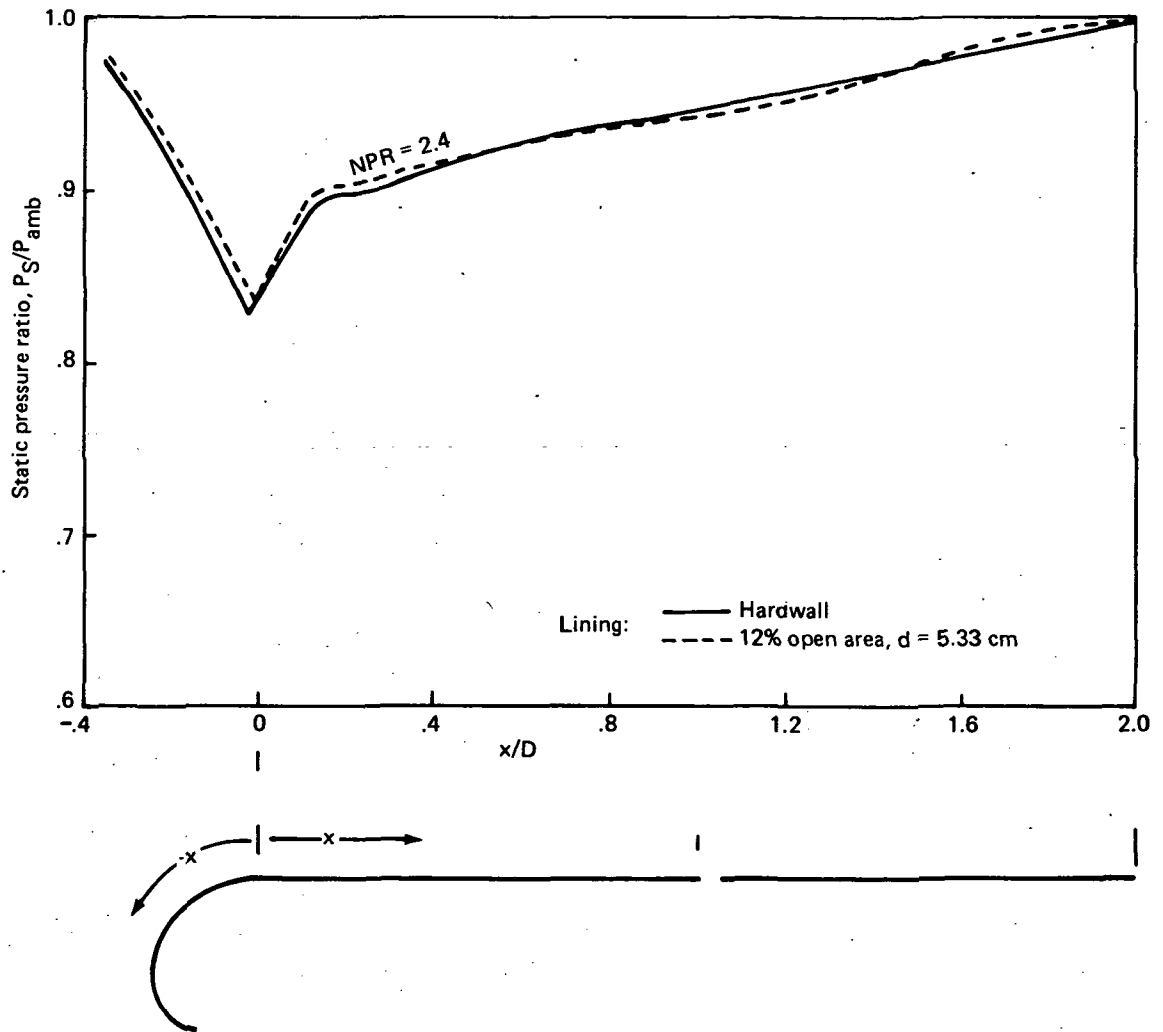
FIGURE 121. — THE EFFECT OF ACOUSTIC LINING ON THE WALL STATIC PRESSURE OF THE FULL-SCALE L/D = 2 EJECTOR

FIGURE 122.– FULL-SCALE VELOCITY AND MACH NUMBER SURVEYS ACROSS THE J-75 ENGINE CONICAL NOZZLE JET AT NPR = 2.4 AND T_T = 823° K
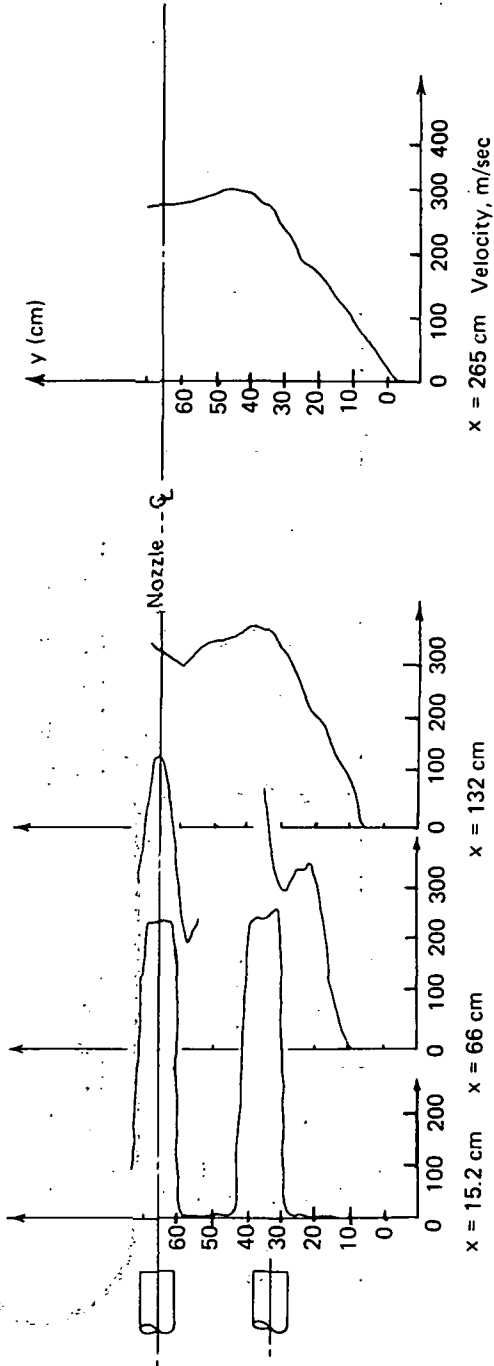
FIGURE 123. — FULL-SCALE VELOCITY AND MACH NUMBER SURVEYS ACROSS THE 37-TUBE NOZZLE JET AT NPR = 2.4 AND T_T = 823° K

209
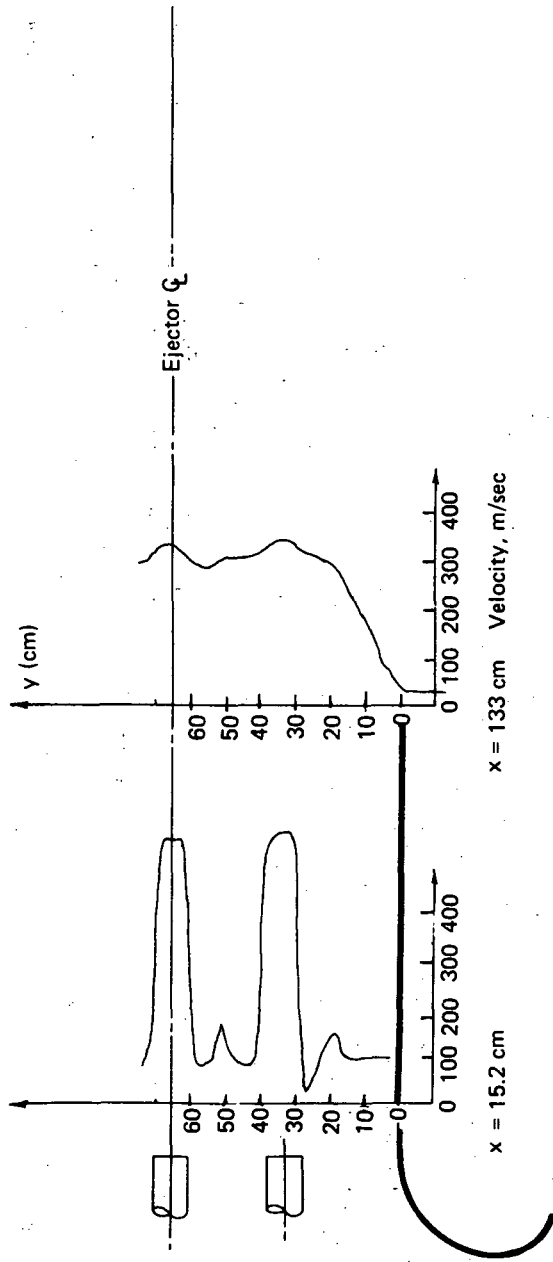
FIGURE 124. – FULL-SCALE VELOCITY AND MACH NUMBER SURVEYS ACROSS THE FLOW OF THE L/D = 1 HARDWALL EJECTOR AT NPR = 2.0 AND T_T = 723° K

Velocity surveys

Mach no. surveys

——— Hardwall
- - - - Lined d = 5.33 cm
12% open area
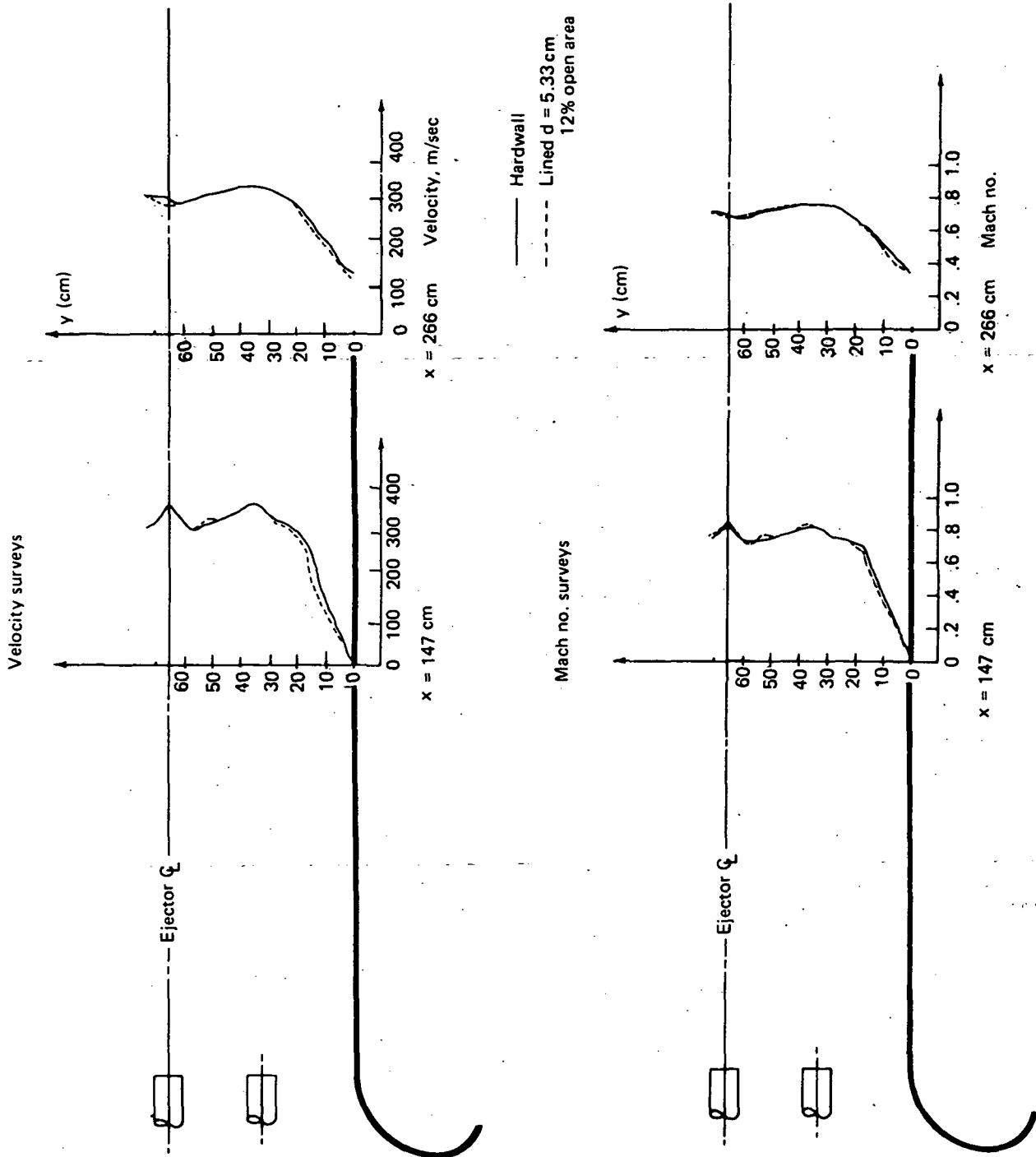
FIGURE 125. – FULL-SCALE VELOCITY AND MACH NUMBER SURVEYS ACROSS THE FLOW OF THE L/D = 2 HARDWALL AND ACOUSTICALLY LINED EJECTORS AT NPR = 2.4 AND T_T = 823° K

211
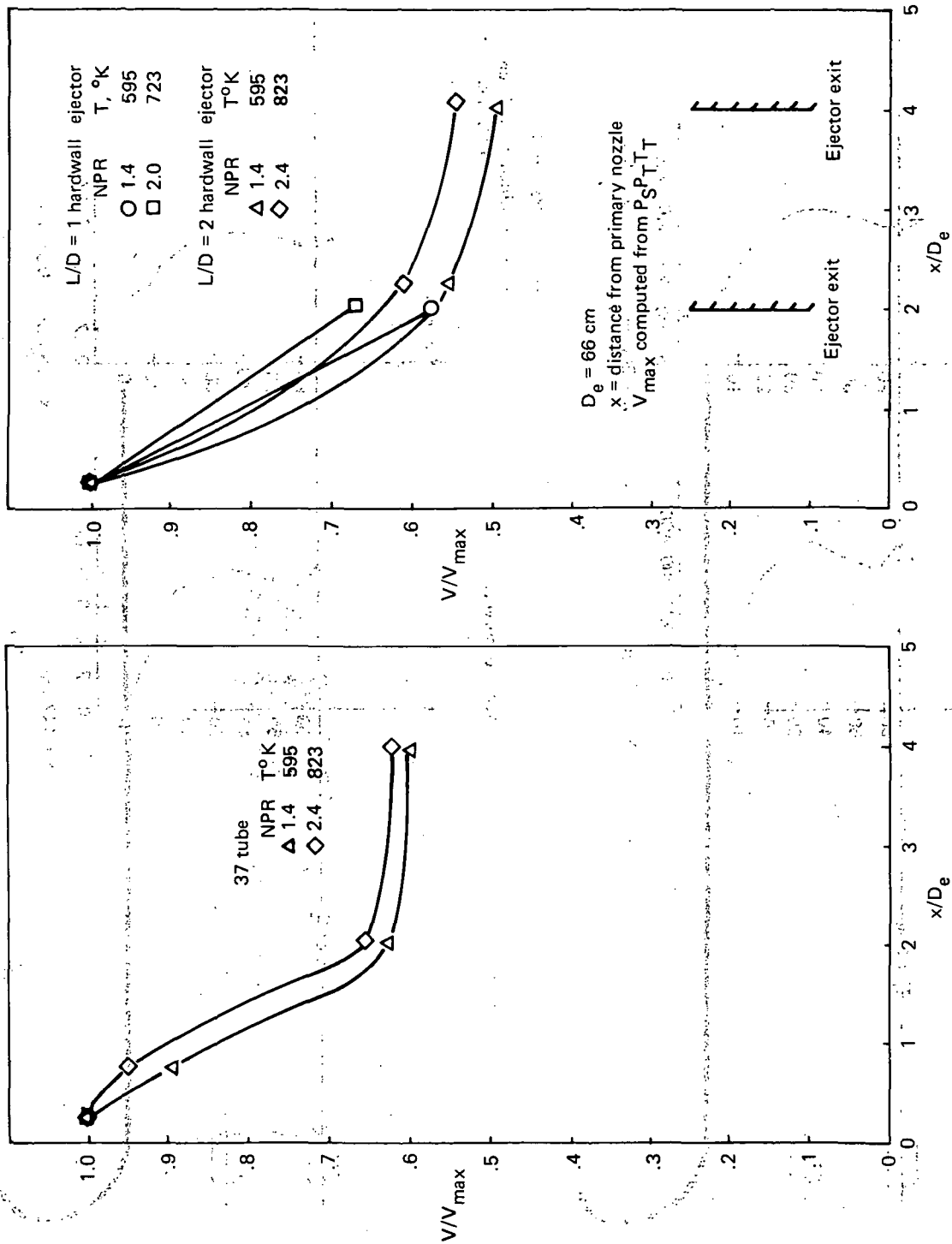
FIGURE 126. — FULL-SCALE JET PEAK VELOCITY DECAY FOR THE 37-TUBE NOZZLE, L/D = 1 AND L/D = 2 EJECTORS
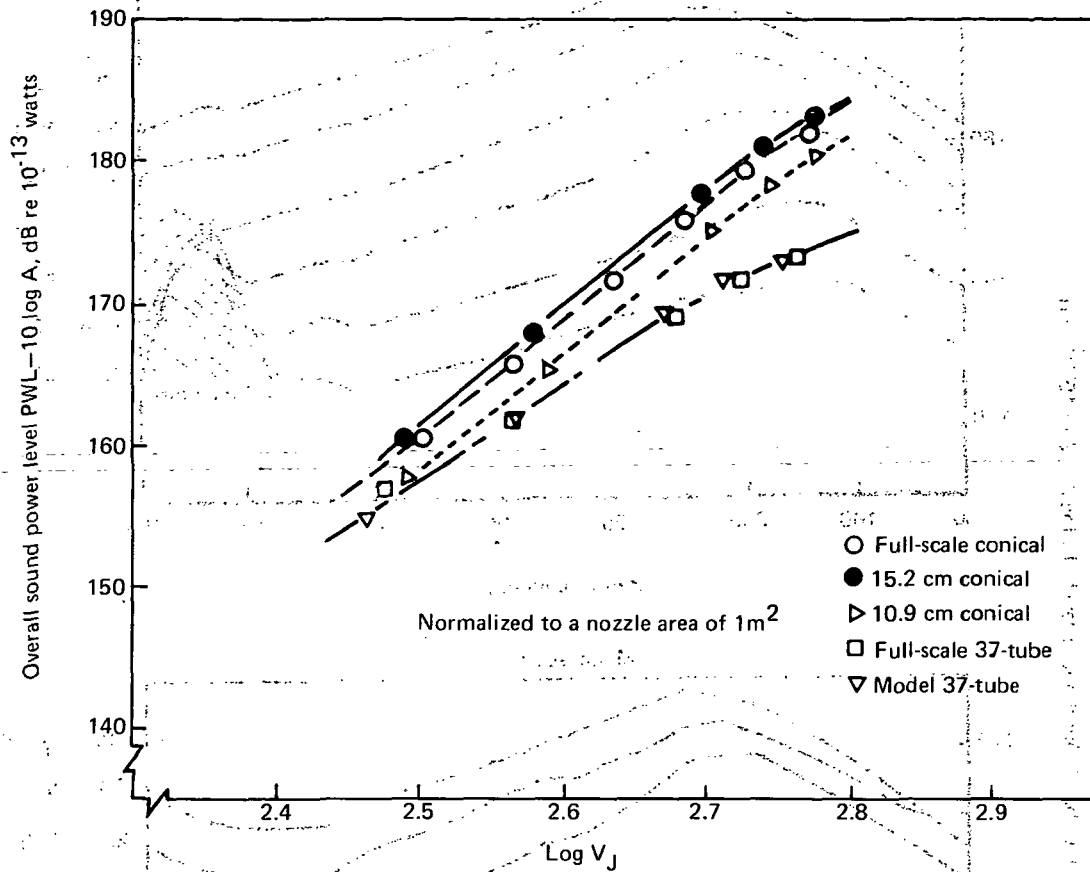
FIGURE 127. —COMPARISON OF MODEL— AND FULL-SCALE CONICAL AND 37-TUBE SOUND POWER LEVELS AS A FUNCTION OF JET VELOCITY (J-75 OPERATING LINE).
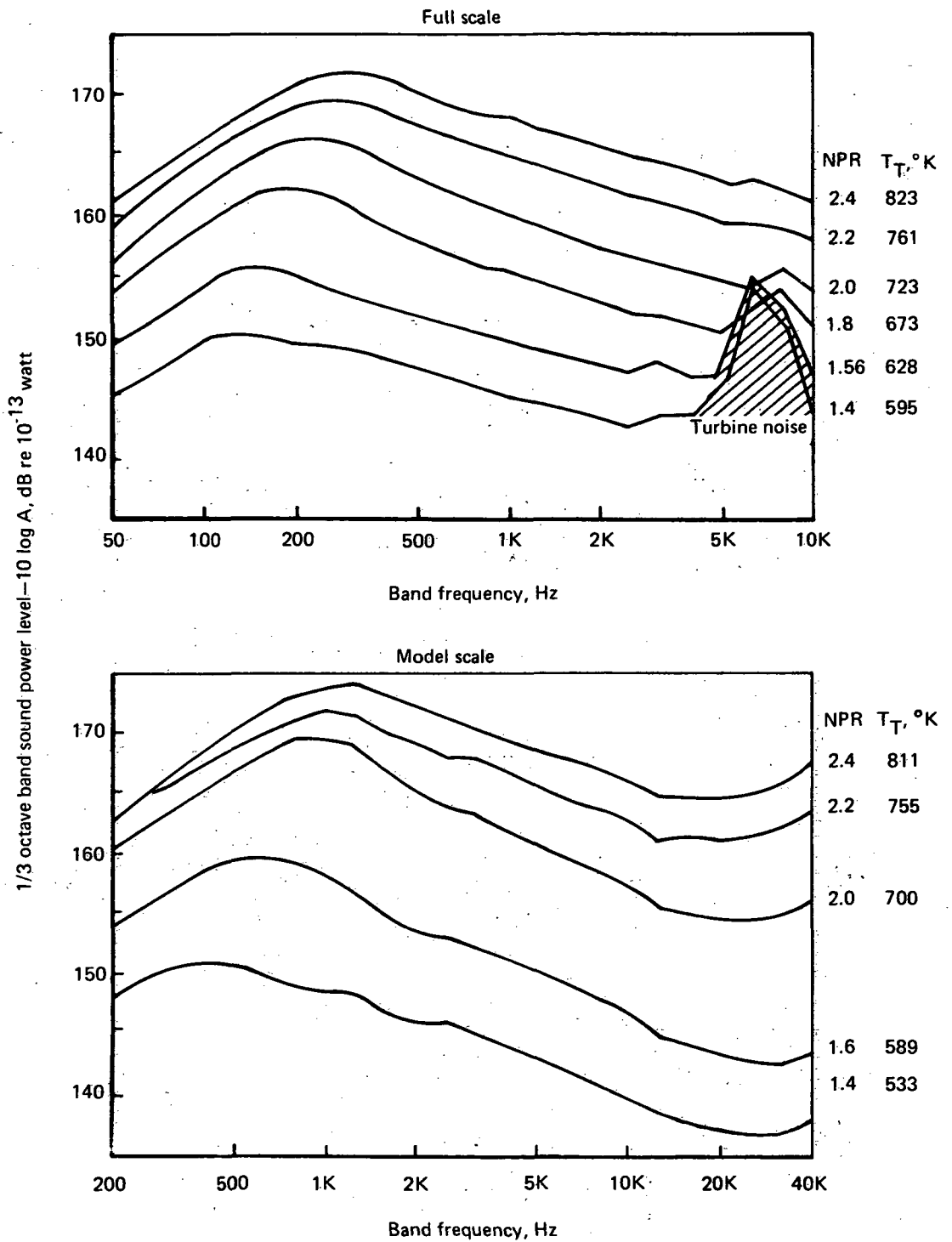
FIGURE 128.—COMPARISON OF MODEL- AND FULL-SCALE CONICAL NOZZLE SOUND POWER SPECTRA
OVER THE J-75 ENGINE OPERATING RANGE (NORMALIZED TO A NOZZLE AREA OF 1 M²)
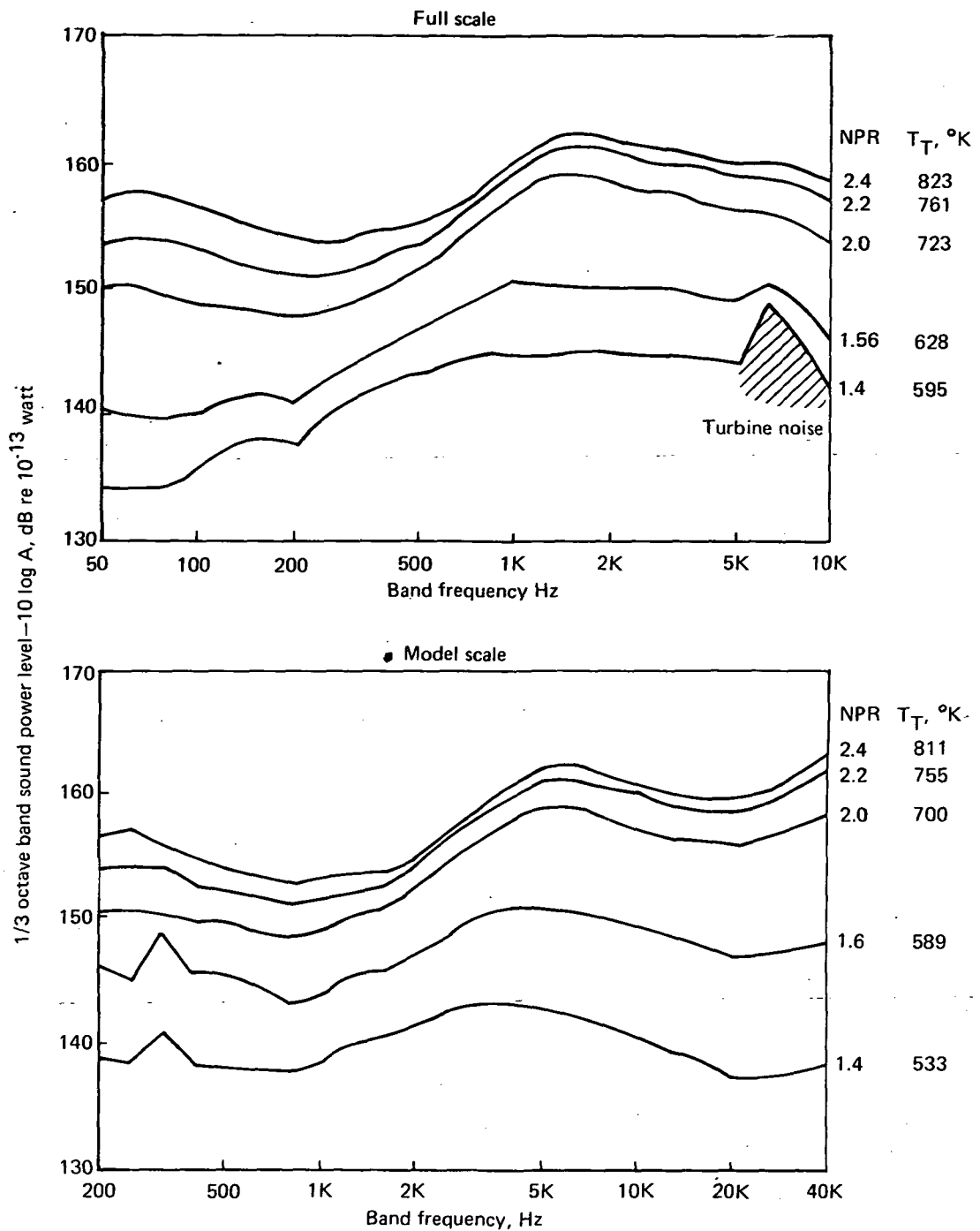
FIGURE 129.—COMPARISON OF MODEL- AND FULL-SCALE 37-TUBE NOZZLE SOUND POWER SPECTRA OVER THE J-75 ENGINE OPERATING RANGE (NORMALIZED TO A NOZZLE AREA OF 1 M^2)
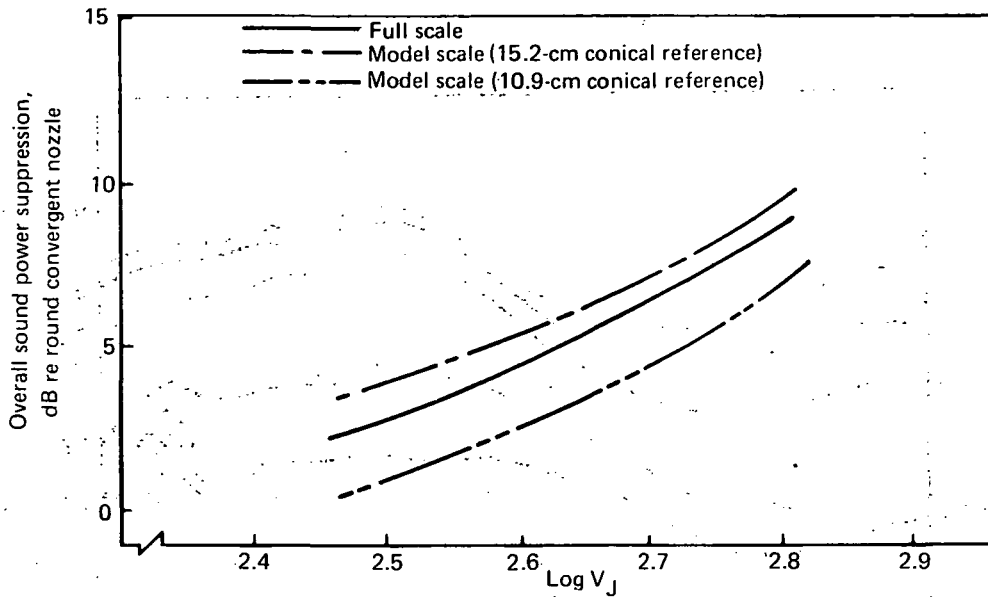
FIGURE 130.—OVERALL SOUND POWER SUPPRESSION FOR MODEL- AND
FULL-SCALE 37-TUBE NOZZLES (J-75 OPERATING LINE)
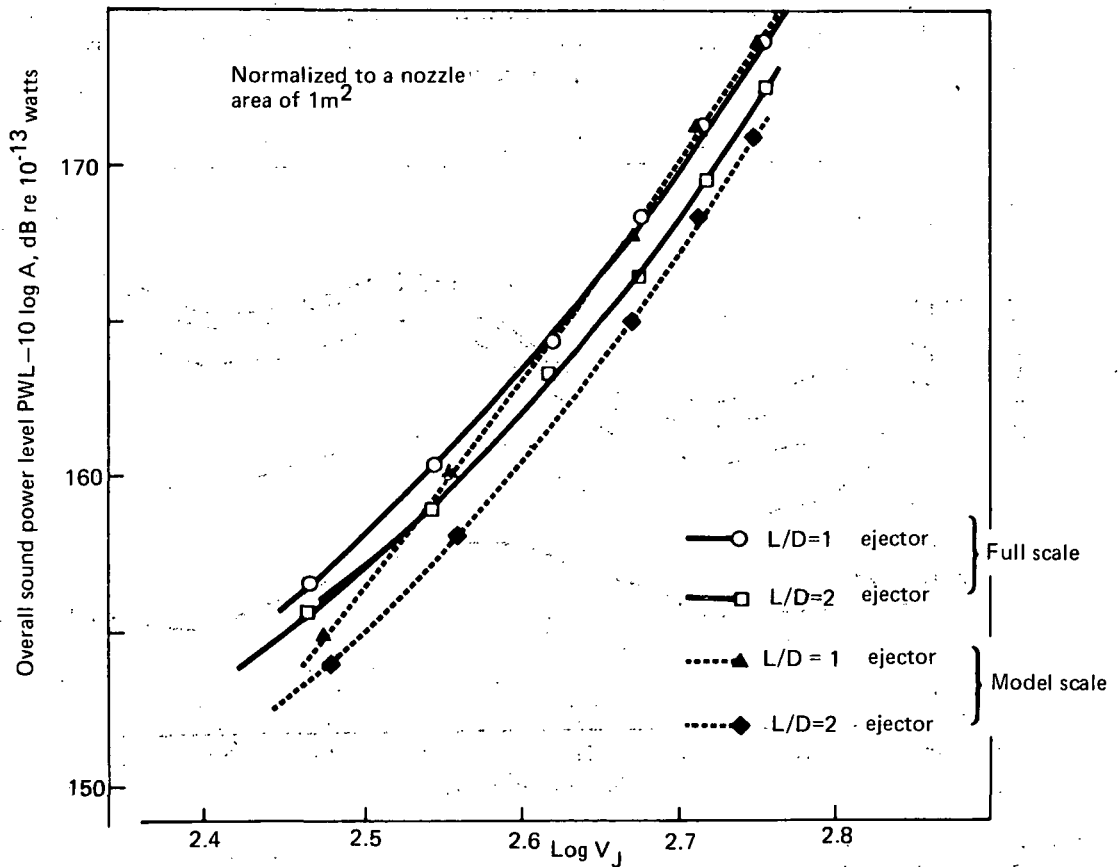
FIGURE 131.—COMPARISON OF OVERALL SOUND POWER LEVELS FOR FULL- AND MODEL-SCALE
L/D = 1 AND L/D = 2 EJECTOR CONFIGURATIONS (J-75 OPERATING LINE)
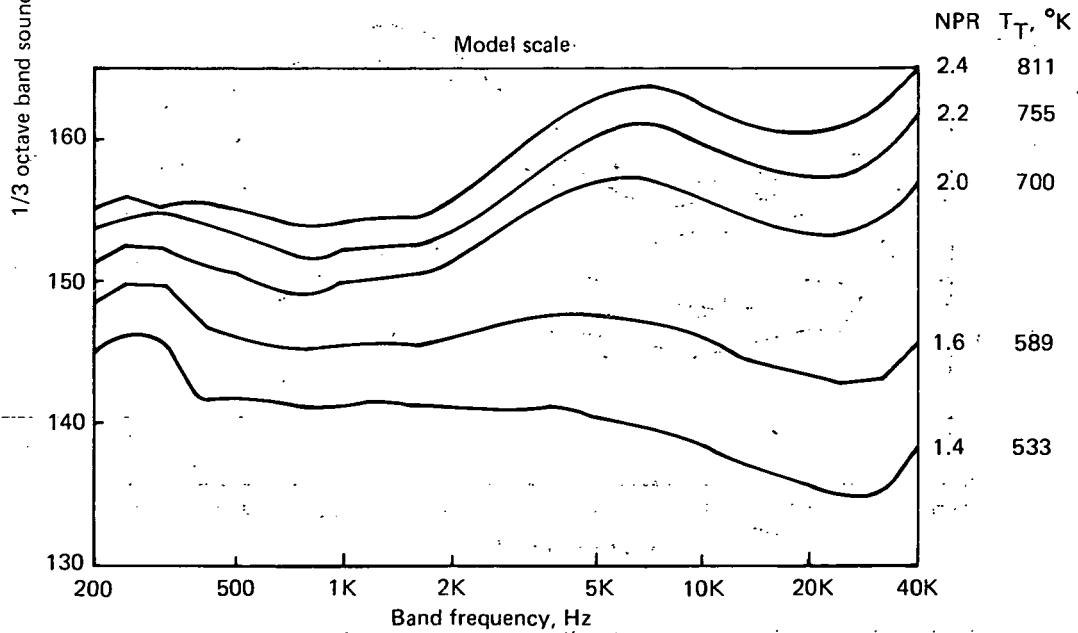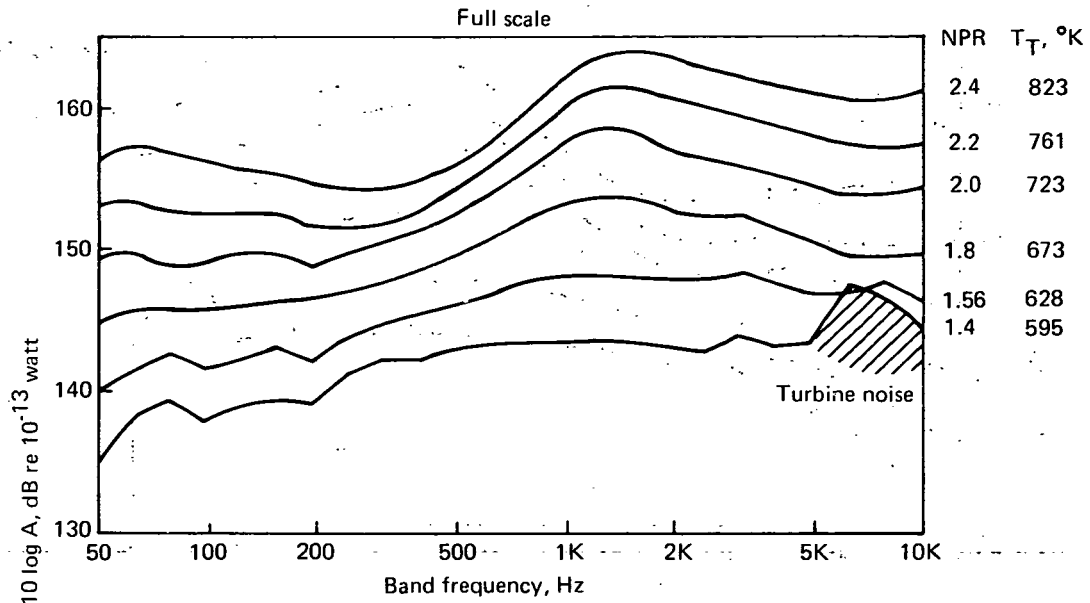
FIGURE 132.—COMPARISON OF MODEL- AND FULL-SCALE, L/D = 1 HARDWALL EJECTOR SOUND POWER SPECTRA OVER THE J-75 ENGINE OPERATING RANGE (NORMALIZED TO A NOZZLE AREA OF 1 M^2)
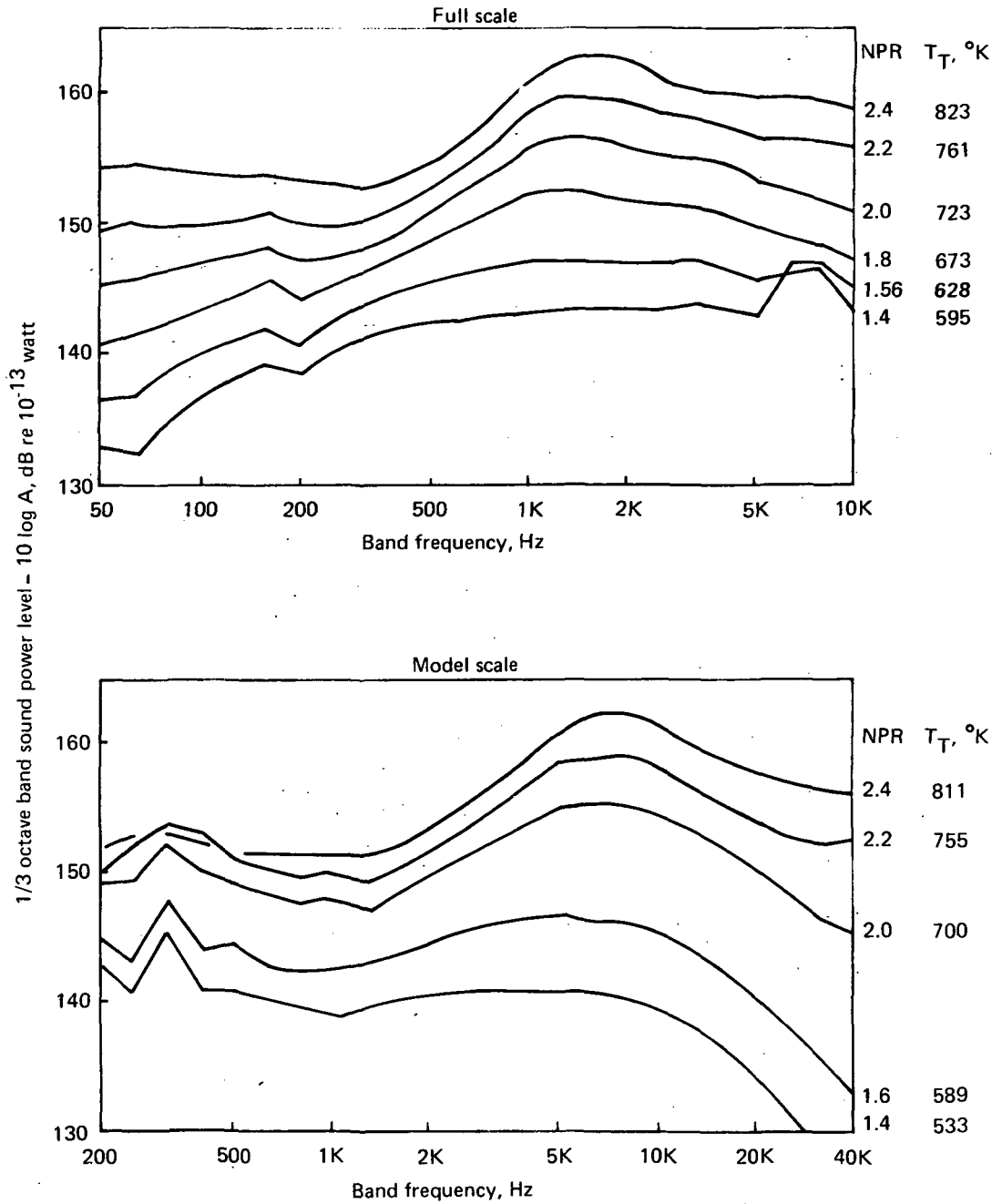
FIGURE 133.—COMPARISON OF MODEL- AND FULL-SCALE, L/D = 2 HARDWALL EJECTOR SOUND POWER SPECTRA OVER THE J-75 ENGINE OPERATING RANGE (NORMALIZED TO A NOZZLE AREA OF 1 M^2)
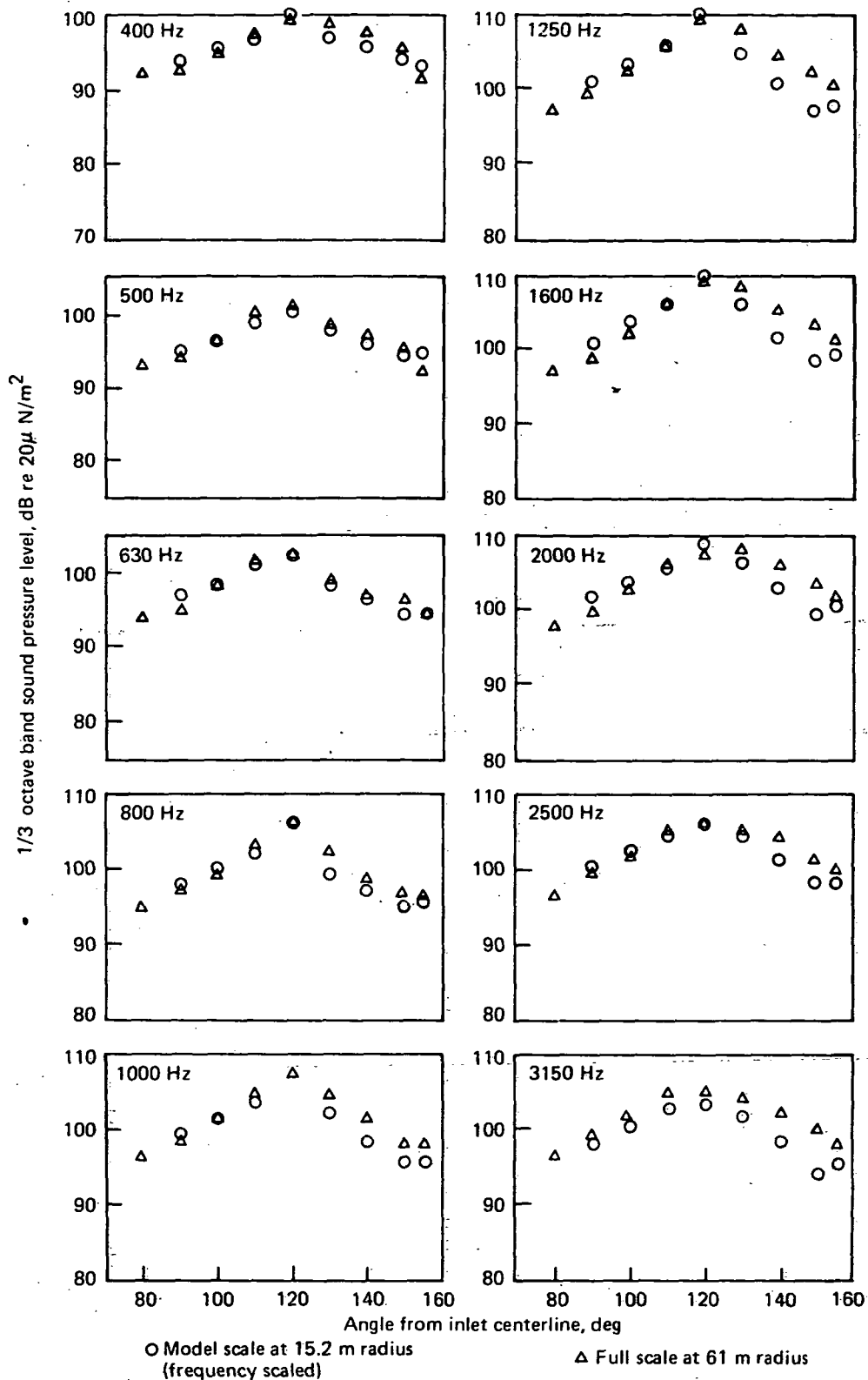
FIGURE 134.—COMPARISON OF SOUND FIELD DIRECTIVITY CHARACTERISTICS FOR MODEL- AND
FULL-SCALE L/D = 1 HARDWALL EJECTORS

O Model scale at 15.2 m radius (frequency scaled)   Δ Full scale at 61 m radius
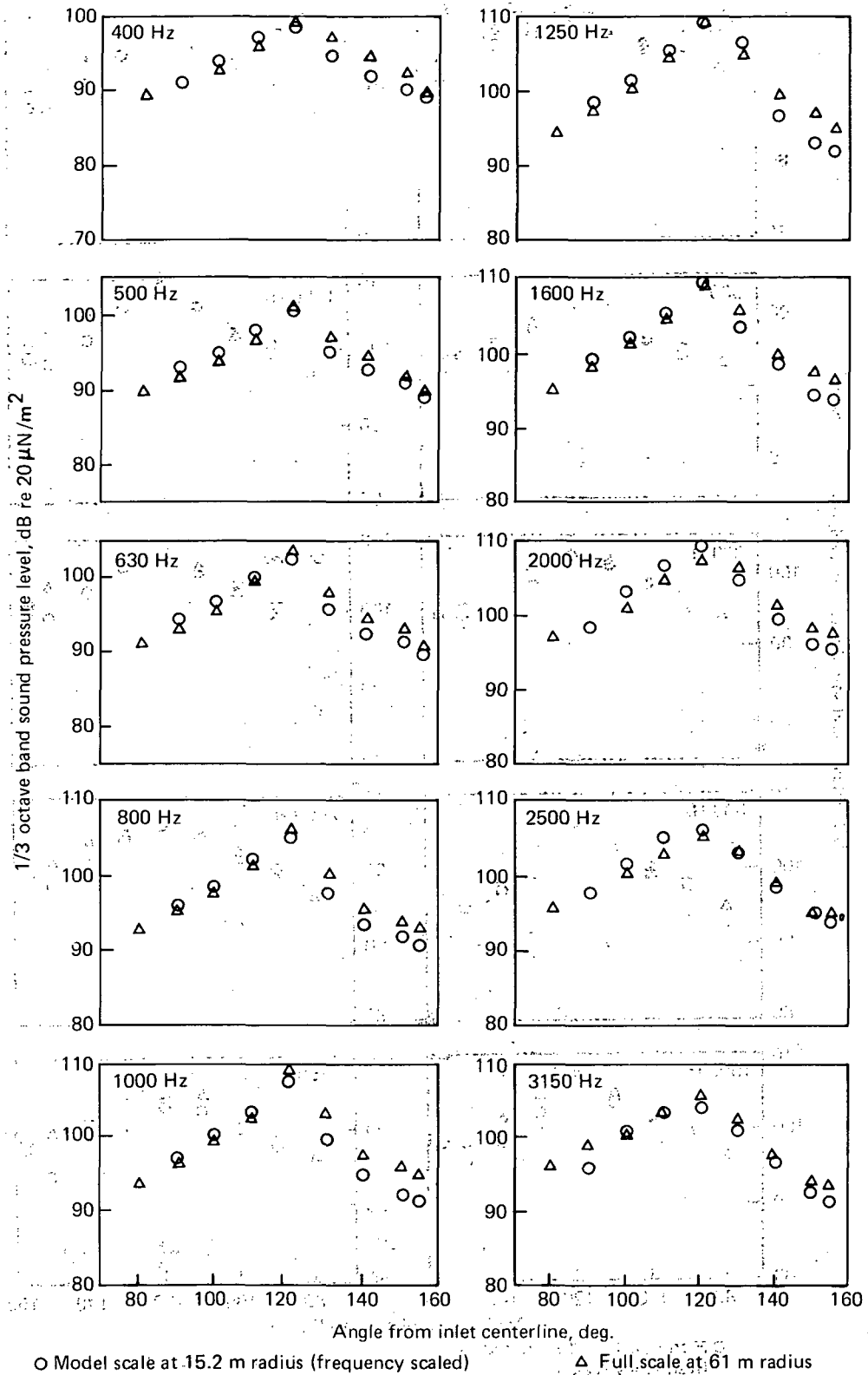
FIGURE 135.—COMPARISON OF SOUND FIELD DIRECTIVITY CHARACTERISTICS FOR MODEL- AND FULL-SCALE L/D = 2 HARDWALL EJECTORS

Ejector

Suppressor nozzle

Mixed flow
(Lower velocity, large diameter jet;
D = ejector exit diameter)

① Noise generated within ejector length
(attenuated by lining)

② Noise generated downstream of ejector exit
(not attenuated by lining)

— — — Hardwall ejector
- - - - - Lined Ejector

Average SPL, dB

Frequency, Hz ⟶

f

Spectrum

SPL, dB

Angle from inlet ⟶

Directivity
(at frequency f)
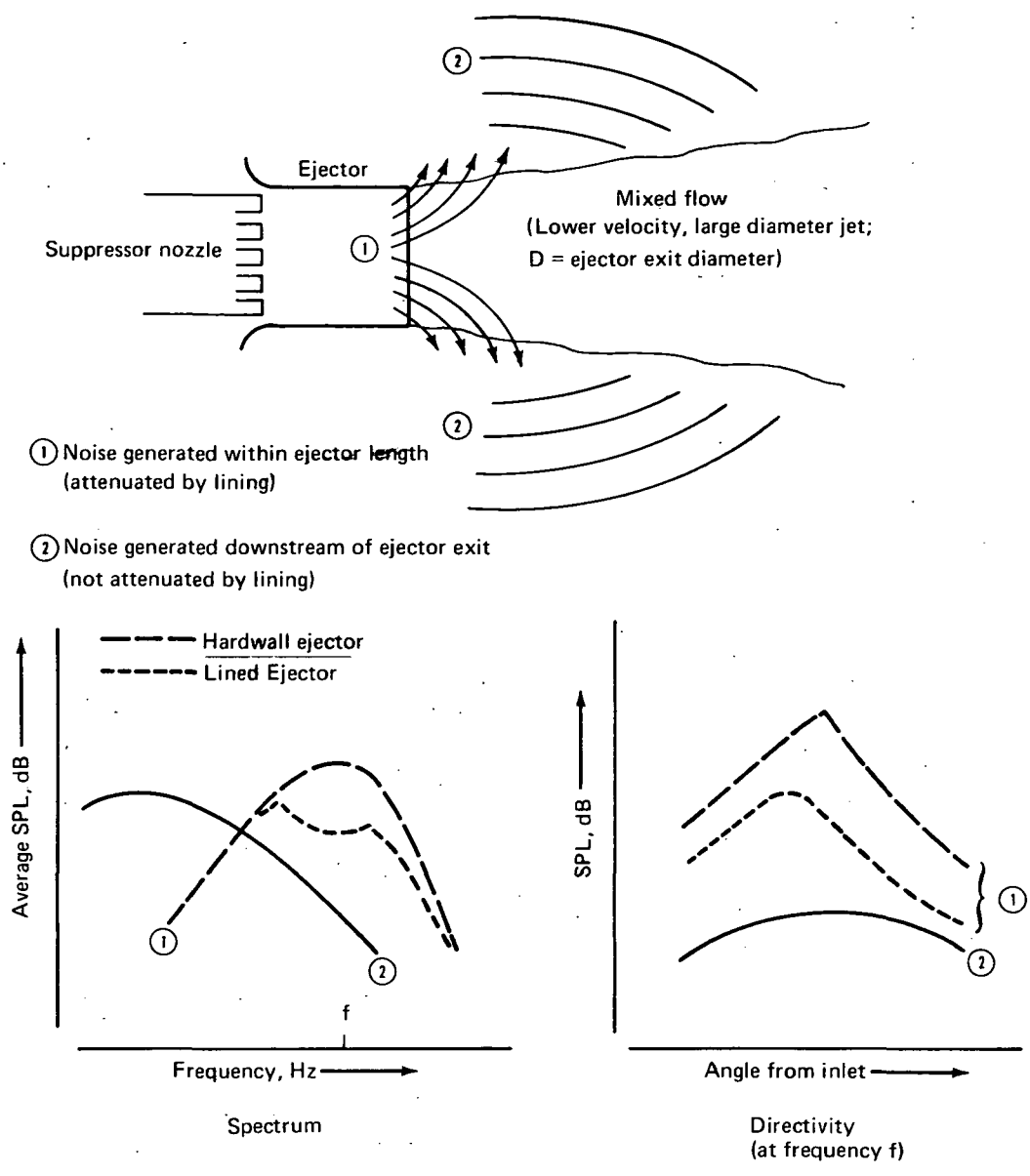
FIGURE 136.—QUALITATIVE REPRESENTATION OF JET NOISE FOR AN EJECTOR CONFIGURATION

221
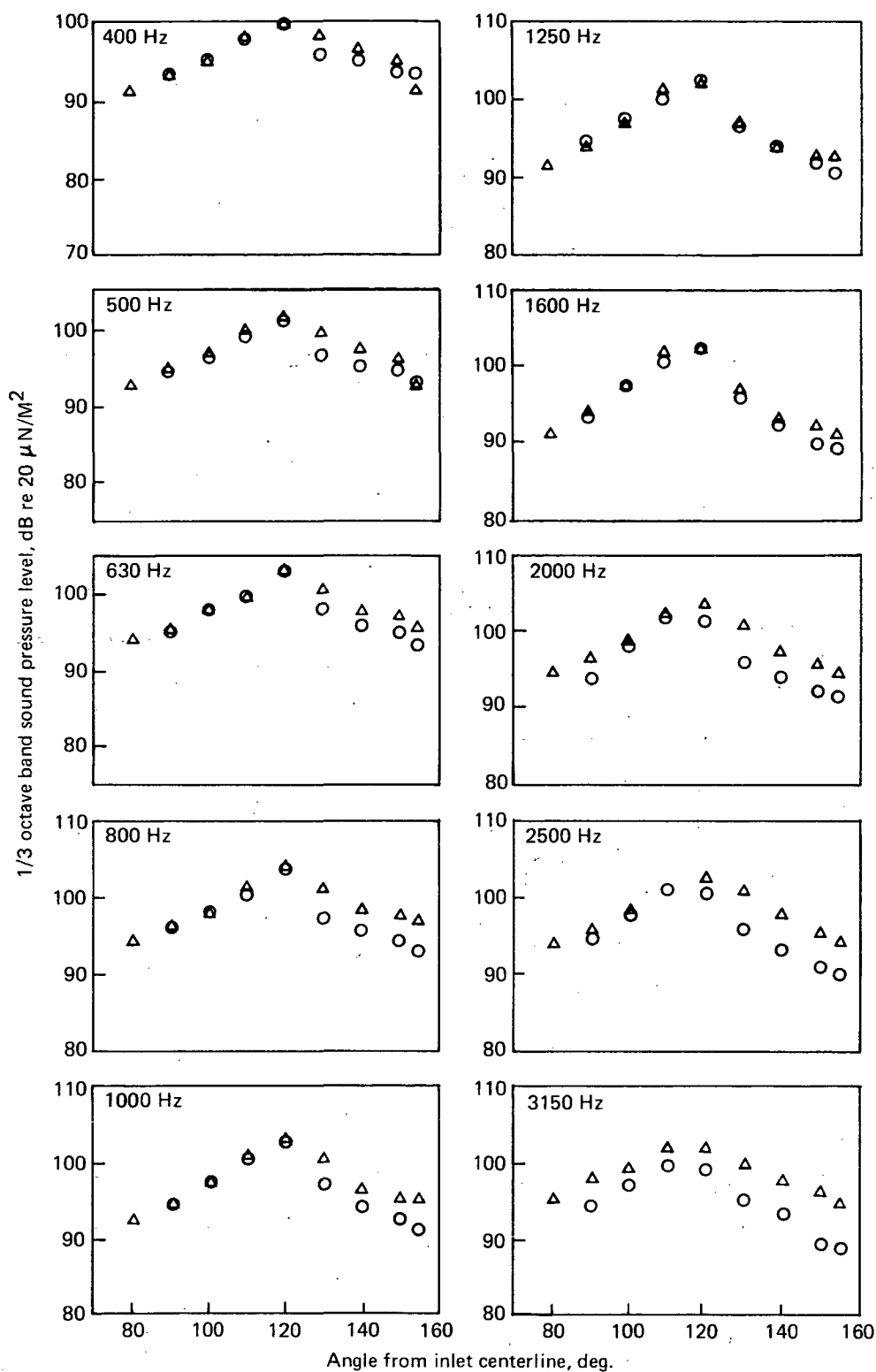
O Model scale at 15.2 m radius (frequency scaled)   △ Full scale at 61 m radius

FIGURE 137.—COMPARISON OF SOUND FIELD DIRECTIVITY CHARACTERISTICS FOR MODEL-
AND FULL-SCALE L/D = 1 LINED EJECTORS (12% OPEN AREA, d = 0.9-CM MODEL
SCALE; 12% OPEN AREA, d = 3.81 CM FULL SCALE)
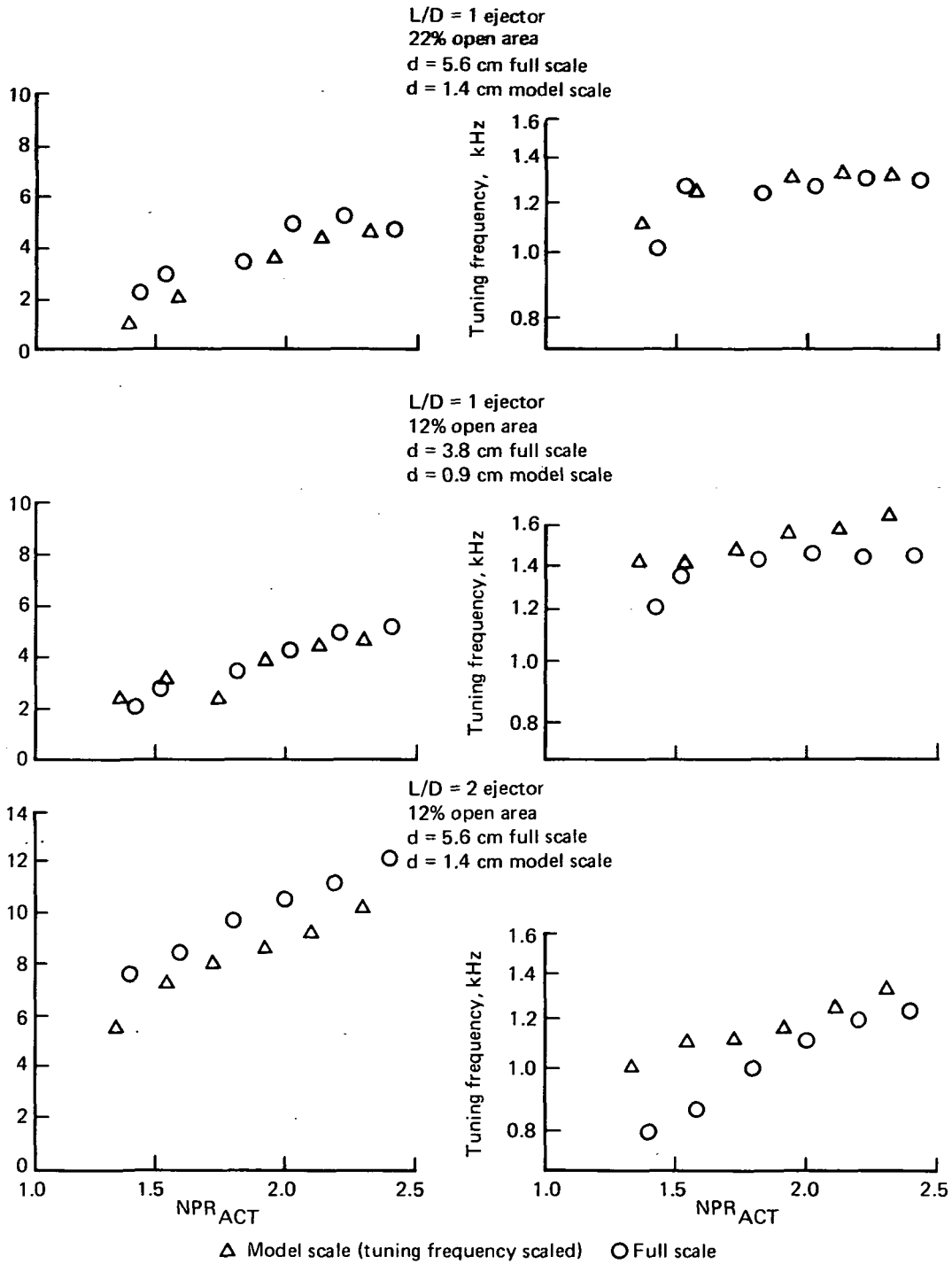
FIGURE 138.—COMPARISON OF MODEL- AND FULL-SCALE LINING PERFORMANCE
(J-75 ENGINE OPERATING LINE)

223
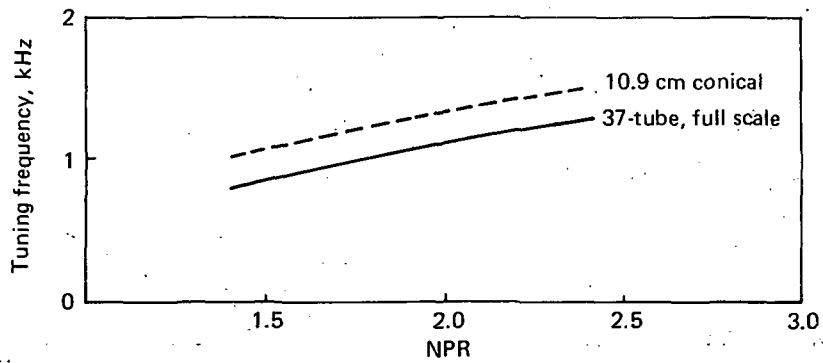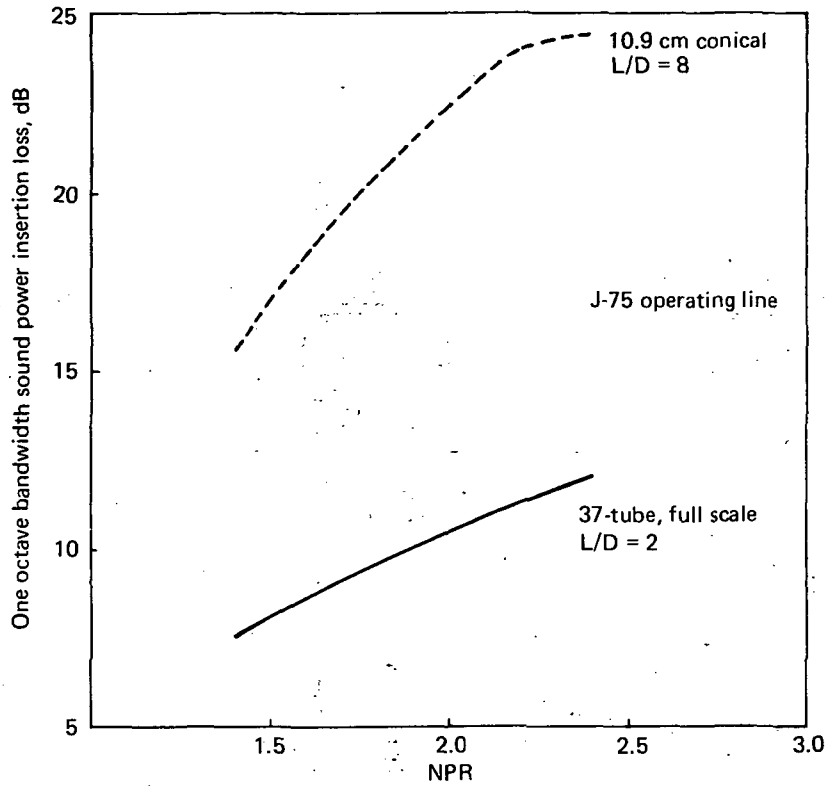
FIGURE 139.—DIRECT COMPARISON OF EJECTOR LINING INSERTION LOSS AND TUNING
FREQUENCY FOR 2.65 M EJECTORS WITH 10.9 CM CONICAL AND FULL-SCALE
37-TUBE NOZZLES
(12% OPEN AREA, d = 5.33 CM FOR 37-TUBE NOZZLE)
(12% OPEN AREA, d = 5.85 CM FOR 10.9 CM NOZZLE)
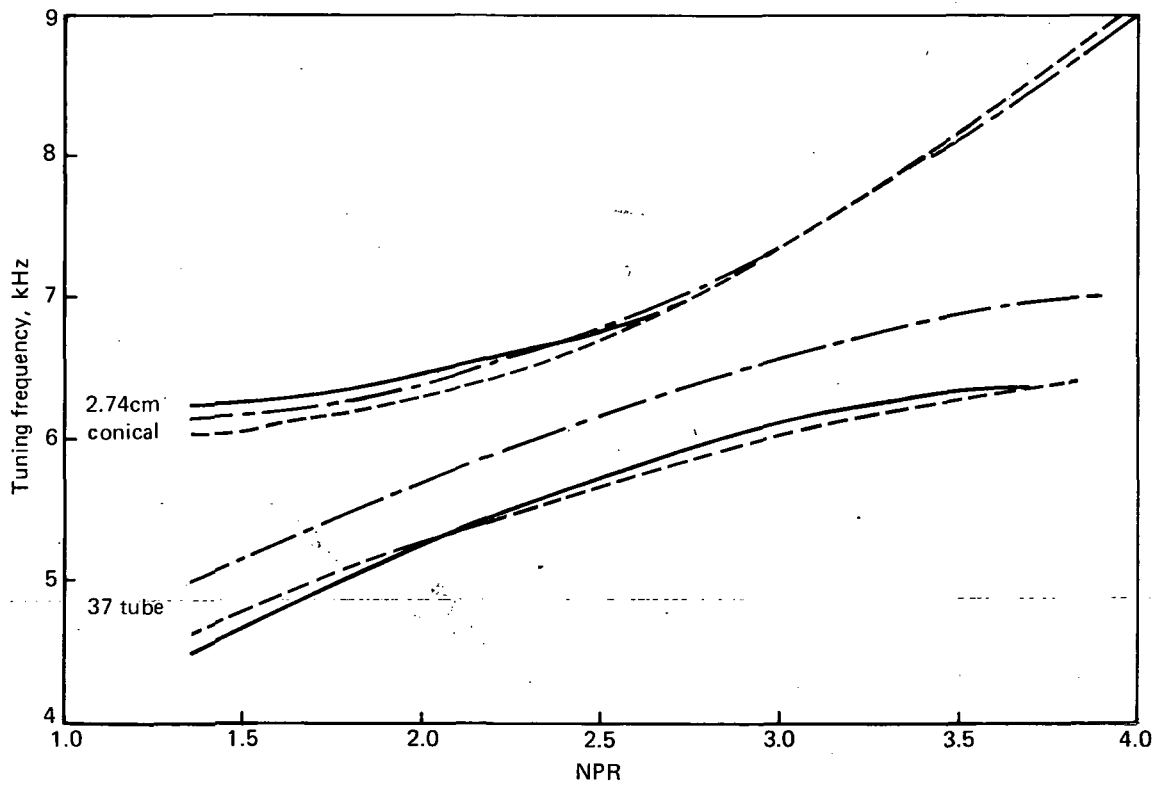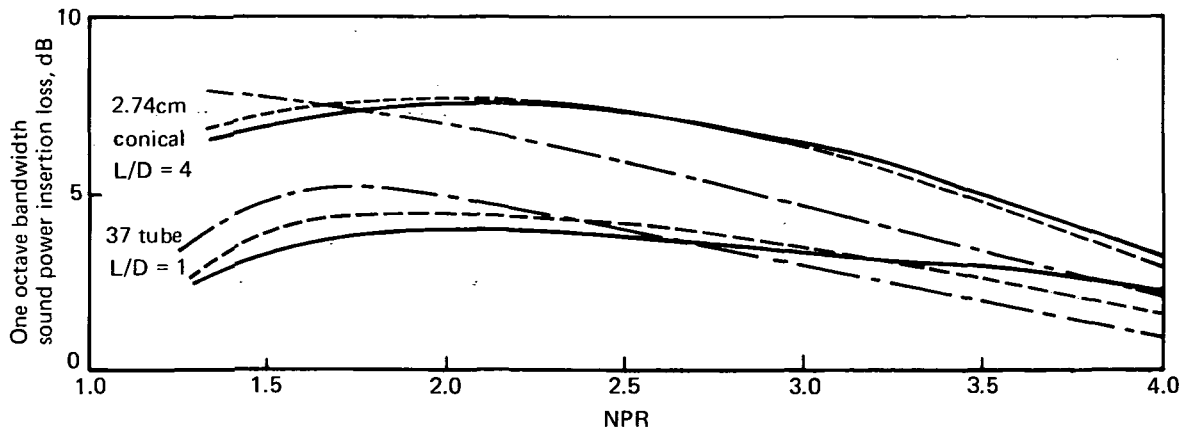
FIGURE 140.—DIRECT COMPARISON OF EJECTOR LINING INSERTION LOSS AND TUNING FREQUENCY FOR 33-CM LINED EJECTORS WITH 2.74-CM CONICAL AND MODEL SCALE 37-TUBE NOZZLES (22% OPEN AREA, d = 1.4-CM LININGS)
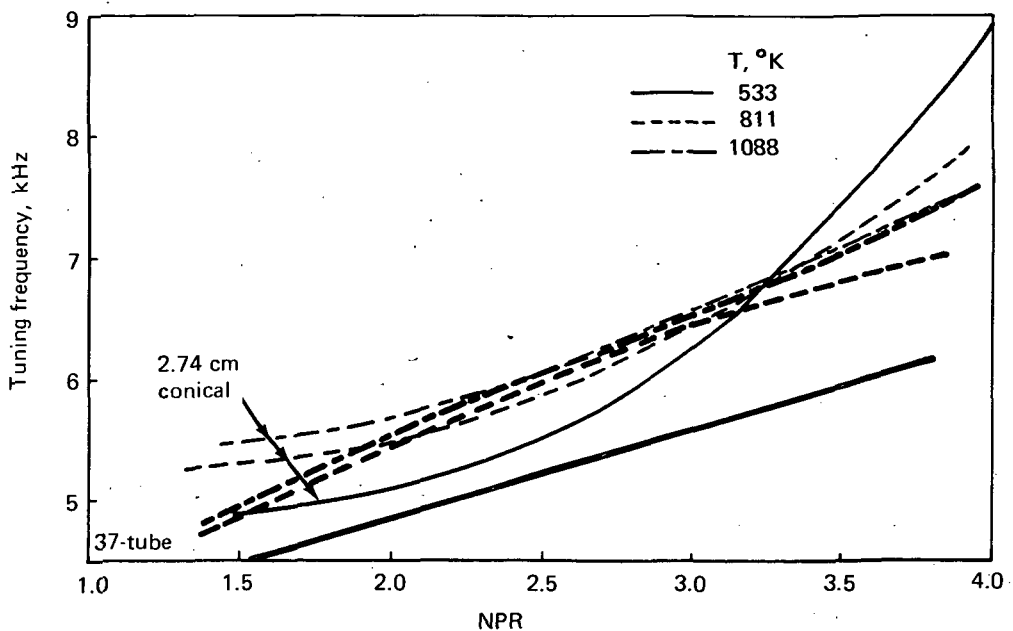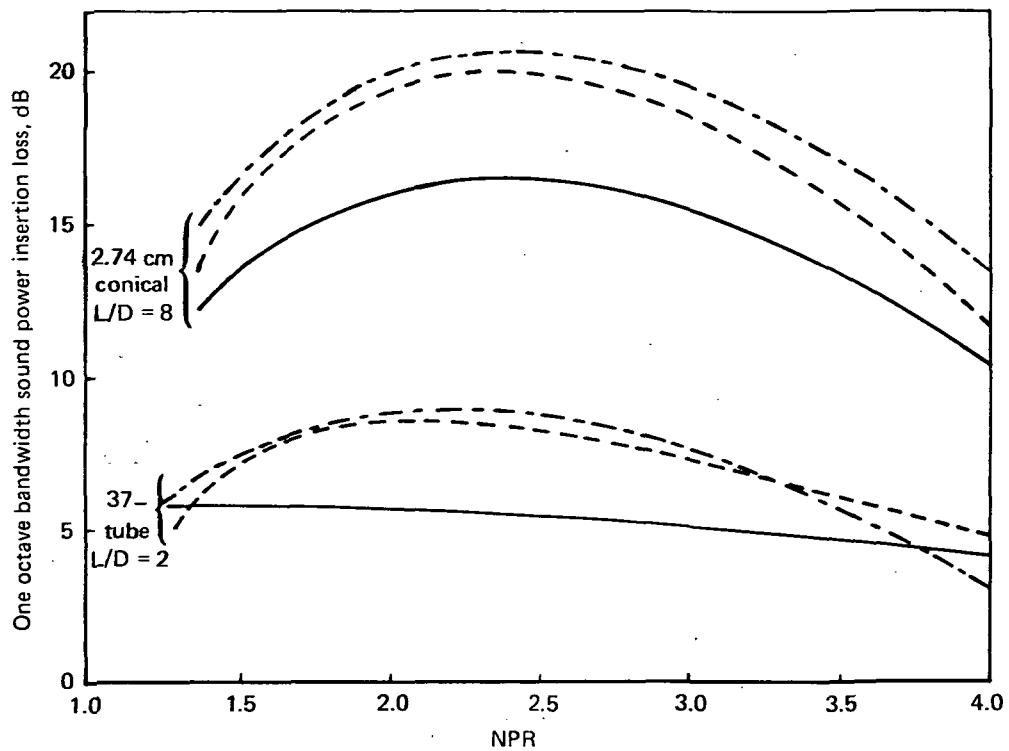
FIGURE 141.–DIRECT COMPARISON OF EJECTOR LINING INSERTION LOSS AND TUNING
FREQUENCY FOR 66-CM LINED EJECTORS WITH 2.74-CM CONICAL AND MODEL-
SCALE 37-TUBE NOZZLES (22% OPEN AREA, 1.4-CM DEEP LININGS)
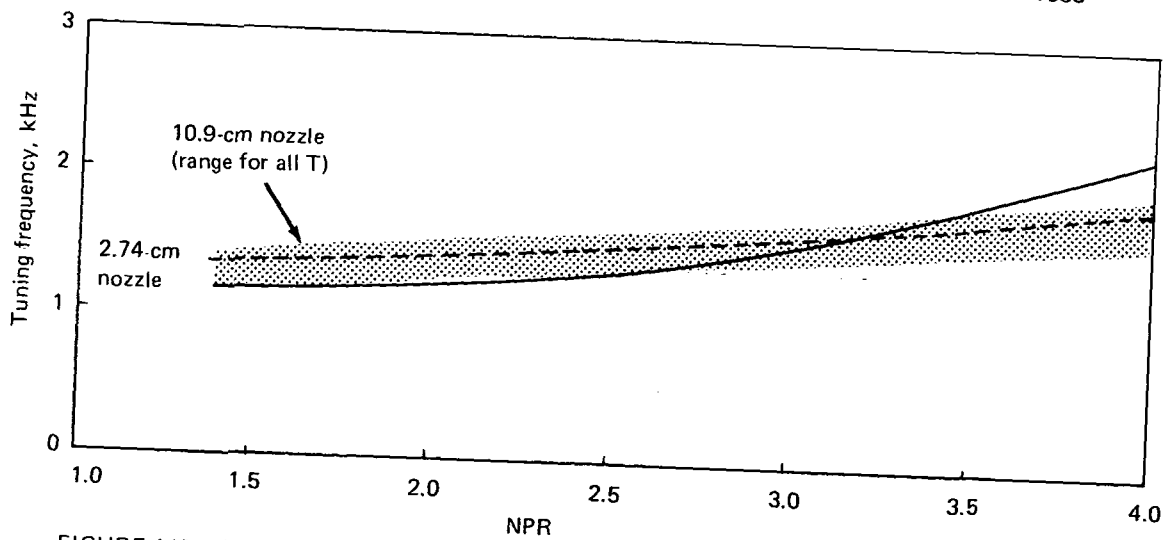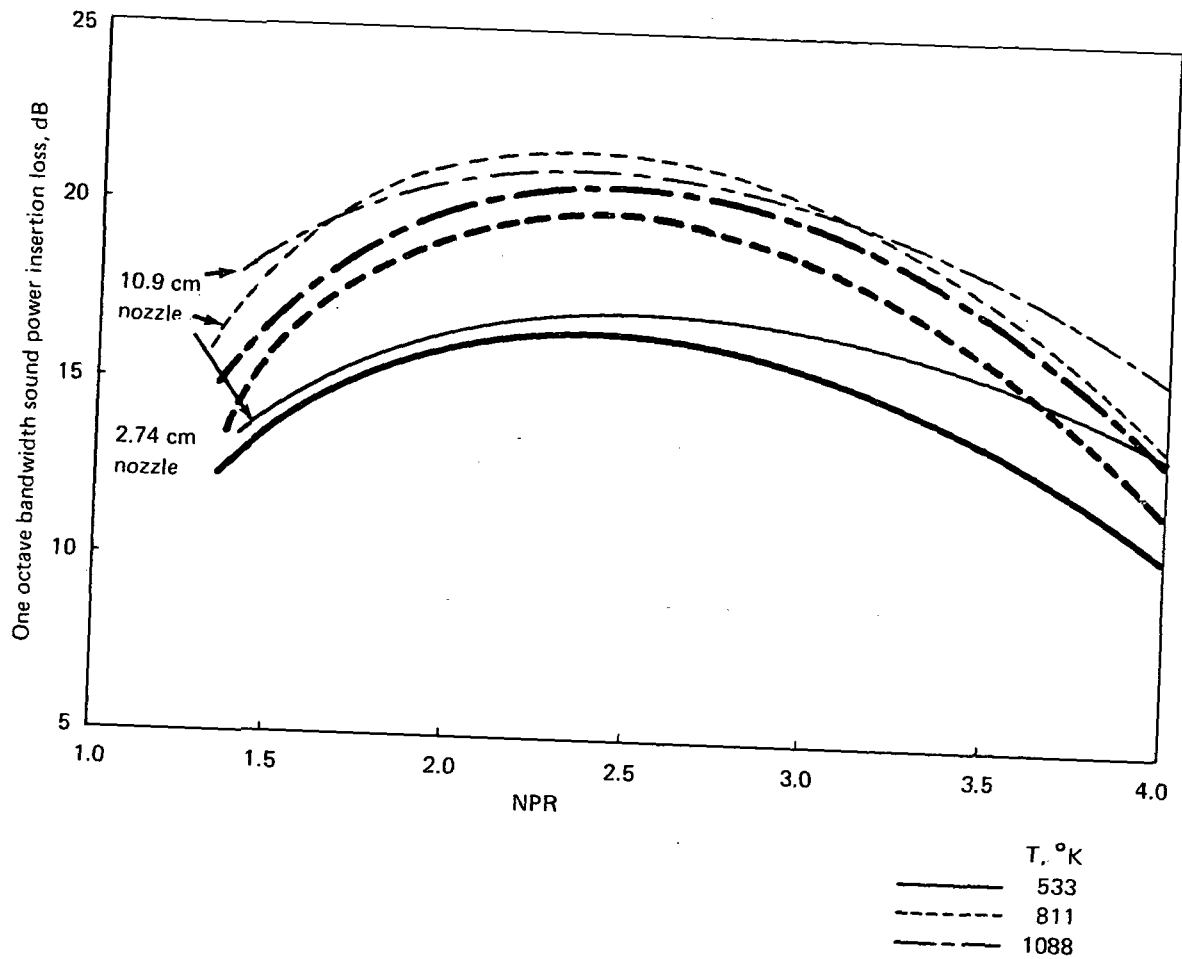
FIGURE 142.—COMPARISON OF LINING INSERTION LOSS AND TUNING FREQUENCY FOR L/D = 8 LINED EJECTORS WITH 2.74-CM- AND 10.9-CM-DIAMETER CONICAL NOZZLES (22% OPEN AREA, d = 5.85 CM FOR 10.9-CM NOZZLE AND d = 1.4 CM FOR 2.74-CM NOZZLE)

227
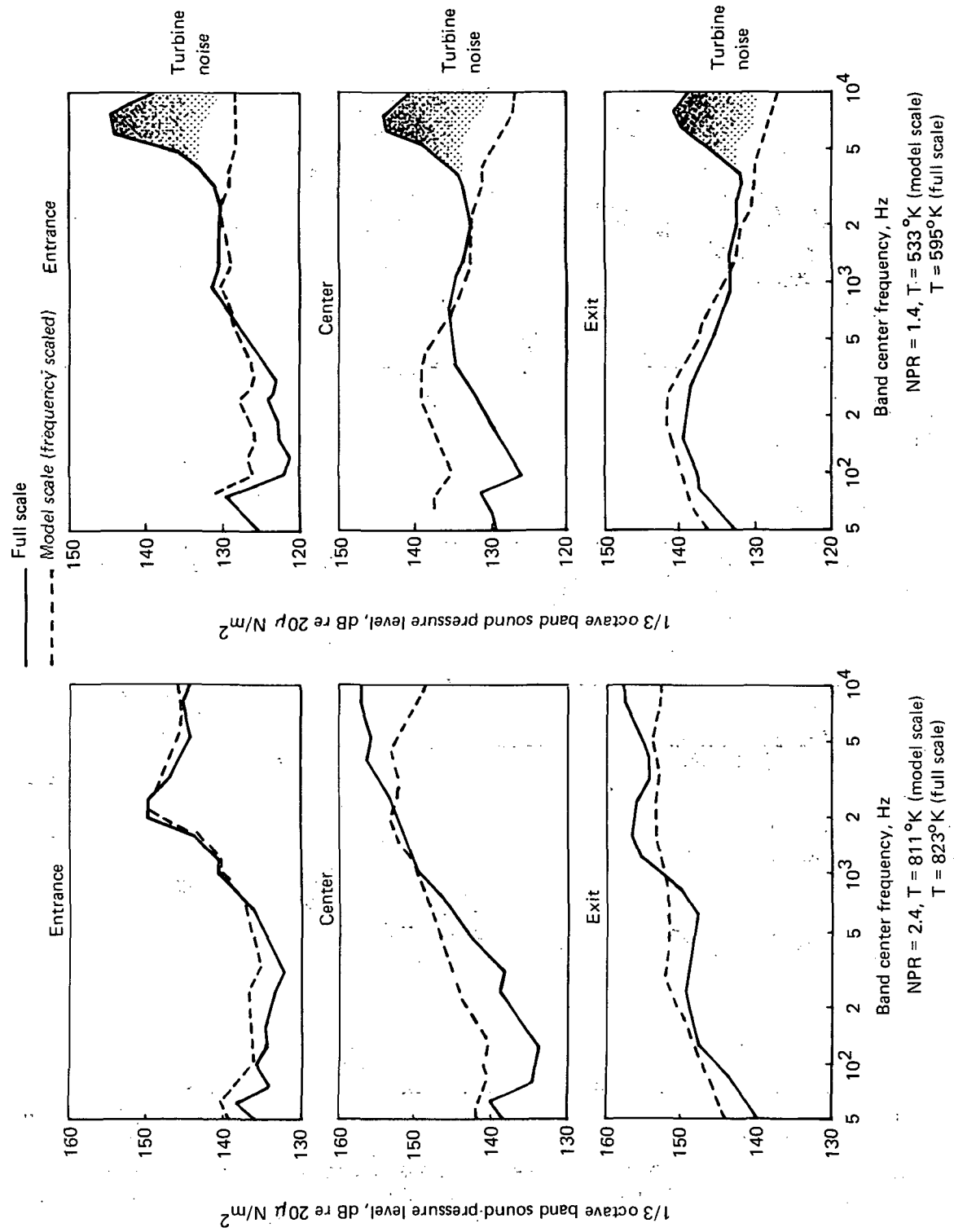
FIGURE 143.— COMPARISON OF MODEL- AND FULL-SCALE EJECTOR WALL SPL SPECTRA FOR THE
L/D = 1 HARDWALL EJECTOR

228
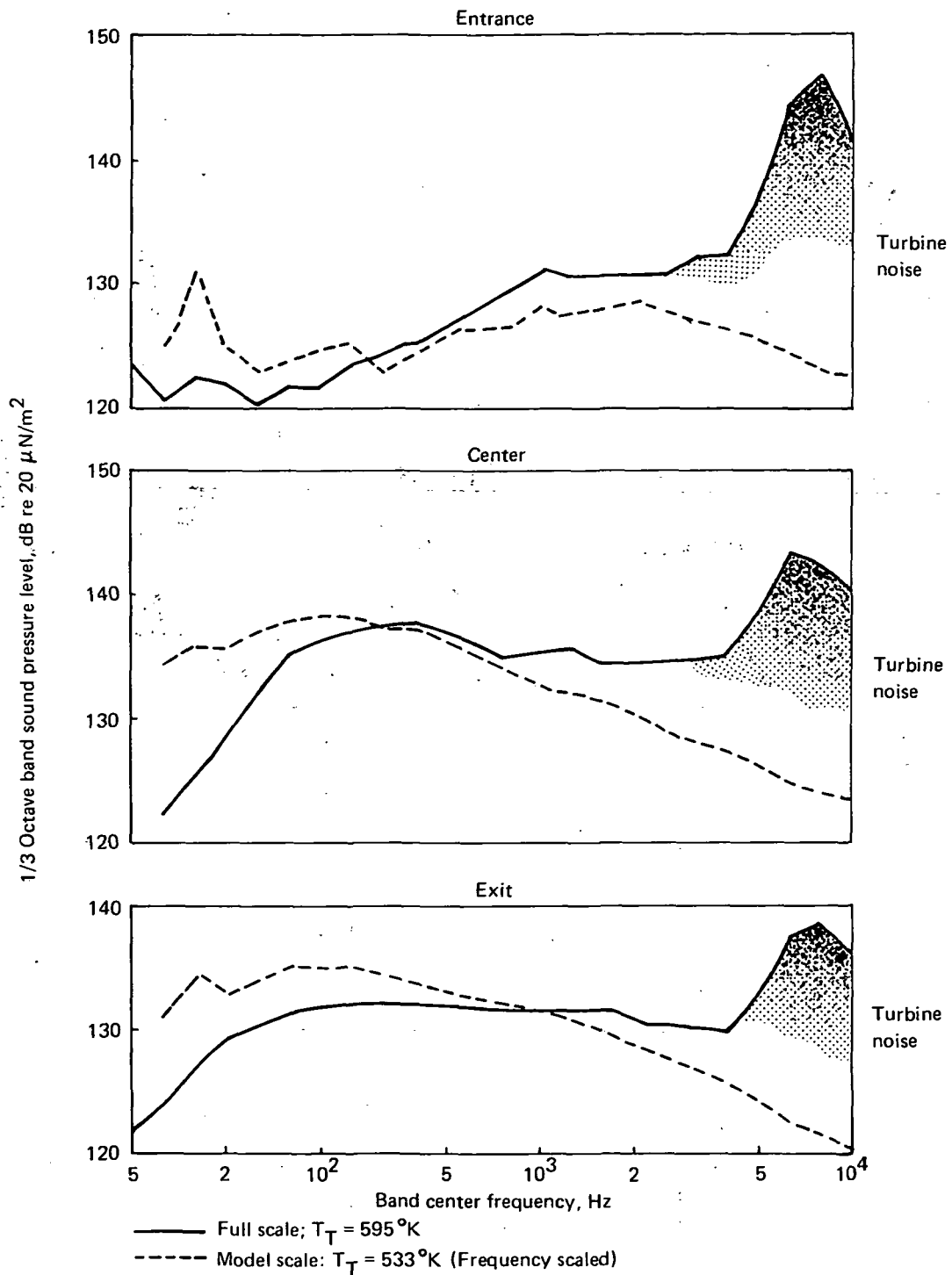
FIGURE 144.– COMPARISON OF MODEL AND FULL SCALE EJECTOR WALL SPL SPECTRA FOR THE L/D = 2 HARDWALL EJECTOR AT NPR = 1.4

229
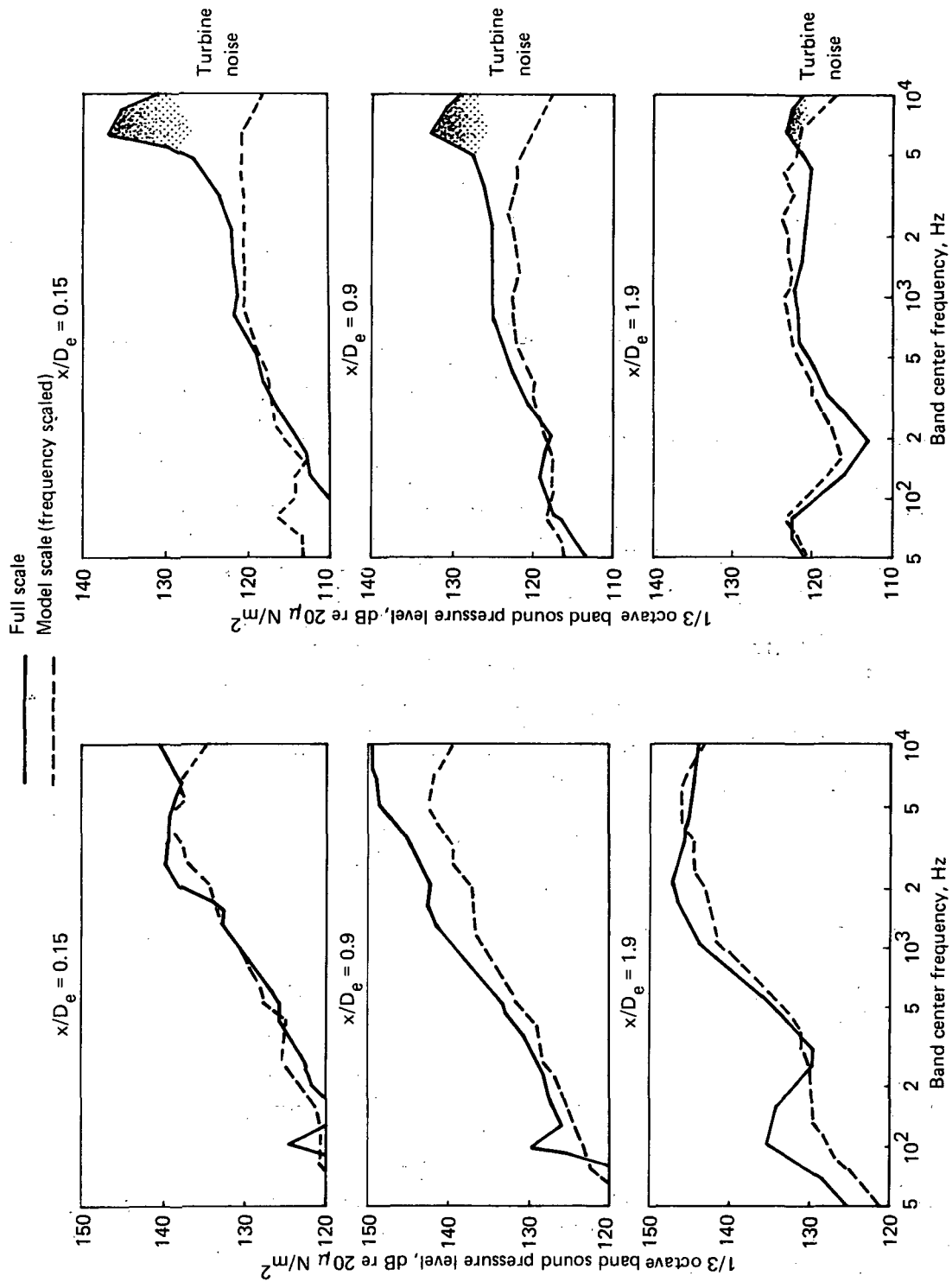
FIGURE 145.—COMPARISON OF MODEL- AND FULL-SCALE NEAR FIELD 37-TUBE NOZZLE JET NOISE ENVIRONMENT AT NPR = 1.4 AND 2.4

230
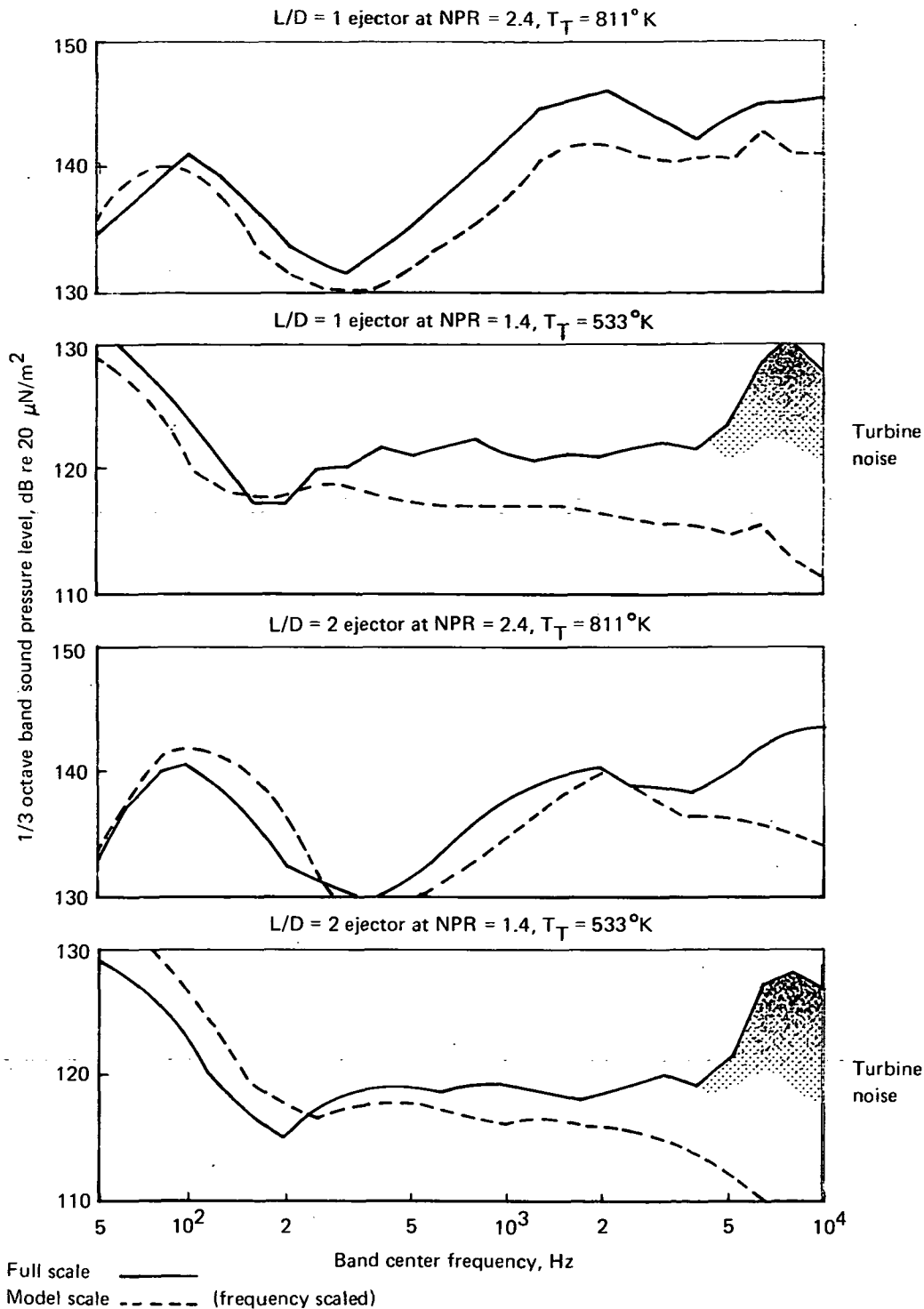
FIGURE 146.—COMPARISON OF MODEL- AND FULL-SCALE NEAR FIELD JET NOISE ENVIRONMENTS AT A STATION $x/D_e = 1$ DOWNSTREAM OF THE HARDWALL EJECTOR EXIT
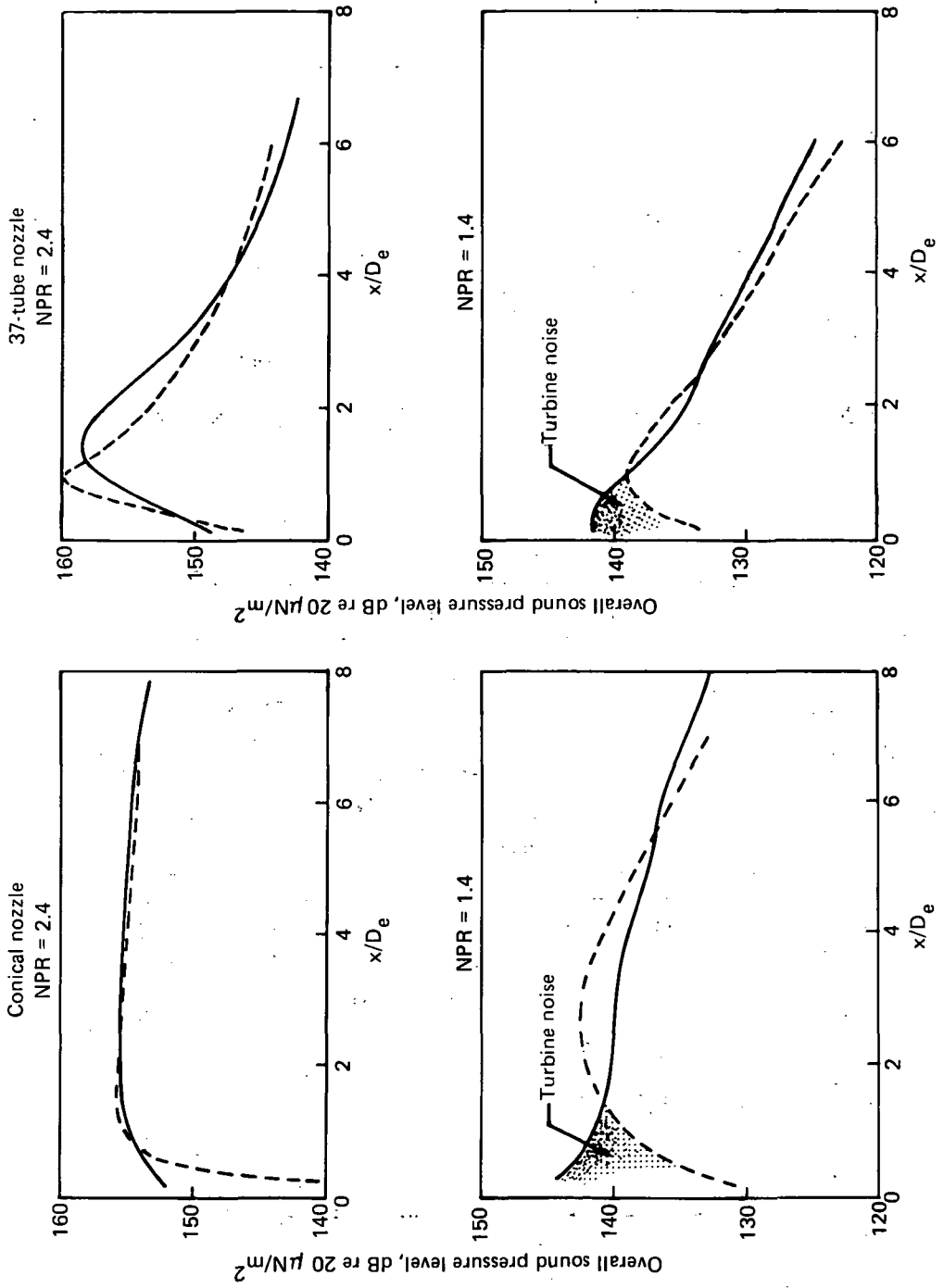
FIGURE 147.—COMPARISON OF MODEL- AND FULL-SCALE NEAR FIELD JET NOISE ENVIRONMENTS AS A FUNCTION OF DISTANCE FROM THE CONICAL AND 37-TUBE NOZZLE EXIT PLANES
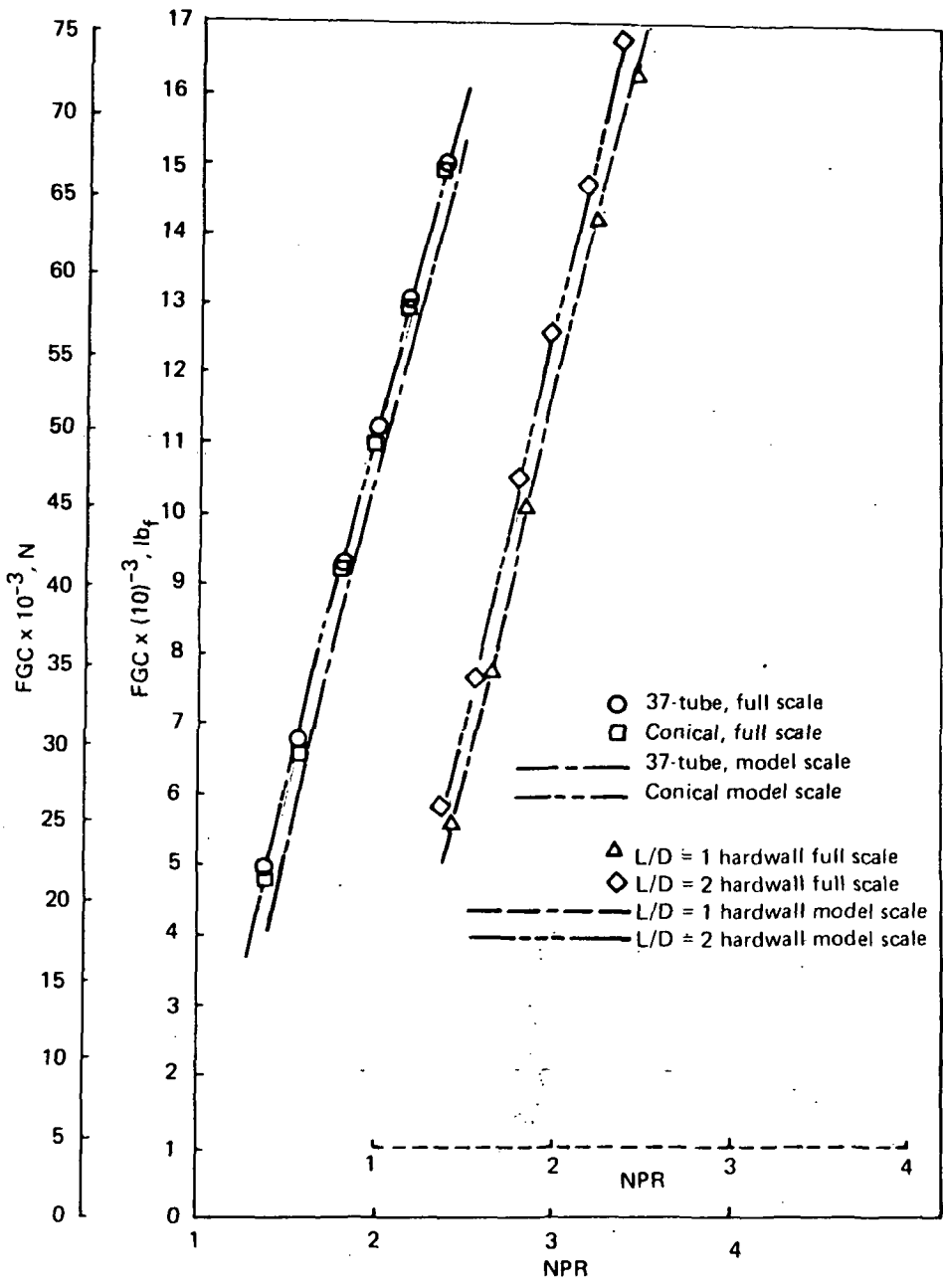
FIGURE 148.— COMPARISON OF FULL-SCALE THRUST RESULTS WITH GEOMETRICALLY SCALED MODEL THRUST RESULTS

233
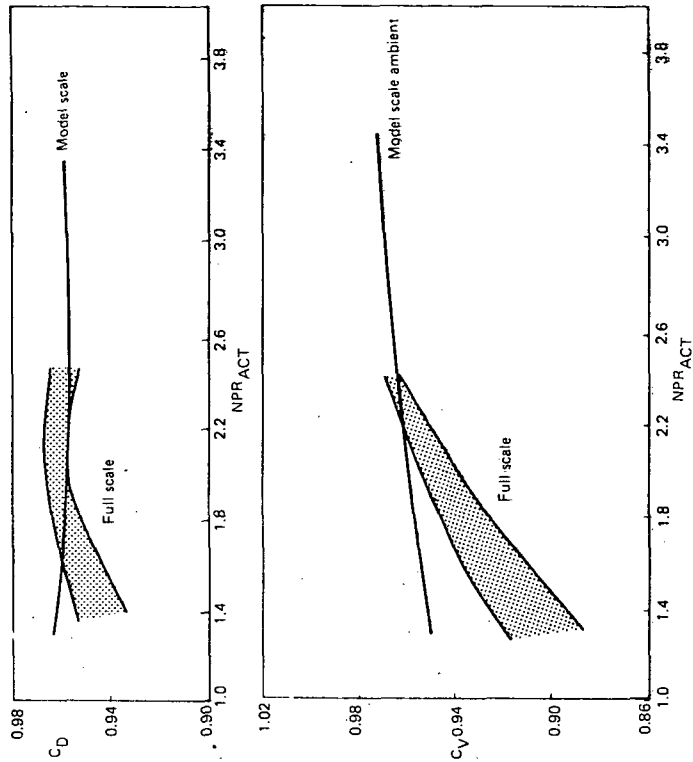
FIGURE 150.— COMPARISON OF MODEL AND FULL SCALE
37-TUBE NOZZLE DISCHARGE AND
VELOCITY COEFFICIENTS
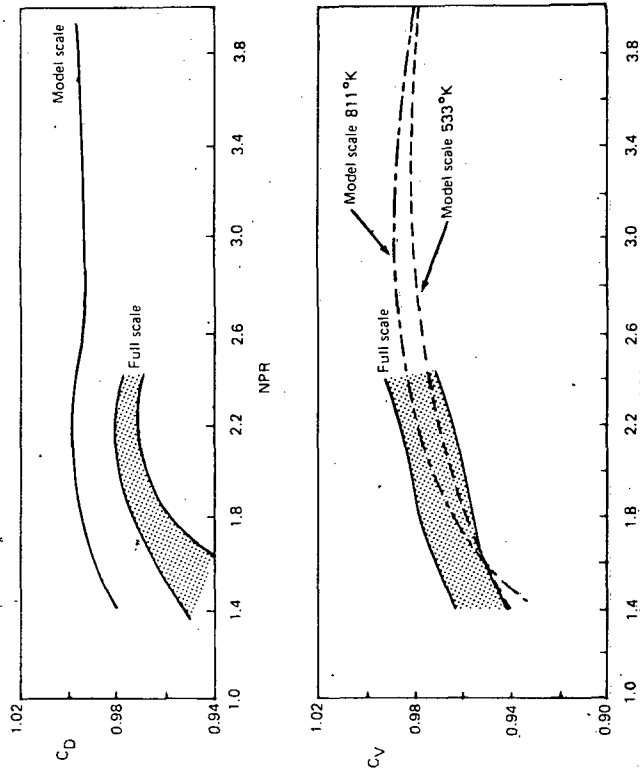
FIGURE 149.—COMPARISON OF MODEL- AND FULL-SCALE
CONICAL NOZZLE DISCHARGE AND
VELOCITY COEFFICIENTS

234
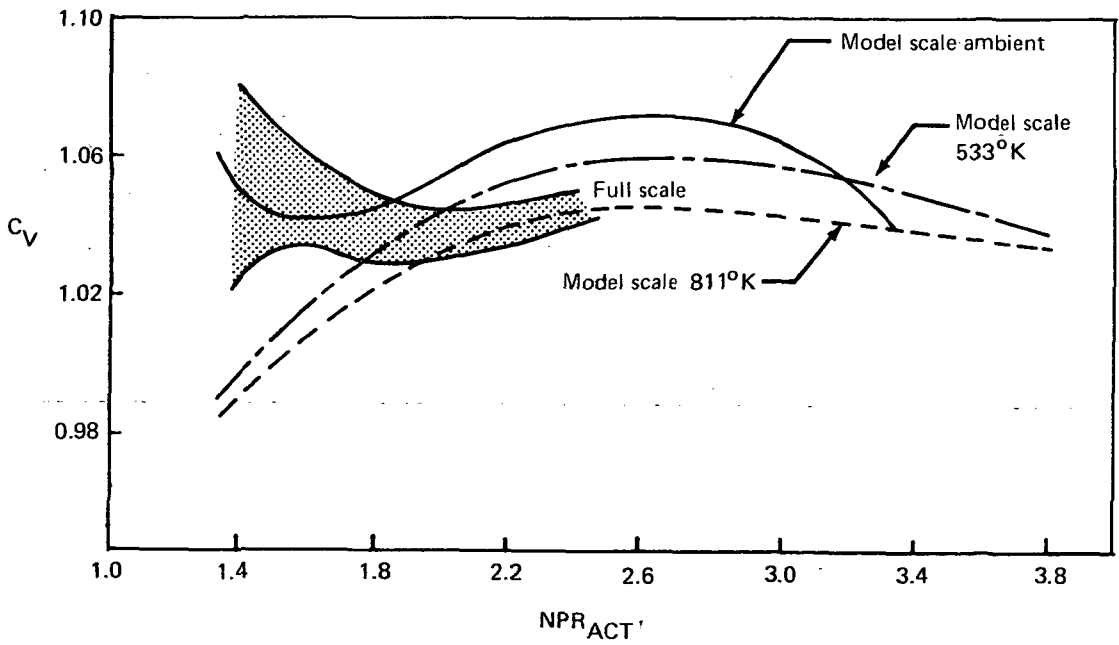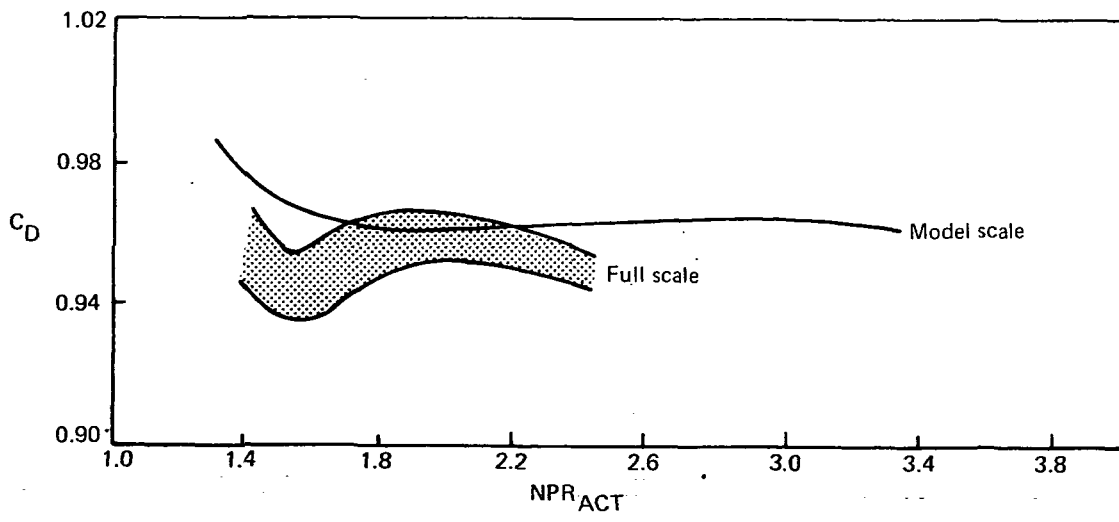
FIGURE 151.—COMPARISON OF MODEL- AND FULL-SCALE 37-TUBE NOZZLE WITH L/D = 1 HARDWALL EJECTOR DISCHARGE AND VELOCITY COEFFICIENTS
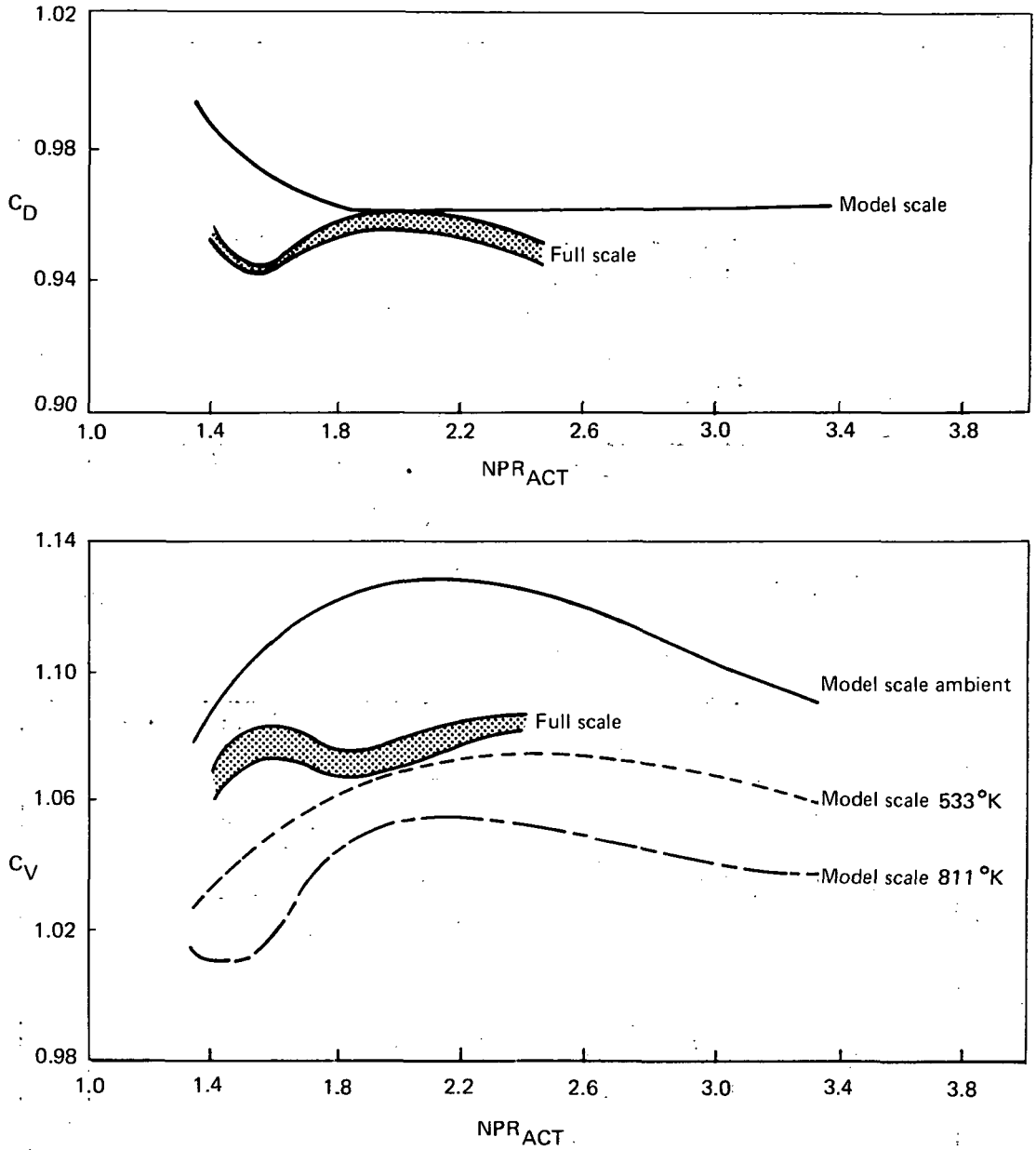
FIGURE 152.—COMPARISON OF MODEL- AND FULL-SCALE 37-TUBE NOZZLE WITH L/D = 2 HARDWALL EJECTOR DISCHARGE AND VELOCITY COEFFICIENTS
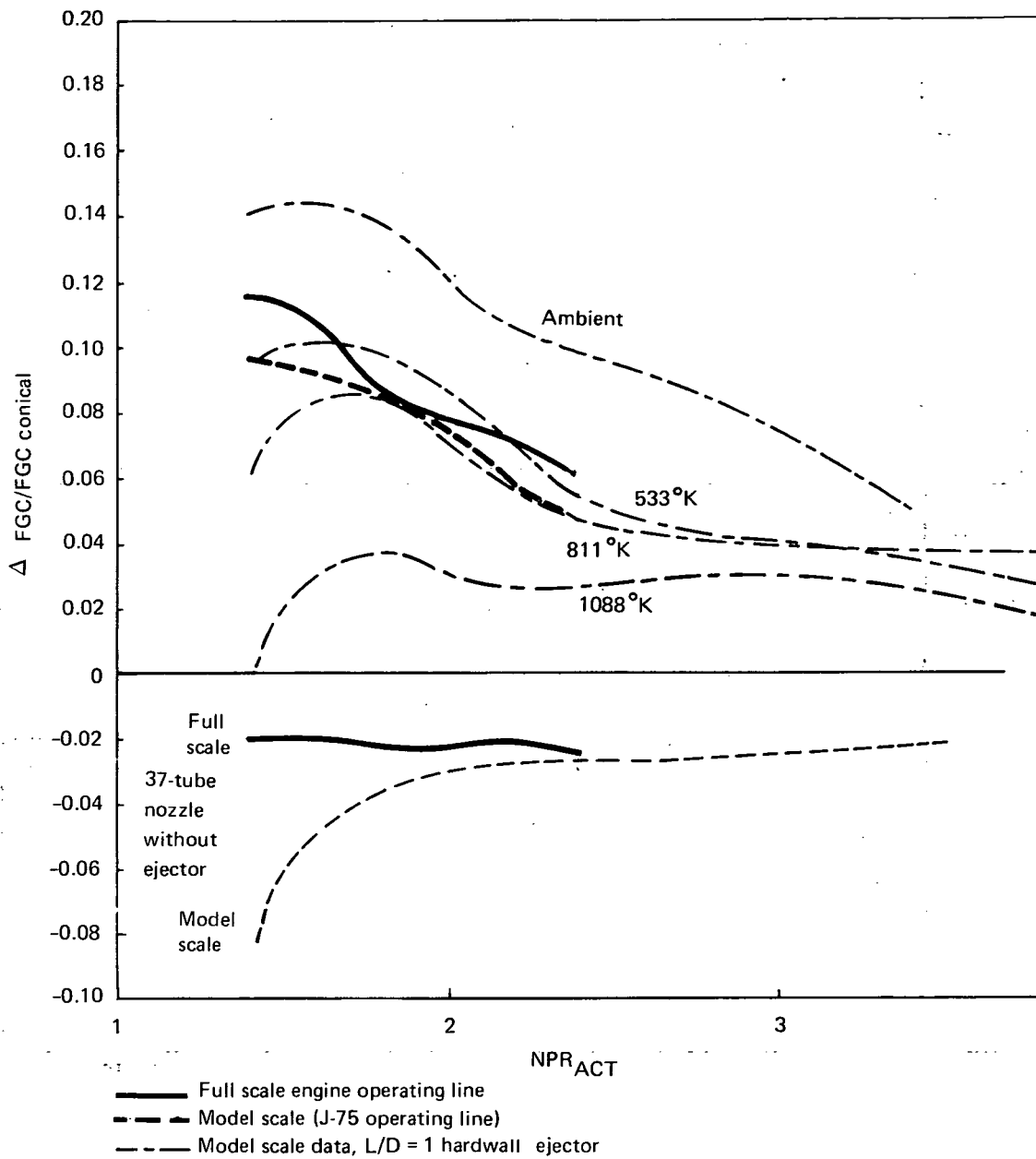
FIGURE 153.—THRUST DIFFERENCES OF MODEL- AND FULL-SCALE 37-TUBE NOZZLES AND L/D = 1 EJECTORS WITH RESPECT TO THE CONICAL NOZZLES
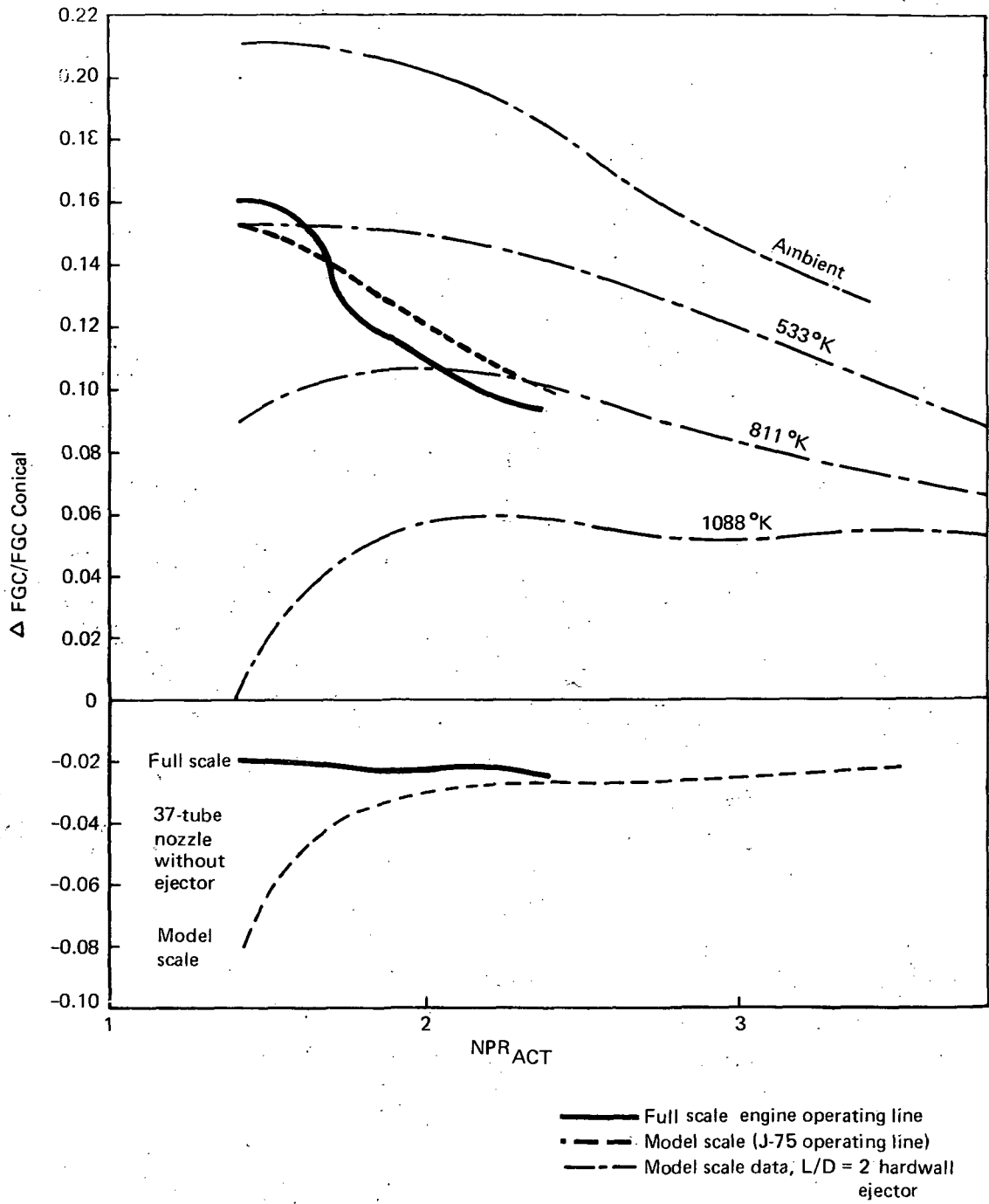
FIGURE 154.—THRUST DIFFERENCES OF MODEL- AND FULL-SCALE 37-TUBE NOZZLES AND
L/D = 2 EJECTORS WITH RESPECT TO THE CONICAL NOZZLES
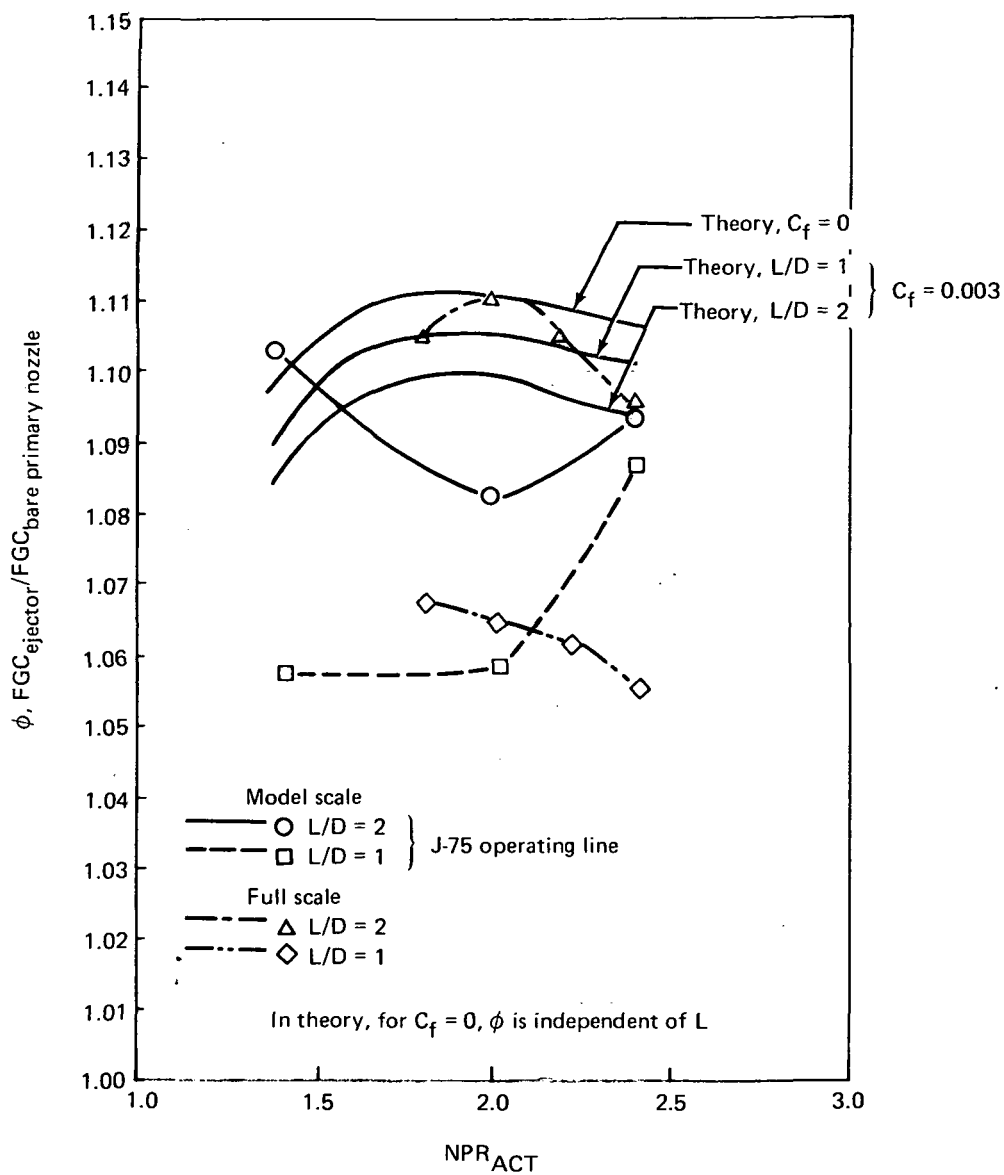
FIGURE 155.—THRUST AUGMENTATION FOR MODEL- AND FULL-SCALE EJECTORS
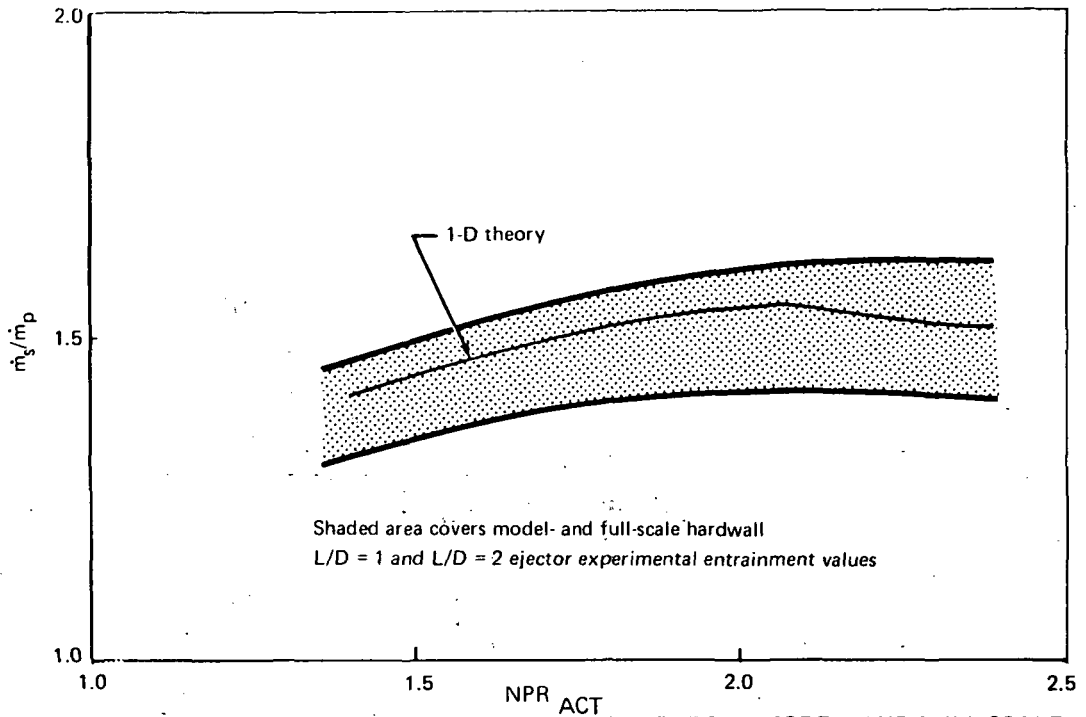
FIGURE 156.—SECONDARY AIRFLOW ENTRAINMENT FOR MODEL- AND FULL-SCALE HARDWALL EJECTORS (J-75 OPERATING LINE)
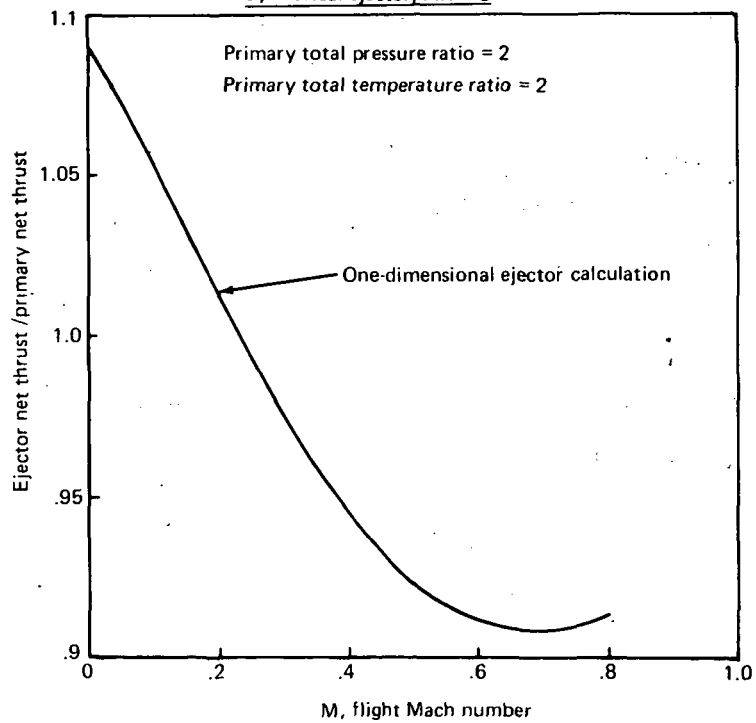
FIGURE 157.— ESTIMATED THRUST VARIATION WITH FORWARD FLIGHT SPEED FOR A TYPICAL EJECTOR
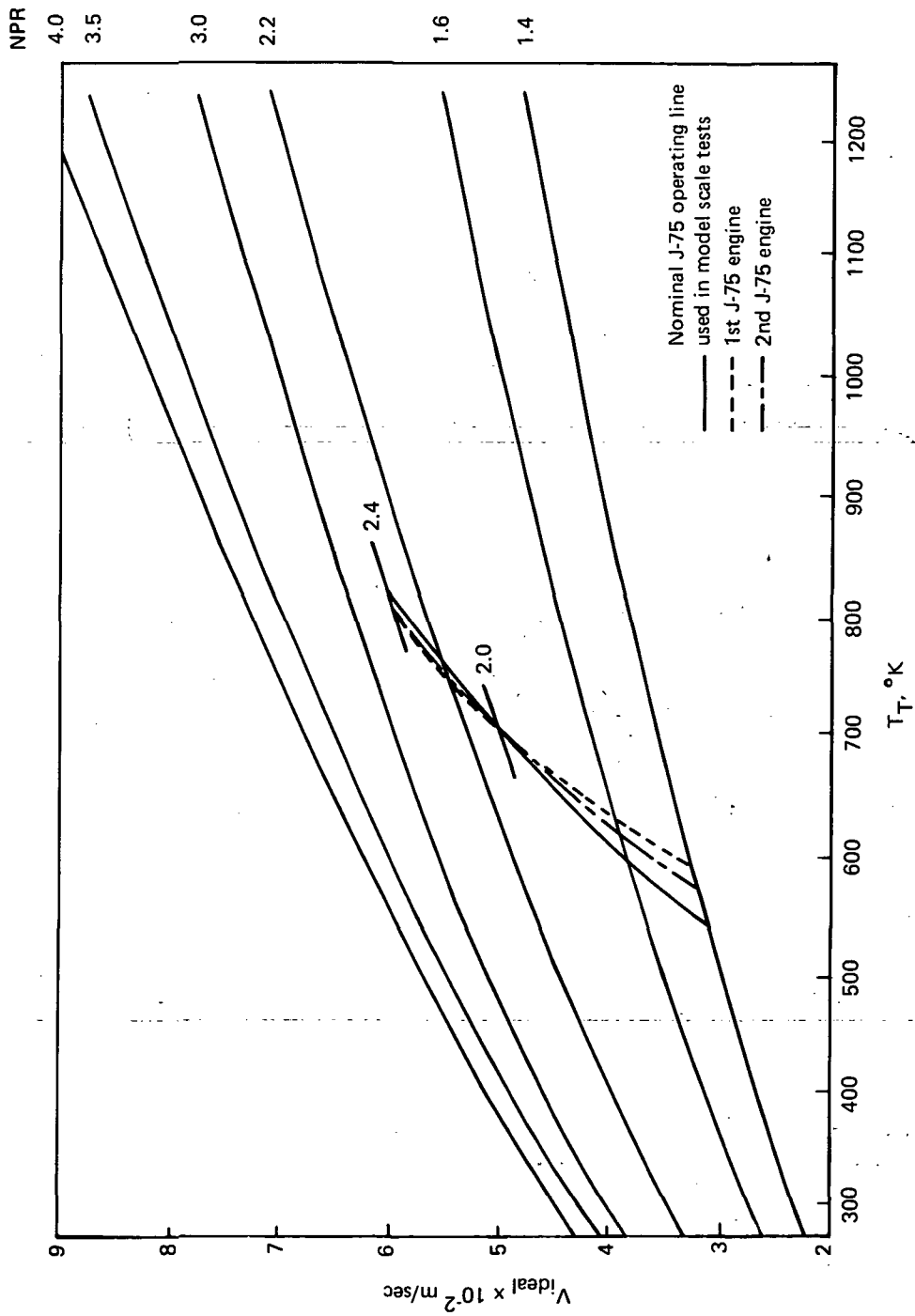
FIGURE 158.— IDEAL JET VELOCITY AS A FUNCTION OF POWER SETTING OVER THE RANGE OF MODEL—AND FULL—SCALE TEST CONDITIONS
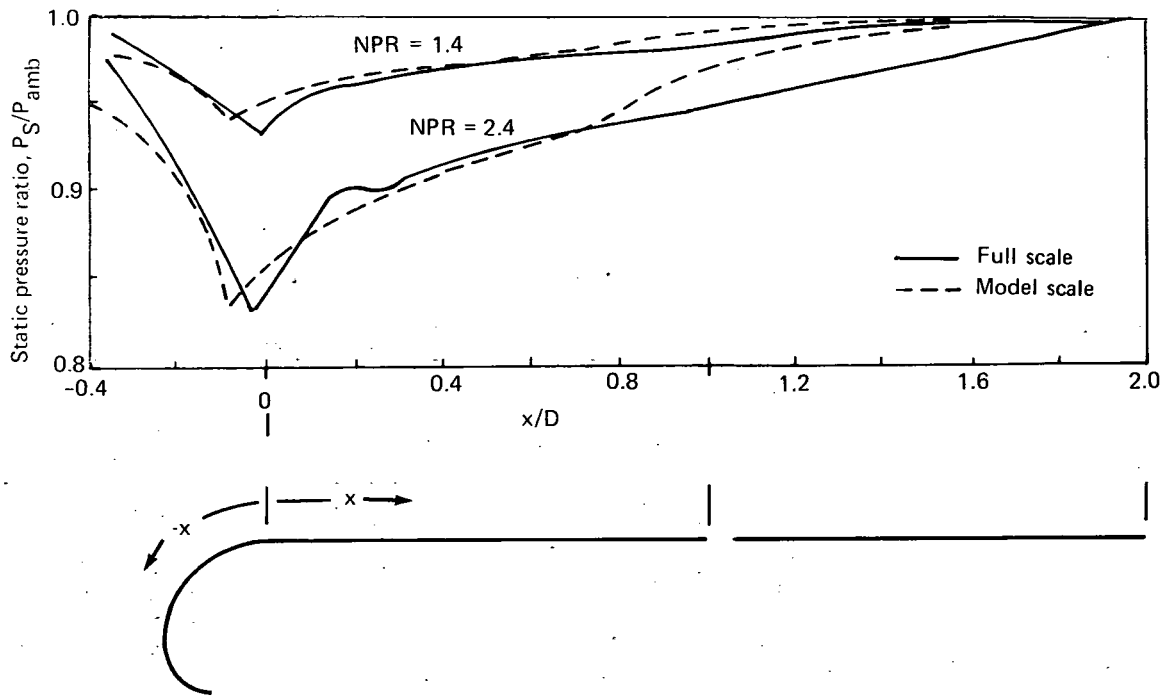
FIGURE 159.— COMPARISON OF EJECTOR WALL STATIC PRESSURE DISTRIBUTIONS BETWEEN MODEL
AND FULL-SCALE L/D = 2 HARDWALL EJECTORS (J-75 NOZZLE OPERATING CONDITIONS)
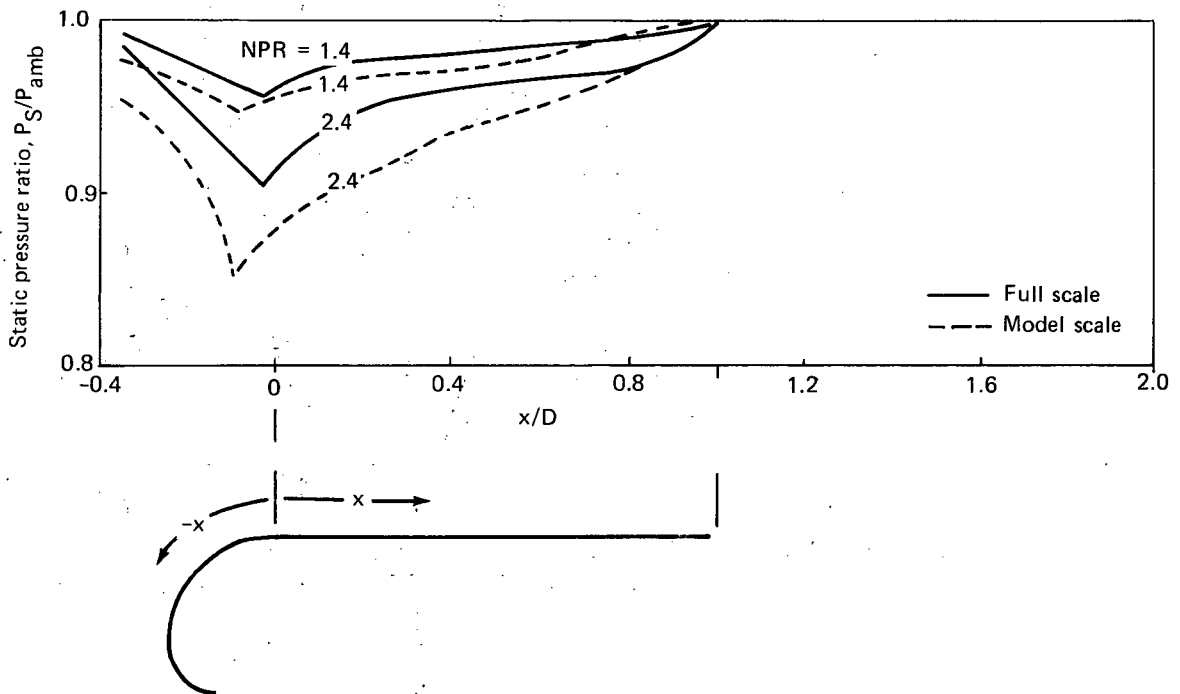
FIGURE 160.— COMPARISON OF EJECTOR WALL STATIC PRESSURE DISTRIBUTIONS BETWEEN MODEL-
AND FULL-SCALE L/D = 1 HARDWALL EJECTORS (J-75 NOZZLE OPERATING CONDITIONS)

242

Velocity Surveys

Full scale 37-tube nozzle with L/D = 1 hardwall ejector

1/4 scale 37-tube nozzle with L/D = 1 hardwall ejector

Mach No. Surveys
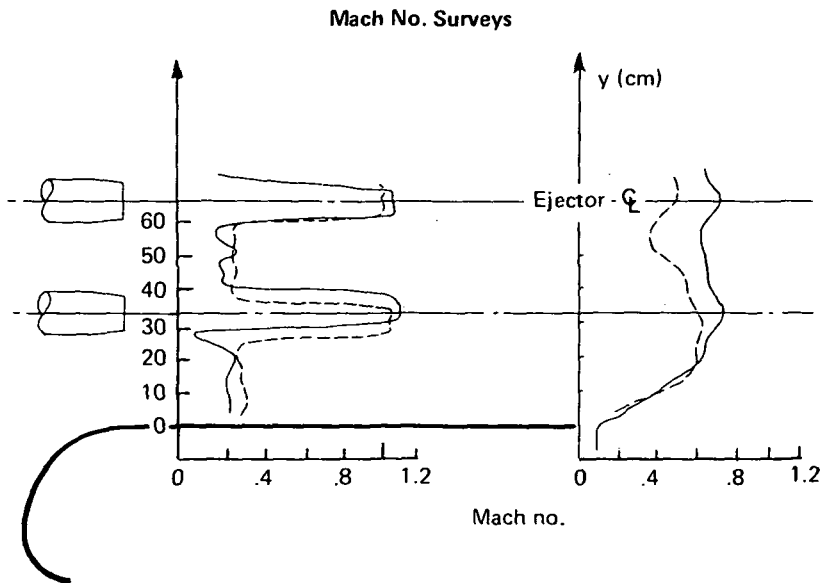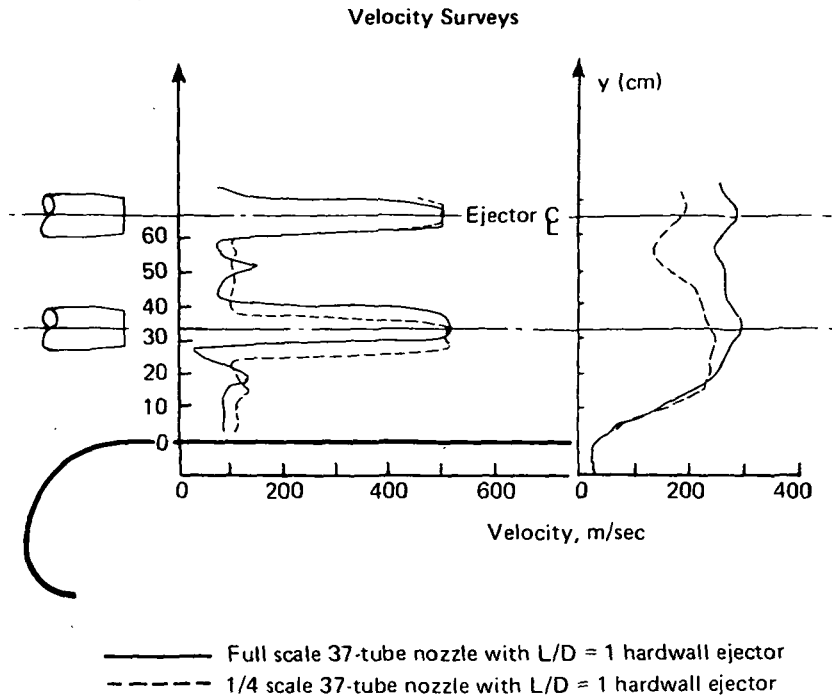
FIGURE 161.—COMPARISON OF MODEL- AND FULL-SCALE FLOW SURVEYS FOR THE L/D = 1 HARDWALL EJECTORS AT NPR = 2.0, T = 700°K
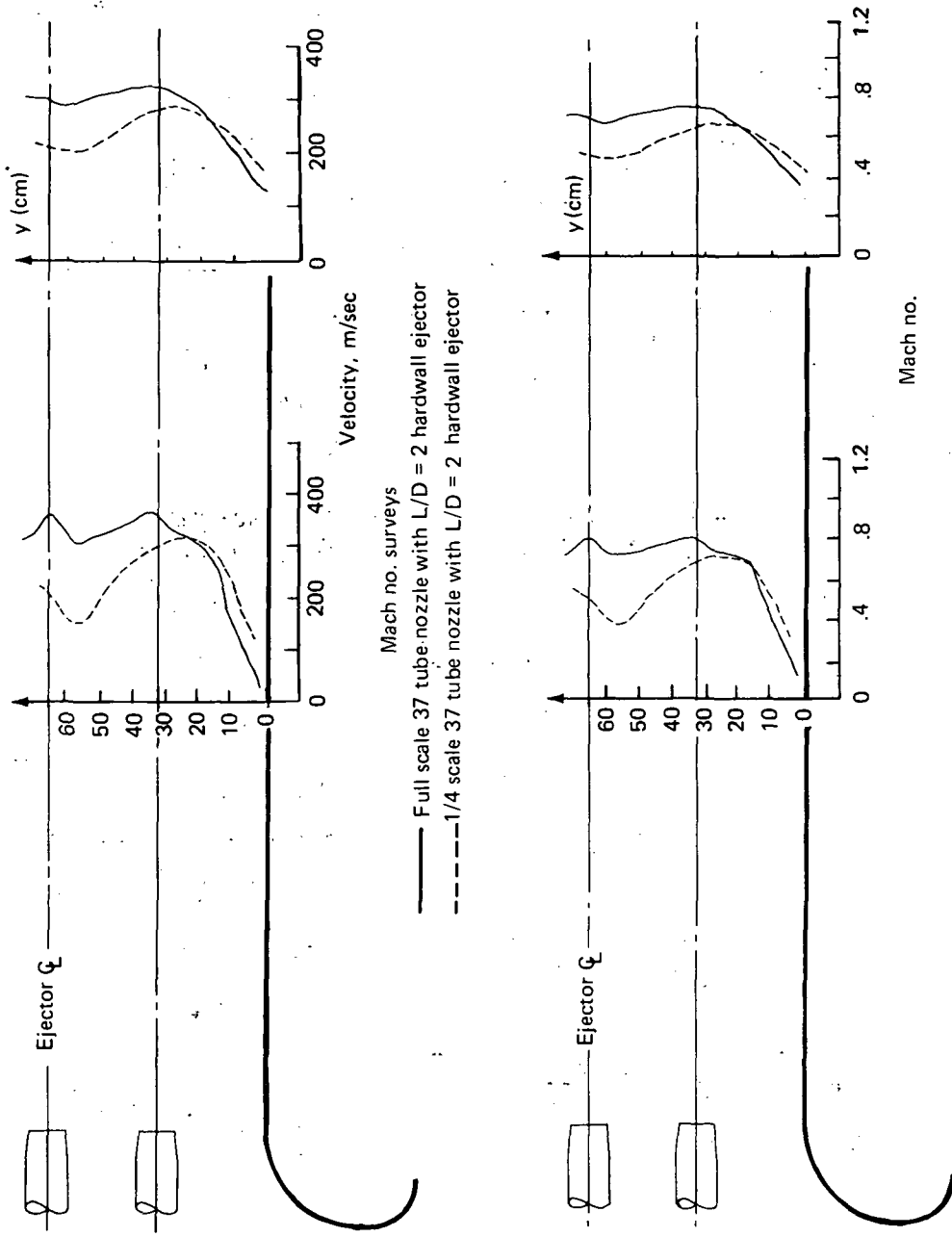
FIGURE 162.—COMPARISON OF MODEL- AND FULL-SCALE FLOW SURVEYS FOR THE L/D = 2 HARDWALL EJECTORS AT NPR = 2.4 AND T_T = 811°K
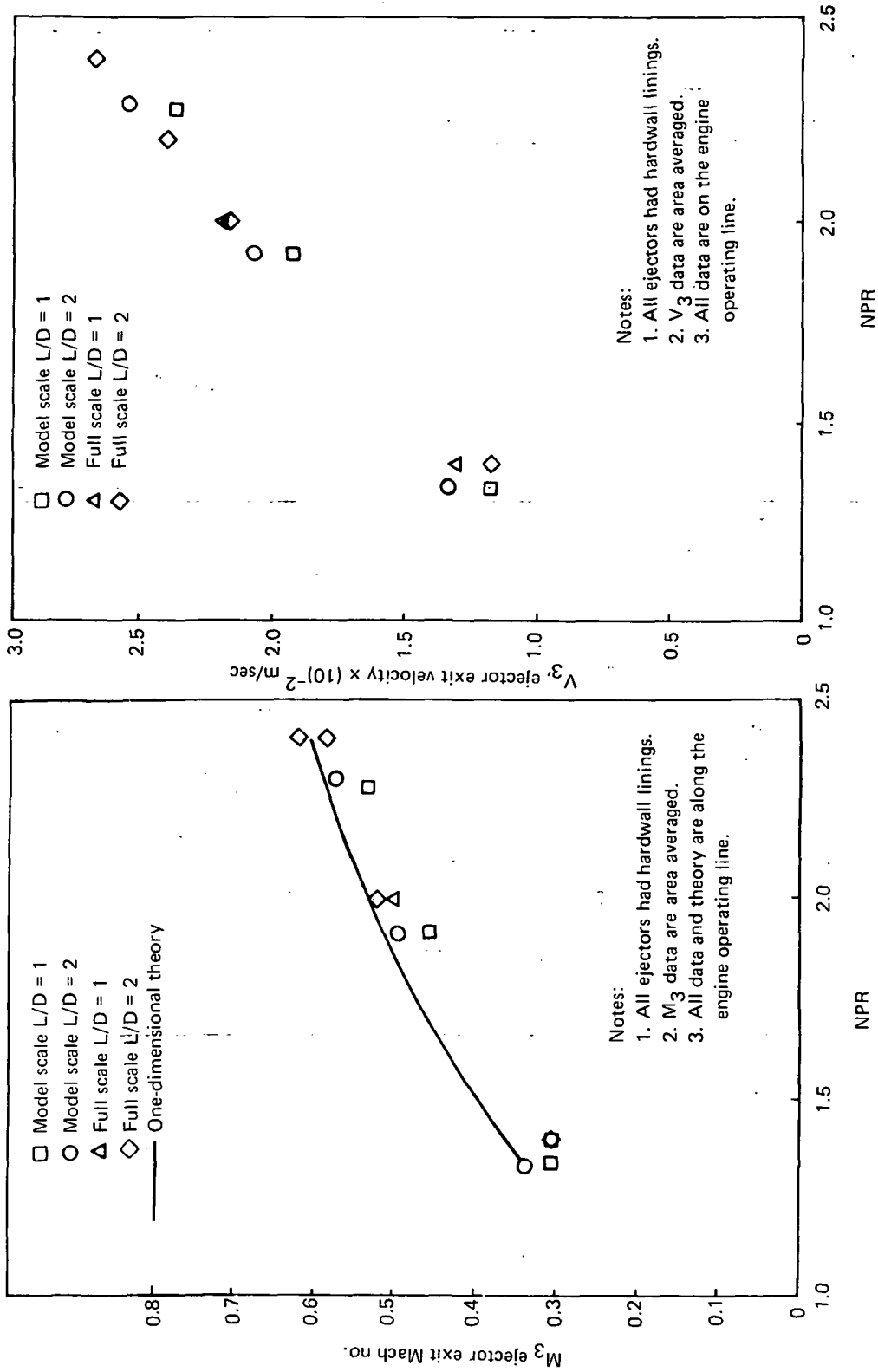
FIGURE 163.—COMPARISON OF MODEL- AND FULL-SCALE EJECTOR EXIT MACH NUMBERS AND VELOCITIES

245
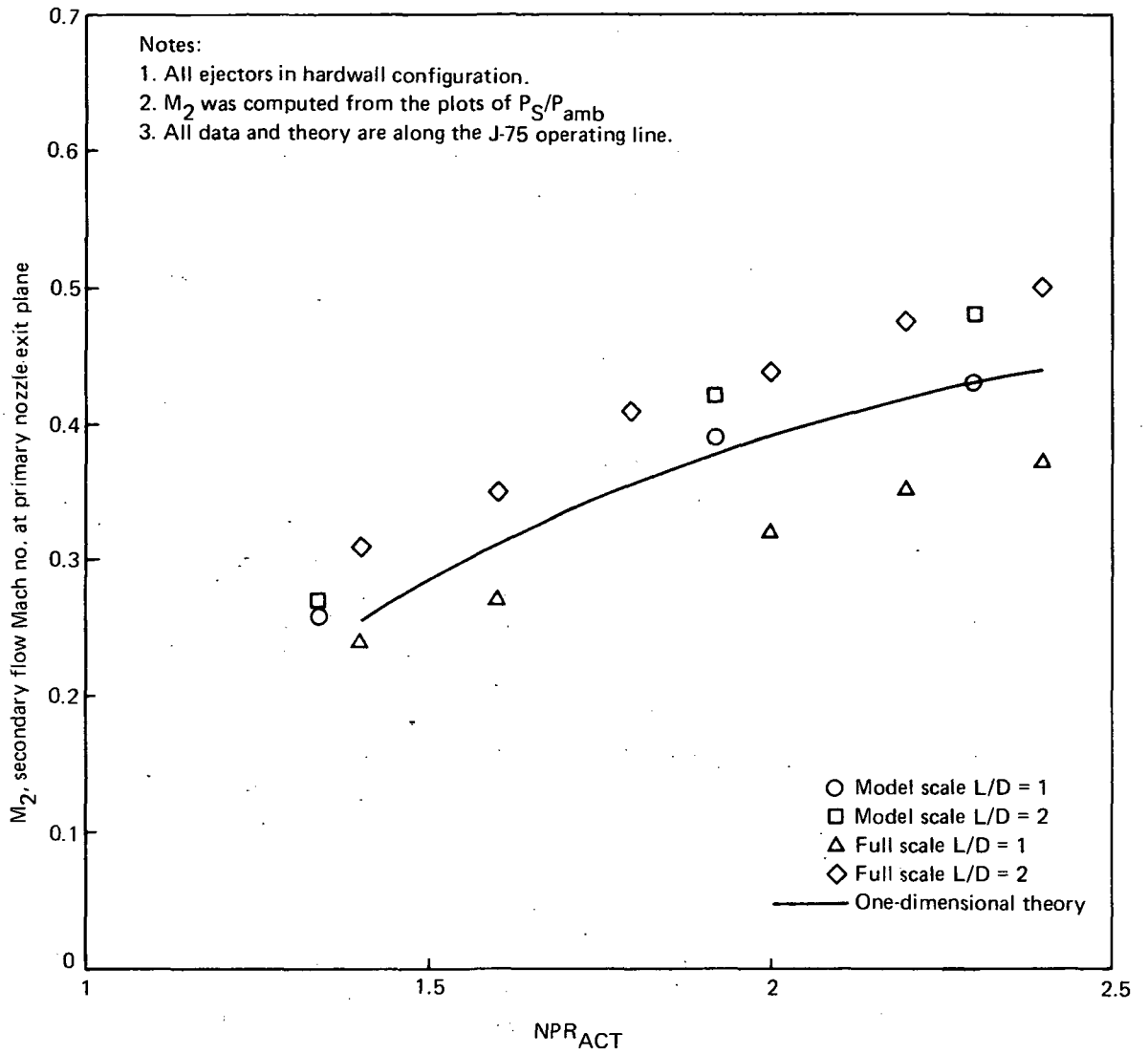
FIGURE 164.—COMPARISON OF MODEL- AND FULL-SCALE EJECTOR SECONDARY FLOW
MACH NUMBERS

FIGURE 166.– COMPARISON OF RESULTS BETWEEN THE "INITIAL" AND "REVISED" LINING PREDICTION PROCEDURES

FIGURE 165.–COMPARISON OF MODEL- AND FULL-SCALE PEAK JET VELOCITY DECAY FOR THE 37-TUBE NOZZLES, L/D = 1 AND L/D = 2 HARDWALL EJECTORS

247
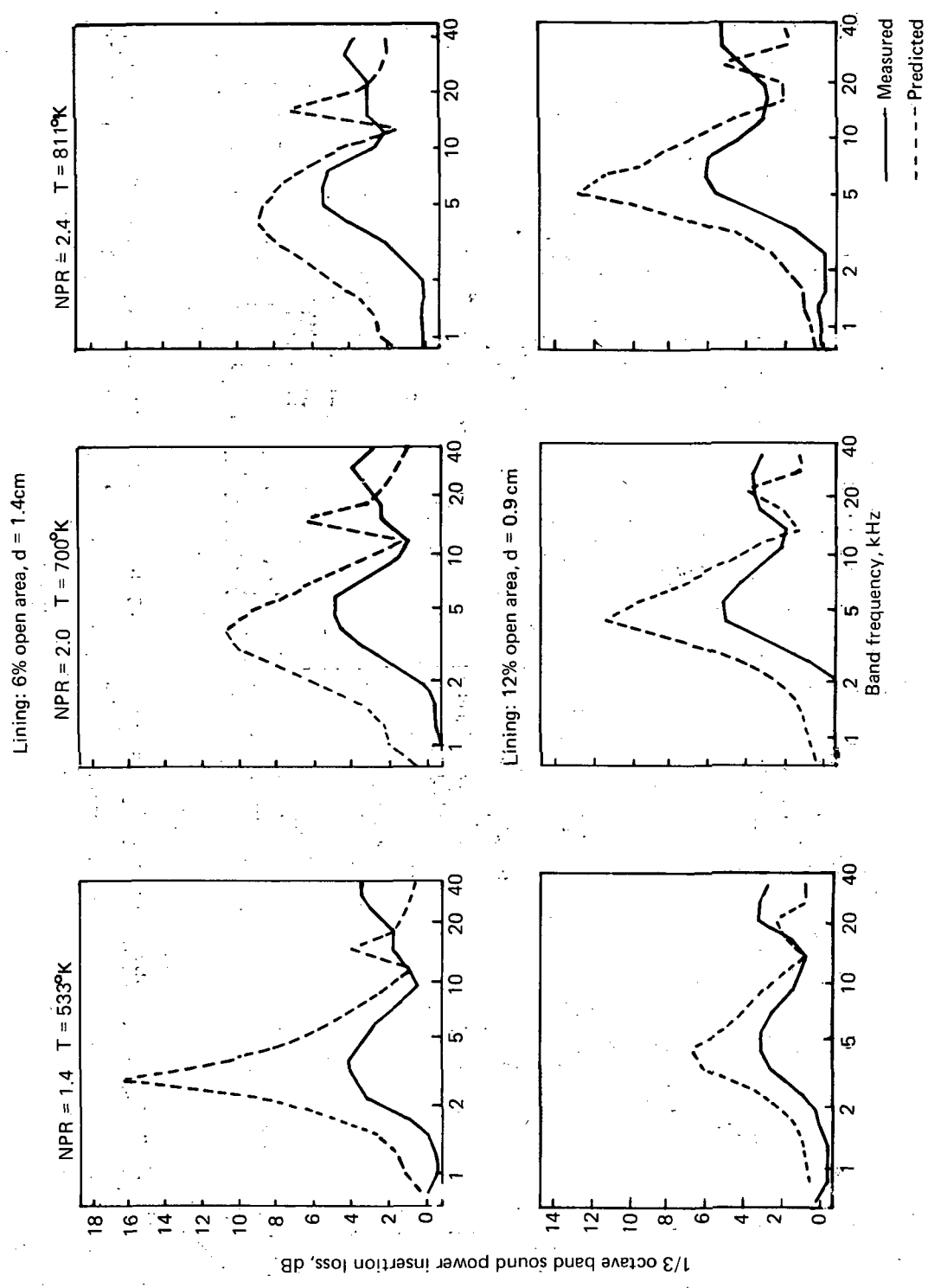
FIGURE 167.—MEASURED AND PREDICTED SOUND POWER INSERTION LOSS SPECTRA FOR MODEL L/D = 1 LINED EJECTOR

248

FIGURE 167.—Continued

Lining: 22% open area, d = 1.4 cm

NPR = 1.4   T = 533°K   NPR = 2.0   T = 700°K   NPR = 2.4   T = 811°K

Lining: 30% open area, d = 1.4 cm

Measured
Predicted

Band frequency, kHz

FIGURE 167.—Concluded
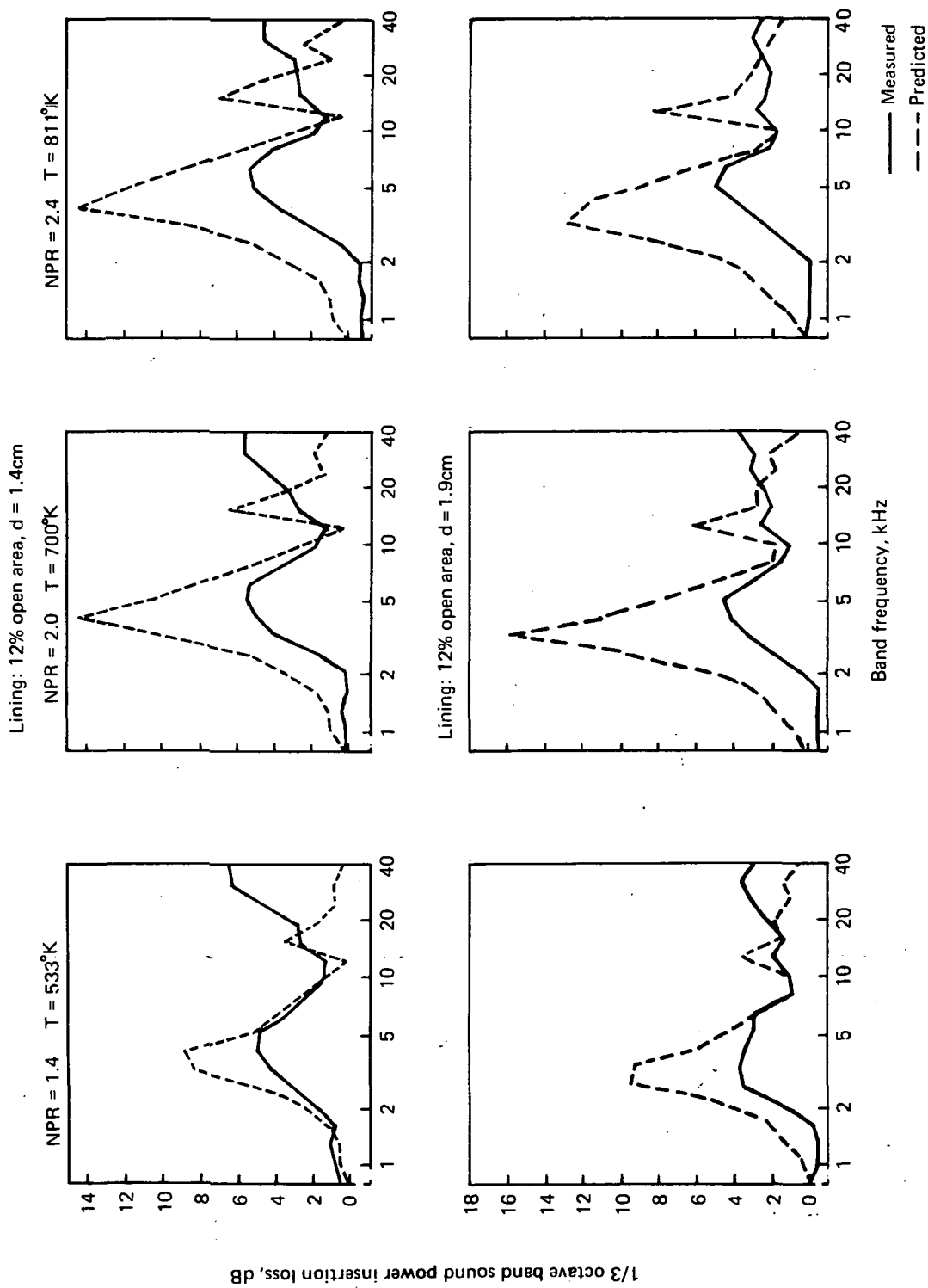
1/3 octave band sound power insertion loss, dB
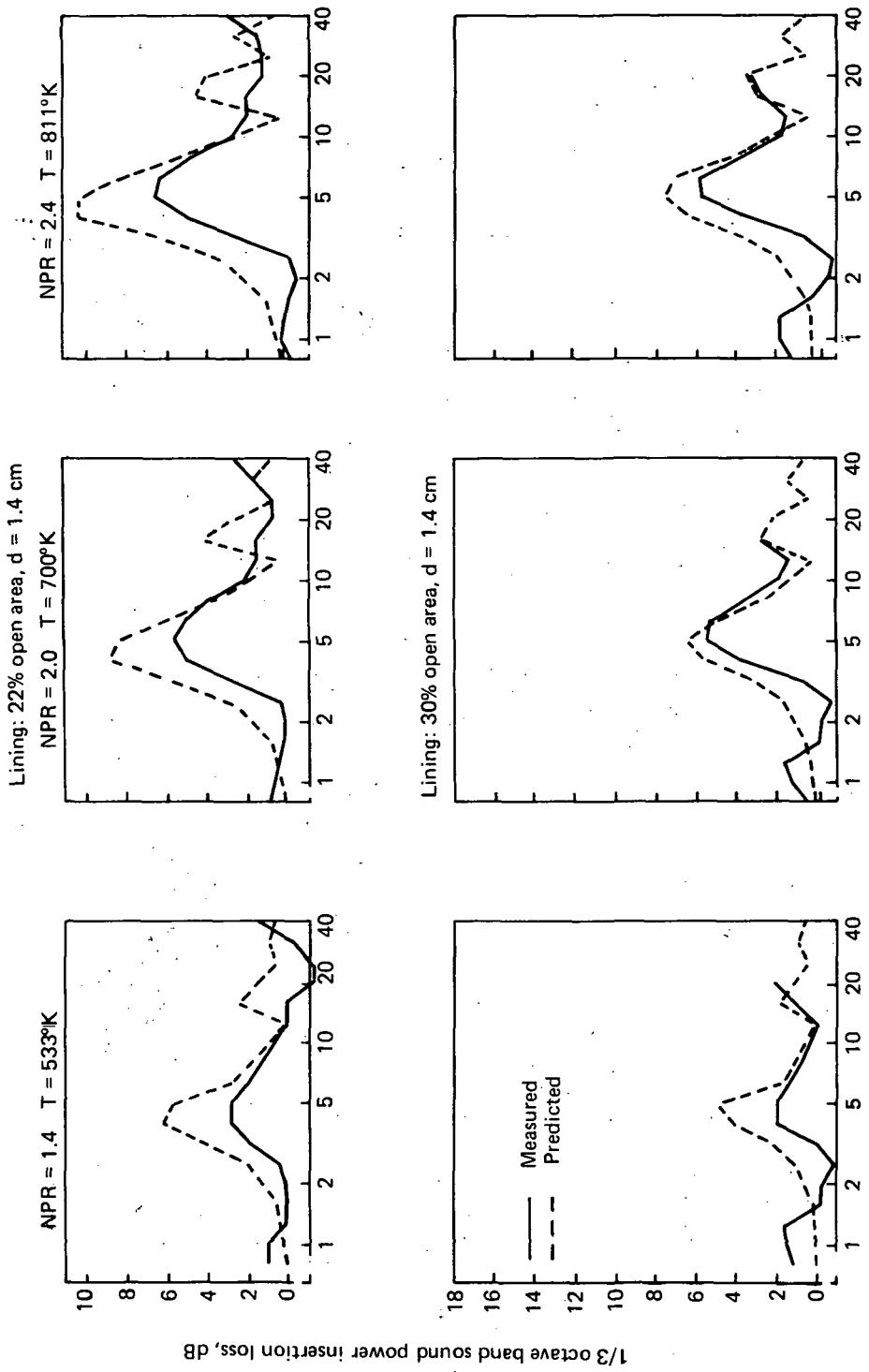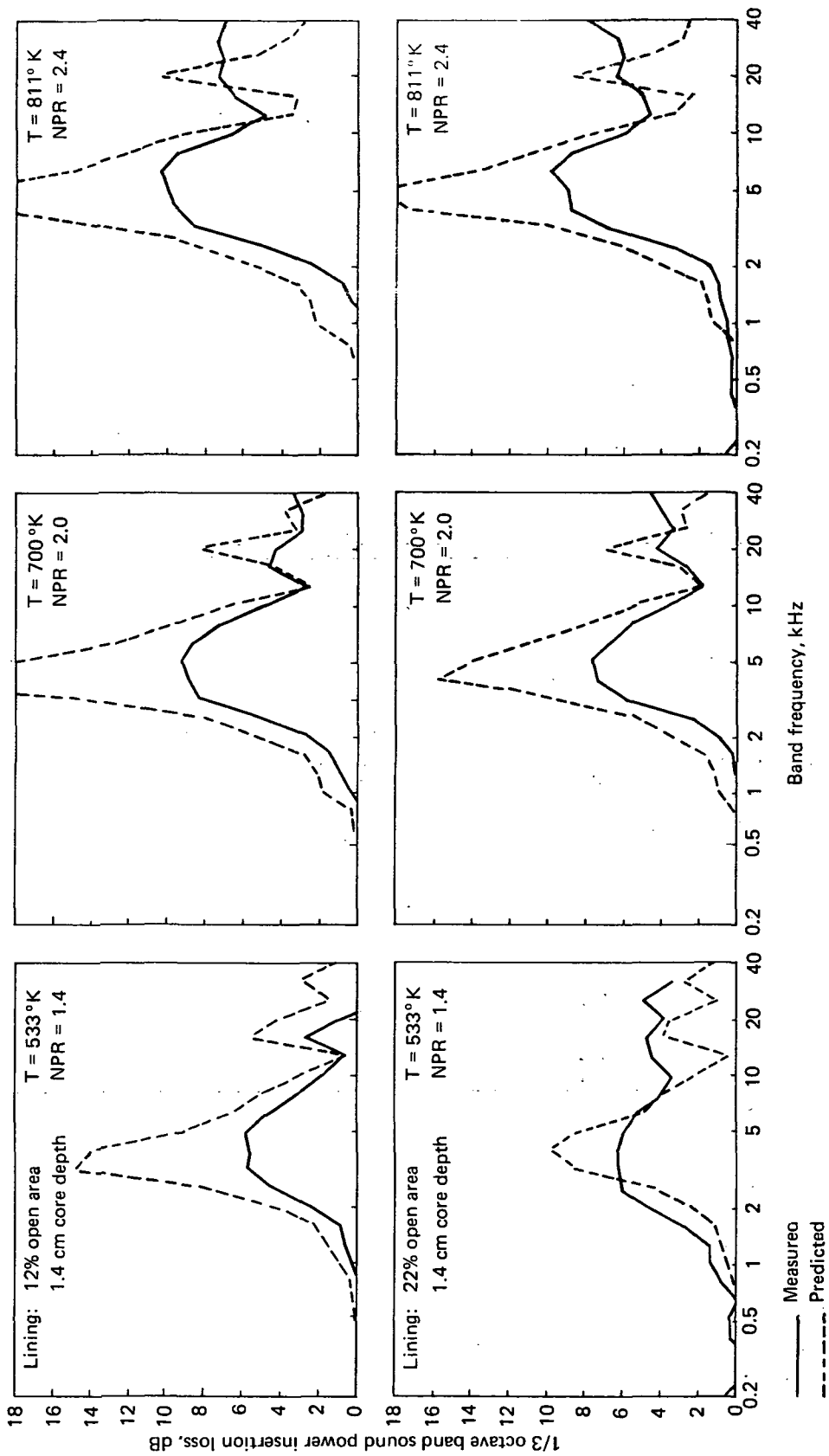
FIGURE 168.— MEASURED AND PREDICTED SOUND POWER INSERTION LOSS SPECTRA
FOR THE MODEL SCALE L/D = 2 LINED EJECTOR

251
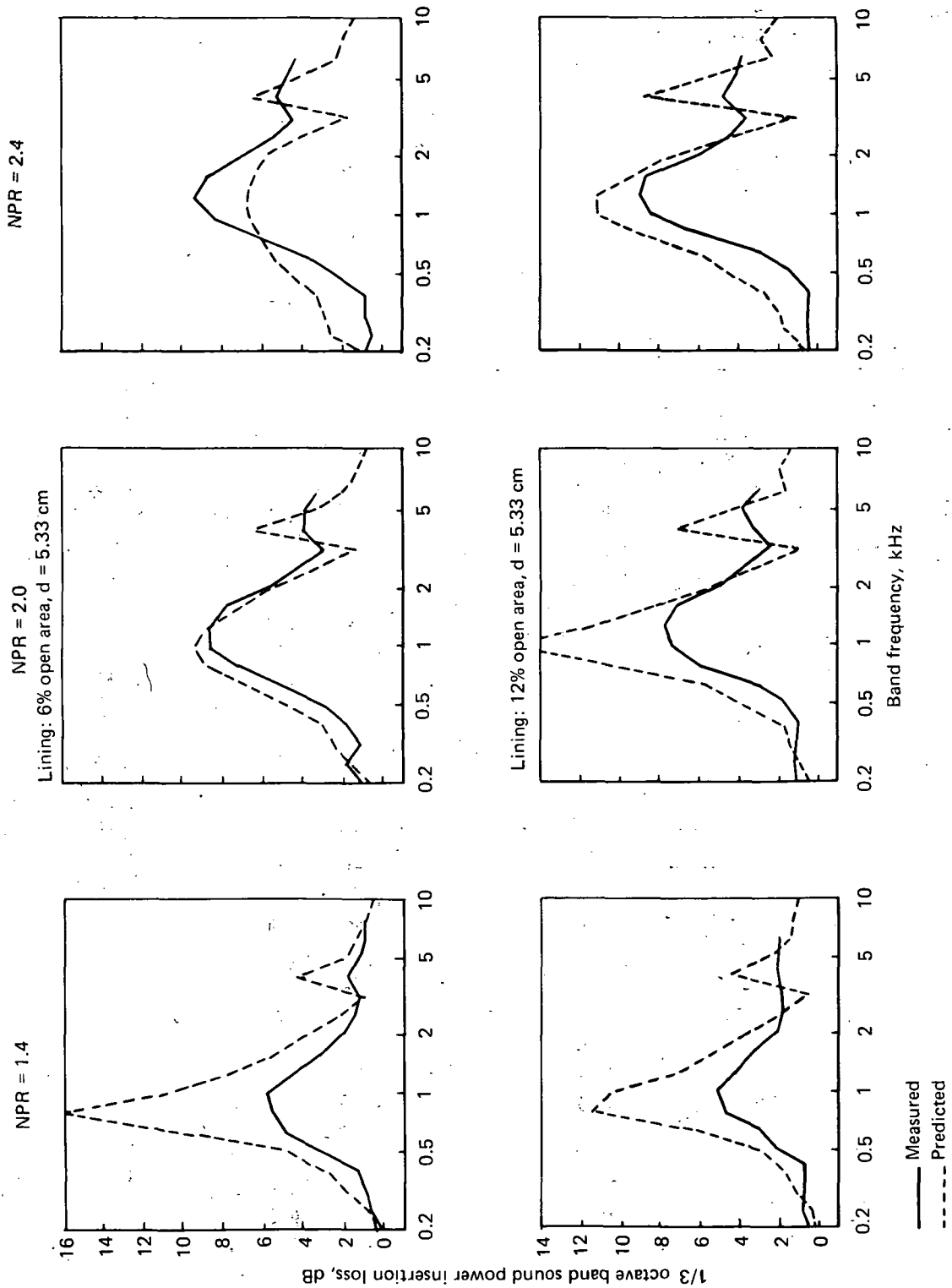
FIGURE 169.– MEASURED AND PREDICTED SOUND POWER INSERTION LOSS SPECTRA
FOR THE FULL-SCALE L/D = 1 LINED EJECTORS
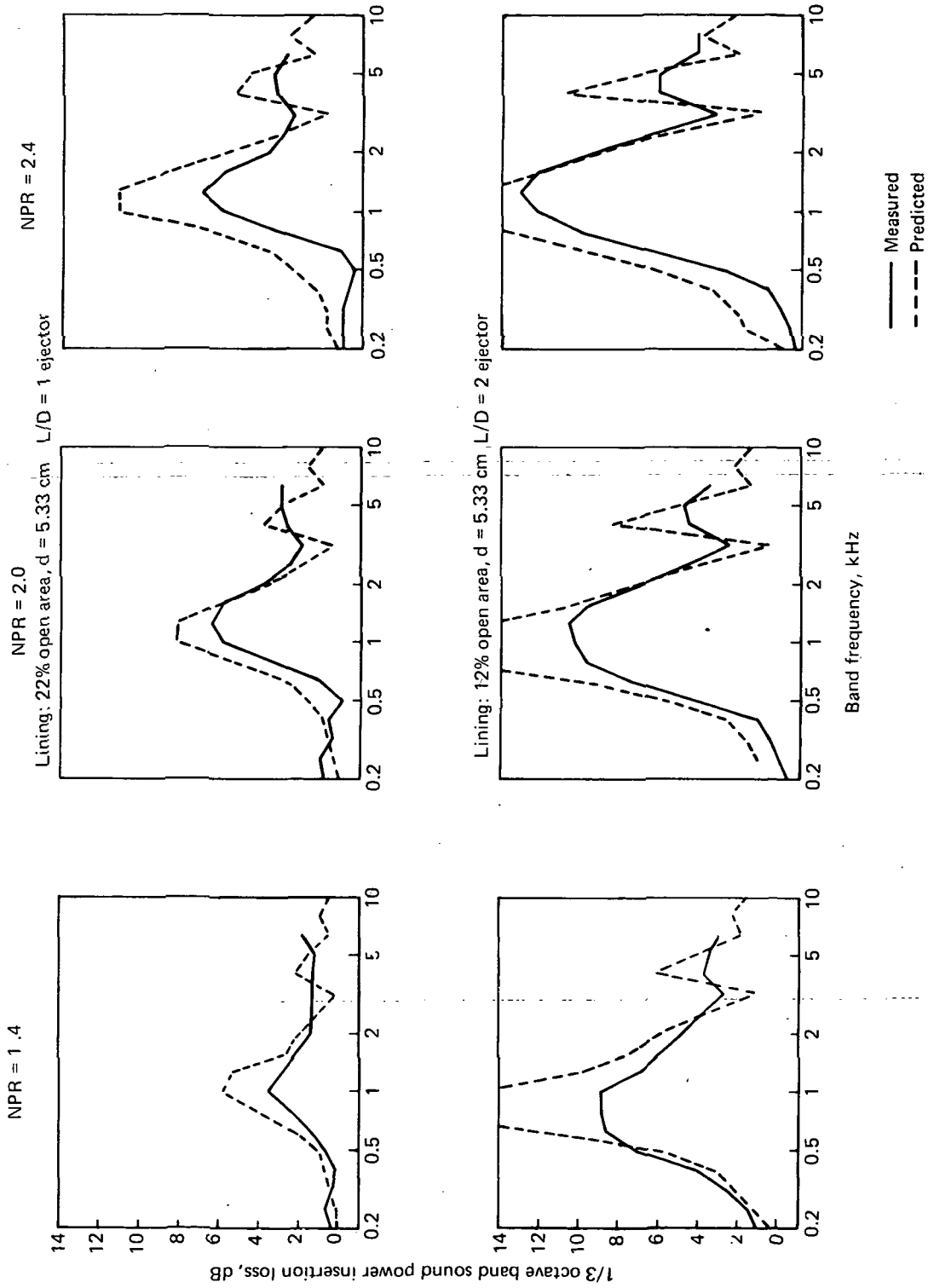
FIGURE 170.— MEASURED AND PREDICTED SOUND POWER INSERTION LOSS SPECTRA
FOR THE FULL-SCALE L/D = 1 AND L/D = 2 LINED EJECTORS
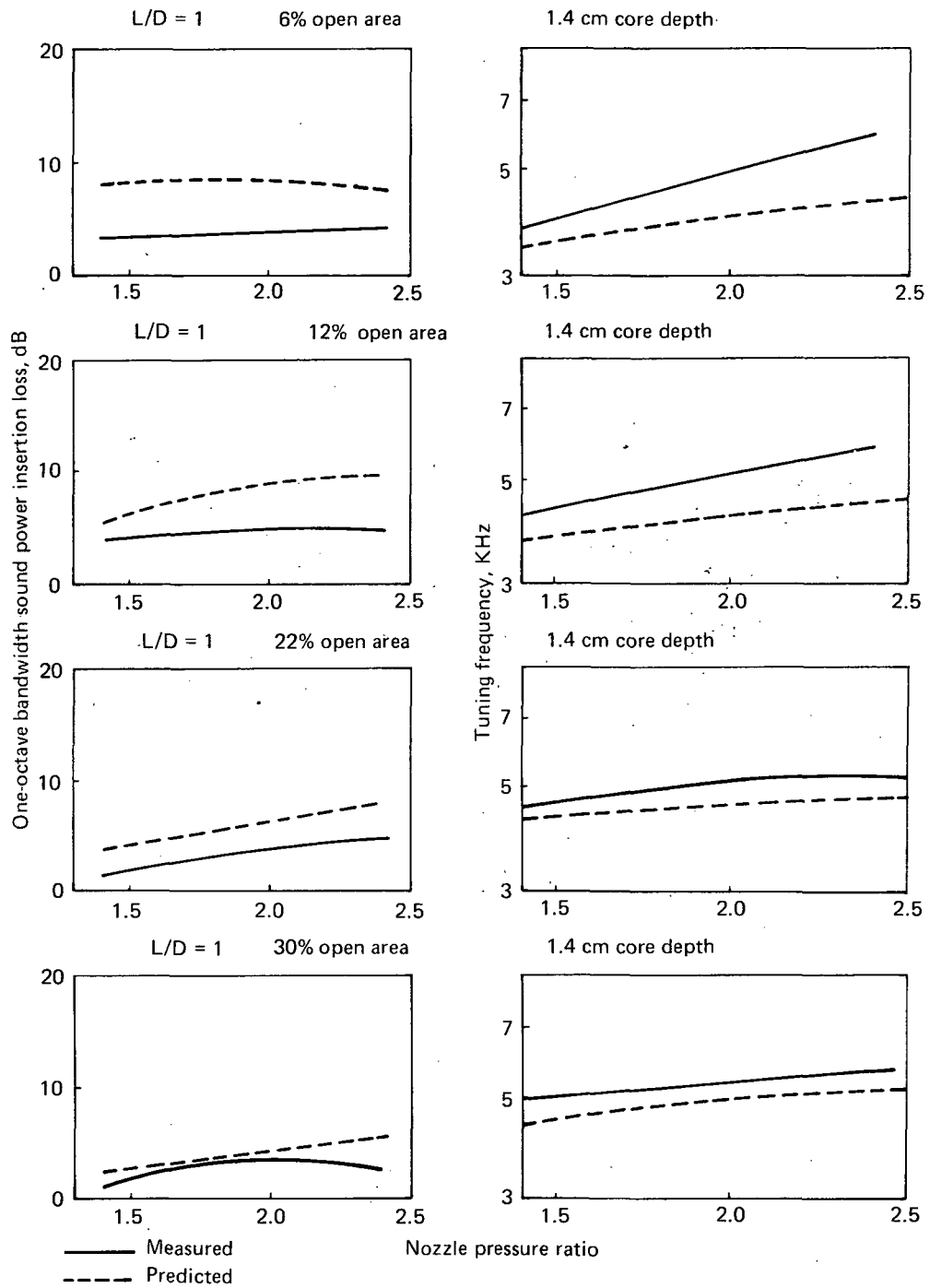
FIGURE 171.—MEASURED AND PREDICTED ACOUSTIC PERFORMANCE OF MODEL SCALE LINED EJECTORS

254
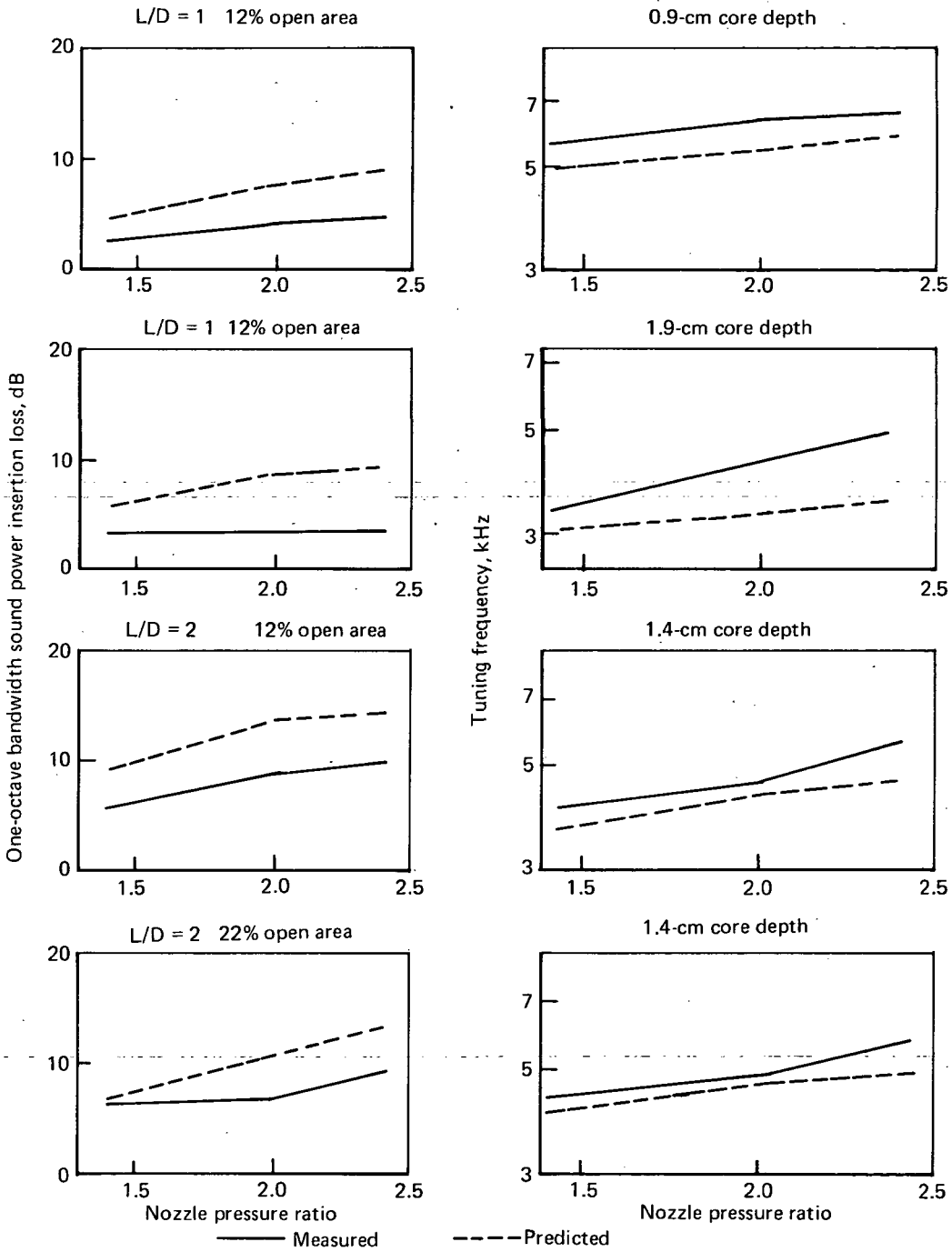
FIGURE 171.—Concluded

255
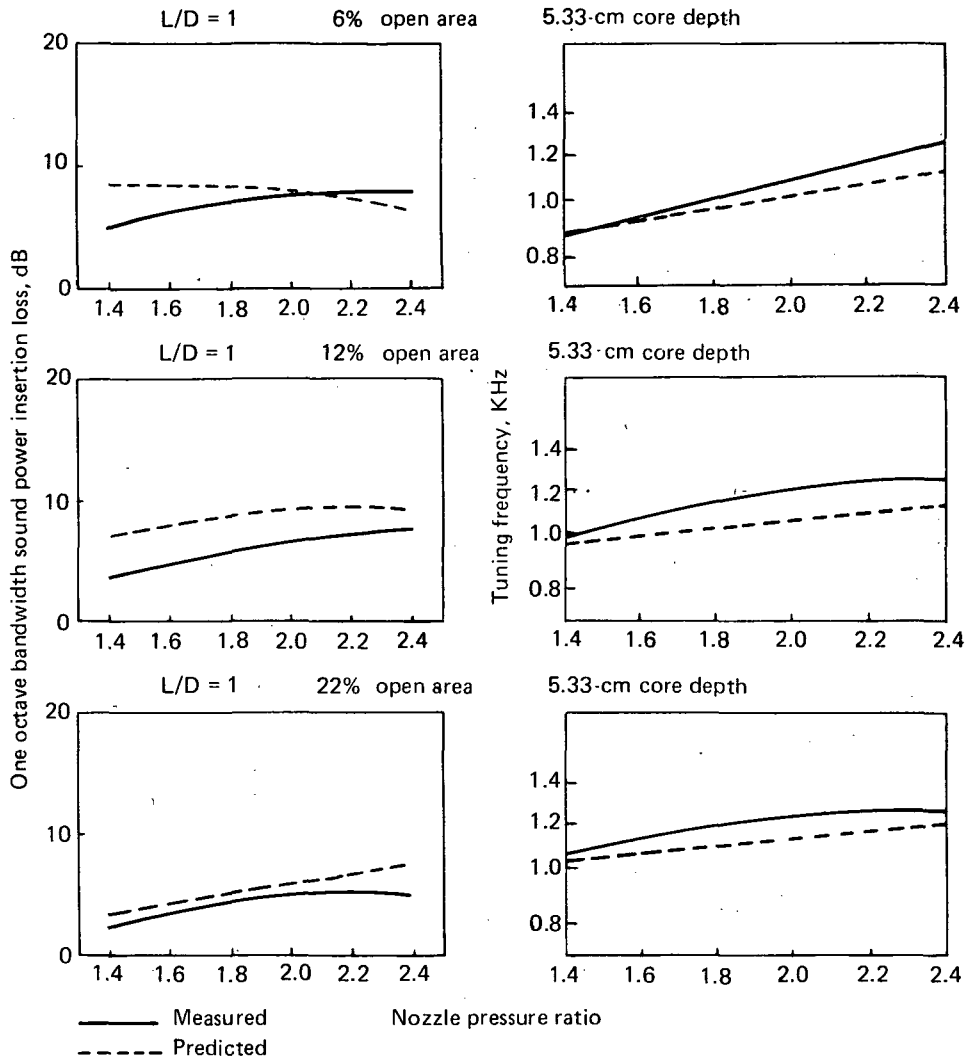
FIGURE 172.—MEASURED AND PREDICTED ACOUSTIC PERFORMANCE
OF FULL-SCALE LINED EJECTORS
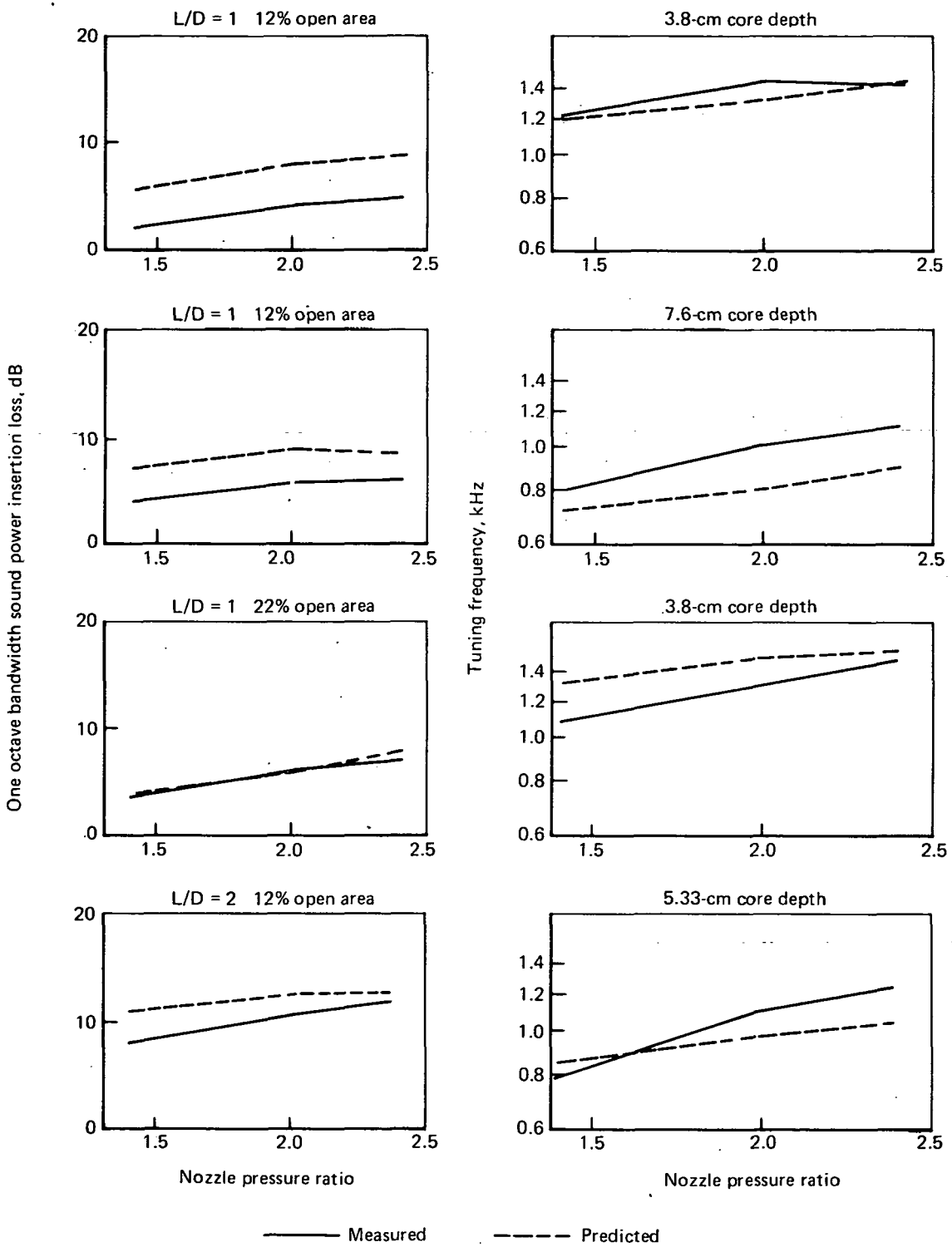
FIGURE 172.--Concluded

257
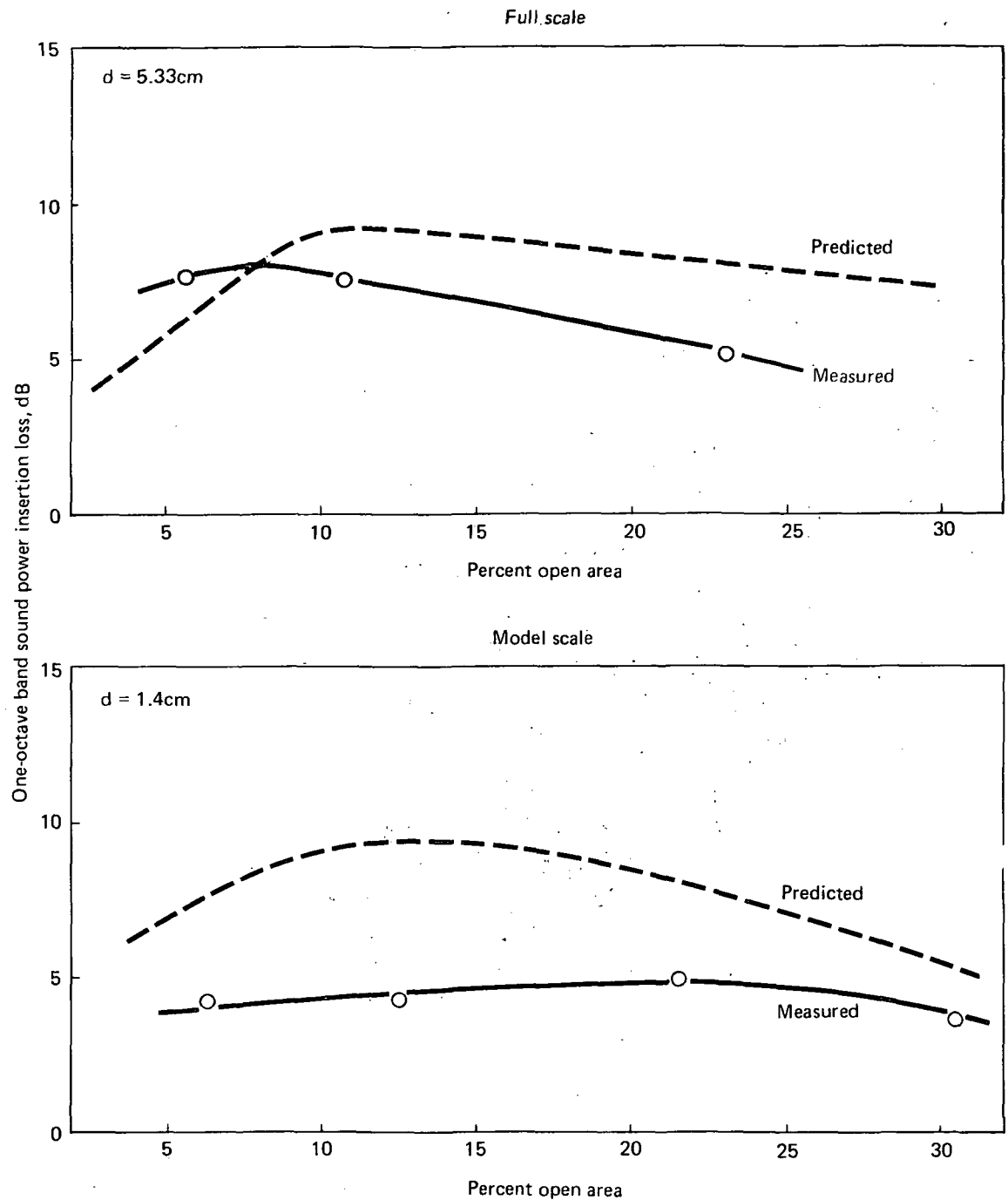
FIGURE 173.—MEASURED AND PREDICTED EJECTOR LINING INSERTION LOSS (L/D = 1) AS A FUNCTION OF LINING PERCENT OPEN AREA AT NPR = 2.4 AND T = 811°K

NPR = 2.40, T = 811°K
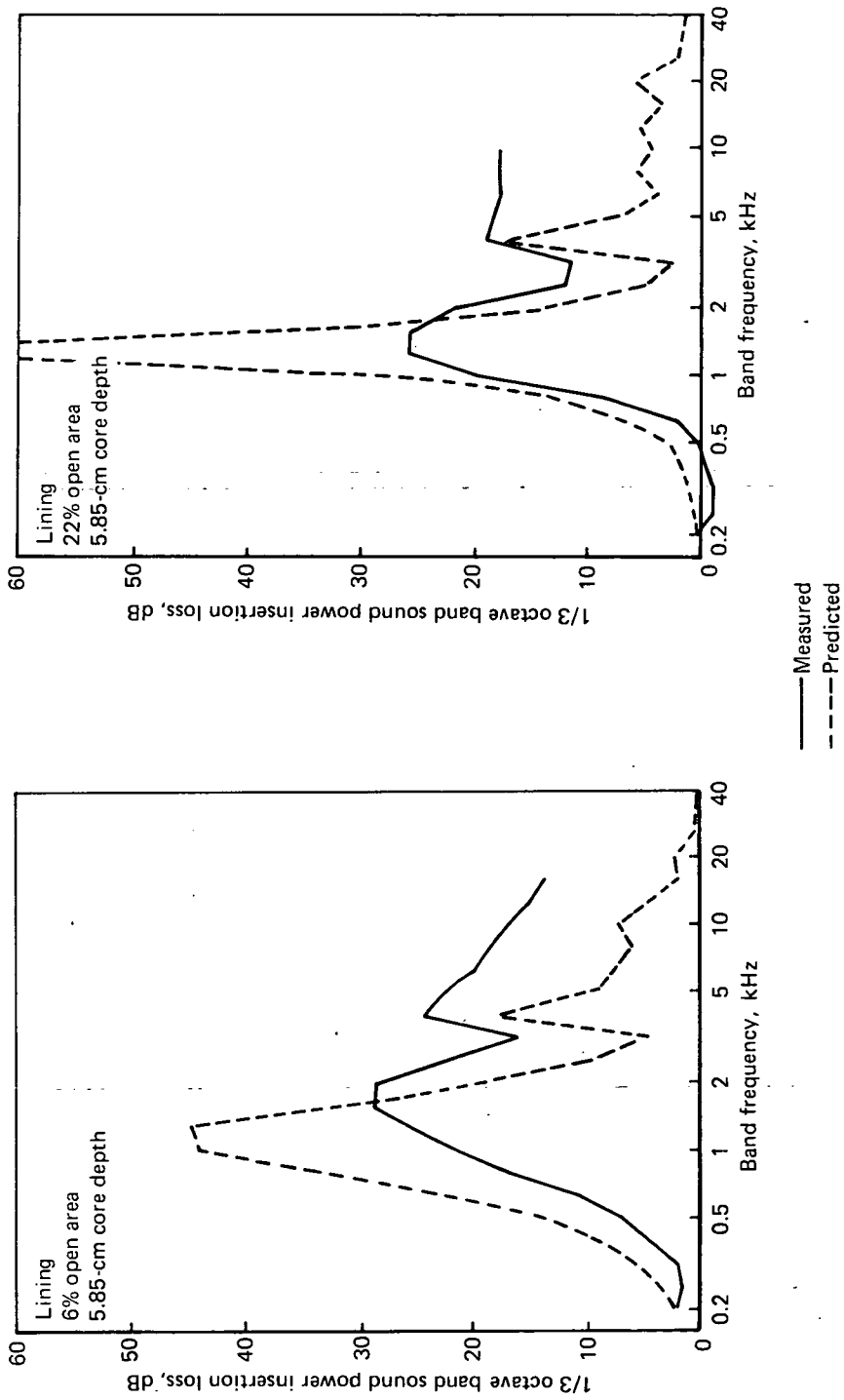
FIGURE 174.—MEASURED AND PREDICTED SOUND POWER INSERTION LOSS
SPECTRA FOR THE 10.9-CM-DIAMETER NOZZLE WITH LINED
L/D = 8 EJECTOR

259
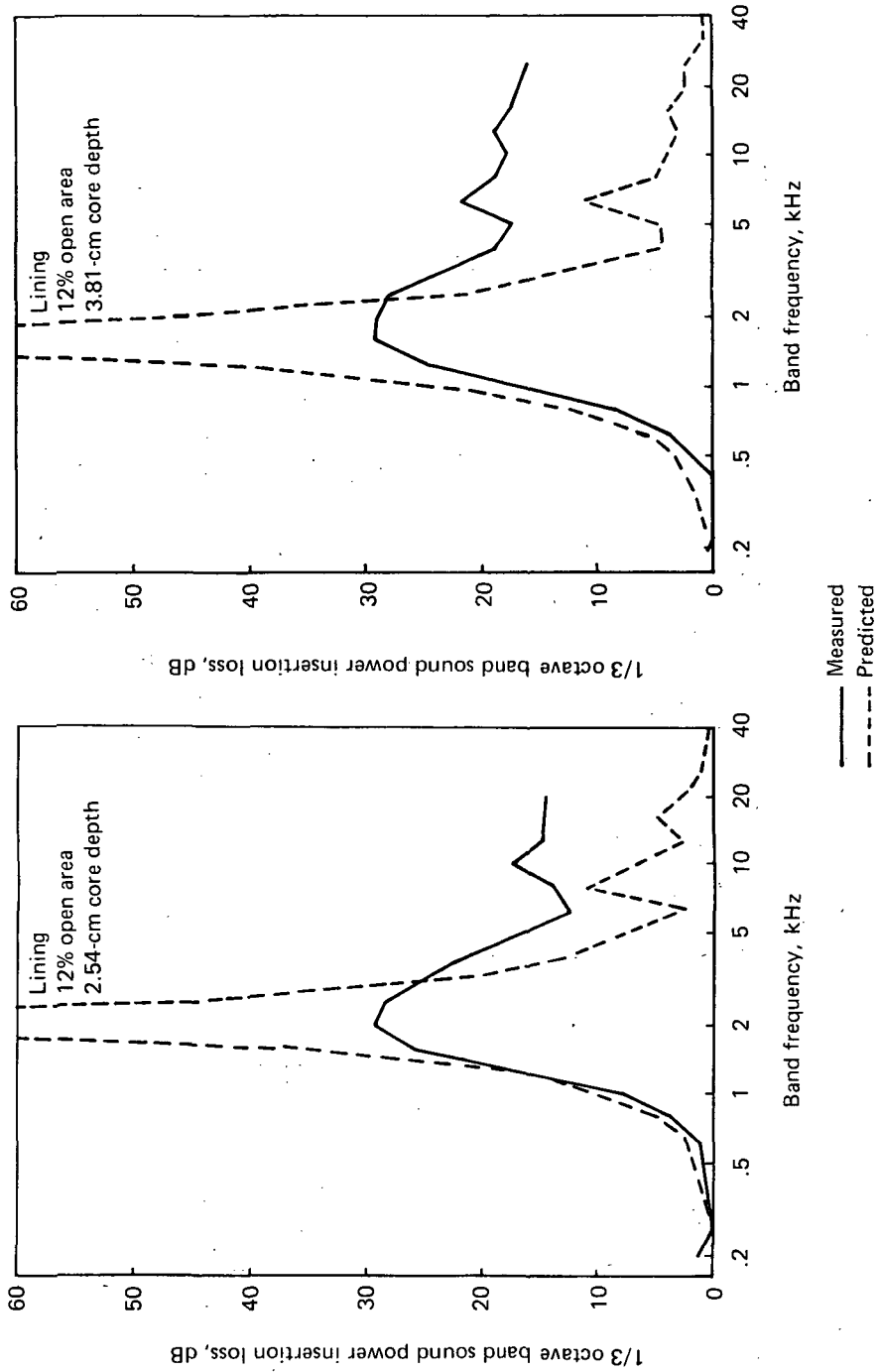
FIGURE 175.— MEASURED AND PREDICTED SOUND POWER INSERTION LOSS SPECTRA FOR THE 10.9-CM-DIAMETER NOZZLE WITH LINED L/D = 8 EJECTOR

260
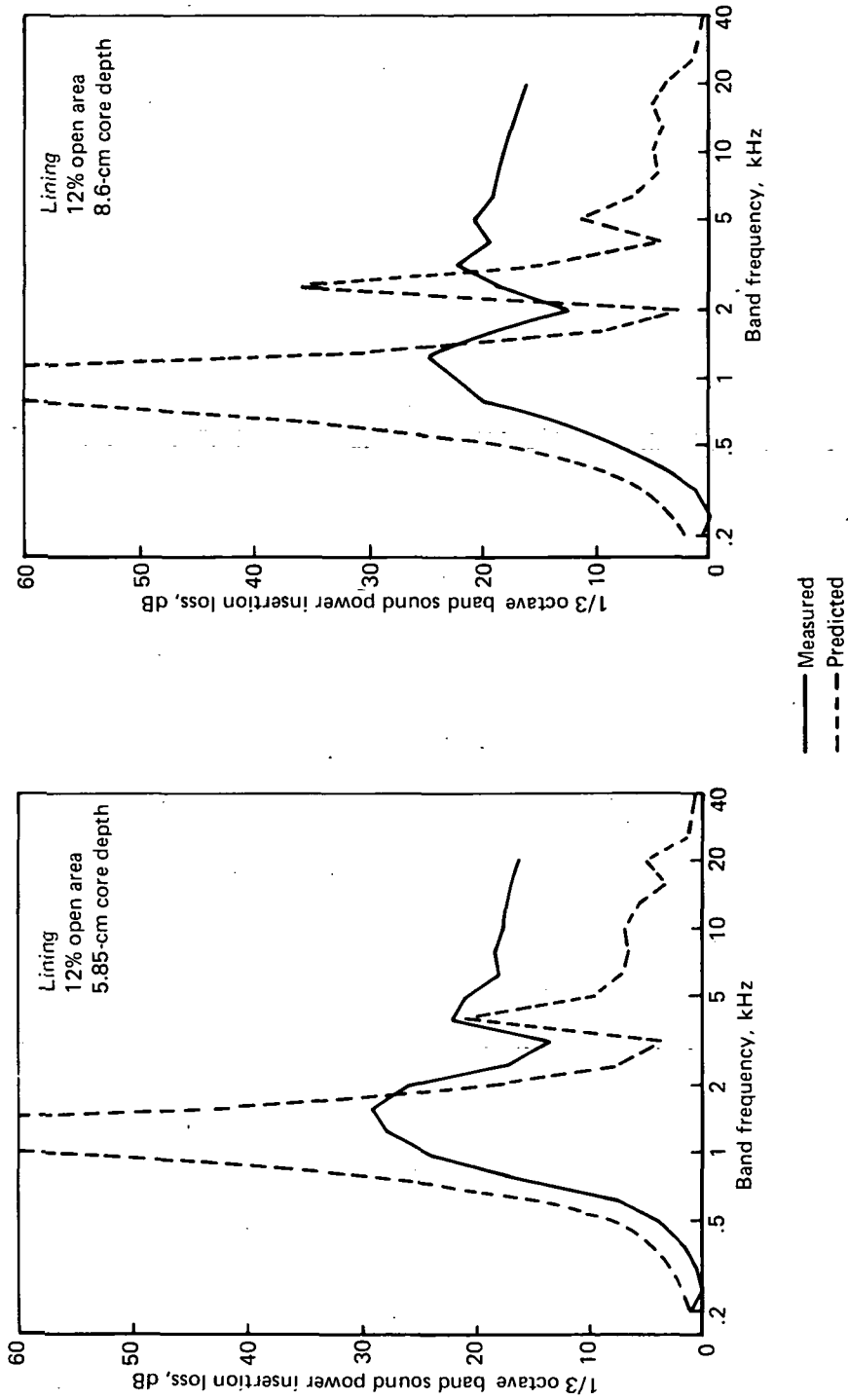
NPR = 2.40, T = 811°K

FIGURE 175.–Concluded

261
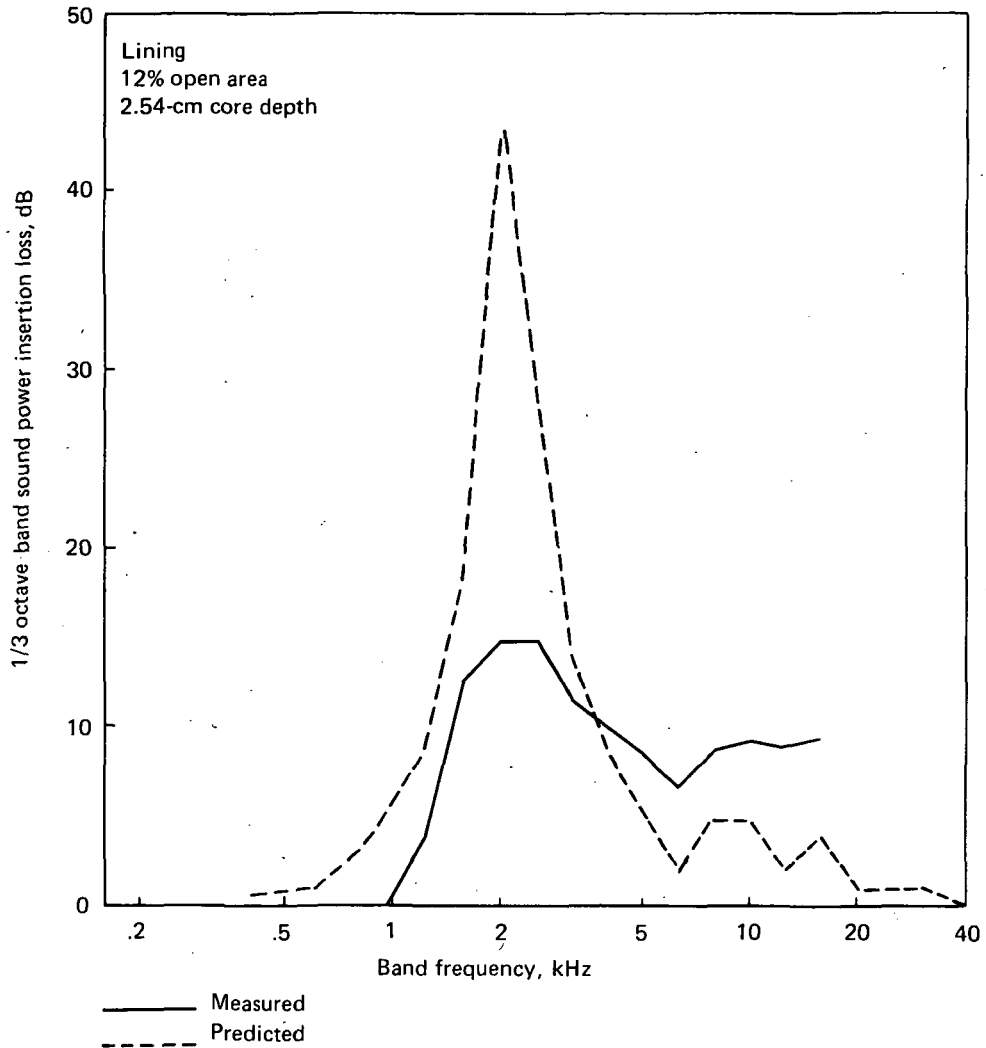
FIGURE 176.— MEASURED AND PREDICTED SOUND POWER INSERTION LOSS SPECTRA FOR THE 10.9-CM-DIAMETER NOZZLE WITH LINED L/D = 4 EJECTOR
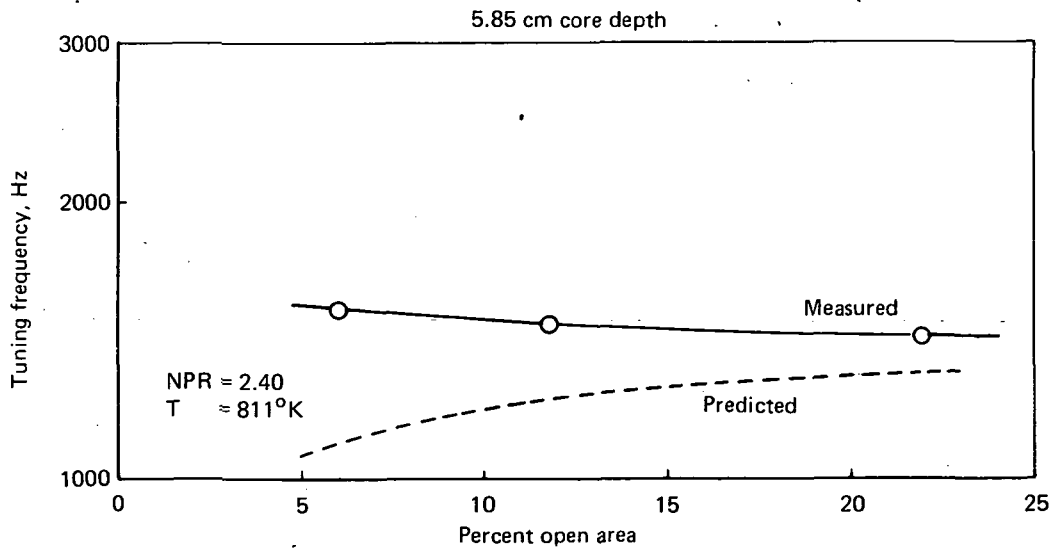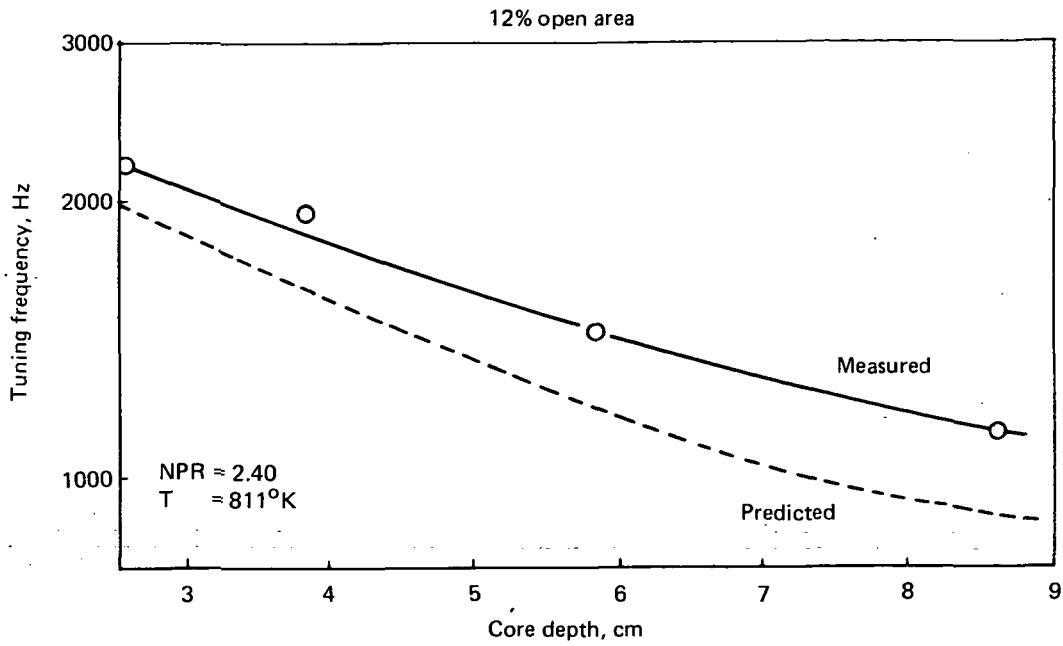
FIGURE 177.—MEASURED AND PREDICTED TUNING FREQUENCY (AS A FUNCTION OF LINING CORE DEPTH AND PERCENT OPEN AREA) FOR THE L/D = 8 EJECTOR (10.9-CM-DIAMETER NOZZLE)
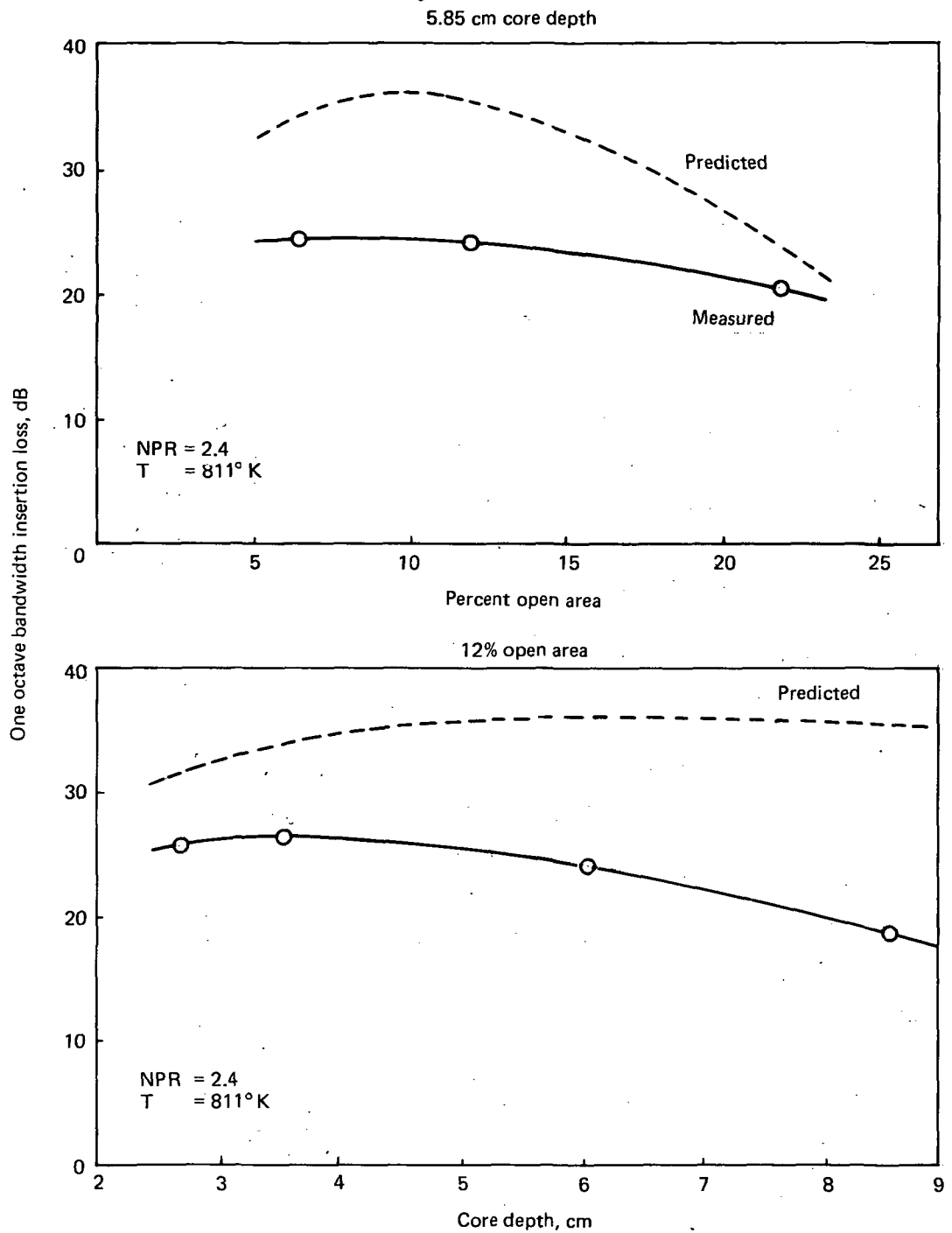
FIGURE 178.—MEASURED AND PREDICTED LINING INSERTION LOSS AS A FUNCTION OF
PERCENT OPEN AREA AND CORE DEPTH FOR THE L/D = 8 EJECTOR
(10.9-CM CONICAL NOZZLE)
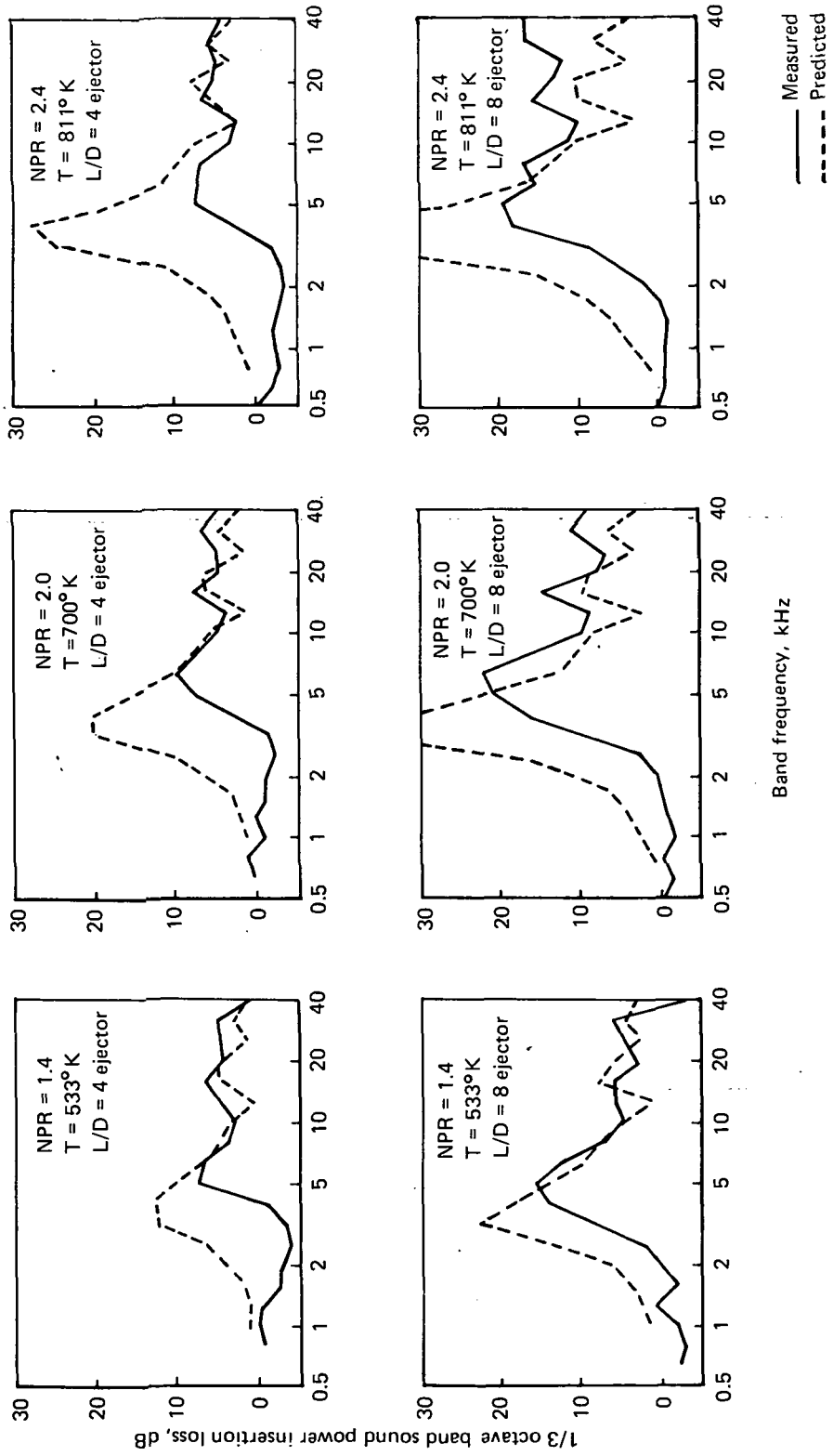
FIGURE 179.— MEASURED AND PREDICTED LINED EJECTOR SOUND POWER INSERTION LOSS SPECTRA FOR THE 2.74-CM-DIAMETER NOZZLE (22% OPEN AREA; 1.4-CM-DEEP LININGS)

265
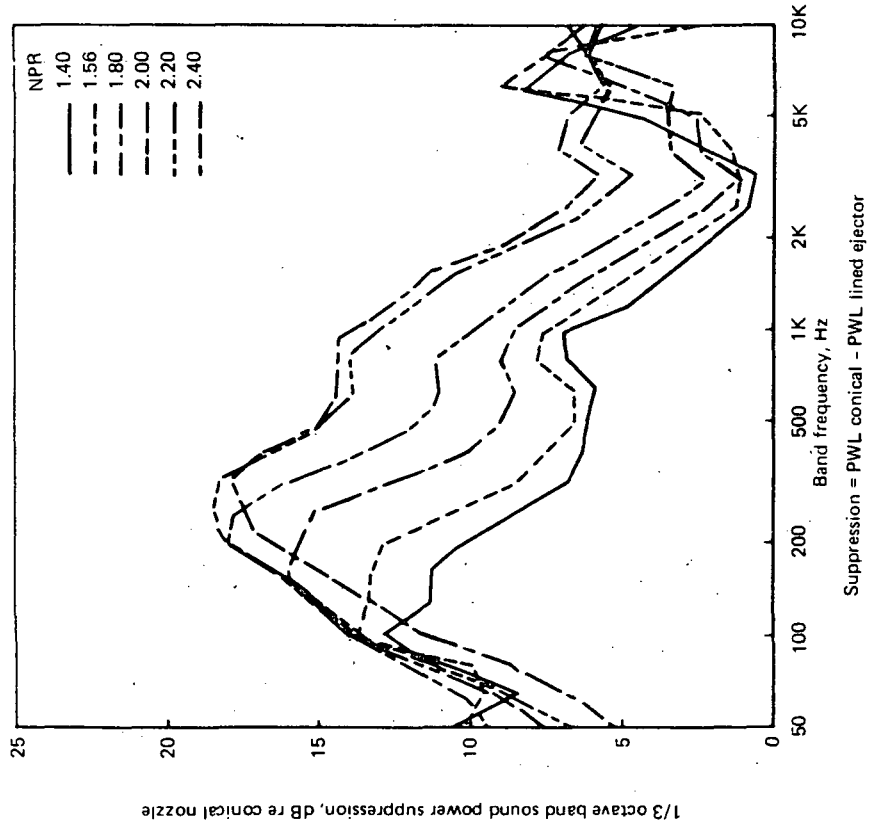
FIGURE 180.— SOUND POWER SUPPRESSION SPECTRA WITH
FULL-SCALE 37-TUBE NOZZLE AND L/D = 1
LINED EJECTOR (12% OPEN AREA,
5.33-CM-DEEP LINING)
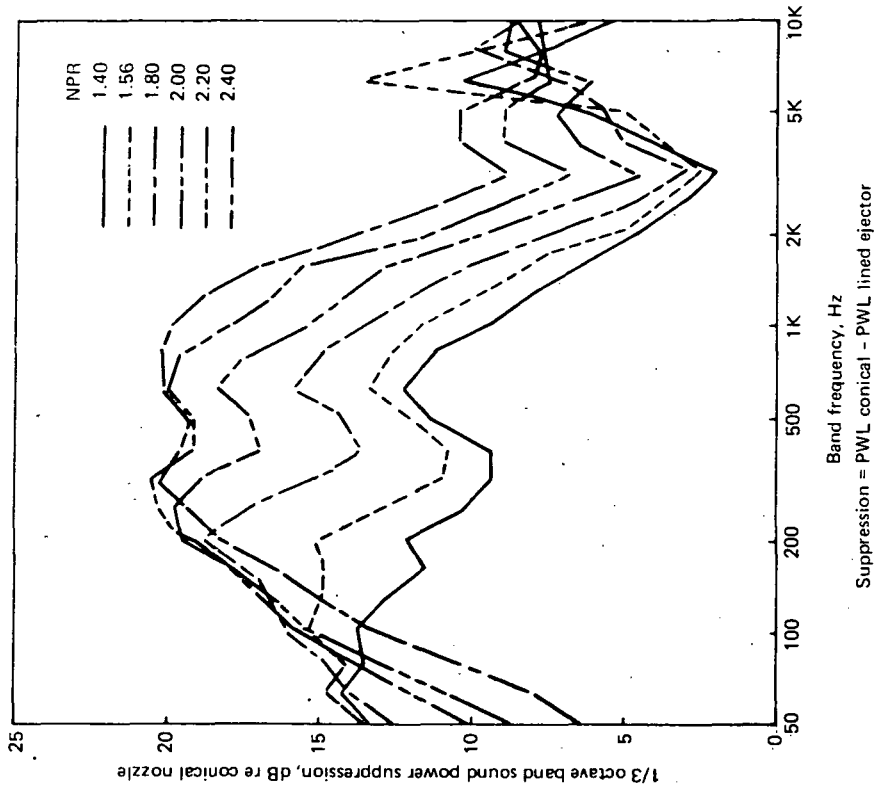
FIGURE 181.— SOUND POWER SUPPRESSION SPECTRA WITH
FULL-SCALE 37-TUBE NOZZLE AND L/D = 2
LINED EJECTOR (12% OPEN AREA,
5.33-CM-DEEP LINING)
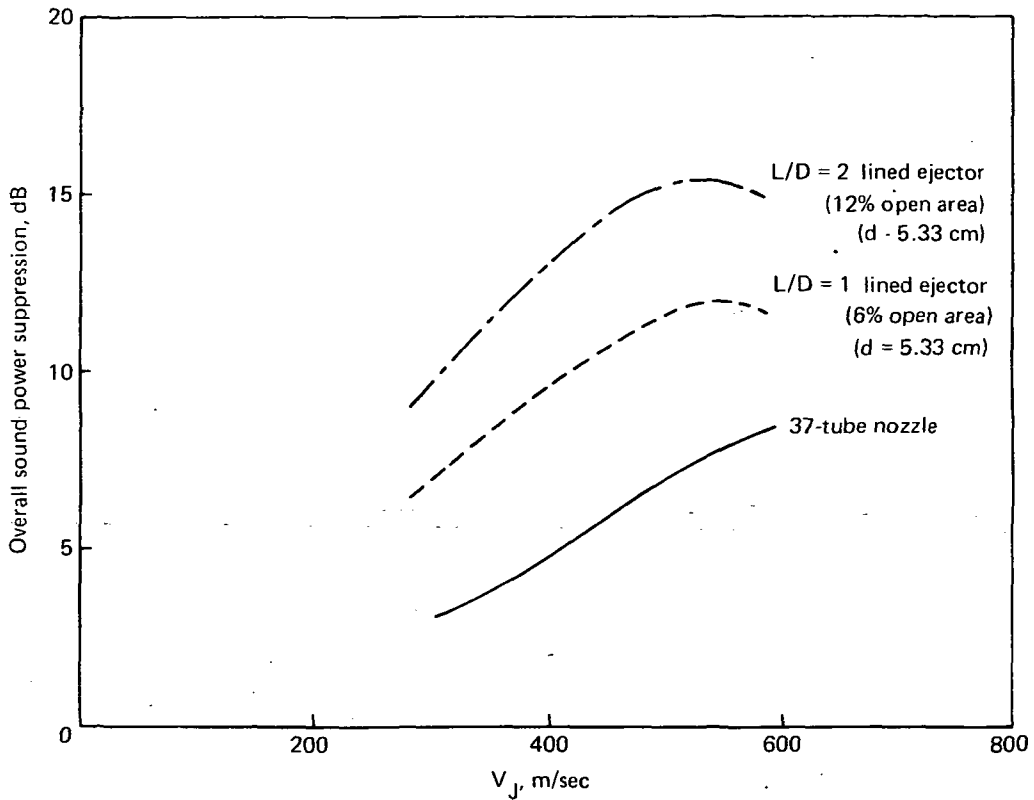
FIGURE 182.—OVERALL SOUND POWER SUPPRESSION FOR THE VARIOUS FULL-SCALE
SUPPRESSOR COMPONENTS RELATIVE TO THE CONICAL NOZZLE

Suppression = PWL conical – PWL 37-tube
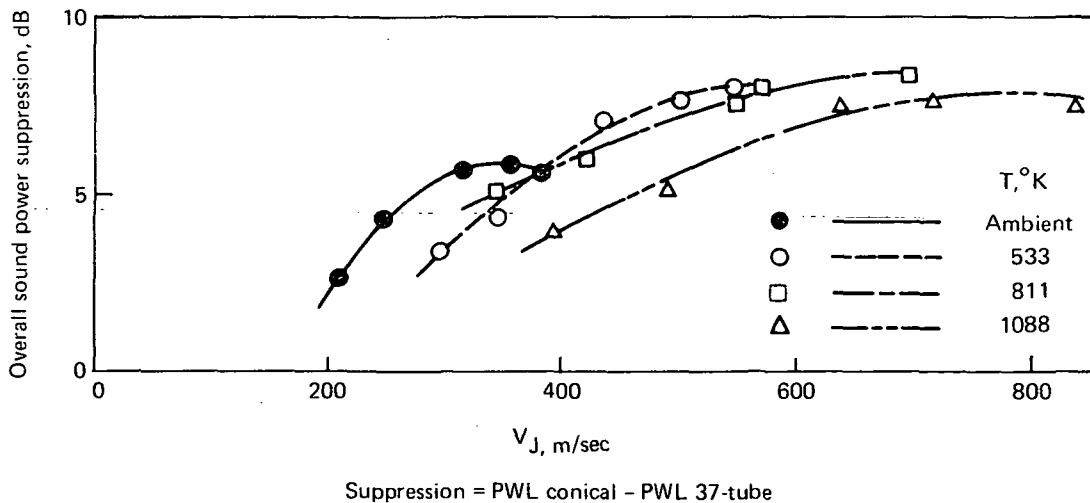
FIGURE 183.—OVERALL SOUND POWER SUPPRESSION FOR THE MODEL-SCALE 37-TUBE
NOZZLE AS A FUNCTION OF JET TEMPERATURE AND VELOCITY
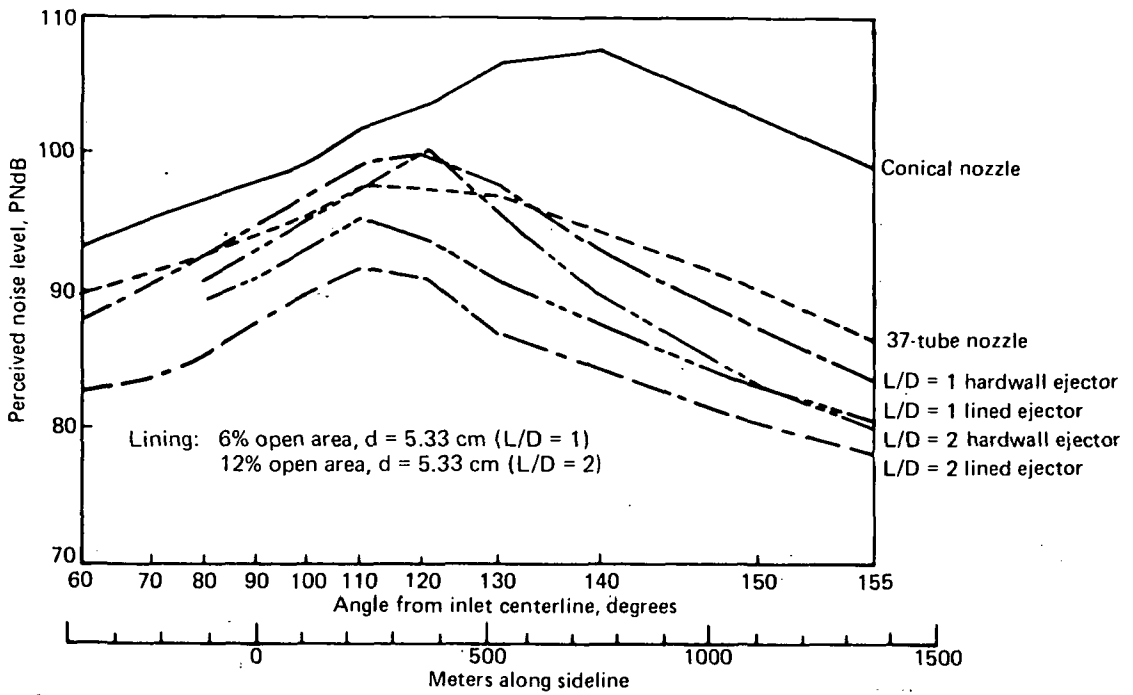
FIGURE 184.—649-M SIDELINE PERCEIVED NOISE DIRECTIVITY FOR THE VARIOUS FULL SCALE
SUPPRESSOR COMPONENTS AT NPR = 2.4 AND T = 823°K
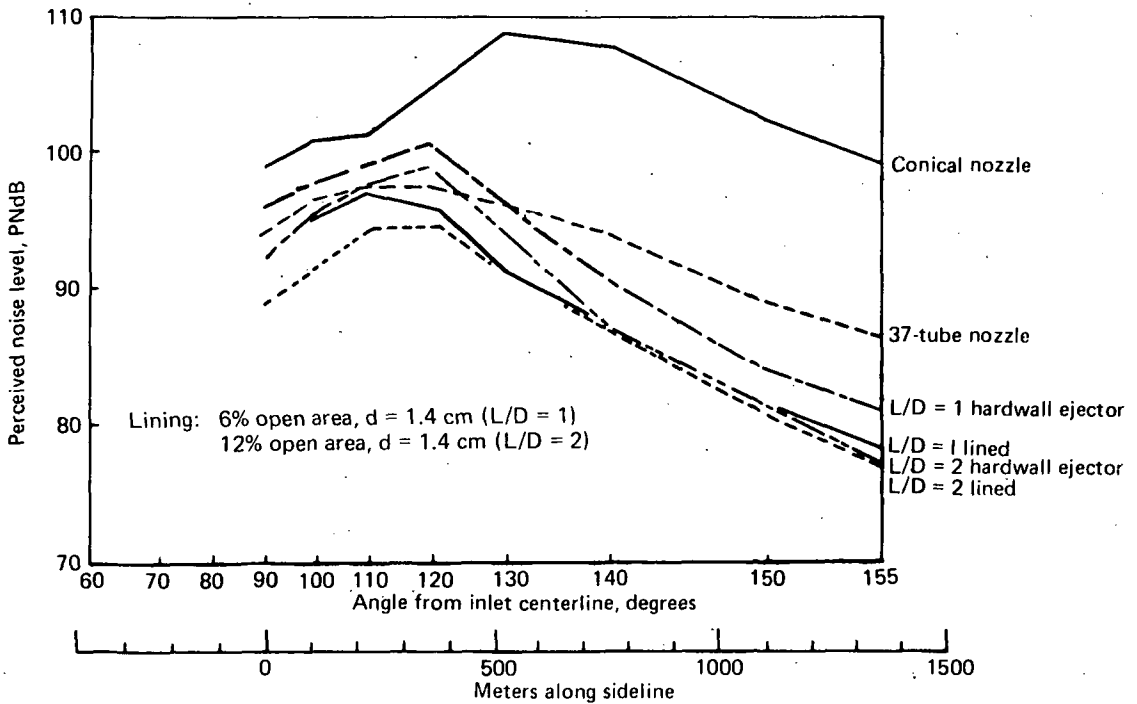
FIGURE 185.—649-M SIDELINE PERCEIVED NOISE DIRECTIVITY FOR THE MODEL-SCALE
SUPPRESSOR COMPONENTS AT NPR = 2.4 AND T = 811°K
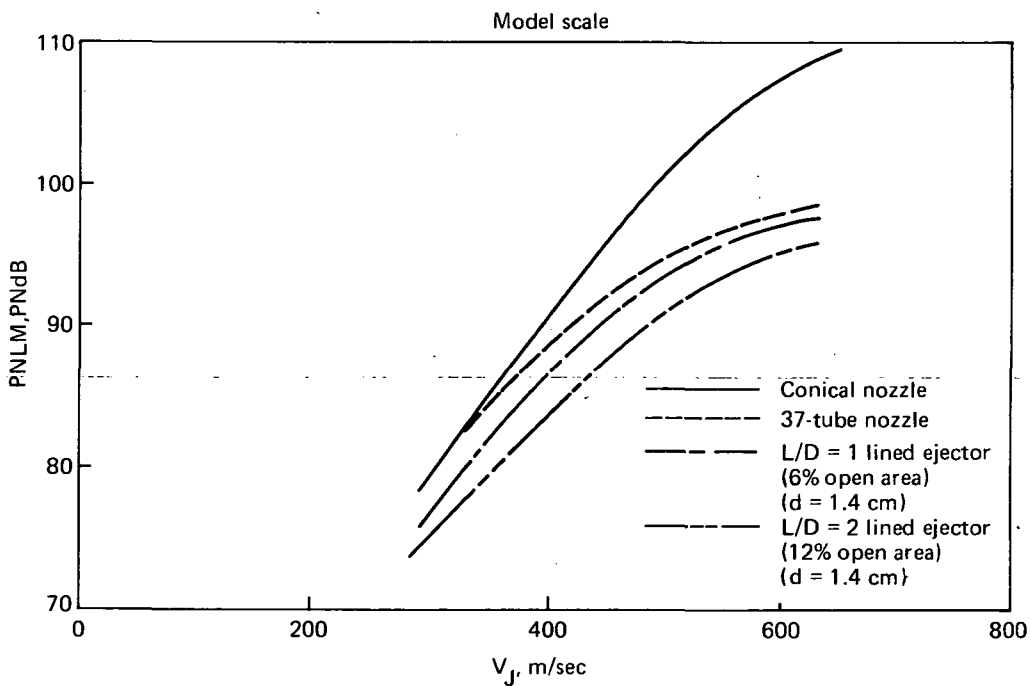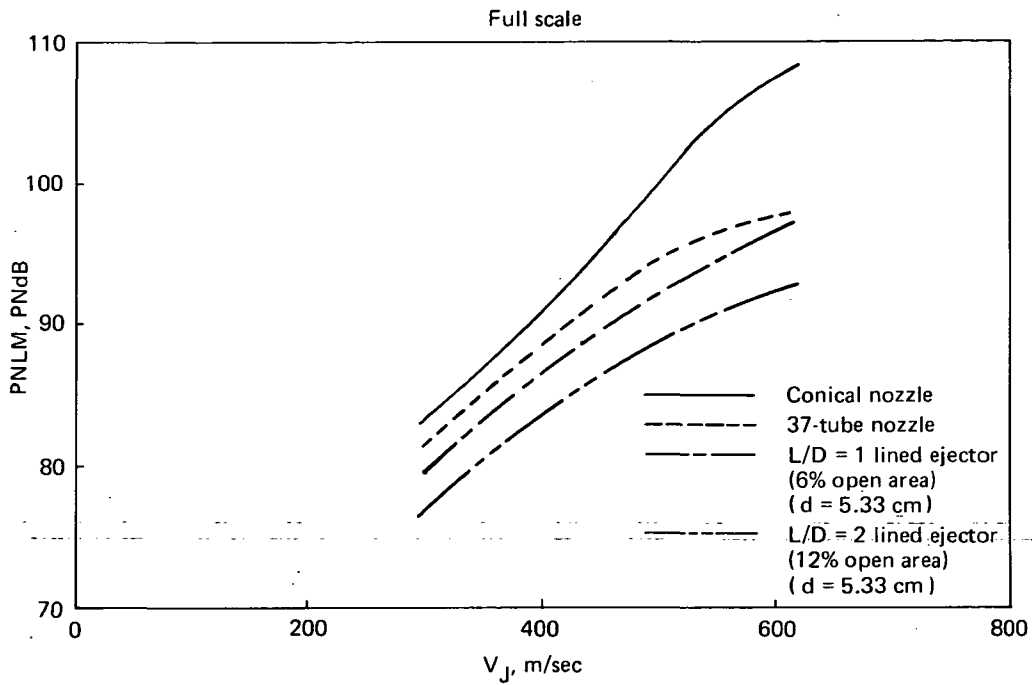
FIGURE 186.—649-M SIDELINE MAXIMUM PERCEIVED NOISE LEVELS FOR THE SUPPRESSOR
COMPONENTS AS A FUNCTION OF THE J-75 ENGINE OPERATING LINE

269
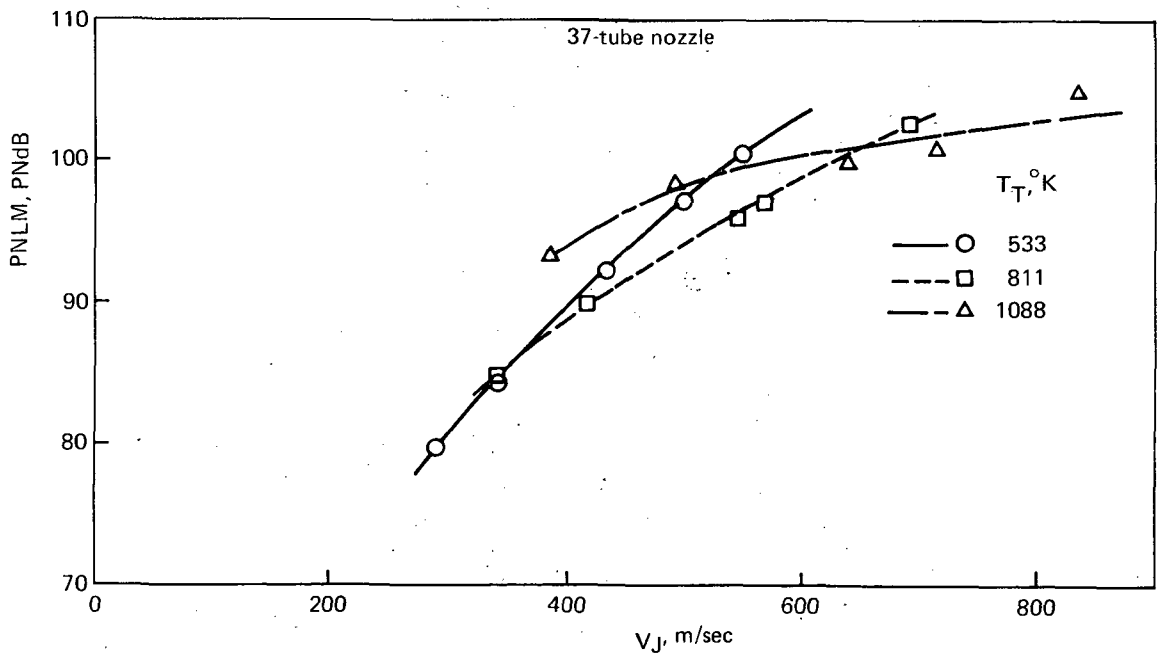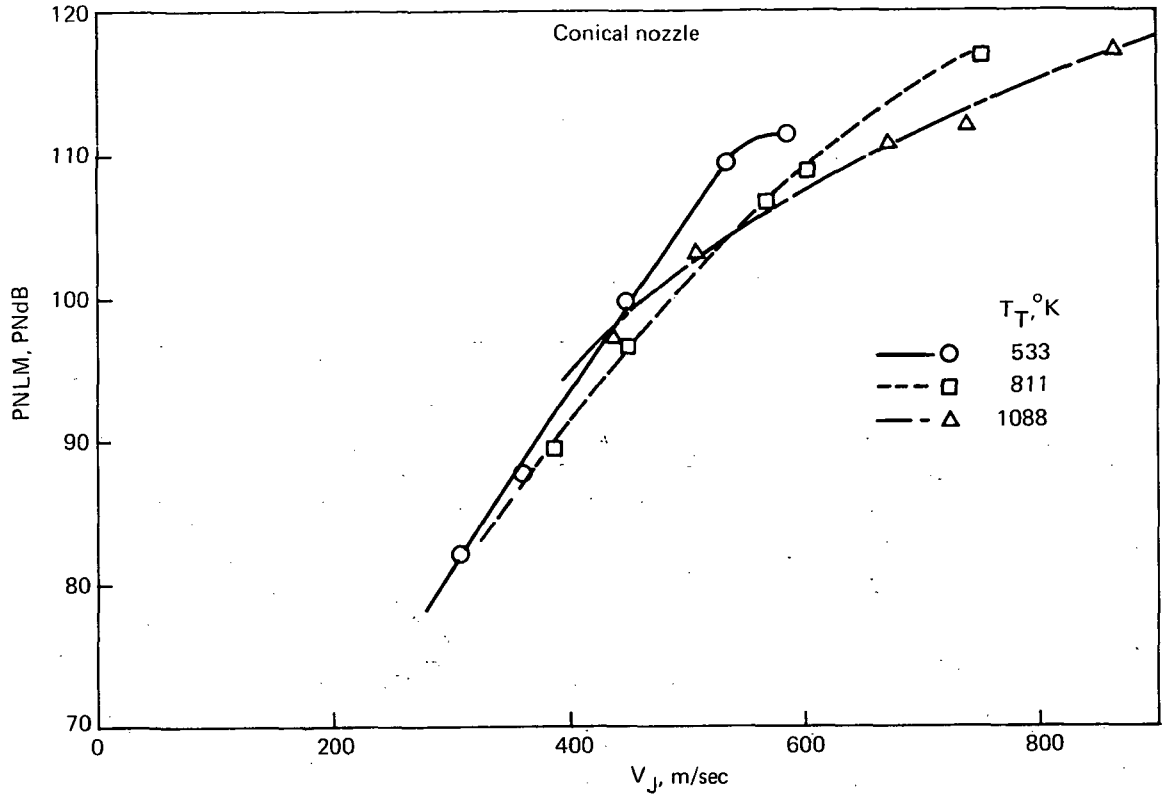
FIGURE 187.—649-M SIDELINE MAXIMUM PERCEIVED NOISE LEVELS FOR THE MODEL-SCALE CONICAL AND 37-TUBE NOZZLES AS A FUNCTION OF JET TEMPERATURE AND VELOCITY
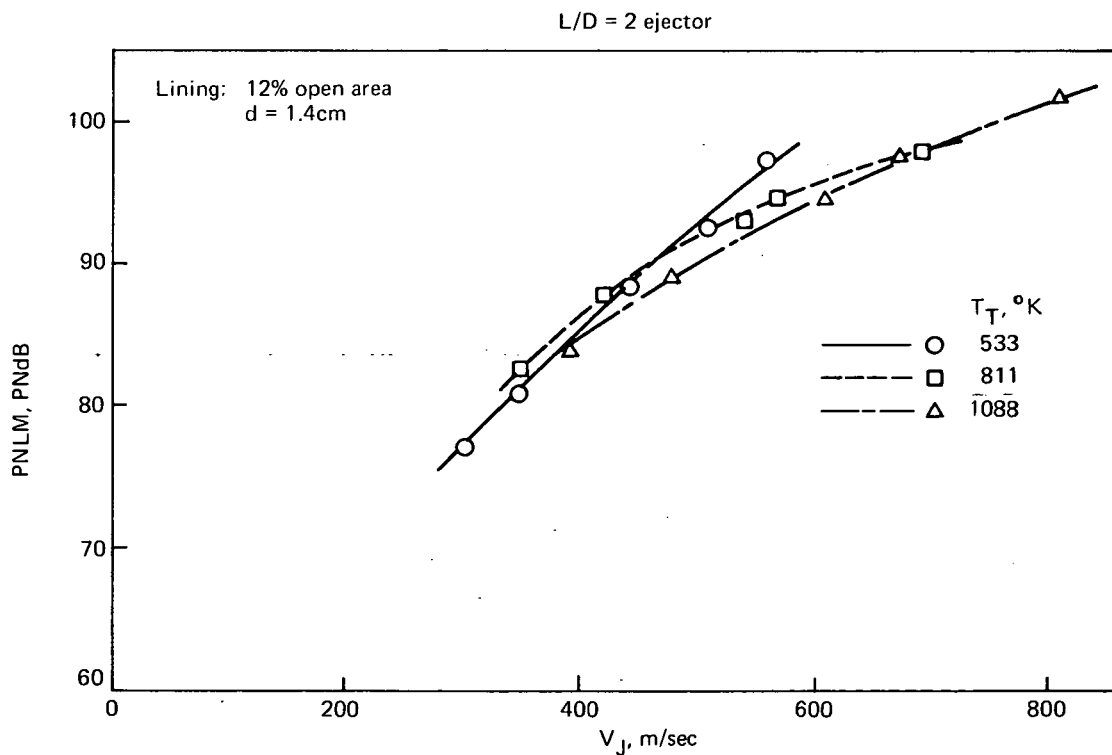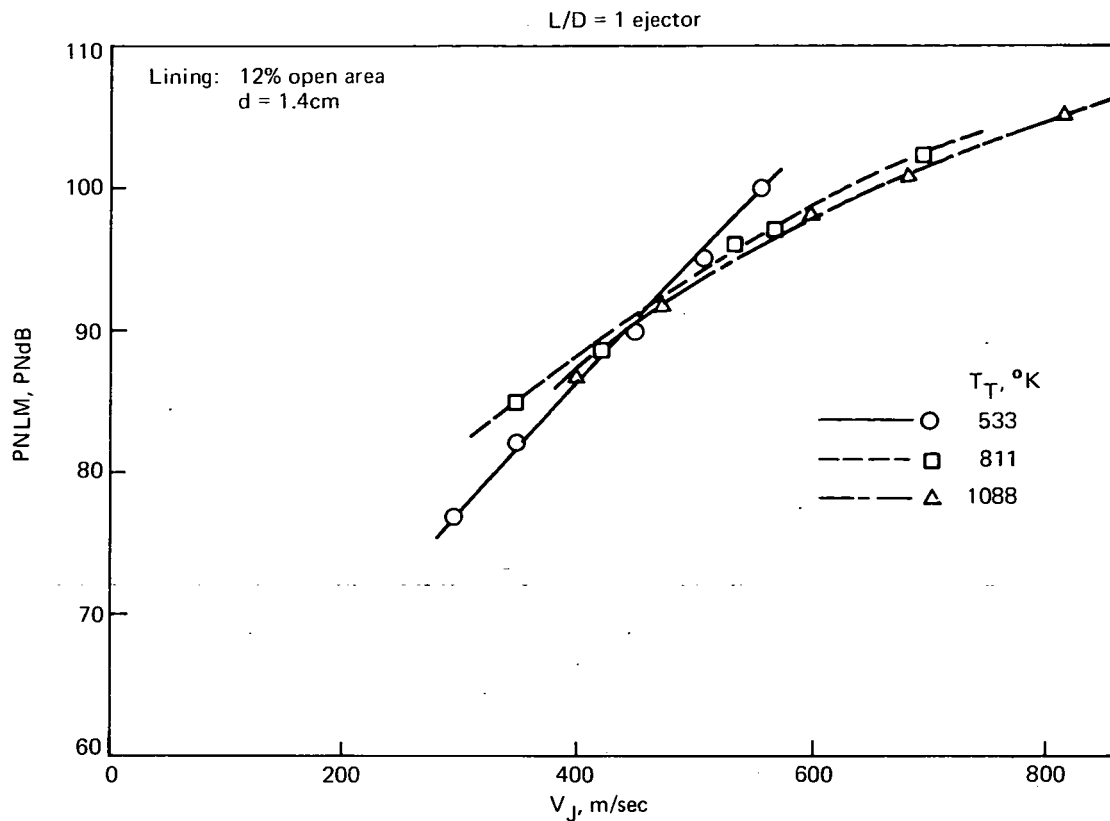
FIGURE 188.—649-M SIDELINE MAXIMUM PERCEIVED NOISE LEVELS FOR THE MODEL-SCALE L/D = 1
AND L/D = 2 LINED EJECTORS AS A FUNCTION OF JET TEMPERATURE AND VELOCITY

271

Full scale

L/D = 2 lined ejector
(12% open area)
(d = 5.33 cm)

L/D = 1 lined ejector
(6% open area)
(d = 5.33 cm)

37-tube nozzle

Model scale

L/2 = 2 lined ejector
(12% open area)
(d - 1.4 cm)

L/D = 1 lined ejector
(6% open area)
(d = 1.4 cm)

37-tube nozzle
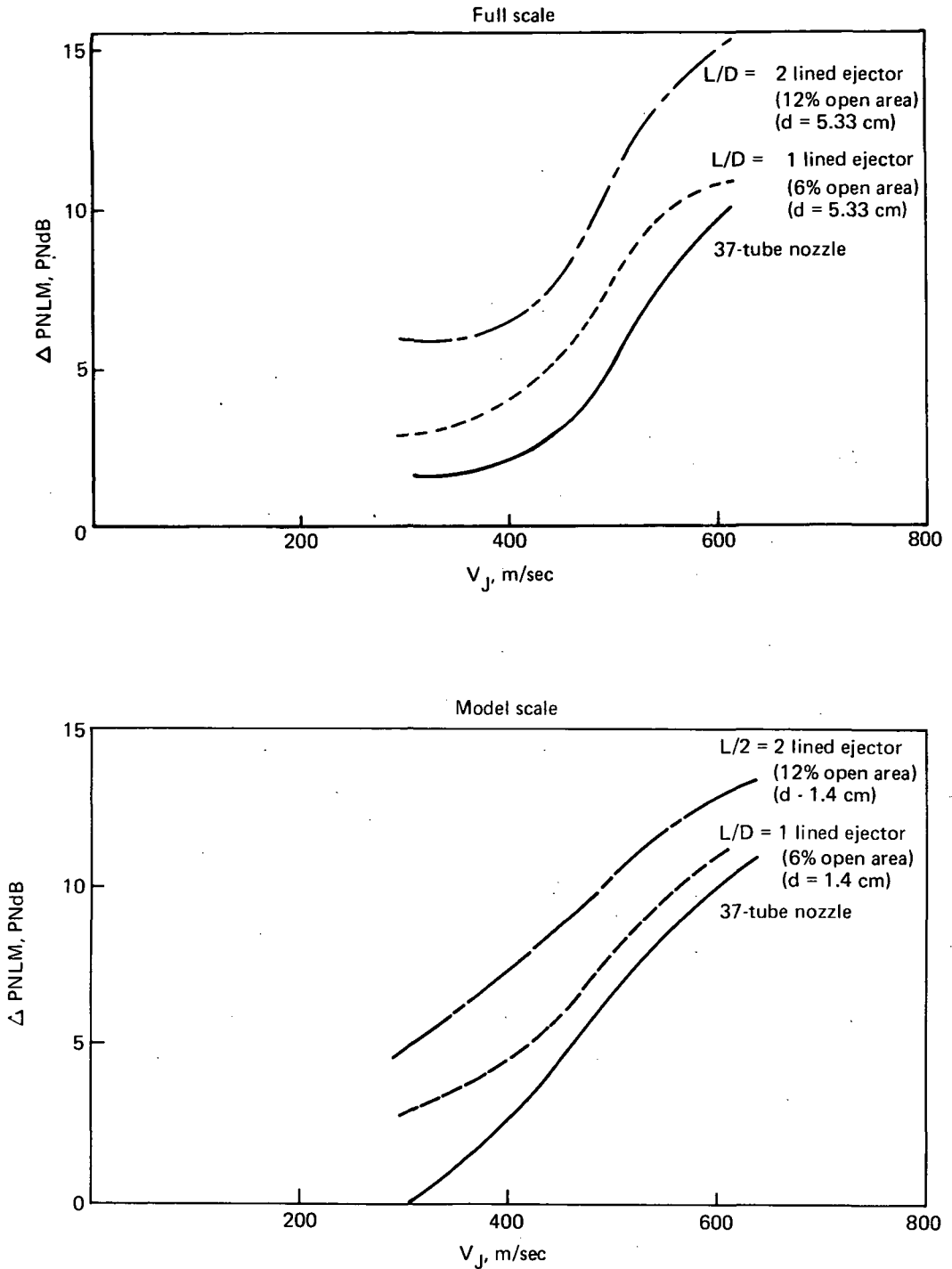
FIGURE 189.—649-M SIDELINE MAXIMUM PERCEIVED NOISE LEVEL REDUCTION FOR THE MODEL-
AND FULL-SCALE SUPPRESSOR COMPONENTS AS A FUNCTION OF THE J-75 ENGINE
OPERATING LINE
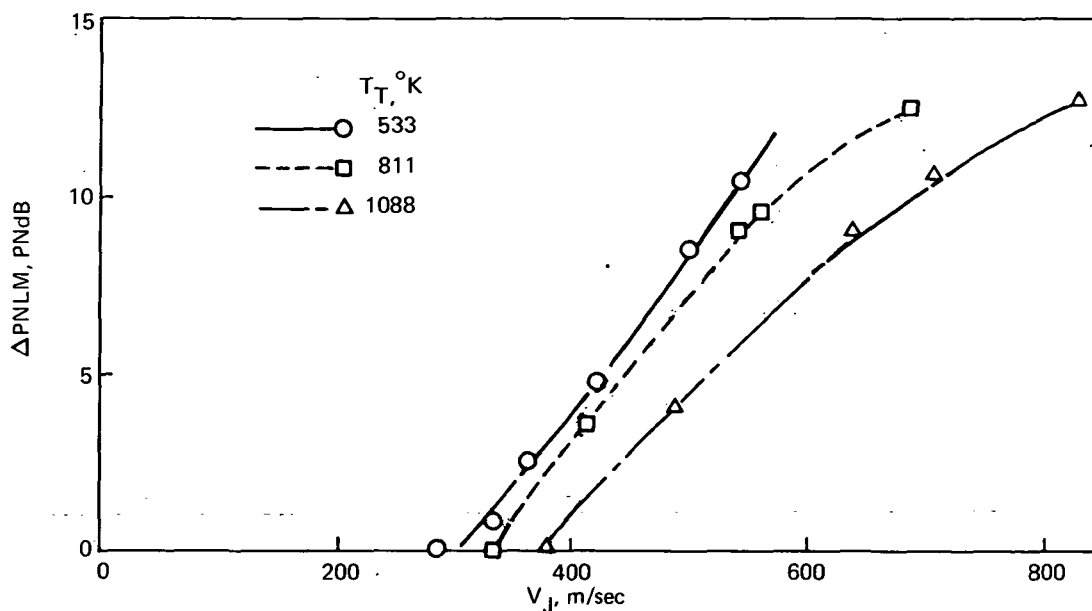
ΔPNLM = PNLM conical – PNLM 37-tube

FIGURE 190.—649m SIDELINE MAXIMUM PERCEIVED NOISE LEVEL REDUCTION BY THE MODEL SCALE 37-TUBE NOZZLE AS A FUNCTION OF JET TEMPERATURE AND VELOCITY
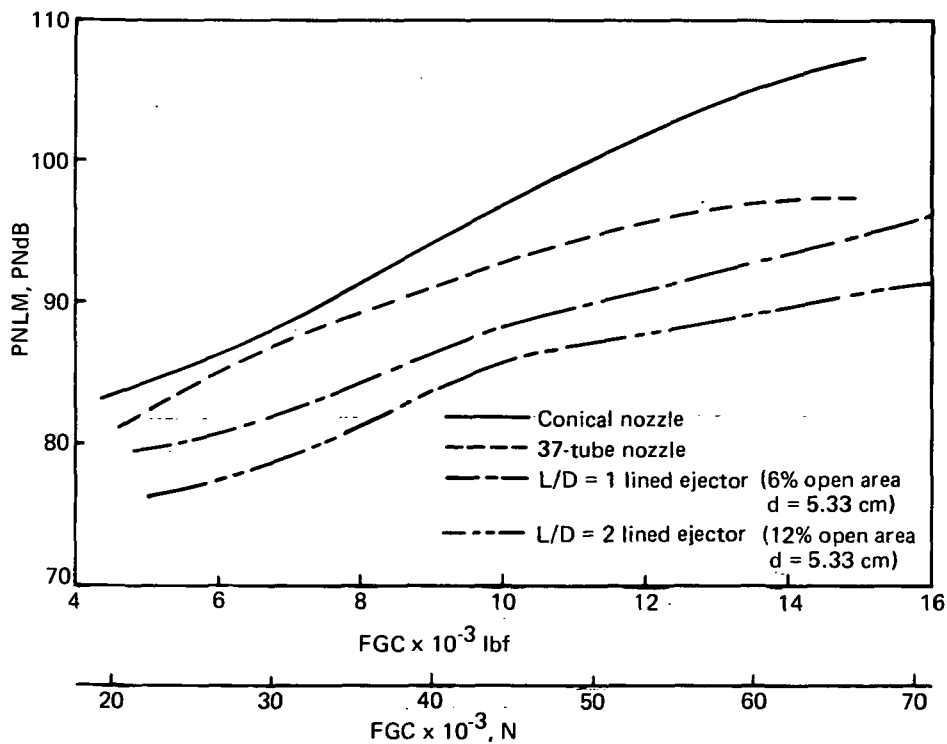
FIGURE 191.—649-M SIDELINE MAXIMUM PERCEIVED NOISE LEVELS FOR THE VARIOUS FULL-SCALE SUPPRESSOR COMPONENTS AS A FUNCTION OF STATIC THRUST

273

Suppressor components

ΔPNLM = PNLM conical
       − PNLM lined ejector

Linings with respect to
hardwall ejectors

ΔPNLM = PNLM hardwall ejector
       − PNLM lined ejector

Percent maximum thrust of conical nozzle

———————— 37-tube nozzle

– – – – – L/D = 1 lined ejector
(6% open area, d = 5.33 cm)

— — — L/D = 2 lined ejector
(12% open area, d = 5.33 cm)
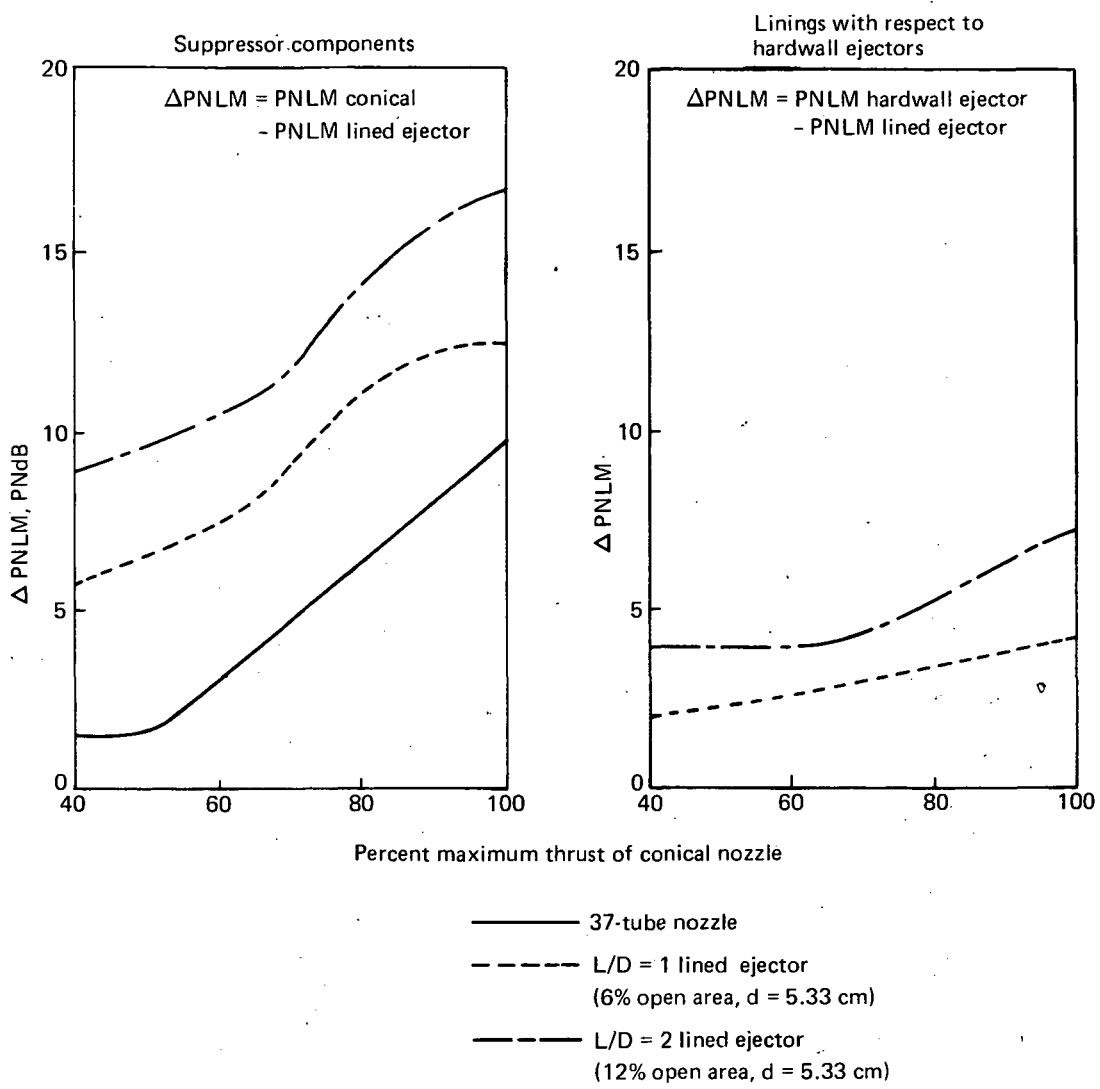
FIGURE 192.—649-M SIDELINE MAXIMUM PERCEIVED NOISE LEVEL REDUCTION FOR THE VARIOI
FULL-SCALE SUPPRESSOR COMPONENTS AS A FUNCTION OF STATIC THRUST

12% open area lining
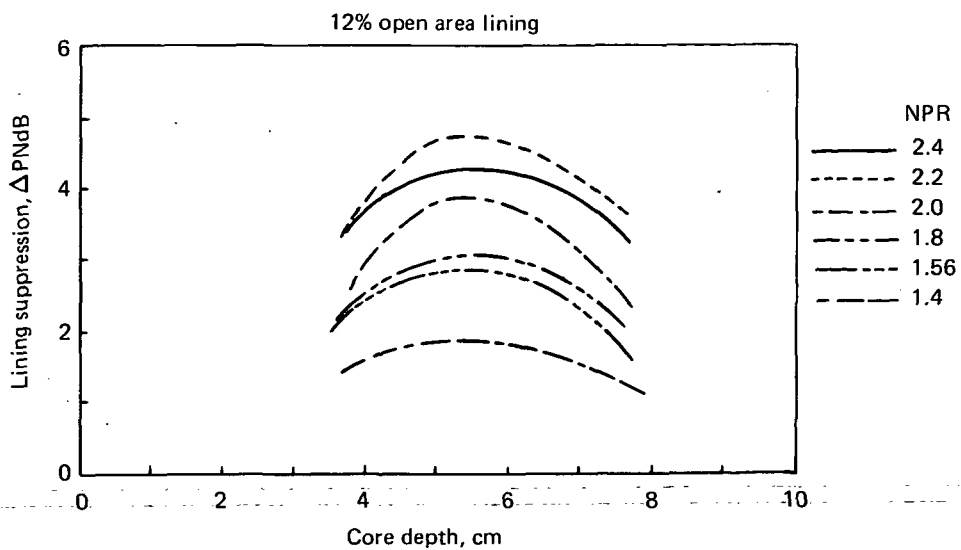
Lining suppression = PNLM hardwall ejector – PNLM lined ejector

5.33-cm deep lining
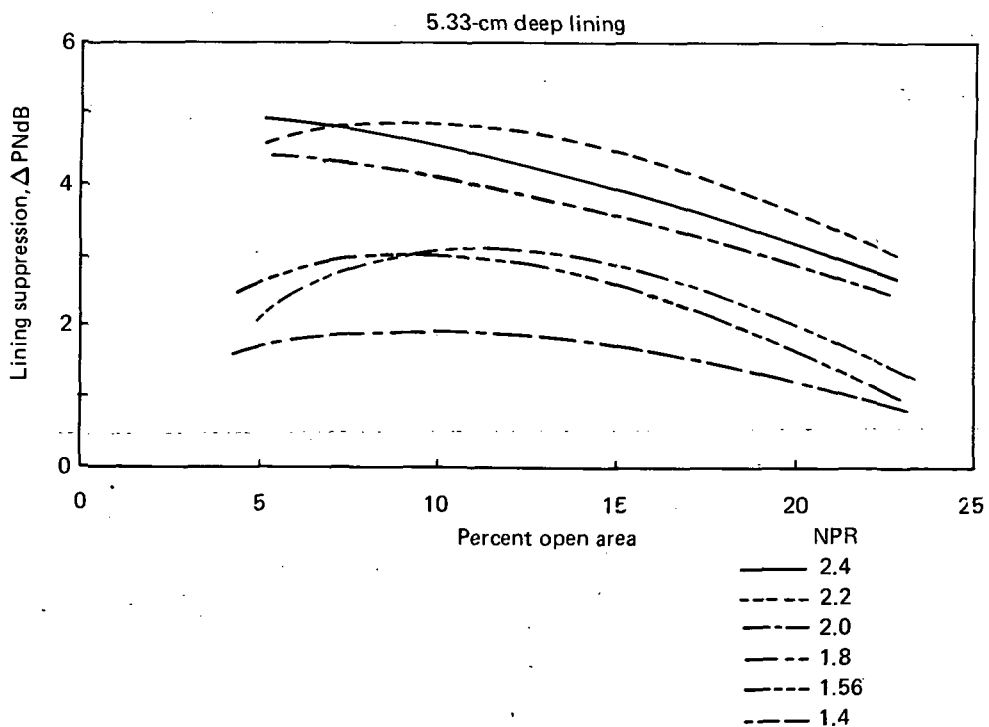
FIGURE 193.–649-M SIDELINE MAXIMUM PERCEIVED NOISE LEVEL REDUCTION DUE TO VARIOUS ACOUSTIC LININGS IN THE FULL-SCALE L/D = 1 EJECTOR

275
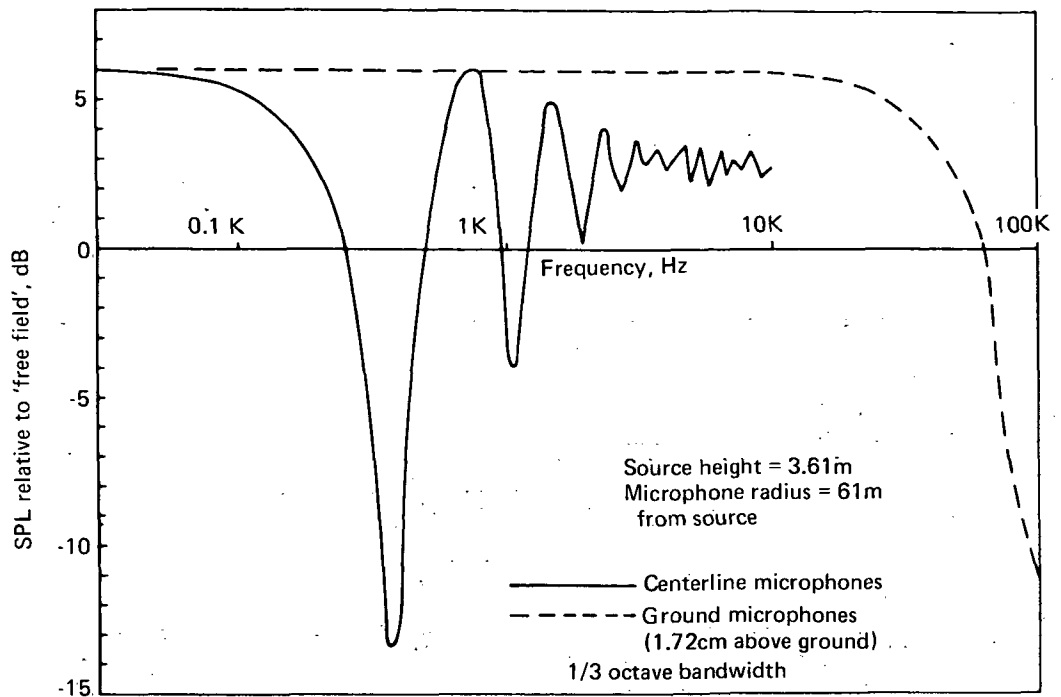
FIGURE A-1.—ESTIMATED GROUND REFLECTION INTERFERENCE ON THE FAR FIELD MEASUREMENTS FROM A POINT SOURCE OF SOUND IN THE FULL-SCALE ACOUSTIC TEST ARENA
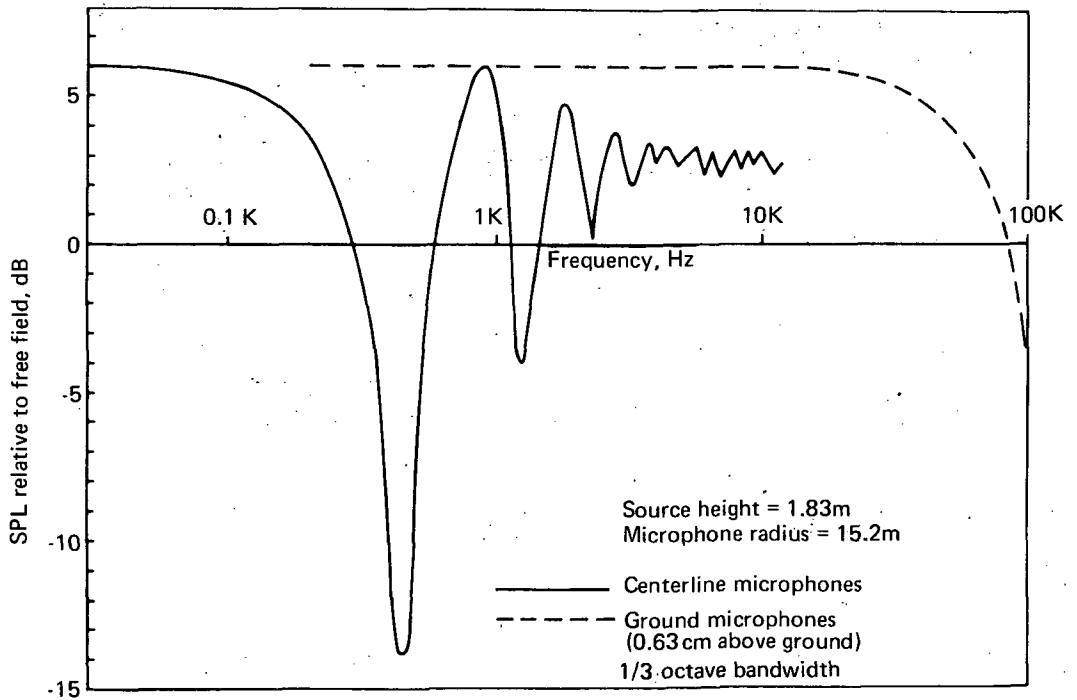
FIGURE A-2.—ESTIMATED GROUND REFLECTION INTERFERENCE ON THE FAR FIELD MEASUREMENTS FROM A POINT SOURCE OF SOUND IN THE MODEL-SCALE ACOUSTIC TEST ARENA
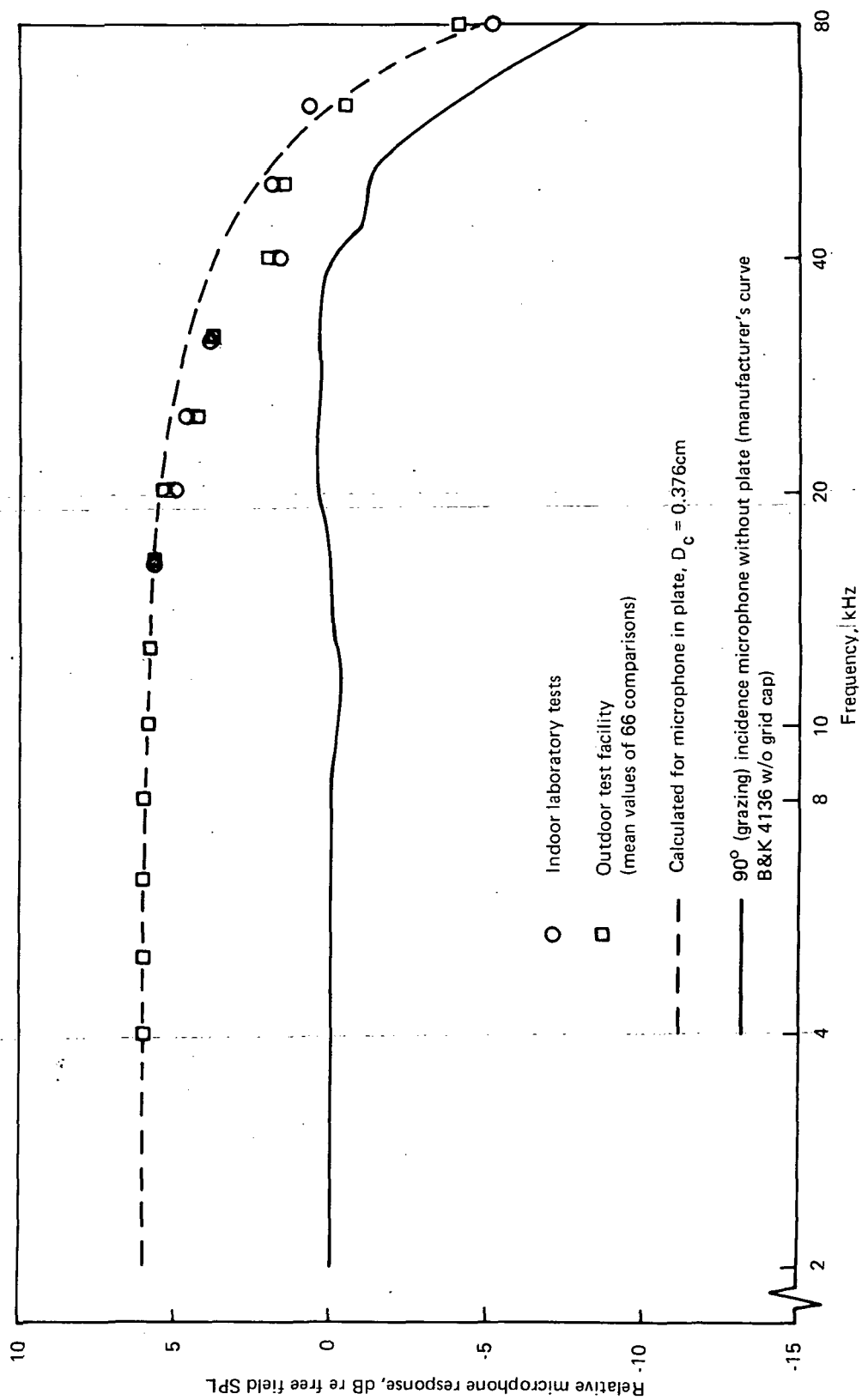
FIGURE A-3.—CALCULATED RESPONSE FOR A FLUSH-MOUNTED MICROPHONE COMPARED WITH MEASURED DATA

277
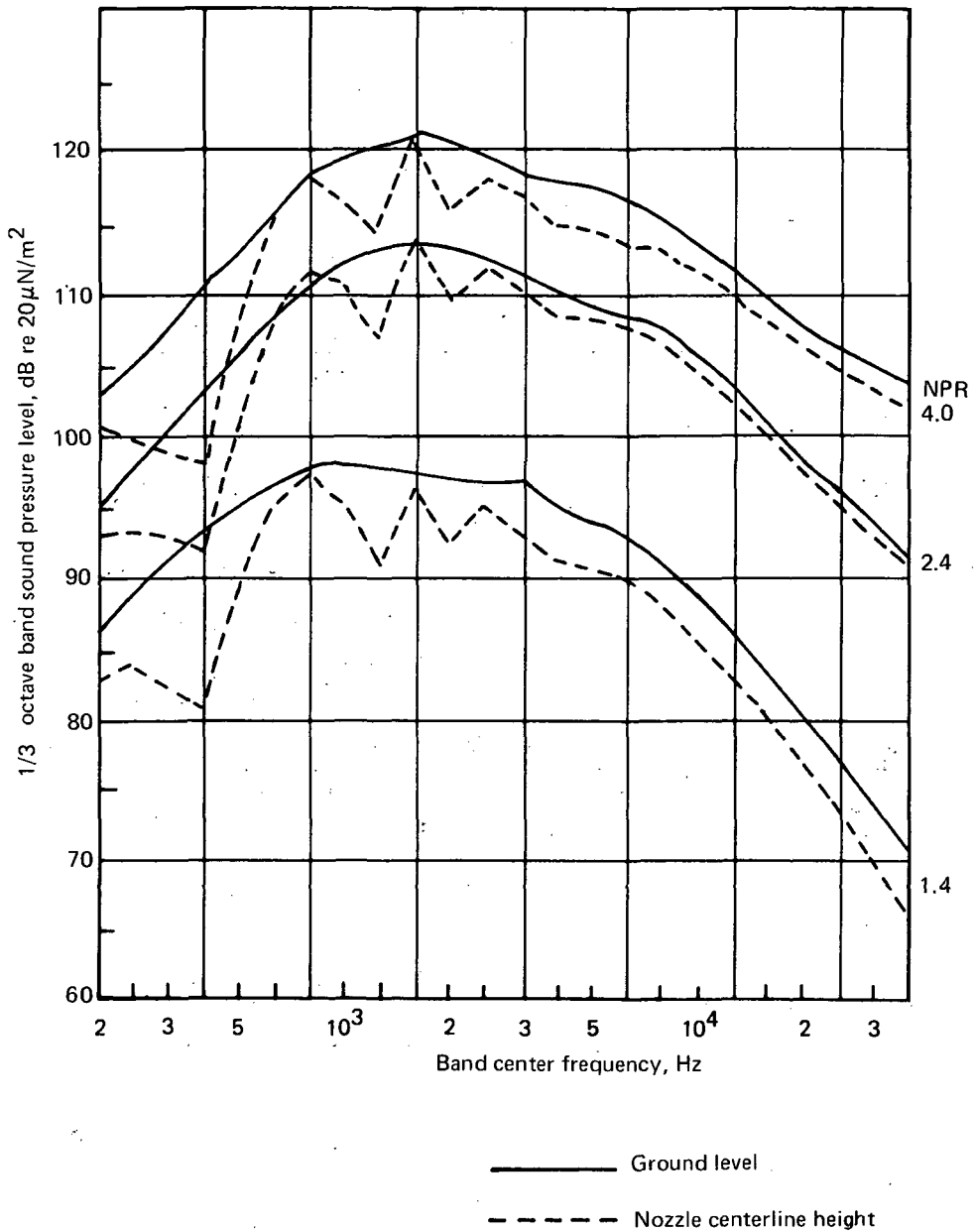
FIGURE A-4.—COMPARISON OF "AS MEASURED" GROUND AND NOZZLE CENTERLINE
   —HEIGHT MICROPHONE SPECTRA FROM THE MODEL-SCALE ACOUSTIC TEST ARENA
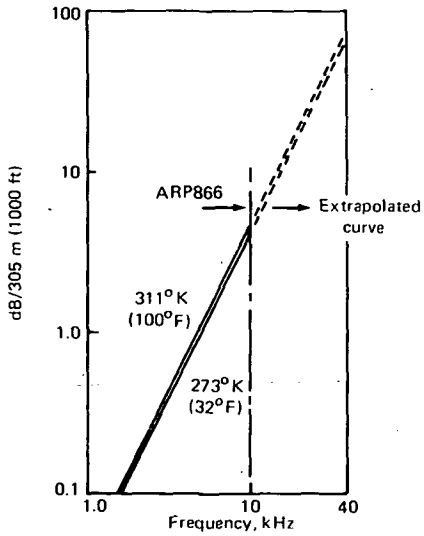
FIGURE B-1.—CLASSICAL ATMOSPHERIC
ABSORPTION OF SOUND
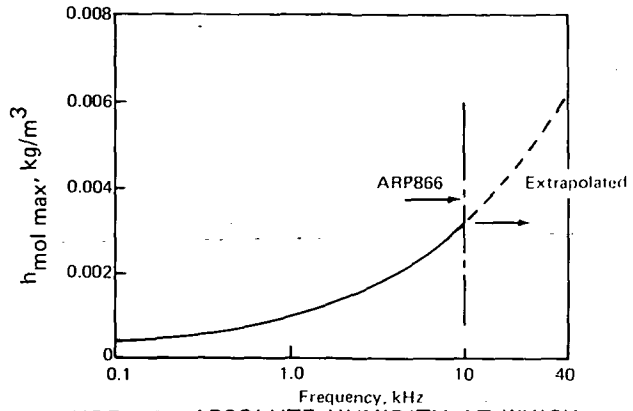
FIGURE B-2.—ABSOLUTE HUMIDITY AT WHICH
MAXIMUM MOLECULAR ABSORPTION
OF SOUND OCCURS AS A FUNCTION
OF FREQUENCY
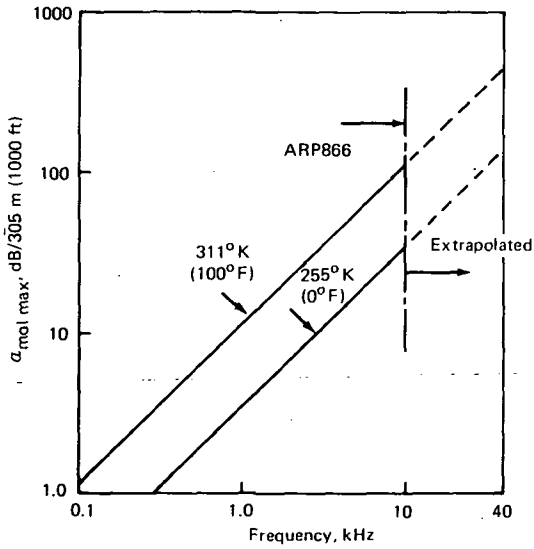
FIGURE B-3.—MAXIMUM MOLECULAR
ABSORPTION OF SOUND AS A
FUNCTION OF FREQUENCY
FOR DIFFERENT TEMPERATURES
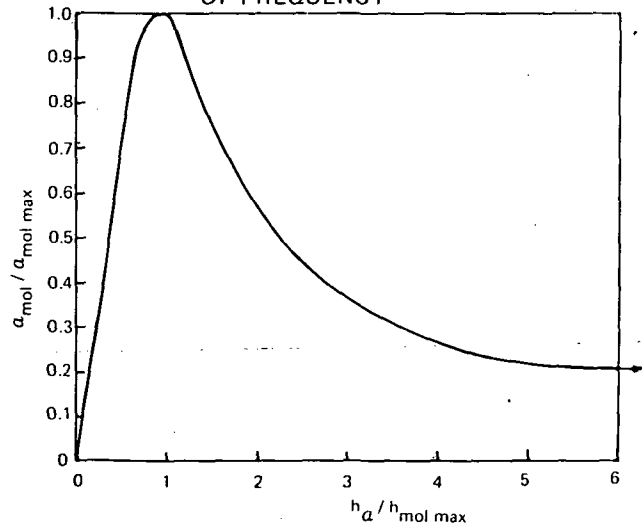
FIGURE B-4.—NORMALIZED MOLECULAR ABSORPTION
AS A FUNCTION OF NORMALIZED
ABSOLUTE HUMIDITY

279
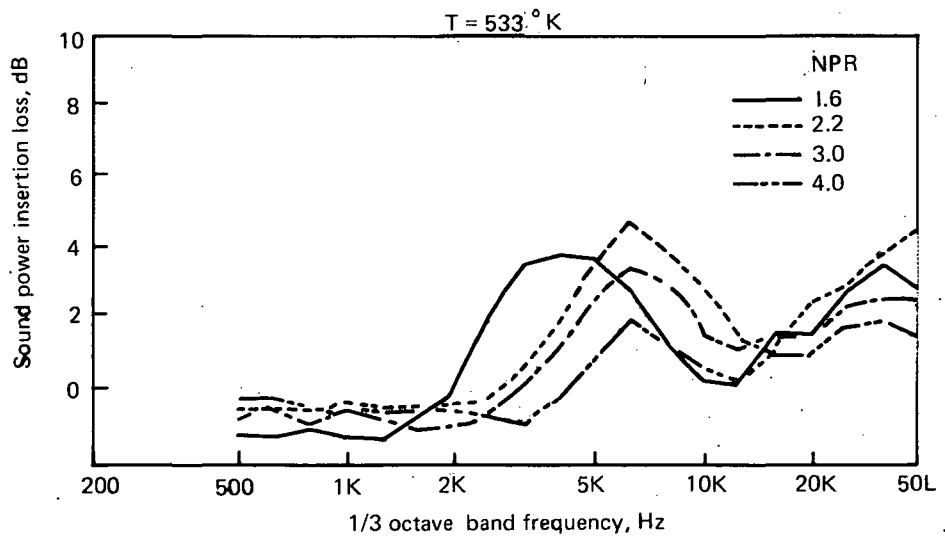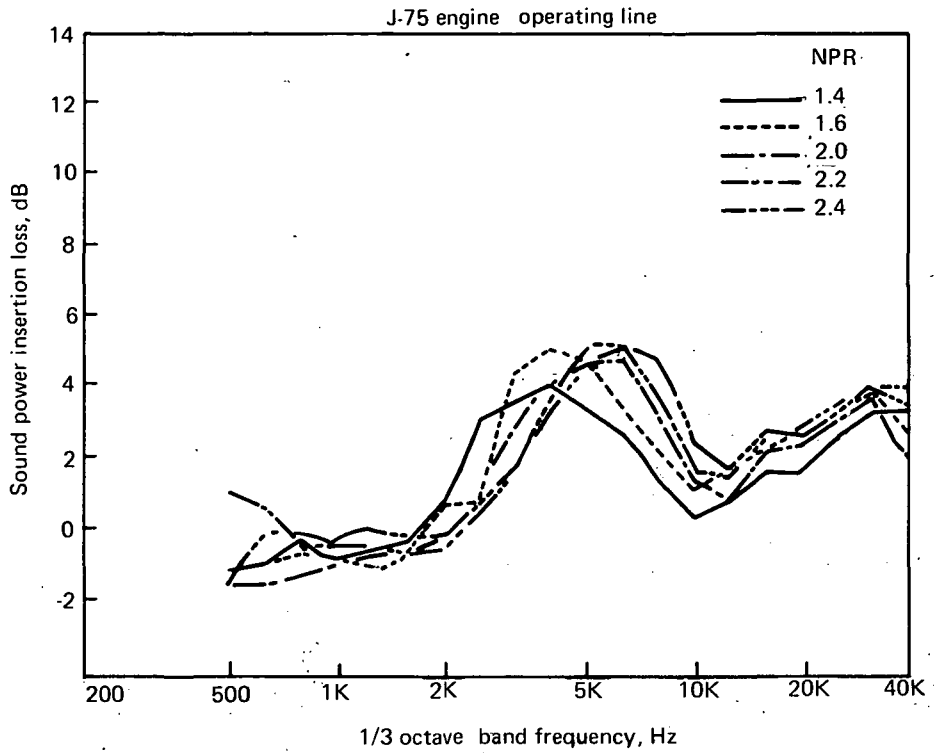
FIGURE C-1.—MODEL-SCALE SOUND POWER INSERTION LOSS SPECTRA FOR A
6% OPEN AREA 1.4-CM-DEEP LINING IN L/D = 1. EJECTOR
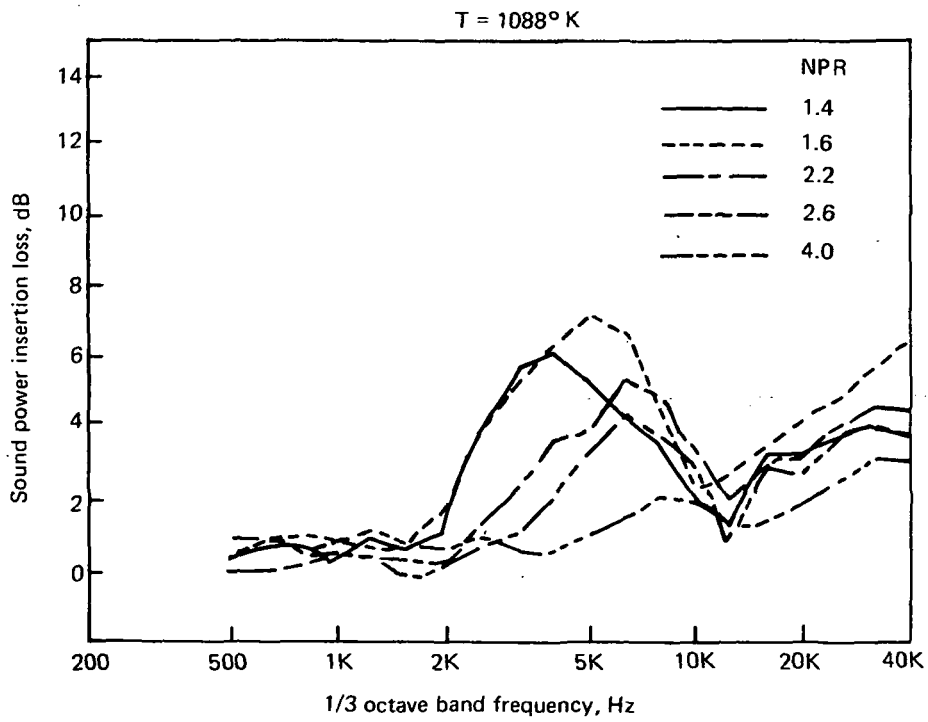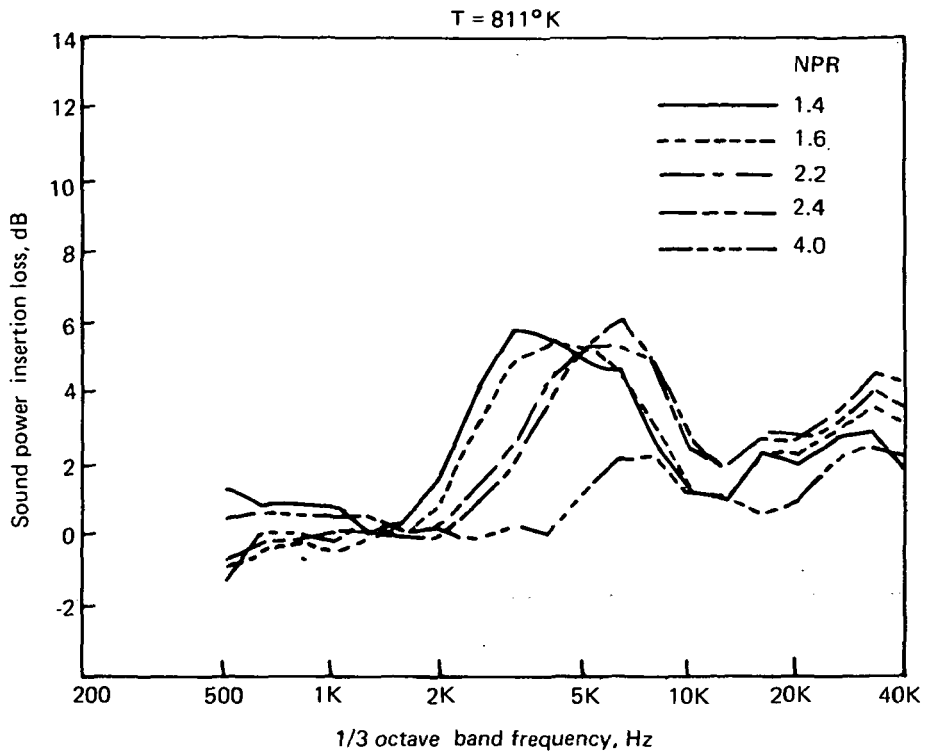
FIGURE C-1.—Concluded

281
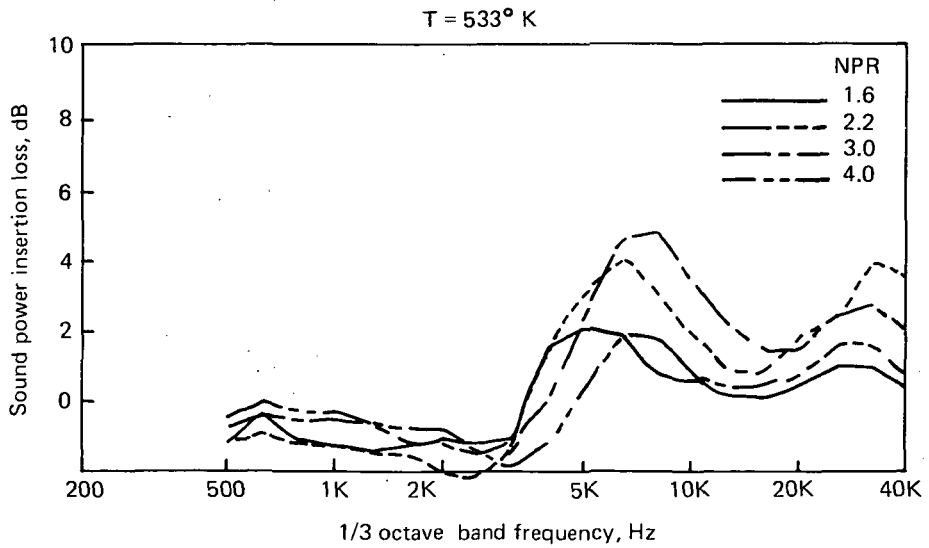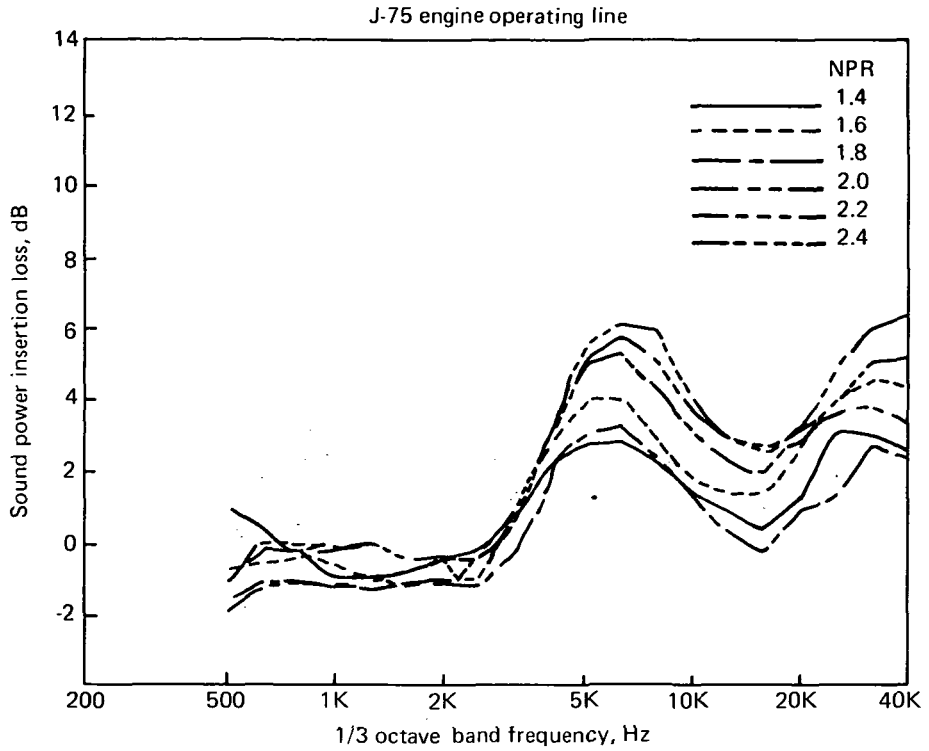
FIGURE C-2.—MODEL-SCALE SOUND POWER INSERTION LOSS SPECTRA FOR A
12% OPEN AREA 0.9-CM-DEEP LINING IN L/D = 1 EJECTOR

T = 811° K

T = 1088° K
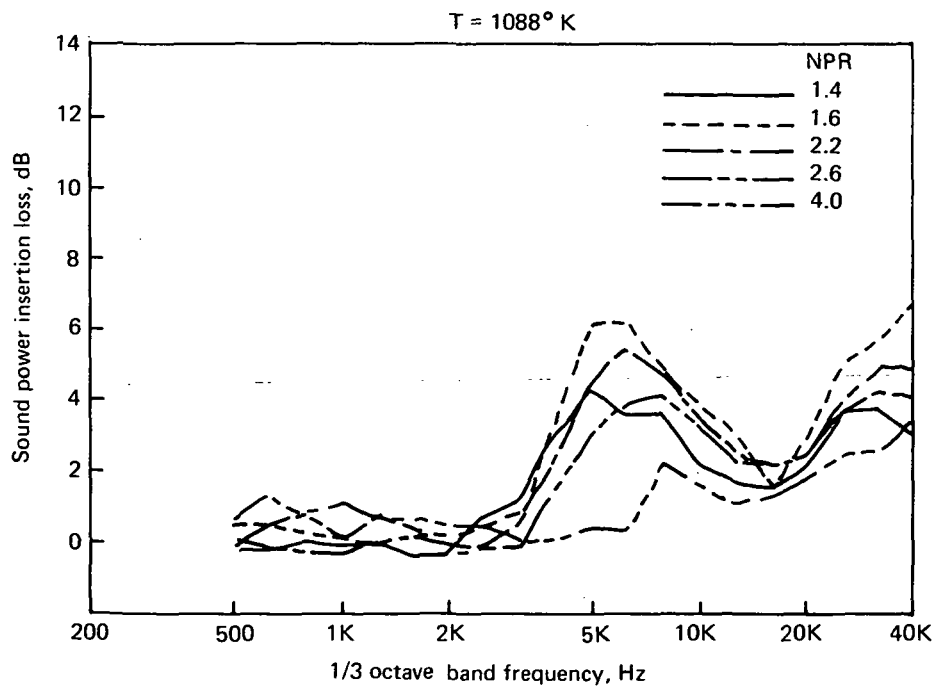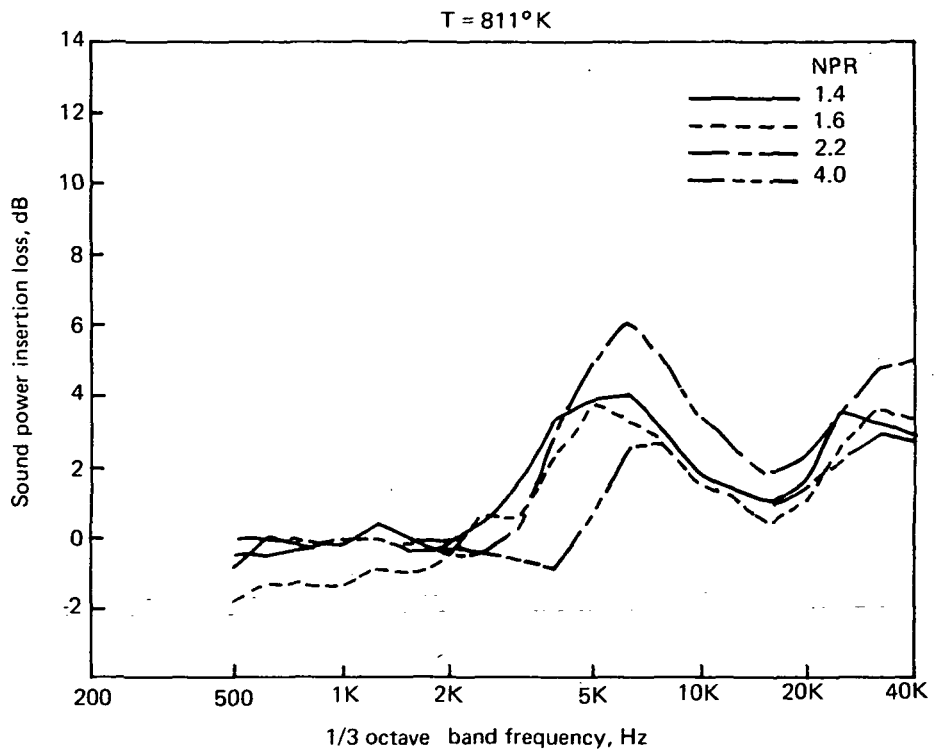
FIGURE C-2.—Concluded
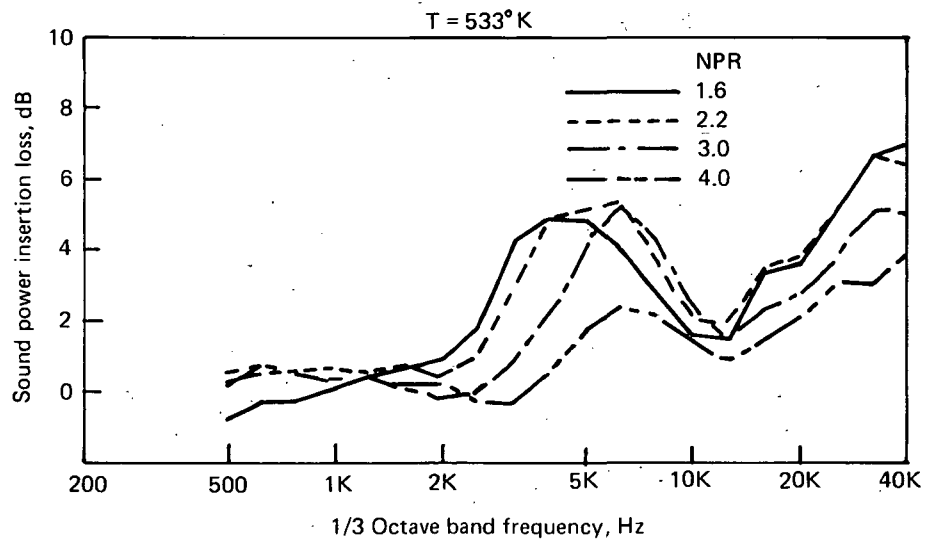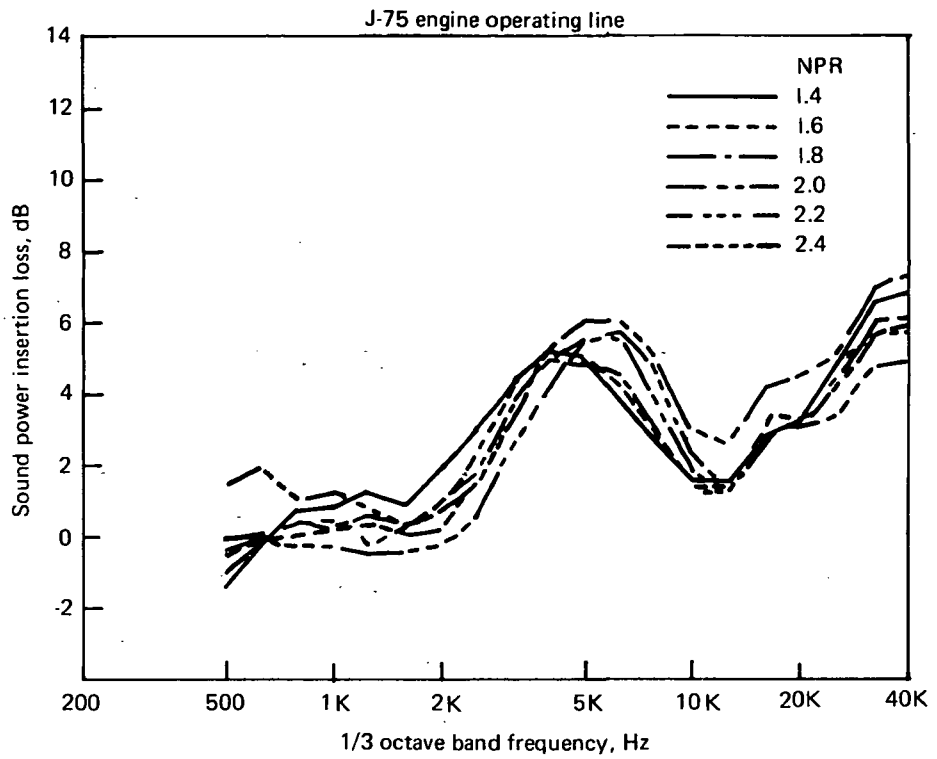
FIGURE C-3.—MODEL-SCALE SOUND POWER INSERTION LOSS SPECTRA FOR A
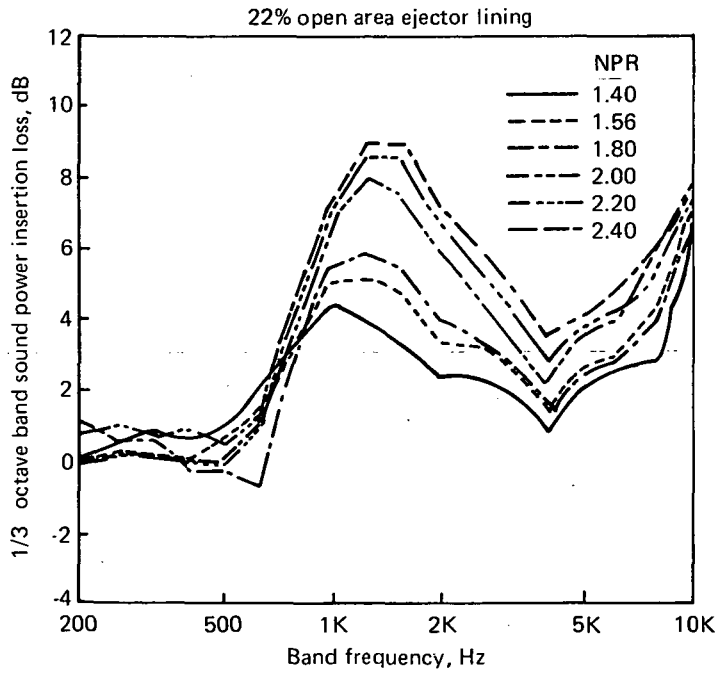12% OPEN AREA 1.4-CM-DEEP LINING IN A L/D = 1 EJECTOR
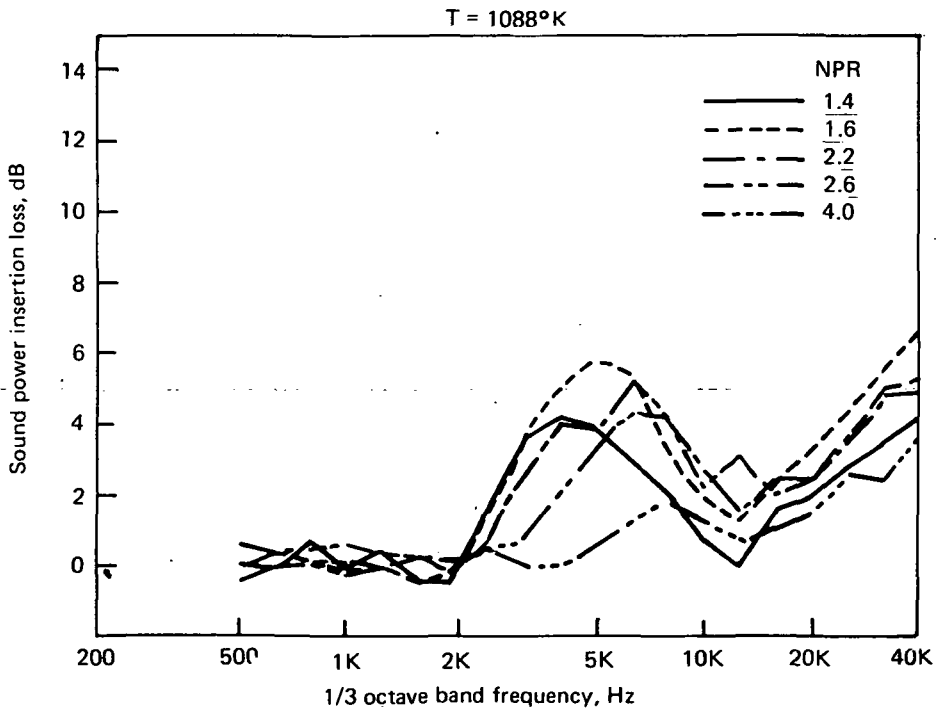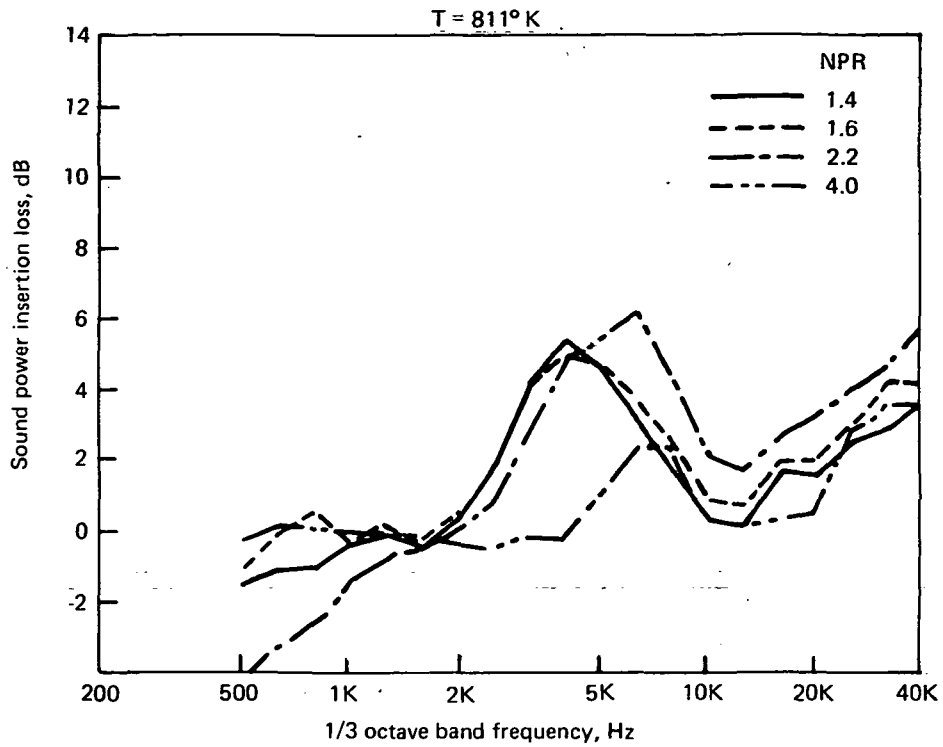
FIGURE C-3.— Concluded
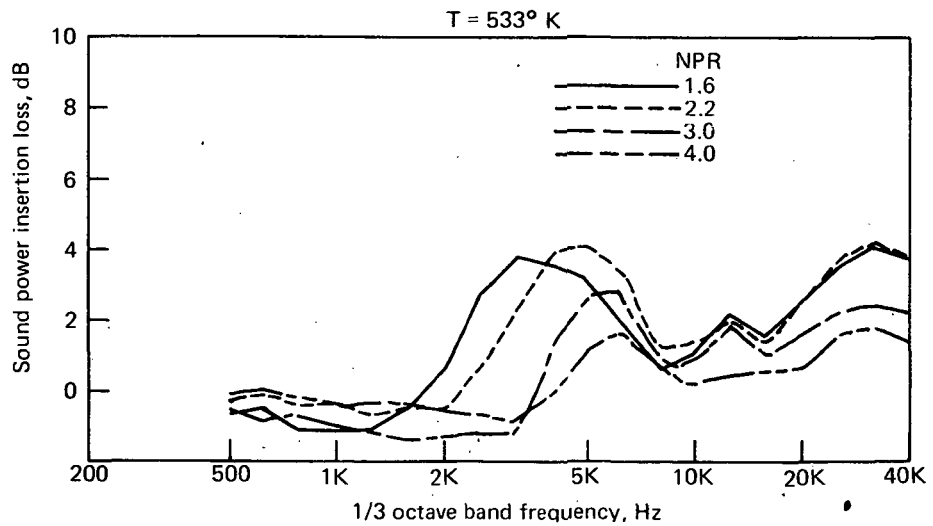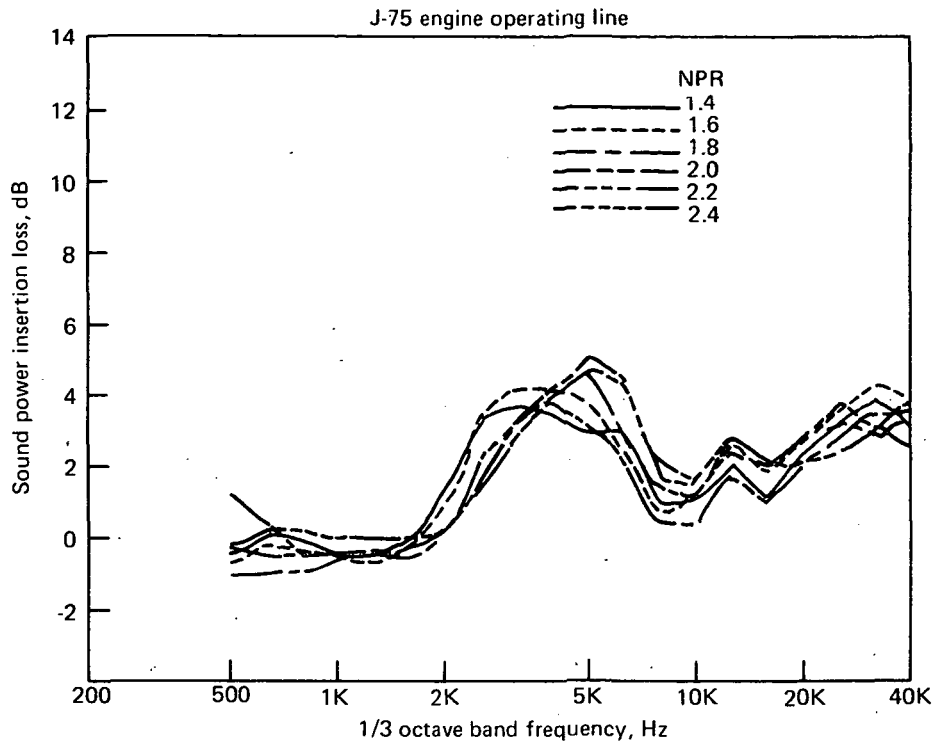
FIGURE C-4.—MODEL-SCALE SOUND POWER INSERTION LOSS SPECTRA FOR A
12% OPEN AREA 1.9-CM-DEEP LINING IN A L/D = 1 EJECTOR

T = 811°K
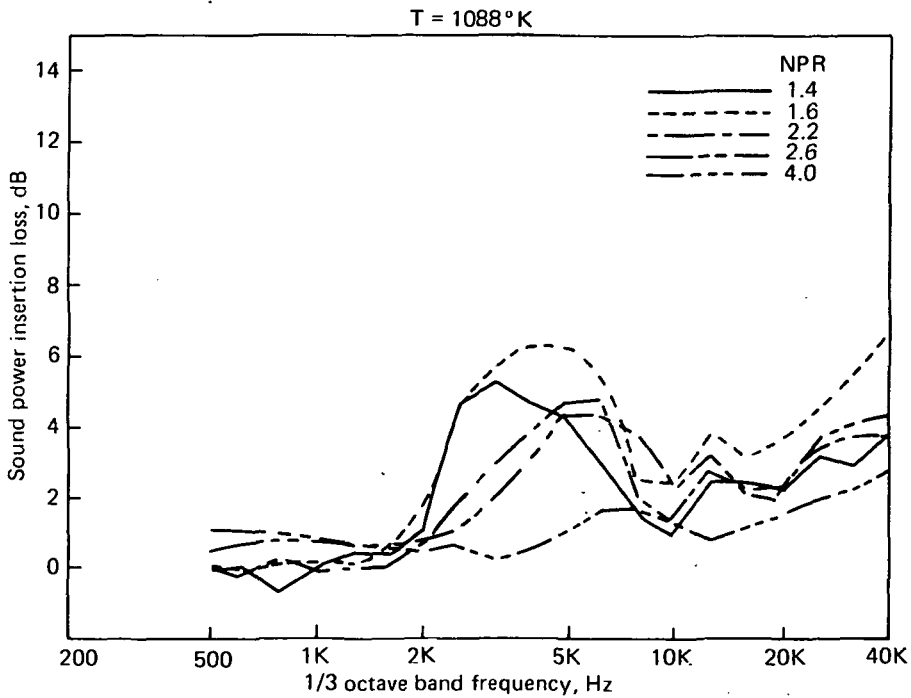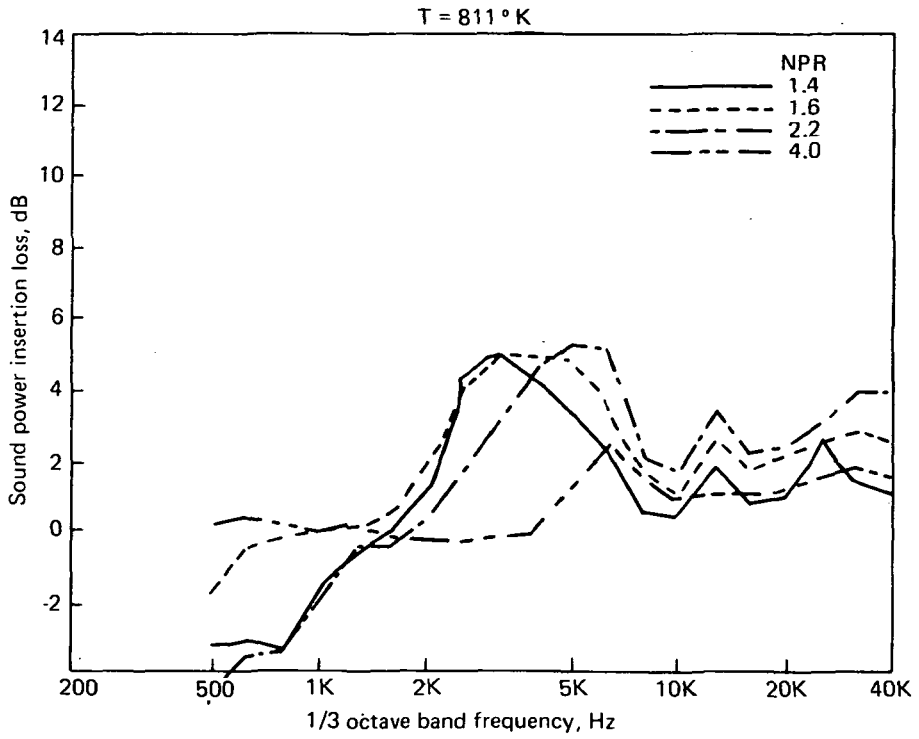
FIGURE C-4.– Concluded

T = 1088°K
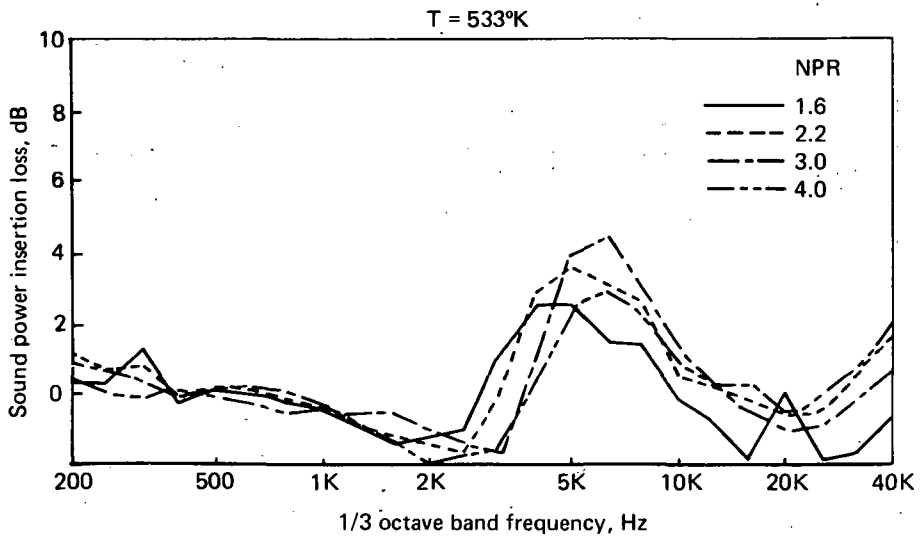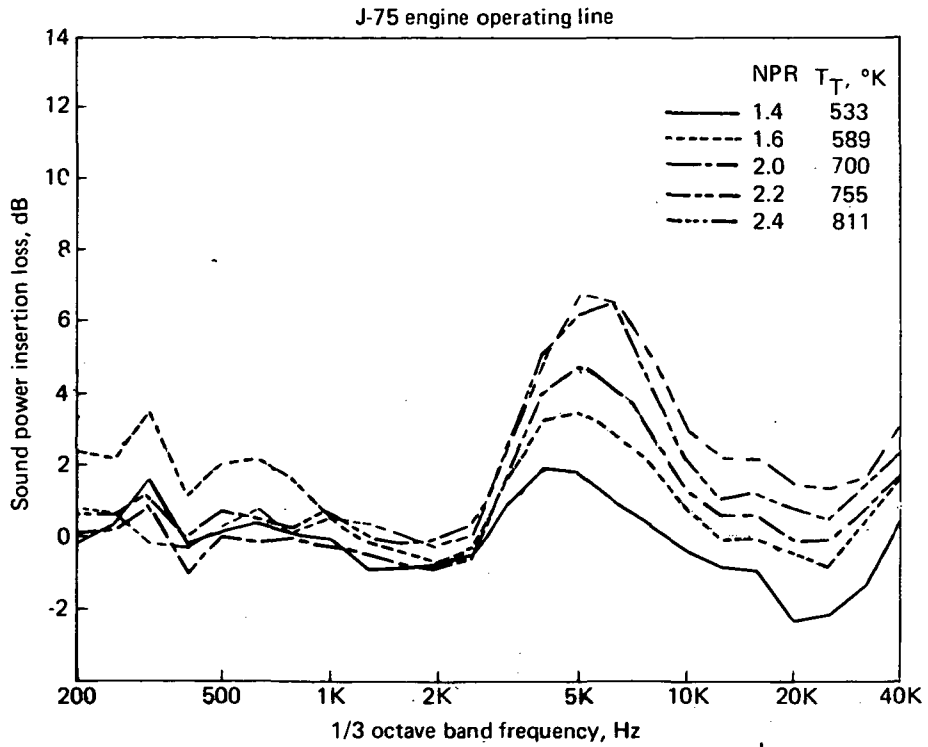
FIGURE C-5.–MODEL–SCALE SOUND POWER INSERTION LOSS SPECTRA FOR A
22% OPEN AREA, 1.4-CM-DEEP LINING IN A L/D = 1 EJECTOR

T = 811°K

T = 1088°K
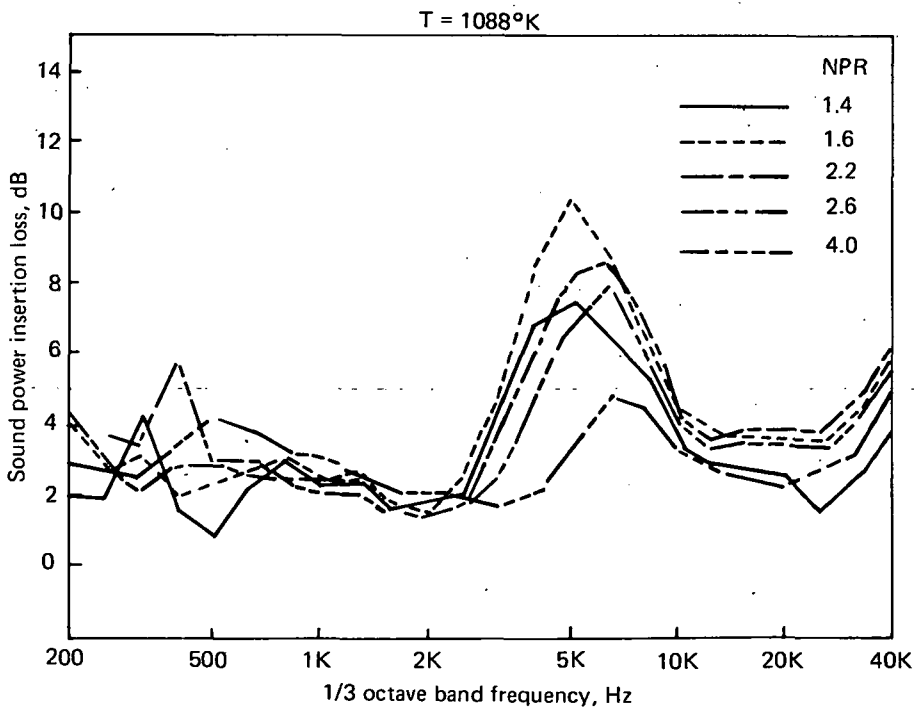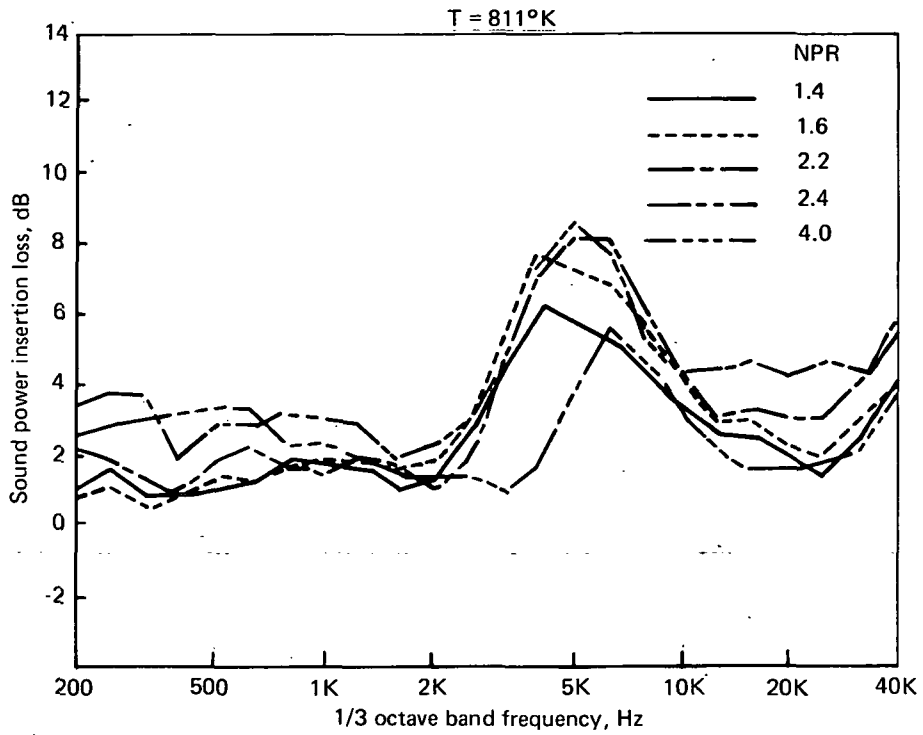
FIGURE C-5.—Concluded
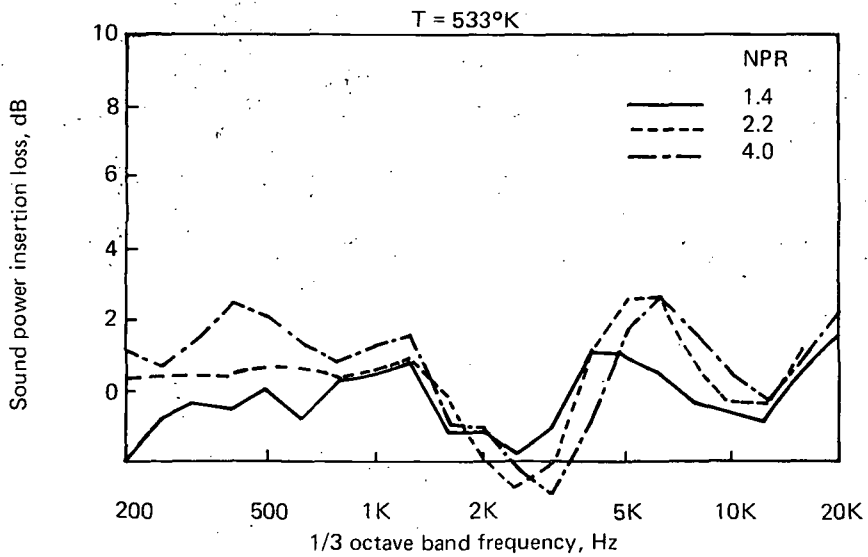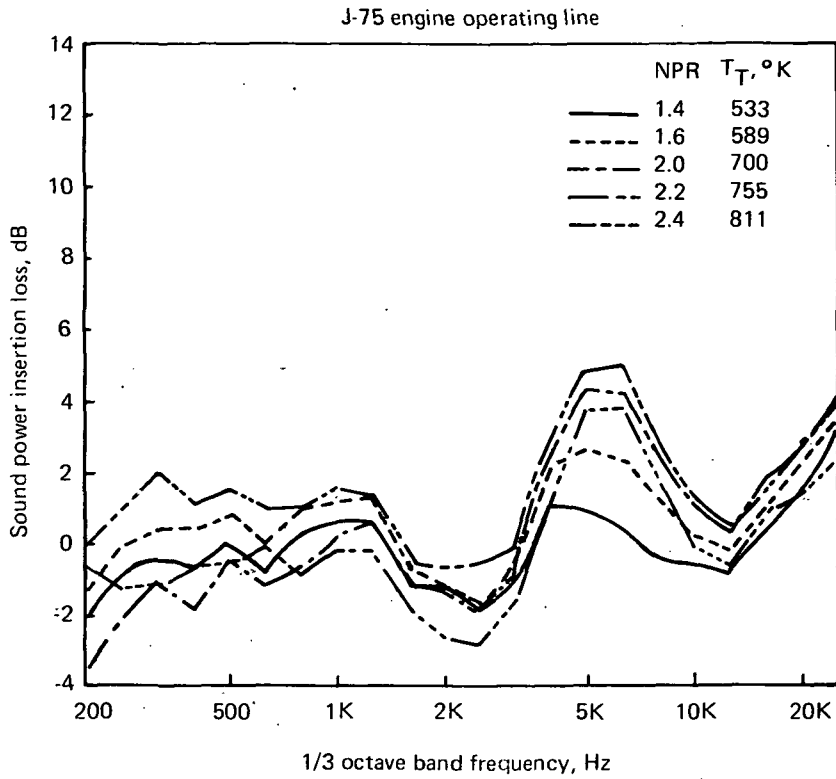
FIGURE C-6.—MODEL-SCALE SOUND POWER INSERTION LOSS SPECTRA FOR
A 30% OPEN AREA, 1.4-CM-DEEP LINING IN A L/D = 1 EJECTOR
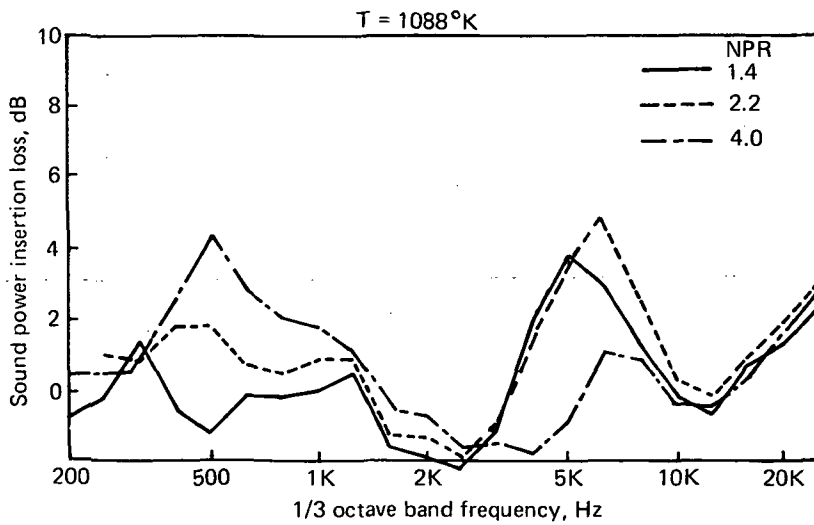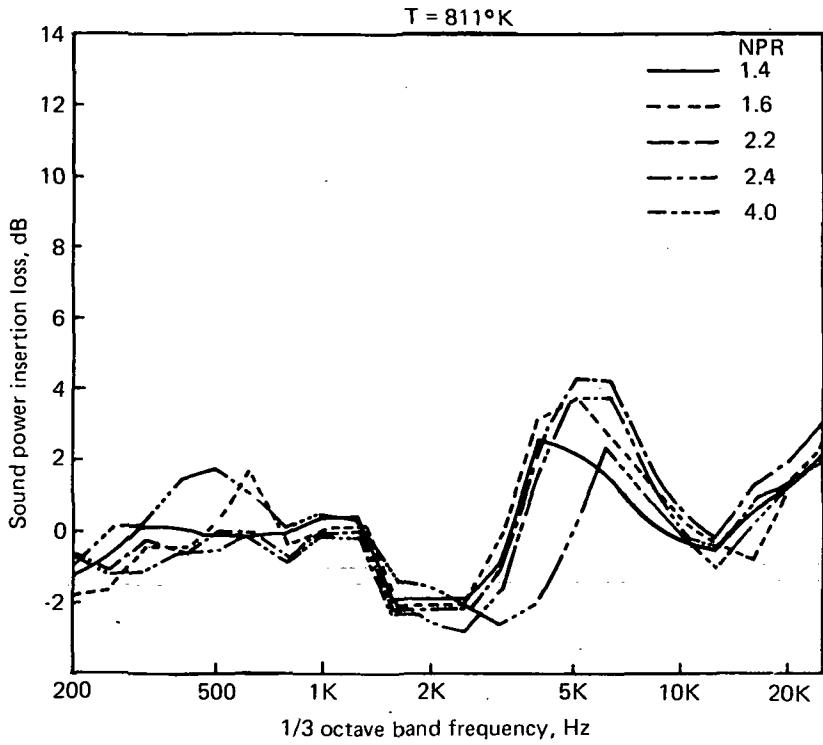
FIGURE C-6.—Concluded
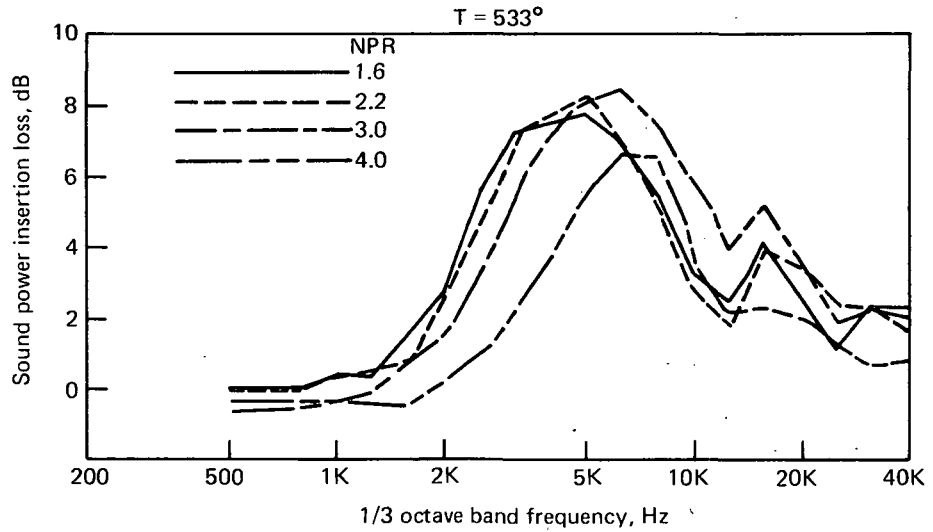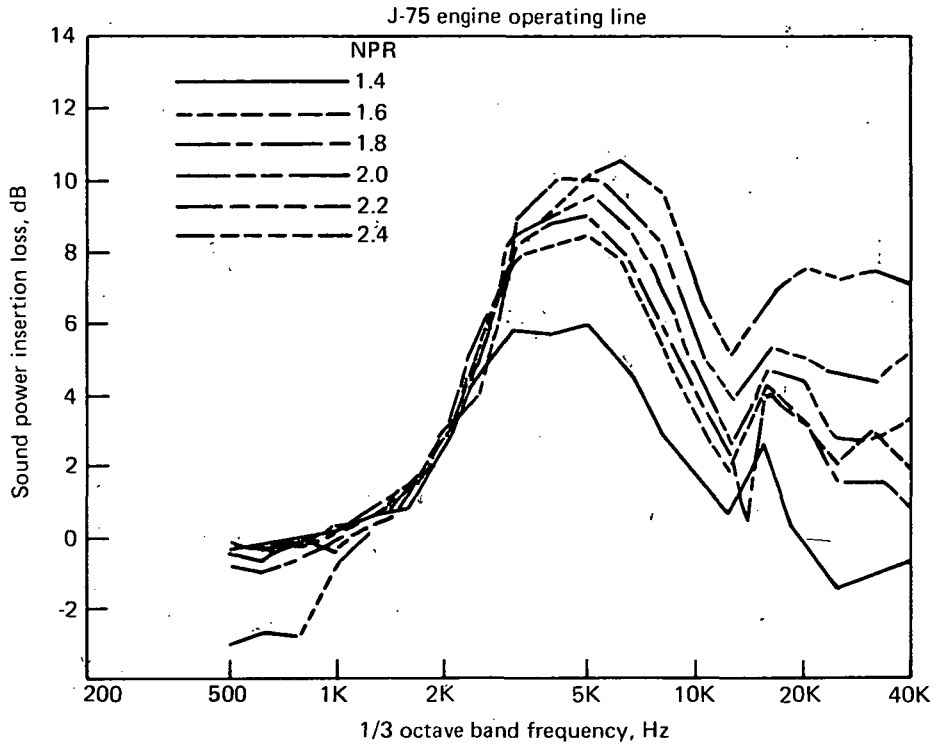
FIGURE C-7.—MODEL-SCALE SOUND POWER INSERTION LOSS SPECTRA FOR A
12% OPEN AREA 1.4-CM-DEEP LINING IN A L/D = 2 EJECTOR
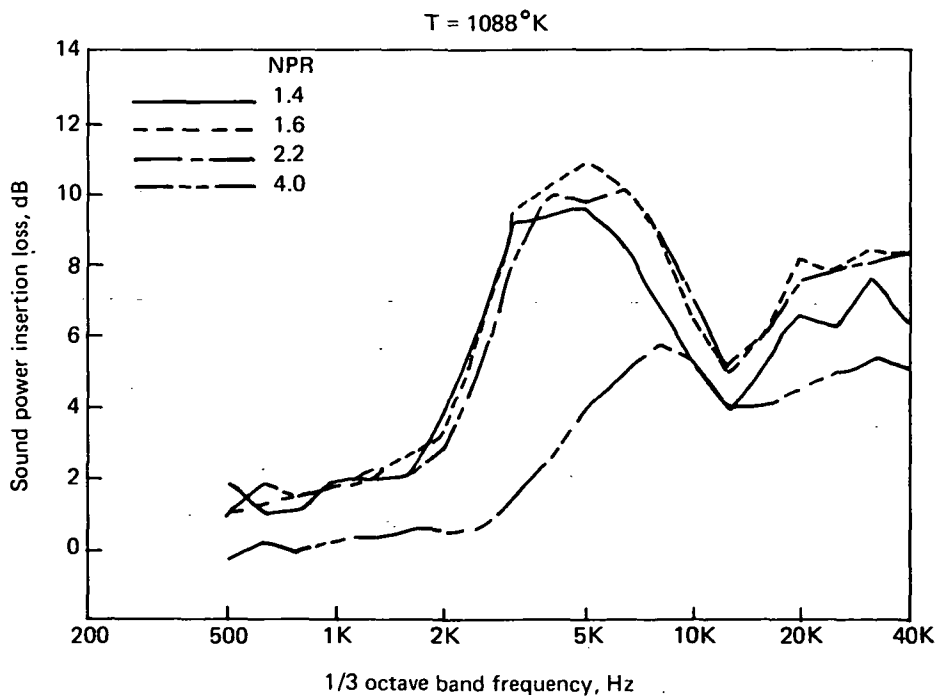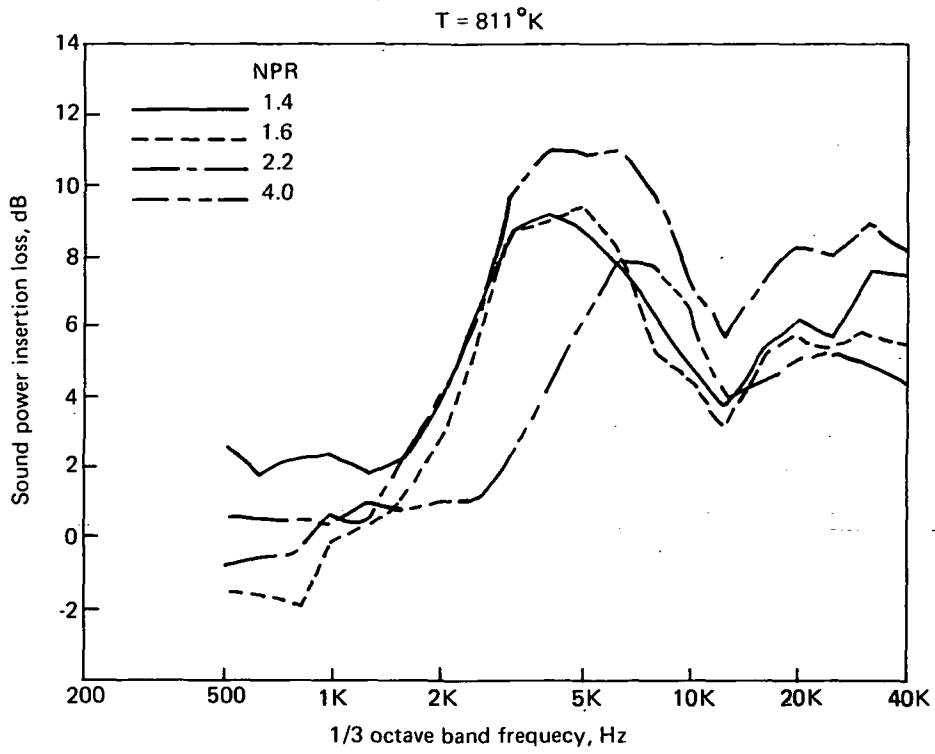
FIGURE C-7.—Concluded
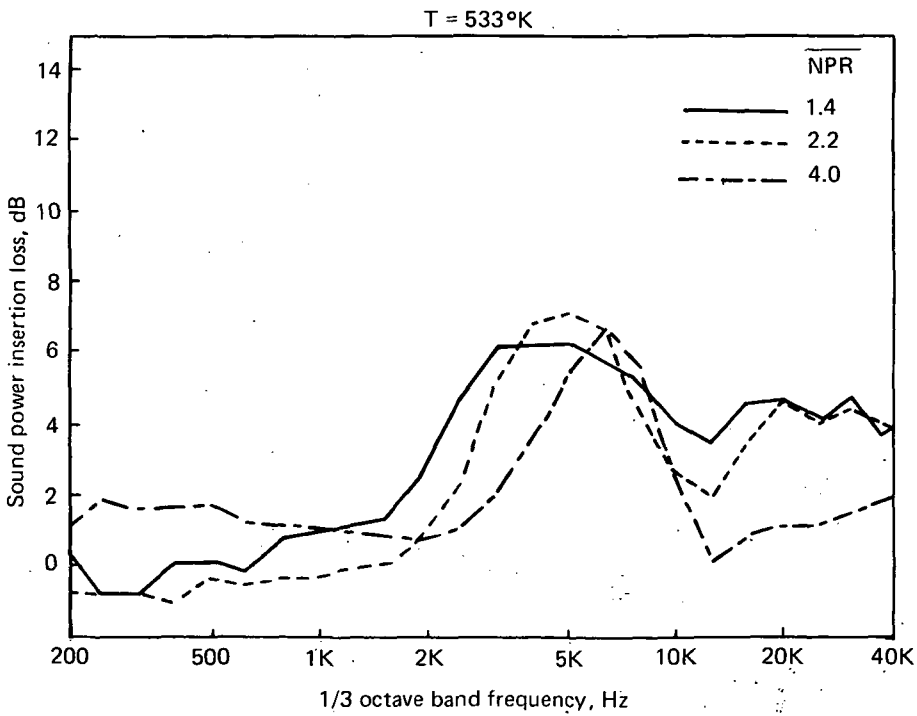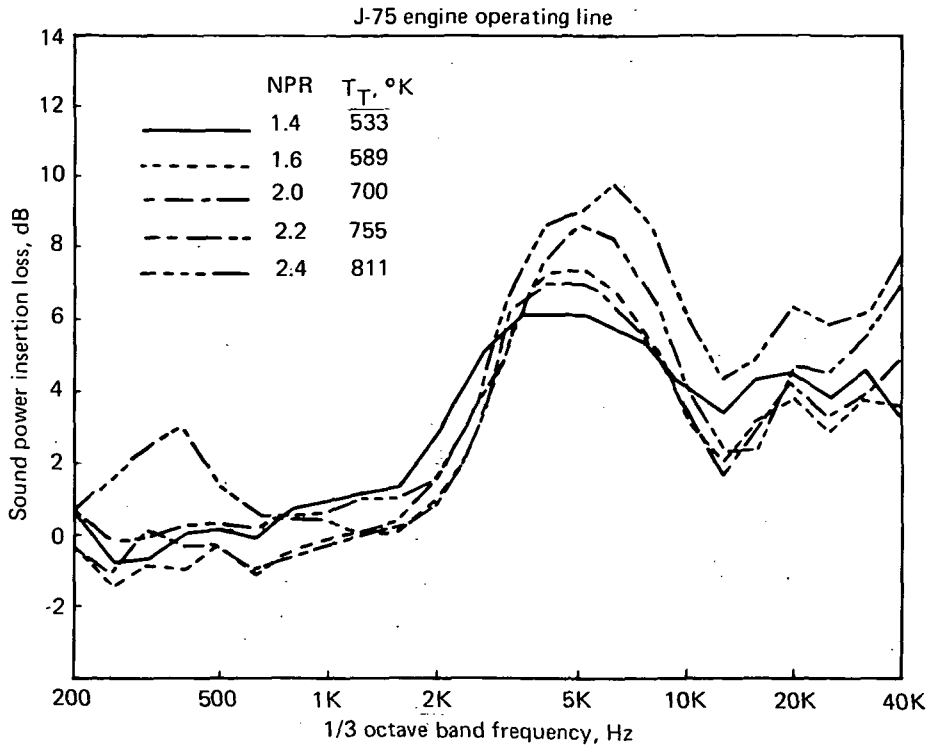
FIGURE C-8.—MODEL–SCALE SOUND POWER INSERTION LOSS SPECTRA FOR A 22% OPEN AREA, 1.4-CM-DEEP LINING IN A L/D = 2 EJECTOR

T = 811°K

T = 1088 °K
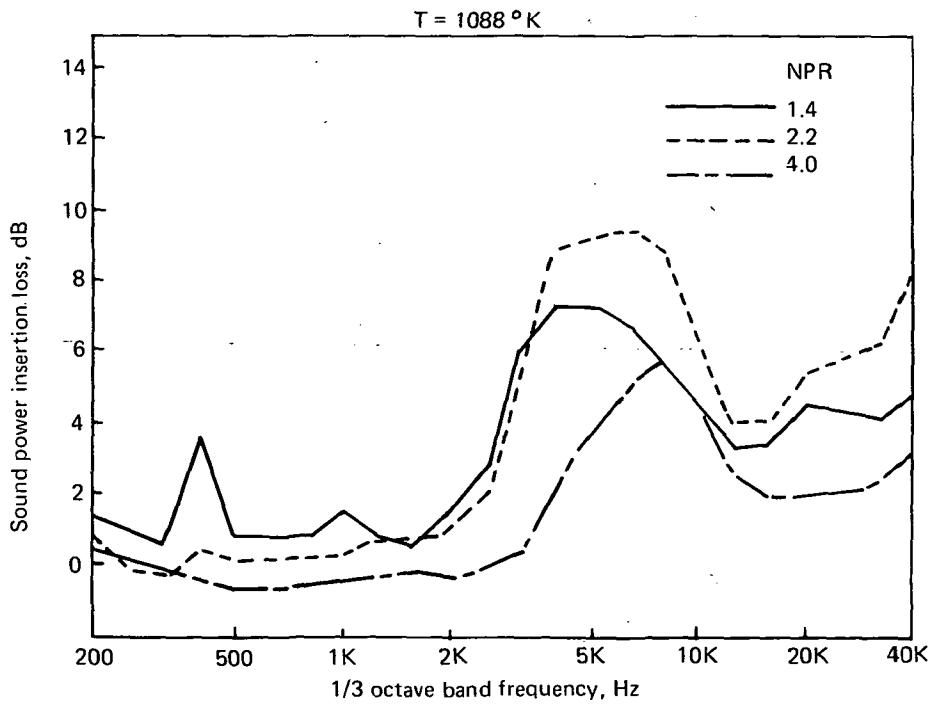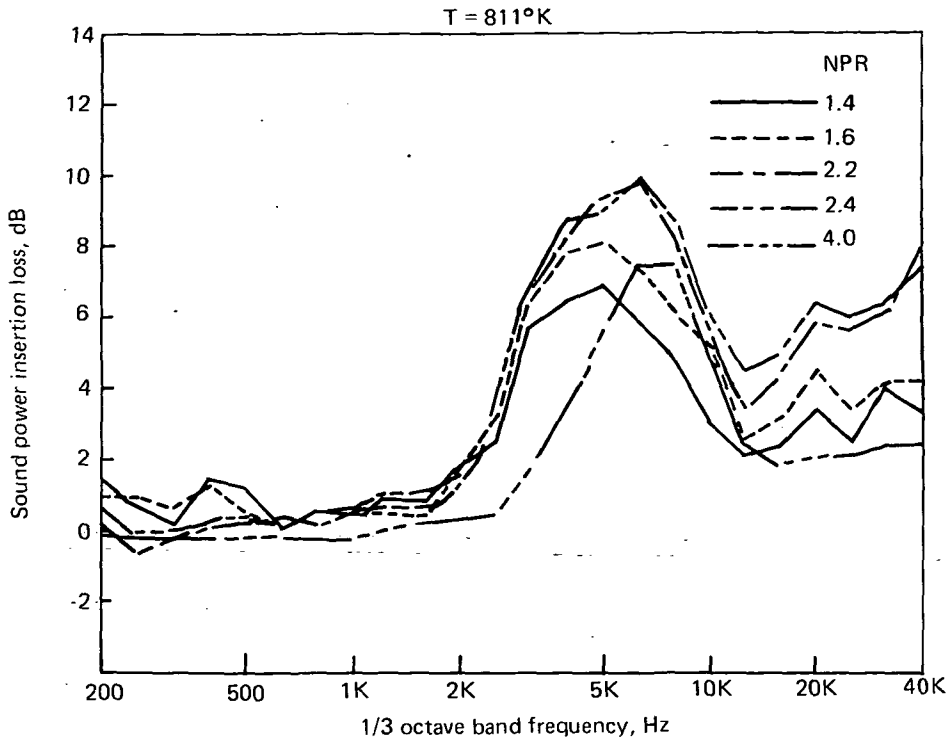
FIGURE C-8.—Concluded
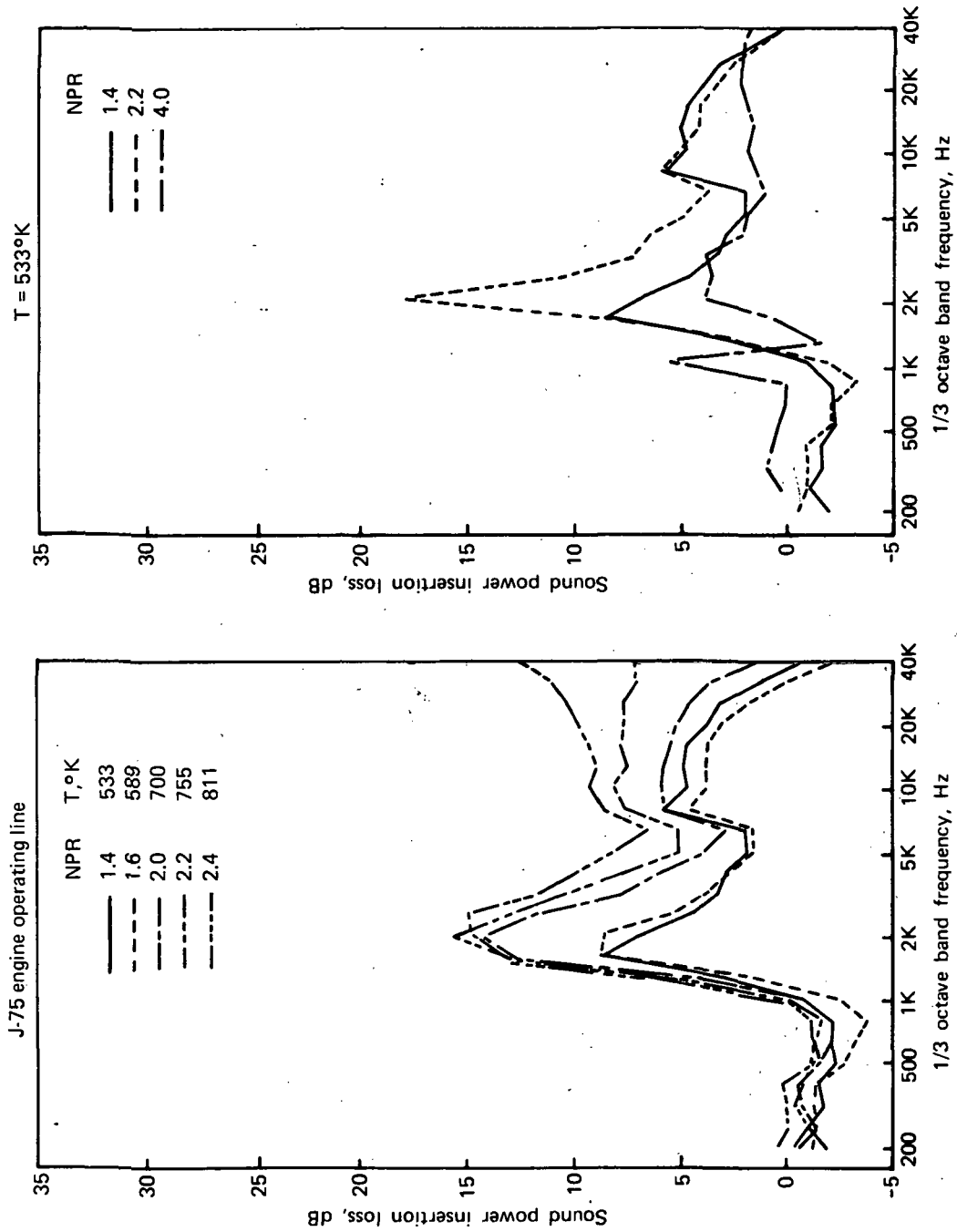
FIGURE C-9.—MODEL-SCALE SOUND POWER INSERTION LOSS SPECTRA FOR A 12% OPEN AREA, 2.54-CM-DEEP LINING IN A L/D = 4 EJECTOR AND 10.9-CM DIAMETER NOZZLE
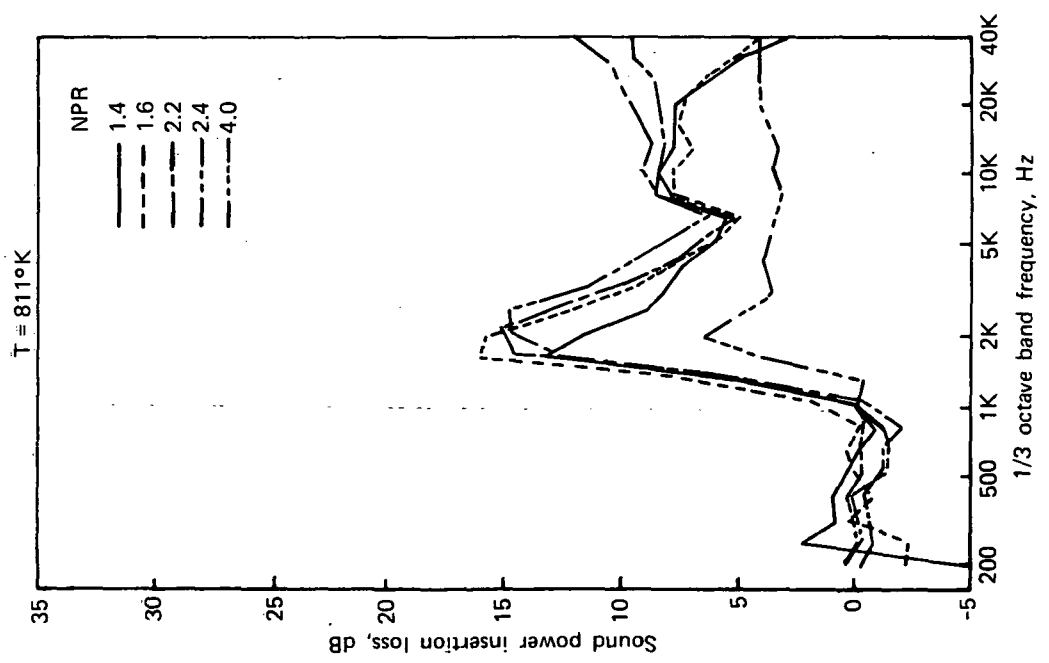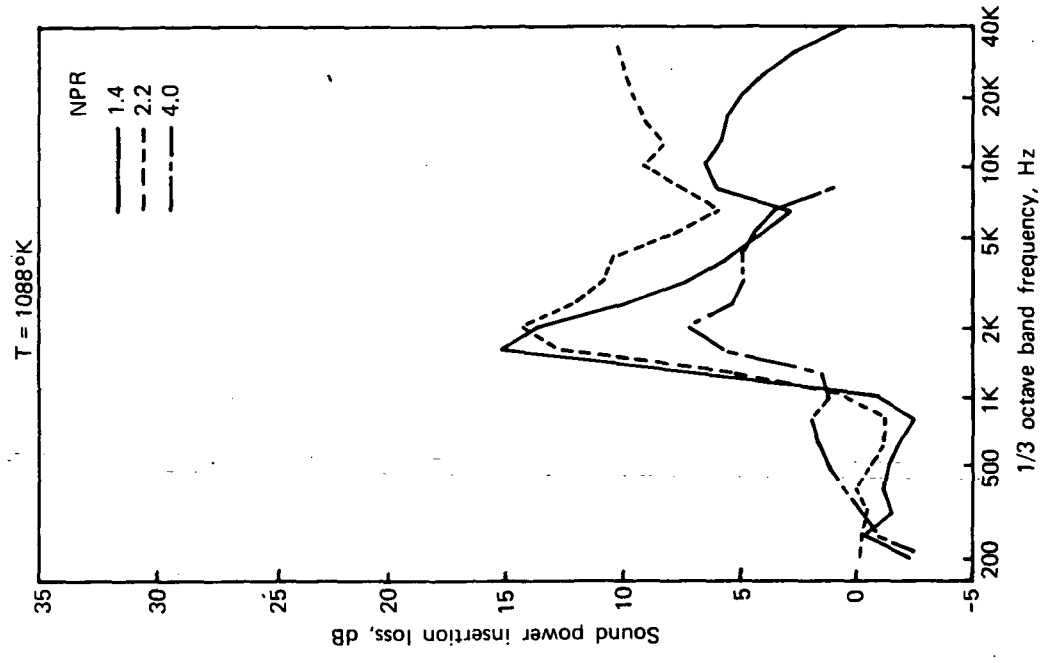
FIGURE C-9.--Concluded

297
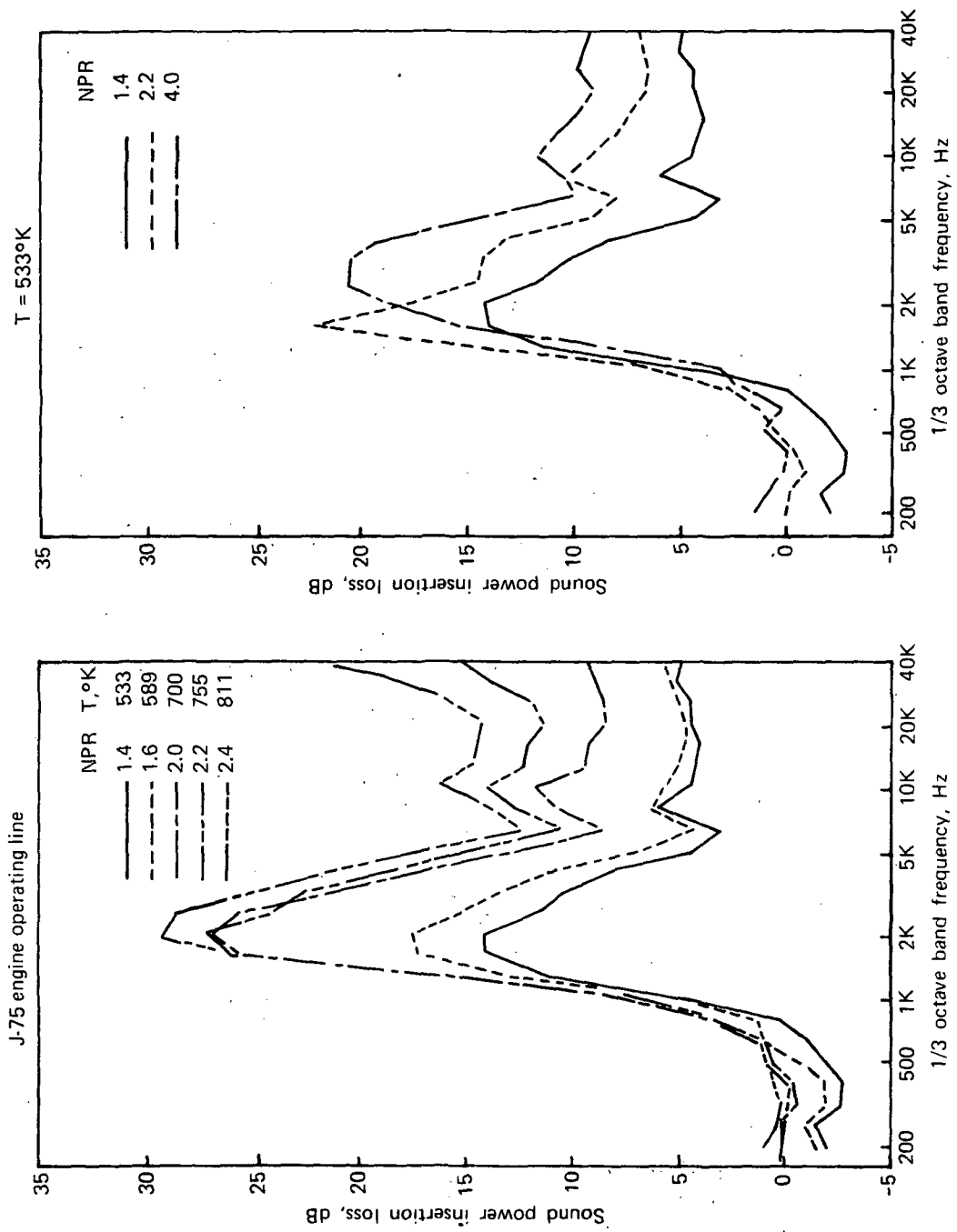
FIGURE C-10.—MODEL-SCALE SOUND POWER INSERTION LOSS SPECTRA FOR A 12% OPEN AREA, 2.54-CM-DEEP LINING IN A L/D = 8 EJECTOR AND 10.9-CM-DIAMETER NOZZLE
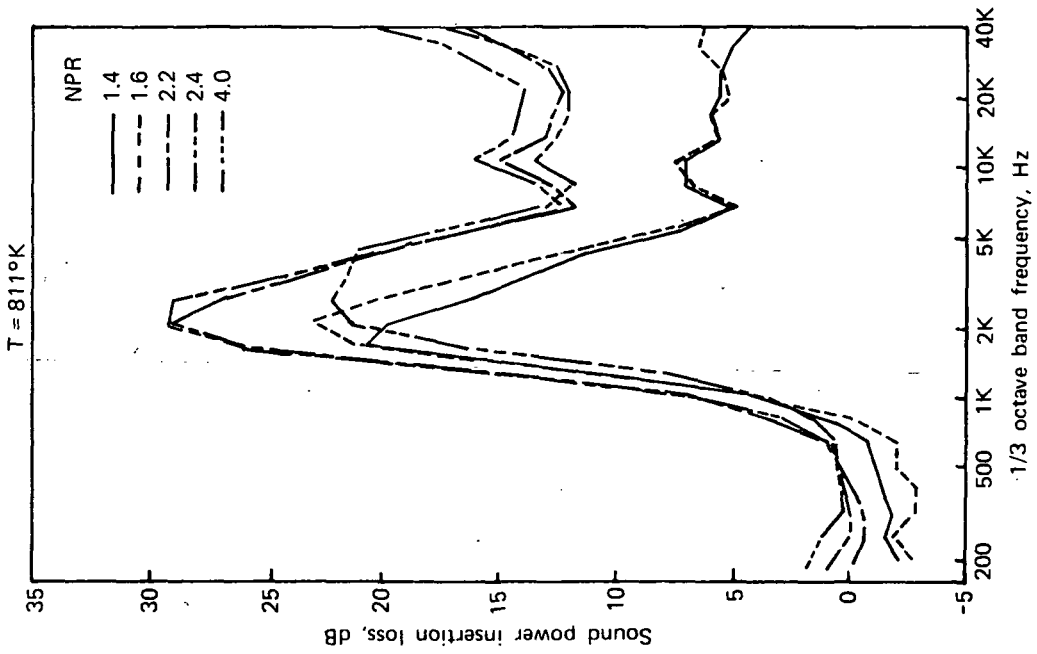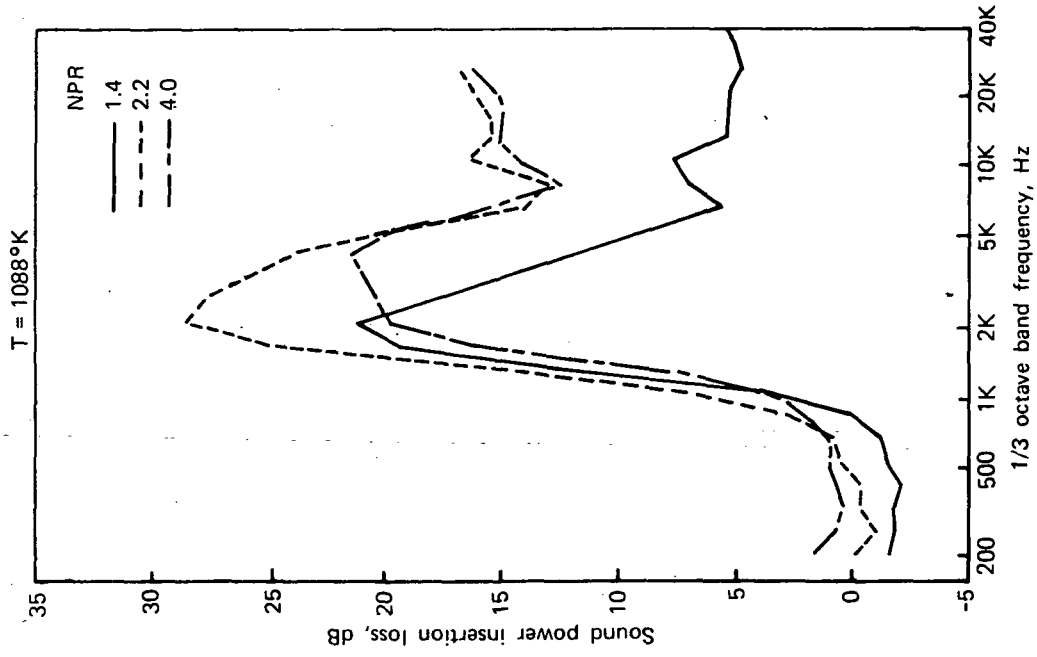
FIGURE C-10.—Concluded

299
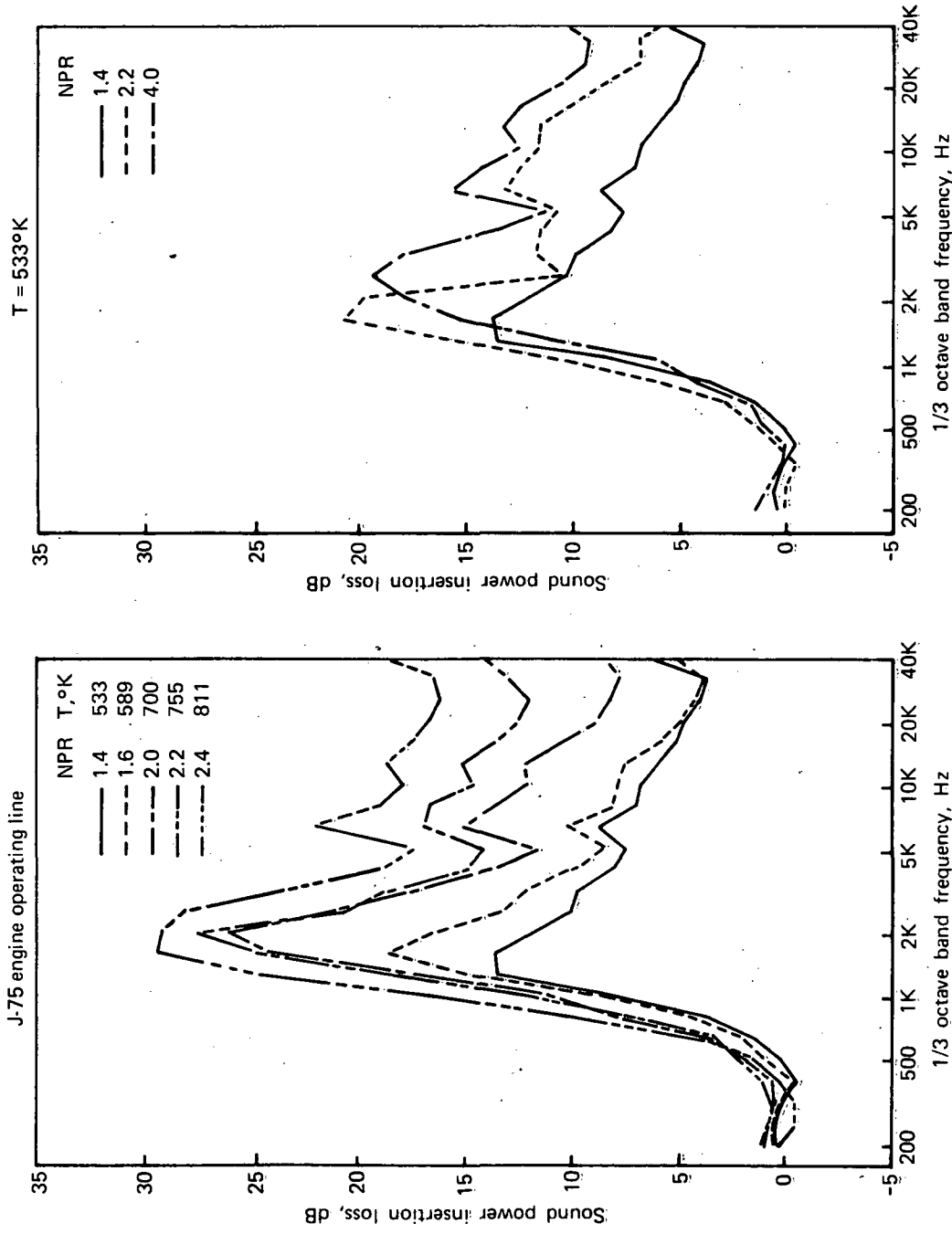
FIGURE C-11.—MODEL-SCALE SOUND POWER INSERTION LOSS SPECTRA FOR A 12% OPEN AREA, 3.8-CM-DEEP LINING IN A L/D = 8 EJECTOR AND 10.9-CM-DIAMETER NOZZLE
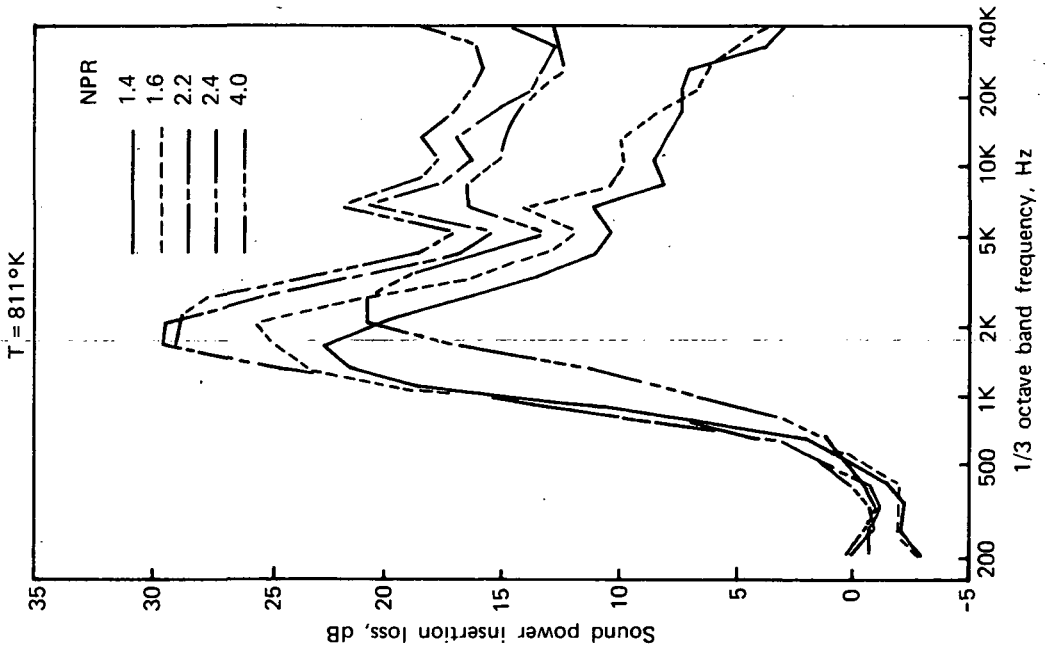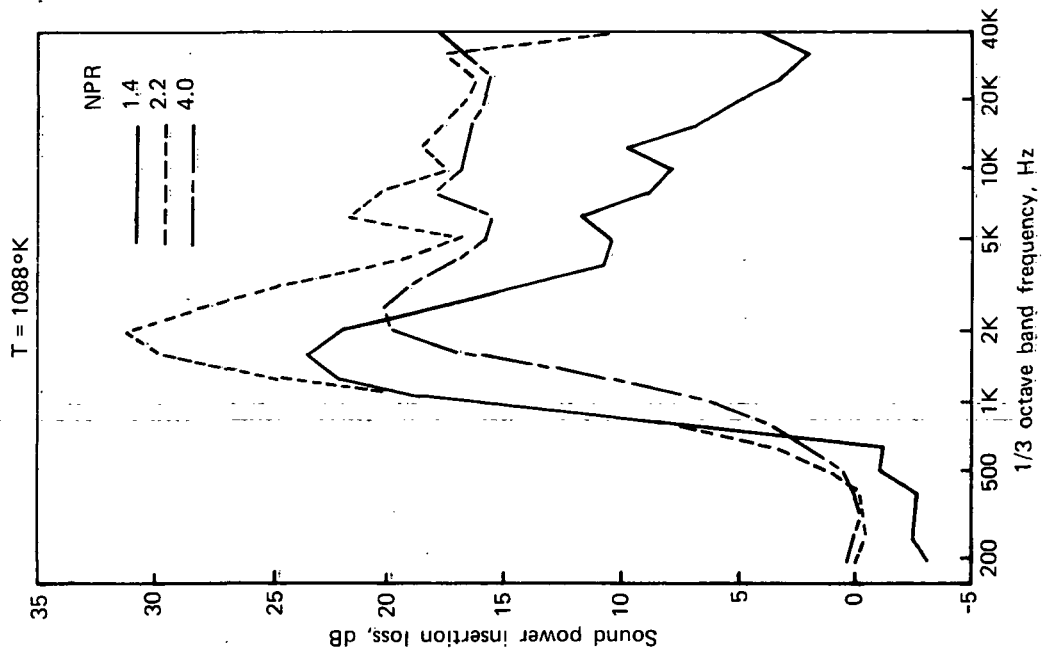
FIGURE C-11.—Continued
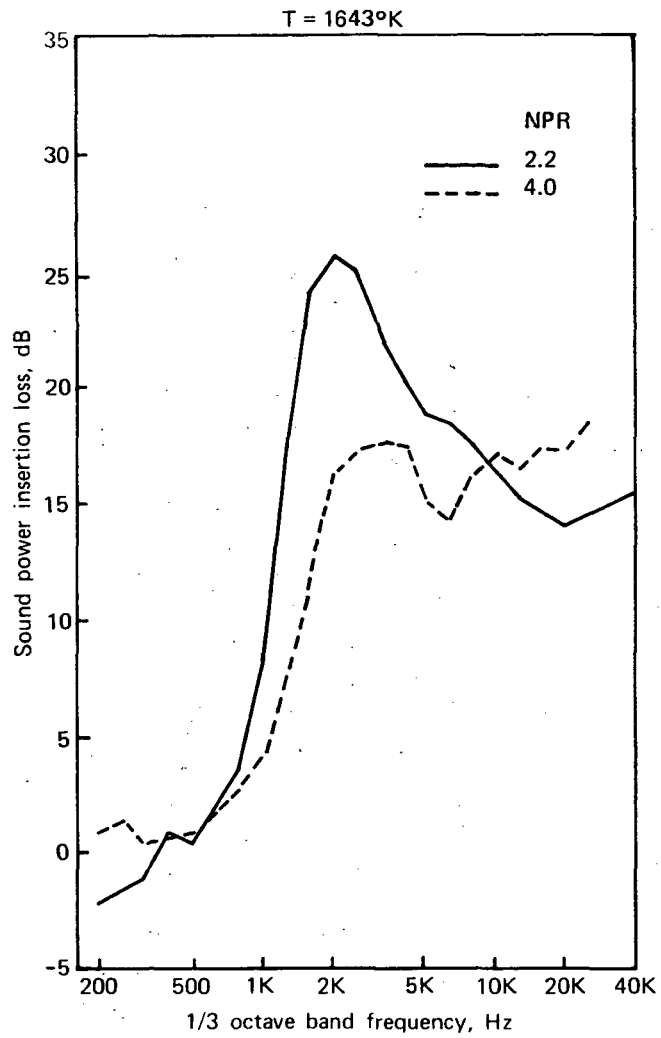
FIGURE C-11.—Concluded
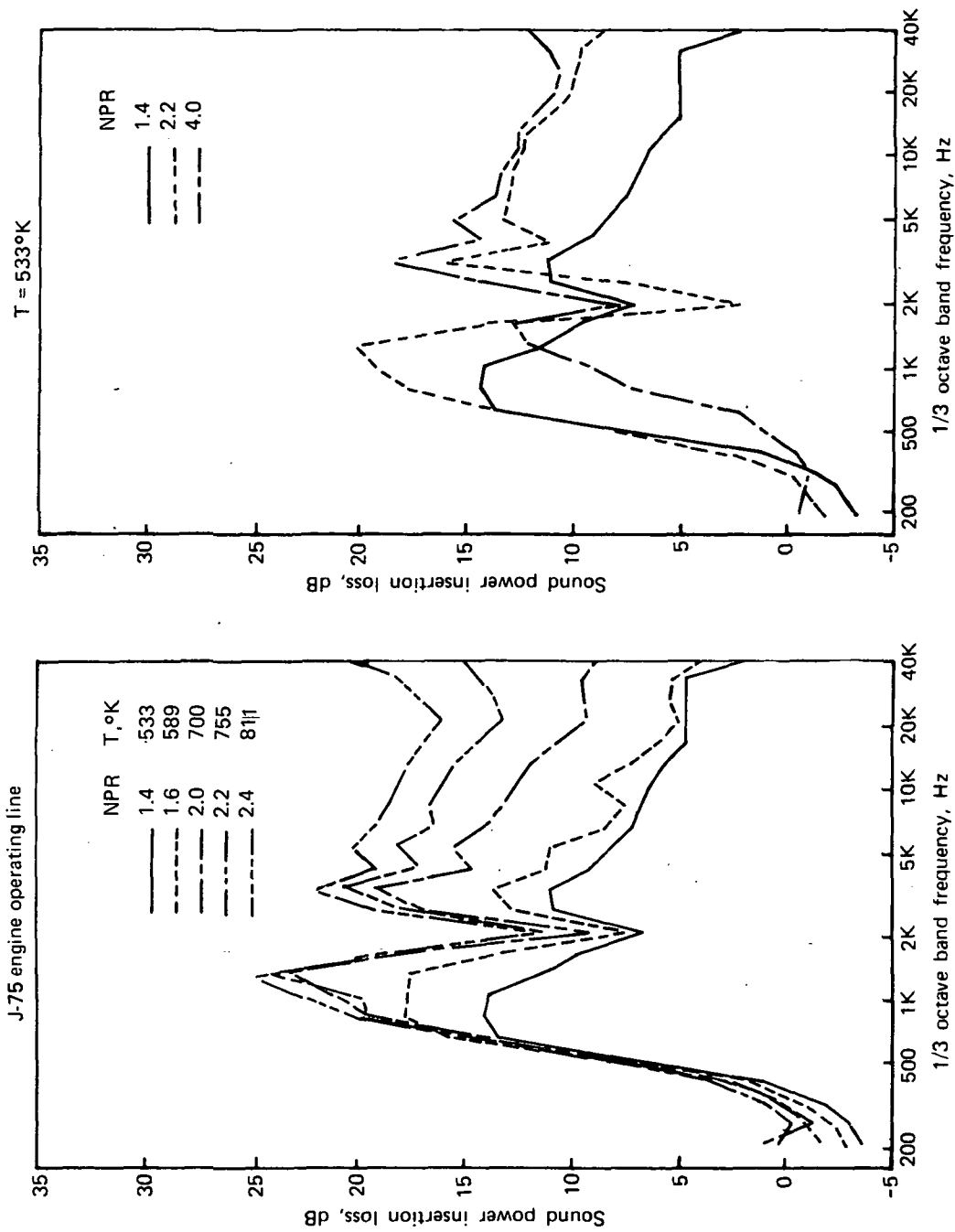
FIGURE C-12.—MODEL-SCALE SOUND POWER INSERTION LOSS SPECTRA FOR A 12% OPEN AREA, 8.6-CM-DEEP LINING IN A L/D = 8 EJECTOR AND 10.9-CM-DIAMETER NOZZLE

303
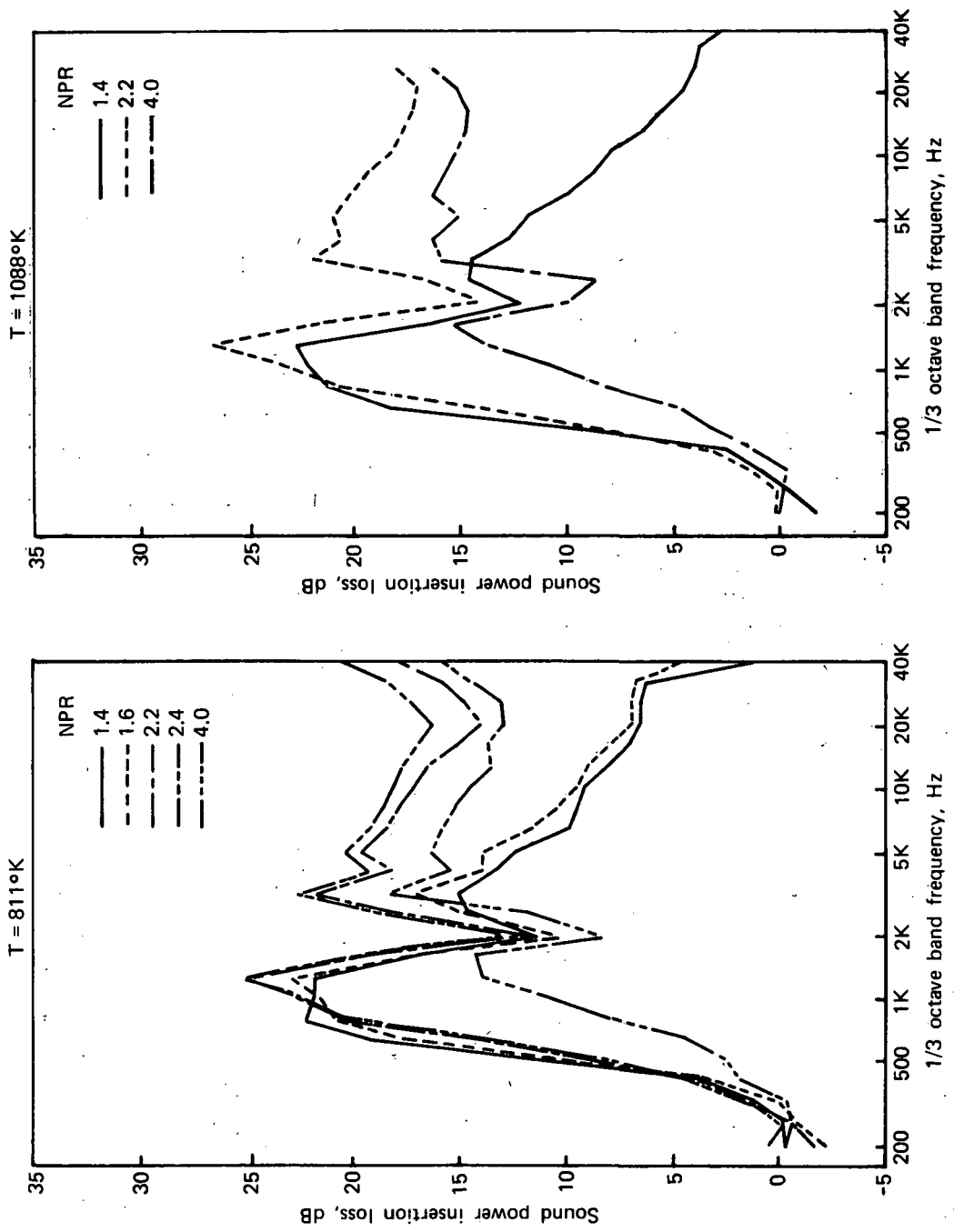
FIGURE C-12.—Concluded
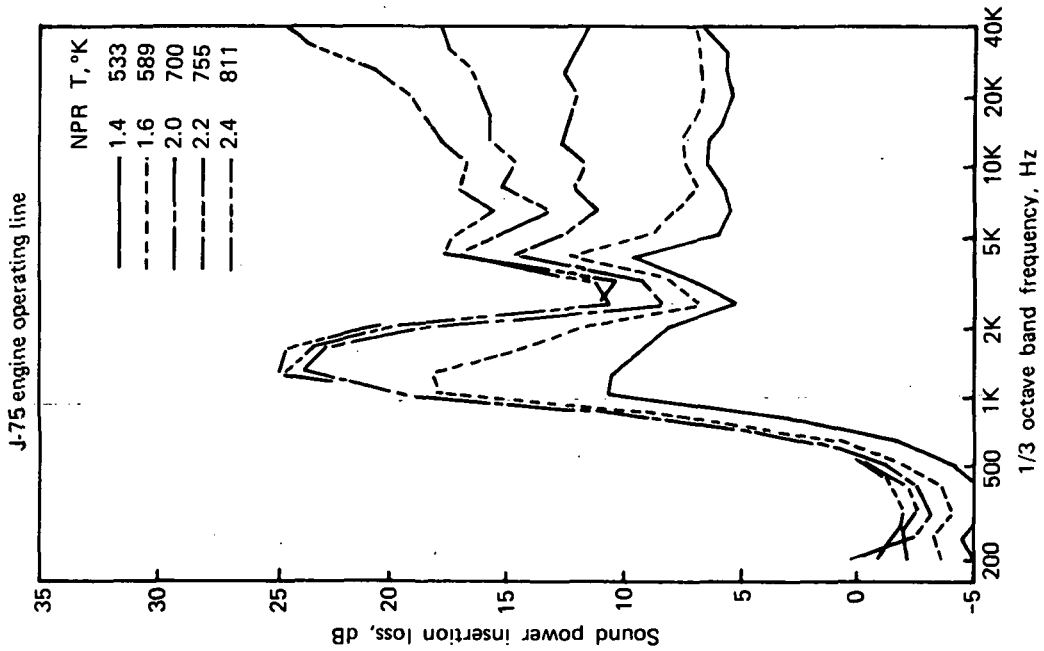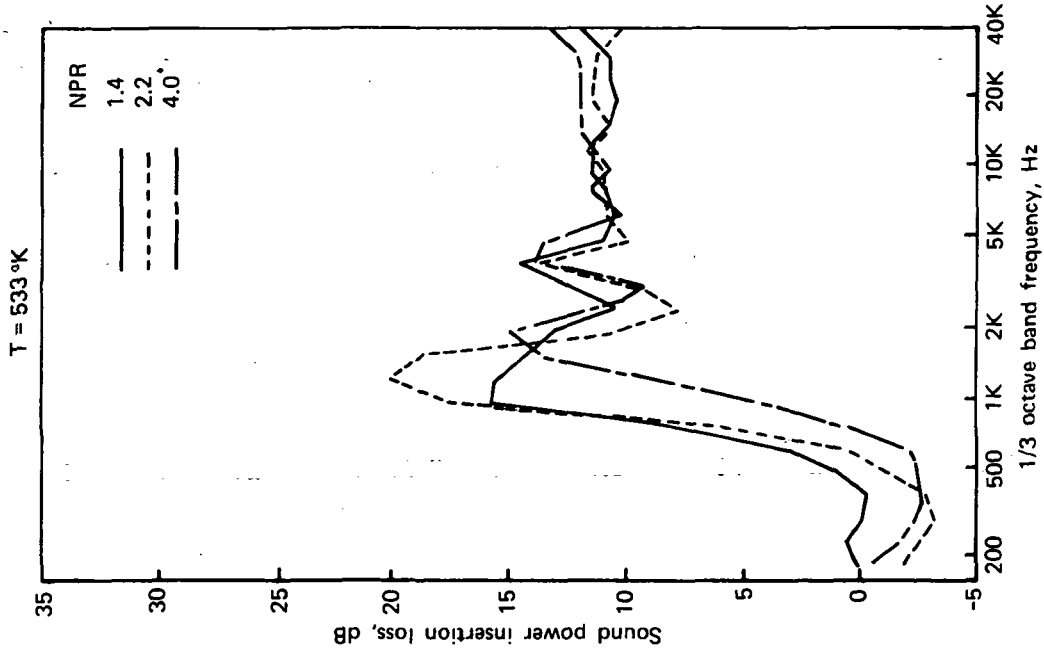
FIGURE C-13.—MODEL-SCALE SOUND POWER INSERTION LOSS SPECTRA FOR A 22% OPEN AREA, 5.85-CM-DEEP LINING IN A L/D = 8 EJECTOR AND 10.9-CM-DIAMETER NOZZLE
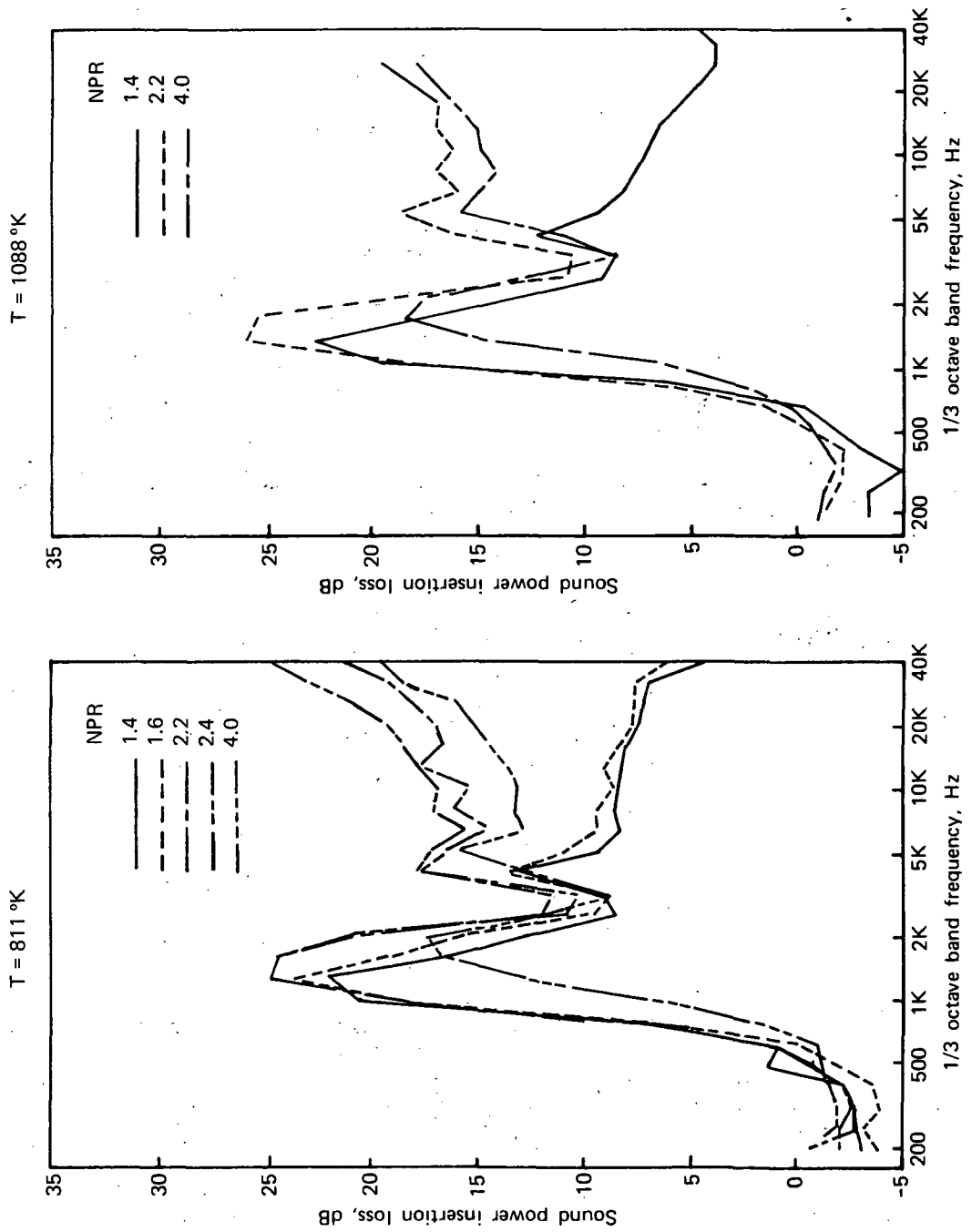
FIGURE C-13.—Concluded
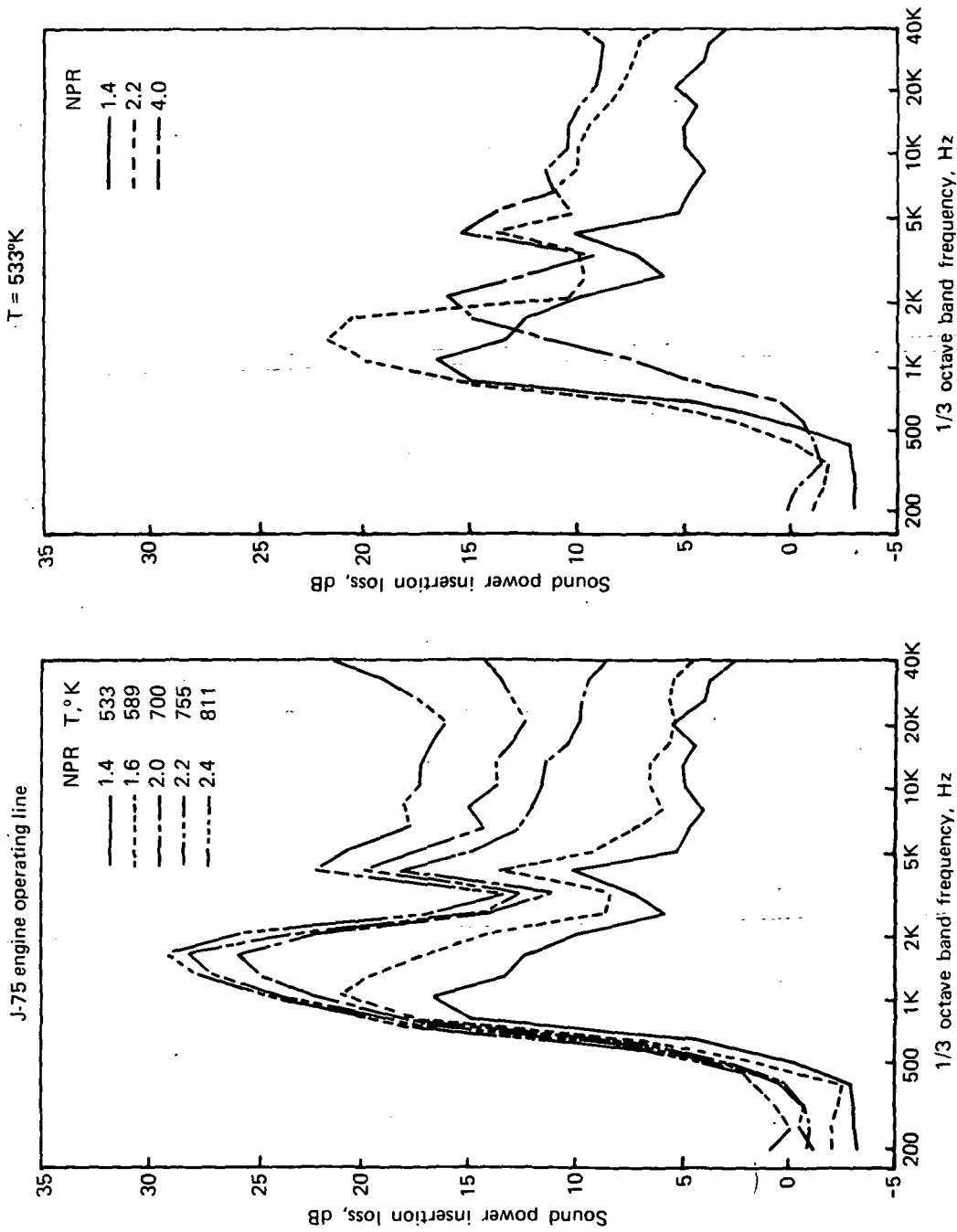
FIGURE C-14.—MODEL-SCALE SOUND POWER INSERTION LOSS SPECTRA FOR A 12% OPEN AREA, 5.85-CM-DEEP LINING IN A L/D = 8 EJECTOR AND 10.9-CM-DIAMETER NOZZLE

307
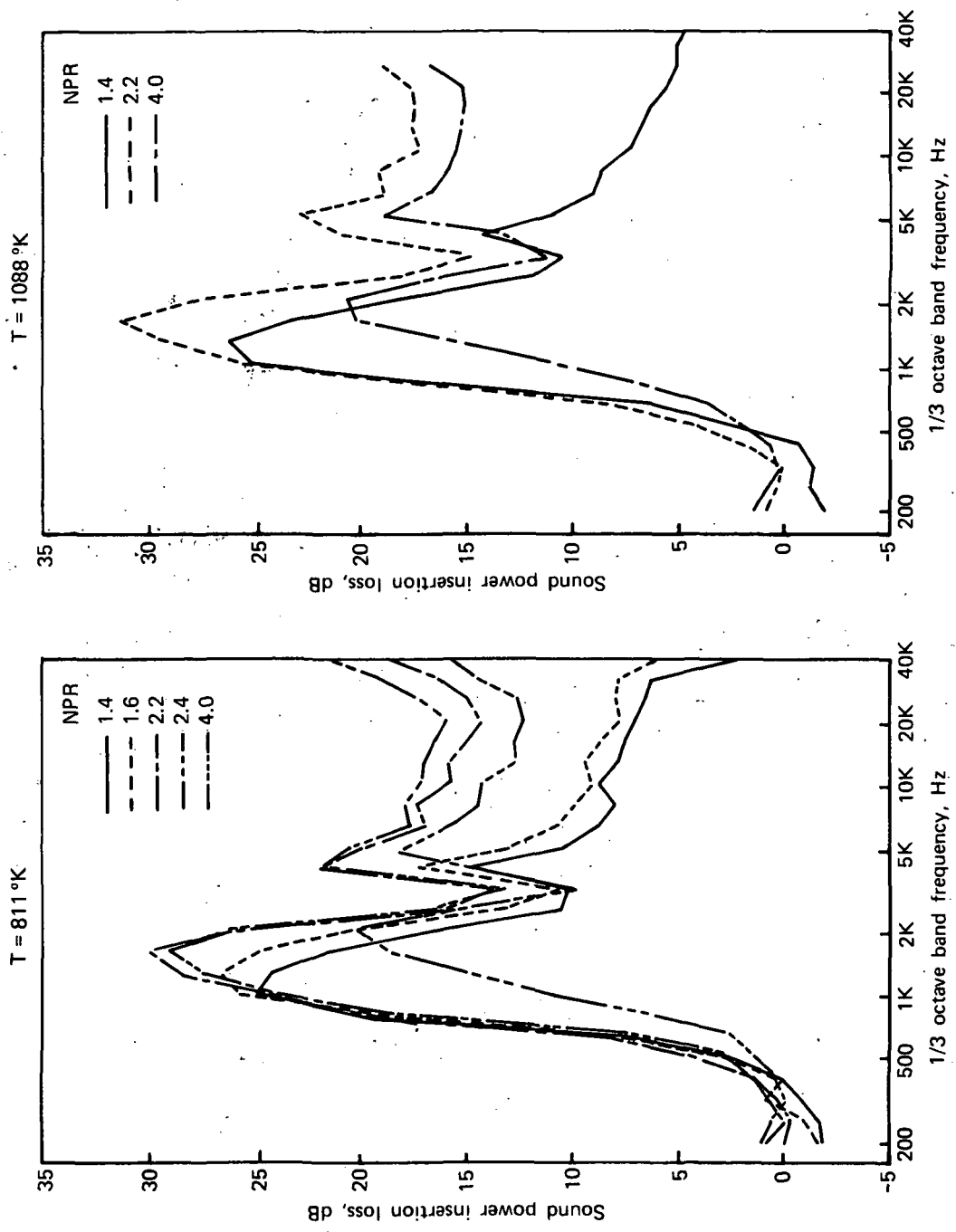
FIGURE C-14.—Concluded
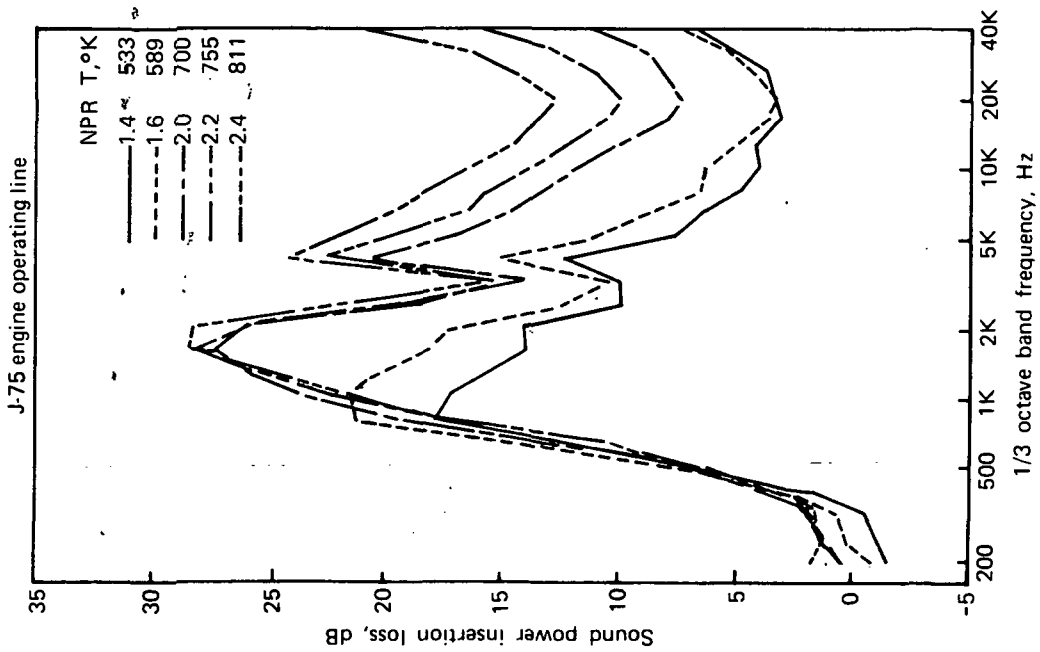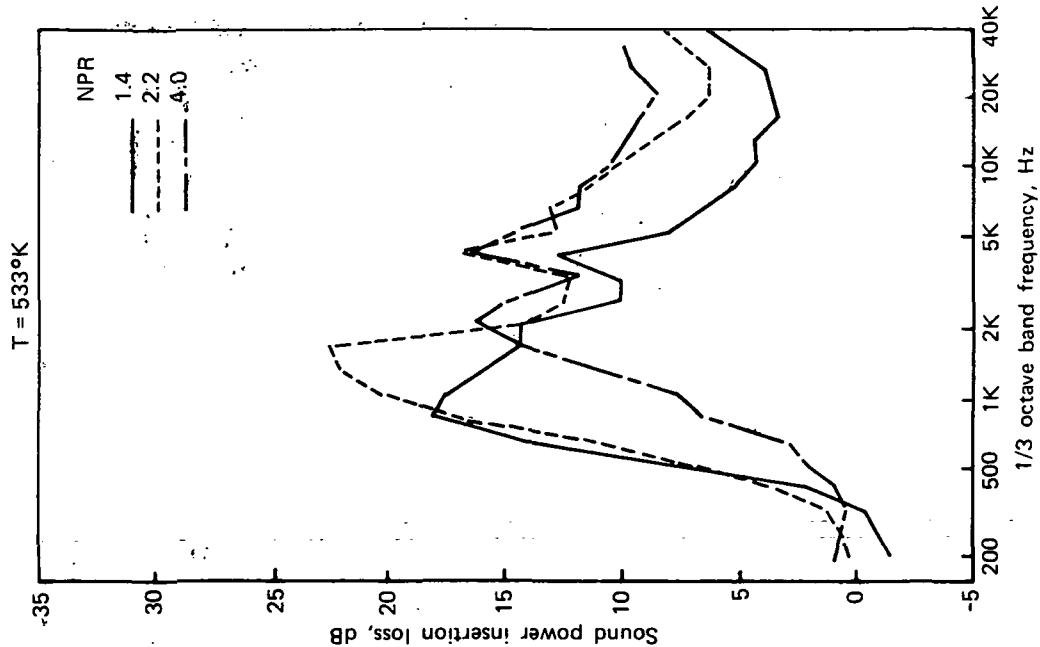
FIGURE C-15.—MODEL-SCALE SOUND POWER INSERTION LOSS SPECTRA FOR A 6% OPEN AREA, 5.85-CM-DEEP LINING IN A L/D = 8 EJECTOR AND 10.9-CM-DIAMETER NOZZLE

309
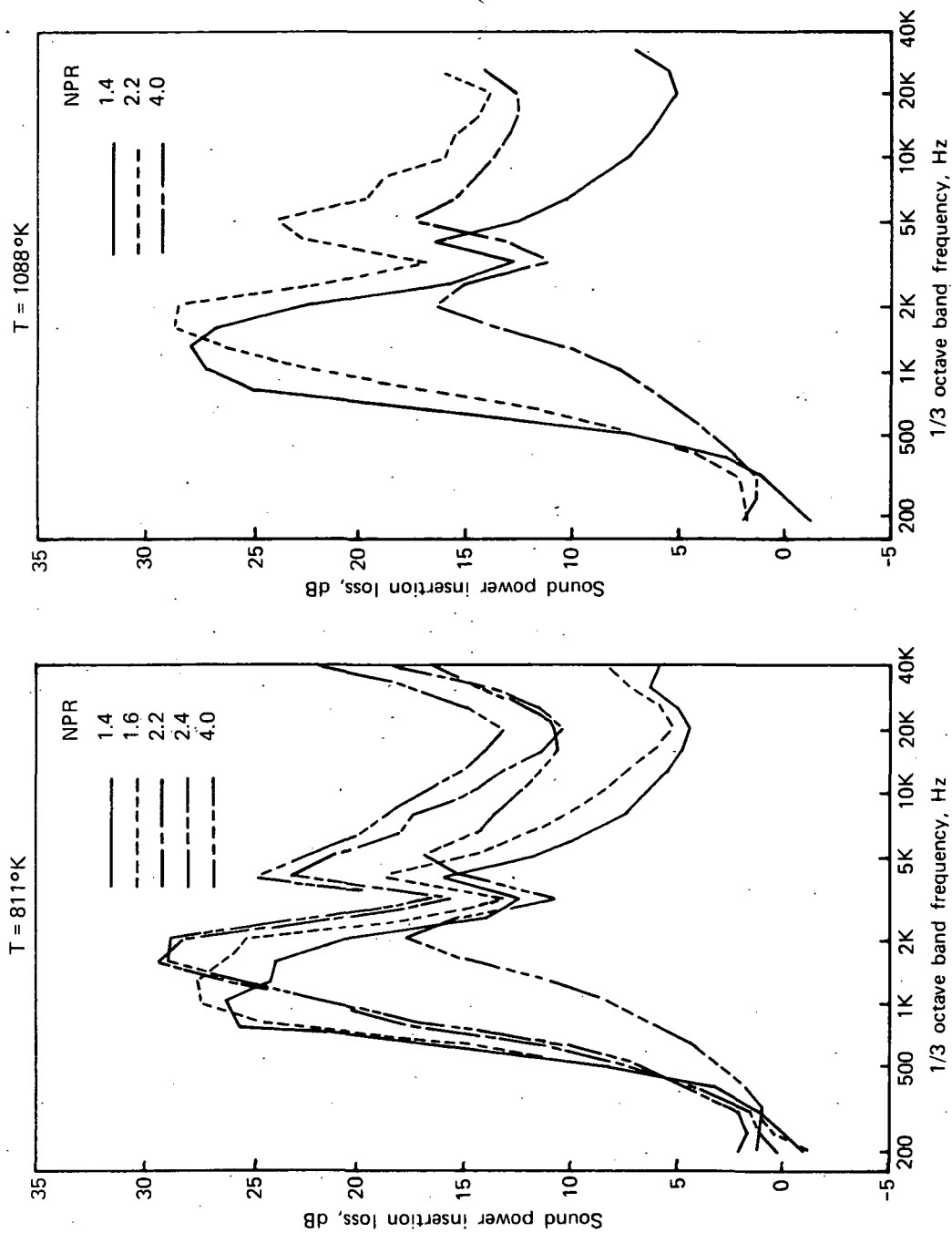
FIGURE C-15.–Concluded
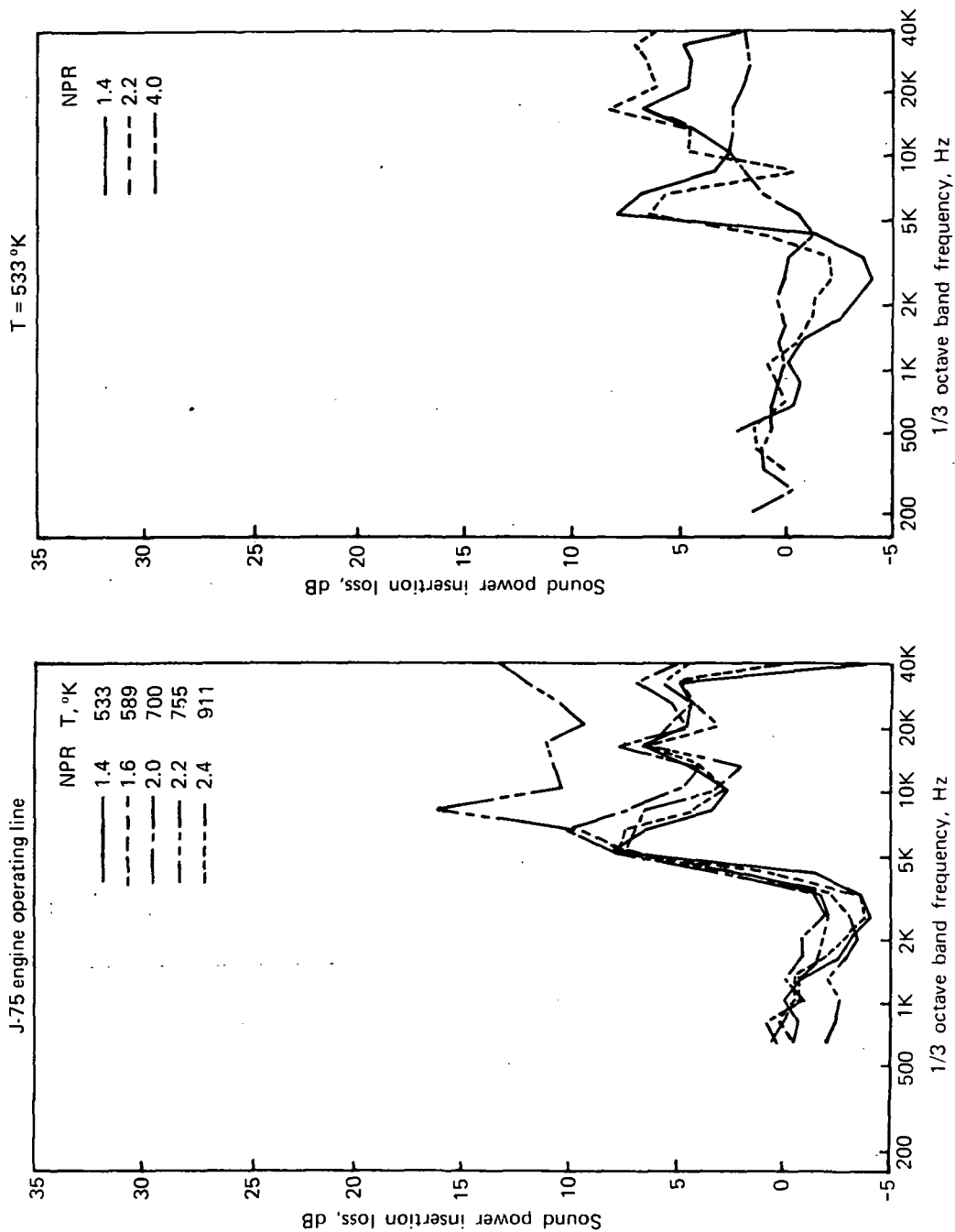
FIGURE C-16.—MODEL-SCALE SOUND POWER INSERTION LOSS SPECTRA FOR A 22% OPEN AREA, 1.4-CM-DEEP LINING IN A L/D = 4 EJECTOR AND 2.74-CM-DIAMETER NOZZLE

311
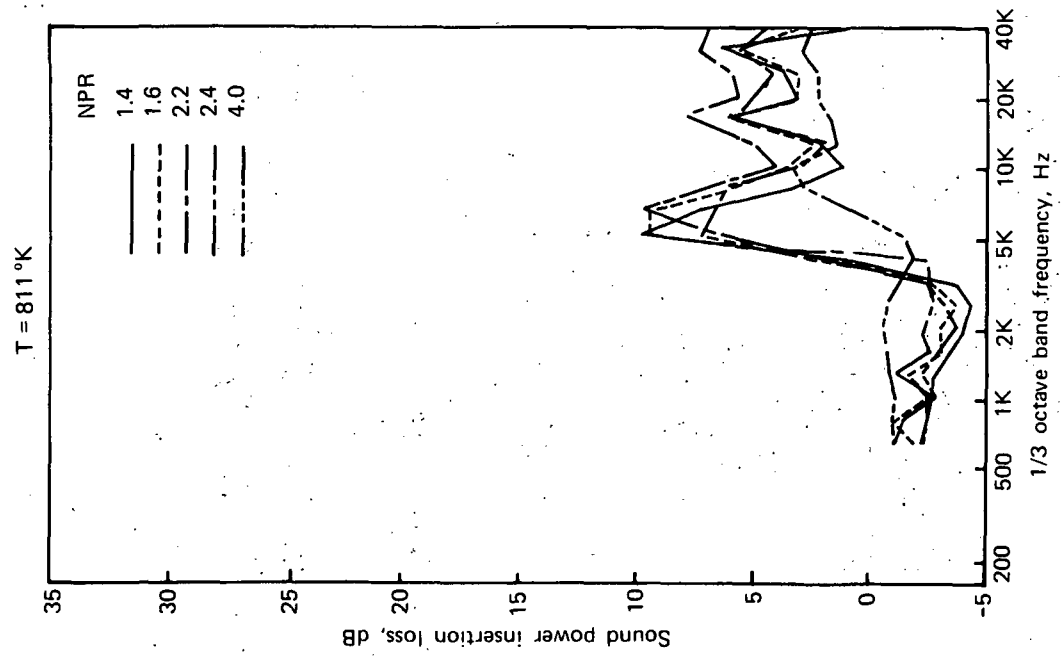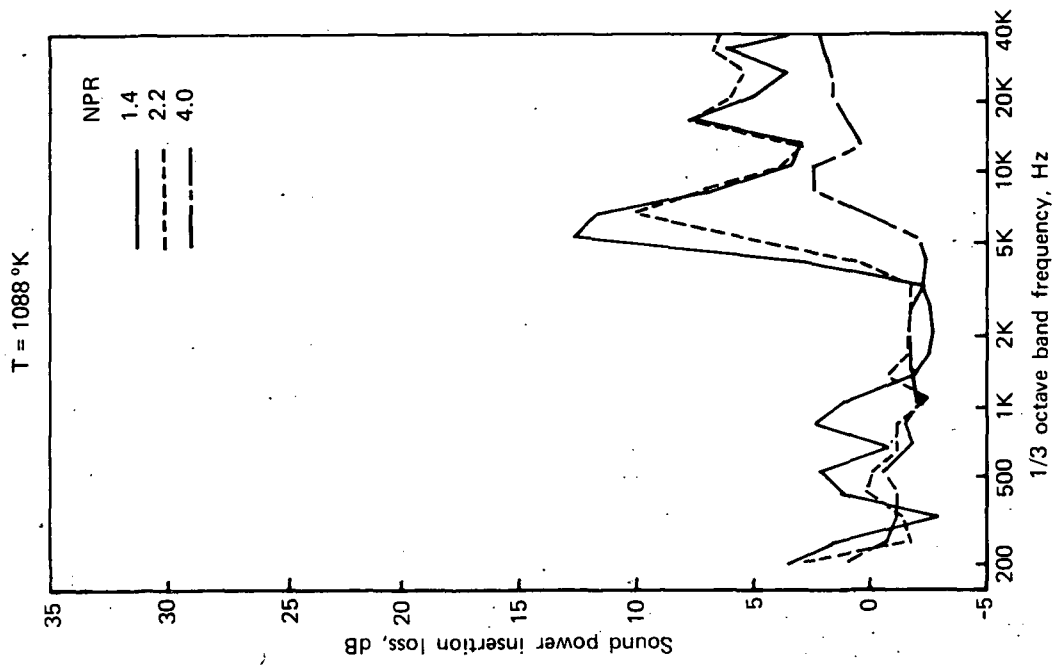
FIGURE C-16.—Concluded

312
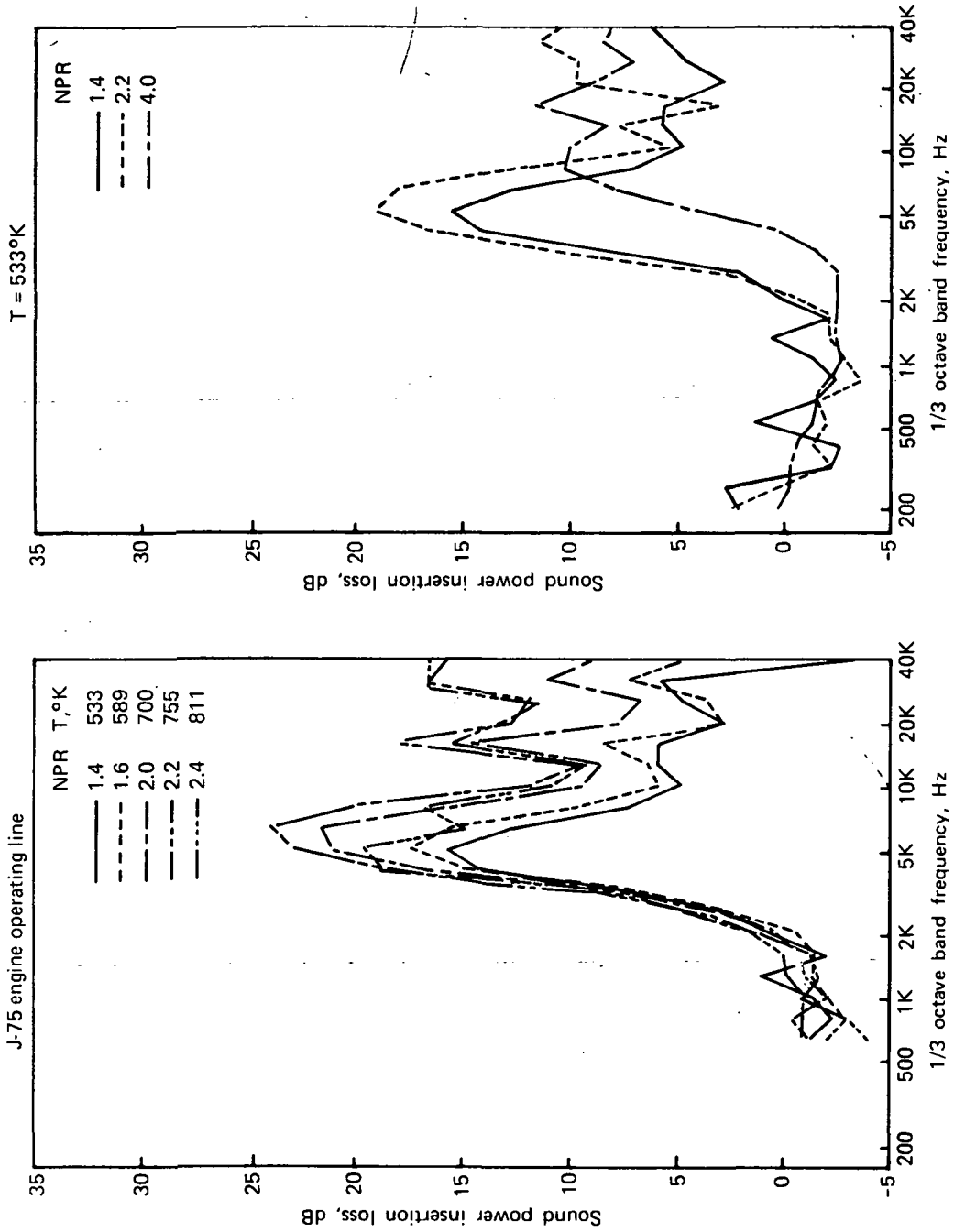
FIGURE C-17.—MODEL–SCALE SOUND POWER INSERTION LOSS SPECTRA FOR A 22% OPEN AREA, 1.4-CM-
DEEP LINING IN A L/D = 8 EJECTOR AND 2.74-CM-DIAMETER NOZZLE
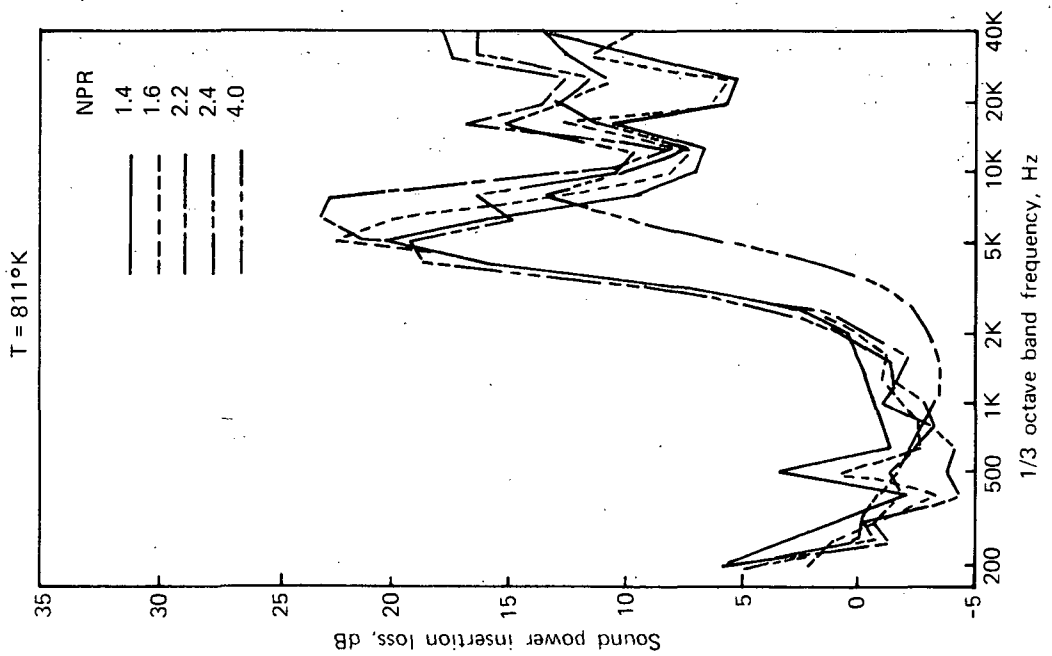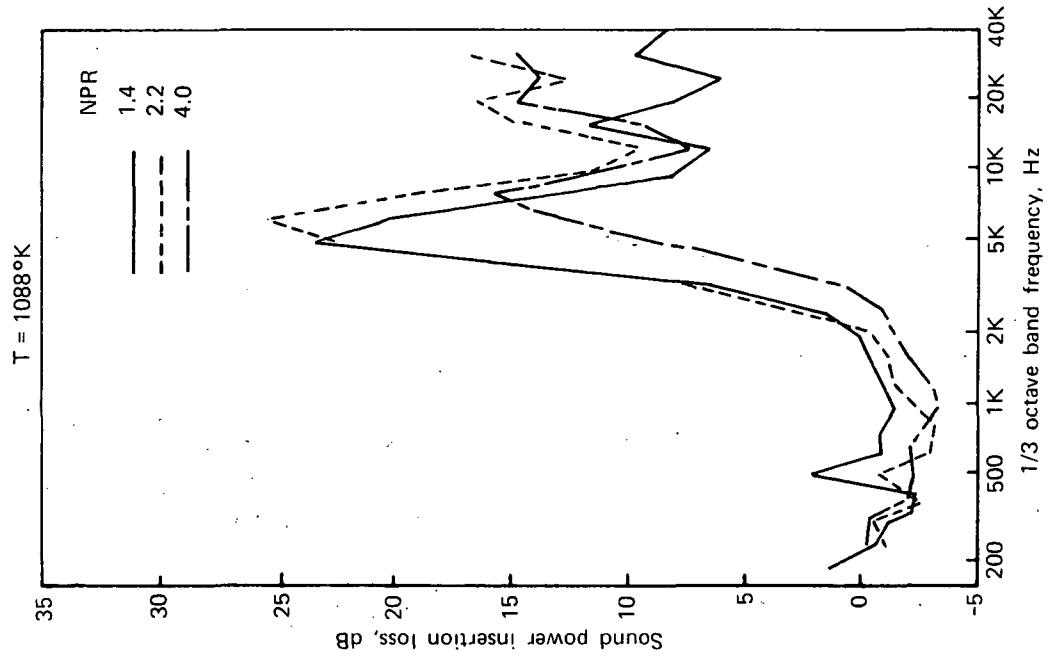
FIGURE C-17.—Concluded
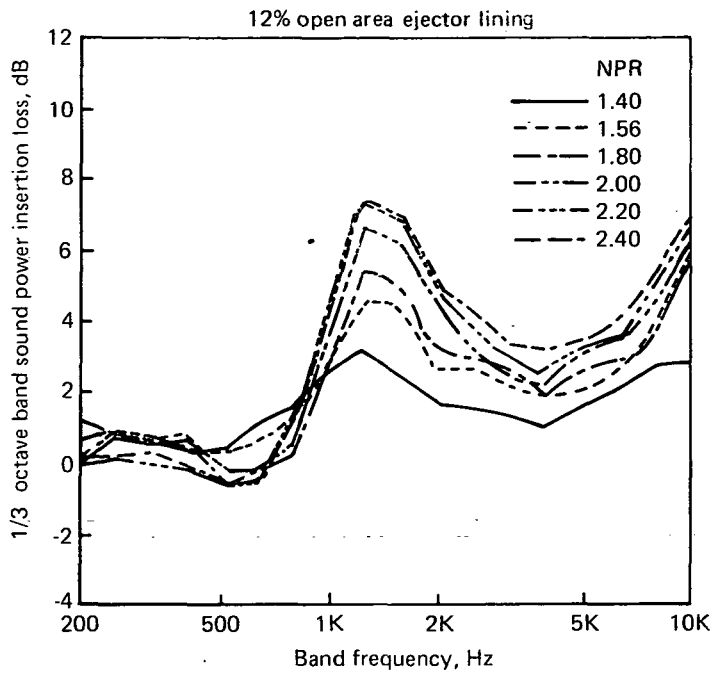
FIGURE C-18.—FULL–SCALE SOUND POWER INSERTION LOSS SPECTRA FOR A 3.8-CM-DEEP
LINING IN A L/D = 1 EJECTOR OVER THE J-75 ENGINE OPERATING LINE
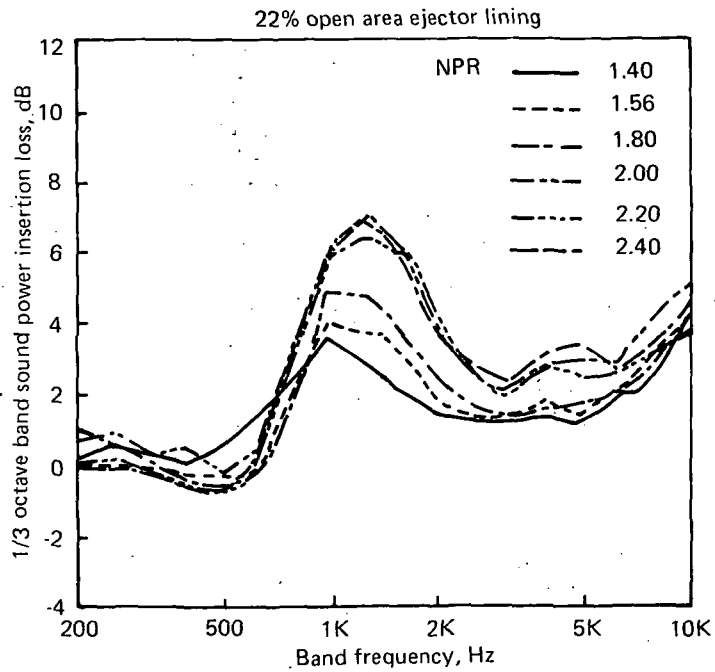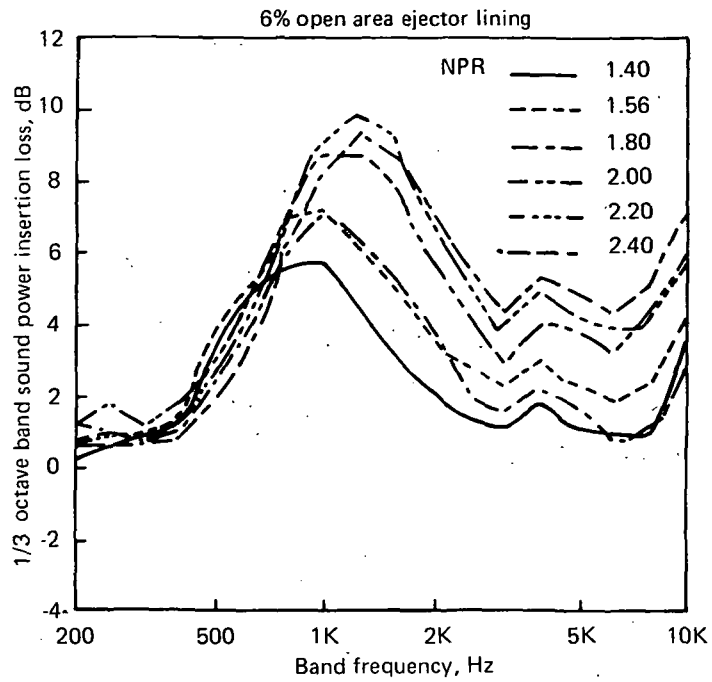
FIGURE C-19.—FULL-SCALE SOUND POWER INSERTION LOSS SPECTRA FOR A 5.3-CM-DEEP
LINING IN A L/D = 1 EJECTOR OVER THE J-75 ENGINE OPERATING LINE
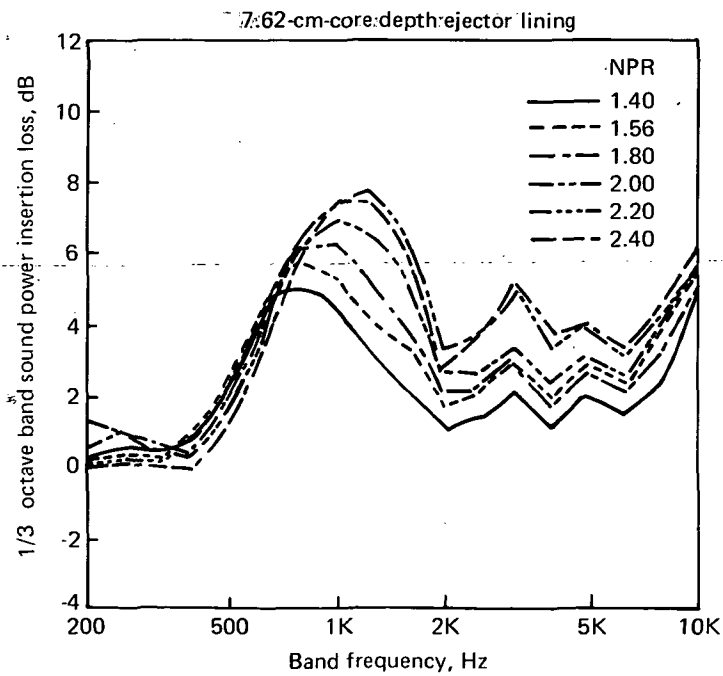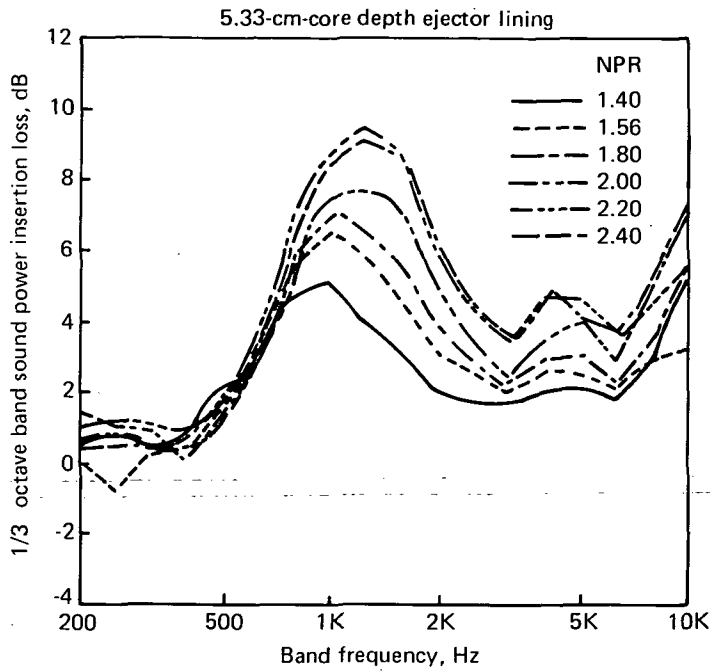
FIGURE C-20.—FULL—SCALE SOUND POWER INSERTION LOSS SPECTRA FOR A 12% OPEN
AREA LINING IN A L/D = 1 EJECTOR OVER THE J-75 ENGINE OPERATING LINE
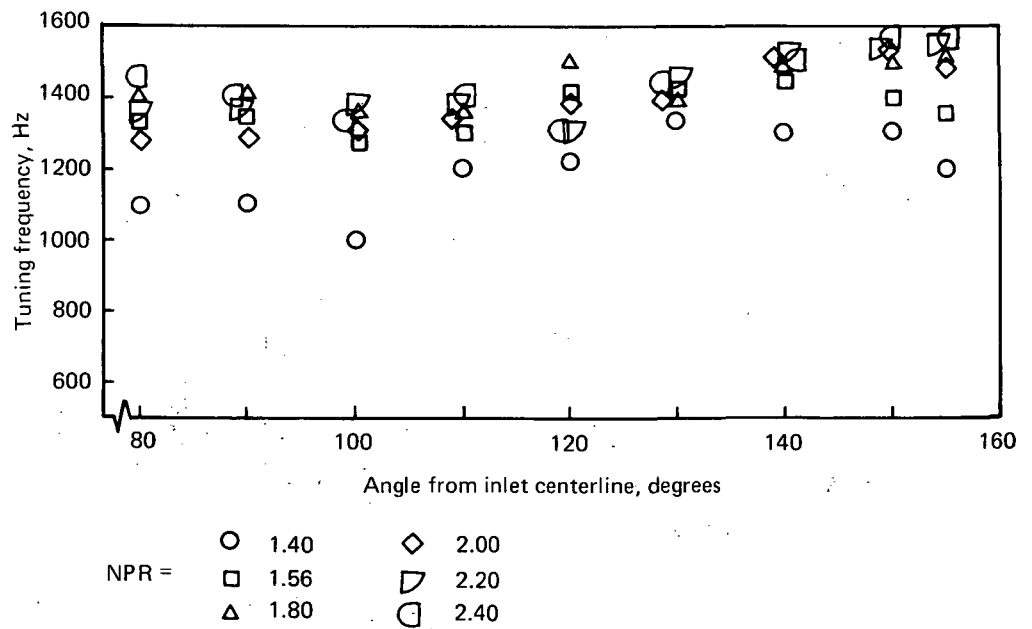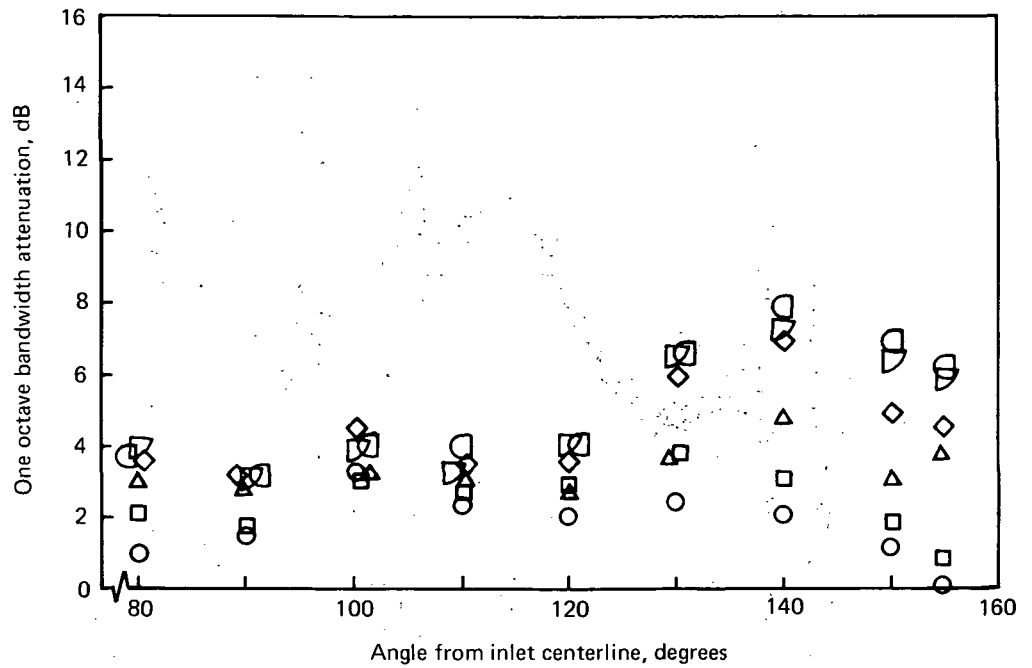
FIGURE C-21.—FULL-SCALE ACOUSTICALLY LINED EJECTOR SUPPRESSION DIRECTIVITY WITH
L/D = 1 EJECTOR AND 12% OPEN AREA, 3.8-CM-DEEP LINING
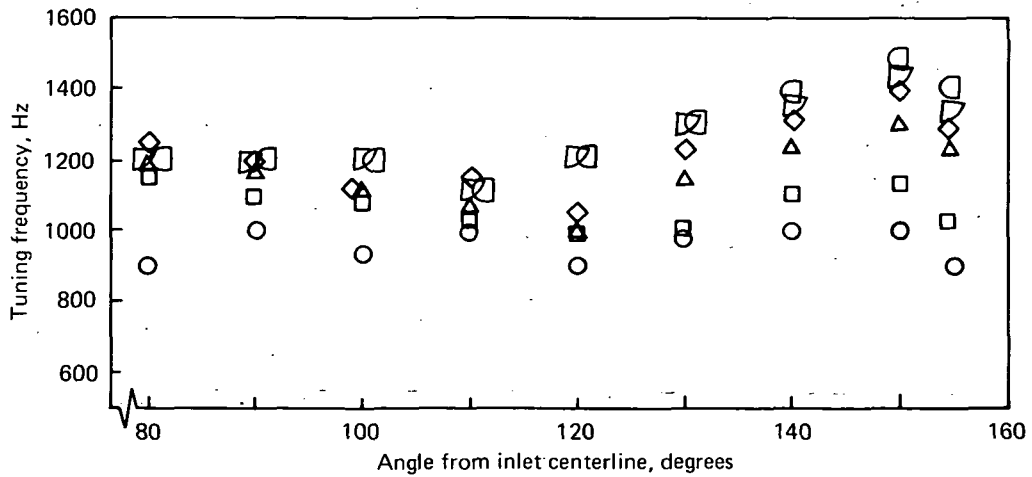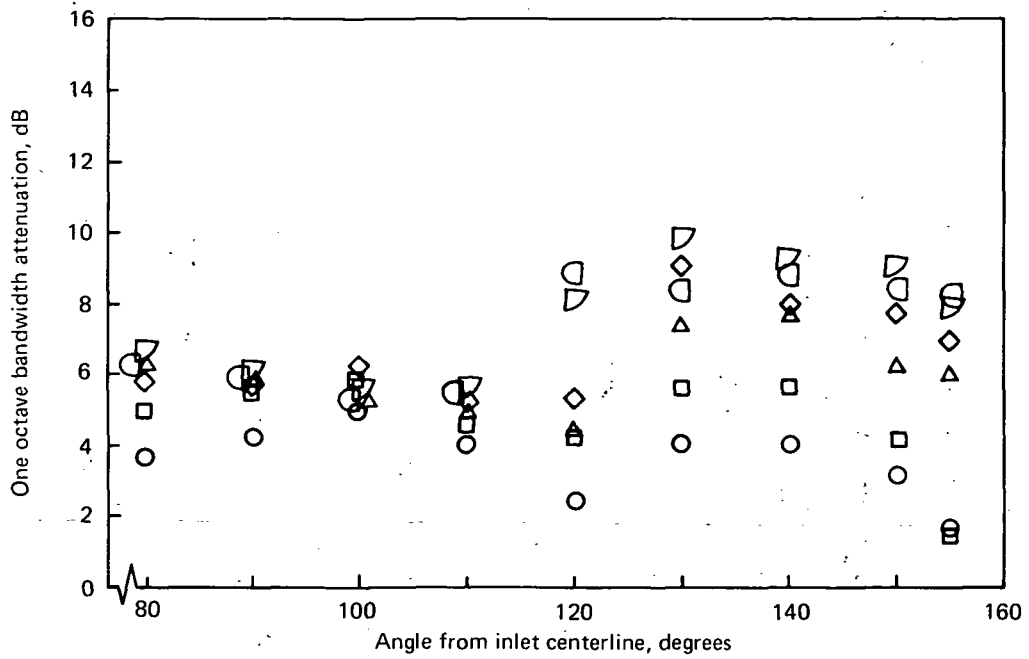
FIGURE C-22.—FULL-SCALE ACOUSTICALLY LINED EJECTOR SUPPRESSION DIRECTIVITY WITH
L/D = 1 EJECTOR AND 12% OPEN AREA, 5.3-CM-DEEP LINING
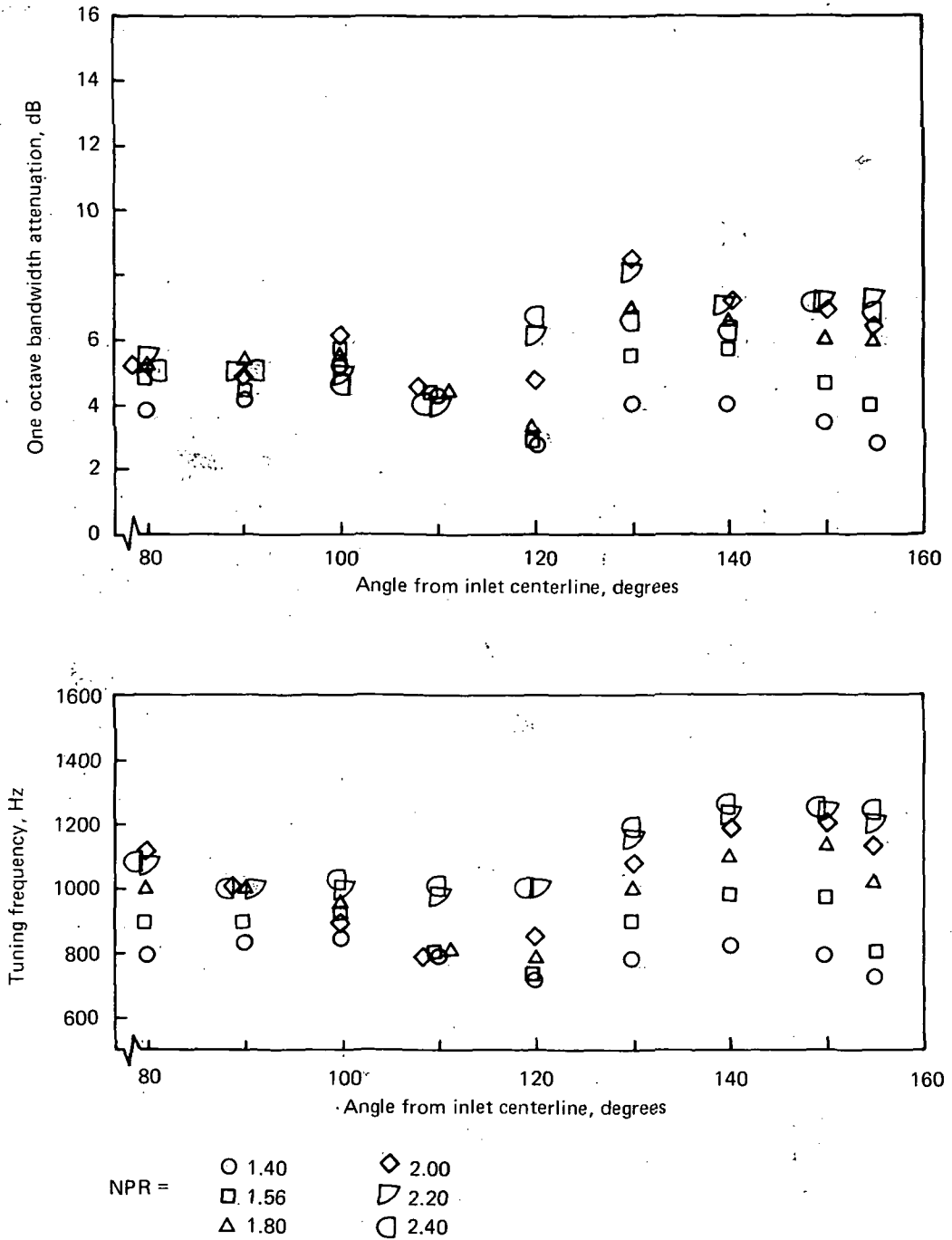
FIGURE C-23.—FULL-SCALE ACOUSTICALLY LINED EJECTOR SUPPRESSION DIRECTIVITY WITH
L/D = 1 EJECTOR AND 12% OPEN AREA, 7.6-CM-DEEP LINING
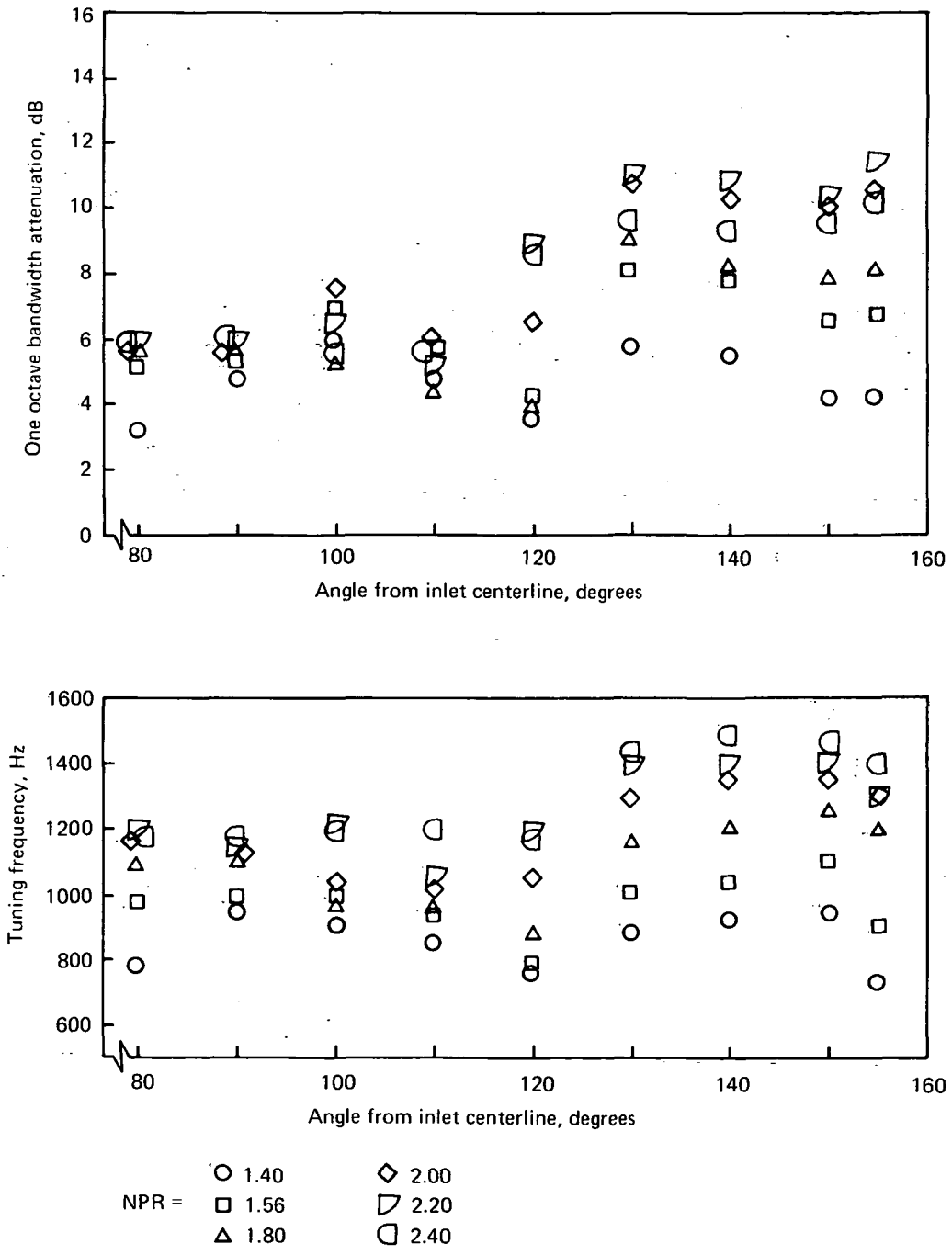
FIGURE C-24.—FULL-SCALE ACOUSTICALLY LINED EJECTOR SUPPRESSION DIRECTIVITY WITH
L/D = 1 EJECTOR AND 6% OPEN AREA, 5.3-CM-DEEP LINING
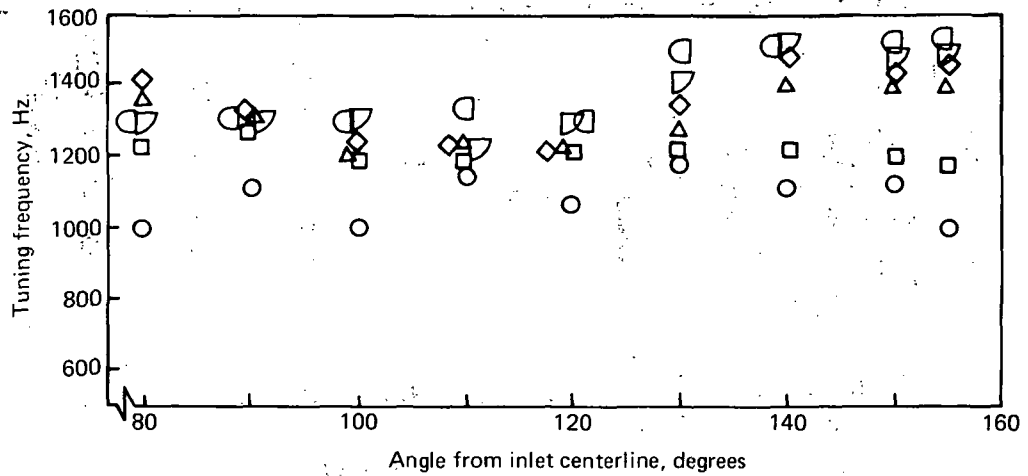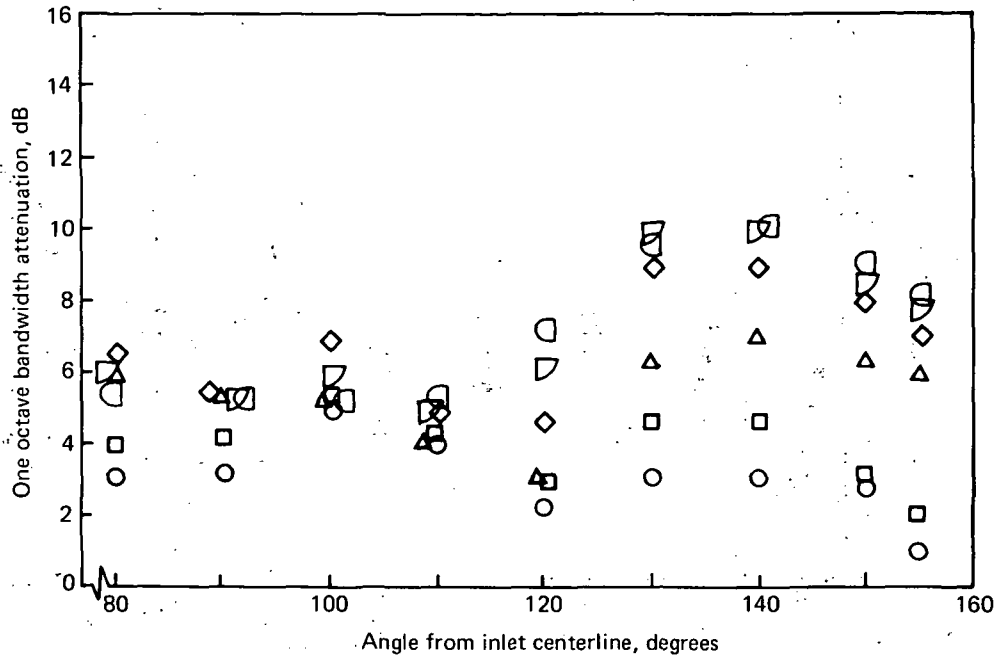
FIGURE C-25.—FULL-SCALE ACOUSTICALLY LINED EJECTOR SUPPRESSION DIRECTIVITY WITH L/D = 1 EJECTOR AND 22% OPEN AREA, 3.8-CM-DEEP LINING
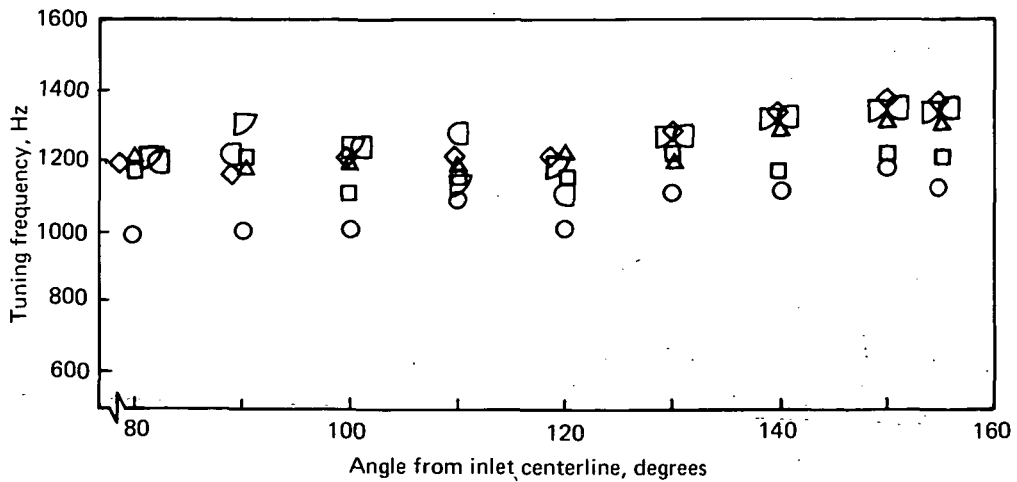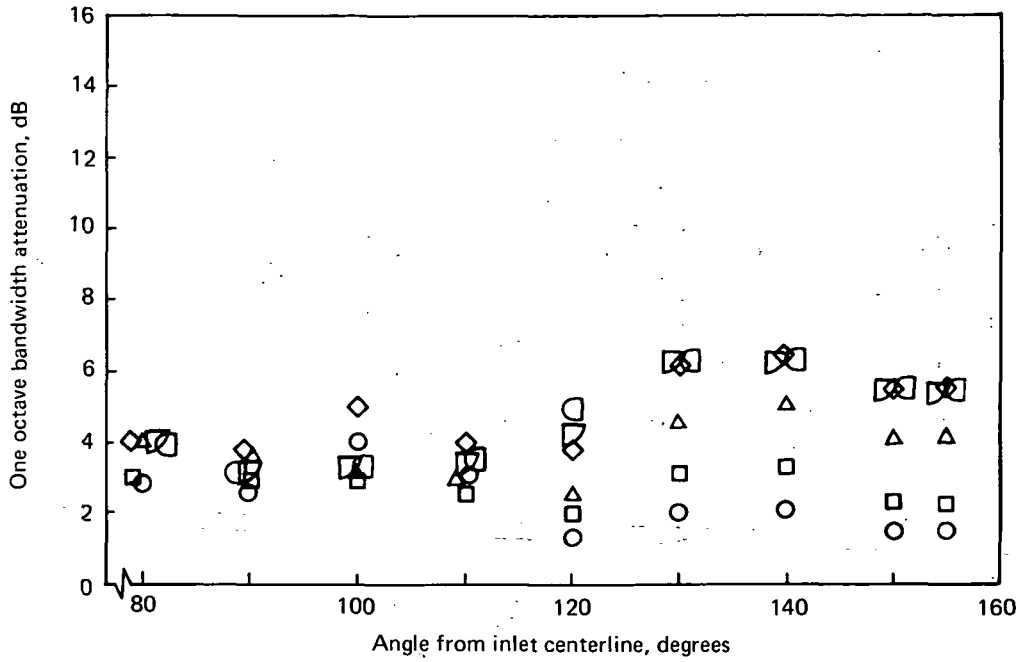
FIGURE C-26.—FULL–SCALE ACOUSTICALLY LINED EJECTOR SUPPRESSION DIRECTIVITY WITH L/D = 1 EJECTOR AND 22% OPEN AREA, 5.3-CM-DEEP LINING

323
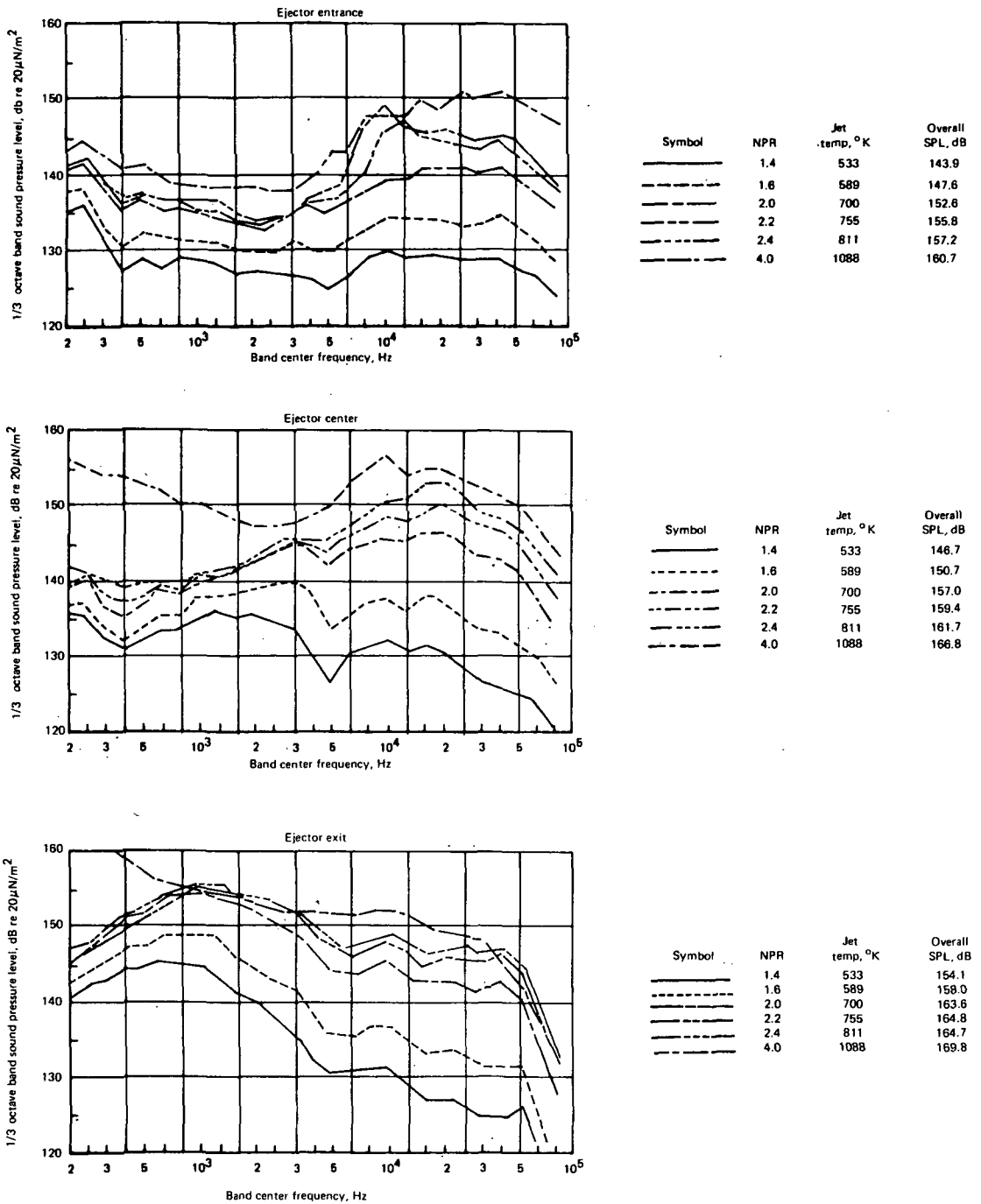
FIGURE C-27.—MODEL-SCALE EJECTOR WALL SPL SPECTRA IN THE L/D = 1 LINED EJECTOR
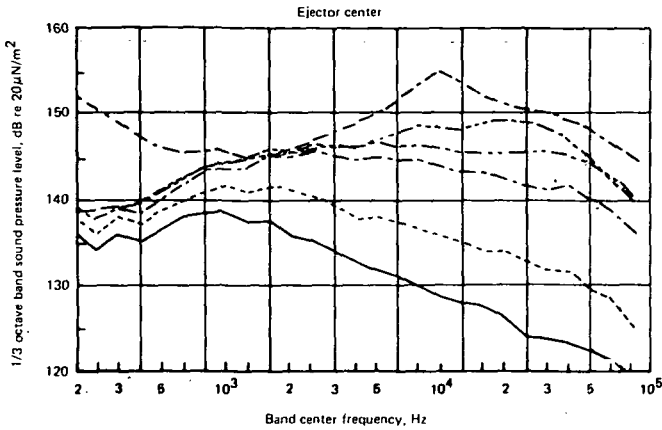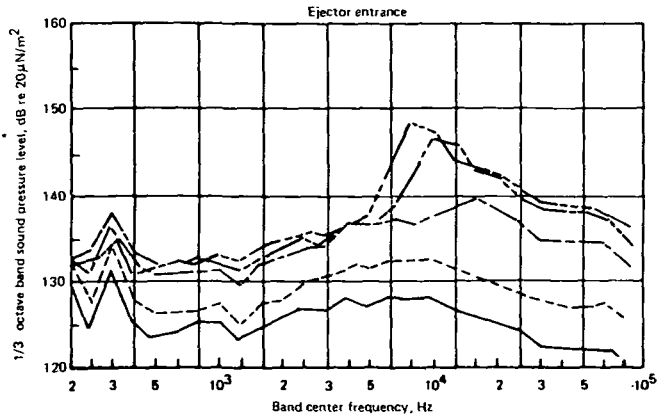(22% OPEN AREA, 1.4-CM-DEEP LINING)

324

Ejector entrance

Symbol	NPR	Jet temp. °K	Overall SPL, dB
	1.4	533	140.5
	1.6	589	144.2
	2.0	700	149.7
	2.2	755	153.8
	2.4	811	155.1

Ejector center

Symbol	NPR	Jet temp. °K	Overall SPL, dB
	1.4	533	148.4
	1.6	589	152.2
	2.0	700	157.5
	2.2	755	159.0
	2.4	811	160.4
	4.0	1088	164.2

Ejector exit

Symbol	NPR	Jet temp. °K	Overall SPL, dB
	1.4	533	145.6
	1.6	589	149.9
	2.0	700	157.7
	2.2	755	159.6
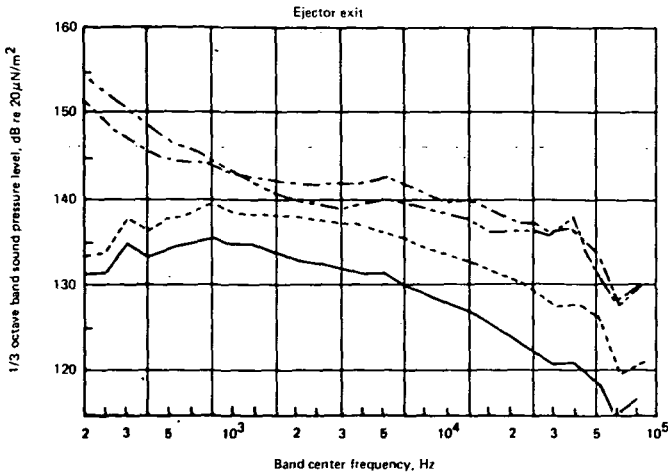
FIGURE C-28.—MODEL-SCALE EJECTOR WALL SPL SPECTRA IN THE L/D = 2 HARDWALL EJECTOR

325

FIGURE C-29.—MODEL-SCALE EJECTOR WALL SPL SPECTRA IN THE L/D = 8 LINED EJECTOR AND 10.9-CM CONICAL NOZZLE 12% OPEN AREA, 3.8-CM-DEEP LINING)

Ejector entrance
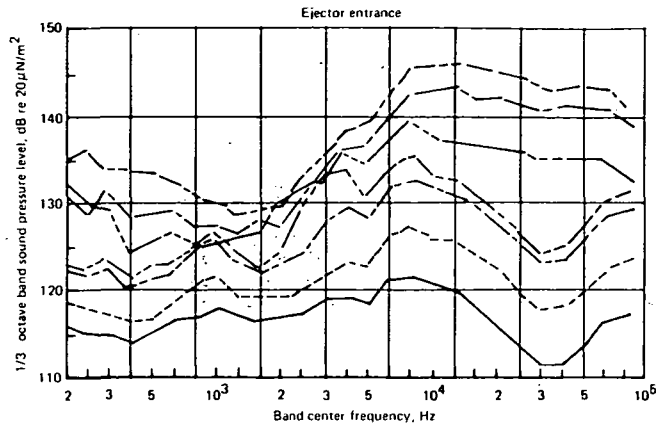
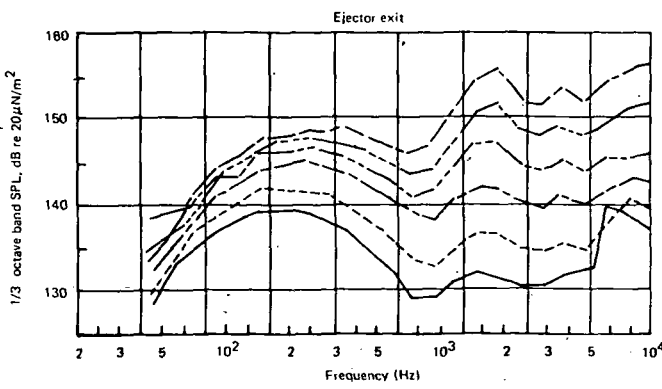| Symbol	NPR	Jet temp, °K	Overall SPL, dB
	1.4	533	131.7
	1.6	589	136.4
	2.0	700	141.5
	2.2	755	144.0
	2.4	811	148.3
	4.0	1088	152.7
	4.0	1643	155.8

Ejector center
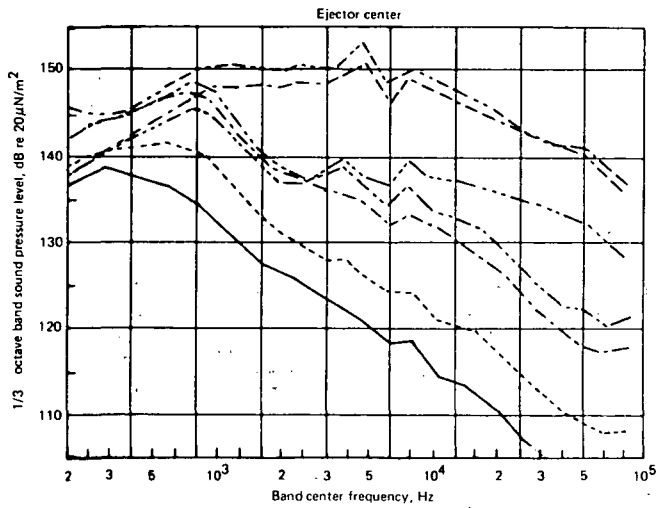
Symbol	NPR	Jet temp, °K	Overall SPL, dB
	1.4	533	145.9
	1.6	589	150.0
	2.0	700	155.3
	2.2	755	156.1
	2.4	811	154.0
	4.0	1088	160.7
	4.0	1643	162.5

Ejector exit
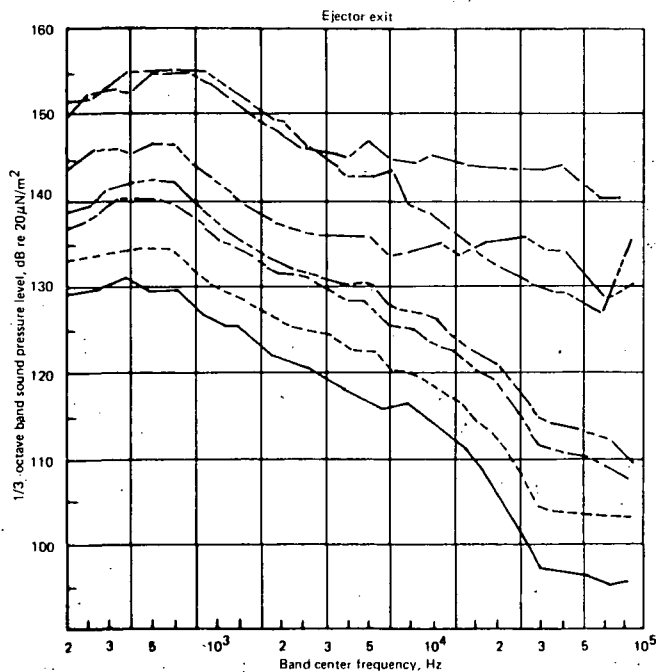
Symbol	NPR	Jet temp, °K	Overall SPL, dB
	1.4	533	138.8
	1.6	589	143.2
	2.0	700	148.6
	2.2	755	150.5
	2.4	811	155.5
	4.0	1088	164.0
	4.0	1643	163.9

Ejector entrance

Symbol	NPR	Jet temp, °K	Overall SPL, dB
	1.4	595	150.5
	1.56	628	150.8
	1.8	673	151.8
	2.0	723	152.8
	2.2	761	155.3
	2.4	823	158.0

Ejector center
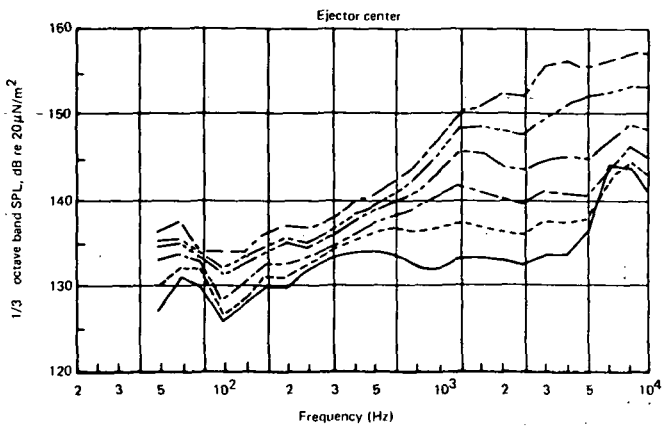
Symbol	NPR	Jet temp, °K	Overall SPL, dB
	1.4	595	151.8
	1.56	628	153.1
	1.8	673	155.6
	2.0	723	158.3
	2.2	761	163.3
	2.4	823	167.1

Ejector exit

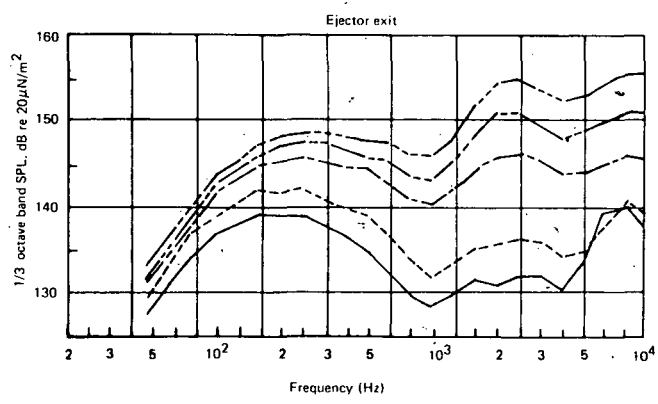| Symbol	NPR	Jet temp, °K	Overall SPL, dB
	1.4	595	151.6
	1.56	628	153.9
	1.8	673	157.1
	2.0	723	160.4
	2.2	761	163.4
	2.4	823	166.9

FIGURE C-30.– FULL-SCALE EJECTOR WALL SPL SPECTRA IN THE L/D = 1 LINED EJECTOR
(12% OPEN AREA, 7.6-CM-DEEP LINING)

327

Ejector entrance
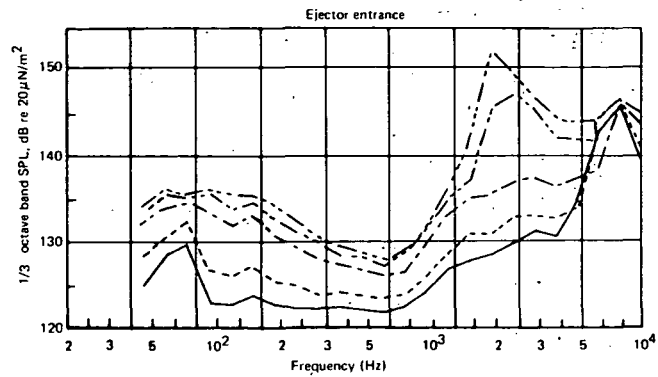
Symbol	NPR	Jet temp, °K	Overall SPL, dB
————	1.4	595	151.5
········	1.56	628	151.0
—·—·—	2.0	723	152.2
—··—··—	2.2	761	156.2
—···—···—	2.4	823	158.7

Ejector center
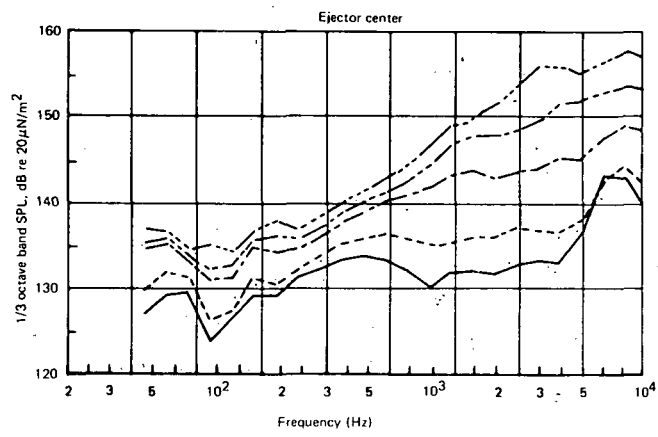
Symbol	NPR	Jet temp, °K	Overall SPL, dB
————	1.4	595	151.1
- - - -	1.56	628	152.6
— — —	2.0	723	158.1
—·—·—	2.2	761	163.1
—··—··—	2.4	823	166.6

Ejector exit

Symbol	NPR	Jet temp, °K	Overall SPL, dB
————	1.4	595	151.0
- - - -	1.56	628	153.7
— — —	2.0	723	159.5
—·—·—	2.2	761	163.2
—··—··—	2.4	823	166.5

FIGURE C-31.— FULL-SCALE EJECTOR WALL SPL SPECTRA IN THE L/D = 1 LINED EJECTOR
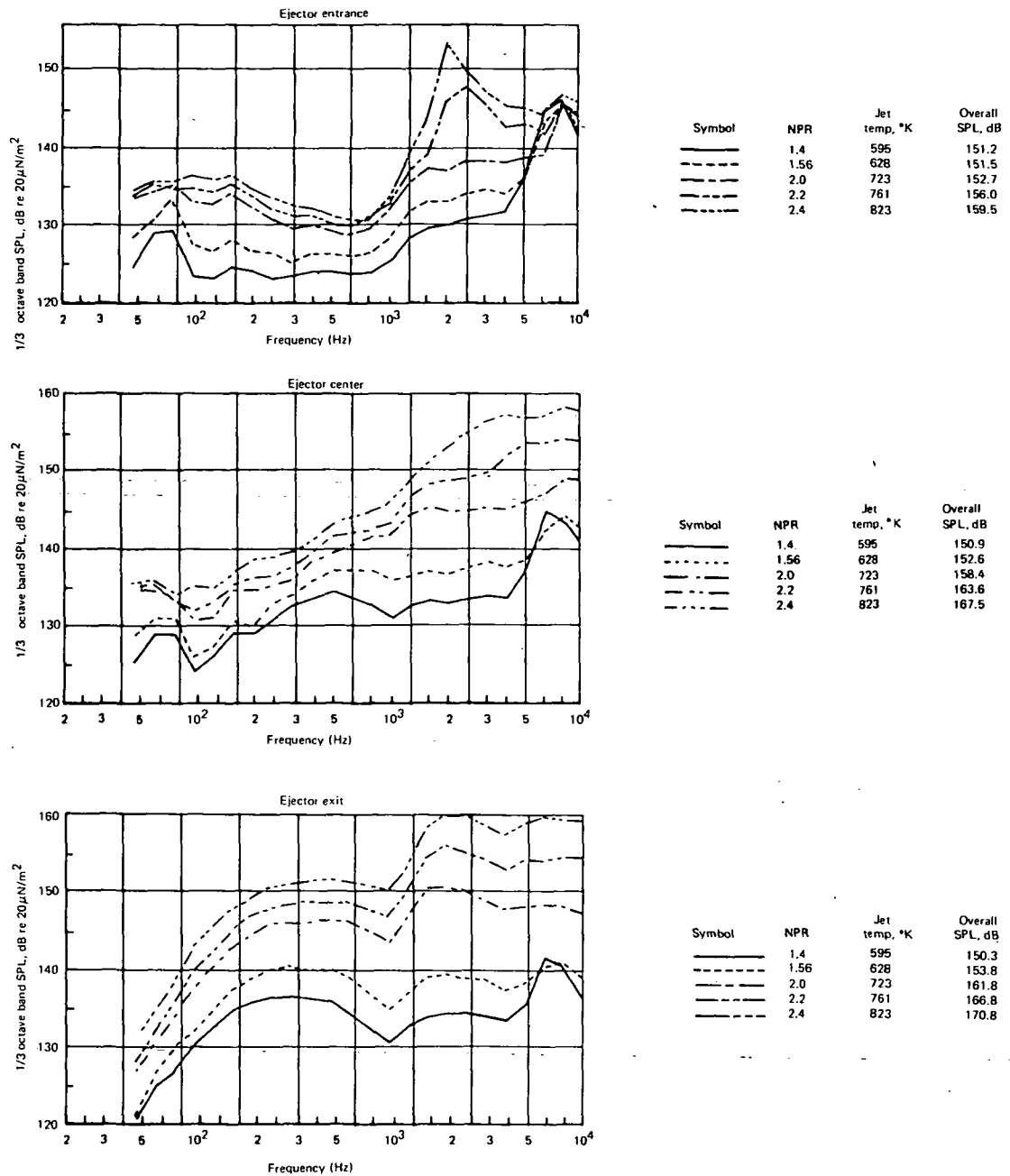(11% OPEN AREA, 5.3-CM-DEEP LINING)

328

FIGURE C-32.—FULL-SCALE EJECTOR WALL SPL SPECTRA IN THE L/D = 1 LINED EJECTOR (22% OPEN AREA, 5.3-CM-DEEP LINING)
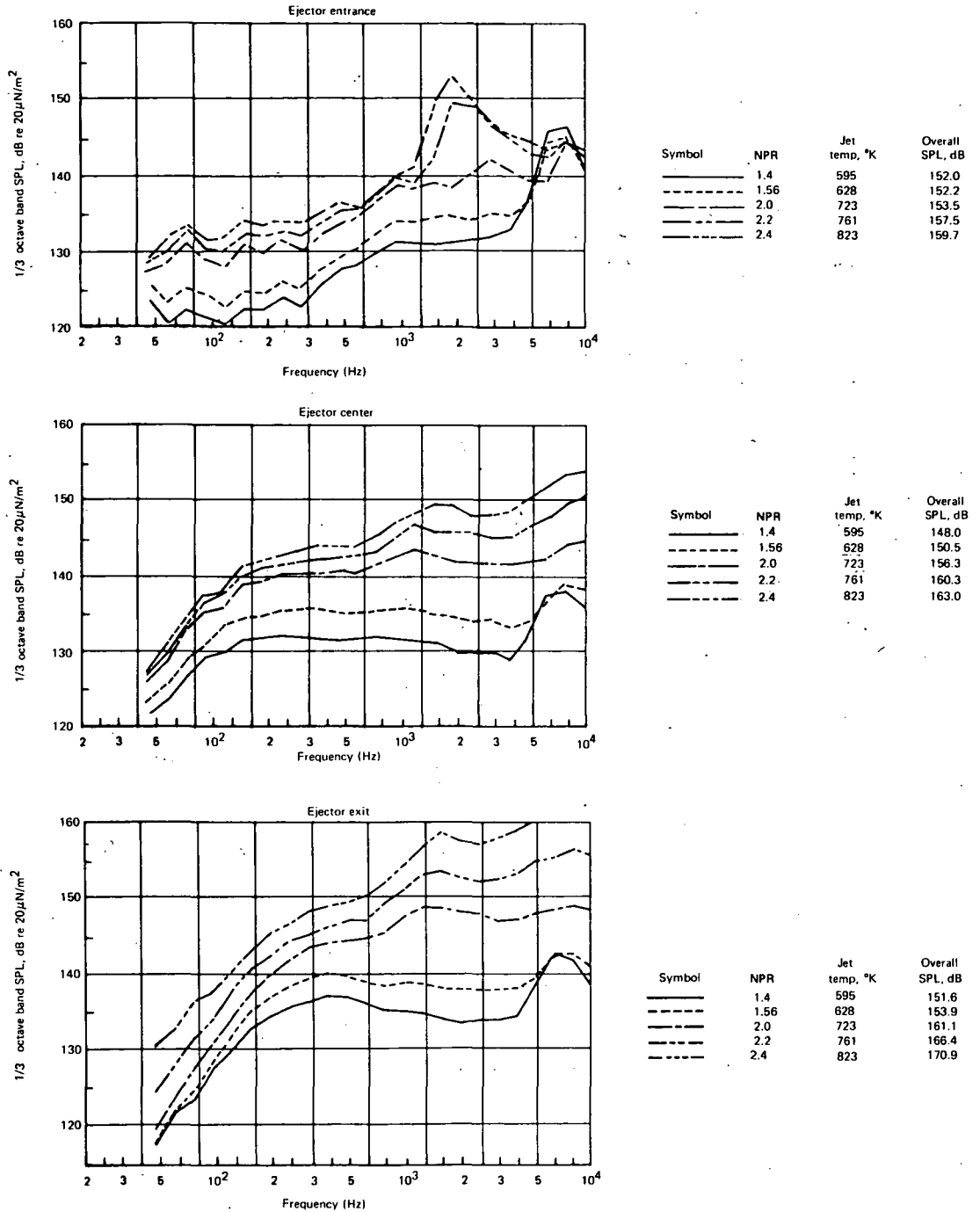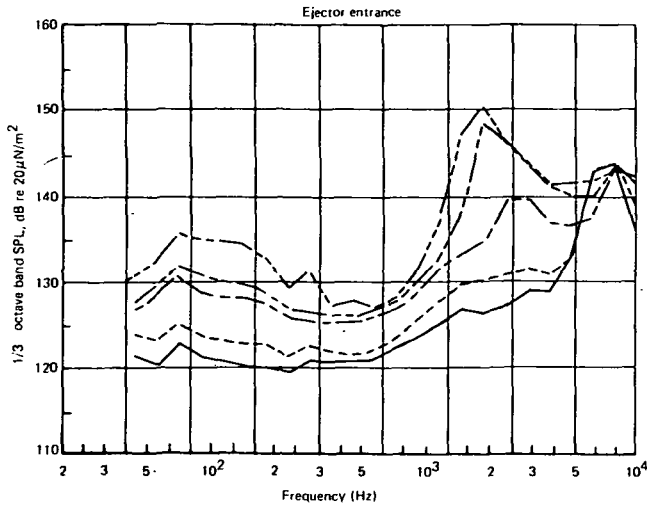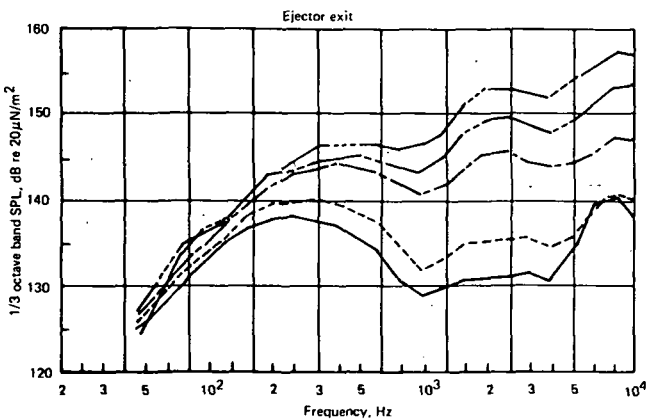
Ejector entrance

Symbol	NPR	Jet temp, °K	Overall SPL, dB
	1.4	595	152.0
	1.56	628	152.2
	2.0	723	153.5
	2.2	761	157.5
	2.4	823	159.7

Ejector center

Symbol	NPR	Jet temp, °K	Overall SPL, dB
	1.4	595	148.0
	1.56	628	150.5
	2.0	723	156.3
	2.2	761	160.3
	2.4	823	163.0

Ejector exit

Symbol	NPR	Jet temp, °K	Overall SPL, dB
	1.4	595	151.6
	1.56	628	153.9
	2.0	723	161.1
	2.2	761	166.4
	2.4	823	170.9

FIGURE C-33.—FULL-SCALE EJECTOR WALL SPL SPECTRA IN THE L/D = 2 HARDWALL EJECTOR

FIGURE C-34.—FULL-SCALE EJECTOR WALL SPL SPECTRA IN THE L/D = 2 LINED EJECTOR (12% OPEN AREA, 5.3-CM-DEEP LINING)

Page Intentionally Left Blank

"The aeronautical and space activities of the United States shall be conducted so as to contribute ... to the expansion of human knowledge of phenomena in the atmosphere and space. The Administration shall provide for the widest practicable and appropriate dissemination of information concerning its activities and the results thereof."
—NATIONAL AERONAUTICS AND SPACE ACT OF 1958

NASA SCIENTIFIC AND TECHNICAL PUBLICATIONS

TECHNICAL REPORTS: Scientific and technical information considered important, complete, and a lasting contribution to existing knowledge.

TECHNICAL NOTES: Information less broad in scope but nevertheless of importance as a contribution to existing knowledge.

TECHNICAL MEMORANDUMS: Information receiving limited distribution because of preliminary data, security classification, or other reasons. Also includes conference proceedings with either limited or unlimited distribution.

CONTRACTOR REPORTS: Scientific and technical information generated under a NASA contract or grant and considered an important contribution to existing knowledge.

TECHNICAL TRANSLATIONS: Information published in a foreign language considered to merit NASA distribution in English.

SPECIAL PUBLICATIONS: Information derived from or of value to NASA activities. Publications include final reports of major projects, monographs, data compilations, handbooks, sourcebooks, and special bibliographies.

TECHNOLOGY UTILIZATION PUBLICATIONS: Information on technology used by NASA that may be of particular interest in commercial and other non-aerospace applications. Publications include Tech Briefs, Technology Utilization Reports and Technology Surveys.

Details on the availability of these publications may be obtained from:

SCIENTIFIC AND TECHNICAL INFORMATION OFFICE

NATIONAL AERONAUTICS AND SPACE ADMINISTRATION
Washington, D.C. 20546